AFRPL-TR-76-11

ANALYTICAL PREDICTION OF MOTOR COMPONENT VIBRATIONS DRIVEN BY ACOUSTIC COMBUSTION INSTABILITY

FINAL REPORT

Hercules Incorporated
Systems Group
Wilmington, Delaware 19899

Author: F. R. JENSEN

MARCH 1976

APPROVED FOR PUBLIC RELEASE

DISTRIBUTION UNLIMITED

AIR FORCE ROCKET PROPULSION LABORATORY
DIRECTOR OF SCIENCE AND TECHNOLOGY
AIR FORCE SYSTEMS COMMAND
EDWARDS AFB, CALIFORNIA 93523

Best Available Copy

FOREWORD

This report constitutes the final report for the original portion of the AFRPL Motor Component Vibration Study, Contract F04611-73-C-0025. The contract was recently amended to include an analysis of the Space Shuttle Booster motors. A separate final report will be issued on the Space Shuttle work. The work reported was accomplished at Hercules Incorporated, Bacchus Works, Magna, Utah.

This report is submitted in accordance with data item B-006 of the referenced contract. Contract F04611-73-C-0025 was issued to Hercules by the Air Force Rocket Propulsion Laboratory, Edwards, CA 93523. Project engineers for the contract have been Mr. D. Thrasher and Dr. D. George. The current project engineer is Mr. W. C. Andrepont.

A subcontract was issued to the MacNeal-Schwendler Corporation for modifications to the NASTRAN computer program. Cyclic symmetry analysis capability was added to the frequency response package (Rigid Format 8), in level 15.0 NASTRAN by MacNeal-Schwendler.

The Lockheed Missiles and Space Company at Sunnyvale, California furnished data on the components that are attached to the aft dome of the C-3 Poseidon SS motor. In addition, Lockheed loaned Hercules an inert Poseidon SS motor for use in the acoustics testing portion of this program. The Aerojet Solid Propulsion Company at Sacramento, California supplied reports and other data on the Minuteman III third stage motor for use in constructing finite element models of the motor.

The following Hercules employees have made significant contributions to this effort: E. Hikida (Task 3), L. West (Task 4), B. Moore (Tasks 8, 10 and 11), D. Wang (Task 11) and F.R. Jensen, Principal Investigator.

W. C. ANDREPONT, GS-14
Project Engineer

WILLIAM D. SIURU, JR., Major USAF
Chief, Supporting Technology Branch

FOR THE COMMANDER

JAMES T. EDWARDS, Deputy Chief
Technology Division

UNCLASSIFIED

SECURITY CLASSIFICATION OF THIS PAGE (When Data Entered)

REPORT DOCUMENTATION PAGE		READ INSTRUCTIONS BEFORE COMPLETING FORM
1. REPORT NUMBER AFRPL-TR-76-11	2. GOVT ACCESSION NO.	3. RECIPIENT'S CATALOG NUMBER
4. TITLE (and Subtitle) ANALYTICAL PREDICTION OF MOTOR COMPONENT VIBRATIONS DRIVEN BY ACOUSTIC COMBUSTION INSTABILITY		5. TYPE OF REPORT & PERIOD COVERED Final Report, Aug 72 — Dec 75
		6. PERFORMING ORG. REPORT NUMBER
7. AUTHOR(s) F. R. Jensen		8. CONTRACT OR GRANT NUMBER(s) F04611-73-C-0025
9. PERFORMING ORGANIZATION NAME AND ADDRESS Hercules Incorporated Wilmington, Delaware		10. PROGRAM ELEMENT, PROJECT, TASK AREA & WORK UNIT NUMBERS JON 57301OBY
11. CONTROLLING OFFICE NAME AND ADDRESS Air Force Rocket Propulsion Laboratory Edwards, CA 93523		12. REPORT DATE February 1976
		13. NUMBER OF PAGES 648
14. MONITORING AGENCY NAME & ADDRESS (if different from Controlling Office) (12) 656		15. SECURITY CLASS. (of this report) UNCLASSIFIED
		15a. DECLASSIFICATION/DOWNGRADING SCHEDULE N/A

16. DISTRIBUTION STATEMENT (of this Report)

APPROVED FOR PUBLIC RELEASE; DISTRIBUTION UNLIMITED

17. DISTRIBUTION STATEMENT (of the abstract entered in Block 20, if different from Report)

18. SUPPLEMENTARY NOTES

19. KEY WORDS (Continue on reverse side if necessary and identify by block number)

Solid rocket motors, structural dynamics analyses, structural response to unstable acoustic oscillations, mechanical impedance applications, cyclic symmetry analysis applications, acoustic/structural testing

20. ABSTRACT (Continue on reverse side if necessary and identify by block number)

A detailed investigation has been conducted on the structural dynamic response of solid rocket motors. The study was particularly concerned with estimating the structural response to unstable acoustic combustion oscillations that often occur in solid motors during motor firing time. Detailed finite element analyses were performed on the Poseidon C-3 second stage motor and on the Minuteman III third stage motor using a NASTRAN computer program. In addition, the response of an inert second stage Poseidon C-3 motor to

DD FORM 1 JAN 73 1473 EDITION OF 1 NOV 65 IS OBSOLETE

UNCLASSIFIED

SECURITY CLASSIFICATION OF THIS PAGE (When Data Entered)

4.

internal acoustic excitation was measured during an experimental task. A significant new analysis tool became available when the MacNeal-Schwendler Company incorporated the cyclic symmetry option into the NASTRAN frequency response rigid format using resources from this project.

Results from the analyses were evaluated by comparing them with test data (from the inert Poseidon C-3 motor) and with actual firing data. Several special analyses were conducted on parts of the motor structure, such as separate grain or dome models, to better define expected overall motor response and to investigate possible modeling simplifications. Mechanical Impedance methods were used in the detailed motor analyses to account for components that are not symmetric about the motor centerline.

Results from the AFRPL Component Vibration program that are given in the final report provide a considerable amount of detail on typical measured and predicted rocket motor response to acoustic combustion oscillations. The information given should be of value to an engineer planning similar analyses on other rocket motor designs. In addition to the experimental and analytical results, specific guidelines for future analysis projects are provided in a modeling techniques manual.

TABLE OF CONTENTS

TABLE OF CONTENTS (Cont)

LIST OF FIGURES

LIST OF TABLES

SECTION I

INTRODUCTION

There were two major objectives of the Component Vibration program: (1) Develop simplified finite element structural modeling techniques for the determination of permissible limiting amplitudes of acoustic pressure oscillations on the basis of motor-mounted hardware vibration limits, and (2) develop criteria for the degree of simplification which can be tolerated in structural modeling of the rocket motor for combustion-instability-related dynamic structural analyses.

Acoustic pressure oscillations in the combustion cavity of a solid propellant rocket motor can impose excessive dynamic loads on structural components and attached auxiliary motor hardware and on hydraulic and electronic equipment. The problem of combustion instability has received renewed emphasis in recent years because of these structural effects. High dynamic loads (accelerations) have been observed on structural components - particularly in high-strength, low-modulus rocket motor cases - at relatively low oscillating pressure amplitudes (<3 psi in the Poseidon second stage). Dynamic response to acoustic pressure oscillations must be predicted to define acceleration levels to be expected on individual components during flight and static firings. This information is then used to indicate possible redesign of the motor or a component, to define component qualification test specifications, or to design a means for shock isolation. Since the analysis method must account for motor design parameters it may be used to assist in redesign efforts.

Nearly all solid propellant rocket motors currently in use in upper stage ballistic missiles exhibit some degree of combustion instability. In strategic missiles, the most vibration-sensitive guidance equipment is placed on or above the upper stage motors. The upper stages are, therefore, of great concern with regard to tolerable levels of acoustic combustion oscillation.

High amplitude vibrations may be detrimental to components that have been designed and qualified to withstand lower levels. For example, MIL-STD-810B requires vibration tests at levels up to a maximum of 50 g's for components mounted on ground-launched or air-launched missiles. Vibration levels over 100 g's have been observed on the Minuteman II third stage motor and vibration levels over 300 g's have been observed on both the Minuteman III third stage and Poseidon C-3 second stage motors.

Guidance and related motor control hardware are normally constructed of lightly-damped metal and plastic materials in comparison to the heavily-damped propellant grain. Hence, vibration amplitudes associated with resonances of these components can be very high. The degree to which combustion instability can be tolerated depends upon the relative resonant frequency ranges of the components and the acoustic cavity, which can often be unstable at several frequencies over a broad range.

The work planned to accomplish the stated objectives was divided into three separate phases, with each phase having its own objective. The work within each phase was further divided into tasks. The three phases and 14 tasks that constitute the total effort are as follows:

Phase I - Establish a Baseline Analysis

Task 1 - Select a Baseline Motor

Task 2 - Baseline Motor Acoustics Analysis

Task 3 - Baseline Motor Structural Dynamics Analysis

Task 4 - Structural Response Testing Using Acoustic Excitation

Task 5 - Baseline Motor Analysis Evaluation

Phase II - Simplified Modeling Studies

Task 6 - Select Simplified Modeling Techniques

Task 7 - Baseline Motor Analysis Using Simplified Techniques

Task 8 - Evaluation of Simplified Model Analyses

Phase III - Verification Motor Analysis

Task 9 - Select Verification Motor(s)

Task 10 - Verification Motor Acoustics Analysis

Task 11 - Structural Dynamics Analysis of the Verification Motor(s)

Task 12 - Evaluation of Verification Motor Analyses

Task 13 - Select Simplified Modeling Techniques

Task 14 - Issue Final Report Including Modeling Techniques Manual

The major purpose of Phase I was to provide a data baseline for evaluation of simplified techniques. Plans called for a detailed analysis of a motor to be conducted with as much detail in the model as could be considered reasonable to provide results that would be as accurate as state-of-the-art modeling would yield. The validity of a modeling simplification could then be evaluated by comparing results from a model using the proposed simplification with results from the detailed analysis.

Phase II was included in the program to develop simplified modeling techniques. Proposed techniques were to be screened in Task 6, based on experience gained during Phase I. The simplified techniques that appeared to be most promising were to be applied in an analysis of the baseline motor in Task 7. Task 8 was intended as an evaluation of simplified model results obtained by comparing Phase I and Task 7 solutions.

The Phase III verification analyses were scheduled to verify the simplified analysis techniques developed in Phase II. The simplified techniques were to be applied to two verification motors and results were to be evaluated by comparing available accelerometer data with analysis results.

The program conducted does not agree exactly with the original program plan as outlined above. Changes and reasons for the changes are given in the body of the report.

A separate section of the report is used to discuss each major task or phase. Much of the work has been documented by task final reports that were written after completion of the individual task. For the work covered by task final reports, only a summary is given under the task heading and the task final report is included as an appendix. For tasks that were not documented by final reports, appropriate detail is included in the main body of this report. Some of the technical details previously published in monthly status reports have been gathered to form another appendix to this report. A report written to Hercules by the MacNeal-Schwendler Corporation (MSC), has also been included as an appendix. The MSC report was written to document the addition of the Cyclic Symmetry capability to the Frequency Response Rigid format in NASTRAN. A final appendix is the Modeling Techniques Manual that is intended to provide guidance to analysts who must analyze solid rocket motors subject to unstable acoustic pressure oscillations. The following appendices are included as a part of this final report:

Appendix A - Task 1 Final Report

Appendix B - Task 2 Final Report

Appendix C - MSC Cyclic Symmetry Report

Appendix D - Task 4 Final Report

Appendix E - Task 5 Final Report

Appendix F - Task 8 Final Report

Appendix G - Excerpts from Monthly Status Reports

Appendix H - Closed Envelope Predictions

Appendix I - Modeling Techniques Manual

Final reports covering the analysis of the C-3 Poseidon SS motor, (Task 3), and the analysis of the Minuteman III TS motor, (Phase III), were not written. Therefore, a detailed discussion of these analyses is included in this report. The report ends with a section containing conclusions and recommendations for additional work.

SECTION II

TASK 1 - SELECTION OF THE BASELINE MOTOR

The major objective of Task 1 was to select a baseline motor. Motors to be considered as candidates for the baseline motor included the Minuteman II and Minuteman III third stage motors and the C-3 Poseidon second stage motor. A secondary objective of Task 1 was to establish error limits to be used for evaluation of the baseline motor analysis.

A. BASELINE MOTOR SELECTION

The following factors were specified in the contract work statement as criteria for selecting the baseline motor:

(1) Availability of component vibration and acoustic pressure oscillation data from static and flight tests

(2) Availability of acoustic mode analysis and dynamic structural analysis results

(3) Degree to which the motor configuration is representative of probable future ballistic missile motor designs

Both the Minuteman and Poseidon motors appeared to have sufficient component vibration data from static and flight tests. In addition, acoustic mode analyses had been performed on each motor by the MacNeal-Schwendler Corporation. Acoustic bench tests had been performed on each motor, with the Poseidon C-3 second stage having the most comprehensive bench test results available. More significant structural dynamic analyses had been performed on the Minuteman III third stage than on either of the other two motors.

After reviewing the qualifications of each candidate motor, it was concluded that either the Minuteman III third stage or the Poseidon C-3 second stage motor could qualify as a baseline motor. The Minuteman II third stage motor was disqualified because the use of four separate nozzles was judged to be not typical of probable future motor designs. Hercules selected the Poseidon C-3 second stage motor to be the baseline motor. The fact that an inert motor would be readily available for the Task 4 test program was a major consideration in selecting the Poseidon motor over the Minuteman III motor. Appendix A provides for a more detailed discussion of the baseline motor selection.

B. ERROR LIMIT DEFINITION

The contract work statement specified that acceptable error limits for predicted component vibration levels be defined prior to the performance of the dynamic structural analyses; that is, a prediction of the accuracy of the analysis results, based on some logical rationale, was desired. Existing component vibration and pressure oscillation data, as well as available results from acoustic mode analyses and structural dynamic analyses were to be considered in defining the error limits. The uncertainty in the applied oscillating pressure loads and the experimental variability in accelerometer measurements was to be taken into account.

To establish the error limits, results from the finite element models were assumed to represent mean values (m). Error limits about m were then based on results from statistical analyses of static firing accelerometer data. The statistical analyses yielded an estimate of the standard deviation (s) and the average acceleration response ($\bar{y}$) for each accelerometer location and for each analysis frequency. The coefficient of variation is the ratio of standard deviation to mean, c.o.v. = $s/\bar{y}$. Using all available accelerometer data, an average c.o.v. = 0.569 was calculated. Assuming that the maximum accelerations at a point on the motor are normally distributed, an acceleration selected at random from the population should be equal to or less than 1.94 times the mean maximum acceleration 95 percent of the time. Therefore, 1.94 m was selected as an upper bound error limit for evaluation of the analysis results.

To use the error limit of 1.94 m, the acceleration response calculated by analyzing finite element models is multiplied by 1.94 for comparison with accelerometer data. If the analysis was accurate, then 95 percent of all accelerometer data points should fall below the 1.94 m error limit.

Additional detail on selection of the error limits can be found in the Task 1 report in Appendix G.

SECTION III

TASK 2 - ACOUSTIC ANALYSIS OF THE BASELINE MOTOR

To calculate the response of a motor undergoing structural vibrations due to unstable acoustic pressure oscillations, it is necessary to know the pressure distribution (mode shape) and frequency for each acoustic mode likely to be unstable. The objective of this task was to define the acoustic mode shapes and frequencies to be used as loading conditions in the structural dynamic analyses. Since analyses at two burn times were required, part of the Task 2 effort consisted of selecting the burn times.

A zero burn time was preselected so that results would be available for comparison with the zero burn inert motor used in the Task 4 acoustics testing. The second burn time was to be selected on the basis of the severity of component vibration indicated by existing accelerometer data. A burn time when both longitudinal and transverse acoustic modes are present was desired. Two longitudinal and two tangential modes at each burn time were desired so that a total of 8 frequency response analyses could be conducted to characterize the motor structural response.

To provide information for selection of the second burn time, accelerometer data from two static firings were analyzed in detail. In addition, a graph showing the frequency activity in the motor as a function of time was studied, (see Figure 9 in Appendix B). A four-second burn time was selected as the required advanced burn time because of motor response to the first and third axial modes and the third tangential mode being present at that time.

Existing data on mode shapes and frequencies from four different sources were reviewed. Existing data were concluded to be adequate for use in the definition of the mode shapes and frequencies and no additional acoustic analyses were required. Data from the MacNeal-Schwendler Corporation NASTRAN analysis, from the Naval Weapons Center acoustics tests on a 1/4 scale model, from the Hercules 2-D analyses, and from Hercules full-scale testing program were reviewed and compared.

Based on the data review, the following mode shapes and frequencies were selected for use in the structural dynamics analyses:

Burn Time (sec)	Mode	Frequency (Hz)
0	A_3	770
	A_4	365*
	T_1	668
	T_3	1327
4	A_1	281
	A_3	805
	T_1	634
	T_2	830

*In air

The 365 Hz fourth longitudinal (axial) mode was selected to provide results for comparison with the Task 4 acoustics testing results. Analyses were also performed during Task 3, at 265 Hz, using the A_3 mode to provide additional data for comparison with Task 4 results.

A more detailed description of the burn time selection and of the acoustic mode selection can be found in Appendix B.

SECTION IV
TASK 3
STRUCTURAL DYNAMICS ANALYSIS OF THE BASELINE MOTOR

This section on the baseline motor analysis has been organized as follows:

- A. Introduction
- B. Approach
    - 1. General
    - 2. Application of Mechanical Impedance
- C. Structural Models
    - 1. Grid Generation
    - 2. Checkouts of Models
    - 3. Data Decks
    - 4. Load Generation

No results or discussions are given in this section. Results are given and evaluated in the Task 5 section.

A. INTRODUCTION

The C-3 Poseidon second stage (SS) motor was selected for use as a baseline motor as discussed in Task 1. Loads on the motor due to acoustic pressure oscillations were defined in Task 2. The objective of this task was to calculate the response of the motor structure, including attached components, to the defined loading distributions.

Rocket motors are often analyzed with the use of two-dimensional (2D) axisymmetric finite element models. The axisymmetric approximation to the motor structure has been found to yield good results in calculating stresses in the motor due to the axisymmetric internal pressure load or due to other axisymmetric loads. Typical motor designs are not axisymmetric. Most motors have slots in the propellant grain and/or miscellaneous hardware (components) attached that prevent them from being truly axisymmetric.

Motion of the unsymmetrically attached components was considered to be important for the Task 3 analyses. In addition, calculation of motor response to the nonaxisymmetric tangential acoustic modes was required. For these reasons, the use of a general 3D solution for structural response calculations was necessary.

When a general 3D finite element model is constructed to represent a structure as complex as a rocket motor, an extremely large number of degrees of freedom are required. In addition, the nature of a 3D problem results in very large bandwidths for the stiffness matrices that represent finite element models. The result is unreasonably long computer run times and unreasonably large computer core requirements.

Because of the problems associated with obtaining general straightforward 3D solutions, special techniques were required to make obtaining such solutions practical.

B. APPROACH

1. General

The use of NASTRAN, level 15, as the basic analysis tool for this program was a contractual requirement. In spite of the capacity that the NASTRAN program has for solving arbitrarily large problems, the need for special treatment of this particular problem was apparent at the beginning. Original plans called for a modal synthesis approach. Separate detailed models were to have been constructed for the various portions of the motor and then effectively combined using modal synthesis. Such an approach was advantageous as considerable detail could be used in the individual models for each portion of the motor. Another advantage was that mode shapes and natural frequencies would be calculated in the course of obtaining the solutions, thus providing valuable insight into the behavior of the motor model. The modal synthesis approach was found to have the disadvantage that the frequency dependence of the propellant grain stiffness could not be accurately modeled.

To obtain a model that could represent the frequency-dependent grain behavior and still maintain reasonable detail in the model, a cyclic symmetry model was used. "Cyclic Symmetry Analysis" is a technique developed by MacNeal Schwendler for efficient analysis of cyclic symmetric structures. A rocket motor that is axisymmetric except for radial grain slots is an example of a cyclic symmetric structure because the geometry repeats around the motor circumference.

A structure is said to be cyclic symmetric when it consists of a set of identical segments located symmetrically about a particular axis. The structure shown in Figure 4-1 is cyclic symmetric when the beam element model is removed. Figure 4-1 shows a simple motor model with three slots. If an r-z plane is passed through the centerline of each slot, the model would be divided into three 120° segments. Since each of the segments would be identical, the motor structure is said to be cyclic symmetric. The model of Figure 4-1 could also be divided into three identical segments so that a slot would be centered in each segment. The type of symmetry discussed to this point is referred to as rotational cyclic symmetry in the MacNeal Schwendler Corporation report included as Appendix C. A structure that possesses rotational cyclic symmetry also possesses

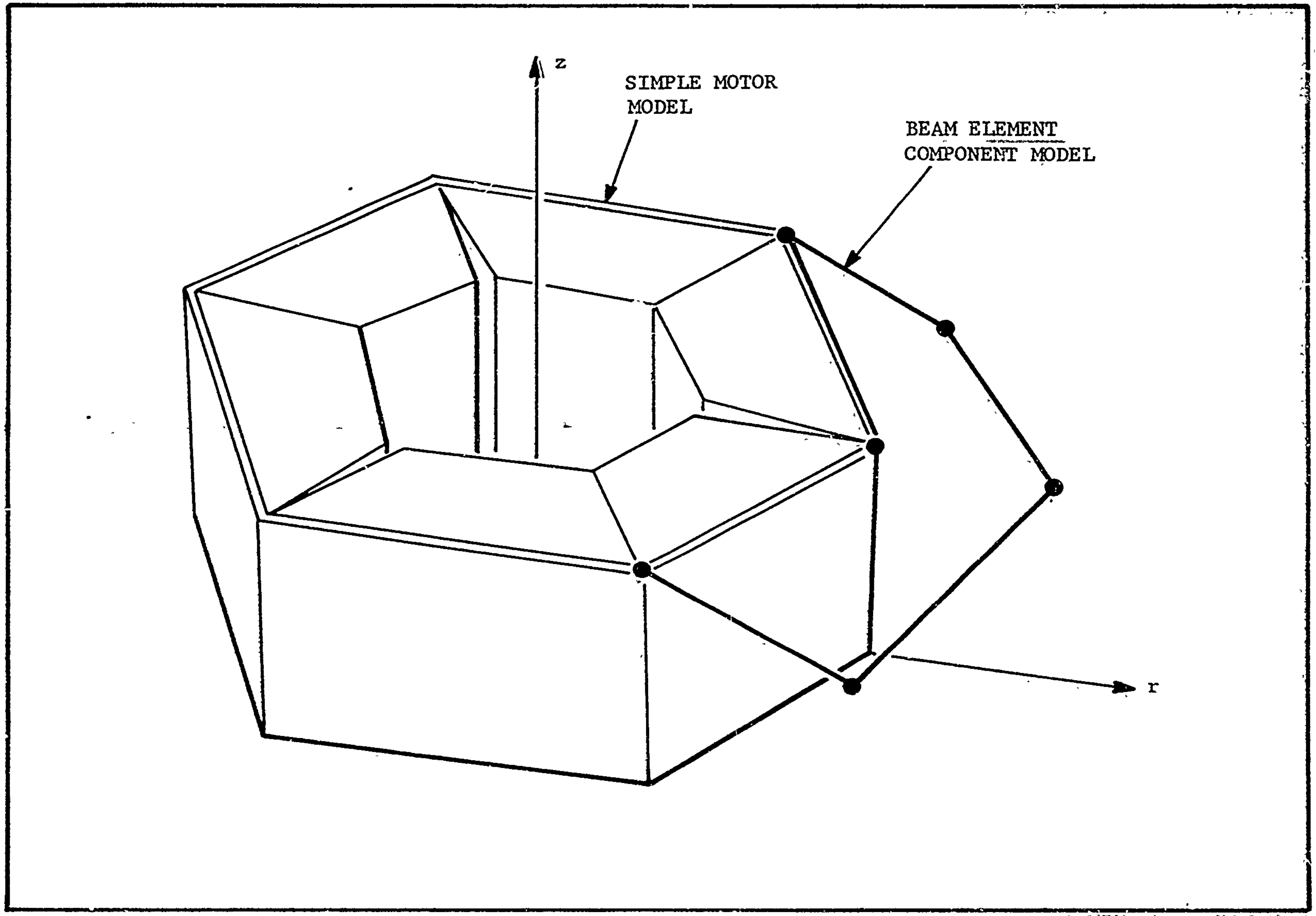

Figure 4-1. Simple Motor Model with Attached Component Used for Checkout

dihedral cyclic symmetry if each segment consists of two subsegments which are mirror images of one another. The model in Figure 4-1 possesses dihedral cyclic symmetry because each 120° segment has a plane of symmetry and can be represented by two 60° segments which are mirror images of one another. Additional discussion on cyclic symmetry can be found in Appendix C.

Using the cyclic symmetry approach, it is possible to obtain a general 3D solution by modeling only the unique portion of the structure (i.e., by modeling only the pie-slice-shaped segment of the motor that, when repeated around the circumference, represents the complete motor). Most rocket motors with slotted grains possess dihedral cyclic symmetry. The use of the dihedral cyclic symmetry option allows the use of a model only one-half as large as that required for rotational cyclic symmetry. The model in Figure 4-1 is represented by only one 60° segment in a dihedral cyclic symmetry analysis.

The theory upon which cyclic symmetry analysis is based is discussed in the MacNeal Schwendler's report (refer to Appendix C). Basically, a coordinate transformation is applied to the one-segment finite element model. The solutions are then obtained in so-called "cyclic coordinates." To obtain a solution for a model represented by n segments, the one-segment model is solved n times. The model in Figure 4-1 could be represented by six segments using dihedral cyclic symmetry. Therefore, the 60° segment model would be solved six times to obtain a general 3-dimensional solution for one applied load set. A cyclic symmetry solution is apparently much more efficient than a standard solution because the problem can be solved one segment at a time. The bandwidth for a cyclic symmetry problem can be significantly smaller than the corresponding bandwidth for a standard solution.

To use the cyclic symmetry approach in the baseline motor analysis, it was necessary to modify the existing NASTRAN program. MacNeal-Schwendler added the cyclic symmetry capability to the Frequency Response rigid format in NASTRAN. Hercules received a computer tape from the MacNeal-Schwendler Corporation (MSC) containing the object code for the special version of NASTRAN that includes cyclic symmetry in Rigid Format 8. Hercules also received the source code that would be required to adapt cyclic symmetry to NASTRAN Level 15.5. According to MSC officials, the cyclic symmetry capability in Rigid Format 8 would be available in the MSC version of NASTRAN which the MSC company supplies to their customers. Since NASTRAN Level 16.0 (soon to be released) will not include cyclic symmetry in Rigid Format 8, the MSC version is apparently the only current location where the general public can access this analysis capability. The MSC NASTRAN program can be used on the Control Data Corporation Cybernet Computer system.

The MSC report in Appendix C describes cyclic symmetry and an added program feature which allows a more efficient analysis to be conducted when solutions are desired at several different frequencies. A table containing the propellant properties as a function of frequency is input to the program. Then, only the portion of the stiffness matrix affected by the changed propellant properties is modified to obtain a solution at a new frequency.

By performing frequency response analyses on a cyclic symmetry finite element model of the motor, it was possible to calculate motor response in a true 3D sense and to account for the frequency-dependent grain properties. However, when components are attached to the motor, the motor becomes unsymmetric. To correctly account for the effects of the attached components, a mechanical impedance technique was applied. The use of mechanical impedance methods to deal with the problem of unsymmetric components was recommended by the MSC.

2. Application of Mechanical Impedance

"Impedance" and "admittance" are terms generally associated with electrical circuits. The terms "mechanical impedance" and "mechanical admittance" are normally used to indicate that an analogy is being made between an electrical circuit and a mechanical system. The literature on mechanical vibration analysis contains a large amount of information on mechanical impedance-type approaches. For example, the Shock and Vibration Bulletin contains many papers on application of mechanical impedance techniques.[1]

Mechanical impedance is a ratio of force to velocity. Mechanical admittance, commonly called "mobility," is the inverse of mechanical impedance, i.e., a ratio of velocity to force. A basic discussion on mechanical impedance and mobility can be found in Reference 2. The term "receptance" is used to denote the ratio of displacement to force. The concept of receptance is discussed in References 2, 3, and 4. Additional discussion on electromechanical analogies are contained in References 5 and 6.

(1) Index to the Shock and Vibration Bulletins, February 1968, The Shock and Vibration Information Center, Naval Research Laboratory, Washington, D.C.

(2) Harris, C. M., and Crede, C. E., Shock and Vibration Handbook, Vol. 1, Chapter 10, McGraw-Hill Book Co., New York, 1961.

(3) Bishop, R. E. D., Gladwell, G. M. L., and Michaelson, S., The Matrix Analysis of Vibration, Section 5.5, Cambridge at the University Press, London, 1965.

(4) Bishop, R. E. D., and Johnson, D. C., The Mechanics of Vibration, Cambridge at the University Press, London, 1960.

(5) Crafton, P. A., Shock and Vibration in Linear Systems, Harper and Brothers, New York, 1961.

(6) MacNeal, R. H., Electric Circuit Analogies for Elastic Structures, Vol 2, John Wiley and Sons, New York, 1962.

The term "immittance" has been used to represent impedance or admittance. Mechanical immittance and transmission matrix concepts are discussed in References 1, 2, and 3.

When a sinusoidal force drives a linear system, the steady state response displacements, velocities, and accelerations are sinusoidal at the frequency of the driving force. For a damped system, the response is out-of-phase with the driving force. The relationship between driving force and response can be expressed by algebraic equations involving complex numbers. The analysis of such a system is called a "frequency response analysis." The use of frequency response-type analyses is implied when mechanical impedance is discussed. The frequency response rigid format in NASTRAN, Rigid Format No. 8, was used for all of the frequency response analysis conducted during this program. The NASTRAN theoretical manual contains a description of the theory pertaining to frequency response analyses (reference 4).

For this discussion consider first a motor with one component attached. The same reasoning is generalized for additional components below. The reason for using the mechanical impedance approach is that it allows the clean motor model (component not attached) and the component model to be analyzed separately, yet results are obtained for the component-mounted-to-motor condition. To make the analysis exact, the component is replaced by the forces that it creates on the clean motor.

As the motor is oscillating in response to a particular unstable acoustic pressure mode, the motor proper is considered to be acted upon by two separate sets of forces; the oscillating pressure forces are applied internally, and inertia forces due to the attached component are applied at the motor-component interface locations. The solution is obtained by superimposing effects of both loading conditions.

The clean motor model is analyzed with only internal pressure loading applied to obtain the velocities $\{V_o\}$ at the motor-component interface. The velocities $\{V_1\}$ at the interface caused by component connection forces $\{F_c\}$ can be expressed by using the motor admittance matrix $[Y]$:

$$\{V_1\} = [Y]\ \{F_c\}$$

The total velocity $\{V_t\}$ is obtained by superimposing the effects of the two loading conditions:

$$\{V_t\} = \{V_o\} + \{V_1\}$$

---

(1) Rubin, S., Review of Mechanical Immittance and Transmission Concepts, Presented at the 71st Meeting of the Acoustical Society of America, Boston, Mass., June 1966.

(2) Rubin, S., Class Notes distributed at UCLA Short Course on Structural Dynamics Analysis, Los Angeles, California, 1967.

(3) Rubin, S., On the Use of Eight-Pole Parameters for Analysis of Beam Systems, Soc. of Automotive Engineers, Reprint 925F, October 1964.

(4) NASTRAN Theoretical Manual, R. H. MacNeal Ed., Scientific and Tecanical Information Office, NASA Administration, Washington, D.C., December 1972.

Substituting from above gives

$$\{V_t\} = \{V_o\} + [Y] \{F_c\}$$

The forces $\{F_c\}$ at the interface are unknown, but they can be expressed in terms of the total velocity by considering the component impedance relationship:

$$\{F_c\} = -[Z_c] \{V_t\}$$

where $[Z_c]$ represents the component impedance matrix. The minus sign occurs because forces applied to the component are equal and opposite to those applied to the motor. Substituting $\{F_c\}$ in the equation for $\{V_t\}$ gives:

$$\{V_t\} = \{V_o\} - [Y] [Z_c] \{V_t\}$$

Rearranging:

$$\{V_t\} = ([I] + [Y] [Z_c])^{-1} \{V_o\}$$

where [I] is the identity matrix. Each matrix must be complex to handle the magnitude and phase information required for characterization of damped systems. The solution represented by the last equation given above for $\{V_t\}$ must be repeated at each frequency of interest.

Application of the mechanical impedance method to this particular rocket motor analysis was discussed above in terms of forces, velocities, impedance matrices, and admittance matrices. As a matter of convenience, the program was actually solved in terms of displacements rather than velocities. Adopting another terminology, receptance matrices replace admittance matrices and inverse receptance matrices replace impedance matrices when displacements are used in the place of velocities. If R_m is the receptance matrix for the motor, and R_c is the set of matrices representing component receptances, then the equation that is solved can be written:

$$\{U_T\} = [I + R_m R_c^{-1}]^{-1} \{U_o\} \qquad (1)$$

The identity matrix is denoted I. The displacements at the component connection points resulting from pressure mode loading with no components attached, is denoted U_o. Then, U_T is the total displacement vector calculated to represent the response of the motor (including components) at the component connection points. For the Poseidon SS motor, U_T has 42 rows.

The receptance matrices are formed by applying a unit force at one coordinate while all other forces are zero. The displacements at all component connection coordinates then form a column in the receptance matrix according to the equation:

$$\{U\} = [R] \{F\} \qquad (2)$$

Solution of equation (1) results in displacements only at component connection points. Some data recovery operations are necessary if displacements at other points are desired. If displacements at U_e coordinates are desired, after U_T has been obtained, then equation (2) can be partitioned and solved for U_e:

$$\begin{Bmatrix} U_T \\ \hline U_e \end{Bmatrix} = \begin{bmatrix} R \\ \hline R_e \end{bmatrix} \{F\} \tag{3}$$

$$\{U_e\} = [R_e]\{F\}$$

In equation (3), R_e is part of the receptance matrix that corresponds to the extra coordinates U_e. The R_e matrix can be formed at the same time as the R matrix. The forces F must include both the pressure loading and the interconnection forces. The most convenient way to obtain U_e is to superimpose $(U_e)_o$ from the pressure load with $(U_e)_i$ resulting from the interconnection forces. Once the interconnection displacements, U_T, are obtained from equation (1), the interconnection forces can be determined from:

$$\{F_i\} = [R_c^{-1}]\{U_T\} \tag{4}$$

Then, superimposing:

$$\{U_e\} = \{U_e\}_o + [R_e][R_c^{-1}]\{U_T\} \tag{5}$$

Equation (5) defines the data recovery operations required to obtain displacements at points other than the component connection points. When three components are attached to the motor instead of just one, then $[R_c^{-1}]$ in equation (1) is replaced by:

$$[R_c^{-1}] = \begin{bmatrix} R_{c_1}^{-1} & & \\ & R_{c_2}^{-1} & \\ & & R_{c_3}^{-1} \end{bmatrix}$$

where the $R_{c_i}^{-1}$'s are the inverse receptance matrices for each component.

To check out the impedance response equation, (1), a very simple problem was analyzed. Figure 4-1 shows a motor model consisting of six propellant elements and six case elements with a four-element beam component model attached. The response of the total model shown in Figure 4-1 was calculated. Loads were applied in the centerbore of the motor model to simulate an acoustic pressure mode. A listing of the NASTRAN deck used to analyze the simple model is given in Table 4-I with solutions obtained.

TABLE 4-I

NASTRAN DATA DECK LISTING FOR SIMPLE MOTOR WITH COMPONENT

```
                                                    FEBRUARY  8, 1974   NASTRAN 12/ 1/73    PAGE    1

        N A S T R A N    E X E C U T I V E    C O N T R O L    D E C K    E C H O


      ID      STOUT,MOTOR
      APP     DISP
      SOL     8,1
      TIME    5
      CEND


                                   C A S E    C O N T R O L    D E C K    E C H O
           CARD
           COUNT
             1       TITLE  #  FREQUENCY RESPONSE ANALYSIS OF STOUT MOTOR USING FULL MODEL
             2       MPC  #   988
             3       SPC    # 999
             4       SDISP#   ALL
             5       FREQ  #  1
             6               SUBCASE 1
             7               DLOAD # 1
             8               LABEL  #  1ST LOAD
             9               SUBCASE 2
            10               DLOAD  #  2
            11               LABEL  #  2ND LOAD
            12       BEGIN BULK


  *** USER INFORMATION MESSAGE 207, BULK DATA NOT SORTED,XSORT WILL RE-ORDER DECK.
```

TABLE 4-I (Cont)

NASTRAN DATA DECK LISTING FOR SIMPLE MOTOR WITH COMPONENT

S O R T E D   B U L K   D A T A   E C H O

CARD COUNT	. 1 ..	2 ..	3 ..	4 ..	5 ..	6 ..	7 ..	8 ..	9 ..	10 .
1-	CBAR	1	19	216	213	4.0	45.	2.0	1	
2-	CBAR	2	19	213	214	5.0	15.	2.0	1	
3-	CBAR	3	19	214	215	5.0	-30.	2.0	1	
4-	CBAR	4	19	215	218	4.0	300.	2.0	1	
5-	CHEXA2	20	20	101	102	112	111	201	202	&20
6-	&20	212	211							
7-	CHEXA2	21	20	111	112	122	120	211	212	&21
8-	&21	222	220							
9-	CHEXA2	22	20	121	122	132	131	221	222	&22
10-	&22	232	231							
11-	CHEXA2	23	20	131	132	142	140	231	232	&23
12-	&23	242	240							
13-	CHEXA2	24	20	141	142	152	151	241	242	&24
14-	&24	252	251							
15-	CHEXA2	25	20	151	152	102	100	251	252	&25
16-	&25	202	200							
17-	CORD2C	10		0.0	0.0	0.0	0.0	0.0	1.	&010
18-	&010	1.0	0.	0.						
19-	CQUAD2	10	10	102	112	212	202			
20-	CQUAD2	11	10	112	122	222	212			
21-	CQUAD2	12	10	122	132	232	222			
22-	CQUAD2	13	10	132	142	242	232			
23-	CQUAD2	14	10	142	152	252	242			
24-	CQUAD2	15	10	152	102	202	252			
25-	DAREA	1	200	1	.8660254	200	2	-.5		
26-	DAREA	1	201	1	.8660254	201	2	.5		
27-	DAREA	2	200	1	.8660254	200	2	-.5		
28-	DAREA	2	201	1	.8660254	201	2	.5		
29-	DAREA	2	211	1	.8660254	211	2	-.5		
30-	DAREA	2	251	1	.8660254	251	2	.5		
31-	EIGR	1	GIV	0.0	1.&8		6			&E1
32-	&E1	MAX								
33-	FREQ	1	1500.							
34-	GRID	100	10	1.0	.0	.0	10			
35-	GRID	101	10	1.0	.0	.0	10			
36-	GRID	102	10	3.0	.0	.0	10			
37-	GRID	111	10	1.0	60.	.0	10			
38-	GRID	112	10	3.0	60.	.0	10			
39-	GRID	120	10	1.0	120.	.0	10			
40-	GRID	121	10	1.0	120.	.0	10			
41-	GRID	122	10	3.0	120.	.0	10			
42-	GRID	131	10	1.0	180.	.0	10			
43-	GRID	132	10	3.0	180.	.0	10			
44-	GRID	140	10	1.0	240.	.0	10			
45-	GRID	141	10	1.0	240.	.0	10			
46-	GRID	142	10	3.0	240.	.0	10			
47-	GRID	151	10	1.0	300.	.0	10			
48-	GRID	152	10	3.0	300.	.0	10			
49-	GRID	200	10	1.0	.0	2.0	10			
50-	GRID	201	10	1.0	.0	2.0	10			

TABLE 4-I (Cont)

NASTRAN DATA DECK LISTING FOR SIMPLE MOTOR WITH COMPONENT

FREQUENCY RESPONSE ANALYSIS OF STOUT MOTOR USING FULL MODEL FEBRUARY 8, 1974 NASTRAN 1. / 1/73 PAGE 4

S O R T E D B U L K D A T A E C H O

CARD COUNT	. 1 ..	2 ..	3 ..	4 ..	5 ..	6 ..	7 ..	8 ..	9 ..	10 .
51-	GRID	202	10	3.0	.0	2.0	10			
52-	GRID	211	10	1.0	60.	2.0	10			
53-	GRID	212	10	3.0	60.	2.0	10			
54-	GRID	213	10	4.0	30.	2.0	10	345		
55-	GRID	214	10	4.0	.0	2.0	10	345		
56-	GRID	215	10	5.0	-45.	2.0	10	345		
57-	GRID	216	10	3.0	60.	2.0	10	345		
58-	GRID	218	10	3.0	300.	2.0	10	345		
59-	GRID	220	10	1.0	120.	2.0	10			
60-	GRID	221	10	1.0	120.	2.0	10			
61-	GRID	222	10	3.0	120.	2.0	10			
62-	GRID	231	10	1.0	180.	2.0	10			
63-	GRID	232	10	3.0	180.	2.0	10			
64-	GRID	240	10	1.0	240.	2.0	10			
65-	GRID	241	10	1.0	240.	2.0	10			
66-	GRID	242	10	3.0	240.	2.0	10			
67-	GRID	251	10	1.0	300.	2.0	10			
68-	GRID	252	10	3.0	300.	2.0	10			
69-	MAT1	10	1.E7		.25	2.-4				
70-	MAT1	18	30.E6		.3	7.32-4			.10	
71-	MAT1	20		860.	.49	1.66-4			.56	
72-	MPC	988	216	1	1.0	212	1	-1.0		
73-	MPC	988	216	2	1.0	212	2	-1.0		
74-	MPC	988	216	6	1.0	212	6	-1.0		
75-	MPC	988	218	1	1.0	252	1	-1.0		
76-	MPC	988	218	2	1.0	252	2	-1.0		
77-	MPC	988	218	6	1.0	252	6	-1.0		
78-	PARAM	COUPMASS1								
79-	PARAM	DECOMOPT2								
80-	PARAM	G	0.0							
81-	PBAR	19	18	.15	.002					
82-	PQUAD2	10	10	.1						
83-	RLOAD1	1	1			1000				
84-	RLOAD1	2	2			1000				
85-	SPC1	999	456	200	201	211	220	221	231	&92
86-	&92	240	241	251						
87-	SPC1	999	123456	100	101	102	111	112	120	&90
88-	&90	121	122	131	132	140	141	142	151	&91
89-	&91	152								
90-	TABLED1	1000								&1000
91-	&1000	0.	1.0	100.	1.0	ENDT				
	ENDDATA									

NO ERRORS FOUND - EXECUTE NASTRAN PROGRAM

TABLE 4-I (Cont)

NASTRAN DATA DECK LISTING FOR SIMPLE MOTOR WITH COMPONENT

FREQUENCY RESPONSE ANALYSIS OF STOUT MOTOR USING FULL MODEL FEBRUARY 8, 1974 NASTRAN 12/ 1/73 PAGE 5

1ST LOAD
FREQUENCY = 1.500000E 03

SUBCASE 1

C O M P L E X D I S P L A C E M E N T V E C T O R (SOLUTION SET)
(REAL/IMAGINARY)

POINT ID.	TYPE	T1	T2	T3	R1	R2	R3
200	G	5.838381E-06 -6.455104E-05	-3.621753E-06 1.410146E-05	-2.891044E-05 -4.610509E-05			
201	G	6.123882E-06 -6.436040E-05	3.925215E-06 -1.385162E-05	-2.901650E-05 -4.660604E-05			
202	G	3.913394E-06 -8.524346E-06	1.465349E-08 1.374520E-07	7.708740E-08 7.467196E-08	-1.671135E-08 -1.364241E-07	2.243877E-06 -4.813138E-06	-2.752548E-08 -8.799740E-07
211	G	2.389934E-06 -2.300118E-05	1.196169E-05 1.517946E-05	-7.588756E-06 1.512123E-05			
212	G	6.639207E-07 -1.715272E-07	-3.535503E-07 1.724168E-06	1.384709E-07 -2.403262E-07	4.536176E-07 -[illegible]67181E-06	6.446407E-07 -5.124065E-07	1.097407E-07 1.652334E-06
213	G	6.698407E-07 6.901162E-07	-4.054413E-08 3.101260E-06				-3.013649E-07 -2.882182E-08
214	G	-8.007090E-07 -7.285023E-06	-7.300872E-08 1.372063E-06				1.360692E-08 -5.531929E-07
215	G	5.975410E-07 -1.590083E-06	2.362601E-07 -6.807401E-07				3.287916E-07 1.684887E-06
220	G	1.924789E-05 -4.252857E-06	1.659183E-05 5.526976E-06	-8.097360E-06 1.991668E-05			
221	G	1.243324E-06 1.829277E-07	1.923902E-07 2.672523E-07	8.580883E-07 -7.967491E-07			
222	G	9.100552E-07 9.187577E-07	-1.592692E-07 4.384847E-07	3.097967E-08 -1.410509E-07	1.754860E-07 -2.019817E-07	4.820379E-07 5.217894E-07	4.389573E-07 -3.242283E-07
231	G	2.542497E-07 5.846378E-07	6.188947E-08 -1.297756E-08	-1.241209E-06 3.512388E-07			
232	G	-7.166333E-07 1.275806E-09	3.453753E-09 6.836867E-10	9.039161E-08 -1.387029E-08	-7.409085E-09 -1.185027E-08	-[illegible]139463E-07 1.446152E-07	-8.901588E-08 1.234923E-07
240	G	1.472047E-06 1.705620E-07	-1.828783E-07 -3.730441E-07	1.031724E-06 -7.789642E-07			
241	G	1.915208E-05 -4.416829E-06	-1.690935E-05 -5.656576E-06	-7.799492E-06 2.042476E-05			
242	G	9.606911E-07 1.075098E-06	1.437096E-07 -5.281071E-07	2.575268E-08 -1.565357E-07	-1.563394E-07 2.940005E-07	5.062819E-07 5.285297E-07	-2.[illegible]46410E-07 -1.438491E-07

TABLE 4-I (Cont)

NASTRAN DATA DECK LISTING FOR SIMPLE MOTOR WITH COMPONENT

1ST LOAD
FREQUENCY = 1.500000E 03 SUBCASE 1

C O M P L E X D I S P L A C E M E N T V E C T O R (SOLUTION SET)
(REAL/IMAGINARY)

POINT ID.	TYPE	T1	T2	T3	R1	R2	R3
251	G	1.624014E-06	-1.202413E-05	-8.035545E-06			
		-2.355591E-05	-1.515717E-05	1.529303E-05			
252	G	5.462359E-07	3.487139E-07	1.425472E-07	-4.459859E-07	5.776417E-07	-1.514637E-07
		-8.731442E-07	-1.642242E-06	-1.758108E-07	1.841348E-06	-9.248662E-07	-2.185999E-07

To determine if the calculated response given in Table 4-I could be duplicated by applying equation (1), the beam component model was separated from the motor model and each was analyzed separately. This time the motor model was analyzed using cyclic symmetry. The simple motor model used for this checkout is the same model used by MSC as an example for a cyclic symmetry solution. The solution for response of the motor to an internal load is discussed in Appendix C. For the purposes of this problem, a DMAP alter was added to the cyclic symmetry alter package to form the $\{U_o\}$ vector and save it on tape. A listing of the run made to obtain $\{U_o\}$ including the DMAP alter is shown in Table 4-II.

The cyclic symmetry motor model was analyzed again to calculate the receptance matrix $[R_m]$ required in equation (1). The analysis was conducted by applying unit loads at each component connection point in each coordinate direction. The $\{U_o\}$ and $[R_m]$ analyses could have been performed more efficiently by combining them into one computer run. The run listing for the $[R_m]$ calculation is shown in Table 4-III. Only the altered portion of the executive control deck is shown. The $[R_m]$ matrix is saved on a tape.

The final run made to check out the mechanical impedance approach served two purposes: (1) The beam component model was analyzed to obtain the inverse component receptance matrix $[R_c^{-1}]$, and (2) the $\{U_T\}$ solution vector was formed by evaluating equation (1). A listing of the NASTRAN run used for the final calculations is shown in Table 4-IV.

A comparison between the results obtained by the direct solution and by evaluation of equation (1) is shown in Table 4-V. The multiplier 10^{-7} has been omitted from values shown in the table. The comparison given by Table 4-V indicates excellent agreement between the two solutions.

C. STRUCTURAL MODELS

For the analysis of the SS Poseidon motor, several different finite element models were created. Models of the clean motor (motor with no components attached) were assembled for a zero burn time and for an advanced (4.0 second) burn time. Clean motor models for the two burn times are shown in Figures 4-2 and 4-3. Two component models were created, one for the flight electronics package, and one to model both the hydraulic power unit and the gas generator. The two nozzle actuators were each modeled with a scalar spring. A sketch of the components attached to the aft adapter ring is shown in Figure 4-4. Dimensions of the motor are given in Figure 4-5. Verification of models was accomplished by comparison to mass and stiffness measurements. Acoustic pressure distributions were applied to the appropriate internal grain igniter and nozzle surfaces. With acoustic loads applied to the mathematical models, accelerations and

TABLE 4-II

NASTRAN DATA DECK LISTING FOR CYCLIC SYMMETRY

SOLUTION OF SIMPLE MOTOR MODEL - UZRO CALCULATION

N A S T R A N   E X E C U T I V E   C O N T R O L   D E C K   E C H O

```
ID  HEXFREQ,DIH
APP  DISP
SOL  8,1  $ FREQUENCY RESPONSE
TIME 2
DIAG 8,13 $ PRINT TRAILERS AND OPEN CORE MESSAGES
DIAG 14   $ PRINT RIGID FORMAT
$- CYCLIC TRANSFORMATION - FREQUENCY RESPONSE --------------------------
$      12/01/73        R I G I D   F O R M A T   8  /  SERIES M
$                                                    /  RLH VERSION
$  CASE CONTROL INPUT
$      A SUBCASE IS USED FOR EACH SUBSTRUCTURE AND LOADING CONDITION.
$      ALL MPC AND SPC REQUESTS MUST BE ABOVE THE SUBCASE LEVEL.
$
$  BULK DATA INPUT
$         PARAMETERS USED ARE...
$       CTYPE %REQUIRED<   ROT # ROTATIONAL
$                          DIH # DIHEDRAL
$                         DSYM # DIH PLUS DEFORMATION SYMMETRY
$                         DANT # DIH PLUS DEFORMATION ANTISYMMETRY
$       N      %REQUIRED<   NUMBER OF SEGMENTS
$       KMIN   %DEFAULT 0 < MIN RANGE OF CYCLIC INDEX K
$       KMAX   %DEFAULT -1< MAX RANGE OF CYCLIC INDEX K %-1 IMPLIES ALL<
$       CYCIO %DEFAULT &1< INPUT/OUTPUT, &1 # PHYSICAL , -1 # SYM COMP
$       CYCSEQ%DEFAULT -1< MATRIX ELEMENT SEQUENCE, 1 # SEPARATE
$                                                -1 # ALTERNATING
$       NLOAD %DEFAULT &1< NUMBER OF LOADING CONDITIONS
$       NOKPRT%DEFAULT -1< IF &1 K WILL BE OUTPUT AT THE TOP OF LOOP
$
$       CYJOIN BULK DATA CARDS ARE REQUIRED.
$
$     THE MODEL MUST CONTAIN K4 STRUCTURAL DAMPING %FOR FREQ DEP MATL<
$     TWO TABLEDX,TR%F< AND TI%F<, ARE SELECTED IN CASE CONTROL VIA
$     SDAMP %THE ID OF TR IS SELECTED, THE ID OF TI MUST BE ONE LARGER<
$     THE STIFFNESS MATRIX %WITH STRUCTURAL DAMPING< WILL BE
$       K * % 1. & I*C < & K4 * % TR%F< & I*TI%F< <
$        WHERE K # STIFFNESS MATRIX , C # PARAM OVERALL DAMPING
$
$ THE ANALYSIS WILL LOOP THRU A RANGE OF THE CYCLIC INDEX K # KMIN,KMAX
$
ALTER 2
FILE       UXVF#APPEND $
COND       ERRORN,N $  IF USER HAS NOT SPECIFIED N %DEFAULT # -1<
COND       FIND,KMAX $
JUMP       KNOWN $
LABEL      FIND $
PARAM      //C,N,DIV/V,Y,KMAX#-1/V,Y,N/C,N,2 $
LABEL      KNOWN $
PARAM      //C,N,NOP/V,Y,CYCIO#1/V,Y,NOKPRT#-1 $
ALTER 92
```

TABLE 4-II (Cont)

NASTRAN DATA DECK LISTING FOR CYCLIC SYMMETRY
SOLUTION OF SIMPLE MOTOR MODEL - UZRO CALCULATION


```
N A S T R A N   E X E C U T I V E   C O N T R O L   D E C K   E C H O

GPCYC    GEOM4,EQDYN,USETD/CYCDD/V,Y,CTYPE/V,N,NOGO $  DATA FOR CYCT2  00000440
CHKPNT   CYCDD $                                                        00000450
ALTER 129,129                                                           00000460
PURGE    K2DD/NOK2PP/M2PP/NOM2PP/B2DD/NOB2PP $                          00000470
ALTER 133,133                                                           00000480
GKAD     USETD,GM,GO,KAA,BAA,MAA,     ,K2PP,M2PP,B2PP/KDD,BDD,MDD,GMD,  00000490
         GOD,K2DD,M2DD,B2DD/C,N,FREQRESP/C,N,DISP/C,N,DIRECT/C,Y,G=0.0/ 00000500
         C,N,0.0/C,N,0.0/V,N,NOK2PP/V,N,NOM2PP/V,N,NOB2PP/   V,N,MPCF1/ 00000510
         V,N,SINGLE/V,N,OMIT/V,N,NOUE/C,N,-1    /V,N,NOBGG/V,N,KDEK2/C, 00000520
         N,-1 $     REMOVE K4                                           00000530
ALTER 139,139 $ ACTUALLY  ALTER 139,141                                 00000540
EQUIV    K4AA,K4DD/NOUE $                                               00000550
CHKPNT   K4DD $                                                         00000560
COND     LBLNOUE,NOUE $                                                 00000570
VEC      USETD/EPV/C,N,D/C,N,../C,N,E $                                 00000580
MERGE    K4AA,,,,EPV,/K4DD $                                            00000590
CHKPNT   K4DD $                                                         00000600
LABEL    LBLNOUE $                                                      00000610
FRLG     CASEXX,USETD,DLT,FRL,GMD,GOD,DIT,/PPF,PSF,PDF,FOL,PHF/         00000620
         C,N,DIRECT  $  COMPUTE LOADS                                   00000630
CHKPNT   PPF,PSF,PDF,FOL  $                                             00000640
EQUIV    PPF,PDF/NOSET $                                                00000650
CHKPNT   PDF $                                                          00000660
EQUIV    PDF,PXF/CYCIO $                                                00000670
CHKPNT   PXF $                                                          00000680
COND     LCYC1,CYCIO $ IF (CYCIO.GE.0) TRANSFORM TO SYMMETRIC COMPONENTS00000690
CYCT1    PDF/PXF,GCYCFF/V,Y,CTYPE/C,N,FORE/V,Y,N/V,Y,KMAX/V,Y,NLOAD/    00000700
         V,Y,KMIN $                                                     00000710
CHKPNT   PXF $                                                          00000720
LABEL    LCYC1 $                                                        00000730
PARAM    //C,N,ADD/V,N,K/C,N,0/V,Y,KMIN=0 $ INITIALIZE K = KMIN         00000740
LABEL    TOPCYC $$$$$$$$$$$$$$  LOOP ON K  $$$$$$$$$$$$$$$$$$$$$$$$$$$$$00000750
COND     NOKPRT,NOKPRT  $                                              $00000760
PRTPARM  //C,N,0/C,N,K $                                               $00000770
LABEL    NOKPRT $                                                      $00000780
ALTER 140,140                                                          $00000790
CYCT2    CYCDD,KDD,MDD,PXF,BDD,K4DD/KKKF,MKKF,PKF,BKKF,K4KKF/C,N,       00000800
         FOREFREQ/V,Y,N=-1/V,N,K/V,Y,CYCSEQ=-1/V,Y,NLOAD=1/V,N,NOGO/    00000810
         V,Y,KMAX/V,Y,KMIN $                                           $00000820
CHKPNT   KKKF,MKKF,PKF,BKKF,K4KKF $                                    $00000830
FRRD1    CASEXX,DIT,KKKF,BKKF,MKKF,K4KKF,PKF,FRL,FOL/UKVF/C,N,DIRECT/   00000840
         V,N,NONCUP/C,Y,DECOMOPT=1 $                                   $00000850
CHKPNT   UKVF $                                                        $00000860
ALTER 141,141                                                          $00000870
CYCT2    CYCDD,,,UKVF,,/,,UXVF,,/C,N,BACKFREQ/V,Y,N/V,N,K/V,Y,CYCSEQ/V, 00000880
         Y,NLOAD/V,N,NOGO/V,Y,KMAX/V,Y,KMIN $                          $00000890
CHKPNT   UXVF $                                                        $00000900
PARAM    //C,N,ADD/V,N,K/V,N,K/C,N,1 $          K = K + 1              $00000910
PARAM    //C,N,SUB/V,N,DONE/V,Y,KMAX/V,N,K $                           $00000920
COND     LCYC2,DONE $  IF (K.GT.KMAX) EXIT LOOP                        $00000930
```

TABLE 4-II (Cont)

NASTRAN DATA DECK LISTING FOR CYCLIC SYMMETRY
SOLUTION OF SIMPLE MOTOR MODEL - UZRO CALCULATION


```
 N A S T R A N   E X E C U T I V E   C O N T R O L   D E C K   E C H O


REPT     TOPCYC,100 $$$$$$$$$$$$$$$$$$$$$$$$$$$$$$$$$$$$$$$$$$$$$$$$$$$$$$$$$$$$$00000940
JUMP     ERROR1 $                                                        00000950
LABEL    LCYC2 $                                                         00000960
EQUIV    UXVF,UDVF/CYCIO $                                               00000970
CHKPNT   UDVF $                                                          00000980
COND     LCYC3,CYCIO $ IF %CYCIO.GE.0< TRANSFORM TO PHYSICAL VARIABLES   00000990
CYCT1    UXVF/UDVF,GCYCBF/V,Y,CTYPE/C,N,BACK/V,Y,N/V,Y,KMAX/V,Y,NLOAD/   00001000
         V,Y,KMIN $                                                      00001010
CHKPNT   UDVF $                                                          00001020
$
$           FRJ  ALTER FOR UZRO CALCULATION
$
MATPRN  UDVF,,,,//    $
PARTN   UDVF,CP1R,/,,U1R,/C,N,1/C,N,3    $
MATPRN  U1R,,,,//   $
PARTN   U1R,,RP1/,UP1,,/C,N,1/C,N,3   $
MATPRN  UP1,,,,//   $
PARTN   UDVF,CP3R,/,,U3R,/C,N,1/C,N,3    $
MATPRN  U3R,,,,//   $
PARTN   U3R,,RP1/,UP2,,/C,N,1/C,N,3   $
MATPRN  UP2,,,,//   $
MERGE   UP1,UP2,,,,RPM/UZRO/C,N,1/C,N,3/C,N,2      $
MATPRN  UZRO,,,,//   $
OUTPUT1 UZRO,,,,//C,N,-1/C,N,0/C,N,RAYTAPE   $
INPUTT1 /,,,,/C,N,-3/C,N,0/C,N,RAYTAPE   $
$
LABEL    LCYC3 $                                                         00001030
$                                                                        00001040
ALTER 199                                                                00001050
LABEL    ERRORN $  FAILED TO SPECIFY PARAM  N.GT.0                       00001060
PRTPARM  //C,N,0/C,N,N $          END OF ALTER                           00001070
ENDALTER
CEND
```

TABLE 4-II (Cont)

NASTRAN DATA DECK LISTING FOR CYCLIC SYMMETRY
SOLUTION OF SIMPLE MOTOR MODEL - UZRO CALCULATION


```
                         C A S E   C O N T R O L   D E C K   E C H O
CARD
COUNT
  1        TITLE # FREQUENCY RESPONSE OF HEX,  DIH METHOD, FREQ DEP MATL
  2        SPC   # 999
  3        FREQ  # 1
  4        SDAMP # 10
  5        SDISP # ALL
  6      SUBCASE 1
  7        LABEL #   SEG 1-R  1ST LOAD
  8        DLOAD # 1
  9      SUBCASE 2
 10        LABEL #   SEG 1-L  1ST LOAD
 11      SUBCASE 3
 12        LABEL #   SEG 2-R  1ST LOAD
 13      SUBCASE 4
 14        LABEL #   SEG 2-L  1ST LOAD
 15      SUBCASE 5
 16        LABEL #   SEG 3-R  1ST LOAD
 17      SUBCASE 6
 18        LABEL #   SEG 3-L  1ST LOAD
 19        DLOAD # 1
 20      BEGIN BULK

*** USER INFORMATION MESSAGE 207, BULK DATA NOT SORTED,XSORT WILL RE-ORDER DECK.
```

TABLE 4-II (Cont)

NASTRAN DATA DECK LISTING FOR CYCLIC SYMMETRY
SOLUTION OF SIMPLE MOTOR MODEL - UZRO CALCULATION

S O R T E D B U L K D A T A E C H O

CARD COUNT	. 1 ..	2 ..	3 ..	4 ..	5 ..	6 ..	7 ..	8 ..	9 ..	10 .
1-	CHEXA2	20	20	101	102	112	111	201	202	&20
2-	&20	212	211							
3-	CORD2C	10		.0	.0	.0	.0	.0	1.0	&C10
4-	&C1C	1.0	0.0	0.0						
5-	CQUAD2	10	10	102	112	212	202			
6-	CYJOIN	1	C	202						
7-	CYJOIN	2	C	211	212					
8-	DAREA	1	201	1	.8660254201		2	.5		
9-	DAREA	2	201	1	.8660254201		2	.5		
10-	DAREA	2	211	1	.8660254211		2	-.5		
11-	DMI	CP1R	0	2	1	1		12	1	
12-	DMI	CP1R	1	2	1.0					
13-	DMI	CP3R	0	2	1	1		12	1	
14-	DMI	CP3R	1	10	1.0					
15-	DMI	RPM	0	2	1	1		6	1	
16-	DMI	RPM	1	4	1.0	1.0	1.0			
17-	DMI	RP1	0	2	1	1		18	1	
18-	DMI	RP1	1	13	1.0	1.0	18	1.0		
19-	EIGR	1	GIV	.0	1.88		6			&E1
20-	&E1	MAX								
21-	FORCE	1	201	10	1.0	.8660254.5				
22-	FORCE	2	201	10	1.0	.8660254.5				
23-	FORCE	2	211	10	1.0	.8660254-.5				
24-	FREQ1	1	.0	1500.	1					
25-	GRID	101	10	1.	0.0	0.0	10			
26-	GRID	102	10	3.	0.0	0.0	10			
27-	GRID	111	10	1.	60.	0.0	10			
28-	GRID	112	10	3.	60.	0.0	10			
29-	GRID	201	10	1.	0.0	2.	10			
30-	GRID	202	10	3.	0.0	2.	10			
31-	GRID	211	10	1.	60.	2.	10			
32-	GRID	212	10	3.	60.	2.	10			
33-	MAT1	10	1.87		.25	2.-4				
34-	MAT1	20		500.	.49	1.66-4			.50	
35-	PARAM	COUPMASS1								
36-	PARAM	CTYPE	DIH							
37-	PARAM	DECOMOPT2								
38-	PARAM	G	.C							
39-	PARAM	N	3							
40-	PARAM	NOKPRT	1							
41-	PQUAD2	10	10	.1						
42-	RLOAD1	1	1			1000				
43-	RLOAD1	2	2			1000				
44-	SPC1	999	456	101	111	201	211			
45-	SPC1	999	173456	101	102	111	112			
46-	TABLED1	10								&T10
47-	&T10	0.0	0.0	1500.	1.44	3000.	2.72	ENDT		
48-	TABLED1	11								&T11
49-	&T11	0.0	0.0	1500.	1.9264	3000.	2.5016	ENDT		
50-	TABLED1	1000								&1000

TABLE 4-II (Cont)

NASTRAN DATA DECK LISTING FOR CYCLIC SYMMETRY
SOLUTION OF SIMPLE MOTOR MODEL - UZRO CALCULATION


```
                         S O R T E D   B U L K   D A T A   E C H O
 CARD
 COUNT      .  1  ..  2  ..  3  ..  4  ..  5  ..  6  ..  7  ..  8  ..  9  ..  10  .
   51-      &1000   0.      1.0     10C.    1.0     ENDT
            ENDDATA
```

TABLE 4-II (Cont)

NASTRAN DATA DECK LISTING FOR CYCLIC SYMMETRY
SOLUTION OF SIMPLE MOTOR MODEL - UZRO CALCULATION

```
FREQUENCY RESPONSE OF HEX,  DIH METHOD, FREQ DEP MATL                JANUARY  25, 1974   NASTRAN 12/ 1/73    PAGE     28


    MATRIX UZRO     %GINO NAME 101 < IS A COMPLEX       1 COLUMN X      6 ROW RECTANG  MATRIX.

COLUMN       1       ROWS       1 THRU      6    --------------------------------------------------

 5.7358E-07R -3.0051E-07I -3.5763E-07R  1.4252E-06I  1.2036E-06R -4.4642E-06I  5.7357E-07R -3.0051E-07I  3.5763E-07R -1.4252E-06I
-1.2036E-06R  4.4642E-06I

THE NUMBER OF NON-ZERO WORDS IN THE LONGEST RECORD #      12

THE DENSITY OF THIS MATRIX IS 100.00 PERCENT.


*** USER INFORMATION MESSAGE 4114,
DATA BLOCK UZRO     WRITTEN ON NASTRAN FILE INPT, TRL #
               101                1                 6                 2                 3                12             10000
```

TABLE 4-III
NASTRAN DATA DECK LISTING FOR CYCLIC SYMMETRY
SOLUTION OF SIMPLE MOTOR MODEL - RMAT CALCULATION

N A S T R A N   E X E C U T I V E   C O N T R O L   D E C K   E C H O

```
ID  HEXFREQ,DIH
APP  DISP
SOL  8,1  $ FREQUENCY RESPONSE
TIME    12
DIAG 8,13 $ PRINT TRAILERS AND OPEN CORE MESSAGES
$- CYCLIC TRANSFORMATION - FREQUENCY RESPONSE ------------------------00000010
$       12/01/73         R I G I D   F O R M A T   8  /  SERIES M      00000020
$                                                      /  RLH VERSION   00000030
$   CASE CONTROL INPUT                                                 00000040
$       A SUBCASE IS USED FOR EACH SUBSTRUCTURE AND LOADING CONDITION.  00000050
$       ALL MPC AND SPC REQUESTS MUST BE ABOVE THE SUBCASE LEVEL.      00000060
$                                                                      00000070
$   BULK DATA INPUT                                                    00000080
$          PARAMETERS USED ARE.                                        00000090
$         CTYPE %REQUIRED<   ROT # ROTATIONAL                          00000100
$                            DIH # DIHEDRAL                            00000110
$                           DSYM # DIH PLUS DEFORMATION SYMMETRY       00000120
$                           DANT # DIH PLUS DEFORMATION-ANTISYMMETRY   00000130
$         N      %REQUIRED<   NUMBER OF SEGMENTS                       00000140
$         KMIN   %DEFAULT 0 < MIN RANGE OF CYCLIC INDEX K              00000150
$         KMAX   %DEFAULT -1< MAX RANGE OF CYCLIC INDEX K %-1 IMPLIES ALL<00000160
$         CYCIO %DEFAULT &1< INPUT/OUTPUT, &1 # PHYSICAL , -1 # SYM COMP 00000170
$         CYCSEQ%DEFAULT -1< MATRIX ELEMENT SEQUENCE, 1 # SEPARATE     00000180
$                                               -1 # ALTERNATING       00000190
$         NLOAD %DEFAULT &1< NUMBER OF LOADING CONDITIONS              00000200
$         NOKPRT%DEFAULT -1< IF &1 K WILL BE OUTPUT AT THE TOP OF LOOP  00000210
$                                                                      00000220
$         CYJOIN BULK DATA CARDS ARE REQUIRED.                         00000230
$                                                                      00000240
$      THE MODEL MUST CONTAIN K4 STRUCTURAL DAMPING %FOR FREQ DEP MATL< 00000250
$      TWO TABLEDX,TR%F< AND TI%F<, ARE SELECTED IN CASE CONTROL VIA    00000260
$      SDAMP %THE ID OF TR IS SELECTED, THE ID OF TI MUST BE ONE LARGER<00000270
$      THE STIFFNESS MATRIX %WITH STRUCTURAL DAMPING< WILL BE          00000280
$         K * % 1. & I*G < & K4 * % TR%F< & I*TI%F< <                  00000290
$          WHERE K # STIFFNESS MATRIX , G # PARAM OVERALL DAMPING      00000300
$                                                                      00000310
$ THE ANALYSIS WILL LOOP THRU A RANGE OF THE CYCLIC INDEX K # KMIN,KMAX 00000320
$                                                                      00000330
ALTER 2                                                                00000340
FILE      UXVF#APPEND $                                                00000350
COND      ERRORN,N $  IF USER HAS NOT SPECIFIED N %DEFAULT & -1<       00000360
COND      FIND,KMAX $                                                  00000370
JUMP      KNOWN $                                                      00000380
LABEL     FIND $                                                       00000390
PARAM     //C,N,DIV/V,Y,KMAX#-1/V,Y,N/C,N,2 $                          00000400
LABEL     KNOWN $                                                      00000410
PARAM     //C,N,NOP/V,Y,CYCIO#1/V,Y,NOKPRT#-1 $                        00000420
ALTER 92                                                               00000430
GPCYC     GEOM4,EQDYN,USETD/CYCDD/V,Y,CTYPE/V,N,NOGO $  DATA FOR CYCT2 00000440
```

TABLE 4-III (Cont)

NASTRAN DATA DECK LISTING FOR CYCLIC SYMMETRY
SOLUTION OF SIMPLE MOTOR MODEL - RMAT CALCULATION

N A S T R A N   E X E C U T I V E   C O N T R O L   D E C K   E C H O

```
CHKPNT   CYCDD $                                                    00000450
ALTER 129,129 $                                                     00000460
PURGE    K2DD/NOK2PP/M2DD/NOM2PP/B2DD/NOB2PP $                      00000470
ALTER 133,133                                                       00000480
GKAD     USETD,GM,GD,KAA,BAA,MAA,     ,K2PP,M2PF,B2PP/KDD,BDD,MDD,GMD, 00000490
         GOD,K2DD,M2DD,B2DD/C,N,FREQRESP/C,N,DISP/C,N,DIRECT/C,Y,G#0.0/ 00000500
         C,N,0.0/C,N,0.0/V,N,NOK2PP/V,N,NOM2PP/V,N,NOB2PP/    V,N,MPCF1/ 00000510
         V,N,SINGLE/V,N,OMIT/V,N,NOUE/C,N,-1     /V,N,NOBGG/V,N,KDEK2/C, 00000520
         N,-1 $     REMOVE K4                                       00000530
ALTER 139,139 $ ACTUALLY  ALTER 139,141                             00000540
EQUIV    K4AA,K4DD/NOUE $                                           00000550
CHKPNT   K4DD $                                                     00000560
COND     LBLNOUE,NOUE $                                             00000570
VEC      USETD/EPV/C,N,D/C,N,A/C,N,E $                              00000580
MERGE    K4AA,,,,EPV,/K4DD $                                        00000590
CHKPNT   K4DD $                                                     00000600
LABEL    LBLNOUE $                                                  00000610
FRLG     CASEXX,USETD,DLT,FRL,GMD,GOD,DIT,/PPF,PSF,PDF,FOL,PHF/     00000620
         C,N,DIRECT  $  COMPUTE LOADS                               00000630
CHKPNT   PPF,PSF,PDF,FOL  $                                         00000640
EQUIV    PPF,PDF/NOSET $                                            00000650
CHKPNT   PDF $                                                      00000660
EQUIV    PDF,PXF/CYCIO $                                            00000670
CHKPNT   PXF $                                                      00000680
COND     LCYC1,CYCIO $ IF %CYCIO.GE.0< TRANSFORM TO SYMMETRIC COMPONENTS00000690
CYCT1    PDF/PXF,GCYCFF/V,Y,CTYPE/C,N,FORE/V,Y,N/V,Y,KMAX/V,Y,NLOAD/ 00000700
         V,Y,KMIN $                                                 00000710
CHKPNT   PXF $                                                      00000720
LABEL    LCYC1 $                                                    00000730
PARAM    //C,N,ADD/V,N,K/C,N,0/V,Y,KMIN#0 $ INITIALIZE K # KMIN     00000740
LABEL    TOPCYC $$$$$$$$$$$$$$$  LOOP ON K  $$$$$$$$$$$$$$$$$$$$$$$$$$$$$$00000750
COND     NOKPRT,NOKPRT  $                                          $00000760
PRTPARM  //C,N,0/C,N,K $                                           $00000770
LABEL    NOKPRT $                                                  $00000780
ALTER 140,140                                                      $00000790
CYCT2    CYCDD,KDD,MDD,PXF,BDD,K4DD/KKKF,MKKF,PKF,BKKF,K4KKF/C,N,   00000800
         FOREFREQ/V,Y,N#-1/V,N,K/V,Y,CYCSEQ#-1/V,Y,NLOAD#1/V,N,NOGO/ 00000810
         V,Y,KMAX/V,Y,KMIN $                                       $00000820
CHKPNT   KKKF,MKKF,PKF,BKKF,K4KKF $                                $00000830
FRRD1    CASEXX,DIT,KKKF,BKKF,MKKF,K4KKF,PKF,FRL,FOL/UKVF/C,N,DIRECT/ 00000840
         V,N,NONCUP/C,Y,DECOMOPT#1 $                               $00000850
CHKPNT   UKVF $                                                    $00000860
ALTER 141,141                                                      $00000870
CYCT2    CYCDD,,,UKVF,,/,,UXVF,,/C,N,BACKFREQ/V,Y,N/V,N,K/V,Y,CYCSEQ/V, 00000880
         Y,NLOAD/V,N,NOGO/V,Y,KMAX/V,Y,KMIN $                      $00000890
CHKPNT   UXVF $                                                    $00000900
PARAM    //C,N,ADD/V,N,K/V,N,K/C,N,1 $          K # K & 1          $00000910
PARAM    //C,N,SUB/V,N,DONE/V,Y,KMAX/V,N,K $                       $00000920
COND     LCYC2,DONE $  IF%K.GT.KMAX< EXIT LOOP                     $00000930
REPT     TOPCYC,100 $$$$$$$$$$$$$$$$$$$$$$$$$$$$$$$$$$$$$$$$$$$$$$$$$$$00000940
```

TABLE 4-III (Cont)

NASTRAN DATA DECK LISTING FOR CYCLIC SYMMETRY
SOLUTION OF SIMPLE MOTOR MODEL - RMAT CALCULATION

N A S T R A N   E X E C U T I V E   C O N T R O L   D E C K   E C H O

```
JUMP      ERROR1 $                                                            00000950
LABEL     LCYC2 $                                                             00000960
EQUIV     UXVF,UDVF/CYCIO $                                                   00000970
CHKPNT    UDVF $                                                              00000980
COND      LCYC3,CYCIO $ IF %CYCIO.GE.0< TRANSFORM TO PHYSICAL VARIABLES       00000990
CYCT1     UXVF/UDVF,GCYCDF/V,Y,CTYPE/C,N,BACK/V,Y,N/V,Y,KMAX/V,Y,NLOAD/       00001000
          V,Y,KMIN $                                                          00001010
CHKPNT    UDVF $                                                              00001020
$
$    $    FRJ  ALTER FOR RMAT CALCULATION
$
PARTN     UDVF,CP1R,/,,U1R,/C,N,1/C,N,3   $
MATPRN    U1R,,,,// $
PARTN     U1R,,RP1/,UP1,,/C,N,1/C,N,3   $
MATPRN    UP1,,,,//   $
PARTN     UDVF,CP3R,/,,U3R,/C,N,1/C,N,3   $
MATPRN    U3R,,,,//   $
PARTN     U3R,,RP1/,UP2,,/C,N,1/C,N,3   $
MATPRN    UP2,,,,//   $
MERGE     UP1,UP2,,,,RPM/RMAT/C,N,1/C,N,3/C,N,2   $
MATPRN    RMAT,,,,// $
INPUTT1   /UZRO,,,,/C,N,-7/C,N,0/C,N,RAYTAPE   $
OUTPUT1   UZRO,RMAT,,,//C,N,-1/C,N,1/C,N,RAYTAPE1   $
INPUTT1   /,,,,/C,N,-3/C,N,1/C,N,RAYTAPE1   $
$
LABEL     LCYC3 $                                                             00001030
$                                                                             00001040
ALTER 199                                                                     00001050
LABEL     ERRORN $  FAILED TO SPECIFY PARAM  N.GT.0                           00001060
PRTPARM   //C,N,0/C,N,N $          END OF ALTER                               00001070
ENDALTER
CEND
```

TABLE 4-III (Cont)

NASTRAN DATA DECK LISTING FOR CYCLIC SYMMETRY
SOLUTION OF SIMPLE MOTOR MODEL - RMAT CALCULATION

```
FREQUENCY RESPONSE OF HEX,  DIH METHOD, FREQ DEP MATL                JANUARY 31, 1974   NASTRAN 12/ 1/73    PAGE    4
    RECEPTANCE MATRIX CALCULATION

                                   C A S E   C O N T R O L   D E C K   E C H O
          CARD
          COUNT
            1        TITLE # FREQUENCY RESPONSE OF HEX,  DIH METHOD, FREQ DEP MATL
            2      SUBTITLE  #      RECEPTANCE MATRIX CALCULATION
            3        SPC   # 999
            4        FREQ  # 1
            5        SDAMP # 10
            6        SDISP # ALL
            7      SUBCASE 1
            8        LABEL #   SEG 1-R   1ST LOAD
            9        DLOAD # 1
           10      SUBCASE 2
           11        LABEL #   SEG 1-L   1ST LOAD
           12      SUBCASE 3
           13        LABEL #   SEG 2-R   1ST LOAD
           14      SUBCASE 4
           15        LABEL #   SEG 2-L   1ST LOAD
           16      SUBCASE 5
           17        LABEL #   SEG 3-R   1ST LOAD
           18      SUBCASE 6
           19        LABEL #   SEG 3-L   1ST LOAD
           20      SUBCASE 7
           21        LABEL #   SEG 1-R   2ND LOAD
           22        DLOAD # 2
           23      SUBCASE 8
           24        LABEL #   SEG 1-L   2ND LOAD
           25      SUBCASE 9
           26        LABEL #   SEG 2-R   2ND LOAD
           27      SUBCASE 10
           28        LABEL #   SEG 2-L   2ND LOAD
           29      SUBCASE 11
           30        LABEL #   SEG 3-R   2ND LOAD
           31      SUBCASE 12
           32        LABEL #   SEG 3-L   2ND LOAD
           33      SUBCASE 13
           34        LABEL #   SEG 1-R   3RD LOAD
           35        DLOAD # 3
           36      SUBCASE 14
           37        LABEL #   SEG 1-L   3RD LOAD
           38      SUBCASE 15
           39        LABEL #   SEG 2-R   3RD LOAD
           40      SUBCASE 16
           41        LABEL #   SEG 2-L   3RD LOAD
           42      SUBCASE 17
           43        LABEL #   SEG 3-R   3RD LOAD
           44      SUBCASE 18
           45        LABEL #   SEG 3-L   3RD LOAD
           46      SUBCASE 19
           47        LABEL #   SEG 1-R   4TH LOAD
           48      SUBCASE 20
           49        LABEL #   SEG 1-L   4TH LOAD
           50      SUBCASE 21
```

TABLE 4-III (Cont)

NASTRAN DATA DECK LISTING FOR CYCLIC SYMMETRY
SOLUTION OF SIMPLE MOTOR MODEL - RMAT CALCULATION


```
                         C A S E   C O N T R O L   D E C K   E C H O
     CARD
     COUNT
      51         LABEL #   SEG 2-R  4TH LOAD
      52       SUBCASE 22
      53         LABEL #   SEG 2-L  4TH LOAD
      54       SUBCASE 23
      55         LABEL #   SEG 3-R  4TH LOAD
      56         DLOAD = 4
      57       SUBCASE 24
      58         LABEL #   SEG 3-L  4TH LOAD
      59       SUBCASE 25
      60         LABEL #   SEG 1-R  5TH LOAD
      61       SUBCASE 26
      62         LABEL #   SEG 1-L  5TH LOAD
      63       SUBCASE 27
      64         LABEL #   SEG 2-R  5TH LOAD
      65       SUBCASE 28
      66         LABEL #   SEG 2-L  5TH LOAD
      67       SUBCASE 29
      68         LABEL #   SEG 3-R  5TH LOAD
      69         DLOAD = 5
      70       SUBCASE 30
      71         LABEL #   SEG 3-L  5TH LOAD
      72       SUBCASE 31
      73         LABEL #   SEG 1-R  6TH LOAD
      74       SUBCASE 32
      75         LABEL #   SEG 1-L  6TH LOAD
      76       SUBCASE 33
      77         LABEL #   SEG 2-R  6TH LOAD
      78       SUBCASE 34
      79         LABEL #   SEG 2-L  6TH LOAD
      80       SUBCASE 35
      81         LABEL #   SEG 3-R  6TH LOAD
      82         DLOAD = 6
      83       SUBCASE 36
      84         LABEL #   SEG 3-L  6TH LOAD
      85       BEGIN BULK

*** USER INFORMATION MESSAGE 207, BULK DATA NOT SORTED,XSORT WILL RE-ORDER DECK.
```

TABLE 4-III (Cont)

NASTRAN DATA DECK LISTING FOR CYCLIC SYMMETRY
SOLUTION OF SIMPLE MOTOR MODEL - RMAT CALCULATION

S O R T E D B U L K D A T A E C H O

CARD COUNT	. 1 ..	2 ..	3 ..	4 ..	5 ..	6 ..	7 ..	8 ..	9 ..	10 .
1-	CHEXA2	20	20	101	102	112	111	201	202	&20
2-	&20	212	211							
3-	CORD2C	10		.0	.0	.0	.0	.0	1.0	&C10
4-	&C10	1.0	0.0	0.0						
5-	CQUAD2	10	10	102	112	212	202			
6-	CYJOIN	1	C	202						
7-	CYJOIN	2	C	211	212					
8-	DAREA	1	201	1	.8660254201		2	.5		
9-	DAREA	2	201	1	.8660254201		2	.5		
10-	DAREA	2	211	1	.8660254211		2	-.5		
11-	DAREA	31	212	1	1.0					
12-	DAREA	32	212	2	1.0					
13-	DAREA	33	212	6	1.0					
14-	DAREA	34	212	1	1.0					
15-	DAREA	35	212	2	1.0					
16-	DAREA	36	212	6	1.0					
17-	DMI	CP1R	0	2	1	1		72	1	
18-	DMI	CP1R	1	2	1.0	14	1.0	26	1.0	&CP1
19-	&CP1	56	1.0	50	1.0	62	1.0			
20-	DMI	CP3R	0	2	1	1		72	1	
21-	DMI	CP3R	1	10	1.0	22	1.0	34	1.0	&CP2
22-	&CP2	46	1.0	58	1.0	70	1.0			
23-	DMI	RPM	0	2	1	1		6	1	
24-	DMI	RPM	1	4	1.0	1.0	1.0			
25-	DMI	RP1	0	2	1	1		18	1	
26-	DMI	RP1	1	13	1.0	1.0	18	1.0		
27-	EIGR	1	GIV	.0	1.E8		6			&E1
28-	&E1	MAX								
29-	FORCE	1	201	10	1.0	.8660254.5				
30-	FORCE	2	201	10	1.0	.8660254.5				
31-	FORCE	2	211	10	1.0	.8660254-.5				
32-	FREQ1	1	.0	1500.	1					
33-	GRID	101	10	1.	0.0	0.0	10			
34-	GRID	102	10	3.	0.0	0.0	10			
35-	GRID	111	10	1.	60.	0.0	10			
36-	GRID	112	10	3.	60.	0.0	10			
37-	GRID	201	10	1.	0.0	2.	10			
38-	GRID	202	10	3.	0.0	2.	10			
39-	GRID	211	10	1.	60.	2.	10			
40-	GRID	212	10	3.	60.	2.	10			
41-	MAT1	10	1.E7		.25	2.-4				
42-	MAT1	20		500.	.49	1.66-4			.50	
43-	~~PARAM~~	~~COUPMASS1~~								
44-	PARAM	CTYPE	DIH							
45-	PARAM	DECOMOPT2								
46-	PARAM	G	.0							
47-	PARAM	N	3							
48-	PARAM	NLOAD	6							
49-	PARAM	NOKPRT	1							
50-	PQUAD2	10	10	.1						

TABLE 4-III (Cont)

NASTRAN DATA DECK LISTING FOR CYCLIC SYMMETRY
SOLUTION OF SIMPLE MOTOR MODEL - RMAT CALCULATION

```
FREQUENCY RESPONSE OF HEX,  CIH METHOD, FREQ DEP MATL                JANUARY  31, 1974   NASTRAN 12/ 1/73    PAGE    7
    RECEPTANCE MATRIX CALCULATION

                                   S O R T E D   B U L K   D A T A   E C H O
  CARD
  COUNT        .   1  ..   2  ..   3  ..   4  ..   5  ..   6  ..   7  ..   8  ..   9  ..  10  .
    51-        RLOAD1  1       31                      1000
    52-        RLOAD1  2       32                      1000
    53-        RLOAD1  3       33                      1000
    54-        RLOAD1  4       34                      1000
    55-        RLOAD1  5       35                      1000
    56-        RLOAD1  6       36                      1000
    57-        SPC1    999     456     101     111     201     211
    58-        SPC1    999     123456  101     102     111     112
    59-        TABLED1 10                                                              &T10
    60-        &T10    0.0     0.0     1500.   1.44    3000.   2.72    ENDT
    61-        TABLED1 11                                                              &T11
    62-        &T11    0.0     0.0     1500.   1.9264  3000.   2.5016  ENDT
    63-        TABLED1 1000                                                            &1000
    64-        &1000   0.      1.0     100.    1.0     ENDT
               ENDDATA

**NO ERRORS FOUND - EXECUTE NASTRAN PROGRAM**
```

COPY AVAILABLE TO DDC DOES NOT PERMIT FULLY LEGIBLE PRODUCTION

TABLE 4-III (Cont)

NASTRAN DATA DECK LISTING FOR CYCLIC SYMMETRY
SOLUTION OF SIMPLE MOTOR MODEL - RMAT CALCULATION


```
 MATRIX RMAT  (GINO NAME 101 < IS A COMPLEX       6 COLUMN X      6 ROW RECTANG  MATRIX.
COLUMN      1        ROWS     1 THRU     6    ----------------------------------------------------
 6.0442E-06R -1.1671E-06I  0.0         0.0      I  9.0949E-13R  0.0       I -8.9737E-08R  2.5789E-08I -1.5496E-06R  4.2415E-08I
 2.5136E-06R -5.8972E-07I
COLUMN      2        ROWS     1 THRU     6    ----------------------------------------------------
 1.5927E-06R -5.6787E-08I -7.0170E-07R  2.0106E-07I  1.5496E-06R -4.2415E-08I -2.7799E-06R  2.6775E-08I  2.7505E-07R -1.0018E-07I
COLUMN      3        ROWS     1 THRU     6    ----------------------------------------------------
-9.0949E-13R  0.0        I -7.0170E-07R  2.0106E-07I  6.4766E-04R -1.0837E-06I -2.5136E-06R  5.8972E-07I  2.7505E-07R -1.0018E-07I
 3.3084E-04R  5.3674E-07I
COLUMN      4        ROWS     1 THRU     6    ----------------------------------------------------
-8.9737E-08R  2.5789E-08I  1.5496E-06R -4.2415E-08I -2.5136E-06R  5.8972E-07I  6.0442E-06R -1.1671E-06I  4.4591E-15R -5.4520E-15I
-3.8564E-13R  7.7913E-14I
COLUMN      5        ROWS     1 THRU     6    ----------------------------------------------------
-1.5496E-06R  4.2415E-08I -2.7799E-06R  2.6775E-08I  2.7505E-07R -1.0018E-07I -4.4591E-15R  5.4520E-15I  1.5927E-06R -5.6787E-08I
-7.0170E-07R  2.0106E-07I
COLUMN      6        ROWS     1 THRU     6    ----------------------------------------------------
 2.5136E-06R -5.8972E-07I  2.7505E-07R -1.0018E-07I  3.3084E-04R  5.3674E-07I  3.8564E-13R -7.7913E-14I -7.0170E-07R  2.0106E-07I
 6.4766E-04R -1.0837E-06I
THE NUMBER OF NON-ZERO WORDS IN THE LONGEST RECORD #      12
THE DENSITY OF THIS MATRIX IS  94.44 PERCENT.

*** USER INFORMATION MESSAGE 4139,    DATA BLOCK UZRO     RETRIEVED FROM USER TAPE INPT %DATA BLOCK COUNT #    1<

*** USER INFORMATION MESSAGE 4114,
DATA BLOCK UZRO      WRITTEN ON NASTRAN FILE INP1, TRL #
            101            1            6            2            3            12            10000

*** USER INFORMATION MESSAGE 4114,
DATA BLOCK RMAT      WRITTEN ON NASTRAN FILE INP1, TRL #
            102            6            6            2            3            12            9444
```

TABLE 4-IV

NASTRAN DATA DECK LISTING FOR BEAM COMPONENT
INVERSE RECEPTANCE MATRIX CALCULATION AND $\{U_T\}$ CALCULATION

N A S T R A N   E X E C U T I V E   C O N T R O L   D E C K   E C H O

```
ID       BEAM,COMPNT
APP      DISP
SOL      8,1
TIME     5
ALTER    141
MPYAD    PDF,UDVF,/RMATC/C,N,1    $
MATPRN   UDVF,PDF,RMATC,,//       $
SOLVE    RMATC,/RIMAT/C,N,0/C,N,1/C,N,2/C,N,3     $
MATPRN   RIMAT,,,,//              $
INPUTT1  /UZRO,RMAT,,,/C,N,-5/C,N,1/C,N,RAYTAPE1          $
MPYAD     RMAT,RIMAT,/PMAT/C,N,0      $
ADD       UNI,PMAT/MAT/C,N,%1.0,0.0</C,N,%1.0,0.0<     $
SOLVE     MAT,/MATI/C,N,0/C,N,1/C,N,2/C,N,3      $
MPYAD     MATI,UZRO,/UTOT/C,N,0      $
MATPRN    UNI,PMAT,MAT,MATI,UTOT//      $
SOLVE    RIMAT,/RCMAT/C,N,0/C,N,1/C,N,2/C,N,3    $
ADD       RCMAT,RMATC/ERMAT/C,N,%1.0,0.</C,N,%-1.0,0.0<      $
MATPRN    ERMAT,,,,//      $
ENDALTER
CEND
```

TABLE 4-IV (Cont)

NASTRAN DATA DECK LISTING FOR BEAM COMPONENT
INVERSE RECEPTANCE MATRIX CALCULATION AND $\{\ddot{U}_T\}$ CALCULATION


```
                                   C A S E    C O N T R O L    D E C K    E C H O
 CARD
 COUNT
   1      TITLE  #  INVERSE RECEPTANCE MATRIX CALCULATION FOR BEAM COMPONENT
   2      FREQ   # 20
   3      OUTPUT
   4                SDISP   #  ALL
   5      SUBCASE 1
   6                LABEL # 1ST LOAD
   7                DLOAD # 1
   8      SUBCASE 2
   9                LABEL # 2ND LOAD
  10                DLOAD # 2
  11      SUBCASE 3
  12                LABEL # 3RD LOAD
  13                DLOAD # 3
  14      SUBCASE 4
  15                LABEL # 4TH LOAD
  16                DLOAD # 4
  17      SUBCASE 5
  18                LABEL # 5TH LOAD
  19                DLOAD # 5
  20      SUBCASE 6
  21                LABEL # 6TH LOAD
  22                DLOAD # 6
  23      BEGIN BULK

*** USER INFORMATION MESSAGE 207, BULK DATA NOT SORTED,XSORT WILL RE-ORDER DECK.
```

TABLE 4-IV (Cont)

NASTRAN DATA DECK LISTING FOR BEAM COMPONENT
INVERSE RECEPTANCE MATRIX CALCULATION AND $\{U_T\}$ CALCULATION

S O R T E D B U L K D A T A E C H O

CARD COUNT	. 1 ..	2 ..	3 ..	4 ..	5 ..	6 ..	7 ..	8 ..	9 ..	10 .
1-	CBAR	1	19	20	21	4.0	45.	2.0	1	
2-	CBAR	2	19	21	22	5.0	15.	2.0	1	
3-	CBAR	3	19	22	23	5.0	-30.	2.0	1	
4-	CBAR	4	19	23	24	4.0	300.	2.C	1	
5-	CORD2C	10		.0	.0	.0	.0	.C	1.0	&C10
6-	&C10	1.0	0.0	0.0						
7-	DAREA	51	20	1	1.0					
8-	DAREA	52	20	2	1.0					
9-	DAREA	53	20	6	1.0					
10-	DAREA	54	24	1	1.0					
11-	DAREA	55	24	2	1.0					
12-	DAREA	56	24	6	1.0					
13-	DMI	UNI	0	2	3	3		6	6	
14-	DMI	UNI	1	1	1.0	.0				
15-	DMI	UNI	2	2	1.0	.0				
16-	DMI	UNI	3	3	1.0	.0				
17-	DMI	UNI	4	4	1.0	.0				
18-	DMI	UNI	5	5	1.0	.0				
19-	DMI	UNI	6	6	1.0	.0				
20-	FREQ	20	1500.							
21-	GRID	20	10	3.0	60.	2.0	10	345		
22-	GRID	21	10	4.0	30.	2.0	10	345		
23-	GRID	22	10	4.0	.0	2.0	10	345		
24-	GRID	23	10	5.0	-45.	2.0	10	345		
25-	GRID	24	10	3.0	-60.	2.0	10	345		
26-	MAT1	18	30.E6		.3	7.32-4			.10	
27-	PARAM	COUPMASS1								
28-	PBAR	19	19	.15	.002					
29-	RLOAD1	1	51			1000				
30-	RLOAD1	2	52			1000				
31-	RLOAD1	3	53			1000				
32-	RLOAD1	4	54			1000				
33-	RLOAD1	5	55			1000				
34-	RLOAD1	6	56			1000				
35-	TABLED1	1000								&T1
36-	&T1	-1000.	1.0	2000.	1.0	ENDT				
	ENDDATA									

NO ERRORS FOUND - EXECUTE NASTRAN PROGRAM

TABLE 4-IV (Cont)

NASTRAN DATA DECK LISTING FOR BEAM COMPONENT
INVERSE ACCEPTANCE MATRIX CALCULATION AND $\{U_T\}$ CALCULATION

```
INVERSE RECEPTANCE MATRIX CALCULATION FOR BEAM COMPONENT              FEBRUARY  7, 1974   NASTRAN 12/ 1/73    PAGE    14


     MATRIX UTOT     %GINO NAME 105 < IS A COMPLEX       1 COLUMN X      6 ROW RECTANG  MATRIX.
COLUMN       1       ROWS       1 THRU       6    ------------------------------------------------------

 6.6393E-078 -1.7153E-07I -2.5355E-078  1.7242E-06I  1.0973E-078  1.6523E-06I  5.4624E-078 -8.7315E-07I  3.4871E-078 -1.6422E-06I
-1.5148E-078 -2.1860E-07I

THE NUMBER OF NON-ZERO WORDS IN THE LONGEST RECORD =       24

THE DENSITY OF THIS MATRIX IS 100.00 PERCENT.

*** USER INFORMATION MESSAGE 3028,      B #     6      BBAR #     5
                                        C #     0      CBAR #     0
                                        R #     5

*** USER INFORMATION MESSAGE 3027, UNSYMMETRIC COMPLEX DECOMPOSITION TIME ESTIMATE IS       0 SECONDS.
```

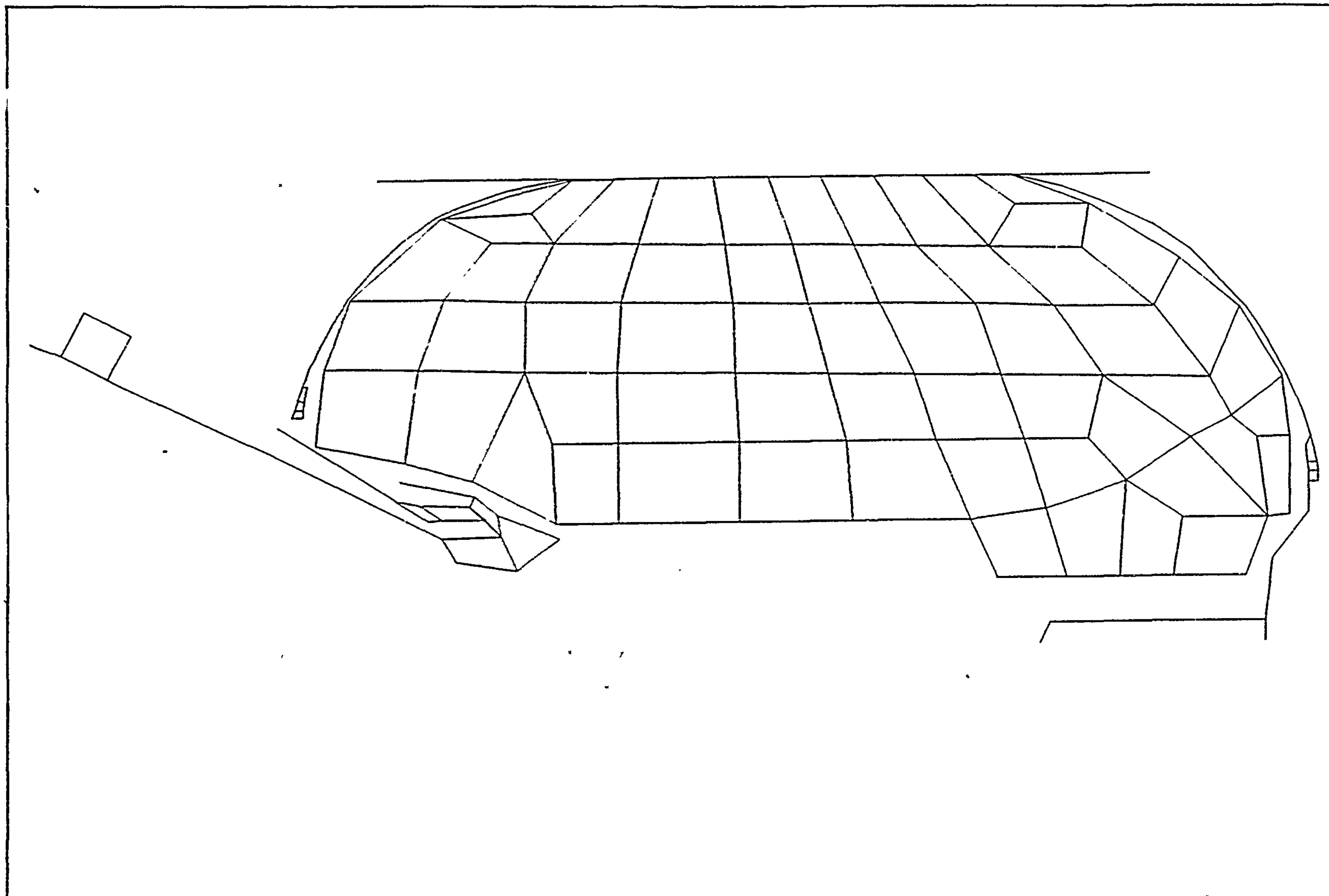

Figure 4-2. Finite Element Grid for the 1/24 Section Zero Burn Time Model, Poseidon C-3 SS motor

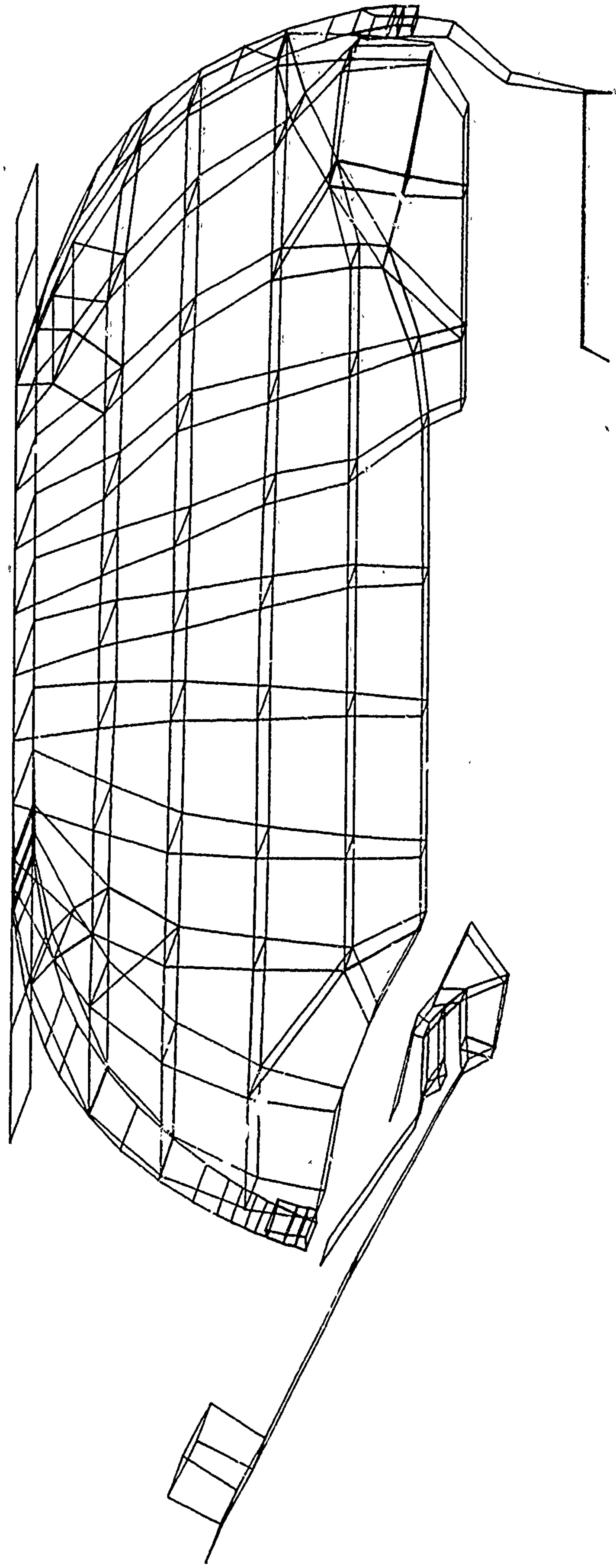

Figure 4-3. Finite-Element Grid for 1/24 Section Advanced (4.0 Second)
Burn Time Model, Poseidon C-3 SS motor

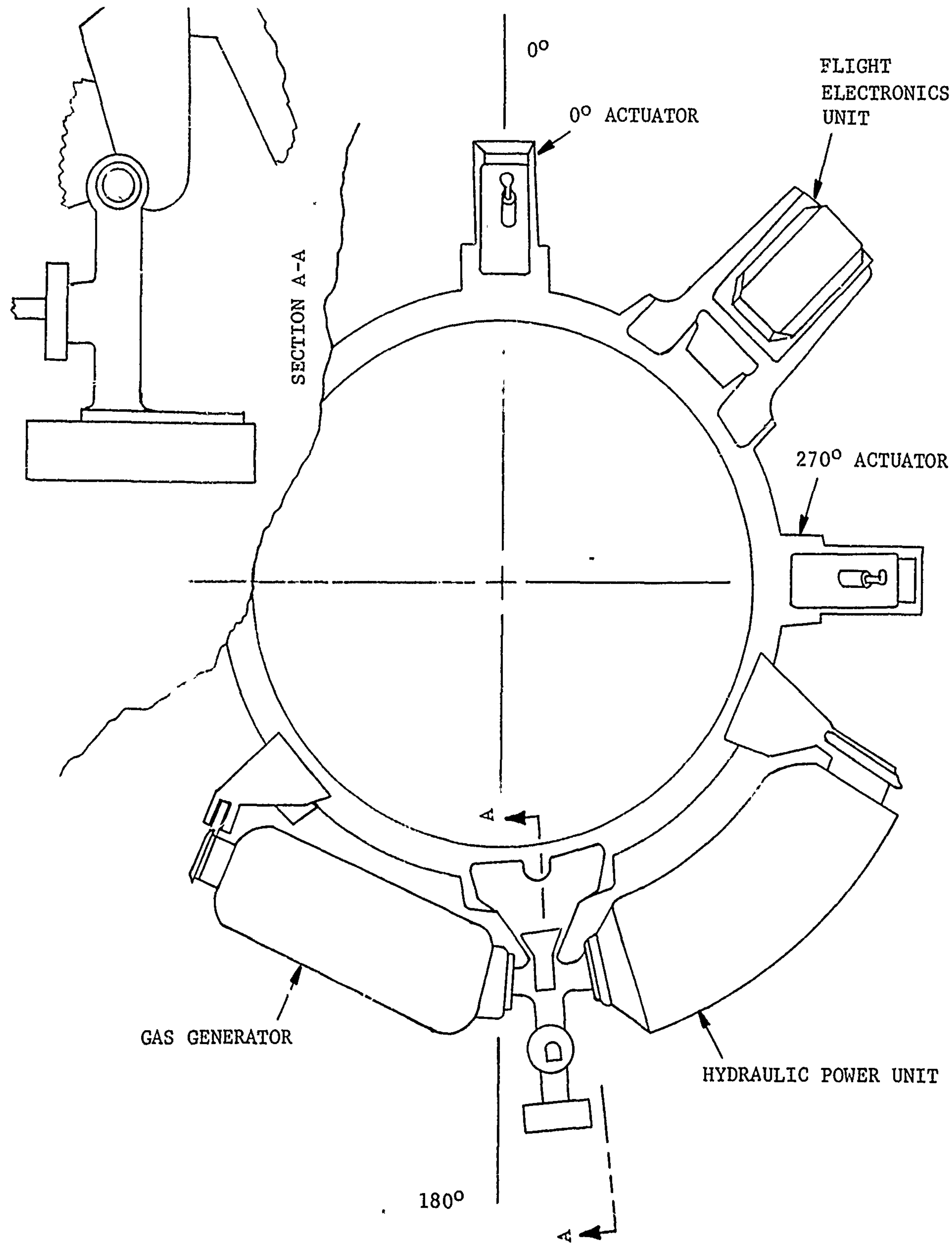

Figure 4-4. Components Mounted on the Nozzle Adapter,
SS Poseidon Aft Dome

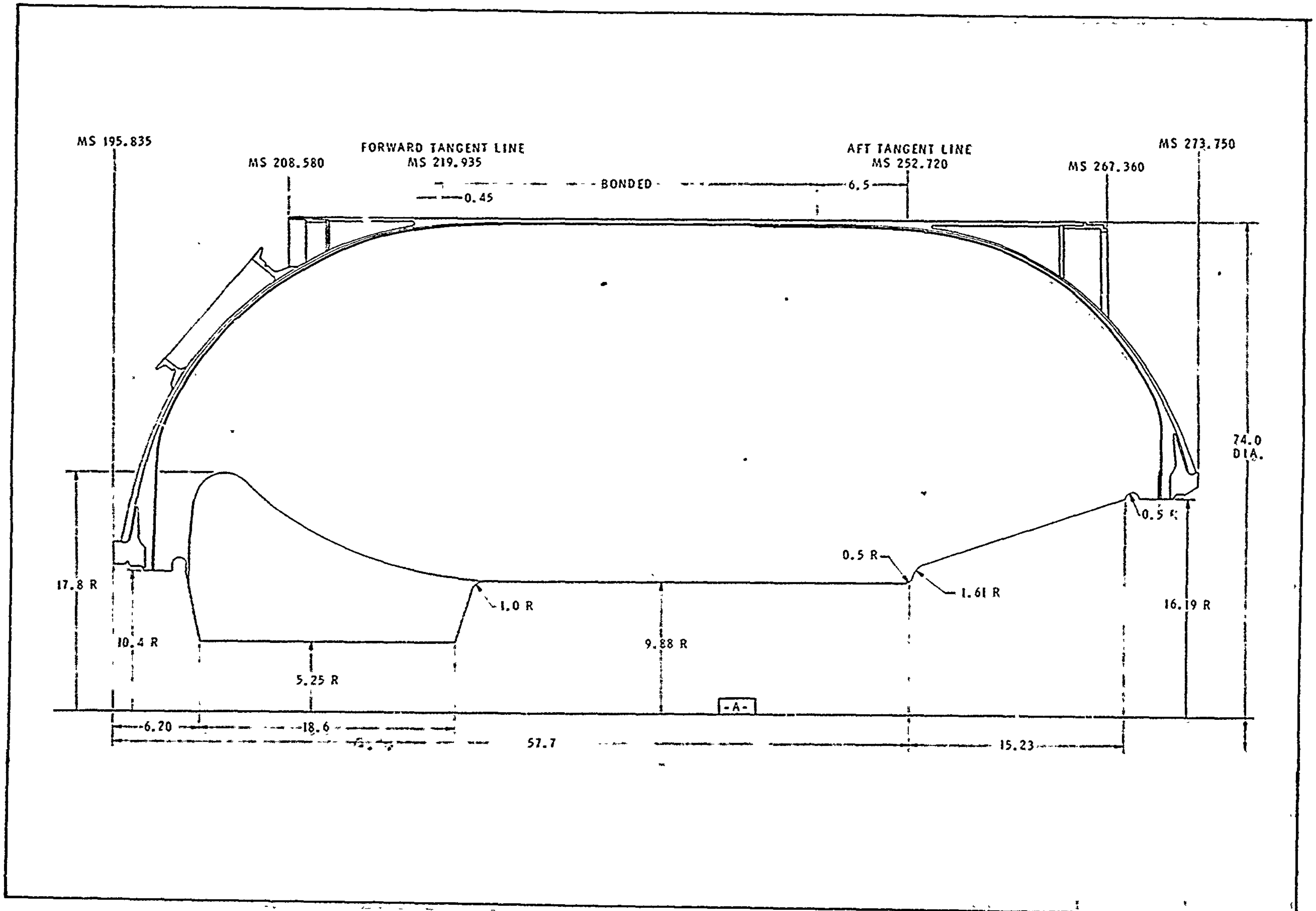

Figure 4-5. Dimensions of the C-3 Poseidon SS Motor

TABLE 4-V

COMPLEX DISPLACEMENT VECTORS
FOR COMPONENT CONNECTION COORDINATES

Direct Solution	Mechanical Impedance
6.639207 - 1.715272i	6.6393 - 1.7153i
-3.535503 + 17.24168i	-3.5355 + 17.242i
1.097407 + 16.52334i	1.0973 + 16.523i
5.462359 - 8.731442i	5.4624 - 8.7315i
3.487139 - 16.42242i	3.4871 - 16.422i
-1.514637 - 2.185999i	-1.5148 - 2.1860i

displacements were predicted at several locations on the model. Receptance matrices were calculated and the total response was obtained by evaluating equation (1). A discussion of the mathematical models, checkouts, modeling techniques, and load generation procedures follows.

1. Grid Generation

A grid for the clean motor model was generated for a 1/24 section. The 1/24 sections shown in Figures 4-2 and 4-3 have 1176 degrees of freedom in the solution set, which is equivalent to 14,112 degrees of freedom in a full motor model. Figures 4-2 and 4-3 show the full motor with wedge elements. All of the Task 3 analyses were completed before the problems with wedge elements were discovered. Effects of wedge elements on the motor analysis results are discussed in Appendix G. As can be seen in Figures 4-2 and 4-3, the 1/24 grid contains elements representing grain, case, igniter, and nozzle.

Checkout for proper operation of the model was accomplished through several comparisons.

2. Checkouts of Models

Because of the importance of an accurate representative case stiffness for prediction of displacements and accelerations, substantial efforts were made for the determination of chamber stiffness. The effective stiffness for a particular panel was calculated with the following procedure. First, the unidirectional, longitudinal, transverse, and shear moduli as well as Poisson's ratios were calculated using relationships established by Eckvall,[1] which have been demonstrated to be accurate for many glass/resin systems. The lamina stiffnesses were rotated to the winding angle, α, at the center of a particular finite element panel. The several lamina stiffnesses were combined, using classical laminate theory, to represent the total laminate stiffnesses. The effective laminate stiffnesses were calculated with a separate computer program, SQ-5.[2,3] The orientation of the finite element panel is determined by special modules within NASTRAN. For verification of mechanical stiffnesses of the chamber, predicted deflections resulting from pressurization were compared to results from an independent analysis.

Evaluation of math models was accomplished through comparison of NASTRAN deformations and predicted deformations of an independent finite element analysis.[4] For a uniform internal pressure of 400 psi, radial deformations at the centerbore and case midcylinder were compared. At the grain centerbore, the NASTRAN model predicted a radial deformation of 0.342 inch, while an independent finite element analysis[4] calculated a deformation of 0.41 inch. Radial growth at midcylinder of the NASTRAN model was predicted to be 0.444 inch radial growth, while another analysis calculated 0.45 inch.

NASTRAN-predicted axial movement (under 400 psi pressurization) of the forward and aft adapters of SS Poseidon motor was compared to measured movements.[5] Measured movements of the forward adapter range from 1.36 to 1.45 inches. Calculated movement, at the 400 psi pressurization, was 1.58 inches. For the aft adapter, measured movements range from 0.97 to 1.68 inches. The calculated movement was 1.53 inches.

---

(1) Eckvall, J. C., Elastic Property Orthotropic Monofilament Laminate, ASME publication No. 61-AV-56.

(2) Reed, D. L., Advanced Composite Technology Point Stress Laminate Analysis, Report FZM-5494 General Dynamics, Fort Worth Division, 1 April 1970.

(3) Laminate Properties Program, Hercules Computer Program 62113, 8 July 1969.

(4) Structural and Thermal Analysis Final Report, SE025-A2A00HTJ-2, Hercules Incorporated, November 1970, pp. 4-57.

(5) Summary of Hydrotest Results, Ref. 17-10203/5/40-74.

The NASTRAN finite-element model for the nozzle and nozzle bucket was checked out. The total model weight was 412.7 pounds. This compares well with the nominal 425 pound nozzle and bucket weight. The movable portion of the model has a weight of 307.8 pounds. Model pitch and yaw moments of inertia are both 17.5 slug-ft^2, compared with a nominal 17.9 slug-ft^2. A nominal roll moment of inertia was not available for comparison. The model center of gravity (CG) is located at missile station (MS) 270.39, compared with a nominal CG location of MS 270.58. It is thus concluded that the NASTRAN nozzle model provides a reasonably accurate mass and inertia representation. Similar comparisons for the total motor and for the grain alone showed equally good agreement between model mass and measured or nominal values.

3. Data Decks

Three distinct types of data decks were used in the analysis of the clean motor and components of the SS Poseidon rocket motor. The data decks were used to: (1) Calculate U_o and R_m (Table 4-VI), (2) calculate R_c^{-1} (Table 4-VII), and (3) read U_o, R_m, and the R_c^{-1} matrices from tape, and evaluate equation (1) to obtain U_T. Details of the calculations were given above under the heading of Approach.

Each time a solution was calculated for one load, 24 subcases were required because a 1/24 segment of the model was used. A total of 1032 subcases were used in the clean motor model. The motor was divided into 12 parts, each of which contained a left and right segment. The result was a 1/24-grid section of a motor. Appendix C contains details of the modeling procedure. A typical bulk data deck for the clean motor is shown in Table 4-VIII.

4. Load Generation

Because the acoustic pressure oscillation is the source of vibration, care was taken to accurately represent the pressure distribution in the centerbore. Acoustic pressure distributions have been described in the Task II report (Appendix B). The pressure longitudinal and tangential acoustic modes for vibrational analyses were applied along the centerbore of the model. For each finite element panel, the acoustic pressure at the center was used to represent the pressure distribution. The equivalent vector nodal forces were computed by NASTRAN and punched onto DAREA cards for vibrational analyses.

A description of the Task 3 analyses has been presented in this section. Results from the analyses as well as an evaluation of the results and conclusions are contained in Section VI, Evaluation of the Baseline Motor Analysis.

TABLE 4-VI

EXECUTIVE CONTROL DECK FOR CALCULATION OF $\{U_o\}$ AND $[R_m]$
FOR THE CLEAN MOTOR MODEL

```
                                                                  MAY  4, 1974   NASTRAN 12/ 1/73    PAGE    1

     N A S T R A N   E X E C U T I V E   C O N T R O L   D E C K   E C H O

ID      BIG,MUMMA
TIME    1000
APP  DISP
DIAG  5,6
DIAG 1,12,14
SOL  8,1  $ FREQUENCY RESPONSE
$- CYCLIC TRANSFORMATION - FREQUENCY RESPONSE -------------------------00000010
$     12/01/73        R I G I D   F O R M A T   8  /  SERIES M         00000020
$                                                  /  RE  VERSION      00000030
$  CASE CONTROL INPUT                                                  00000040
$      A SUBCASE IS USED FOR EACH SUBSTRUCTURE AND LOADING CONDITION.  00000050
$      ALL MPC AND SPC REQUESTS MUST BE ABOVE THE SUBCASE LEVEL.       00000060
$                                                                      00000070
$  BULK DATA INPUT                                                     00000080
$        PARAMETERS USED ARE...                                        00000090
$       CTYPE %REQUIRED<   ROT # ROTATIONAL                            00000100
$                          DIH # DIHEDRAL                              00000110
$                         DSYM # DIH PLUS DEFORMATION SYMMETRY         00000120
$                         DANT # DIH PLUS DEFORMATION ANTISYMMETRY     00000130
$       N      %REQUIRED<  NUMBER OF SEGMENTS                          00000140
$       KMIN   %DEFAULT 0 < MIN RANGE OF CYCLIC INDEX K                00000150
$       KMAX   %DEFAULT -1< MAX RANGE OF CYCLIC INDEX K &-1 IMPLIES ALL<00000160
$       CYCIO %DEFAULT &1< INPUT/OUTPUT, &1 # PHYSICAL , -1 # SYM COMP  00000170
$       CYCSEQ%DEFAULT -1< MATRIX ELEMENT SEQUENCE, 1 # SEPARATE       00000180
$                                                 -1 # ALTERNATING     00000190
$       NLOAD %DEFAULT &1< NUMBER OF LOADING CONDITIONS                00000200
$       NOKPRT%DEFAULT -1< IF &1 K WILL BE OUTPUT AT THE TOP OF LOOP   00000210
$                                                                      00000220
$       CYJOIN BULK DATA CARDS ARE REQUIRED.                           00000230
$                                                                      00000240
$      THE MODEL MUST CONTAIN K4 STRUCTURAL DAMPING %FOR FREQ DEP MATL< 00000250
$      TWO TABLEDX,TR%F< AND TI%F<, ARE SELECTED IN CASE CONTROL VIA   00000260
$      SDAMP %THE ID OF TR IS SELECTED, THE ID OF TI MUST BE ONE LARG-R<00000270
$      THE STIFFNESS MATRIX WITH STRUCTURAL DAMPING< WILL B.           00000280
$        K # % 1. & I*G < & K4 # % TR%F< & I*TI%F< <                   00000290
$        WHERE K # STIFFNESS MATRIX , G # PARAM OVERALL DAMPING        00000300
$                                                                      00000310
$ THE ANALYSIS WILL LOOP THRU A RANGE OF THE CYCLIC INDEX K # KMIN,KMAX 00000320
$                                                                      00000330
ALTER 2                                                                [illegible]
FILE    UXVF#APPEND $                                                  [illegible]
COND    ERRORN,N $  IF USER HAS NOT SPECIFIED N DEFAULT # -1<          [illegible]
COND    FIND,KMAX $                                                    [illegible]
JUMP    KNOWN $                                                        [illegible]
LABEL   FIND $                                                         [illegible]
PARAM   //C,N,DIV/V,Y,KMAX#-1/V,Y,N/ , ,2 $                            [illegible]
LABEL   KNOWN $                                                        [illegible]
PARAM   //C,N,NOP/V,Y,CYCIO#1/V,Y,NOKPRT#-1 $                          [illegible]
ALTER 92                                                               [illegible]
```

TABLE 4-VI (Cont)

EXECUTIVE CONTROL DECK FOR CALCULATION OF $\{U_o\}$ AND $[R_m]$
FOR THE CLEAN MOTOR MODEL

N A S T R A N   E X E C U T I V E   C O N T R O L   D E C K   E C H O

```
GPCYC    GEOM4,EQDYN,USLTD/CYCDD/V,Y,CTYPE/V,N,NOGO $  DATA FOR CYCT2   00000440
CHKPNT   CYCDD $                                                       00000450
ALTER 129,129 $                                                        00000460
PURGE    K2DD/NOK2PP/M2DD/NOM2PP/B2DD/NOB2PP $                          00000470
ALTER 133,133                                                          00000480
GKAD     USETD,GM,GO,KAA,BAA,MAA,    ,K2PP,M2PP,B2PP/KDD,BDD,MDD,GMD,  00000490
         GOD,K2DD,M2DD,B2DD/C,N,FREQRESP/C,N,DISP/C,N,DIRECT/C,Y,G#0.0/ 00000500
         C,N,0.0/C,N,0.0/V,N,NOK2PP/V,N,NOM2PP/V,N,NOB2PP/   V,N,MPCF1/ 00000510
         V,N,SINGLE/V,N,OMIT/V,N,NOUE/C,N,-1    /V,N,NOBGG/V,N,KDEK2/C, 00000520
         N,-1 $      REMOVE K4                                         00000530
ALTER 139,139 $ ACTUALLY  ALTER 139,141                                00000540
EQUIV    K4AA,K4DD/NOUE $                                              00000550
CHKPNT   K4DD $                                                        00000560
COND     LBLNOUE,NOUE $                                                00000570
VEC      USETD/EPV/C,N,D/C,N,A/C,N,E $                                 00000580
MERGE    K4AA,,,,EPV,/K4DD $                                           00000590
CHKPNT   K4DD $                                                        00000600
LABEL    LBLNOUE $                                                     00000610
FRLG     CASEXX,USETD,DLT,FRL,GMD,GOD,DIT,/PPF,PSF,PDF,FOL,PHF/         00000620
         C,N,DIRECT  $  COMPUTE LOADS                                  00000630
CHKPNT   PPF,PSF,PDF,FOL  $                                            00000640
EQUIV    PPF,PDF/NOSET $                                               00000650
CHKPNT   PDF $                                                         00000660
EQUIV    PDF,PXF/CYCIO $                                               00000670
CHKPNT   PXF $                                                         00000680
COND     LCYC1,CYCIO $ IF %CYCIO.GE.0< TRANSFORM TO SYMMETRIC COMPONENTS00000690
CYCT1    PDF/PXF,GCYCFF/V,Y,CTYPE/C,N,FORE/V,Y,N/V,Y,KMAX/V,Y,NLOAD/    00000700
         V,Y,KMIN $                                                    00000710
CHKPNT   PXF $                                                         00000720
LABEL    LCYC1 $                                                       00000730
PARAM    //C,N,ADD/V,N,K/C,N,0/V,Y,KMIN#0 $ INITIALIZE K # KMIN        00000740
LABEL    TOPCYC $$$$$$$$$$$$$$$  LOOP ON K  $$$$$$$$$$$$$$$$$$$$$$$$$$$$00000750
COND     NOKPRT,NOKPRT  $                                             $00000760
PRTPARM  //C,N,0/C,N,K $                                              $00000770
LABEL    NOKPRT $                                                     $00000780
ALTER 140,140                                                         $00000790
CYCT2    CYCDD,KDD,MDD,PXF,BDD,K4DD/KKKF,MKKF,PKF,BKKF,K4KKF/C,N,       00000800
         FOREFREQ/V,Y,N#-1/V,N,K/V,Y,CYCSEQ#-1/V,Y,NLOAD#1/V,N,NOGO/   00000810
         V,Y,KMAX/V,Y,KMIN $                                          $00000820
CHKPNT   KKKF,MKKF,PKF,BKKF,K4KKF $                                   $00000830
FRRD1    CASEXX,DIT,KKKF,BKKF,MKKF,K4KKF,PKF,FRL,FOL/UKVF/C,N,DIRECT/   00000840
         V,N,NONCUP/C,Y,DECOMOPT#1 $                                  $00000850
CHKPNT   UKVF $                                                       $00000860
ALTER 141,141                                                         $00000870
CYCT2    CYCDD,,,UKVF,,/,,UXVF,,/C,N,BACKFREQ/V,Y,N/V,N,K/V,Y,CYCSEQ/V, 00000880
         Y,NLOAD/V,N,NOGO/V,Y,KMAX/V,Y,KMIN $                         $00000890
CHKPNT   UXVF $                                                       $00000900
PARAM    //C,N,ADD/V,N,K/V,N,K/C,N,1 $           K # K & 1 .          $00000910
PARAM    //C,N,SUB/V,N,DONE/V,Y,KMAX/V,N,K $                          $00000920
COND     LCYC2,DONE $  IF%K.GT.KMAX< EXIT LOOP                        $00000930
```

TABLE 4-VI (Cont)

EXECUTIVE CONTROL DECK FOR CALCULATION OF $\{U_o\}$ AND $[R_m]$ FOR THE CLEAN MOTOR MODEL

```
                                                          MAY   1974   NASTRAN 12/ 1/72   PAGE    3

   N A S T R A N   E X E C U T I V E   C O N T R O L   D E C K   E C H O

REPT      TOPCYC,100 $$$$$$$$$$$$$$$$$$$$$$$$$$$$$$$$$$$$$$$$$$$$$$$00000940
JUMP      ERROR1 $                                                00000950
LABEL     LCYC2 $                                                 00000960
EQUIV     UXVF,UDVF/CYCIO .                                       00000970
CHKPNT    UDVF $                                                  00000980
COND      LCYC3,CYCIO $ IF XCYCIO.GE.0< TRANSFORM TO PHYSICAL VARIABLES 00000990
CYCT1     UXVF/UDVF,GCYCBF/V,Y,CTYPE/C,N,BACK/V,Y,N/V,Y,KMAX/V,Y,NLOAD/ 00001000
          V,Y,KMIN $                                              00001010
CHKPNT    UDVF $                                                  00001020
OUTPUT1 UDVF,,,,//C,N,-1/C,N,2/C,N,HIKIDA $
$
$           FRJ  ALTER FOR RMAT  FOR FULL MOTOR MODEL
PARTN     UDVF,CP1R,/,,U1R,/C,N,1/C,N,3         $
PARTN     U1R,,RP1/,UP1,,/C,N,1/C,N,3           $
PARTN     UDVF,CP5R,/,,U5R,/C,N,1/C,N,3         $
PARTN     U5R,,RP2/,UP2,,/C,N,1/C,N,3           $
MERGE     UP1,UP2,,,,RP12/RM12/C,N,1/C,N,4/C,N,2  $
PARTN     UDVF,CP7R,/,,U7R,/C,N,1/C,N,3         $
PARTN     U7R,,RP3/,UP3,,/C,N,1/C,N,3           $
MERGE     RM12,UP3,,,,RP13/RM13/C,N,1/C,N,4/C,N,2  $
PARTN     UDVF,CP9R,/,,U9R,/C,N,1/C,N,3         $
PARTN     U9R,,RP3/,UP4,,/C,N,1/C,N,3           $
MERGE     RM13,UP4,,,,RP14/RM14/C,N,1/C,N,4/C,N,2  $
PARTN     UDVF,CP10,/,,U10,/C,N,1/C,N,3         $
PARTN     U10,,RP1/,UP5,,/C,N,1/C,N,3           $
MERGE     RM14,UP5,,,,RP15/RM15/C,N,1/C,N,4/C,N,2 $
PARTN     UDVF,CP11,/,,U11,/C,N,1/C,N,3         $
PARTN     U11,,RP3/,UP6,,/C,N,1/C,N,3           $
MERGE     RM15,UP6,,,,RP16/RM16/C,N,1/C,N,4/C,N,2 $
PARTN     UDVF,CP12,/,,U12,/C,N,1/C,N,3         $
PARTN     U12,,RP3/,UP7,,/C,N,1/C,N,3           $
MERGE     RM16,UP7,,,,RP17/RMAT/C,N,1/C,N,4/C,N,2 $
MATPRN    RMAT,,,,//         $
OUTPUT1 RMAT,,,,//C,N,-1/C,N,0/C,N,RAYTAPE        $
$
$      UZRO EXTRACTOR-KEEP OUT OF REACH OF CHILDREN
PARTN     UDVF,CP1RR,/,,U1RR,/C,N,1/C,N,3     $
PARTN     U1RR,,RP1/,UP1R,,/C,N,1/C,N,3       $
PARTN     UDVF,CP5RR,/,,U5RR,/C,N,1/C,N,3     $
PARTN     U5RR,,RP2/,UP2R,,/C,N,1/C,N,3       $
MERGE     UP1R,UP2R,,,,RP12/RM12R/C,N,1/C,N,4/C,N,2    $
PARTN     UDVF,CP7RR,/,,U7RR,/C,N,1/C,N,3     $
PARTN     U7RR,,RP3/,UP3R,,/C,N,1/C,N,3       $
MERGE     RM12R,UP3R,,,,RP13/RM13R/C,N,1/C,N,4/C,N,2    $
PARTN     UDVF,CP9RR,/,,U9RR,/C,N,1/C,N,3     $
PARTN     U9RR,,RP3/,UP4R,,/C,N,1/C,N,3       $
MERGE     RM13R,UP4R,,,,RP14/RM14R/C,N,1/C,N,4/C,N,2 $
PARTN     UDVF,CP10R,/,,U10R,/C,N,1/C,N,3     $
PARTN     U10R,,RP1/,UP5R,,/C,N,1/C,N,3       $
MERGE     RM14R,UP5R,,,,RP15/RM15R/C,N,1/C,N,4/C,N,2 $
```

TABLE 4-VI (Cont)

EXECUTIVE CONTROL DECK FOR CALCULATION OF $\{U_o\}$ AND $[R_m]$
FOR THE CLEAN MOTOR MODEL

```
N A S T R A N   E X E C U T I V E   C O N T R O L   D E C K   E C H O

PARTN    UDVF,CP11R,/,,U11R,/C,N,1/C,N,2  $
PARTN    U11R,,RP3/,UP6R,,/C,N,1/C,N,3    $
MERGE    KM15R,UP6R,,,,RP16/RM16R/C,N,1/C,N,4/C,N,2  $
PARTN    UDVF,CP12R,/,,U12F,/C,N,1/C,N,2  $
PARTN    U12R,,RP./,UP7R,,/C,N,1/C,N,2    $
MERGE    RM16R,UP7R,,,,RP17/UZRO/C,N,1/C,N,4/C,N,2  $
MATPRN   UZRO,,,,//   $
OUTPUT1  UZRO,,,,//C,N,-1/C,N,1/C,N,MODEDL  $
$
LABEL     LOYCS $                                          00001030
$                                                          00001040
ALTER 199                                                  00001050
LABEL     ERRURN $  FAILED TO SPECIFY PARAM  N.GT.0        00001060
PRTPARM  //C,N,0/C,N,N $         END OF ALTER              00001070
ENDALTER
CEND
```

TABLE 4-VII

EXECUTIVE CONTROL DECK FOR CALCULATION OF $[R_c^{-1}]$

N A S T R A N   E X E C U T I V E   C O N T R O L   D E C K   E C H O

```
ID       HIKIDAS, MODEL
SOL      8,1
DIAG 8,13 $ PRINT TRAILERS AND OPEN CORE MESSAGES
DIAG 14   $ PRINT RIGID FORMAT
TIME 30
APP      DISP
ALTER    141
MPYAD    PDF,UDVF,/RMATH/C,N,1   $
MATPRN   UDVF,PDF,RMATH,,//      $
SOLVE    RMATH,/RIMATH/C,N,0/C,N,1/C,N,2/C,N,3   $
MATPRN   RIMATH,,,,//      $
OUTPUT1  RIMATH,,,,//C,N,-1/C,N,0/C,N,RAYTAPE     $
INPUTT1  /,,,,/C,N,-3/C,N,0/C,N,RAYTAPE       $
ENDALTER
CEND
```

TABLE 4-VIII

TYPICAL BULK DATA DECK FOR THE CLEAN
MOTOR MODEL FOR POSEIDON C-3 SS MOTOR

S O R T E D   B U L K   D A T A   E C H O

CARD COUNT	. 1 ..	2 ..	3 ..	4 ..	5 ..	6 ..	7 ..	8 ..	9 ..	10 .
1-	CBAR	301	301	16	15	1.0	.0	.0	1	&CB1
2-	&CB1			-0.7	0.0	-.35	-0.7	0.0	-.35	
3-	CBAR	302	302	256	255	1.0	.0	.0	1	&CB2
4-	&CB2			-0.8	0.0	1.35	-0.8	0.0	1.35	
5-	CELAS2	351	8000.	209	3	237	3			
6-	CELAS2	352	8000.	210	3	238	3			
7-	CELAS2	353	8000.	207	3	229	3			
8-	CELAS2	354	8000.	208	3	230	3			
9-	CELAS2	355	8000.	205	3	225	3			
10-	CELAS2	356	8000.	206	3	226	3			
11-	CHEXA2	101	1000	67	83	81	65	68	84	&GR1
12-	&GR1	82	66							
13-	CHEXA2	102	1000	65	81	79	63	66	82	&GR2
14-	&GR2	80	64							
15-	CHEXA2	104	1000	63	77	75	61	64	78	&GR4
16-	&GR4	76	62							
17-	CHEXA2	105	1000	61	75	73	59	62	76	&GR5
18-	&GR5	74	60							
19-	CHEXA2	110	1000	85	99	97	83	86	100	&GR10
20-	&GR10	98	84							
21-	CHEXA2	111	1000	83	97	95	81	84	98	&GR11
22-	&GR11	96	82							
23-	CHEXA2	113	1000	79	95	93	77	80	96	&GR13
24-	&GR13	94	78							
25-	CHEXA2	114	1000	77	93	91	75	78	94	&GR14
26-	&GR14	92	76							
27-	CHEXA2	115	1000	75	91	89	73	76	92	&GR15
28-	&GR15	90	74							
29-	CHEXA2	117	1000	71	89	87	69	72	90	&GR17
30-	&GR17	88	70							
31-	CHEXA2	118	1000	99	117	101	97	100	118	&GR18
32-	&GR18	102	98							
33-	CHEXA2	123	1000	101	115	113	103	102	116	&GR23
34-	&GR23	114	104							
35-	CHEXA2	124	1000	103	113	111	93	104	114	&GR24
36-	&GR24	112	94							
37-	CHEXA2	125	1000	93	111	109	91	94	112	&GR25
38-	&GR25	110	92							
39-	CHEXA2	126	1000	91	109	107	89	92	110	&GR26
40-	&GR26	108	90							
41-	CHEXA2	127	1000	89	107	105	87	90	108	&GR27
42-	&GR27	106	88							
43-	CHEXA2	128	1000	115	117	131	129	116	118	&GR28
44-	&GR28	132	130							
45-	CHEXA2	129	1000	113	115	129	127	114	116	&GR29
46-	&GR29	130	128							
47-	CHEXA2	130	1000	111	113	127	125	112	114	&GR30
48-	&GR30	128	126							
49-	CHEXA2	131	1000	109	111	125	123	110	112	&GR31
50-	&GR31	126	124							

TABLE 4-VIII (Cont)

TYPICAL BULK DATA DECK FOR THE CLEAN
MOTOR MODEL FOR POSEIDON C-3 SS MOTOR

S O R T E D B U L K D A T A E C H O

CARD COUNT	. 1 ..	2 ..	3 ..	4 ..	5 ..	6 ..	7 ..	8 ..	9 ..	10 .
51-	CHEXA2	132	1000	107	109	123	121	108	110	&CH32
52-	&CH32	124	122							
53-	CHEXA2	133	1000	105	107	121	119	106	108	&CH33
54-	&CH33	122	120							
55-	CHEXA2	134	1000	127	129	143	141	128	130	&CH34
56-	&CH34	144	142							
57-	CHEXA2	135	1000	125	127	141	139	126	128	&CH35
58-	&CH35	142	140							
59-	CHEXA2	136	1000	123	125	139	137	124	126	&CH36
60-	&CH36	140	138							
61-	CHEXA2	137	1000	121	123	137	135	122	124	&CH37
62-	&CH37	138	136							
63-	CHEXA2	138	1000	119	121	135	133	120	122	&CH38
64-	&CH38	136	134							
65-	CHEXA2	139	1000	141	143	155	153	142	144	&CH39
66-	&CH39	156	154							
67-	CHEXA2	140	1000	139	[illegible]	153	151	140	142	&CH40
68-	&CH40	154	[illegible]							
69-	CHEXA2	141	1000	137	139	151	149	138	140	&CH41
70-	&CH41	152	150							
71-	CHEXA2	142	1000	135	137	149	147	136	138	&CH42
72-	&CH42	150	148							
73-	CHEXA2	143	1000	133	135	147	145	134	136	&CH43
74-	&CH43	148	146							
75-	CHEXA2	144	1000	153	155	167	165	154	156	&CH44
76-	&CH44	168	166							
77-	CHEXA2	145	1000	151	153	165	163	152	154	&CH45
78-	&CH45	166	164							
79-	CHEXA2	146	1000	149	151	163	161	150	152	&CH46
80-	&CH46	164	162							
81-	CHEXA2	147	1000	147	149	161	159	148	150	&CH47
82-	&CH47	162	160							
83-	CHEXA2	148	1000	145	147	159	157	146	148	&CH48
84-	&CH48	160	158							
85-	CHEXA2	149	1000	165	167	181	179	166	168	&CH49
86-	&CH49	182	180							
87-	CHEXA2	150	1000	163	165	179	177	164	166	&CH50
88-	&CH50	180	178							
89-	CHEXA2	151	1000	161	163	177	175	162	164	&CH51
90-	&CH51	178	176							
91-	CHEXA2	152	1000	159	161	175	173	160	162	&CH52
92-	&CH52	176	174							
93-	CHEXA2	153	1000	157	159	173	171	158	160	&CH53
94-	&CH53	174	172							
95-	CHEXA2	155	1000	179	183	197	195	180	184	&CH55
96-	&CH55	198	196							
97-	CHEXA2	157	1000	175	177	195	193	176	178	&CH57
98-	&CH57	196	194							
99-	CHEXA2	158	1000	173	175	193	191	174	176	&CH58
100-	&CH58	194	192							

TABLE 4-VIII (Cont)

TYPICAL BULK DATA DECK FOR THE CLEAN MOTOR MODEL FOR POSEIDON C-3 SS MOTOR

S O R T E D B U L K D A T A E C H O

CARD COUNT	. 1 ..	2 ..	3 ..	4 ..	5 ..	6 ..	7 ..	8 ..	9 ..	10 .
101-	CHEXA2	160	1000	171	173	189	187	172	174	&CH60
102-	&CH60	190	188							
103-	CHEXA2	161	1000	195	197	211	209	196	198	&CH61
104-	&CH61	212	210							
105-	CHEXA2	162	1000	193	195	209	207	194	196	&CH62
106-	&CH62	210	208							
107-	CHEXA2	163	1000	191	193	207	205	192	194	&CH63
108-	&CH63	208	206							
109-	CHEXA2	164	1000	189	191	205	203	190	192	&CH64
110-	&CH64	206	204							
111-	CHEXA2	165	1000	187	189	203	201	188	190	&CH65
112-	&CH65	204	202							
113-	CHEXA2	166	604	21	17	15	19	22	18	&CH66
114-	&CH66	16	20							
115-	CHEXA2	167	603	25	21	19	23	26	22	&CH67
116-	&CH67	20	24							
117-	CHEXA2	168	602	29	25	23	27	30	26	&CH68
118-	&CH68	24	28							
119-	CHEXA2	169	604	251	255	253	249	252	256	&CH69
120-	&CH69	254	250							
121-	CHEXA2	170	603	247	251	249	243	248	252	&CH70
122-	&CH70	250	244							
123-	CHEXA2	171	602	245	247	243	241	246	248	&CH71
124-	&CH71	244	242							
125-	CHEXA2	173	6	269	267	265	261	270	268	&CH73
126-	&CH73	266	262							
127-	CHEXA2	174	2	275	277	269	273	276	278	&CH74
128-	&CH74	270	274							
129-	CHEXA2	175	7	279	281	277	275	280	282	&CH75
130-	&CH75	278	276							
131-	CHEXA2	176	7	277	281	285	283	278	282	&CH76
132-	&CH76	286	284							
133-	CORD2C	1	0	.0	.0	.0	.0	.0	1.0	222
134-	&222	1.0	0.0	0.0						
135-	CQUAD1	1	1	2	1	3	4			
136-	CQUAD1	2	2	4	3	5	6			
137-	CQUAD1	3	3	6	5	9	10			
138-	CQUAD1	4	4	7	8	10	9			
139-	CQUAD1	5	5	9	10	12	11			
140-	CQUAD1	6	6	11	12	14	13			
141-	CQUAD1	7	7	13	14	16	15			
142-	CQUAD1	8	8	15	16	20	19			
143-	CQUAD1	9	9	19	20	24	23			
144-	CQUAD1	10	10	23	24	28	27			
145-	CQUAD1	11	101	17	18	22	21	90.0		
146-	CQUAD1	12	102	21	22	26	25	90.0		
147-	CQUAD1	13	103	25	26	30	29	90.0		
148-	CQUAD1	14	104	29	30	32	31	90.0		
149-	CQUAD1	15	105	31	32	34	33	90.0		
150-	CQUAD1	17	107	35	36	38	37	90.0		

TABLE 4-VIII (Cont)

TYPICAL BULK DATA DECK FOR THE CLEAN
MOTOR MODEL FOR POSEIDON C-3 SS MOTOR

FULL MOTOR MODEL *** FIRST LONG. MODE / ADV. BURN SEPTEMBER 14, 1974 NASTRAN 12/ 1/73 PAGE 51

S O R T E D B U L K D A T A E C H O

CARD COUNT	. 1 ..	2 ..	3 ..	4 ..	5 ..	6 ..	7 ..	8 ..	9 ..	10 .
151-	CQUAD1	18	108	37	38	40	39	90.0		
152-	CQUAD1	20	110	41	42	44	43	90.0		
153-	CQUAD1	21	111	43	44	46	45	90.0		
154-	CQUAD1	22	112	45	46	48	47	90.0		
155-	CQUAD1	23	113	47	48	50	49	90.0		
156-	CQUAD1	24	114	49	50	56	55	90.0		
157-	CQUAD1	25	115	51	52	54	53	90.0		
158-	CQUAD1	26	116	53	54	56	55	90.0		
159-	CQUAD1	27	117	55	56	70	69	90.0		
160-	CQUAD1	28	118	69	70	88	87	90.0		
161-	CQUAD1	29	118	87	88	106	105	90.0		
162-	CQUAD1	30	118	105	106	120	119	90.0		
163-	CQUAD1	31	118	119	120	134	133	90.0		
164-	CQUAD1	32	118	133	134	146	145	90.0		
165-	CQUAD1	33	118	145	146	158	157	90.0		
166-	CQUAD1	34	118	157	158	170	169	90.0		
167-	CQUAD1	35	118	169	170	186	185	90.0		
168-	CQUAD1	36	119	185	186	200	199	90.0		
169-	CQUAD1	37	120	199	200	216	215	90.0		
170-	CQUAD1	38	120	215	216	218	217	90.0		
171-	CQUAD1	39	121	214	213	199	200	90.0		
172-	CQUAD1	40	122	220	219	213	214	90.0		
173-	CQUAD1	41	123	222	221	219	220	90.0		
174-	CQUAD1	42	124	224	223	221	222	90.0		
175-	CQUAD1	43	125	226	225	223	224	90.0		
176-	CQUAD1	44	126	228	227	225	226	90.0		
177-	CQUAD1	45	127	230	229	227	228	90.0		
178-	CQUAD1	46	128	232	231	229	230	90.0		
179-	CQUAD1	47	129	234	233	231	232	90.0		
180-	CQUAD1	48	130	236	235	233	234	90.0		
181-	CQUAD1	49	131	238	237	235	236	90.0		
182-	CQUAD1	50	132	240	239	237	238	90.0		
183-	CQUAD1	51	133	242	241	239	240	90.0		
184-	CQUAD1	52	134	244	243	241	242	90.0		
185-	CQUAD1	53	135	250	249	243	244	90.0		
186-	CQUAD1	54	136	254	253	249	250	90.0		
187-	CQUAD1	55	137	248	247	245	246			
188-	CQUAD1	56	138	252	251	247	248			
189-	CQUAD1	57	139	256	255	251	252			
190-	CQUAD1	58	140	260	259	257	258			
191-	CQUAD1	59	141	262	261	259	260			
192-	CQUAD1	60	142	268	267	269	270			
193-	CQUAD1	61	143	278	277	267	268			
194-	CQUAD1	62	144	284	283	277	278			
195-	CQUAD1	63	145	272	271	273	274			
196-	CQUAD1	64	146	290	289	287	288			
197-	CQUAD1	65	147	292	291	289	290			
198-	CQUAD1	66	148	298	297	291	292			
199-	CQUAD1	67	149	292	291	293	294			
200-	CQUAD1	68	149	296	295	293	294			

TABLE 4-VIII (Cont)

TYPICAL BULK DATA DECK FOR THE CLEAN
MOTOR MODEL FOR POSEIDON C-3 SS MOTOR

S O R T E D B U L K D A T A E C H O

CARD COUNT	. 1 ..	2 ..	3 ..	4 ..	5 ..	6 ..	7 ..	8 ..	9 ..	10 .
201-	COQUAD1	69	149	298	297	295	296			
202-	COQUAD1	70	150	300	299	297	298			
203-	COQUAD1	201	201	36	35	33	34	90.0		
204-	COQUAD1	202	202	42	41	39	40	90.0		
205-	CWEDGE	103	1000	64	80	78	63	79	77	
206-	CWEDGE	106	1000	59	73	57	60	74	58	
207-	CWEDGE	107	1000	57	73	71	58	74	72	
208-	CWEDGE	108	1000	57	71	55	58	72	56	
209-	CWEDGE	109	1000	55	71	69	56	72	70	
210-	CWEDGE	112	1000	81	95	79	82	96	80	
211-	CWEDGE	116	1000	73	89	71	74	90	72	
212-	CWEDGE	119	1000	97	101	95	98	102	96	
213-	CWEDGE	120	1000	95	101	103	96	102	104	
214-	CWEDGE	121	1000	95	103	93	96	104	94	
215-	CWEDGE	122	1000	101	117	115	102	118	116	
216-	CWEDGE	154	1000	179	181	183	180	182	184	
217-	CWEDGE	156	1000	177	179	195	178	180	196	
218-	CWEDGE	159	1000	173	191	189	174	192	190	
219-	CWEDGE	172	2	265	263	261	266	264	262	
220-	CWEDGE	177	5	283	285	287	284	286	288	
221-	CYJOIN	1	C	1	3	5	7	9	11	&CY1
222-	&CY1	13	15	17	19	21	23	25	27	&CY2
223-	&CY2	29	31	33	35	37	39	41	43	&CY3
224-	&CY3	45	47	49	51	53	55	57	59	&CY4
225-	&CY4	61	63	65	67	69	71	73	75	&CY5
226-	&CY5	77	79	81	83	87	89	91	93	&CY6
227-	&CY6	95	101	103	105	107	109	111	113	&CY7
228-	&CY7	115	119	121	123	125	127	129	133	&CY8
229-	&CY8	135	137	139	141	143	145	147	149	&CY9
230-	&CY9	151	153	155	157	159	161	163	165	&CY10
231-	&CY10	167	169	171	173	175	177	179	181	&CY11
232-	&CY11	183	185	187	189	191	193	195	197	&CY12
233-	&CY12	199	201	203	205	207	209	211	213	&CY13
234-	&CY13	215	217	219	221	223	225	227	229	&CY14
235-	&CY14	231	233	235	237	239	241	243	245	&CY15
236-	&CY15	247	249	251	253	255	257	259	261	&CY16
237-	&CY16	263	265	267	269	271	273	275	277	&CY17
238-	&CY17	279	281	283	285	287	289	291	293	&CY18
239-	&CY18	295	297	299						
240-	CYJOIN	2	C	2	4	6	8	10	12	&CY20
241-	&CY20	14	16	18	20	22	24	26	28	&CY21
242-	&CY21	30	32	34	36	38	40	42	44	&CY22
243-	&CY22	46	48	50	52	54	56	58	60	&CY23
244-	&CY23	62	64	66	68	70	72	74	76	&CY24
245-	&CY24	78	80	82	84	88	90	92	94	&CY25
246-	&CY25	96	102	104	106	108	110	112	114	&CY26
247-	&CY26	116	120	122	124	126	128	130	134	&CY27
248-	&CY27	136	138	140	142	144	146	148	150	&CY28
249-	&CY28	152	154	156	158	160	162	164	166	&CY29
250-	&CY29	168	170	172	174	176	178	180	182	&CY30

TABLE 4-VIII (Cont)

TYPICAL BULK DATA DECK FOR THE CLEAN
MOTOR MODEL FOR POSEIDON C-3 SS MOTOR

S O R T E D B U L K D A T A E C H O

CARD COUNT	. 1	.. 2	.. 3	.. 4	.. 5	.. 6	.. 7	.. 8	.. 9	.. 10 .
251-	&CY30	184	186	188	190	192	194	196	198	&CY31
252-	&CY31	200	202	204	206	208	210	212	214	&CY32
253-	&CY32	216	218	220	222	224	226	228	230	&CY33
254-	&CY33	232	234	236	238	240	242	244	246	&CY34
255-	&CY34	248	250	252	254	256	258	260	262	&CY35
256-	&CY35	264	266	268	270	272	274	276	278	&CY36
257-	&CY36	280	282	284	286	288	290	292	294	&CY37
258-	&CY37	296	298	300	86	98	100	118	132	
259-	DAREA	100	1	1	.0158	1	2	.0021		
260-	DAREA	100	1	3	.0339					
261-	DAREA	100	2	1	.0158	2	2	-0.0021		
262-	DAREA	100	2	3	.0339					
263-	DAREA	100	3	1	.6637	3	2	.0874		
264-	DAREA	100	3	3	.0651					
265-	DAREA	100	4	1	.6637	4	2	-0.0874		
266-	DAREA	100	4	3	.0651					
267-	DAREA	100	5	1	1.3410	5	2	.1765		
268-	DAREA	100	5	3	.0					
269-	DAREA	100	6	1	1.3410	6	2	-0.1765		
270-	DAREA	100	6	3	.0					
271-	DAREA	100	9	1	.8369	9	2	.1102		
272-	DAREA	100	9	3	1.0245					
273-	DAREA	100	10	1	.8369	10	2	-0.1102		
274-	DAREA	100	10	3	1.0245					
275-	DAREA	100	11	1	1.5669	11	2	.2063		
276-	DAREA	100	11	3	3.3625					
277-	DAREA	100	12	1	1.5669	12	2	-0.2063		
278-	DAREA	100	12	3	3.3625					
279-	DAREA	100	13	1	1.5955	13	2	.2101		
280-	DAREA	100	13	3	3.7788					
281-	DAREA	100	14	1	1.5955	14	2	-0.2101		
282-	DAREA	100	14	3	3.7788					
283-	DAREA	100	15	1	.0	15	2	.0		
284-	DAREA	100	15	3	1.7462					
285-	DAREA	100	16	1	.0	16	2	.0		
286-	DAREA	100	16	3	1.7462					
287-	DAREA	100	67	1	-0.1339	67	2	-0.0176		
288-	DAREA	100	67	3	.0					
289-	DAREA	100	68	1	-0.1339	68	2	.0176		
290-	DAREA	100	68	3	.0					
291-	DAREA	100	83	1	-2.2591	83	2	.0		
292-	DAREA	100	83	3	-1.4376					
293-	DAREA	100	84	1	-2.2591	84	2	.2974		
294-	DAREA	100	84	3	-1.4376					
295-	DAREA	100	85	1	-4.5926	85	2	-12.5291		
296-	DAREA	100	85	3	-1.3349					
297-	DAREA	100	86	1	-4.5926	86	2	.6046		
298-	DAREA	100	86	3	-1.3349					
299-	DAREA	100	97	1	.0	97	2	-43.3853		
300-	DAREA	100	97	3	.0					

TABLE 4-VIII (Cont)

TYPICAL BULK DATA DECK FOR THE CLEAN
MOTOR MODEL FOR POSEIDON C-3 SS MOTOR

S O R T E D   B U L K   D A T A   E C H O

CARD COUNT	. 1 ..	2 ..	3 ..	4 ..	5 ..	6 ..	7 ..	8 ..	9 ..	10 .
301-	DAREA	100	99	1	-6.0243	99	2	-21.8685		
302-	DAREA	100	99	3	.0					
303-	DAREA	100	100	1	-6.0243	100	2	.7931		
304-	DAREA	100	100	3	.0					
305-	DAREA	100	117	1	-4.6908	117	2	-15.2540		
306-	DAREA	100	117	3	.0					
307-	DAREA	100	118	1	-4.6908	118	2	.6176		
308-	DAREA	100	118	3	.0					
309-	DAREA	100	129	1	-2.1289	129	2	.0		
310-	DAREA	100	129	3	.6690					
311-	DAREA	100	130	1	-2.1289	130	2	.2803		
312-	DAREA	100	130	3	.6690					
313-	DAREA	100	131	1	-1.5842	131	2	-3.9042		
314-	DAREA	100	131	3	.6376					
315-	DAREA	100	132	1	-1.5842	132	2	.2086		
316-	DAREA	100	132	3	.6376					
317-	DAREA	100	143	1	-2.1093	143	2	-0.2777		
318-	DAREA	100	143	3	-0.0186					
319-	DAREA	100	144	1	-2.1093	144	2	.2777		
320-	DAREA	100	144	3	-0.0186					
321-	DAREA	100	155	1	1.3410	155	2	.1765		
322-	DAREA	100	155	3	.0					
323-	DAREA	100	156	1	1.3410	156	2	-0.1765		
324-	DAREA	100	156	3	.0					
325-	DAREA	100	167	1	3.0342	167	2	.3995		
326-	DAREA	100	167	3	.0					
327-	DAREA	100	168	1	3.0342	168	2	-0.3995		
328-	DAREA	100	168	3	.0					
329-	DAREA	100	181	1	4.2018	181	2	.5532		
330-	DAREA	100	181	3	-1.4772					
331-	DAREA	100	182	1	4.2018	182	2	-0.5532		
332-	DAREA	100	182	3	-1.4772					
333-	DAREA	100	183	1	6.8715	183	2	.9047		
334-	DAREA	100	183	3	-2.9906					
335-	DAREA	100	184	1	6.8715	184	2	-0.9047		
336-	DAREA	100	184	3	-2.9906					
337-	DAREA	100	197	1	10.0310	197	2	1.3206		
338-	DAREA	100	197	3	-2.5936					
339-	DAREA	100	198	1	10.0310	198	2	-1.3206		
340-	DAREA	100	198	3	-2.5936					
341-	DAREA	100	211	1	6.1970	211	2	.8159		
342-	DAREA	100	211	3	-1.1737					
343-	DAREA	100	212	1	6.1970	212	2	-0.8158		
344-	DAREA	100	212	3	-1.1737					
345-	DAREA	100	257	1	-7.0415	257	2	-0.9270		
346-	DAREA	100	257	3	4.7239					
347-	DAREA	100	258	1	-7.0415	258	2	.9270		
348-	DAREA	100	258	3	4.7239					
349-	DAREA	100	259	1	-7.1717	259	2	-0.9442		
350-	DAREA	100	259	3	4.3580					

TABLE 4-VIII (Cont)

TYPICAL BULK DATA DECK FOR THE CLEAN
MOTOR MODEL FOR POSEIDON C-3 SS MOTOR

S O R T E D B U L K D A T A E C H O

CARD COUNT	. 1 ..	2 ..	3 ..	4 ..	5 ..	6 ..	7 ..	8 ..	9 ..	10 .
351-	DAREA	100	260	1	-7.1717	260	2	.9442		
352-	DAREA	100	260	3	4.3580					
353-	DAREA	100	261	1	-2.7994	261	2	-0.3685		
354-	DAREA	100	261	3	.2693					
355-	DAREA	100	262	1	-2.7994	262	2	.3685		
356-	DAREA	100	262	3	.2693					
357-	DAREA	100	269	1	-1.9511	269	2	-0.2569		
358-	DAREA	100	269	3	-0.3089					
359-	DAREA	100	270	1	-1.9511	270	2	.2569		
360-	DAREA	100	270	3	-0.3089					
361-	DAREA	100	273	1	-0.9419	273	2	-0.1240		
362-	DAREA	100	273	3	.2839					
363-	DAREA	100	274	1	-0.9419	274	2	.1240		
364-	DAREA	100	274	3	.2839					
365-	DAREA	100	275	1	-2.3350	275	2	-0.3074		
366-	DAREA	100	275	3	1.3081					
367-	DAREA	100	276	1	-2.3350	276	2	.3074		
368-	DAREA	100	276	3	1.3081					
369-	DAREA	100	279	1	-0.6688	279	2	-0.0881		
370-	DAREA	100	279	3	1.2788					
371-	DAREA	100	280	1	-0.6688	280	2	.0880		
372-	DAREA	100	280	3	1.2788					
373-	DAREA	100	281	1	.7280	281	2	.0958		
374-	DAREA	100	281	3	.5707					
375-	DAREA	100	282	1	.7280	282	2	-0.0958		
376-	DAREA	100	282	3	.5707					
377-	DAREA	301	257	1	1.0					
378-	DAREA	302	257	2	1.0					
379-	DAREA	303	257	3	1.0					
380-	DAREA	304	257	4	1.0					
381-	DAREA	305	257	5	1.0					
382-	DAREA	306	257	6	1.0					
383-	DAREA	307	258	1	1.0					
384-	DAREA	308	258	2	1.0					
385-	DAREA	309	258	3	1.0					
386-	DAREA	310	258	4	1.0					
387-	DAREA	311	258	5	1.0					
388-	DAREA	312	258	6	1.0					
389-	DAREA	313	293	1	1.0					
390-	DAREA	314	293	2	1.0					
391-	DAREA	315	293	3	1.0					
392-	DMI	CP1R	0	2	1	1		1032	1	
393-	DMI	CP1R	1	1	1.0	25	1.0	49	1.0	&1R1
394-	&1R1	7	1.0	97	1.0	121	1.0	145	1.0	&1R2
395-	&1R2	169	1.0	193	1.0	217	1.0	241	1.0	&1R3
396-	&1R3	265	1.0	289	1.0	313	1.0	337	1.0	&1R4
397-	&1R4	361	1.0	385	1.0	409	1.0	433	1.0	&1R5
398-	&1R5	457	1.0	481	1.0	505	1.0	529	1.0	&1R6
399-	&1R6	553	1.0	577	1.0	601	1.0	625	1.0	&1R7
400-	&1R7	649	1.0	673	1.0	697	1.0	721	1.0	&1R8

TABLE 4-VIII (Cont)

TYP^^AL BULK DATA DECK FOR THE CLEAN
MOTOR MODEL FOR POSEIDON C-3 SS MOTOR

S O R T E D B U L K D A T A E C H O

CARD COUNT	. 1	.. 2	.. 3	.. 4	.. 5	.. 6	.. 7	.. 8	.. 9	.. 10 .
401-	&1R8	745	1.0	769	1.0	793	1.0	817	1.0	&1R9
402-	&1R9	841	1.0	865	1.0	889	1.0	913	1.0	&1RA
403-	&1RA	937	1.0	961	1.0	985	1.0			
404-	DMI	CP1RR	0	2	1	1		1032	1	
405-	DMI	CP1RR	1	1009	1.0					
406-	DMI	CP10	0	2	1	1		1032	1	
407-	DMI	CP10	1	19	1.0	43	1.0	67	1.0	&101
408-	&101	91	1.0	115	1.0	139	1.0	163	1.0	&102
409-	&102	187	1.0	211	1.0	235	1.0	259	1.0	&103
410-	&103	283	1.0	307	1.0	331	1.0	355	1.0	&104
411-	&104	379	1.0	403	1.0	427	1.0	451	1.0	&105
412-	&105	475	1.0	499	1.0	523	1.0	547	1.0	&106
413-	&106	571	1.0	595	1.0	619	1.0	643	1.0	&107
414-	&107	667	1.0	691	1.0	715	1.0	739	1.0	&108
415-	&108	763	1.0	787	1.0	811	1.0	835	1.0	&109
416-	&109	859	1.0	883	1.0	907	1.0	931	1.0	&10A
417-	&10A	955	1.0	979	1.0	1003	1.0			
418-	DMI	CP10R	0	2	1	1		1032	1	
419-	DMI	CP10R	1	1027	1.0					
420-	DMI	CP11	0	2	1	1		1032	1	
421-	DMI	CP11	1	21	1.0	45	1.0	69	1.0	&111
422-	&111	93	1.0	117	1.0	141	1.0	165	1.0	&112
423-	&112	189	1.0	213	1.0	237	1.0	261	1.0	&113
424-	&113	285	1.0	309	1.0	333	1.0	357	1.0	&114
425-	&114	381	1.0	405	1.0	429	1.0	453	1.0	&115
426-	&115	477	1.0	501	1.0	525	1.0	549	1.0	&116
427-	&116	573	1.0	597	1.0	621	1.0	645	1.0	&117
428-	&117	669	1.0	693	1.0	717	1.0	741	1.0	&118
429-	&118	765	1.0	789	1.0	813	1.0	837	1.0	&119
430-	&119	861	1.0	885	1.0	909	1.0	933	1.0	&11A
431-	&11A	957	1.0	981	1.0	1005	1.0			
432-	DMI	CP11R	0	2	1	1		1032	1	
433-	DMI	CP11R	1	1029	1.0					
434-	DMI	CP12	0	2	1	1		1032	1	
435-	DMI	CP12	1	23	1.0	47	1.0	71	1.0	&121
436-	&121	95	1.0	119	1.0	143	1.0	167	1.0	&122
437-	&122	191	1.0	215	1.0	239	1.0	263	1.0	&123
438-	&123	287	1.0	311	1.0	335	1.0	359	1.0	&124
439-	&124	383	1.0	407	1.0	431	1.0	455	1.0	&125
440-	&125	479	1.0	503	1.0	527	1.0	551	1.0	&126
441-	&126	575	1.0	599	1.0	623	1.0	647	1.0	&127
442-	&127	671	1.0	695	1.0	719	1.0	743	1.0	&128
443-	&128	767	1.0	791	1.0	815	1.0	839	1.0	&129
444-	&129	863	1.0	887	1.0	911	1.0	935	1.0	&12A
445-	&12A	959	1.0	983	1.0	1007	1.0			
446-	DMI	CP12R	0	2	1	1		1032	1	
447-	DMI	CP12R	1	1031	1.0					
448-	DMI	CP5R	0	2	1	1		1032	1	

TABLE 4-VIII (Cont)

TYPICAL BULK DATA DECK FOR THE CLEAN MOTOR MODEL FOR POSEIDON C-3 SS MOTOR

S O R T E D   B U L K   D A T A   E C H O

CARD COUNT	. 1	.. 2	.. 3	.. 4	.. 5	.. 6	.. 7	.. 8	.. 9	.. 10 .
451-	&5R2	177	1.0	201	1.0	225	1.0	249	1.0	&5R3
452-	&5R3	273	1.0	297	1.0	321	1.0	345	1.0	&5R4
453-	&5R4	369	1.0	393	1.0	417	1.0	441	1.0	&5R5
454-	&5R5	465	1.0	489	1.0	513	1.0	537	1.0	&5R6
455-	&5R6	561	1.0	585	1.0	609	1.0	633	1.0	&5R7
456-	&5R7	657	1.0	681	1.0	705	1.0	729	1.0	&5R8
457-	&5R8	753	1.0	777	1.0	801	1.0	825	1.0	&5R9
458-	&5R9	849	1.0	873	1.0	897	1.0	921	1.0	&5RA
459-	&5RA	945	1.0	969	1.0	993	1.0			
460-	DMI	CP5RR	0	2	1	1		1032	1	
461-	DMI	CP5RR	1	1017	1.0					
462-	DMI	CP7R	0	2	1	1		1032	1	
463-	DMI	CP7R	1	13	1.0	37	1.0	61	1.0	&7R1
464-	&7R1	85	1.0	109	1.0	133	1.0	157	1.0	&7R2
465-	&7R2	181	1.0	205	1.0	229	1.0	253	1.0	&7R3
466-	&7R3	277	1.0	301	1.0	325	1.0	349	1.0	&7R4
467-	&7R4	373	1.0	397	1.0	421	1.0	445	1.0	&7R5
468-	&7R5	469	1.0	493	1.0	517	1.0	541	1.0	&7R6
469-	&7R6	565	1.0	589	1.0	613	1.0	637	1.0	&7R7
470-	&7R7	661	1.0	685	1.0	709	1.0	733	1.0	&7R8
471-	&7R8	757	1.0	781	1.0	805	1.0	829	1.0	&7R9
472-	&7R9	853	1.0	877	1.0	901	1.0	925	1.0	&7RA
473-	&7RA	949	1.0	973	1.0	997	1.0			
474-	DMI	CP7RR	0	2	1	1		1032	1	
475-	DMI	CP7RR	1	1021	1.0					
476-	DMI	CP9R	0	2	1	1		1032	1	
477-	DMI	CP9R	1	17	1.0	41	1.0	65	1.0	&9R1
478-	&9R1	89	1.0	113	1.0	137	1.0	161	1.0	&9R2
479-	&9R2	185	1.0	209	1.0	233	1.0	257	1.0	&9R3
480-	&9R3	281	1.0	305	1.0	329	1.0	353	1.0	&9R4
481-	&9R4	377	1.0	401	1.0	425	1.0	449	1.0	&9R5
482-	&9R5	473	1.0	497	1.0	521	1.0	545	1.0	&9R6
483-	&9R6	569	1.0	593	1.0	617	1.0	641	1.0	&9R7
484-	&9R7	665	1.0	689	1.0	713	1.0	737	1.0	&9R8
485-	&9R8	761	1.0	785	1.0	809	1.0	833	1.0	&9R9
486-	&9R9	857	1.0	881	1.0	905	1.0	929	1.0	&9RA
487-	&9RA	953	1.0	977	1.0	1001	1.0			
488-	DMI	CP9RR	0	2	1	1		1032	1	
489-	DMI	CP9RR	1	1025	1.0					
490-	DMI	RP1	0	2	1	1		1176	1	
491-	DMI	RP1	1	972	1.0	981	1.0	982	1.0	&RP1
492-	&RP1	1131	1.0	1132	1.0	1132	1.0			
493-	DMI	RP12	0	2	1	1		12	1	
494-	DMI	RP12	1	7	1.0	1.0	1.0	1.0	1.0	&RP11
495-	&RP11	1.0								
496-	DMI	RP13	0	2	1	1		18	1	
497-	DMI	RP13	1	13	1.0	1.0	1.0	1.0	1.0	&RP12
498-	&RP12	1.0								
499-	DMI	RP14	0	2	1	1		24	1	
500-	DMI	RP14	1	19	1.0	1.0	1.0	1.0	1.0	&RP13

TABLE 4-VIII (Cont)

TYPICAL BULK DATA DECK FOR THE CLEAN
MOTOR MODEL FOR POSEIDON C-3 SS MOTOR

S O R T E D B U L K D A T A E C H O

CARD COUNT	. 1 ..	2 ..	3 ..	4 ..	5 ..	6 ..	7 ..	8 ..	9 ..	10 .
501-	&RP13	1.0								
502-	DMI	RP15	0	2	1	1		30	1	
503-	DMI	RP15	1	25	1.0	1.0	1.0	1.0	1.0	&RP14
504-	&RP14	1.0								
505-	DMI	RP16	0	2	1	1		36	1	
506-	DMI	RP16	1	31	1.0	1.0	1.0	1.0	1.0	&RP15
507-	&RP15	1.0								
508-	DMI	RP17	0	2	1	1		42	1	
509-	DMI	RP17	1	37	1.0	1.0	1.0	1.0	1.0	&RP6
510-	&RP6	1.0								
511-	DMI	RP2	0	2	1	1		1176	1	
512-	DMI	RP2	1	977	1.0	986	1.0	987	1.0	&RP2
513-	&RP2	988	1.0	989	1.0	990	1.0			
514-	DMI	RP3	0	2	1	1		1176	1	
515-	DMI	RP3	1	972	1.0	981	1.0	982	1.0	&RP3
516-	&RP3	983	1.0	984	1.0	985	1.0			
517-	FREQ	1	281.0							
518-	GRID	1	1	.05	.0	21.67	1			
519-	GRID	2	1	.05	15.0	21.67	1			
520-	GRID	3	1	1.75	.0	20.88	1			
521-	GRID	4	1	1.75	15.0	20.88	1			
522-	GRID	5	1	1.75	.0	12.00	1			
523-	GRID	6	1	1.75	15.0	12.00	1			
524-	GRID	7	1	.05	.0	4.90	1			
525-	GRID	8	1	.05	15.0	4.90	1			
526-	GRID	9	1	1.75	.0	4.90	1			
527-	GRID	10	1	1.75	15.0	4.90	1			
528-	GRID	11	1	6.50	.0	4.30	1			
529-	GRID	12	1	6.50	15.0	4.30	1			
530-	GRID	13	1	10.20	.0	1.55	1			
531-	GRID	14	1	10.20	15.0	1.55	1			
532-	GRID	15	1	12.50	.0	1.55	1			
533-	GRID	16	1	12.50	15.0	1.55	1			
534-	GRID	17	1	12.50	.0	.85	1			
535-	GRID	18	1	12.50	15.0	.85	1			
536-	GRID	19	1	13.38	.0	1.60	1			
537-	GRID	20	1	13.38	15.0	1.60	1			
538-	GRID	21	1	13.38	.0	.85	1			
539-	GRID	22	1	13.38	15.0	.85	1			
540-	GRID	23	1	14.00	.0	1.65	1			
541-	GRID	24	1	14.00	15.0	1.65	1			
542-	GRID	25	1	14.00	.0	1.00	1			
543-	GRID	26	1	14.00	15.0	1.00	1			
544-	GRID	27	1	15.30	.0	1.75	1			
545-	GRID	28	1	15.30	15.0	1.75	1			
546-	GRID	29	1	16.11	.0	1.45	1			
547-	GRID	30	1	16.11	15.0	1.45	1			
548-	GRID	31	1	17.87	.0	1.95	1			
	[illegible]	[illegible]	1	17.87	15.0	1.95	1			

TABLE 4-VIII (Cont)

TYPICAL BULK DATA DECK FOR THE CLEAN
MOTOR MODEL FOR POSEIDON C-3 SS MOTOR

S O R T E D B U L K D A T A E C H O

CARD COUNT	. 1 ..	2 ..	3 ..	4 ..	5 ..	6 ..	7 ..	8 ..	9 ..	10 .
551-	GRID	34	1	20.80	15.0	3.05	1			
552-	GRID	35	1	23.66	.0	4.45	1			
553-	GRID	36	1	23.66	15.0	4.45	1			
554-	GRID	37	1	26.35	.0	6.18	1			
555-	GRID	38	1	26.35	15.0	6.18	1			
556-	GRID	39	1	29.58	.0	8.90	1			
557-	GRID	40	1	29.58	15.0	8.90	1			
558-	GRID	41	1	30.95	.0	10.29	1			
559-	GRID	42	1	30.95	15.0	10.29	1			
560-	GRID	43	1	32.95	.0	13.00	1			
561-	GRID	44	1	32.95	15.0	13.00	1			
562-	GRID	45	1	34.85	.0	16.80	1			
563-	GRID	46	1	34.85	15.0	16.80	1			
564-	GRID	47	1	35.95	.0	19.75	1			
565-	GRID	48	1	35.95	15.0	19.75	1			
566-	GRID	49	1	36.60	.0	21.95	1			
567-	GRID	50	1	36.60	15.0	21.95	1			
568-	GRID	51	1	36.875	.0	13.14	1			
569-	GRID	52	1	36.875	15.0	13.14	1			
570-	GRID	53	1	36.875	.0	18.32	1			
571-	GRID	54	1	36.875	15.0	18.32	1			
572-	GRID	55	1	36.875	.0	23.50	1			
573-	GRID	56	1	36.875	15.0	23.50	1			
574-	GRID	57	1	34.60	.0	17.80	1			
575-	GRID	58	1	34.60	15.0	17.80	1			
576-	GRID	59	1	30.29	.0	11.1	1			
577-	GRID	60	1	30.29	15.0	11.1	1			
578-	GRID	61	1	26.35	.0	6.65	1			
579-	GRID	62	1	26.35	15.0	6.65	1			
580-	GRID	63	1	20.80	.0	3.40	1			
581-	GRID	64	1	20.80	15.0	3.40	1			
582-	GRID	65	1	16.11	.0	3.0	1			
583-	GRID	66	1	16.11	15.0	3.0	1			
584-	GRID	67	1	11.5	.0	3.0	1			
585-	GRID	68	1	11.5	15.0	3.0	1			
586-	GRID	69	1	36.875	.0	26.30	1			
587-	GRID	70	1	36.875	15.0	26.30	1			
588-	GRID	71	1	34.60	.0	23.30	1			
589-	GRID	72	1	34.60	15.0	23.30	1			
590-	GRID	73	1	31.20	.0	18.30	1			
591-	GRID	74	1	31.20	15.0	18.30	1			
592-	GRID	75	1	26.50	.0	12.90	1			
593-	GRID	76	1	26.50	15.0	12.90	1			
594-	GRID	77	1	20.90	.0	8.80	1			
595-	GRID	78	1	20.90	15.0	8.80	1			
596-	GRID	79	1	19.75	.0	7.0	1			
597-	GRID	80	1	19.75	15.0	7.0	1			
598-	GRID	81	1	16.75	.0	3.80	1			
599-	GRID	82	1	16.75	15.0	3.80	1			
600-	GRID	83	1	11.5	.0	3.20	1			

TABLE 4-VIII (Cont)

TYPICAL BULK DATA DECK FOR THE CLEAN
MOTOR MODEL FOR POSEIDON C-3 SS MOTOR

S O R T E D B U L K D A T A E C H O

CARD COUNT	1	2	3	4	5	6	7	8	9	10
601-	GRID	84	1	11.50	15.0	3.20	1			
602-	GRID	85	1	9.20	.0	6.60	1			
603-	GRID	86	1	9.20	15.0	6.60	1			
604-	GRID	87	1	36.875	.0	30.2	1			
605-	GRID	88	1	36.875	15.0	30.2	1			
606-	GRID	89	1	31.30	.0	25.28	1			
607-	GRID	90	1	31.30	15.0	25.28	1			
608-	GRID	91	1	26.64	.0	20.4	1			
609-	GRID	92	1	26.64	15.0	20.4	1			
610-	GRID	93	1	21.08	.0	16.8	1			
611-	GRID	94	1	21.08	15.0	16.8	1			
612-	GRID	95	1	17.55	.0	10.9	1			
613-	GRID	96	1	17.55	15.0	10.9	1			
614-	GRID	97	1	13.00	.0	11.40	1			
615-	GRID	98	1	13.00	15.0	11.40	1			
616-	GRID	99	1	9.20	.0	11.6	1			
617-	GRID	100	1	9.20	15.0	11.6	1			
618-	GRID	101	1	14.15	.0	16.05	1			
619-	GRID	102	1	14.15	15.0	16.05	1			
620-	GRID	103	1	16.11	.0	16.0	1			
621-	GRID	104	1	16.11	15.0	16.0	1			
622-	GRID	105	1	36.875	.0	33.8	1			
623-	GRID	106	1	36.875	15.0	33.8	1			
624-	GRID	107	1	31.40	.0	30.6	1			
625-	GRID	108	1	31.40	15.0	30.6	1			
626-	GRID	109	1	26.80	.0	26.34	1			
627-	GRID	110	1	26.80	15.0	26.34	1			
628-	GRID	111	1	21.20	.0	24.46	1			
629-	GRID	112	1	21.20	15.0	24.46	1			
630-	GRID	113	1	16.11	.0	22.80	1			
631-	GRID	114	1	16.11	15.0	22.80	1			
632-	GRID	115	1	12.20	.0	21.40	1			
633-	GRID	116	1	12.20	15.0	21.40	1			
634-	GRID	117	1	9.20	.0	20.4	1			
635-	GRID	118	1	9.20	15.0	20.4	1			
636-	GRID	119	1	36.875	.0	37.8	1			
637-	GRID	120	1	36.875	15.0	37.8	1			
638-	GRID	121	1	31.50	.0	35.4	1			
639-	GRID	122	1	31.50	15.0	35.4	1			
640-	GRID	123	1	26.90	.0	33.50	1			
641-	GRID	124	1	26.90	15.0	33.50	1			
642-	GRID	125	1	21.36	.0	30.89	1			
643-	GRID	126	1	21.36	15.0	30.89	1			
644-	GRID	127	1	16.11	.0	29.40	1			
645-	GRID	128	1	16.11	15.0	29.40	1			
646-	GRID	129	1	11.55	.0	26.00	1			
647-	GRID	130	1	11.55	15.0	26.00	1			
648-	GRID	131	1	9.20	.0	24.90	1			
649-	GRID	132	1	9.20	15.0	24.90	1			
650-	GRID	133	1	36.875	.0	41.70	1			

TABLE 4-VIII (Cont)

TYPICAL BULK DATA DECK FOR THE CLEAN
MOTOR MODEL FOR POSEIDON C-3 SS MOTOR

S O R T E D   B U L K   D A T A   E C H O

CARD COUNT	. 1 ..	2 ..	3 ..	4 ..	5 ..	6 ..	7 ..	8 ..	9 ..	10 .
651-	GRID	134	1	36.875	15.0	41.70	1			
652-	GRID	135	1	31.60	.0	39.90	1			
653-	GRID	136	1	31.60	15.0	39.90	1			
654-	GRID	137	1	27.00	.0	38.80	1			
655-	GRID	138	1	27.00	15.0	38.80	1			
656-	GRID	139	1	21.48	.0	37.32	1			
657-	GRID	140	1	21.48	15.0	37.32	1			
658-	GRID	141	1	16.11	.0	36.0	1			
659-	GRID	142	1	16.11	15.0	36.0	1			
660-	GRID	143	1	11.45	.0	35.7	1			
661-	GRID	144	1	11.45	15.0	35.7	1			
662-	GRID	145	1	36.875	.0	45.8	1			
663-	GRID	146	1	36.875	15.0	45.8	1			
664-	GRID	147	1	31.60	.0	45.0	1			
665-	GRID	148	1	31.60	15.0	45.0	1			
666-	GRID	149	1	27.06	.0	44.4	1			
667-	GRID	150	1	27.06	15.0	44.4	1			
668-	GRID	151	1	21.60	.0	44.20	1			
669-	GRID	152	1	21.60	15.0	44.20	1			
670-	GRID	153	1	16.11	.0	44.00	1			
671-	GRID	154	1	16.11	15.0	44.00	1			
672-	GRID	155	1	11.45	.0	44.00	1			
673-	GRID	156	1	11.45	15.0	44.00	1			
674-	GRID	157	1	36.875	.0	49.80	1			
675-	GRID	158	1	36.875	15.0	49.80	1			
676-	GRID	159	1	31.80	.0	51.40	1			
677-	GRID	160	1	31.80	15.0	51.40	1			
678-	GRID	161	1	27.2	.0	52.70	1			
679-	GRID	162	1	27.2	15.0	52.70	1			
680-	GRID	163	1	21.70	.0	53.00	1			
681-	GRID	164	1	21.70	15.0	53.00	1			
682-	GRID	165	1	16.11	.0	53.00	1			
683-	GRID	166	1	16.11	15.0	53.00	1			
684-	GRID	167	1	11.45	.0	52.90	1			
685-	GRID	168	1	11.45	15.0	52.90	1			
686-	GRID	169	1	36.875	.0	53.20	1			
687-	GRID	170	1	36.875	15.0	53.20	1			
688-	GRID	171	1	36.775	.0	53.20	1			
689-	GRID	172	1	36.775	15.0	53.70	1			
690-	GRID	173	1	31.90	.0	57.80	1			
691-	GRID	174	1	31.90	15.0	57.80	1			
692-	GRID	175	1	27.34	.0	59.80	1			
693-	GRID	176	1	27.34	15.0	59.80	1			
694-	GRID	177	1	21.80	.0	60.0	1			
695-	GRID	178	1	21.80	15.0	60.0	1			
696-	GRID	179	1	16.11	.0	60.0	1			
697-	GRID	180	1	16.11	15.0	60.0	1			
698-	GRID	181	1	11.45	.0	57.25	1			
699-	GRID	182	1	11.45	15.0	57.25	1			
700-	GRID	183	1	14.65	.0	63.35	1			

TABLE 4-VIII (Cont)

TYPICAL BULK DATA DECK FOR THE CLEAN
MOTOR MODEL FOR POSEIDON C-3 SS MOTOR

S O R T E D   B U L K   D A T A   E C H O

CARD COUNT	. 1 ..	2 ..	3 ..	4 ..	5 ..	6 ..	7 ..	8 ..	9 ..	10 .
701-	GRID	184	1	14.65	15.0	63.35	1			
702-	GRID	185	1	36.875	.0	55.0	1			
703-	GRID	186	1	36.875	15.0	55.0	1			
704-	GRID	187	1	36.775	.0	55.0	1			
705-	GRID	188	1	36.775	15.0	55.0	1			
706-	GRID	189	1	34.20	.0	59.40	1			
707-	GRID	190	1	34.20	15.0	59.40	1			
708-	GRID	191	1	32.00	.0	62.40	1			
709-	GRID	192	1	32.00	15.0	62.40	1			
710-	GRID	193	1	27.50	.0	65.90	1			
711-	GRID	194	1	27.50	15.0	65.90	1			
712-	GRID	195	1	22.00	.0	68.00	1			
713-	GRID	196	1	22.00	15.0	68.00	1			
714-	GRID	197	1	16.65	.0	68.85	1			
715-	GRID	198	1	16.65	15.0	68.85	1			
716-	GRID	199	1	36.875	.0	56.28	1			
717-	GRID	200	1	36.875	15.00	56.28	1			
718-	GRID	201	1	36.775	.0	56.28	1			
719-	GRID	202	1	36.775	15.00	56.28	1			
720-	GRID	203	1	35.60	.0	61.0	1			
721-	GRID	204	1	35.60	15.00	61.0	1			
722-	GRID	205	1	32.005	.0	69.0	1			
723-	GRID	206	1	32.005	15.00	69.0	1			
724-	GRID	207	1	27.580	.0	73.00	1			
725-	GRID	208	1	27.500	15.00	73.00	1			
726-	GRID	209	1	22.14	.0	75.00	1			
727-	GRID	210	1	22.14	15.0	75.00	1			
728-	GRID	211	1	17.90	.0	75.45	1			
729-	GRID	212	1	17.90	15.0	75.45	1			
730-	GRID	213	1	36.635	.0	57.73	1			
731-	GRID	214	1	36.635	15.0	57.73	1			
732-	GRID	215	1	36.875	.0	64.00	1			
733-	GRID	216	1	36.875	15.0	64.00	1			
734-	GRID	217	1	36.875	.0	70.92	1			
735-	GRID	218	1	36.875	15.0	70.92	1			
736-	GRID	219	1	36.025	.0	61.31	1			
737-	GRID	220	1	36.025	15.0	61.31	1			
738-	GRID	221	1	34.75	.0	64.873	1			
739-	GRID	222	1	34.75	15.0	64.873	1			
740-	GRID	223	1	33.87	.0	66.62	1			
741-	GRID	224	1	33.87	15.0	66.62	1			
742-	GRID	225	1	32.005	.0	69.19	1			
743-	GRID	226	1	32.005	15.0	69.19	1			
744-	GRID	227	1	29.955	.0	71.28	1			
745-	GRID	228	1	29.955	15.0	71.28	1			
746-	GRID	229	1	27.58	.0	73.175	1			
747-	GRID	230	1	27.58	15.0	73.175	1			
748-	GPID	231	1	25.46	.0	74.515	1			
749-	GRID	232	1	25.46	15.0	74.515	1			
750-	GRID	233	1	23.982	.0	75.29	1			

TABLE 4-VIII (Cont)

TYPICAL BULK DATA DECK FOR THE CLEAN
MOTOR MODEL FOR POSEIDON C-3 SS MOTOR

S O R T E D   B U L K   D A T A   E C H O

CARD COUNT	. 1 ..	2 ..	3 ..	4 ..	5 ..	6 ..	7 .. 8 .. 9 .. 10 .
751-	GRID	234	1	23.962	15.0	75.29	1
752-	GRID	235	1	23.05	.0	75.74	1
753-	GRID	236	1	23.05	15.0	75.74	1
754-	GRID	237	1	22.14	.0	76.16	1
755-	GRID	238	1	22.14	15.0	76.16	1
756-	GRID	239	1	21.484	.0	76.445	1
757-	GRID	240	1	21.484	15.0	76.445	1
758-	GRID	241	1	20.80	.0	76.683	1
759-	GRID	242	1	20.80	15.0	76.683	1
760-	GRID	243	1	19.75	.0	77.03	1
761-	GRID	244	1	19.75	15.0	77.03	1
762-	GRID	245	1	20.90	.0	76.26	1
763-	GRID	246	1	20.90	15.0	76.26	1
764-	GRID	247	1	19.60	.0	76.53	1
765-	GRID	248	1	19.60	15.0	76.53	1
766-	GRID	249	1	19.00	.0	77.26	1
767-	GRID	250	1	19.00	15.0	77.26	1
768-	GRID	251	1	18.95	.0	76.61	1
769-	GRID	252	1	18.95	15.0	76.61	1
770-	GRID	253	1	18.35	.0	77.43	1
771-	GRID	254	1	18.35	15.0	77.43	1
772-	GRID	255	1	18.35	.0	76.63	1
773-	GRID	256	1	18.35	15.0	76.63	1
774-	GRID	257	1	17.55	.0	78.48	1
775-	GRID	258	1	17.55	15.0	78.48	1
776-	GRID	259	1	11.70	.0	69.76	1
777-	GRID	260	1	11.70	15.0	69.76	1
778-	GRID	261	1	11.30	.0	67.96	1
779-	GRID	262	1	11.30	15.0	67.96	1
780-	GRID	263	1	10.05	.0	67.26	1
781-	GRID	264	1	10.05	15.0	67.26	1
782-	GRID	265	1	10.20	.0	66.31	1
783-	GRID	266	1	10.20	15.0	66.31	1
784-	GRID	267	1	10.20	.0	63.06	1
785-	GRID	268	1	10.20	15.0	63.06	1
786-	GRID	269	1	11.20	.0	64.16	1
787-	GRID	270	1	11.20	15.0	64.16	1
788-	GRID	271	1	13.20	.0	69.36	1
789-	GRID	272	1	13.20	15.0	69.36	1
790-	GRID	273	1	12.00	.0	63.81	1
791-	GRID	274	1	12.00	15.0	63.81	1
792-	GRID	275	1	10.55	.0	62.06	1
793-	GRID	276	1	10.55	15.0	62.06	1
794-	GRID	277	1	8.93	.0	61.81	1
795-	GRID	278	1	8.93	15.0	61.81	1
796-	GRID	279	1	8.60	.0	57.56	1
797-	GRID	280	1	8.60	15.0	57.56	1
798-	GRID	281	1	6.17	.0	60.66	1
799-	GRID	282	1	6.17	15.0	60.66	1
800-	GRID	283	1	8.93	.0	64.76	1

TABLE 4-VIII (Cont)

TYPICAL BULK DATA DECK FOR THE CLEAN
MOTOR MODEL FOR POSEIDON C-3 SS MOTOR

S O R T E D B U L K D A T A E C H O

CARD COUNT	. 1 ..	2 ..	3 ..	4 ..	5 ..	6 ..	7 ..	8 ..	9 ..	10 .
801-	GRID	284	1	8.93	15.0	64.76	1			
802-	GRID	285	1	6.90	.0	65.26	1			
803-	GRID	286	1	6.90	15.0	65.26	1			
804-	GRID	287	1	8.76	.0	66.32	1			
805-	GRID	288	1	8.76	15.0	66.32	1			
806-	GRID	289	1	15.60	.0	79.16	1			
807-	GRID	290	1	15.60	15.0	79.16	1			
808-	GRID	291	1	21.55	.0	91.30	1			
809-	GRID	292	1	21.55	15.0	91.30	1			
810-	GRID	293	1	25.00	.0	89.54	1			
811-	GRID	294	1	25.00	15.0	89.54	1			
812-	GRID	295	1	26.80	.0	93.00	1			
813-	GRID	296	1	26.80	15.0	93.00	1			
814-	GRID	297	1	23.40	.0	94.8	1			
815-	GRID	298	1	23.40	15.0	94.8	1			
816-	GRID	299	1	24.40	.0	97.14	1			
817-	GRID	300	1	24.40	15.0	97.14	1			
818-	MAT1	2	3.30E&06		.22	1.71E-04				
819-	MAT1	3	3.62E&06		.2465	1.65E-04				
820-	MAT1	4	4.25E&06		.251	1.69E-04				
821-	MAT1	5	5.24E&06		.26	1.84E-04				
822-	MAT1	6	3.34E&04		.49	4.34E-04				
823-	MAT1	7	2.00E&06		.22	1.34E-04				
824-	MAT1	600	1.03E&07		.33	2.53E-04.0				
825-	MAT1	601	30.0E&06		.32	7.48E-04				
826-	MAT1	602	5125.	2560.	.49	1.00E-09				
827-	MAT1	603	8200.	4100.	.49	1.00E-09				
828-	MAT1	604	9560.	4780.	.49	1.00E-09				
829-	MAT1	610	1000.	100.	.49	1.00E-09				
830-	MAT1	1000		333.0	.49	1.76E-04			.38051	
831-	MAT2	11	.294E&07.109E&07			.407E&07		.125E&07.00018		
832-	MAT2	25	.317E&07.111E&07			.369E&07		.126E&07.00018		
833-	MAT2	26	.384E&07.144E&07			.183E&07		.155E&07.00018		
834-	MAT2	27	.375E&07.147E&07			.185E&07		.158E&07.00018		
835-	MAT2	28	.391E&07.149E&07			.183E&07		.162E&07.00018		
836-	MAT2	29	4.64E&061.55E&06			1.70E&06		1.71E&06.000186		
837-	MAT2	210	4.20E&061.67E&06			1.89E&06		1.83E&06.000186		
838-	MAT2	211	3.65E&061.79E&06			2.20E&06		1.95E&06.000186		
839-	MAT2	212	3.02E&061.87E&06			2.68E&06		2.03E&06.000186		
840-	MAT2	213	2.48E&061.85E&06			2.26E&06		2.01E&06.000186		
841-	MAT2	501	.294E&07.109E&07			.407E&07		.125E&07.000183		
842-	MAT2	515	.450E&07.274E&06			.277E&07		.355E&06.000186		
843-	MAT2	518	.335E&07.859E&06			.485E&07		.106E&07.000186		
844-	MAT2	520	.374E&07.320E&06			.463E&07		.475E&06.000186		
845-	MAT2	528	.375E&07.147E&07			.186E&07		.158E&07.000186		
846-	MAT2	529	.498E&07.143E&07			.158E&07		.160E&07.000186		
847-	MAT2	530	.484E&07.149E&07			.163E&07		.165E&07.000186		
848-	MAT2	532	.455E&07.158E&07			.174E&07		.174E&07.000186		
849-	MAT2	534	[illegible]							

TABLE 4-VIII (Cont)

TYPICAL BULK DATA DECK FOR THE CLEAN
MOTOR MODEL FOR POSEIDON C-3 SC MOTOR

```
FULL MOTOR MODEL   ***  FIRST LONG. MODE / ADV. BURN              SEPTEMBER  14, 1974   NASTRAN 12/ 1/73    PAGE     65

                                    S O R T E D   B U L K   D A T A   E C H O
          CARD
          COUNT          .  1  ..  2  ..  3  ..  4  ..  5  ..  6  ..  7  ..  8  ..  9  ..  10  .
           851-          MAT2   539    .358E&07.181E&07         .225E&07         .197E&07.000186
           852-          MAT2   545    .285E&07.187E&07         .285E&07         .203E&07.000186
           853-          MAT2   552    .216E&07.178E&07         .371E&07         .194E&07.000186
           854-          MAT2   563    .149E&07.134E&07         .527E&07         .150E&07.000186
           855-          MAT2   574    .124E&07.761E&06         .668E&07         .921E&06.000186
           856-          MAT2   585    .119E&07.373E&06         .750E&07         .534E&06.000186
           857-          MAT2   2141   2.11E&061.77E&06         3.79E&06         1.93E&06.000186
           858-          MAT2   2142   1.86E&061.65E&06         4.28E&06         1.81E&06.000186
           859-          MAT2   2151   1.65E&061.51E&06         4.76E&06         1.67E&06.000186
           860-          MAT2   2152   1.51E&061.35E&06         5.22E&06         1.51E&06.000186
           861-          MAT2   2153   1.38E&061.15E&06         5.75E&06         1.31E&06.000186
           862-          MAT2   2161   1.21E&06.582E&06         7.07E&06         .742E&06.000186
           863-          MAT2   2162   1.19E&06.357E&06         7.53E&06         .517E&06.000186
           864-          MAT2   5285   .372E&07.148E&07         .187E&07         .160E&07.000186
           865-          MAT2   5532   .329E&07.146E&07         .204E&07         .155E&07.000183
           866-          MAT2   5534   .219E&07.148E&07         .208E&07         .158E&07.000183
           867-          MAT2   5536   .209E&07.151E&07         .214E&07         .161E&07.000183
           868-          MAT2   5539   .294E&07.154E&07         .223E&07         .164E&07.000183
           869-          MPC    1      13      1      1.0      15      1      -1.0
           870-          MPC    1      13      2      1.0      15      2      -1.0
           871-          MPC    1      13      3      1.0      15      3      -1.0                  &MPF1
           872-          &MPF1         15      5      -2.3
           873-          MPC    1      13      4      1.0      15      4      -1.0
           874-          MPC    1      13      5      1.0      15      5      -1.0
           875-          MPC    1      13      6      1.0      15      6      -1.0
           876-          MPC    1      14      1      1.0      16      1      -1.0
           877-          MPC    1      14      2      1.0      16      2      -1.0
           878-          MPC    1      14      3      1.0      16      3      -1.0                  &MPF2
           879-          &MPF2         16      5      -2.3
           880-          MPC    1      14      4      1.0      16      4      -1.0
           881-          MPC    1      14      5      1.0      16      5      -1.0
           882-          MPC    1      14      6      1.0      16      6      -1.0
           883-          MPC    1      15      2      1.0      17      2      -1.0
           884-          MPC    1      16      2      1.0      18      2      -1.0
           885-          MPC    1      19      2      1.0      21      2      -1.0
           886-          MPC    1      20      2      1.0      22      2      -1.0
           887-          MPC    1      23      2      1.0      25      2      -1.0
           888-          MPC    1      24      2      1.0      26      2      -1.0
           889-          MPC    1      27      2      1.0      29      2      -1.0
           890-          MPC    1      28      2      1.0      30      2      -1.0
           891-          MPC    1      29      3      1.0      65      3      -1.0
           892-          MPC    1      30      3      1.0      66      3      -1.0
           893-          MPC    1      33      3      1.0      63      3      -1.0
           894-          MPC    1      34      3      1.0      64      3      -1.0
           895-          MPC    1      37      3      1.0      61      3      -1.0
           896-          MPC    1      38      3      1.0      62      3      -1.0
           897-          MPC    1      41      3      1.0      59      3      -1.0
           898-          MPC    1      42      3      1.0      60      3      -1.0
           899-          MPC    1      45      3      1.0      57      3      -1.0
           900-          MPC    1      46      3      1.0      58      3      -1.0
```

TABLE 4-VIII (Cont)

TYPICAL BULK DATA DECK FOR THE CLEAN
MOTOR MODEL FOR POSEIDON C-3 SS MOTOR

S O R T E D B U L K D A T A E C H O

CARD COUNT	. 1 ..	2 ..	3 ..	4 ..	5 ..	6 ..	7 ..	8 ..	9 ..	10 .
901-	MPC	1	169	1	1.0	171	1	-1.0		
902-	MPC	1	169	2	1.0	171	2	-1.0		
903-	MPC	1	169	3	1.0	171	3	-1.0		
904-	MPC	1	169	5	1.0	171	5	-1.0		
905-	MPC	1	169	6	1.0	171	6	-1.0		
906-	MPC	1	170	1	1.0	172	1	-1.0		
907-	MPC	1	170	2	1.0	172	2	-1.0		
908-	MPC	1	170	3	1.0	172	3	-1.0		
909-	MPC	1	170	5	1.0	172	5	-1.0		
910-	MPC	1	170	6	1.0	172	6	-1.0		
911-	MPC	1	185	1	1.0	187	1	-1.0		
912-	MPC	1	185	2	1.0	187	2	-1.0		
913-	MPC	1	185	3	1.0	187	3	-1.0		
914-	MPC	1	186	1	1.0	188	1	-1.0		
915-	MPC	1	186	2	1.0	188	2	-1.0		
916-	MPC	1	186	3	1.0	188	3	-1.0		
917-	MPC	1	199	1	1.0	201	1	-1.0		
918-	MPC	1	199	2	1.0	201	2	-1.0		
919-	MPC	1	199	3	1.0	201	3	-1.0		
920-	MPC	1	200	1	1.0	202	1	-1.0		
921-	MPC	1	200	2	1.0	202	2	-1.0		
922-	MPC	1	200	3	1.0	202	3	-1.0		
923-	MPC	1	245	2	1.0	241	2	-1.0		
924-	MPC	1	246	2	1.0	242	2	-1.0		
925-	MPC	1	247	2	1.0	243	2	-1.0		
926-	MPC	1	248	2	1.0	244	2	-1.0		
927-	MPC	1	251	2	1.0	249	2	-1.0		
928-	MPC	1	252	2	1.0	250	2	-1.0		
929-	MPC	1	255	2	1.0	253	2	-1.0		
930-	MPC	1	256	2	1.0	254	2	-1.0		
931-	MPC	1	257	1	1.0	255	1	-1.0		
932-	MPC	1	257	2	1.0	255	2	-1.0		
933-	MPC	1	257	3	1.0	255	3	-1.0		&MPA1
934-	&MPA1		255	5	-2.015					
935-	MPC	1	257	4	1.0	255	4	-1.0		
936-	MPC	1	257	5	1.0	255	5	-1.0		
937-	MPC	1	257	6	1.0	255	6	-1.0		
938-	MPC	1	258	1	1.0	256	1	-1.0		
939-	MPC	1	258	2	1.0	256	2	-1.0		
940-	MPC	1	258	3	1.0	256	3	-1.0		&MPA2
941-	&MPA2		256	5	-2.015					
942-	MPC	1	258	4	1.0	256	4	-1.0		
943-	MPC	1	258	5	1.0	256	5	-1.0		
944-	MPC	1	258	6	1.0	256	6	-1.0		
945-	MPC	1	267	1	1.0	269	1	-0.5		&MPN1
946-	&MPN1		277	1	-0.5					
947-	MPC	1	267	2	1.0	269	2	-1.0		
948-	MPC	1	267	3	1.0	269	3	-0.5		&MPN3
949-	&MPN3		277	3	-0.5					
950-	MPC	1	[illegible]	[illegible]	[illegible]	[illegible]				

TABLE 4-VIII (Cont)

TYPICAL BULK DATA DECK FOR THE CLEAN
MOTOR MODEL FOR POSEIDON C-3 SS MOTOR

S O R T E D B U L K D A T A E C H O

CARD COUNT	. 1 ..	2 ..	3 ..	4 ..	5 ..	6 ..	7 ..	8 ..	9 ..	10 .
951-	&MPN4		277	4	-0.5					
952-	MPC	1	267	5	1.0	269	5	-0.5		&MPN5
953-	&MPN5		277	5	-0.5					
954-	MPC	1	267	6	1.0	269	6	-0.5		&MPN6
955-	&MPN6		277	6	-0.5					
956-	MPC	1	268	1	1.0	270	1	-0.5		&MPN7
957-	&MPN7		278	1	-0.5					
958-	MPC	1	268	2	1.0	266	2	-1.0		
959-	MPC	1	268	3	1.0	270	3	-0.5		&MPN9
960-	&MPN9		278	3	-0.5					
961-	MPC	1	268	4	1.0	270	4	-0.5		&MPN10
962-	&MPN10		278	4	-0.5					
963-	MPC	1	268	5	1.0	270	5	-0.5		&MPN11
964-	&MPN11		278	5	-0.5					
965-	MPC	1	268	6	1.0	270	6	-0.5		&MPN12
966-	&MPN12		278	6	-0.5					
967-	MPC	1	269	2	1.0	261	2	-1.0		
968-	MPC	1	270	2	1.0	262	2	-1.0		
969-	PARAM	COUPMASS1								
970-	PARAM	CTYPE	DIH							
971-	PARAM	DECOMOPT2								
972-	PARAM	G	.06							
973-	PARAM	N	12							
974-	PARAM	NLOAD	43							
975-	PBAR	301	600	3.91	1.725	.941	2.05			&PB1
976-	&PB1	1.0	1.0	1.0	1.0	1.0	1.0	1.0	1.0	&PB2
977-	&PB2	.8333	.8333							
978-	PBAR	302	600	4.32	1.025	.972	2.325			&PB3
979-	&PB3	1.0	1.0	1.0	1.0	1.0	1.0	1.0	1.0	&PB4
980-	&PB4	.8333	.8333							
981-	PQUAD1	1	518	.40	518	5.333E-3			1.10E-05	
982-	PQUAD1	2	518	.125	518	1.628E-4			1.10E-05	
983-	PQUAD1	3	518	.25	518	1.302E-3			4.95E-05	
984-	PQUAD1	4	601	.50	601	.010417				
985-	PQUAD1	5	600	.53	600	.012406				
986-	PQUAD1	6	600	.60	600	.018				
987-	PQUAD1	7	600	.50	600	.010417			5.85E-05	
988-	PQUAD1	8	600	.575	600	.015842			1.13E-04	
989-	PQUAD1	9	600	.45	600	7.594E-3			1.20E-04	
990-	PQUAD1	10	600	.275	600	1.733E-3			1.21E-04	
991-	PQUAD1	101	585	.76	585	.036581				
992-	PQUAD1	102	574	.61	574	.018915				
993-	PQUAD1	103	563	.344	563	3.392E-3				
994-	PQUAD1	104	552	.2495	552	1.294E-3			1.30E-04	
995-	PQUAD1	105	545	.235	545	1.10E-03			6.48E-05	
996-	PQUAD1	107	545	.2296	545	1.001E-3				
997-	PQUAD1	108	530	.215	530	8.282E-4				
998-	PQUAD1	110	530	.1021	530	8.869E-5			1.94E-05	
999-	PQUAD1	111	529	.0937	529	6.856E-5			1.73E-05	
1000-	PQUAD1	112	5285	.217	5285	8.515E-4			1.62E-05	

TABLE 4-VIII (Cont)

TYPICAL BULK DATA DECK FOR THE CLEAN
MOTOR MODEL FOR POSEIDON C-3 SS MOTOR

S O R T E D   B U L K   D A T A   E C H O

CARD COUNT	. 1 ..	2 ..	3 ..	4 ..	5 ..	6 ..	7 ..	8 ..	9 ..	10 .
1001-	PQUAD1	113	528	.216	528	8.398E-4			1.35E-05	
1002-	PQUAD1	114	528	.2144	528	8.213E-4			8.64E-06	
1003-	PQUAD1	115	515	.20	515	6.677E-4				
1004-	PQUAD1	116	515	.20	515	6.667E-4				
1005-	PQUAD1	117	501	.30	501	2.250E-3			8.64E-06	
1006-	PQUAD1	118	518	.20	518	6.667E-4			8.64E-06	
1007-	PQUAD1	119	11	.185	11	5.276E-4			6.48E-06	
1008-	PQUAD1	120	520	.185	520	5.276E-4			6.48E-06	
1009-	PQUAD1	121	25	.1342	25	2.014E-4			8.10E-06	
1010-	PQUAD1	122	26	.1970	26	6.371E-4			8.65E-06	
1011-	PQUAD1	123	27	.1733	27	4.337E-4			1.08E-05	
1012-	PQUAD1	124	28	.1661	28	3.819E-4			1.35E-05	
1013-	PQUAD1	125	29	.1408	29	2.326E-4			1.40E-05	
1014-	PQUAD1	126	210	.1192	210	1.411E-4			1.73E-05	
1015-	PQUAD1	127	211	.1285	211	1.768E-4			1.84E-05	
1016-	PQUAD1	128	212	.1545	212	3.073E-4			2.16E-05	
1017-	PQUAD1	129	213	.1916	213	5.861E-4			2.70E-05	
1018-	PQUAD1	130	2141	.2168	2141	8.492E-4			4.32E-05	
1019-	PQUAD1	131	2142	.2239	2142	9.354E-4			5.94E-05	
1020-	PQUAD1	132	2151	.2572	2151	1.418E-3			8.64E-05	
1021-	PQUAD1	133	2152	.3320	2152	3.049E-3			9.07E-05	
1022-	PQUAD1	134	2153	.4685	2153	8.569E-3				
1023-	PQUAD1	135	2161	.625	2161	.0203451				
1024-	PQUAD1	136	2162	.6450	2162	.0223613				
1025-	PQUAD1	137	600	.43	600	6.626E-3			8.10E-05	
1026-	PQUAD1	138	600	.68	600	.026203			8.10E-05	
1027-	PQUAD1	139	600	1.025	600	.089741			8.10E-05	
1028-	PQUAD1	140	600	.70	600	.028583			6.60E-04	
1029-	PQUAD1	141	600	1.0	600	.083333			6.60E-04	
1030-	PQUAD1	142	600	.56	600	.014635				
1031-	PQUAD1	143	600	.45	600	7.594E-3				
1032-	PQUAD1	144	600	.30	600	2.250E-3				
1033-	PQUAD1	145	2	.65	2	.022885				
1034-	PQUAD1	146	3	.82	3	.045947				
1035-	PQUAD1	147	4	.55	4	.013865				
1036-	PQUAD1	148	5	.55	5	.013865				
1037-	PQUAD1	149	600	.10	600	8.333E-5				
1038-	PQUAD1	150	4	.55	4	.013865				
1039-	PQUAD1	201	545	.23	545	1.0E-03			3.03E-05	
1040-	PQUAD1	202	530	.101	530	8.85E-05			2.16E-05	
1041-	RLOAD1	1	100			1				
1042-	RLOAD1	2	100			2				
1043-	RLOAD1	3	100			3				
1044-	RLOAD1	4	100			4				
1045-	RLOAD1	5	100			5				
1046-	RLOAD1	6	100			6				
1047-	RLOAD1	7	100			7				
1048-	RLOAD1	8	100			8				
1049-	RLOAD1	9	100			9				
1050-	RLOAD1	10	100			10				

TABLE 4-VIII (Cont)

TYPICAL BULK DATA DECK FOR THE CLEAN
MOTOR MODEL FOR POSEIDON C-3 SS MOTOR

S O R T E D B U L K D A T A E C H O

CARD COUNT	. 1 ..	2 ..	3 ..	4 ..	5 ..	6 .. 7 .. 8 .. 9 .. 10 .
1051-	RLOAD1	11	100			11
1052-	RLOAD1	12	100			12
1053-	RLOAD1	101	301			201
1054-	RLOAD1	102	302			201
1055-	RLOAD1	103	303			201
1056-	RLOAD1	104	304			201
1057-	RLOAD1	105	305			201
1058-	RLOAD1	106	306			201
1059-	RLOAD1	107	307			201
1060-	RLOAD1	108	308			201
1061-	RLOAD1	109	309			201
1062-	RLOAD1	110	310			201
1063-	RLOAD1	111	311			201
1064-	RLOAD1	112	312			201
1065-	RLOAD1	113	313			201
1066-	RLOAD1	114	314			201
1067-	RLOAD1	115	315			201
1068-	SPC1	1	4	39	40	
1069-	SPC1	1	4	45	46	
1070-	SPC1	1	4	51	THRU	54
1071-	SPC1	1	4	69	70	
1072-	SPC1	1	4	87	88	
1073-	SPC1	1	4	105	106	
1074-	SPC1	1	4	119	120	
1075-	SPC1	1	4	133	134	
1076-	SPC1	1	4	145	146	
1077-	SPC1	1	4	157	158	
1078-	SPC1	1	4	169	170	
1079-	SPC1	1	4	171	172	
1080-	SPC1	1	4	185	186	
1081-	SPC1	1	4	213	THRU	218
1082-	SPC1	1	4	235	THRU	238
1083-	SPC1	1	4	241	THRU	244
1084-	SPC1	1	4	253	254	
1085-	SPC1	1	4	261	262	
1086-	SPC1	1	4	271	THRU	274
1087-	SPC1	1	4	283	284	
1088-	SPC1	1	4	287	THRU	290
1089-	SPC1	1	5	5	6	
1090-	SPC1	1	6	7	8	
1091-	SPC1	1	6	17	18	
1092-	SPC1	1	6	23	THRU	30
1093-	SPC1	1	6	41	42	
1094-	SPC1	1	6	231	THRU	234
1095-	SPC1	1	6	245	246	
1096-	SPC1	1	6	269	270	
1097-	SPC1	1	6	299	300	
1098-	SPC1	1	124	1	2	
1099-	SPC1	1	456	57	THRU	68
1100-	SPC1	1	456	71	THRU	86

TABLE 4-VIII (Cont)

TYPICAL BULK DATA DECK FOR THE CLEAN
MOTOR MODEL FOR POSEIDON C-3 SS MOTOR

S O R T E D B U L K D A T A E C H O

CARD COUNT	. 1 ..	2 ..	3 ..	4 ..	5 ..	6 ..	7 ..	8 ..	9 ..	10 .
1101-	SPC1	1	456	89	THRU	104				
1102-	SPC1	1	456	107	THRU	118				
1103-	SPC1	1	456	121	THRU	132				
1104-	SPC1	1	456	135	THRU	144				
1105-	SPC1	1	456	147	THRU	156				
1106-	SPC1	1	456	159	THRU	168				
1107-	SPC1	1	456	171	THRU	184				
1108-	SPC1	1	456	187	THRU	198				
1109-	SPC1	1	456	201	THRU	212				
1110-	SPC1	1	456	263	THRU	266				
1111-	SPC1	1	456	275	276					
1112-	SPC1	1	456	279	THRU	282				
1113-	SPC1	1	456	285	286					
1114-	SPC1	1	1236	51	52					
1115-	TABLED1	1								&TB1
1116-	&TB1	0.0	1.0	3000.	1.0	ENDT				
1117-	TABLED1	2								&TB2
1118-	&TB2	0.0	.88	3000.	.88	ENDT				
1119-	TABLED1	3								&TB3
1120-	&TB3	0.0	.65	3000.	.65	ENDT				
1121-	TABLED1	4								&TB4
1122-	&TB4	0.0	.21	3000.	.21	ENDT				
1123-	TABLED1	5								&TB5
1124-	&TB5	0.0	-.35	3000.	-.35	ENDT				
1125-	TABLED1	6								&TB6
1126-	&TB6	0.0	-.80	3000.	-.80	ENDT				
1127-	TABLED1	7								&TB7
1128-	&TB7	0.0	-1.0	3000.	-1.0	ENDT				
1129-	TABLED1	8								&TB8
1130-	&TB8	0.0	-.90	3000.	-.90	ENDT				
1131-	TABLED1	9								&TB9
1132-	&TB9	0.0	-.61	3000.	-.61	ENDT				
1133-	TABLED1	10								&TB10
1134-	&TB10	0.0	-.10	3000.	-.10	ENDT				
1135-	TABLED1	11								&TB11
1136-	&TB11	0.0	.350	3000.	.350	ENDT				
1137-	TABLED1	12								&TB12
1138-	&TB12	0.0	.800	3000.	.800	ENDT				
1139-	TABLED1	201								&T99
1140-	&T99	0.0	1.0	3000.	1.0	ENDT				
1141-	TABLED1	2000								&FKM1
1142-	&FKM1	0.0	0.0	1.0	1.183	10.0	3.416	50.0	6.045	&FKM2
1143-	&FKM2	100.0	7.621	400.0	11.301	700.0	12.352	1000.0	13.14	&FKM3
1144-	&FKM3	1500.	14.453	ENDT						
1145-	TABLED1	2001								&FKM4
1146-	&FKM4	0.0	.8935	1.0	1.7871	10.0	3.390	50.0	5.361	&FKM5
1147-	&FKM5	100.0	6.1497	400.0	8.252	700.0	9.0406	1000.0	9.5662	&FKM6
1148-	[illegible]	[illegible]	[illegible]							

SECTION V

TASK 4 - STRUCTURAL RESPONSE TESTING USING ACOUSTIC EXCITATION

Solid rocket motor acoustic pressure oscillations that occur during motor operation cause structural vibrations that can be measured and recorded by accelerometers. However, analysis of typical accelerometer data indicates that the structure is probably responsing to several different loads during motor operation time. Determination of the portion of the measured response which is due to acoustic pressure oscillations and that portion which is due to other forcing functions is sometimes difficult. Another factor to be considered in interpretation of motor static firing or flight data is the large motor-to-motor variability in the data as discussed under Task I, Section II.

The objective of the experimental work described in this section was to measure the structural response of a solid rocket motor to a known loading distribution. This experiment was intended to provide "clean" data (by comparison to hot firing data), for evaluation of analytical models.

Use of experimental data from the program had the following advantages over accelerometer data from static firing for evaluation of finite element models:

(1) The measured response of the motor structure represents the response to a single well-defined forcing function; whereas, static firing data contain response information for several ill-defined forcing functions.

(2) Since the testing was conducted under carefully controlled laboratory conditions, variability in the data for repeated test sequences was small; whereas, the variability in accelerometer data from motor firing tests is large.

(3) Measurement and mapping of the acoustic mode shapes resulted in good definition of the loading distributions; whereas, motor static firing tests typically have only one pressure measurement made at one location.

(4) Use of double-backed adhesive tape and a movable accelerometer made possible the mapping of structural response mode shapes in considerable detail. Because data channels are limited in number, only four to six accelerometers are normally recorded during a routine static firing. Even specially instrumented motors generally have only one to two dozen accelerometer measurements.

Results from this testing program were intended to complement static firing data rather than replace it for use in evaluation of analysis results. Filtering and other data reduction techniques were used to obtain meaningful comparisons between analytical results and static firing data.

The following shortcomings were associated with the testing program:

(1) The applied loads and corresponding responses are of very small magnitude compared to those that occur during motor operation. Therefore, nonlinearities are unaccounted for by this test procedure.

(2) Dynamic properties of the inert propellant (HDLK) were not the same as those of the live propellant (FKM).

(3) Boundary conditions used for the acoustics testing do not exactly match those of the static firing or flight test conditions.

In spite of these shortcomings, the testing program produced useful motor response data.

The objective was achieved by measuring the response of an inert Poseidon C-3 second stage motor to acoustic excitation provided by a loudspeaker in the motor combustion cavity. The cone-type loudspeaker was placed in the centerbore of the motor. An oscillator was attached to the loudspeaker through an audio amplifier. Frequency sweeps were conducted by varying the oscillator frequency in the range from 0 to 1000 Hz. A microphone was placed in the combustion cavity to monitor pressure oscillation amplitudes. The microphone was mounted on a shaft that could be moved along the motor centerline to map the acoustic pressure mode shapes. An accelerometer was used on the motor structure and components to map structural mode shapes.

The motor was pressurized to 50 psi so that the dome of the case would be forced out away from the propellant grain. Nitrogen gas was used to pressurize the motor for most of the testing; however, some studies were made using helium gas to change the frequency at which various acoustic modes occurred. Since structural natural frequencies remain constant, variation of the acoustic natural frequencies simplified the problem of separating structural resonance from acoustic resonance in the test data.

Two types of tests were conducted: (1) Frequency response, and (2) mode mapping. The frequency response tests were conducted by recording the accelerometer output on an x-y plotter while the frequency was varied slowly over a certain frequency range. The accelerometer was then moved to another point and the frequency response test repeated. By examining results from the frequency response tests, major resonance frequencies were selected for mode shape mapping. The mode shape mapping was conducted by turning the oscillator to a particular frequency and then moving the accelerometer from one structural point to another to map the mode of response. The accelerometer signal amplitude and phase were recorded at each point.

Results from this experimental project are presented by way of frequency response plots and mode shape plots. The acoustic cavity resonances compare well with those determined previously by test and by analysis. No data were available for evaluation of the structural response results. The testing report that discusses the test setup, procedure, and results is presented in Appendix D.

SECTION VI

TASK 5 - BASELINE MOTOR ANALYSIS EVALUATION

The purpose of Task 5 was to compare analysis results with experimental results, and to make a judgment on the adequacy of the analysis results based on the error limits defined in Task 1. Two types of experimental results were used in evaluating the accuracy of the analytical results: (1) Accelerometer data from static firings, and (2) structural response data from the Task 4 testing. The accelerometer data comparisons are basically comparisons between calculated and measured magnitudes. The Task 4 response data comparisons are basically mode shape comparisons. Each evaluation is discussed separately and more detail is given in the Task 5 final report included as Appendix E.

A. COMPARISONS WITH TASK 4 COLD GAS TEST RESULTS

A typical comparison between NASTRAN model calculated response and Task 4 measured response is shown in Figure 6-1. Both mode shapes shown in the figure have been normalized to have a maximum deformation of unity. The general shapes of the modes shown in Figure 6-1 are similar (each shape has only one crossover from positive to negative deformation). Other than the general similarities, the mode shapes do not show good agreement. Additional aft dome mode shape comparison plots may be found in the August 20, 1974 monthly report also included in Appendix G.

The work of Phase II, discussed in Section VII, may provide some insight into the reasons for lack of agreement between measured and calculated dome mode shapes. The fact that the mode of response is very dependent on the loading distribution was illustrated during Phase II of the program. Since the mode shapes in Figure 6-1 are not in good agreement, the correspondence between load distributions is questionable.

In Task 4, the shape of the pressure mode along the centerbore was measured with reasonable accuracy and a corresponding pressure distribution was applied along the centerbore of the NASTRAN model. Likely problem areas are the cavities between the domes and the grain. Since both domes in the second stage Poseidon motor are unbonded, dome cavities are formed when the chamber is pressurized causing the domes to move out away from the grain. The pressure distribution in the cavities was not measured in Task 4. Scalar springs were used in the NASTRAN model in place of a cavity pressure distribution. There is no reason to expect the equivalent pressure distribution applied to the dome by the scalar springs to simulate the actual pressure distribution in the dome cavity. The forces in the scalar springs are determined by the relative motion between the domes and the grain, whereas the actual acoustic mode pressure distribution is a function of dome cavity geometry and the coupling between dome cavity and main combustion cavity. Poor simulation of dome cavity pressure distributions is, therefore, a likely contribution to poor agreement between measured and calculated mode shapes.

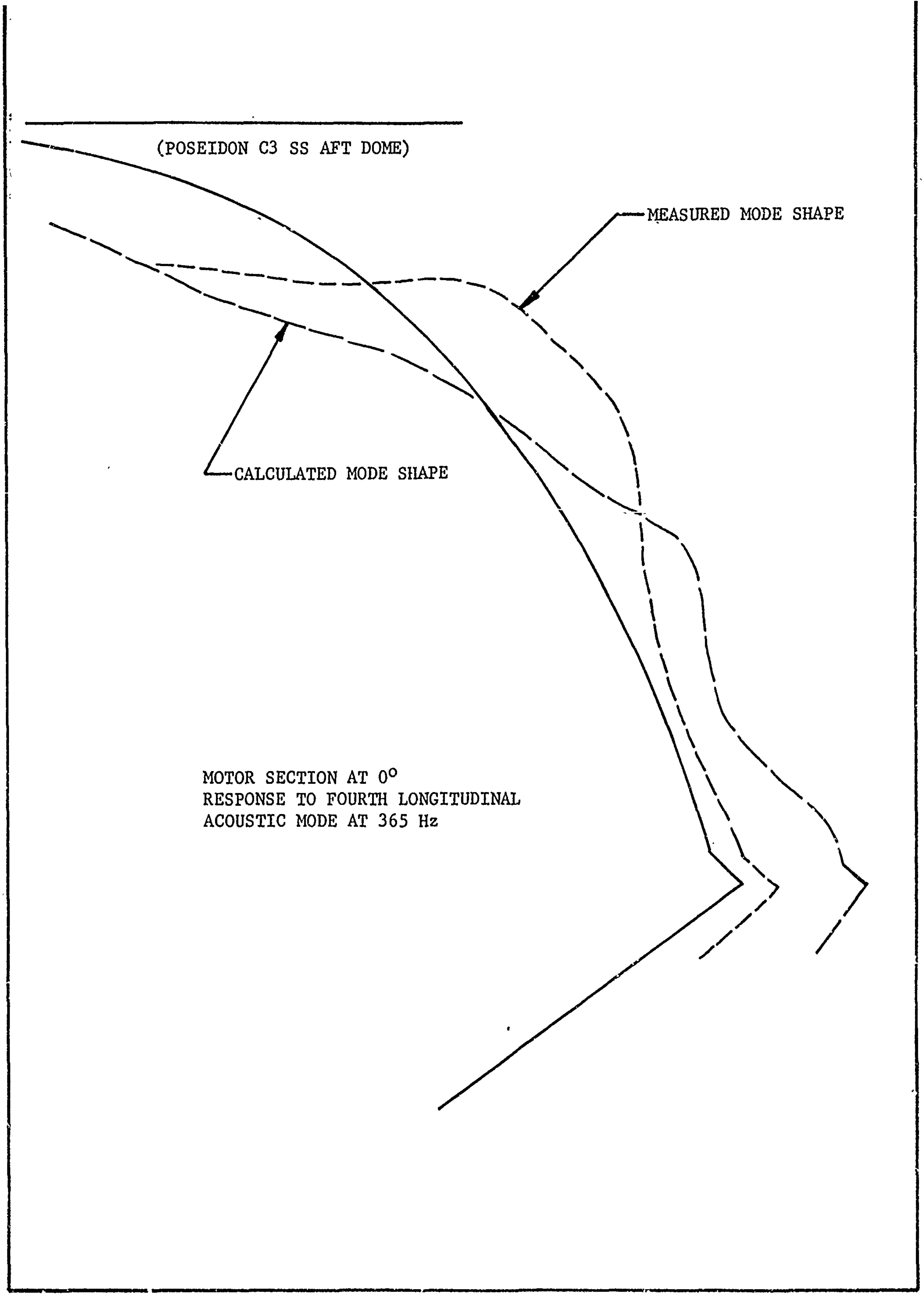

Figure 6-1. Typical Mode Shape Comparison Using Results from Task 4 Testing

Another possible reason for the poor mode shape agreement has to do with the characteristics of the NASTRAN finite element model. Work in Phase II indicated that the use of a 15 degree grid slice may result in a grid too coarse to accurately represent the dome modes. A comparison between dome modes calculated for a 5° and 15° slice is shown in Figure 6-2. The 5° slice should provide the most accurate results because the circular motor geometry is more accurately modeled by a series of 5° segments.

The first natural mode shapes shown in Figure 6-2 have similar shapes for both the 5° and 15° grids, but the frequency is in error by about 10 percent for the 15° grid. The second mode shapes are also similar, but the frequency of 304 Hz for the 15° grid is considerably larger than the 251 Hz calculated for the 5° grid. Higher frequency mode shapes appear to show greater differences in shape and in frequency.

The mode shape in which a structure responds depends on both the load distribution and the frequency of load application. In the model, the dome probably responds to the force distribution applied by the scalar springs and the radial motion at the Y-joint. The radial motion at the Y-joint probably tends to excite the natural modes nearest the forcing frequency that have some modal deformation in a radial direction at the Y-joint. The spring forces tend to excite modes that are shaped most similar to the distribution of forces in the scalar springs. A response mode shape may be made up of the sum of various natural mode shapes in the manner that a Fourier series uses a sum of sinusoidal waves to represent a more complex wave. The measured mode shape shown in Figure 6-1 appears to contain components of the f_3, f_4, and f_5 mode shapes for the 5° slice shown in Figure 6-2, based on the location of the major bulge in the measured mode shape.

A significant difference between the actual rocket motor and the finite element model is probably due to the fact that the actual motor responds to the acoustic pressure distribution in the dome cavities rather than to forces in scalar springs. From this discussion, it is concluded that dome response is a rather complex function of model characteristics (natural mode shapes), and applied loading distributions, and that the differences between the 5° slice model and the 15° slice model could account for some of the difference between measured and calculated modes in Figure 6-1.

B. COMPARISONS WITH ACCELEROMETER DATA

During Task 2, a detailed analysis was performed on data from a representative aft dome accelerometer (AC-250). The analyzed data were obtained from the static firings of Poseidon second stage motors SP-0131 and SP-0160. Results from the data analyses are plotted in the Task 2 report in Appendix B. Acceleration levels are plotted as a function of time for several frequencies of interest. Each frequency range of interest was mapped by covering the frequency range in increments of 10 Hz. The analyses were conducted by playing accelerometer data from the FM tape through a Quantech frequency analyzer.

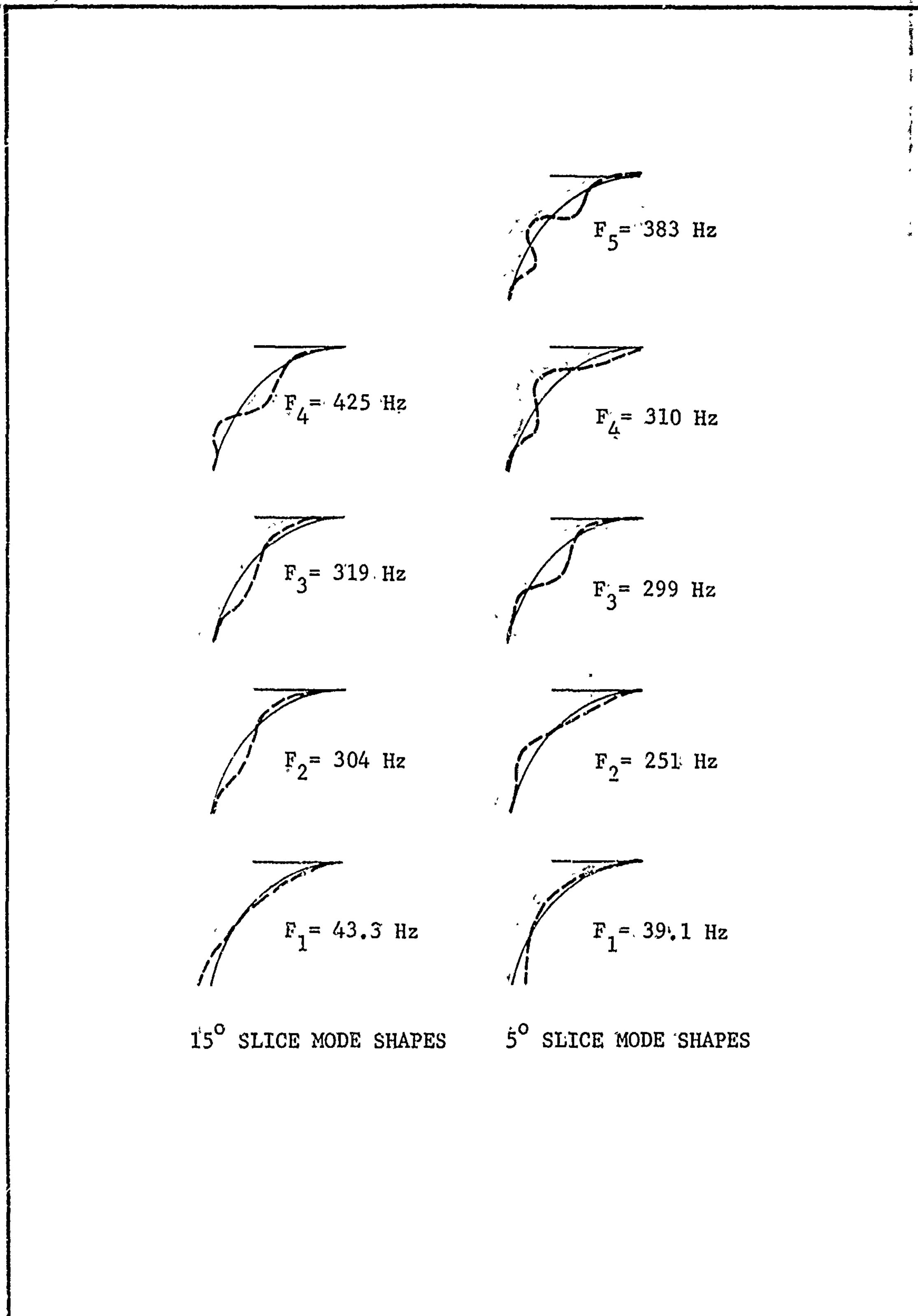

Figure 6-2. Aft Dome Mode Shapes Calculated for 5° and 15° Slice Finite Element Grids

Identification of the characteristic motor frequencies was simplified by the curves shown in Appendix B (Figures 10 through 19). The curves also show that measured response at early times occurs over a broad frequency band. The significance of broad band noise in the accelerometer signal is that care must be taken in interpreting the data for comparison with results from NASTRAN analyses. In the NASTRAN analyses, a single frequency (purely sinusoidal) load was applied and the model responded only at the forcing frequency. Therefore, accelerometer data that show the response to a pure sinusoidal pressure oscillation would be desirable for use in comparison with NASTRAN analysis results. The aft dome accelerometer data analyzed during Task 2 were not "clean". Therefore, data filtering techniques were employed in an effort to isolate only the portions of the signals that occurred at the frequencies of interest. Significant errors in magnitude occur when a composite (unfiltered) accelerometer response is used in place of the filtered signal.

The curves shown in Figure 6-3 illustrate the reduction in magnitude that can occur when data are filtered. The top curve of the figure is essentially unfiltered response data. The middle curve, obtained using a 100 Hz bandwith filter has considerably reduced amplitudes. The reduction in amplitude is typical for filtered broad band or random vibration data.

To obtain data for evaluation of the NASTRAN analyses, accelerometer records from three different motor static firings were analyzed. A report on the data analysis is included in Appendix G, the Task 5 report issued with the December 20, 1974 monthly status report. The Task 5 report in Appendix G contains curves showing filtered pressure gage response and corresponding filtered accelerometer response. Both the 10 Hz and the 100 Hz filter bandwidths were used. Although a typical acoustic mode has a shifting frequency, fixed frequencies that matched the NASTRAN analysis frequencies were used in the accelerometer data analysis.

When an acoustic mode at the analysis frequency is present in the motor, the curves representing pressure as a function of time exhibit peaks. For the three motors included in the study, a special Kistler pressure gage was used to measure the pressure oscillation amplitudes. By plotting filtered accelerometer response on the same graph as pressure gage response, it was easy to read off the acceleration response (in g's) corresponding to a particular pressure oscillation peak (in psi). To present the data in a compact form, the acceleration responses were normalized by dividing peak values by the corresponding peak pressure amplitude levels to obtain (g's/psi). A table showing the resulting (g's/psi) is shown in the Task 5 report in Appendix G.

The NASTRAN analyses resulted in the response displacements and accelerations at the component attachment points (the usual static firing instrumentation for the Poseidon SS motor does not include aft dome accelerometers). Accelerometers AC-250 and AC-261 were located on the nozzle adapter near component attachment points. The rationale used in comparing static firing data and NASTRAN analysis results is given in the Task 5 Final Report of

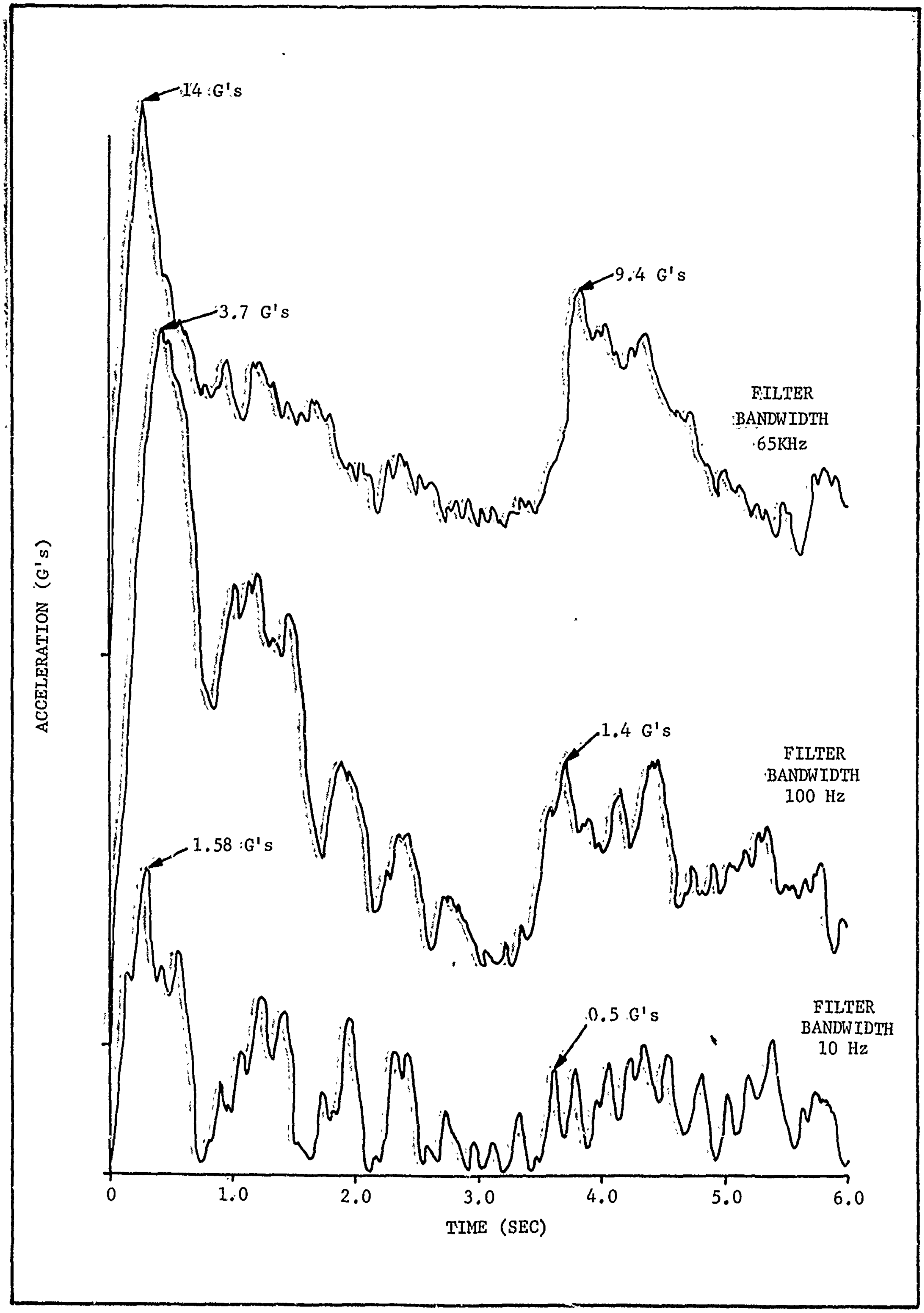

Figure 6-3. Filtered Accelerometer Data for Poseidon SS Motor SP-0115, Aft Dome Accelerometer AC-250, at 680 Hz

Appendix E. The comparisons made in the Task 5 Final Report are reproduced in Tables 6-I and 6-II for easy reference.

TABLE 6-I

COMPARISON BETWEEN STATIC FIRING DATA
AND NASTRAN ANALYSIS RESULTS[(1)]

Frequency (Hz)	Acceleration Response (g's/psi) For Unit Head End Pressure Amplitude			
	Analysis Results for Point 4	AC-250 Static Firing Data	Analysis Results For Point 8	AC-261 Static Firing Data
281	0.74	--	0.29	23.38
634	2.09	1.45 to 3.14	1.53	1.71
668/680*	5.10	1.57 to 3.05	3.21	0.79 to 2.43
770	2.01	2.95	1.23	2.00
1327	2.69	1.86 to 5.39	0.68	1.05 to 1.87

*The NASTRAN analysis was conducted at 668 Hz. The static firing data analysis was erroneously conducted at 680 Hz.

TABLE 6-II

EVALUATION OF ANALYSIS RESULTS USING
ERROR LIMIT FACTOR 1.94[(1)]
(Acceleration Levels in g's)

Frequency (Hz)	Calculated 1.94 x 4	Maximum Measured AC-250	Calculated 1.94 x 8	Maximum Measured AC-261
281	1.46	--	0.56	23.38
634	4.05	3.14	2.97	1.71
668/680	9.89	3.05	6.23	2.43
770	3.90	2.95	2.39	2.00
1327	5.22	5.39	1.32	1.87

(1) Tables 6-I and 6-II were taken from the Task 5 Final Report - refer to Appendix E.

In Table 6-I, calculated values are compared with the range of measured values. In Table 6-II, a factor of 1.94 is applied to the calculated values for comparison with the maximum measured acceleration values in accordance with the error limits established under Task 1. The comparison is favorable to the analysis results as calculated values either approximate or exceed maximum measured values in each case except one. The exception is the 23.38 g's measured by AC-261 at 281 Hz. No reason has been found for the large discrepancy between the measured and calculated response at 281 Hz. The measurement at 281 Hz was available from only one motor at one location. Similar measurements should be made on future static firings to establish that 23 g's is a representative response at 281 Hz.

SECTION VII

PHASE II - SIMPLIFIED MODELS

Phase II of the program was conducted to develop simplified modeling techniques. Changes in grid refinement and the use of a half motor model were studied as possible modeling simplifications. In addition, a study of scalar springs was conducted. The scalar spring study was intended to provide some insight into the general behavior of the motor model. It was reasoned that modeling simplifications would be easier to develop when the model behavior was better understood.

Phase II consisted of three tasks:

Task 6 - Selection of Simplified Modeling Techniques

Task 7 - Analyses Using Simplified Models

Task 8 - Evaluation of Simplified Model Analyses

All three tasks are covered in this section of the report. In Task 6, several options for simplified models were proposed to AFRPL. The three studies covered in this section were selected by AFRPL. The work of analyzing the simplified models was performed under Task 7. The work of Task 8 consisted of writing a Task 8 Final Report to document the simplified analyses and to evaluate the results. The work of Phase II is reported in detail in the Task 8 Final Report which is included as Appendix F. This section includes only brief comments on each of the three main studies.

A. HALF MOTOR MODEL

The decision on whether or not to use a half motor model for a particular situation was left to the analyst. To provide background data and assist the analyst in making a decision, comparative results were given showing how a half motor model responds compared to a full motor model. In addition, the use of different boundary conditions and the corresponding modeling implications were discussed. The conclusion was reached that, in general, a full motor model is to be preferred even if half of the model is very coarse.

B. SCALAR SPRING STUDY

The scalar spring study was performed to investigate the effects of using scalar springs in the dome cavities to represent the combustion gases. Originally, scalar springs were used because of a work statement requirement. The probable intent of the work statement was that scalar springs be used only when unbonded dome cavities are sealed off from the main combustion cavity, as in the case of the third stage Minuteman III motor. Because the intent of the work statement was misunderstood, scalar springs were used in the dome cavities of the Poseidon second stage motor model. The conclusion that scalar springs should not be used to model dome gases in motors similar to the Poseidon was made at the end of the study.

The most beneficial part of the scalar spring study was the insight gained into general dome structural dynamic behavior. In particular, the study of the radial-to-axial motion transfer and the study of dome response to different load distributions provided results of interest.

C. GRID REFINEMENT STUDY

The grid refinement study was conducted in an effort to relate the refinement used in a finite element grid with the highest frequency for which the grid would provide reasonably accurate results. The study resulted in a better understanding of the relationship between response mode shapes and loading distributions, as well as loading frequencies.

It was proposed to use the number of nodes that are available to form a half wave in the mode shape as a measure of mode shape quality. A beam model was used to show that natural mode shapes and natural frequencies are probably sufficiently accurate when three nodes are available to form each half wave of the deformed shape. Some accuracy is lost when only two nodes define a half wave in the mode shape and one node per half wave is definitely undesirable. To apply this criterion to a three-dimensional structure, the mode shape in various convenient planes (such as radial-axial or radial-tangential planes) must be examined.

When a real eigenvalue analysis is performed, natural frequencies and mode shapes are obtained. The higher frequency modes always have more closely spaced waves, (deformation waves of shorter wave length). Inspection of the mode shapes to determine which modes have less than three nodes per half wave is usually an easy matter. Therefore, the frequency at which unacceptable mode shapes are obtained is easily determined for real eigenvalue analyses. Results indicated that the aft dome model for the Poseidon SS was accurate at frequencies up to 400 to 500 Hz for real eigenvalue analyses. The grain becomes inaccurate at lower frequencies, possibly 200 to 300 Hz.

The valid frequency range for a finite element grid used in frequency response analyses is not the same as that for a grid used for real eigenvalue analyses. Apparently, the concept of relating the usefulness of the grid to a particular maximum frequency is not applicable for frequency response analyses. A maximum useful frequency cannot be assigned to a particular grid because the mode of response can depend heavily on the load distribution as well as on the load frequency. For an undamped structure, the response may always be in exactly one mode if the loading distribution exactly matches the mode shape, no matter what forcing frequency is applied. In a more practical situation where the load distribution does not exactly match any natural mode, the mode of response is determined by a combination of the load distribution and the applied load frequency.

The grain surface along the centerbore of the motor was shown to deform with four separate half waves, (Appendix F, Figure 2),in response to the third longitudinal acoustic mode at 770 Hz. Since only two nodes were available to define the first half wave and the last half wave, the grid refinement would be judged as marginal for this analysis. It should be noted that the valid frequency for the grain model in a frequency response analysis is considerably larger than that quoted above for a real eigenvalue analysis. The high valid frequency range occurs because the load distribution does not excite the higher frequency natural modes.

Based on this grid refinement study, the accuracy of frequency response results obtained from a finite element model should be evaluated by examining the response mode shape. If three or more nodes are available to define each half wave of the deformed shape, then the model probably contains reasonable refinement for that particular analysis.

SECTION VIII

PHASE III - VERIFICATION MOTOR ANALYSIS

This section on analysis of the verification motor has been organized as follows:

(1) Introduction

(2) Approach

(3) Models

(4) Closed Envelope Predictions

(5) Evaluation of Verification Motor Analysis

The complete structural dynamics verification motor analysis is discussed in this section.

Phase III of the program was designed to provide a check on modeling techniques selected on the basis of the Phase I and Phase II analyses. The Minuteman III third stage motor, which was manufactured by the Aerojet Solid Propulsion Company, was selected as the motor to be analyzed for verification of the applicability of the proposed modeling techniques. The attributes of the Minuteman third stage motor that make it well suited as a verification motor were covered in the Task 1 Final Report (Appendix A). Two of the major advantages of using the Minuteman III motor were considered to be: (1) The motor design was typical of present and probable future upper stage ballistic missile motors, and (2) a considerable amount of accelerometer data was available.

A. APPROACH

The basic approach used was the same as that used for the baseline motor analysis as explained in Section IV. Only the significant differences in approach are discussed in this section.

The Minuteman motor has six slots in the propellant grain. Using the dihedral symmetry option in the cyclic symmetry procedure, a 30^{o} slice model was required to represent the motor. Use of case elements with a 30^{o} included angle was shown to produce inaccurate results in Phase II. Therefore, the 30^{o} slice was constructed by using two 15^{o} slices. Since two slices were required in the model, a reduction in the number of degrees-of-freedom per slice was necessary to maintain reasonable computer run times. A trial run with the two slice model required 180 minutes (CPU) time using a 600K core on the Hercules IBM 370 model 155 computer. The trial run produced the total solutions for six unit loads applied at a component connection point. All values of the cyclic symmetry K index were used in the trial run.

Run time for the trial run was judged to be excessive. To reduce such time, one of the 15^{o} slices was removed from the model. Removing the slice had the effect of increasing the number of slots in the motor model from 6 to 12. Run time for the 12 slot model was about 90 minutes CPU time.

The propellant grain cannot carry any load in the hoop (tangential) direction in the slotted area. The lack of load-carrying capacity is the same for 6 or 12 slot designs. The radial and axial load carrying capacity of the grain in the slotted area should also be about the same for 6 or 12 slot models. Therefore, the load carrying capacity of the 6 and 12 slot models should be approximately the same. In addition, structural response in an area of the motor removed from the slotted area should be quite similar for both 6 and 12 slot models. This rationale was used to justify the use of a 12 slot model in place of the original 6 slot model. The reasoning was based on equivalent loads being applied to both models. An effort was made to apply loads to the 12 slot model that would simulate those applied to the 6 slot model. Loads were applied in all slots in the hoop directions according to the slot surface areas and local pressure levels. For the tangential modes, a hoop variation in pressure according to PCos θ was used. Radial and axial pressure variations were obtained from acoustic mode analysis results. Radial and axial loads applied in the slotted area were based on assumed exposed surface areas. To simulate the 6 slot model, every other slot was assumed to have zero exposed surface area for application of radial and axial loads. Thus, except for the hoop direction loading, the 12 slot model was loaded as a 6 slot model would have been loaded.

The use of a 12 slot model to represent a 6 slot motor is considered to be a modeling simplification. Unfortunately, this simplification was neither investigated nor evaluated in Phase II. A comparison between the 6 and 12 slot model responses to a unit load at a component attach point showed very little difference between the two models. A comparison of responses to an acoustic mode, preferably a tangential mode, would have been more meaningful, but pressure loads were never obtained for the 6 slot model. The 6 and 12 slot model configurations are shown in Figure 8-1.

The receptance matrices were calculated in a somewhat different way than those calculated for the Poseidon second stage motor. In an effort to reduce computer run times, the unit load solutions required in forming the receptance matrices were obtained from loads only applied at one component connection point. Six unit loads, one in each coordinate direction (rotations and translations), were applied at the component connection point in Section 1R (Figure 8-1). Matrix partitioning and merging operations were then used to rotate the results to apply at other component connection points.

A unit force in the radial direction at the component connection point in Section 2R should result in approximately the same radial displacement that would result at the component connection point in section 1R due to a unit radial load applied at 1R. That is, a radial unit load applied

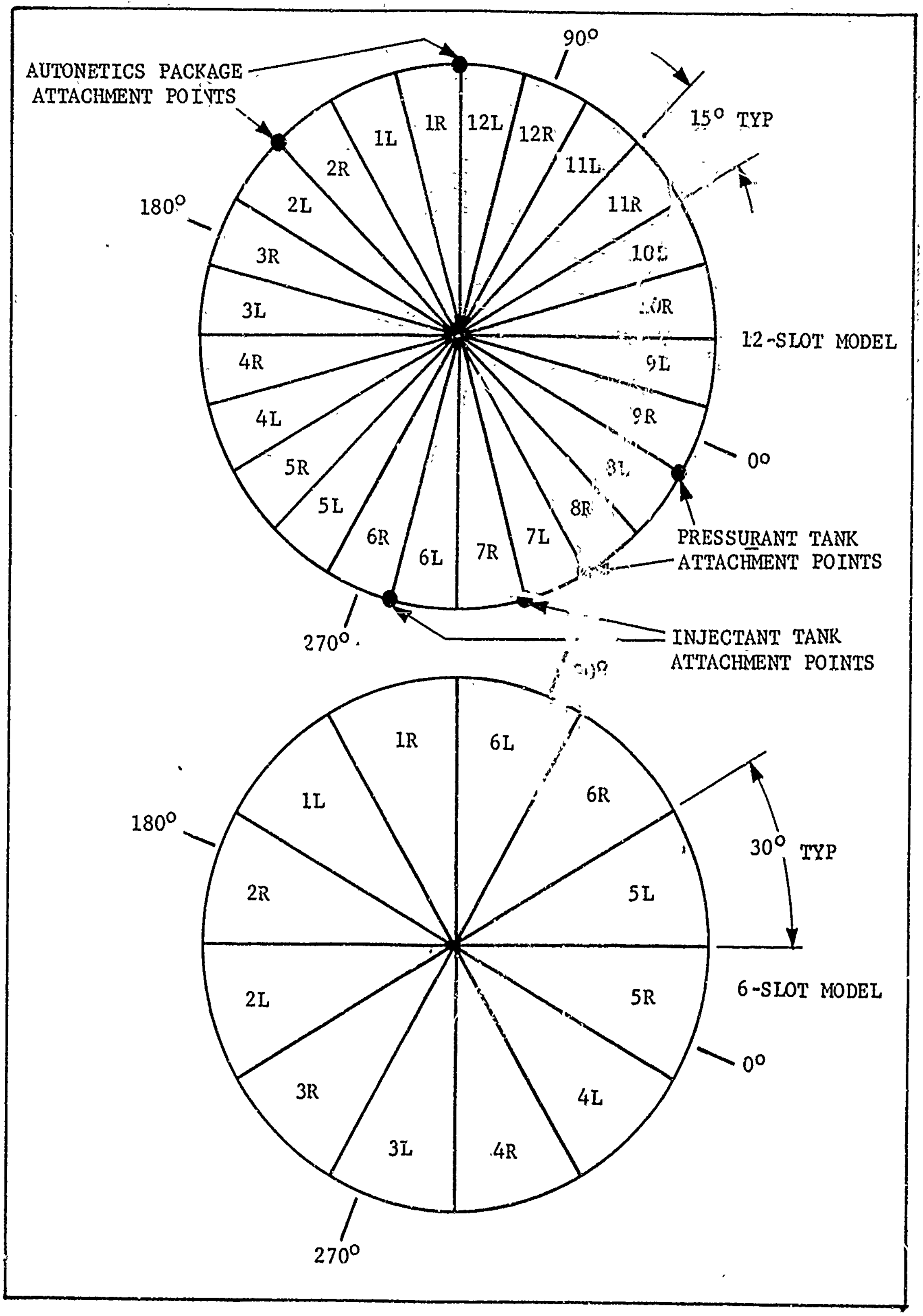

Figure 8-1 Cyclic Symmetry Models of the Minuteman III Third Stage Motor, (view looking aft)

anywhere around the circumference of the motor should cause about the same maximum deformations and deformed shape regardless of circumferential location of the applied load. The same reasoning can also apply to loads in other directions. The locations of the grain slots with respect to loads applied to the case appear to have very little effect on the calculated displacements. A unit load applied on a radial line corresponding with a slot centerline results in about the same case deflections as a unit load applied on a radial line half way between two slots.

The total receptance matrix was obtained by applying only six unit loads at one component connection point. Using the procedure used in the baseline motor analysis, 36 unit loads would have been applied. No comparison results are available to show whether any time was saved by using the 6 load solution in place of the 36 load solution. Solving for 6 unit loads and a pressure load, 168 subcases were required. A total of 888 subcases would have been required for the full 36 unit loads plus pressure load solution. However, considerable matrix partitioning was required to convert the 6 load solution into a 36 load solution.

The Aerojet Minuteman motor has been analyzed previously using NASTRAN. The analyses were performed by the MacNeal Schwendler Corporation working with the Aerojet Solid Propulsion Company. A detailed description of the MSC/ASPC analyses was given in a report(1). Information in the ASPC report was used as much as possible in the work on this project. The acoustic modes and frequencies defined were used as input to the cyclic symmetry model analyses. The same frequencies selected for analysis by ASPC were also used for this project. Data on component models given in the ASPC report were also used to create the models in this program. The MSC/ASPC analysis was conducted without the benefit of cyclic symmetry and thus did not include the full motor in a model.

B. FINITE ELEMENT MODELS

Initially, a model of the Aerojet Minuteman III third stage motor was constructed by using two 15° slices for a cyclic symmetry solution. A computer plot showing the two slice model is shown in Figure 8-2. The single slice model was obtained by removing one slice from the two slice model. Therefore, the bottom plot in Figure 8-2 represents the single slice model.

The propellant grain in the Aerojet Minuteman motor is bonded to the aft dome of the motor case. The forward dome is not bonded. MPC's were used in the NASTRAN analysis to effectively connect the propellant to the

---

(1) Minuteman III Third Stage Pressure Oscillation Study Final Report, 1387-01F, AD888219, Aerojet Solid Propulsion Company, Sacramento, Calif, August 1971.

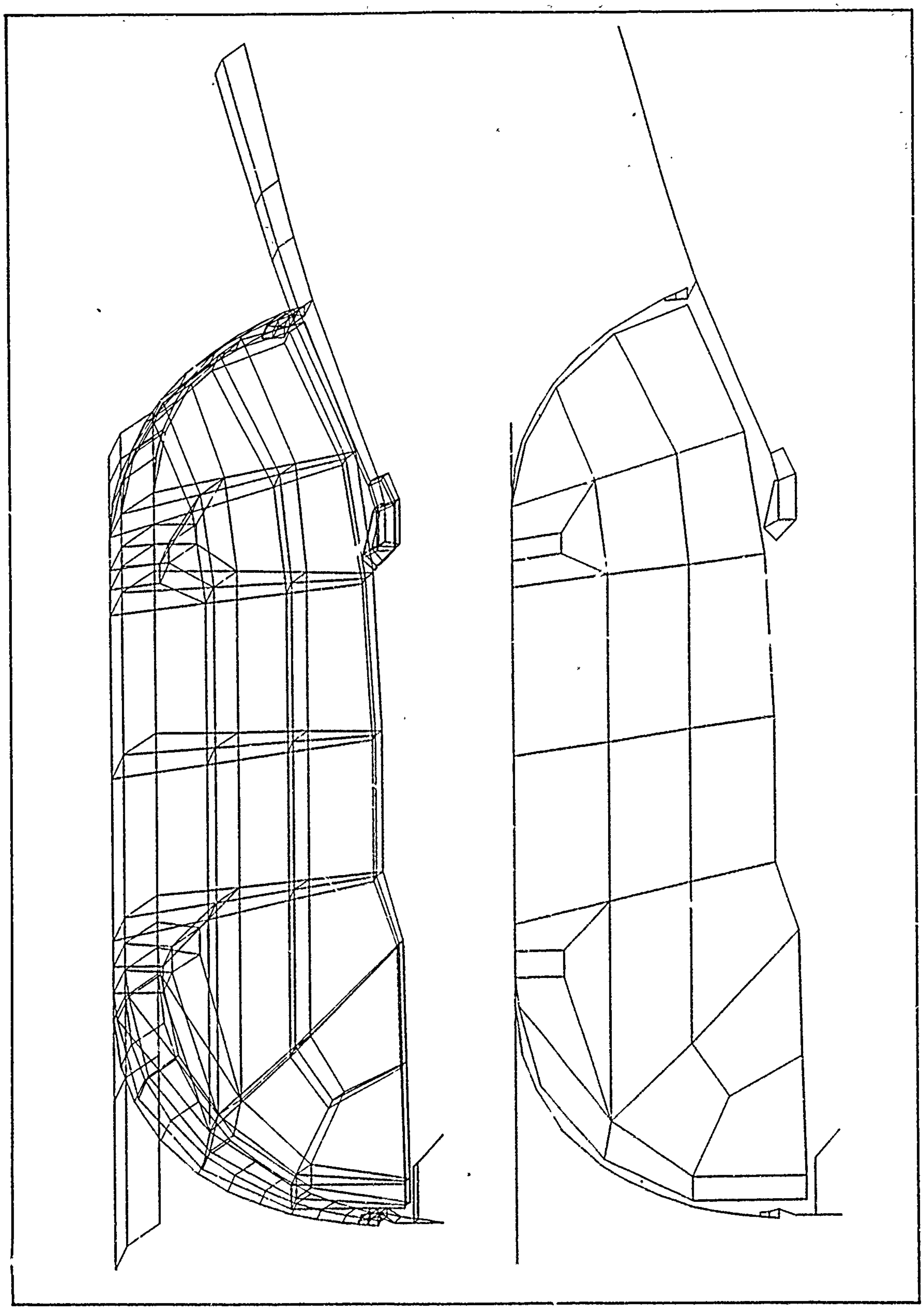

Figure 8-2. Minuteman III Third Stage Finite Element Grid

aft dome. In the model, scalar springs were used in the forward dome cavity to connect the dome to the propellant. When the motor is fired, the grain is forced down around the igniter closing off the forward dome cavity. Scalar springs were used to represent the effect of gases trapped in the forward dome cavity.

The grids shown in Figure 8-2 are for a zero burn time. The zero burn time grid was modified to represent a 6-second burn time by relocating some of the nodes near the center of the grain model. The zero burn time was used for calculating response to the tangential mode. The advanced burn time model was used for calculation of response to the longitudinal mode. The zero burn time model was analyzed at frequencies of 760 Hz, 800 Hz, and 840 Hz using the first tangential mode ($n = 1$). The model representing the 6-second burn time was analyzed at frequencies of 200 Hz, 240 Hz, and 300 Hz using the first longitudinal mode.

Component models were created for the three major components, the Autonetics package, the injectant tank, and the pressurant tank. All three components are mounted to an adapter ring around the circumference of the nozzle. The circumferential locations of the attachment points are shown in Figure 8-1. Data used to create the component models was taken from the ASPC final report[1]. The component models consist of beam elements to model mounting brackets and lumped masses and inertias to represent the main component body.

Rather than giving additional detail on geometry or material properties used in the analyses, copies of the NASTRAN bulk data decks for typical model configurations are given. The bulk data for the motor model is shown in Table 8-I. Bulk data for the three component models are given in Tables 8-II, 8-III, and 8-IV.

C. ANALYSIS RESULTS - CLOSED ENVELOPE PREDICTIONS

The work statement for this program called for "closed envelope" submittal of Phase III analysis results to the AFRPL prior to evaluation of the results by Hercules. This requirement was met by submittal of the "Closed Envelope Predictions" report shown in Appendix H. Accelerations in g's are given for various points on the forward dome and at the component attachment points on the nozzle. The accelerations at the component connection points on the nozzle are shown for both the with and without components-attached solutions. Attaching the components apparently has a rather small effect on the response accelerations.

---

[1] Ibid.

TABLE 8-I

NASTRAN BULK DATA DECK USED IN THE ANALYSIS OF THE THIRD STAGE MINUTEMAN III MOTOR

S O R T E D   B U L K   D A T A   E C H O

CARD COUNT	. 1 ..	2 ..	3 ..	4 ..	5 ..	6 ..	7 ..	8 ..	9 ..	10 .
1-	CBAR	202	201	15	14	1.0	.0	.0	1	&CB2
2-	&CB2			-0.65	0.0	-0.12	-0.65	0.0	-0.12	
3-	CBAR	204	203	225	224	1.0	.0	.0	1	&CB4
4-	&CB4			-0.7386	0.0	-0.4924	-0.7386	0.0	-0.4924	
5-	CHEXA2	101	100	71	72	84	83	68	69	&CH1
6-	&CH1	66	65							
7-	CHEXA2	103	100	74	75	87	86	71	72	&CH3
8-	&CH3	84	83							
9-	CHEXA2	105	100	77	78	90	89	74	75	&CH5
10-	&CH5	87	86							
11-	CHEXA2	107	100	86	87	96	95	83	84	&CH7
12-	&CH7	108	107							
13-	CHEXA2	109	100	89	90	99	98	86	87	&CH9
14-	&CH9	96	95							
15-	CHEXA2	111	100	98	99	111	110	95	96	&CH11
16-	&CH11	108	107							
17-	CHEXA2	113	100	83	84	93	92	65	66	&CH13
18-	&CH13	81	80							
19-	CHEXA2	115	100	92	93	105	104	80	81	&CH15
20-	&CH15	102	101							
21-	CHEXA2	117	100	104	105	117	116	101	102	&CH17
22-	&CH17	114	113							
23-	CHEXA2	119	100	83	84	117	116	92	93	&CH19
24-	&CH19	105	104							
25-	CHEXA2	121	100	107	108	120	119	83	84	&CH21
26-	&CH21	117	116							
27-	CHEXA2	123	100	110	111	123	122	107	108	&CH23
28-	&CH23	120	119							
29-	CHEXA2	125	100	116	117	129	128	113	114	&CH25
30-	&CH25	126	125							
31-	CHEXA2	127	100	119	120	132	131	116	117	&CH27
32-	&CH27	129	128							
33-	CHEXA2	129	100	122	123	135	134	119	120	&CH29
34-	&CH29	132	131							
35-	CHEXA2	131	100	128	129	141	140	125	126	&CH31
36-	&CH31	138	137							
37-	CHEXA2	133	100	131	132	144	143	128	129	&CH33
38-	&CH33	141	140							
39-	CHEXA2	135	100	134	135	147	146	131	132	&CH35
40-	&CH35	144	143							
41-	CHEXA2	137	100	140	141	153	152	137	138	&CH37
42-	&CH37	150	149							
43-	CHEXA2	139	100	152	153	159	158	149	150	&CH39
44-	&CH39	156	155							
45-	CHEXA2	141	100	158	159	165	164	155	156	&CH41
46-	&CH41	162	161							
47-	CHEXA2	143	100	143	144	168	167	140	141	&CH43
48-	&CH43	165	164							
49-	CHEXA2	145	100	146	147	171	170	143	144	&CH45
50-	&CH45	168	167							

TABLE 8-I (Cont)

NASTRAN BULK DATA DECK USED IN THE ANALYSIS OF THE THIRD STAGE MINUTEMAN III MOTOR

FULL LENGTH MOTOR MODEL AT 200 CPS FREQUENCY   JUNE 8, 1975   NASTRAN 12/ 1/73   PAGE 13

S O R T E D   B U L K   D A T A   E C H O

CARD COUNT	. 1 ..	2 ..	3 ..	4 ..	5 ..	6 ..	7 ..	8 ..	9 ..	10 .
51-	CHEXA2	147	100	164	165	183	182	161	162	&CH47
52-	&CH47	180	179							
53-	CHEXA2	149	100	167	168	186	185	164	165	&CH49
54-	&CH49	183	182							
55-	CHEXA2	151	100	140	141	165	164	152	153	&CH51
56-	&CH51	159	158							
57-	CHEXA2	153	100	170	171	189	188	167	168	&CH53
58-	&CH53	186	185							
59-	CHEXA2	155	110	11	12	15	14	17	18	&CH55
60-	&CH55	21	20							
61-	CHEXA2	157	111	17	18	21	20	23	24	&CH57
62-	&CH57	27	26							
63-	CHEXA2	159	120	224	225	228	227	218	219	&CH59
64-	&CH59	222	221							
65-	CHEXA2	161	121	218	219	222	221	212	213	&CH61
66-	&CH61	216	215							
67-	CHEXA2	163	130	254	255	246	245	251	252	&CH63
68-	&CH63	243	242							
69-	CHEXA2	165	131	263	264	255	254	260	261	&CH65
70-	&CH65	252	251							
71-	CHEXA2	167	132	260	261	252	251	257	258	&CH67
72-	&CH67	249	248							
73-	CHEXA2	169	133	266	267	264	263	257	258	&CH69
74-	&CH69	261	260							
75-	CORD2C	1		.0	.0	.0	.0	.0	1.0	&C1
76-	&C1	1.0	0.0	0.0						
77-	CQUAD1	1	1	11	12	18	17	90.0		
78-	CQUAD1	3	2	17	18	24	23	90.0		
79-	CQUAD1	5	3	23	24	30	29	90.0		
80-	CQUAD1	7	4	29	30	33	32	90.0		
81-	CQUAD1	9	5	32	33	36	35	90.0		
82-	CQUAD1	11	6	35	36	39	38	90.0		
83-	CQUAD1	13	7	38	39	42	41	90.0		
-	CQUAD1	15	8	41	42	45	44	90.0		
85-	CQUAD1	17	9	44	45	48	47	90.0		
86-	CQUAD1	19	10	47	48	51	50	90.0		
87-	CQUAD1	21	11	50	51	54	53	90.0		
88-	CQUAD1	23	12	53	54	63	62	90.0		
89-	CQUAD1	25	13	56	57	60	59	90.0		
90-	CQUAD1	27	14	59	60	63	62	90.0		
91-	CQUAD1	29	15	62	63	81	80	90.0		
92-	CQUAD1	31	16	80	81	102	101	90.0		
93-	CQUAD1	33	17	101	102	114	113	90.0		
94-	CQUAD1	35	18	113	114	126	125	90.0		
95-	CQUAD1	37	19	125	126	138	137	90.0		
96-	CQUAD1	39	20	137	138	150	149	90.0		
97-	CQUAD1	41	21	149	150	156	155	90.0		
98-	CQUAD1	43	22	155	156	162	161	90.0		
99-	CQUAD1	45	23	161	162	174	173	90.0		
100-	CQUAD1	47	24	173	174	177	176	90.0		

TABLE 8-I (Cont)

NASTRAN BULK DATA DECK USED IN THE ANALYSIS OF THE THIRD STAGE MINUTEMAN III MOTOR

FULL LENGTH MOTOR MODEL AT 200 CPS FREQUENCY JUNE 8, 1975 NASTRAN 12/ 1/73 PAGE 14

S O R T E D   B U L K   D A T A   E C H O

CARD COUNT	. 1 ..	2 ..	3 ..	4 ..	5 ..	6 ..	7 ..	8 ..	9 ..	10 .
101-	CQUAJ1	49	25	161	162	192	191	90.0		
102-	CQUA 1	51	26	191	192	195	194	90.0		
103-	CQUAD1	53	27	194	195	198	197	90.0		
104-	CQUAD1	55	28	197	198	201	200	90.0		
105-	CQUAD1	57	29	200	201	204	203	90.0		
106-	CQUAD1	59	30	203	204	207	206	90.0		
107-	CQUAD1	61	31	206	207	210	209	90.0		
108-	CQUAD1	63	32	209	210	216	215	90.0		
109-	CQUAD1	65	33	215	216	222	221	90.0		
110-	CQUAD1	67	34	221	222	228	227	90.0		
111-	CQUAD1	69	35	14	15	21	20			
112-	CQUAD1	71	36	20	21	27	26			
113-	CQUAD1	73	37	212	213	219	218			
114-	CQUAD1	75	38	218	219	225	224			
115-	CQUAD1	77	39	230	231	234	233	90.0		
116-	CQUAD1	79	40	233	234	237	236	90.0		
117-	CQUAD1	81	41	236	237	240	239			
118-	CQUAD1	83	42	239	240	243	242			
119-	CQUAD1	85	43	242	243	252	251			
120-	CQUAD1	87	44	251	252	261	260			
121-	CQUAD1	89	45	1	2	4	3			
122-	CQUAD1	90	46	3	4	8	7			
123-	CQUAD1	91	47	5	6	8	7			
124-	CQUAD1	92	48	7	8	10	9			
125-	CQUA 1	93	49	9	10	15	14			
126-	CYJOIN	1	C	1	3	5	7	9	11	&CY1
127-	&CY1	14	17	20	23	26	29	32	35	&CY2
128-	&CY2	38	41	44	47	50	53	56	59	&CY3
129-	&CY3	62	65	68	71	74	77	80	83	&CY4
130-	&CY4	86	89	92	263	266	101	104	107	&CY5
131-	&CY5	110	113	116	119	122	125	128	131	&CY6
132-	&CY6	134	137	140	143	146	149	152	155	&CY7
133-	&CY7	158	161	164	167	170	173	176	179	&CY8
134-	&CY8	182	185	188	191	194	197	200	203	&CY9
135-	&CY9	206	209	212	215	218	221	224	227	&CY10
136-	&CY10	230	233	236	239	242	245	248	251	&CY11
137-	&CY11	254	257	260						
138-	CYJOIN	2	C	2	4	6	8	10	12	&CY12
139-	&CY12	267	15	18	21	24	27	30	33	&CY13
140-	&CY13	36	39	42	45	48	51	54	57	&CY14
141-	&CY14	60	63	66	69	72	75	78	81	&CY15
142-	&CY15	84	87	90	93	96	99	102	105	&CY16
143-	&CY16	108	111	114	117	120	123	126	129	&CY17
144-	&CY17	132	135	138	141	144	147	150	153	&CY18
145-	&CY18	156	159	162	165	168	171	174	177	&CY19
146-	&CY19	180	183	186	189	192	195	198	201	&CY20
147-	&CY20	204	207	210	213	216	219	222	225	&CY21
148-	&CY21	228	231	234	237	240	243	246	249	&CY22
149-	&CY22	252	255	258	261	264				
150-	DAREA	301	236	1	1.0					

TABLE 8-I (Cont)

NASTRAN BULK DATA DECK USED IN THE ANALYSIS OF THE THIRD STAGE MINUTEMAN III MOTOR

FULL LENGTH MOTOR MODEL AT 200 CPS FREQUENCY JUNE 8, 1975 NASTRAN 12/ 1/73 PAGE 15

S O R T E D B U L K D A T A E C H O

CARD COUNT	. 1 ..	2 ..	3 ..	4 ..	5 ..	6 ..	7 ..	8 ..	9 ..	10 .
151-	DAREA	302	236	2	1.0					
152-	DAREA	303	236	3	1.0					
153-	DAREA	304	236	4	1.0					
154-	DAREA	305	236	5	1.0					
155-	DAREA	306	236	6	1.0					
156-	FREQ	1	200.0							
157-	GRDSET		1				1			
158-	GRID	1		.05	.0	12.85				
159-	GRID	2		.05	15.0	12.85				
160-	GRID	3		2.2	.0	10.4				
161-	GRID	4		2.2	15.0	10.4				
162-	GRID	5		.05	.0	6.1				
163-	GRID	6		.05	15.0	6.1				
164-	GRID	7		2.2	.0	6.1				
165-	GRID	8		2.2	15.0	6.1				
166-	GRID	9		3.9	.0	6.1				
167-	GRID	10		3.9	15.0	6.1				
168-	GRID	11		5.2	.0	5.9				
169-	GRID	12		5.2	15.0	5.9				
170-	GRID	14		5.2	.0	6.6				
171-	GRID	15		5.2	15.0	6.6				
172-	GRID	17		6.0	.0	6.0				
173-	GRID	18		6.0	15.0	6.0				
174-	GRID	20		6.0	.0	6.4				
175-	GRID	21		6.0	15.0	6.4				
176-	GRID	23		6.75	.0	6.05				
177-	GRID	24		6.75	15.0	6.05				
178-	GRID	26		6.75	.0	6.3				
179-	GRID	27		6.75	15.0	6.3				
180-	GRID	29		8.0	.0	6.2				
181-	GRID	30		8.0	15.0	6.2				
182-	GRID	32		10.0	.0	6.45				
183-	GRID	33		10.0	15.0	6.45				
184-	GRID	35		12.0	.0	6.85				
185-	GRID	36		12.0	15.0	6.85				
186-	GRID	38		14.5	.0	7.7				
187-	GRID	39		14.5	15.0	7.7				
188-	GRID	41		17.0	.0	8.75				
189-	GRID	42		17.0	15.0	8.75				
190-	GRID	44		19.3	.0	10.05				
191-	GRID	45		19.3	15.0	10.05				
192-	GRID	47		22.25	.0	12.65				
193-	GRID	48		22.25	15.0	12.65				
194-	GRID	50		24.3	.0	15.65				
195-	GRID	51		24.3	15.0	15.65				
196-	GRID	53		25.35	.0	18.3				
197-	GRID	54		25.35	15.0	18.3				
198-	GRID	56		25.86	.0	2.8				
199-	GRID	57		25.86	15.0	2.8				
200-	GRID	59		25.86	.0	15.7				

TABLE 8-I (Cont)

NASTRAN BULK DATA DECK USED IN THE ANALYSIS OF THE THIRD STAGE MINUTEMAN III MOTOR

S O R T E D B U L K D A T A E C H O

CARD COUNT	. 1 ..	2 ..	3 ..	4 ..	5 ..	6 ..	7 ..	8 ..	9 ..	10 .
201-	GRID	60		25.86	15.0	15.7				
202-	GRID	62		25.86	.0	21.95				
203-	GRID	63		25.86	15.0	21.95				
204-	GRID	65		25.6	.0	21.95				
205-	GRID	66		25.6	15.0	21.95				
206-	GRID	68		24.0	.0	15.9				
207-	GRID	69		24.0	15.0	15.9				
208-	GRID	71		19.0	.0	10.45				
209-	GRID	72		19.0	15.0	10.45				
210-	GRID	74		12.0	.0	7.3				
211-	GRID	75		12.0	15.0	7.3				
212-	GRID	77		3.05	.0	7.3				
213-	GRID	78		3.05	15.0	7.3				
214-	GRID	80		25.86	.0	24.0				
215-	GRID	81		25.86	15.0	24.0				
216-	GRID	83		18.35	.0	13.3				
217-	GRID	84		18.35	15.0	13.3				
218-	GRID	86		12.0	.0	9.1				
219-	GRID	87		12.0	15.0	9.1				
220-	GRID	89		3.05	.0	9.1				
221-	GRID	90		3.05	15.0	9.1				
222-	GRID	92		22.0	.0	24.0				
223-	GRID	93		22.0	15.0	24.0				
224-	GRID	95		9.0	.0	15.0				
225-	GRID	96		9.0	15.0	15.0				
226-	GRID	98		3.3	.0	18.0				
227-	GRID	99		3.3	15.0	18.0				
228-	GRID	101		25.86	.0	26.0				
229-	GRID	102		25.86	15.0	26.0				
230-	GRID	104		22.0	.0	26.0				
231-	GRID	105		22.0	15.0	26.0				
232-	GRID	107		12.0	.0	18.95				
233-	GRID	108		12.0	15.0	18.95				
234-	GRID	110		3.5	.0	27.35				
235-	GRID	111		3.5	15.0	27.35				
236-	GRID	113		25.86	.0	28.0				
237-	GRID	114		25.86	15.0	28.0				
238-	GRID	116		18.35	.0	29.6				
239-	GRID	117		18.35	15.0	29.6				
240-	GRID	119		12.0	.0	31.0				
241-	GRID	120		12.0	15.0	31.0				
242-	GRID	122		5.35	.0	32.4				
243-	GRID	123		5.35	15.0	32.4				
244-	GRID	125		25.86	.0	40.5				
245-	GRID	126		25.86	15.0	40.5				
246-	GRID	128		18.35	.0	41.5				
247-	GRID	129		18.35	15.0	41.5				
248-	GRID	131		12.0	.0	42.4				
249-	GRID	132		12.0	15.0	42.4				
250-	GRID	134		5.35	.0	43.25				

TABLE 8-I (Cont)

NASTRAN BULK DATA DECK USED IN THE ANALYSIS OF THE THIRD STAGE MINUTEMAN III MOTOR

FULL LENGTH MOTOR MODEL AT 200 CPS FREQUENCY   JUNE 8, 1975   NASTRAN 12/ 1/73   PAGE 17

S O R T E D   B U L K   D A T A   E C H O

CARD COUNT	. 1 ..	2 ..	3 ..	4 ..	5 ..	6 ..	7 ..	8 ..	9 ..	10 .
251-	GRID	135		5.35	15.0	43.25				
252-	GRID	137		25.86	.0	53.0				
253-	GRID	138		25.86	15.0	53.0				
254-	GRID	140		18.35	.0	53.9				
255-	GRID	141		18.35	15.0	53.9				
256-	GRID	143		12.0	.0	54.6				
257-	GRID	144		12.0	15.0	54.6				
258-	GRID	146		6.0	.0	55.3				
259-	GRID	147		6.0	15.0	55.3				
260-	GRID	149		25.86	.0	55.0				
261-	GRID	150		25.86	15.0	55.0				
262-	GRID	152		22.0	.0	55.5				
263-	GRID	153		22.0	15.0	55.5				
264-	GRID	155		25.86	.0	56.5				
265-	GRID	156		25.86	15.0	56.5				
266-	GRID	158		22.0	.0	57.0				
267-	GRID	159		22.0	15.0	57.0				
268-	GRID	161		25.86	.0	59.0				
269-	GRID	162		25.86	15.0	59.0				
270-	GRID	164		19.4	.0	60.9				
271-	GRID	165		19.4	15.0	60.9				
272-	GRID	167		12.9	.0	62.8				
273-	GRID	168		12.9	15.0	62.8				
274-	GRID	170		7.5	.0	64.4				
275-	GRID	171		7.5	15.0	64.4				
276-	GRID	173		25.86	.0	63.2				
277-	GRID	174		25.86	15.0	63.2				
278-	GRID	176		25.86	.0	65.2				
279-	GRID	177		25.86	15.0	65.2				
280-	GRID	179		24.7	.0	63.8				
281-	GRID	180		24.7	15.0	63.8				
282-	GRID	182		22.35	.0	67.75				
283-	GRID	183		22.35	15.0	67.75				
284-	GRID	185		17.75	.0	71.75				
285-	GRID	186		17.75	15.0	71.75				
286-	GRID	188		12.0	.0	73.85				
287-	GRID	189		12.0	15.0	73.85				
288-	GRID	191		25.6	.0	61.7				
289-	GRID	192		25.6	15.0	61.7				
290-	GRID	194		24.95	.0	63.9				
291-	GRID	195		24.95	15.0	63.9				
292-	GRID	197		23.8	.0	66.2				
293-	GRID	198		23.8	15.0	66.2				
294-	GRID	200		22.5	.0	68.05				
295-	GRID	201		22.5	15.0	68.05				
296-	GRID	203		20.4	.0	70.25				
297-	GRID	204		20.4	15.0	70.25				
298-	GRID	206		18.0	.0	72.1				
299-	GRID	207		18.0	15.0	72.1				
300-	GRID	209		15.9	.0	73.3				

TABLE 8-I (Cont)

NASTRAN BULK DATA DECK USED IN THE ANALYSIS OF THE THIRD STAGE MINUTEMAN III MOTOR

S O R T E D   B U L K   D A T A   E C H O

CARD COUNT	. 1 ..	2 ..	3 ..	4 ..	5 ..	6 ..	7 ..	8 ..	9 ..	10 .
301-	GRID	210		15.9	15.0	73.3				
302-	GRID	212		13.75	.0	74.2				
303-	GRID	213		13.75	15.0	74.2				
304-	GRID	215		13.75	.0	74.4				
305-	GRID	216		13.75	15.0	74.4				
306-	GRID	218		12.9	.0	74.25				
307-	GRID	219		12.9	15.0	74.25				
308-	GRID	221		12.9	.0	74.75				
309-	GRID	222		12.9	15.0	74.75				
310-	GRID	224		12.0	.0	74.3				
311-	GRID	225		12.0	15.0	74.3				
312-	GRID	227		12.0	.0	75.1				
313-	GRID	228		12.0	15.0	75.1				
314-	GRID	230		17.25	.0	94.45				
315-	GRID	231		17.25	15.0	94.45				
316-	GRID	233		14.2	.0	84.45				
317-	GRID	234		14.2	15.0	84.45				
318-	GRID	236		12.25	.0	78.3				
319-	GRID	237		12.25	15.0	78.3				
320-	GRID	239		11.25	.0	75.65				
321-	GRID	240		11.25	15.0	75.65				
322-	GRID	242		5.5	.0	62.75				
323-	GRID	243		5.5	15.0	62.75				
324-	GRID	245		4.5	.0	63.15				
325-	GRID	246		4.5	15.0	63.15				
326-	GRID	248		5.2	.0	60.7				
327-	GRID	249		5.2	15.0	60.7				
328-	GRID	251		4.9	.0	60.7				
329-	GRID	252		4.9	15.0	60.7				
330-	GRID	254		3.5	.0	61.25				
331-	GRID	255		3.5	15.0	61.25				
332-	GRID	257		6.1	.0	57.2				
333-	GRID	258		6.1	15.0	57.2				
334-	GRID	260		4.9	.0	57.8				
335-	GRID	261		4.9	15.0	57.8				
336-	GRID	263		3.5	.0	57.8				
337-	GRID	264		3.5	15.0	57.8				
338-	GRID	266		5.1	.0	56.3				
339-	GRID	267		5.1	15.0	56.3				
340-	MAT1	100		500.	.49	1.6537-4		.50		
341-	MAT1	101	16.0E6		.33	4.140E-4				
342-	MAT1	110	12000.0	3975.0	.49	1.351E-5				
343-	MAT1	111	8000.0	2650.0	.49	2.326E-5				
344-	MAT1	120	7067.0	2341.0	.49	2.633E-5				
345-	MAT1	121	4133.0	1369.0	.49	4.502E-5				
346-	MAT1	130	1.1 E6	.5 E6		1.630E-4				
347-	MAT1	131	1.1 E6	.5 E6		1.630E-4				
348-	MAT1	132	1.2 E6		.25	1.398E-4				
349-	MAT1	133	1.2 E6		.25	1.398E-4				
350-	MAT1	1000	10.3E6		.33	2.614E-4				

TABLE 8-I (Cont)

NASTRAN BULK DATA DECK USED IN THE ANALYSIS OF THE THIRD STAGE MINUTEMAN III MOTOR

FULL LENGTH MOTOR MODEL AT 200 CPS FREQUENCY JUNE 8, 1975 NASTRAN 12/ 1/73 PAGE 19

SORTED BULK DATA ECHO

CARD COUNT	1	2	3	4	5	6	7	8	9	10
351-	MAT2	1	.16038E7	.05284E7		.46347E7		.06442E7	.000122	
352-	MAT2	2	.26144E7	.13987E7		.16657E7		.16155E7	.000123	
353-	MAT2	3	.28968E7	.18085E7		.10772E7		.19932E7	.000134	
354-	MAT2	4	.44806E7	.21428E7		.14391E7		.23625E7	.000139	
355-	MAT2	5	.54595E7	.19162E7		.29278E7		.21370E7	.000146	
356-	MAT2	6	.61709E7	.16724E7		.27077E7		.18922E7	.000152	
357-	MAT2	7	.67374E7	.14448E7		.25962E7		.16647E7	.000161	
358-	MAT2	8	.70252E7	.13203E7		.25571E7		.15403E7	.000168	
359-	MAT2	9	.72808E7	.12055E7		.25313E7		.14255E7	.000177	
360-	MAT2	10	.74541E7	.11256E7		.25181E7		.13454E7	.000185	
361-	MAT2	11	.75633E7	.10742E7		.25114E7		.12941E7	.000190	
362-	MAT2	12	.76577E7	.10293E7		.25067E7		.12493E7	.000192	
363-	MAT2	13	.32627E7	.14851E7		.59904E7		.17050E7	.000192	
364-	MAT2	14	.32627E7	.14851E7		.59904E7		.17050E7	.000192	
365-	MAT2	15	.42053E7	.10542E7		.59094E7		.12741E7	.000192	
366-	MAT2	16	.41621E7	.09898E7		.60814E7		.12097E7	.000192	
367-	MAT2	17	.40356E7	.08827E7		.61520E7		.11027E7	.000192	
368-	MAT2	18	.44428E7	.07749E7		.52429E7		.09894E7	.000192	
369-	MAT2	19	.44428E7	.07749E7		.52429E7		.09894E7	.000192	
370-	MAT2	20	.43059E7	.08826E7		.61521E7		.11025E7	.000192	
371-	MAT2	21	.41623E7	.09893E7		.60822E7		.12092E7	.000192	
372-	MAT2	22	.42053E7	.10541E7		.59094E7		.12741E7	.000192	
373-	MAT2	23	.33387E7	.15706E7		.57430E7		.17906E7	.000192	
374-	MAT2	24	.34165E7	.16580E7		.54905E7		.18780E7	.000192	
375-	MAT2	25	.75322E7	.10888E7		.25130E7		.13087E7	.000192	
376-	MAT2	26	.71680E7	.12569E7		.25414E7		.14768E7	.000189	
377-	MAT2	27	.67127E7	.14558E7		.25989E7		.16757E7	.000185	
378-	MAT2	28	.61482E7	.16821E7		.27104E7		.19021E7	.000180	
379-	MAT2	29	.53293E7	.19600E7		.29737E7		.21799E7	.000170	
380-	MAT2	30	.43628E7	.21732E7		.35134E7		.23932E7	.000162	
381-	MAT2	31	.37012E7	.21959E7		.41301E7		.24158E7	.000149	
382-	MAT2	32	.25450E7	.16420E7		.45429E7		.18220E7	.000134	
383-	MAT2	33	.24062E7	.10726E7		.70059E7		.12781E7	.000126	
384-	MAT2	34	.20934E7	.06574E7		.65730E7		.08350E7	.000125	
385-	MAT2	39	3.77E6	.68E6		6.72E6		1.68E6	.000186	
386-	MAT2	40	3.77E6	.68E6		6.72E6		1.68E6	.000186	
387-	MPC	1	179	1	1.0	194	1	-1.0		
388-	MPC	1	179	2	1.0	194	2	-1.0		
389-	MPC	1	179	3	1.0	194	3	-1.0		
390-	MPC	1	180	1	1.0	195	1	-1.0		
391-	MPC	1	180	2	1.0	195	2	-1.0		
392-	MPC	1	180	3	1.0	195	3	-1.0		
393-	MPC	1	182	1	1.0	200	1	-1.0		
394-	MPC	1	182	2	1.0	200	2	-1.0		
395-	MPC	1	182	3	1.0	200	3	-1.0		
396-	MPC	1	183	1	1.0	201	1	-1.0		
397-	MPC	1	183	2	1.0	201	2	-1.0		
398-	MPC	1	183	3	1.0	201	3	-1.0		
399-	MPC	1	185	1	1.0	206	1	-1.0		
400-	MPC	1	185	2	1.0	206	2	-1.0		

TABLE 8-I (Cont)

NASTRAN BULK DATA DECK USED IN THE ANALYSIS OF THE THIRD STAGE MINUTEMAN III MOTOR

S O R T E D   B U L K   D A T A   E C H O

CARD COUNT	. 1 ..	2 ..	3 ..	4 ..	5 ..	6 ..	7 ..	8 ..	9 ..	10 .
401-	MPC	1	185	3	1.0	206	3	-1.0		
402-	MPC	1	186	1	1.0	207	1	-1.0		
403-	MPC	1	186	2	1.0	207	2	-1.0		
404-	MPC	1	186	3	1.0	207	3	-1.0		
405-	MPC	1	188	1	1.0	224	1	-1.0		
406-	MPC	1	188	2	1.0	224	2	-1.0		
407-	MPC	1	188	3	1.0	224	3	-1.0		
408-	MPC	1	189	1	1.0	225	1	-1.0		
409-	MPC	1	189	2	1.0	225	2	-1.0		
410-	MPC	1	189	3	1.0	225	3	-1.0		
411-	MPC	1	239	1	1.0	224	1	-1.0		
412-	MPC	1	239	2	1.0	224	2	-1.0		
413-	MPC	1	239	3	1.0	224	3	-1.0		&MPA1
414-	&MPA1		224	5	-1.5443					
415-	MPC	1	239	4	1.0	224	4	-1.0		
416-	MPC	1	239	5	1.0	224	5	-1.0		
417-	MPC	1	239	6	1.0	224	6	-1.0		
418-	MPC	1	240	1	1.0	225	1	-1.0		
419-	MPC	1	240	2	1.0	225	2	-1.0		
420-	MPC	1	240	3	1.0	225	3	-1.0		&MPA2
421-	&MPA2		225	5	-1.5443					
422-	MPC	1	240	4	1.0	225	4	-1.0		
423-	MPC	1	240	5	1.0	225	5	-1.0		
424-	MPC	1	240	6	1.0	225	6	-1.0		
425-	PARAM	COUPMASS1								
426-	PARAM	CTYPE	DIH							
427-	PARAM	DECOMOPT2								
428-	PARAM	G	.04							
429-	PARAM	N	12							
430-	PARAM	NLOAD	6							
431-	PBAR	201	1000	1.118	.1575	.0689	.1626			
432-	PBAR	203	1000	2.29	.2862	1.0063	.5573			
433-	PQUAD1	1	1	.64	1	2.185E-2			6.13E-5	
434-	PQUAD1	2	2	.55	2	1.386E-2			6.13E-5	
435-	PQUAD1	3	3	.3687	3	4.177E-3			4.76E-5	
436-	PQUAD1	4	4	.1971	4	6.381E-4			4.59E-5	
437-	PQUAD1	5	5	.15	5	2.813E-4			4.47E-5	
438-	PQUAD1	6	6	.1246	6	1.612E-4			4.42E-5	
439-	PQUAD1	7	7	.1	7	8.333E-5			4.42E-5	
440-	PQUAD1	8	8	.087	8	5.488E-5			4.30E-5	
441-	PQUAD1	9	9	.075	9	3.516E-5			4.19E-5	
442-	PQUAD1	10	10	.066	10	2.396E-5			4.08E-5	
443-	PQUAD1	11	11	.0622	11	2.005E-5			4.02E-5	
444-	PQUAD1	12	12	.0603	12	1.827E-5			2.94E-5	
445-	PQUA.1	13	13	.20151	13	6.819E-4			1.31E-5	
446-	PQUAD1	14	14	.20151	14	6.819E-4			1.31E-5	
447-	PQUAD1	15	15	.22896	15	1.000E-3			2.28E-5	
448-	PQUAD1	16	16	.22097	16	8.991E-4			2.11E-5	
449-	PQUAD1	17	17	.1886	17	5.590E-4			1.82E-5	
450-	PQUAD1	18	18	.16073	18	3.460E-4			9.71E-6	

TABLE 8-I (Cont)

NASTRAN BULK DATA DECK USED IN THE ANALYSIS OF THE THIRD STAGE MINUTEMAN III MOTOR

S O R T E D   B U L K   D A T A   E C H O

CARD COUNT	. 1 ..	2 ..	3 ..	4 ..	5 ..	6 ..	7 ..	8 ..	9 ..	10 .
451-	PQUAD1	19	19	.16073	19	3.460E-4			9.71E-6	
452-	PQUAD1	20	20	.1886	20	5.590E-4			1.03E-5	
453-	PQUAD1	21	21	.22097	21	8.991E-4			1.03E-5	
454-	PQUAD1	22	22	.22727	22	9.782E-4			1.54E-5	
455-	PQUAD1	23	23	.15473	23	3.087E-4			1.80E-5	
456-	PQUA 1	24	24	.24829	24	1.276E-3			1.80E-5	
457-	PQUAD1	25	25	.0605	25	1.845E-5			1.80E-5	
458-	PQUAD1	26	26	.0626	26	2.044E-5			1.74E-5	
459-	PQUAD1	27	27	.066	27	2.396E-5			2.31E-5	
460-	PQUAD1	28	28	.072	28	3.110E-5			2.60E-5	
461-	PQUAD1	29	29	.084	29	4.939E-5			3.16E-5	
462-	PQUA 1	30	30	.0991	30	8.110E-5			3.34E-5	
463-	PQUAD1	31	31	.1354	31	2.069E-4			3.85E-5	
464-	PQUAD1	32	32	.245	32	1.226E-3			5.67E-5	
465-	PQUAD1	33	33	.4095	33	5.722E-3			6.35E-5	
466-	PQUAD1	34	34	.46	34	8.111E-3			6.35E-5	
467-	PQUAD1	35	1000	.40	1000	5.333E-3				
468-	PQUA 1	36	1000	.15	1000	2.813E-4				
469-	PQUAD1	37	1000	.26	1000	1.465E-3				
470-	PQUAD1	38	1000	.67	1000	2.506E-3				
471-	PQUAD1	39	39	.06	39	1.800E-5			3.78E-5	
472-	PQUAD1	40	40	.15	40	2.813E-4			4.20E-5	
473-	PQUAD1	41	1000	.22	1000	8.873E-4			4.20E-5	
474-	PQUA 1	42	1000	.22	1000	8.873E-4			1.42E-4	
475-	PQUAD1	43	101	.1	101	8.333E-5			8.33E-5	
476-	PQUAD1	44	101	.05	101	1.042E-5			6.62E-4	
477-	PQUAD1	45	1000	.1	1000	8.333E-5				
478-	PQUAD1	46	1000	.1	1000	8.333E-5			1.39E-4	
479-	PQUAD1	47	1000	.5	1000	1.042E-2			9.38E-4	
480-	PQUA 1	48	1000	.7	1000	2.858E-2			6.83E-5	
481-	PQUAD1	49	1000	.4	1000	5.333E-3			6.83E-5	
482-	RLOAD1	101	301			1				
483-	RLOAD1	102	302			1				
484-	RLOAD1	103	303			1				
485-	RLOAD1	104	304			1				
486-	RLOAD1	105	305			1				
487-	RLOAD1	106	306			1				
488-	SPC1	1	1	1	2	5	6			
489-	SPC1	1	3	56	57					
490-	SPC1	1	6	5	6					
491-	SPC1	1	456	65	66	68	69	71	72	&SP1
492-	&SP1	74	75	77	78	83	84	86	87	&SP2
493-	&SP2	89	90	92	93	95	96	98	99	&SP3
494-	&SP3	104	105	107	108	110	111	116	117	&SP4
495-	&SP4	119	120	122	123	128	129	131	132	&SP5
496-	&SP5	134	135	140	141	143	144	146	147	&SP6
497-	&SP6	152	153	158	159	164	165	167	168	&SP7
498-	&SP7	170	171	179	180	182	183	185	186	&SP8
499-	&SP8	188	189	245	246	248	249	254	255	&SP9
500-	&SP9	257	258	263	264	266	267			

TABLE 8-I (Cont)

NASTRAN BULK DATA DECK USED IN THE ANALYSIS OF THE THIRD STAGE MINUTEMAN III MOTOR

S O R T E D   B U L K   D A T A   E C H O

CARD COUNT	. 1 ..	2 ..	3 ..	4 ..	5 ..	6 ..	7 ..	8 ..	9 ..	10 .
501-	TABLED1	1								&CL1
502-	&CL1	0.0	1.0	3000.0	1.0	ENDT				
503-	TABLED1	2000								&TR1
504-	&TR1	0.0	0.0	3.0	0.16	6.0	0.50	10.0	0.96	&TR2
505-	&TR2	15.0	1.44	20.0	1.88	40.0	3.28	60.0	4.48	&TR3
506-	&TR3	80.0	5.40	100.0	6.20	150.0	7.60	200.0	8.60	&TR4
507-	&TR4	300.0	10.20	400.0	11.40	500.0	12.0	600.0	12.80	&TR5
508-	&TR5	700.0	13.20	800.0	13.40	900.0	13.60	1000.0	14.00	&TR6
509-	&TR6	ENDT								
510-	TABLED1	2001								&TI1
511-	&TI1	0.0	0.0	3.0	0.87696	6.0	1.2175	10.0	1.60432	&TI2
512-	&TI2	15.0	1.9264	20.0	2.134	40.0	2.7456	60.0	3.26592	&TI3
513-	&TI3	80.0	3.626	100.0	3.936	150.0	4.4736	200.0	4.7912	&TI4
514-	&TI4	300.0	5.3314	400.0	5.6950	500.0	5.768	600.0	5.994	&TI5
515-	&TI5	700.0	6.08	800.0	6.0676	900.0	6.084	1000.0	6.144	&TI6
516-	&TI6	ENDT								
	ENDDATA									

TABLE 8-I (Cont)

NASTRAN BULK DATA DECK USED IN THE ANALYSIS OF THE THIRD STAGE MINUTEMAN III MOTOR

```
                                                                              JUNE   8, 1975   NASTRAN 12/ 1/73   PAGE

     N A S T R A N   E X E C U T I V E   C O N T R O L   D E C K   E C H O


ID      MM, THIRD
CHKPNT  YES
TIME    330
APP  DISP
DIAG 8,13,14
SOL  8,1  $ FREQUENCY RESPONSE
$- CYCLIC TRANSFORMATION - FREQUENCY RESPONSE ----------------------------00000010
$       12/01/73        R I G I D   F O R M A T   8  /  SERIES M          00000020
$                                                    /  RLH VERSION       00000030
$  CASE CONTROL INPUT                                                     00000040
$       A SUBCASE IS USED FOR EACH SUBSTRUCTURE AND LOADING CONDITION.    00000050
$       ALL MPC AND SPC REQUESTS MUST BE ABOVE THE SUBCASE LEVEL.         00000060
$                                                                         00000070
$  BULK DATA INPUT                                                        00000080
$          PARAMETERS USED ARE...                                         00000090
$         CTYPE %REQUIRED<   ROT # ROTATIONAL                             00000100
$                            DIH # DIHEDRAL                               00000110
$                           DSYM # DIH PLUS DEFORMATION SYMMETRY          00000120
$                           DANT # DIH PLUS DEFORMATION ANTISYMMETRY      00000130
$         N      %REQUIRED<   NUMBER OF SEGMENTS                          00000140
$         KMIN   %DEFAULT 0 < MIN RANGE OF CYCLIC INDEX K                 00000150
$         KMAX   %DEFAULT -1< MAX RANGE OF CYCLIC INDEX K %-1 IMPLIES ALL<00000160
$         CYCIO %DEFAULT &1< INPUT/OUTPUT, &1 # PHYSICAL , -1 # SYM COMP 00000170
$         CYCSEQ%DEFAULT -1< MATRIX ELEMENT SEQUENCE, 1 # SEPARATE        00000180
$                                                -1 # ALTERNATING         00000190
$         NLOAD %DEFAULT &1< NUMBER OF LOADING CONDITIONS                 00000200
$         NOKPRT%DEFAULT -1< IF &1 K WILL BE OUTPUT AT THE TOP OF LOOP    00000210
$                                                                         00000220
$         CYJOIN BULK DATA CARDS ARE REQUIRED.                            00000230
$                                                                         00000240
$       THE MODEL MUST CONTAIN K4 STRUCTURAL DAMPING %FOR FREQ DEP MATL<  00000250
$       TWO TABLEDX,TR%F< AND TI%F<, ARE SELECTED IN CASE CONTROL VIA     00000260
$       SDAMP %THE ID OF TR IS SELECTED, THE ID OF TI MUST BE ONE LARGER<00000270
$       THE STIFFNESS MATRIX %WITH STRUCTURAL DAMPING< WILL BE            00000280
$         K * % 1. & I*G < & K4 * % TR%F< & I*TI%F< <                     00000290
$          WHERE K # STIFFNESS MATRIX , G # PARAM OVERALL DAMPING         00000300
$                                                                         00000310
$ THE ANALYSIS WILL LOOP THRU A RANGE OF THE CYCLIC INDEX K # KMIN,KMAX  00000320
$                                                                         00000330
ALTER 2                                                                   00000340
FILE      UXVF*APPEND $                                                   00000350
COND      ER    ,N $  IF USER HAS NOT SPECIFIED N %DEFAULT # -1<          00000360
COND      E    ,KMAX $                                                    00000370
JUMP      F  ,N $                                                         00000380
LABEL     :ND $                                                           00000390
PARAM     //C,N,DIV/V,Y,KMAX#-1/V,Y,N/C,N,2 $                             00000400
LABEL     KNOWN $                                                         00000410
PARAM     //C,N,NOP/V,Y,CYCIO#1/V,Y,NOKPRT#-1 $                           00000420
ALTER 92                                                                  00000430
```

TABLE 8-I (Cont)

NASTRAN BULK DATA DECK USED IN THE ANALYSIS OF THE THIRD STAGE MINUTEMAN III MOTOR

N A S T R A N   E X E C U T I V E   C O N T R O L   D E C K   E C H O

```
GPCYC    GEOM4,EQDYN,USETD/CYCDD/V,Y,CTYPE/V,N,NOGO $  DATA FOR CYCT2     00000440
CHKPNT   CYCDD $                                                           00000450
ALTER 129,129 $                                                            00000460
PURGE    K2DD/NOK2PP/M2DD/NOM2PP/B2DD/NOB2PP $                             00000470
ALTER 133,133                                                              00000480
GKAD     USETD,GM,GO,KAA,BAA,MAA,    ,K2PP,M2PP,B2PP/KDD,BDD,MDD,GMD,      00000490
         GOD,K2DD,M2DD,B2DD/C,N,FREQRESP/C,N,DISP/C,N,DIRECT/C,Y,G#0.0/    00000500
         C,N,0.0/C,N,0.0/V,N,NOK2PP/V,N,NOM2PP/V,N,NOB2PP/   V,N,MPCF1/    00000510
         V,N,SINGLE/V,N,OMIT/V,N,NOUE/C,N,-1    /V,N,NOBGG/V,N,KDEK2/C,    00000520
         N,-1 $     REMOVE K4                                              00000530
ALTER 139,139 $ ACTUALLY  ALTER 139,141                                    00000540
EQUIV    K4AA,K4DD/NOUE $                                                  00000550
CHKPNT   K4DD $                                                            00000560
COND     LBLNOUE,NOUE $                                                    00000570
VEC      USETD/EPV/C,N,D/C,N,A/C,N,E $                                     00000580
MERGE    K4AA,,,,EPV,/K4DD $                                               00000590
CHKPNT   K4DD $                                                            00000600
LABEL    LBLNOUE $                                                         00000610
FRLG     CASEXX,USETD,DLT,FRL,GMD,GOD,DIT,/PPF,PSF,PDF,FOL,PHF/            00000620
         C,N,DIRECT  $  COMPUTE LOADS                                      00000630
CHKPNT   PPF,PSF,PDF,FOL  $                                                00000640
EQUIV    PPF,PDF/NOSET $                                                   00000650
CHKPNT   PDF $                                                             00000660
EQUIV    PDF,PXF/CYCIO $                                                   00000670
CHKPNT   PXF $                                                             00000680
COND     LCYC1,CYCIO $ IF %CYCIO.GE.0< TRANSFORM TO SYMMETRIC COMPONENTS00000690
CYCT1    PDF/PXF,GCYCFF/V,Y,CTYPE/C,N,FORE/V,Y,N/V,Y,KMAX/V,Y,NLOAD/       00000700
         V,Y,KMIN $                                                        00000710
CHKPNT   PXF $                                                             00000720
LABEL    LCYC1 $                                                           00000730
PARAM    //C,N,ADD/V,N,K/C,N,0/V,Y,KMIN#0 $ INITIALIZE K # KMIN            00000740
LABEL    TOPCYC $$$$$$$$$$$$$$  LOOP ON K  $$$$$$$$$$$$$$$$$$$$$$$$$$$$$$00000750
COND     NOKPRT,NOKPRT  $                                                 $00000760
PRTPARM  //C,N,0/C,N,K  $                                                 $00000770
LABEL    NOKPRT $                                                         $00000780
ALTER 140,140                                                             $00000790
CYCT2    CYCDD,KDD,MDD,PXF,BDD,K4DD/KKKF,MKKF,PKF,BKKF,K4KKF/C,N,          00000800
         FOREFREQ/V,Y,N#-1/V,N,K/V,Y,CYCSEQ#-1/V,Y,NLOAD#1/V,N,NOGO/       00000810
         V,Y,KMAX/V,Y,KMIN $                                              $00000820
CHKPNT   KKKF,MKKF,PKF,BKKF,K4KKF $                                       $00000830
FRRD1    CASEXX,DIT,KKKF,BKKF,MKKF,K4KKF,PKF,FRL,FOL/UKVF/C,N,DIRECT/      00000840
         V,N,NONCUP/C,Y,DECOMOPT#1 $                                      $00000850
CHKPNT   UKVF $                                                           $00000860
ALTER 141,141                                                             $00000870
CYCT2    CYCDD,,,UKVF,,/,,UXVF,,/C,N,BACKFREQ/V,Y,N/V,N,K/V,Y,CYCSEQ/V,    00000880
         Y,NLOAD/V,N,NOGO/V,Y,KMAX/V,Y,KMIN $                             $00000890
CHKPNT   UXVF $                                                           $00000900
PARAM    //C,N,ADD/V,N,K/V,N,K/C,N,1 $          K # K & 1                 $00000910
PARAM    //C,N,SUB/V,N,DONE/V,Y,KMAX/V,N,K $                              $00000920
COND     LCYC2,DONE $  IF%K.GT.KMAX< EXIT LOOP                            $00000930
```

TABLE 8-I (Cont)

NASTRAN BULK DATA DECK USED IN THE ANALYSIS OF THE THIRD STAGE MINUTEMAN III MOTOR

```
                                                     JUNE   8, 1975   NASTRAN 12/ 1/73    PAGE

     N A S T R A N    E X E C U T I V E    C O N T R O L   D E C K   E C H O

REPT     TOPCYC,100 $$$$$$$$$$$$$$$$$$$$$$$$$$$$$$$$$$$$$$$$$$$$$$$$$$$$$$$$$00000940
JUMP     ERROR1 $                                                        00000950
LABEL    LCYC2 $                                                         00000960
EQUIV    UXVF,UDVF/CYCIO $                                               00000970
CHKPNT   UDVF $                                                          00000980
COND     LCYC3,CYCIO $ IF %CYCIO.GE.0< TRANSFORM TO PHYSICAL VARIABLES   00000990
CYCT1    UXVF/UDVF,GCYCBF/V,Y,CTYPE/C,N,BACK/V,Y,N/V,Y,KMAX/V,Y,NLOAD/   00001000
         V,Y,KMIN $                                                      00001010
CHKPNT   UDVF $                                                          00001020
OUTPUT1 UDVF,,,,//C,N,-1/C,N,2/C,N,WANG $
$
LABEL    LCYC3 $                                                         00001030
$                                                                        00001040
ALTER 199                                                                00001050
LABEL    ERRORN $  FAILED TO SPECIFY PARAM  N.GT.0                       00001060
PRTPARM  //C,N,0/C,N,N $          END OF ALTER                           00001070
ENDALTER
CEND
```

TABLE 8-II

NASTRAN DATA DECK FOR THE INJECTANT TANK COMPONENT


```
N A S T R A N   E X E C U T I V E   C O N T R O L   D E C K   E C H O

ID INJFCT, TANK
SOL 8,1
DIAG 8,13,14,21,22,1
TIME 30
APP DISP
ALTER 141
MPYAD    PDF,UDVF,/RMATB2/C,N,1  $
MATPRN   UDVF,PDF,RMATB2,,//     $
SOLVE    RMATB2,/RIMATB2/C,N,0/C,N,1/C,N,2/C,N,3  $
MATPRN   RIMATB2,,,,//    $
OUTPUT1  RIMATB2,,,,//C,N,-1/C,N,2/C,N,BMTAP2    $
INPUTT1  /,,,,/C,N,-3/C,N,2/C,N,BMTAP2   $
ENDALTER
CEND
```

TABLE 8-II (Cont)

NASTRAN DATA DECK FOR THE INJECTANT TANK COMPONENT

```
MMIII   INJECTANT TANK                                                  JULY  11, 1975   NASTRAN 12/ 1/73    PAGE
INVERSE RECEPTANCE MATRIX CALCUL-TION

                                   C A S E   C O N T R O L   D E C K   E C H O
          CARD
          COUNT
           1       TITLE # MMIII   INJECTANT TANK
           2       SUBTITLE # INVERSE RECEPTANCE MATRIX CALCULATION
           3       FREQ # 1
           4       SPC  #  1
           5       OUTPUT
           6       DISP # ALL
           7       SUBCASE 1
           8       LABEL # 1ST LOAD
           9               DLOAD # 1
          10       SUBCASE 2
          11       LABEL # 2ND LOA'
          12               DLOAD # 2
          13       SUBCASE 3
          14       LABEL # 3RD LOAD
          15               DLOAD # 3
          16       SUBCASE 4
          17       LABEL # 4TH LOA'
          18               DLOAD # 4
          19       SUBCASE 5
          20       LABEL # 5TH LOAD
          21               DLOAD # 5
          22       SUBCASE 6
          23       LABEL # 6TH LOA'
          24               DLOAD # 6
          25       SUBCASE 7
          26       LABEL # 7TH LOAD
          27               DLOAD # 7
          28       SUBCASE 8
          29       LABEL # 8TH LOAD
          30               DLOAD #8
          31       SUBCASE 9
          32       LABEL # 9TH LOAD
          33               DLOAD # 9
          34       SUBCASE 10
          35       LABEL  # 10TH LOAD
          36               DLOAD #10
          37       SUBCASE 11
          38       LABEL #11TH LAOD
          39               DLOAD # 11
          40       SUBCASE 12
          41       LABEL #12TH LOA:
          42               DLOAD # 12
          43       BEGIN BULK

*** USER INFORMATION MESSAGE 207- BULK DATA NOT SORTED,XSORT WILL RE-ORDER DECK.
```

TABLE 8-II (Cont)

NASTRAN DATA DECK FOR THE INJECTANT TANK COMPONENT

MMII1 INJECTANT TANK
INVERSE RECEPTANCE MATRIX CALCULATION

JULY 11, 1975 NASTRAN 12/31/73 PAGE 3

S O R T E D B U L K D A T A E C H O

CARD COUNT	. 1 ..	2 ..	3 ..	4 ..	5 ..	6 ..	7 ..	8 ..	9 ..	10 .
1-	CBAR	1	101	1	5	51			2	
2-	CBAR	2	101	5	6	4.0	.0	.5	1	
3-	CBAR	3	101	6	7	5.0	.0	1.2	1	
4-	CBAR	4	101	7	8	7.0	.0	2.0	1	
5-	CBAR	5	101	8	9	8.0	.0	4.0	1	
6-	CBAR	6	101	9	4	9.0	.0	6.0	1	
7-	CBAR	7	101	4	10	41			2	
8-	CBAR	8	101	10	11	7.0	.0	10.0	1	
9-	CBAR	9	101	11	12	5.0	.0	11.0	1	
10-	CBAR	10	101	12	13	4.0	.0	12.0	1	
11-	CBAR	11	101	13	2	1.5	.0	12.0	1	
12-	CBAR	15	101	1	50	510			2	
13-	CBAR	20	101	50	60	4.0	.0	.5	1	
14-	CBAR	30	101	60	70	5.0	.0	1.2	1	
15-	CBAR	40	101	70	80	7.0	.0	2.0	1	
16-	CBAR	50	101	80	90	8.0	.0	4.0	1	
17-	CBAR	60	101	90	3	9.0	.0	6.0	1	
18-	CBAR	70	101	3	100	410			2	
19-	CBAR	80	101	100	110	7.0	.0	10.0	1	
20-	CBAR	90	101	110	120	5.0	.0	11.0	1	
21-	CBAR	100	101	120	130	4.0	.0	12.0	1	
22-	CBAR	110	101	130	2	1.5	.0	12.0	1	
23-	CBAR	1001	1000	1	1000	1003			2	
24-	CBAR	1002	1000	2	1000	1003			2	
25-	CONM2	100012	1000	1	.1545					&C10012
26-	&C10012	.881		.881			.881			
27-	CORD1R	2	1	2	4					
28-	CORD1R	2	1	2	3					
29-	CORD2C	1	0	.0	.0	.0	.0	.0	1.0	&222
30-	&222	1.0	0.0	0.0						
31-	DAREA	10	3	1	1.0					
32-	DAREA	20	3	2	1.0					
33-	DAREA	30	3	3	1.0					
34-	DAREA	40	3	4	1.0					
35-	DAREA	50	3	5	1.0					
36-	DAREA	60	3	6	1.0					
37-	DAREA	70	4	1	1.0					
38-	DAREA	80	4	2	1.0					
39-	DAREA	90	4	3	1.0					
40-	DAREA	100	4	4	1.0					
41-	DAREA	110	4	5	1.0					
42-	DAREA	120	4	6	1.0					
43-	FREQ	1	200.							
44-	FREQ	3	300.							
45-	FREQ	4	760.							
46-	FREQ	5	800.							
47-	FREQ	6	840.							
48-	GRID	1	1	13.63	181.5	83.78	1			
49-	GRID	2	1	19.86	181.5	72.12	1			
50-	GRID	3	1	12.31	165.	76.47	1			

TABLE 8-II (Cont)

NASTRAN DATA DECK FOR THE INJECTANT TANK COMPONENT

```
MMIII    INJECTANT TANK                                                  JULY  11, 1975   NASTRAN 12/ 1/73    PAGE
INVERSE RECEPTANCE MATRIX CALCULATION

                                  S O R T E D   B U L K   D A T A   E C H O
 CARD
 COUNT        .  1  ..  2  ..  3  ..  4  ..  5  ..  6  ..  7  ..  8  ..  9  ..  10  .
   51-        GRID    4       1               12.31   195.    76.47   1
   52-        GRID    5       2               2.2     0.0     .45     1
   53-        GRID    6       2               4.0     .0      1.1     1
   54-        GRID    7       2               5.6     .0      2.0     1
   55-        GRID    8       2               7.1     .0      3.3     1
   56-        GRID    9       2               7.65    .0      5.1     1
   57-        GRID    10      2               7.5     .0      8.6     1
   58-        GRID    11      2               6.0     .0      9.0     1
   59-        GRID    12      2               4.2     .0      10.7    1
   60-        GRID    13      2               2.3     0.0     11.2    1
   61-        GRID    41      2               9.0     .0      8.0     1
   62-        GRID    50      3               2.2     0.0     .45     1
   63-        GRID    51      2               1.0     .0      .0      1
   64-        GRID    60      3               4.0     .0      1.1     1
   65-        GRID    70      3               5.6     .0      2.0     1
   66-        GRID    80      3               7.1     .0      3.3     1
   67-        GRID    90      3               7.8     .0      5.1     1
   68-        GRID    100     3               7.5     .0      8.6     1
   69-        GRID    110     3               6.0     .0      9.0     1
   70-        GRID    120     3               4.2     .0      10.7    1
   71-        GRID    130     3               2.3     0.0     11.2    1
   72-        GRID    410     3               9.0     .0      8.0     1
   73-        GRID    510     3               1.0     .0      .0      1
   74-        GRID    1000    1               18.94   181.5   79.10   1
   75-        GRID    1003    1               19.0    296.5   79.1    1
   76-        MAT1    101     16.E6                   .3
   77-        MAT1    1000    1.E12                   .3
   78-        PBAR    101     101             .356    .011    .034    .0098
   79-        PBAR    1000    1000            .356    100.    100.    50.
   80-        RLOAD1  1       10                              3
   81-        RLOAD1  2       20                              3
   82-        RLOAD1  3       30                              3
   83-        RLOAD1  4       40                              3
   84-        RLOAD1  5       50                              3
   85-        RLOAD1  6       60                              3
   86-        RLOAD1  7       70                              3
   87-        RLOAD1  8       80                              3
   88-        RLOAD1  9       90                              3
   89-        RLOAD1  10      100                             3
   90-        RLOAD1  11      110                             3
   91-        RLOAD1  12      120                             3
   92-        SPC1    1       123456  1003    41      51      410     510
   93-        TABLED1 3                                                               &TB3
   94-        &TB3    -1000.  1.0     2000.   1.0     ENDT
              ENDDATA
```

TABLE 8-III

NASTRAN DATA DECK FOR THE PRESSURANT TANK COMPONENT

JULY 8, 1975 NASTRAN 5/13/72 PAGE 1

```
N A S T R A N   E X E C U T I V E   C O N T R O L   D E C K   E C H O

ID PRESSU, TANK
SOL 8,1
DIAG 8,13,14,21,22
TIME 30
APP DISP
ALTER 141
MPYAD   PDF,UDVF,/RMATB3/C,N,1  $
MATPRN  UDVF,PDF,RMATB3,,//     $
SOLVE   RMATB3,/RIMATB3/C,N,0/C,N,1/C,N,2/C,N,3  $
MATPRN  RIMATB3,,,,//    $
OUTPUT1 RIMATB3,,,,//C,N,-1/C,N,2/C,N,BMTAP3    $
INPUTT1 /,,,,/C,N,-3/C,N,2/C,N,BMTAP3   $
ENDALTER
CEND
```

TABLE -III (Cont)

NASTRAN DATA DECK FOR THE PRESSURANT TANK COMPONENT

```
MMIII PRESSURANT TANK                                                    JULY   8, 1975   NASTRAN  5/13/72    PAGE
INVERSE RECEPTANCE MATRIX CALCULATION


                              C A S E   C O N T R O L   D E C K   E C H O
        CARD
        COUNT
          1      TITLE # MMIII PRESSURANT TANK
          2      SUBTITLE # INVERSE RECEPTANCE MATRIX CALCULATION
          3      SPC # 1
          4      FREQ # 1
          5      OUTPUT
          6      DISP # ALL
          7      SUBCASE 1
          8      LABEL # 1ST LOAD
          9              DLOAD # 1
         10      SUBCASE 2
         11      LABEL # 2ND LOAD
         12              DLOAD # 2
         13      SUBCASE 3
         14      LABEL # 3RD LOAD
         15              DLOAD # 3
         16      SUBCASE 4
         17      LABEL # 4TH LOAD
         18              DLOAD # 4
         19      SUBCASE 5
         20      LABEL # 5TH LOAD
         21              DLOAD # 5
         22      SUBCASE 6
         23      LABEL # 6TH LOAD
         24              DLOAD # 6
         25      SUBCASE 7
         26      LABEL # 7TH LOAD
         27              DLOAD # 7
         28      SUBCASE 8
         29      LABEL # 8TH LOAD
         30              DLOAD #8
         31      SUBCASE 9
         32      LABEL # 9TH LOAD
         33              DLOAD # 9
         34      SUBCASE 10
         35      LABEL  # 10TH LOAD
         36              DLOAD #10
         37      SUBCASE 11
         38      LABEL #11TH LOAD
         39              DLOAD # 11
         40      SUBCASE 12
         41      LABEL #12TH LOAD
         42              DLOAD # 12
         43      BEGIN BULK


*** USER INFORMATION MESSAGE 207, BULK DATA NOT SORTED,XSORT WILL RE-ORDER DECK.
```

TABLE 8-III (Cont)

NASTRAN DATA DECK FOR THE PRESSURANT TANK COMPONENT

MMIII PRESSURANT TANK   JULY 8, 1975   NASTRAN 5/13/72   PAGE 3
INVERSE RECEPTANCE MATRIX CALCULATION

S O R T E D   B U L K   D A T A   E C H O

CARD COUNT	1	2	3	4	5	6	7	8	9	10
1-	CBAR	105	100	5	10	51			2	
2-	CBAR	116	100	6	11	61			2	
3-	CBAR	711	10	7	11	71			2	
4-	CBAR	810	10	8	10	81			2	
5-	CBAR	2005	100	5	200	2001			2	
6-	CBAR	2006	100	6	200	2001			2	
7-	CONM2	200	200	1	.0313					&CM
8-	&CM	.429		.429			.429			
9-	CORD2C	1	0	.0	.0	.0	.0	.0	1.	&222
10-	&222	1.0	0.0	0.0						
11-	DAREA	10	7	1	1.0					
12-	DAREA	20	7	2	1.0					
13-	DAREA	30	7	3	1.0					
14-	DAREA	40	7	4	1.0					
15-	DAREA	50	7	5	1.0					
16-	DAREA	60	7	6	1.0					
17-	DAREA	70	8	1	1.0					
18-	DAREA	80	8	2	1.0					
19-	DAREA	90	8	3	1.0					
20-	DAREA	100	8	4	1.0					
21-	DAREA	110	8	5	1.0					
22-	~~DAREA~~	~~120~~	8	6	1.0					
23-	FREQ	1	200							
24-	~~FREQ~~	~~3~~	~~300.~~							
25-	FREQ	4	760.							
26-	FREQ	5	800.							
27-	FREQ	6	840.							
28-	GRID	5	1	20.52	241.0	78.26	1			
29-	GRID	6	1	20.52	209.	78.26	1			
30-	GRID	7	1	12.31	215.	76.47	1			
31-	GRID	8	1	12.31	235.0	76.47	1			
32-	GRID	10	1	19.005	240.29	77.93	1			
33-	GRID	11	1	19.005	209.71	77.93	1			
34-	GRID	51	1	20.52	241.	78.15	1			
35-	GRID	61	1	20.52	209.	78.15	1			
36-	GRID	71	1	12.31	215.	76.35	1			
37-	GRID	81	1	12.31	235.	76.35	1			
38-	GRID	200	1	19.8	225.	78.26	1			
39-	GRID	2001	1	19.80	225.	78.15	1			
40-	MAT1	10	1.&7		.3					
41-	MAT1	100	1.&12		.3					
42-	PARAM	GRDPNT	200							
43-	PBAR	10	10	.34	.23	.086	7.38-4			
44-	PBAR	100	100	.34	100.	100.	30.			
45-	RLOAD1	1	10			3				
46-	RLOAD1	2	20			3				
47-	RLOAD1	3	30			3				
48-	RLOAD1	4	40			3				
49-	RLOAD1	5	50			3				
50-	RLOAD1	6	60			3				

TABLE 8-III (Cont)

NASTRAN DATA DECK FOR THE PRESSURANT TANK COMPONENT

```
MMIII PRESSURANT TANK                                                  JULY   8, 1975   NASTRAN  5/13/72    PAGE
INVERSE RECEPTANCE MATRIX CALCULATION

                                 S O R T E D   B U L K   D A T A   E C H O
CARD
COUNT        .  1  ..  2  ..  3  ..  4  ..  5  ..  6  ..  7  ..  8  ..  9  ..  10  .
  51-        RLOAD1  7       70                      3
  52-        RLOAD1  8       80                      3
  53-        RLOAD1  9       90                      3
  54-        RLOAD1  10      100                     3
  55-        RLOAD1  11      110                     3
  56-        RLOAD1  12      120                     3
  57-        SPC1    1       123456  81      71      61      51      2001
  58-        TABLED1 3                                                               &TB3
  59-        &TB3    -1000.  1.0     2000.   1.0     ENDT
             ENDDATA
```

TABLE 8-IV

NASTRAN DATA DECK FOR THE AUTONETICS PACKAGE COMPONENT

```
                                                       JULY   9, 1975   NASTRAN 12/ 1/73   PAGE   1

     N A S T R A N   E X E C U T I V E   C O N T R O L   D E C K   E C H O

ID AUTONEPD, FREQ
SOL 8,1
DIAC 8,13,14,21,22
TIME 30
APP DISP
ALTER 141
MPYAD    PDF,UDVF,/RMATB1/C,N,1  $
MATPRN   UDVF,PDF,RMATB1,,//     $
SOLVE    RMATB1,/RIMATB1/C,N,0/C,N,1/C,N,2/C,N,3  $
MATPRN   RIMATB1,,,,//    $
OUTPUT1 RIMATB1,,,,//C,N,-1/C,N,2/C,N,BMTAP1    $
INPUTT1 /,,,,/C,N,-3/C,N,2/C,N,BMTAP1   $
ENDALTER
CEND
```

TABLE 8-IV (Cont)

NASTRAN DATA DECK FOR THE AUTONETICS PACKAGE COMPONENT

```
MMIII   AUTONETICS PACKAGE MODEL                                      JULY   9, 1975   NASTRAN 12/ 1/73   PAGE
INVERSE RECEPTANCE MATRIX CALCULATION

                                C A S E   C O N T R O L   D E C K   E C H O
      CARD
      COUNT
        1       TITLE = M III   AUTONETICS PACKAGE MODEL
        2       SUBTITLE = INVERSE RECEPTANCE MATRIX CALCULATION
        3       FREQ = 1
        4       SPC  =  1
        5       MPC = 1
        6       OUTPUT
        7       DISP = ALL
        8       SUBCASE 1
        9       LABEL = 1ST LOAD
       10                 DLOAD = 1
       11       SUBCASE 2
       12       LABEL = 2ND LOAD
       13                 DLOAD = 2
       14       SUBCASE 3
       15       LABEL = 3RD LOAD
       16                 DLOAD = 3
       17       SUBCASE 4
       18       LABEL = 4TH LOAD
       19                 DLOAD = 4
       20       SUBCASE 5
       21       LABEL = 5TH LOAD
       22                 DLOAD = 5
       23       SUBCASE 6
       24       LABEL = 6TH LOAD
       25                 DLOAD = 6
       26       SUBCASE 7
       27       LABEL = 7TH LOAD
       28                 DLOAD = 7
       29       SUBCASE 8
       30       LABEL = 8TH LOAD
       31                 DLOAD =8
       32       SUBCASE 9
       33       LABEL = 9TH LOAD
       34                 DLOAD = 9
       35       SUBCASE 10
       36       LABEL  = 10TH LOAD
       37                 DLOAD =10
       38       SUBCASE 11
       39       LABEL =11TH LOAD
       40                 DLOAD = 11
       41       SUBCASE 12
       42       LABEL =12TH LOAD
       43                 DLOAD = 12
       44       BEGIN BULK

*** USER INFORMATION MESSAGE 207, BULK DATA NOT SORTED.XSORT WILL RE-ORDER DECK.
```

TABLE 8-IV (Cont)

NASTRAN DATA DECK FOR THE AUTONETICS PACKAGE COMPONENT

S O R T E D   B U L K   D A T A   E C H O

CARD COUNT	. 1 ..	2 ..	3 ..	4 ..	5 ..	6 ..	7 ..	8 ..	9 ..	10 .
1-	CBAR	119	119	9	11	500			2	
2-	CBAR	1210	119	10	12	500			2	
3-	CELAS2	331	1000.	9	4					
4-	CELAS2	332	1000.	10	4					
5-	CONM2	498	10	1	1.16-3					&C498
6-	&C498	1.38-2		3.675-3			1.718-2			
7-	CONM2	499	9	1	1.16-3					&C499
8-	&C499	1.38-2		3.675-3			1.718-2			
9-	CONM2	5000	500	1	.0465					&CN2
10-	&CN2	.554		.147			.687			
11-	CORD2C	1	0	0.0	0.0	0.0	0.0	0.0	1.	&RTZ
12-	&RTZ	1.0	0.	0.						
13-	DAREA	10	9	1	1.0					
14-	DAREA	20	9	2	1.0					
15-	DAREA	30	9	3	1.0					
16-	DAREA	40	9	4	1.0					
17-	DAREA	50	9	5	1.0					
18-	DAREA	60	9	6	1.0					
19-	DAREA	70	10	1	1.0					
20-	DAREA	80	10	2	1.0					
21-	DAREA	90	10	3	1.0					
22-	DAREA	100	10	4	1.0					
23-	DAREA	110	10	5	1.0					
24-	DAREA	120	10	6	1.0					
25-	FREQ	1	200.							
26-	FREQ	3	300.							
27-	FREQ	4	760.							
28-	FREQ	5	800.							
29-	FREQ	6	840.							
30-	GENEL	911		11	1	11	2	11	3	&E11
31-	&E11	11	5							&E12
32-	&E12	UD		9	1	9	2	9	3	&E13
33-	&E13	9	5	9	6					&E14
34-	&E14	Z	.921-6	0.	0.	0.0	54.4-6	0.0	0.0	&E15
35-	&E15	23.5-6	-6.87-6	2.1875-6						&E16
36-	&E16	S	1.0	0.	0.	0.	0.	0.	1.0	&E17
37-	&E17	0.	0.	54.89	0.	0.	1.0	-4.89	0.	&E18
38-	&E18	0.	0.	0.	1.	0.				
39-	GENEL	1012		12	1	12	2	12	3	&E21
40-	&E21	12	5							&E22
41-	&E22	UD		10	1	10	2	10	3	&E23
42-	&E23	10	5	10	6					&E24
43-	&E24	Z	.921-6	0.	0.	0.0	54.4-6	0.0	0.0	&E25
44-	&E25	23.5-6	-6.87-6	2.1875-6						&E26
45-	&E26	S	1.0	0.	0.	0.	0.	0.	1.0	&E27
46-	&E27	0.	0.	54.89	0.	0.	1.0	-4.89	0.	&E28
47-	&E28	0.	0.	0.	1.0	0.				
48-	GRID	9	1	12.31	.0	76.47	1			
49-	GRID	10	1	12.31	40.	76.47	1			
50-	GRID	11	1	17.20	.0	76.47	1			

TABLE 8-IV (Cont)

NASTRAN DATA DECK FOR THE AUTONETICS PACKAGE COMPONENT

MMIII AUTONETICS PACKAGE MODEL   JULY 9, 1975   NASTRAN 12/ 1/73   PAGE
INVERSE RECEPTANCE MATRIX CALCULATION

S O R T E D   B U L K   D A T A   E C H O

CARD COUNT	. 1 ..	2 ..	3 ..	4 ..	5 ..	6 ..	7 ..	8 ..	9 ..	10 .
51-	GRID	12	1	17.20	40.	76.47	1			
52-	GRID	500	1	17.20	20.	76.47	1			
53-	MAT1	119	1.&7		.3					
54-	MPC	1	11	1	1.0	500	1	-.93969		&M111
55-	&M111		500	2	&.34202	500	6	-5.88		
56-	MPC	1	11	2	1.0	500	1	-.34202		&M112
57-	&M112		500	2	-.93969	500	6	-1.038		
58-	MPC	1	11	3	1.0	500	3	-1.0		&M113
59-	&M113		500	4	5.97	500	5	-1.038		
60-	MPC	1	11	5	1.0	500	4	-.34202		&M114
61-	&M114		500	5	-.93969					
62-	MPC	1	11	6	1.	500	6	-1.		
63-	MPC	1	12	1	1.0	500	1	-.93969		&M121
64-	&M121		500	2	-.34202	500	6	&5.88		
65-	MPC	1	12	2	1.0	500	1	&.34202		&M122
66-	&M122		500	2	-.93969	500	6	-1.038		
67-	MPC	1	12	3	1.0	500	3	-1.0		&M123
68-	&M123		500	4	-5.88	500	5	-1.038		
69-	MPC	1	12	5	1.0	500	4	&.34202		&M124
70-	&M124		500	5	-.93969					
71-	MPC	1	12	6	1.	500	6	-1.		
72-	PARAM	COUPMASS1								
73-	PARAM	GRDPNT	500							
74-	PBAR	119	119		.069					
75-	RLOAD1	1	10			3				
76-	RLOAD1	2	20			3				
77-	RLOAD1	3	30			3				
78-	RLOAD1	4	40			3				
79-	RLOAD1	5	50			3				
80-	RLOAD1	6	60			3				
81-	RLOAD1	7	70			3				
82-	RLOAD1	8	80			3				
83-	RLOAD1	9	90			3				
84-	RLOAD1	10	100			3				
85-	RLOAD1	11	110			3				
86-	RLOAD1	12	120			3				
87-	SPC1	1	4	11	12					
88-	TABLED1	3								&TB3
89-	&TB3	-1000.	1.0	2000.	1.0	ENDT				
	ENDDATA									

D. EVALUATION OF VERIFICATION MOTOR ANALYSIS RESULTS

The Aerojet acoustics study final report[1] contains a considerable amount of accelerometer data. A summary of the data is given in the figures on pages 17 and 18 of the referenced report. The data from page 17 is reproduced here as Figure 8-3 for ease of reference. The upper graph in Figure 8-3 shows how the maximum envelope acceleration varies with radial distance along the forward dome for the first tangential mode. The lower graph of Figure 8-3 shows the corresponding data for the first longitudinal mode.

To put the accelerometer data in a better form for comparison with analysis results, two different times were selected for each acoustic mode and the acceleration level was replotted as a function of radius at each time for each mode. For the first longitudinal mode, burn times of 6 seconds and 8 seconds were selected. The data for 6 seconds and 8 seconds were plotted in Figure 8-4 as a function of radius. The closed envelope predictions were also plotted in Figure 8-4. The geometry of the advanced burn NASTRAN model was designed to be most accurate at 6 seconds. The maximum response to the longitudinal mode occurred at 240 Hz; therefore, the 240 Hz analysis results were plotted for comparison with the accelerometer data. Data in the closed envelope predictions were given for a maximum acoustic mode pressure of 1.0 psi. The MSC/ASPC analysis was conducted by using a value of 2.03 psi for the maximum pressure of the longitudinal mode[2]. Therefore, the closed envelope predictions for the 240 Hz mode were multiplied by 2.0 to obtain response at a 2 psi level for comparison with accelerometer data in Figure 8-4.

The shapes of the plots for measured and predicted levels shown in Figure 8-4 are similar as all plots are somewhat bell-shaped with a maximum at about 14.0 inches radius. The predicted maximum amplitude compares quite well with measured maximum amplitudes. If the Task I error limits were applied, calculated values would be multiplied by 1.94 for comparison with measured maximum values. Using the error limits, the predicted maximum of about 50 g's includes the measured maximums of less than 30 g's. These comparisons for the longitudinal mode analysis results are considered to be good, even though predicted levels at radii less than 12 inches and greater than 17 inches appear to be too low.

For the first tangential mode, burn times of 1/2 second and 1 second were selected for crossplotting of the data from Figure 8-3. The crossplotted accelerometer envelope data are shown in Figure 8-5. Plots for the tangential mode are different from plots for the longitudinal mode

---

[1] Ibid, pg 17 and 18.

[2] Ibid, pg 119.

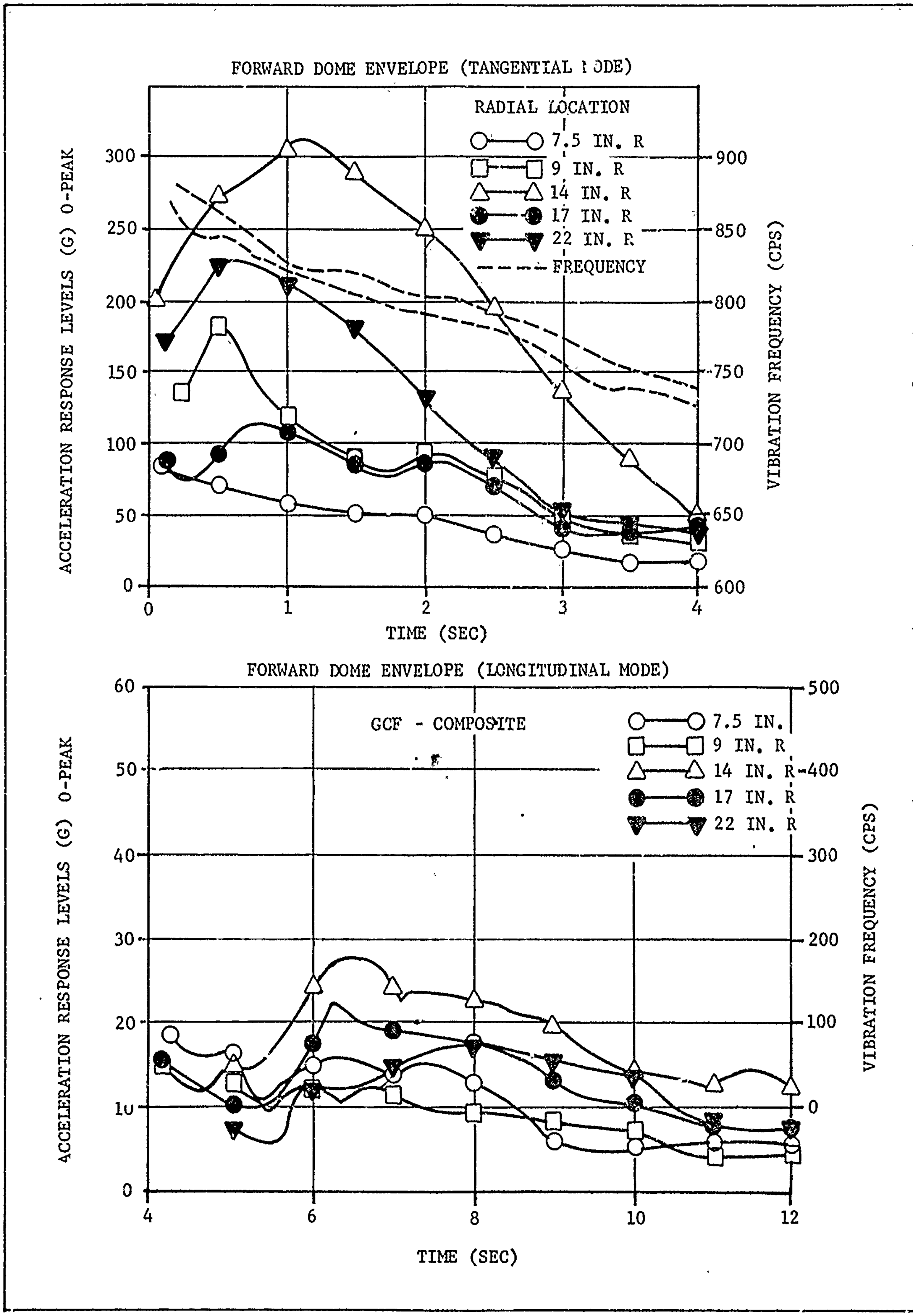

Figure 8-3. Accelerometer Data for the Minuteman III Motor Taken From Reference 1

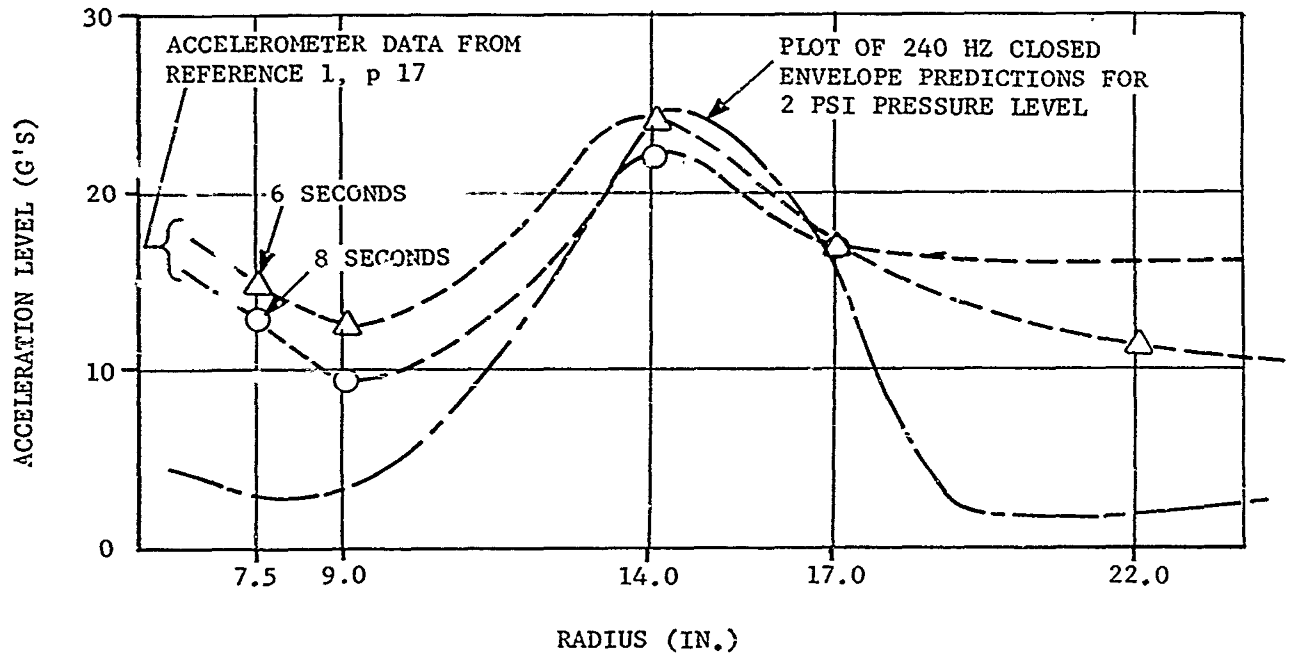

Figure 8-4. Accelerometer Data Compared with Closed Envelope Predicted Levels for the First Longitudinal Mode

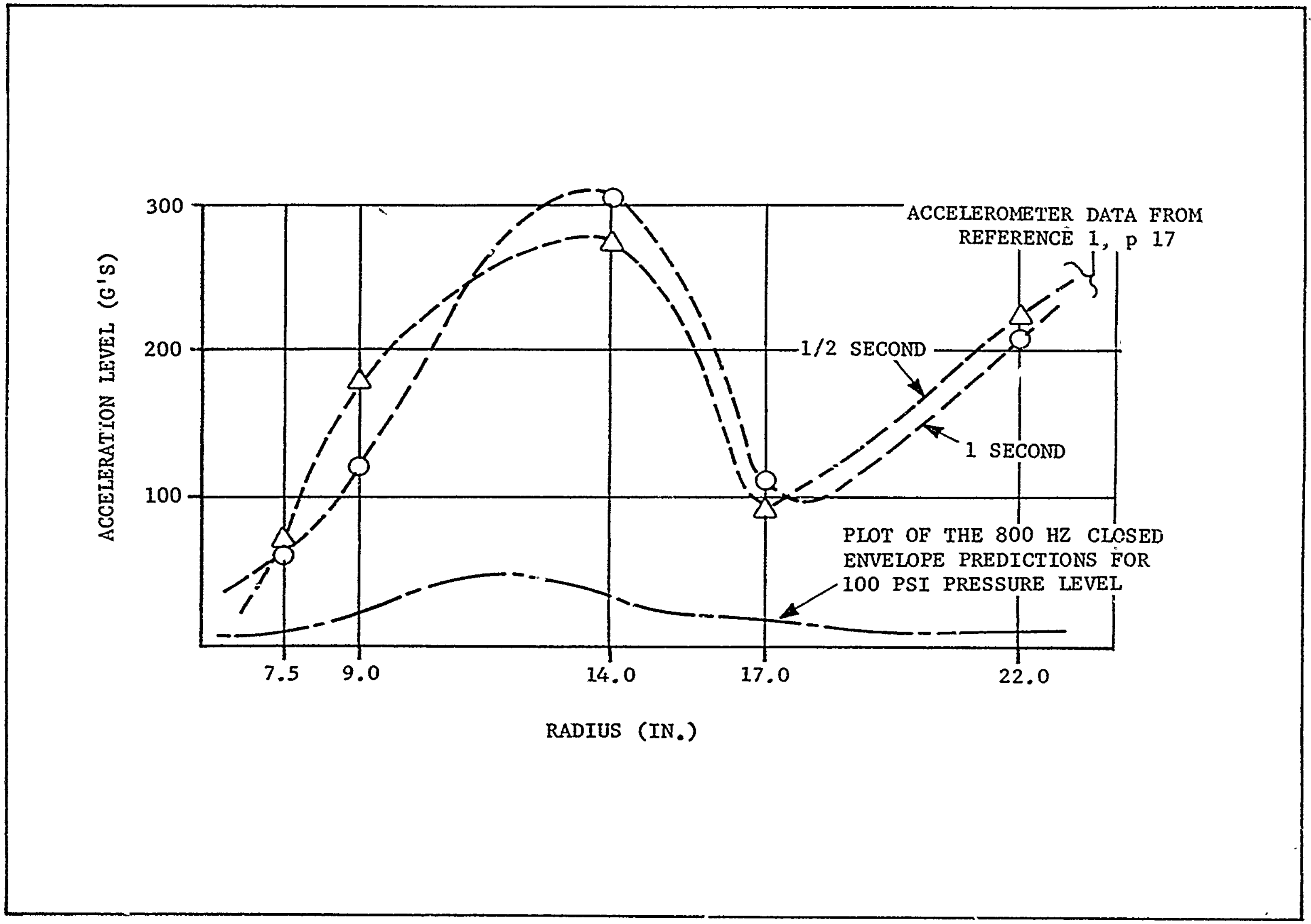

Figure 8-5. Accelerometer Data Compared with Closed Envelope Predicted Levels for the First Tangential Mode

because both loading distributions and frequencies are different. Due to the nature of the tangential mode, the motor centerline should be a node in the response mode shape. The accelerometer data shown in Figure 8-5 appear to approach zero for small radii and increase to reach a maximum at 14.0 inches. The maximum calculated response to the tangential mode occurred at 800 Hz. Therefore, the 800 Hz closed envelope predictions were plotted in Figure 8-5 for comparison with the measured data. The closed envelope predictions show a peak at a radius of 12 inches with a magnitude only slightly over 40 g's. The measured data envelope has a peak over 300 g's.

As a result of the poor agreement between accelerometer data and closed envelope predictions for the tangential mode, the AFRPL requested that the tangential mode solution be studied to determine reasons for the noted discrepancies.

Examination of the curves in Figure 8-3 shows that the response is at a maximum between 1 and 1-1/2 seconds for the tangential acoustic mode. The loads applied to the model were calculated based on a zero burn time geometry. The pressure distribution for the tangential mode has a maximum value of 100 psi at the slot tips and smaller values at the centerbore. An increase in slot tip area due to advanced burn time results in significantly greater forces being applied to the NASTRAN model.

Another computer run was made to calculate the response of the model to an 840 Hz tangential mode. The following changes were made with respect to the configuration used to obtain the closed envelope predictions: (1) Increased loads were applied to correspond to a 1-1/2 second burn time, (2) an error in the bulk data deck that resulted in use of a low grain modulus was corrected, and (3) the scalar springs were removed from the dome cavity. The frequency of 840 Hz was used because of the possibility that the stiffer grain would cause a maximum response at 840 Hz instead of 800 Hz. The grain shear modulus was increased from 500 to 3900 psi through correction of the error. The scalar spring elements were removed from the model to ensure that the springs did not restrict the dome response. Results from the analysis showed very low dome accelerations, a peak of 14 g's at a 10 inch radius, and another peak of 15-1/2 g's at a 22-inch radius. Some points on the grain exhibited accelerations greater than 200 g's.

A second modified computer run was made in an attempt to obtain higher dome accelerations. Examination of the previous run results indicated the need for a more direct load path to transmit grain motions to the case. The radial-to-axial motion transfer discussed in Phase II is apparently not very effective for this tangential mode. The following changes were made for the second modified computer run: (1) The scalar springs were installed, (2) the frequency was changed to 800 Hz, (3) the 1-1/2 second load system was applied, (4) forces were applied to the igniter, and (5) the pair of springs connecting the dome to the grain nearest to the igniter were stiffened considerably to model friction between the grain and the igniter. Forces on the igniter due to the acoustic pressure mode had been inadvertently omitted from previous runs. Forces applied to the igniter are effective in driving the dome because they are not transmitted through the propellant. The forward dome cavity is considered to be sealed off from the main combustion cavity because the grain is forced down around the igniter. While the grain is forced around the igniter, a friction force would tend to restrict relative motion between the grain and the igniter in the axial direction. This friction force was modeled in a crude way by increasing the stiffness of the pair of scalar springs nearest to the igniter.

Results from the second modified computer run showed a dramatic increase in the acceleration levels on the forward dome. The levels are plotted as a function of radius in Figure 8-6. A peak acceleration level of 307 g's was predicted at a radius of 10 inches. The curve has three peaks. The shape of the curve does not correspond to the shape of the measured responses. The conclusion from this analysis is that forces that occur during the 100 psi tangential mode are sufficient to cause accelerations on the dome in the 200 to 300 g range. The discrepancy between calculated and measured acceleration distributions is probably due to poor modeling of load transmission from combustion cavity to dome. No attempt was made to obtain a more accurate load transmission model.

The evaluation of the Minuteman motor did not follow the pattern used for evaluation of the Poseidon motor because the accelerometer data were available in a different form. The pressure oscillation levels were assumed to be 2 psi for the longitudinal mode and 100 psi for the tangential mode in accordance with the Aerojet report[1]. No pressure oscillation data were examined. No attempt was made to evaluate the aft dome response predictions because no filtered data were available. The forward dome data were reported to be sinusoidal and therefore not in need of filtering.

---

[1] Ibid.

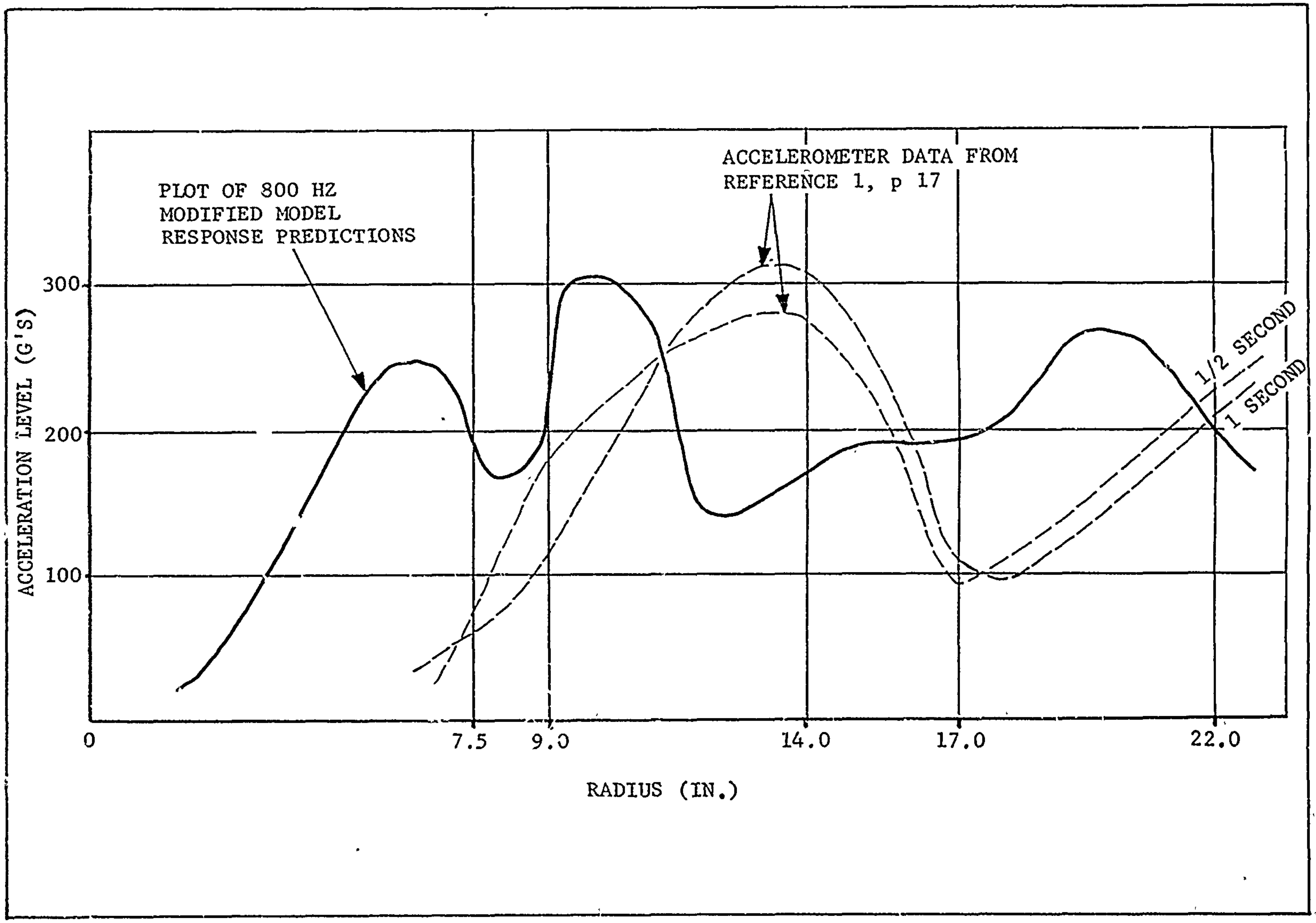

Figure 8-6. Accelerometer Data Compared with Modified Model Response Predictions

SECTION IX

SUMMARY, CONCLUSIONS, AND RECOMMENDATIONS

A. TASK 1

The objective of Task 1 was to select a baseline motor. Application of specified criteria to three candidate motors resulted in the conclusion that either the Minuteman III third stage or the Poseidon C-3 second stage motors could be satisfactorily used as baseline. The Poseidon motor was selected mainly because an inert motor was available for acoustics testing and because of the Hercules familiarity with the C-3 design.

A secondary objective of Task 1 was to establish error limits for use in evaluation of analysis results. This work resulted in the recommendation that an error limit of 1.94 times the calculated value be used. If the analysis was satisfactorily accurate, 95 percent of the test data (maximum acceleration at a point) would be lower than the error limit.

B. TASK 2

The objective of Task 2 was to define the acoustic natural modes and frequencies of the baseline motor. No acoustic analyses were performed because a review of existing experimental data and analysis results indicated that acoustic modes and frequencies were already sufficiently well defined. Based on the review of existing information, the required number of acoustic modes were selected and defined for use as loads in the structural analysis.

C. TASK 4

The objective of Task 4 was to provide experimental data on structural response to acoustic loads. The testing program was considered to be successful. The following conclusions were reached as a result of the Task 4 work:

(1) A vertical testing attitude and motor pressurization are necessary in the testing to obtain separation between the propellant and a motor dome.

(2) Double-backed adhesive tape provides a satisfactory accelerometer mounting system for the low acceleration levels encountered in the tests.

(3) A loudspeaker placed in the centerbore of a sealed motor cavity can excite acoustic cavity modes which, in turn, cause a structural response at a measurable level.

(4) Different gases can be used in the motor cavity to obtain different natural frequencies for the same acoustic mode shapes. The change of frequencies is useful to separate structural resonances in the test data.

(5) The test procedure used in Task 4 can be recommended to characterize motor structural response to well-defined acoustic mode loading conditions.

D. TASK 5

The objective of Task 5 was to evaluate the results of the baseline motor analysis. The results were evaluated in two different ways:

(1) Analytical results were compared with measured static firing data.

(2) Analytical results were compared with measured Task 4 experimental data.

The comparison with static firing data was based on the error limits defined under Task 1. Reasonable agreement was obtained when the comparison was made, with only one of nine measurements grossly exceeding the predicted level and two other measurements exceeding the predicted levels. The fact that component vibration data were available from only four static firings led to the conclusion that additional data should be obtained and reviewed before a firm decision was made about the accuracy of the analysis technique. The one measurement that showed the worst comparison with the analysis data was taken from a single static firing.

Response mode shapes measured during the Task 4 testing were compared with analytically predicted mode shapes. In most cases, reasonable comparative agreement was achieved. No error limits had been specified for mode shape comparison, so quality judgments were somewhat subjective.

Based on the comparisons and evaluations made in Task 5, the basic conclusion that the analysis was sufficiently accurate for program continuation was reached. However, recommendations for use of additional static firing data and for improvements in the baseline motor model were made.

Part of the work in Task 5 consisted of analyzing motor static firing data from Poseidon C-3 second stage firings. The data analysis was conducted to obtain a relationship between measured pressure oscillation levels and acceleration response levels. Because of relatively high noise levels in the response, i.e., response over broad frequency ranges, results obtained by using unfiltered data were found to be misleading. It was therefore concluded that corresponding pressure and acceleration records should be filtered at the frequency of interest to obtain a measure of the response level that could be attributed to the measured pressure oscillation level. This conclusion would not apply to a motor with clean, essentially single-frequency, pressure and response measurements.

E. PHASE II, TASKS 6, 7, AND 8

The purpose of Phase II was to study simplified modeling techniques. The work of Phase II contributed significantly toward obtaining a better understanding of the general structural dynamic behavior of a solid rocket motor. The work was based on the philosophy that simplifications could only be developed after the motor behavior was better understood. The following conclusions were reached as a result of the Phase II work:

(1) Use of a half-motor model for general analysis work is not recommended. Special situations where a half-motor model may be satisfactory are discussed in the text.

(2) Scalar springs should not be used to represent gases in dome cavities that are open to the combustion chamber such as the dome cavities in the second stage Poseidon motor. A scheme involving scalar springs, scalar-masses, and multiple point constraint relations can apparently be used to represent gases trapped in a dome cavity that is physically sealed off from the combustion cavity such as in the Minuteman III third stage motor during the first 2 seconds of firing. The scheme referred to was used by the MacNeal-Schwendler Corporation in a previous analysis and was not studied here.

(3) Because of the curvature in a dome, a radial motion at a Y-joint can result in a significant axial motion at the center of the dome. A radial motion input at the dome Y-joint can excite a large number of dome modes in the 0 to 1000 Hz frequency range.

(4) The mode of response of a dome is likely to be heavily dependent on the applied loading distribution; therefore, the load distribution should be specified as accurately as possible if accurate dome response is desirable. If acoustic cavities are analyzed to determine acoustic mode shapes, then the dome cavities should be included in the cavity finite element model.

(5) The choice of grid refinement should be based on considerations of both structure natural modes and applied loading distribution.

(6) Based on the rule-of-thumb that three nodes be available to define each half wave of the deformed shape, the aft dome model for the second stage Poseidon C-3 motor becomes inaccurate above 500 to 600 Hz.

(7) Based on comparisons between analyses of dome models using different slice sizes, the 15 degree slice model fails to accurately predict the second dome mode which occurs at about 250 Hz. Therefore, a 15 degree slice grid is too coarse for analyses that require accurate response in the higher frequency modes.

(8) A fairly coarse grid can be used for the grain in the motor model. The limiting factor appears to be the requirement that sufficient nodes be available to obtain reasonable definition of the input load distribution.

(9) The WEDGE and HEXA1 elements in NASTRAN are unsatisfactory for the type of analyses conducted during this program. Both element types give unsymmetric responses when subjected to symmetric load distributions.

F. PHASE III

The Minuteman III third stage motor was analyzed during the work of Phase III. The objective of the Minuteman analysis was to verify the analysis techniques recommended at the conclusion of Phase II. Results from the initial analysis were transmitted to the AFRPL on a closed envelope basis. An evaluation of the closed envelope data led to the conclusion that response predictions were reasonably accurate for the longitudinal mode, but predicted levels for the tangential mode were much too low.

When the problem with the tangential mode response was identified, a study was conducted to determine if errors had been made in modeling the motor and to determine if modeling improvements could be made. Some errors were discovered and corrected and changes were made to improve the modeling. The result was a fairly accurate prediction of maximum acceleration amplitudes but a poor prediction of the response mode.

The basic conclusion reached as a result of the Phase III work was that analysis quality can depend to a large extent on the ability of the analyst to visualize the essential structural features of a motor and to include these features in a model. Apparently, the analyst must be quite meticulous in his preparation of the model to avoid making modeling errors, especially when no test data are available to verify the adequacy of the model.

G. GENERAL SUMMARY AND CONCLUSIONS

The calculation of the response of a rocket motor to internal acoustic pressure oscillations is a complex procedure. The three-dimensional nature of the motor structure and typical loading systems have required a detailed three-dimensional finite element model with many degrees-of-freedom. One objective of the program was to simplify the existing complex analysis procedure. A major fundamental analysis simplification resulted from the program. The addition of cyclic symmetry capability to the frequency response rigid format in NASTRAN has made analysis of very complex three-dimensional models practical. The MacNeal-Schwendler Corporation was responsible for the development of the cyclic symmetry concept. The required modifications to NASTRAN were made by MacNeal-Schwendler under contract with Hercules Incorporated. The subcontract work was funded by this program.

To take advantage of the cyclic symmetry capability in analyzing motors with components attached, an approach was adopted using mechanical impedance methods. Components attached to a motor generally spoil the cyclic symmetric character of the bare motor case and grain. By using the mechanical impedance approach, the theoretically correct response for the motor-components combination can be calculated. A specific mechanical impedance approach was formulated and checked out for use in conjunction with cyclic symmetry. The approach was implemented by using the direct matrix abstraction (DMAP) option in NASTRAN. Use of cyclic symmetry in conjunction with the mechanical impedance procedure can now be recommended for any analysis where the response of a coupled motor-component system is desired.

One of the most important contributions made by the program is the practical analysis experience and the insight into motor structural dynamic behavior that was gained. Various analysis approaches were tried and results were evaluated by comparing them with actual static firing data and with special acoustic test results. The analysis experience gained is presented by way of a modeling techniques manual included as Appendix I. Information in the modeling techniques manual is intended to be of value to the prospective analyst who is faced with the problem of calculating response of any solid rocket motor to internal acoustic pressure oscillations.

The acoustic testing work conducted led to the conclusion that structural response to acoustic modes can be successfully measured in a simple bench test. The testing proved to be worthwhile because of the detailed mode mapping that could be performed and because the input was clean and well defined.

The original intent of the program was to develop simplified modeling techniques that could be used during the design phase of motor development programs to predict the load levels input to attached components. Experience gained indicates that no general guidelines can be expected to cover all of the different special problems that each different motor design will create. The quality of future analyses is likely to depend strongly on the ability of the individual analyst to visualize the motor response and to model the significant structural features. A record of past analysis experience may be the prospective analyst's most valuable guide.

Based on the work of the program, four recommendations for future work are made:

(1) Only two different motors were analyzed. Somewhat different techniques were used on each motor. Results from future similar analyses should be reported in sufficient detail so that a catalogue of techniques can be formed and so that confidence can be built for some techniques while others are rejected. Additional comparisons between analytic results and measured data would be helpful to the prospective analyst.

(2) Experiments conducted during the program indicated that rather small increments must be used for hoop direction grid refinement when a curved motor case is modeled with flat plate elements. An improved element for modeling the motor case or better modeling techniques using existing elements is needed to keep overall problem size as small as possible.

(3) More high frequency pressure gage data and accelerometer data are needed from static and flight tests for evaluation of analysis results. Data filtering techniques should be used to isolate the significant characteristics of the data.

(4) A three-dimensional acoustics element coupled with the cyclic symmetry analysis concept could provide a more general acoustics cavity analysis capability.

REFERENCES

The references cited below appear on individual pages throughout the report and are compiled here for handy reference.

Index to the Shock and Vibration Bulletins, February 1968, The Shock and Vibration Information Center, Naval Research Laboratory, Washington, D. C.

Harris, C. M., and Crede, C. E., Shock and Vibration Handbook, Vol. 1, Chapter 10, McGraw-Hill Book Co., New York, 1961.

Bishop, R. E. D., Gladwell, G. M. L., and Michaelson, S., The Matrix Analysis of Vibration, Section 5.5, Cambridge at the University Press, London, 1965.

Bishop, R. E. D., and Johnson, D. C., The Mechanics of Vibration, Cambridge at the University Press, London, 1960.

Crafton, P. A., Shock and Vibration in Linear Systems, Harper and Brothers, New York, 1961.

MacNeal, R. H., Electric Circuit Analogies for Elastic Structures, Vol 2, John Wiley and Sons, New York, 1962.

Rubin, S., Review of Mechanical Immittance and Transmission Concepts, Presented at the 71st Meeting of the Acoustical Society of America, Boston, Mass., June 1966.

Rubin, S., Class Notes distributed at UCLA Short Course on Structural Dynamics Analysis, Los Angeles, California, 1967.

Rubin, S., On the Use of Eight-Pole Parameters for Analysis of Beam Systems, Soc. of Automotive Engineers, Reprint 925F, October 1964.

NASTRAN Theoretical Manual, R. H. MacNeal Ed., Scientific and Technical Information Office, NASA Administration, Washington, D.C., December 1972.

Eckvall, J. C., Elastic Property Orthotropic Monofilament Laminate, ASME Publication No. 61-AV-56.

Reed, D. L., Advanced Composite Technology Point Stress Laminate Analysis, Report FZM-5494 General Dynamics, Fort Worth Division, 1 April 1970.

Laminate Properties Program, Hercules Computer Program 62113, 8 July 1969.

Structural and Thermal Analysis Final Report, SE025-A2A00HTJ-2, Hercules Incorporated, November 1970, pp. 4-57.

Minuteman III Third Stage Pressure Oscillation Study Final Report, 1387-01F, AD888219, Aerojet Solid Propulsion Company, Sacramento, Calif, August 1971.

Minuteman II Stage III Oscillatory Burning Studies and Final CYH Powder Lot Categorization Report, Weapon System 133B, AF Contract 04(694)-903 Hercules Incorporated, Magna, Utah, for SAMSO, Norton AFB California, August 1970.

Final Report, Quality Assurance Test Number VI-QA-82,(Ground Level Test), MTO-1134-14, M57A1 Operational Rocket Motor, Weapon System 133B, AF04(694)-903, Hercules Incorporated, Magna, Utah, 31 December 1969.

Oscillatory Burning and Vibration Analysis Summary, Stage III Minuteman, Weapon System 133B, AF 04(694)-903, Hercules Incorporated, Magna, Utah, 5 May 1969.

Final Report, Transportation and Handling Program for the Stage III Minuteman Motor, Weapon System 133A, Contract AF 04(647)-243, MTO-21, Hercules Powder Company, Magna, Utah, 30 June 1964.

Final Report on the Investigation of Pressure Oscillations During Firing of the Minuteman II Stage III Motor, MTO-1124-34, Vol. III, Hercules Incorporated, Magna, Utah, January 1971.

Anderson, J. M., and Durrant, S. O., "A Finite Element Solution for Acoustic Mode Shapes and Frequencies in Rocket Motor Combustion Cavities," 7th JANNAF Combustion Meeting, CPIA, Pub. 204, Vol. I, February 1971.

Anderson, J. M., "Structural Damping of Acoustic Oscillations in Solid Propellant Rocket Motors," 8th JANNAF Combustion Meeting, CPIA, Pub. 220, Vol. I, November 1971.

Jessen, E. C., Bangerter, C D., and Tew, B. E., "Sold-Propellant Motor Acoustic Model Testing," 7th JANNAF Combustion Meeting, CPIA, Pub. 204, Vol. I, February 1971.

Final Report on the Poseidon Second Stage Acoustics Investigation, Doc. No. SH015-B3A00HTJ-1, Contract No. N0003066C0186, Hercules/Thiokol (A Joint Venture), Volume I, March 1971.

Thacher, J. H., and Dickinson, B. B., "Relationship Between Motor Parameters and Oscillatory Response in the Poseidon Second Stage Motor," 8th JANNAF Solid-Propellant Combustion Meeting, September 1971.

Herting, D. N., Joseph, J. A., Kussinen, L. R., and MacNeal, R. H., Acoustic Analysis of Solid Rocket Motor Cavities by a Finite Element Method, AFRPL-TR-71-96, for Edwards Air Force Base, Rocket Propulsion Laboratory, August 1971.

Poseidon Second Stage Acoustics Investigation, Final Report, Vol. II, Resonant Conditions and Combustion Driving of Pressure Oscillations, SH015-B3A00HTJ-1, Hercules/Thiokol, Joint Venture, Hercules Incorporated, Bacchus Works, Magna, Utah, March 1971.

Poseidon SS Motor Vibrations Studies, Final Report, SA015-B3A00HTJ-23, Contract N0003073C0012, Subcontract AX10A0270M, Hercules/Thiokol Joint Venture, Hercules Incorporated, Bacchus Works, Magna, Utah, 28 June 1973.

Program Plan for Analytical Prediction of Motor Component Vibrations Driven by Acoustic Combustion Instability, 8 January 1973, for AFFTC, Edwards AFB, California, by Hercules Incorporated, Bacchus Works, Magna, Utah.

Jensen, F. R., and Christiansen, H. N., "An Application of Component Mode Synthesis to Rocket Motor Vibration Analysis," The Shock and Vibration Bulletin, The 41st Symposium on Shock, Vibration, and Associated Environments, Naval Research Laboratory, Washington, D. C., October 1970.

APPENDIX A

BASELINE MOTOR SELECTION FOR THE ANALYTICAL PREDICTION OF MOTOR COMPONENT VIBRATIONS DRIVEN BY COMBUSTION INSTABILITY PROGRAM

AS PREVIOUSLY PUBLISHED

HERCULES INCORPORATED
INDUSTRIAL SYSTEMS DEPARTMENT · SYSTEMS GROUP
P. O. BOX 98, MAGNA, UTAH 84044 · TELEPHONE: 297-5911

In Reply Refer To:
MISC/6/40-3382

1 February 1973

Air Force Rocket Propulsion Laboratory
Edwards Air Force Base, California 93523

Attention: DYSC/Dr. D. George

Subject: Task 1 Report, Contract No. F04611-73-C-0025

Dear Sir:

The subject report is enclosed for your information. Three copies have been forwarded to the PCO under separate cover with a request for PCO approval of the Poseidon C3 second stage as the baseline motor selection. The subject report is not a required contract data item. The report was prepared in response to your request that Hercules Incorporated provide back-up data for the baseline motor selection. Please contact the writer if you desire additional detail.

Also enclosed is a copy of Hercules' writeup on the Potential Energy program which is being used to analyze the 3-D check problem. Additional information may be found in the references listed on page 37 of the program writeup.

Very truly yours,

F. Ray Jensen

F. Ray Jensen

FRJ/pj

Enclosures

TASK 1

BASELINE MOTOR SELECTION FOR THE ANALYTICAL PREDICTION OF MOTOR COMPONENT VIBRATIONS DRIVEN BY COMBUSTION INSTABILITY PROGRAM

Prepared for

DEPARTMENT OF THE AIR FORCE (AFSC)
HEADQUARTERS, AIR FORCE FLIGHT TEST CENTER
Edwards Air Force Base, California

Prepared by

HERCULES INCORPORATED
SYSTEMS GROUP
Bacchus Works   Magna, Utah

1 February 1973

FOREWORD

This report presents the results of Task 1 for Contract F04611-73-C-0025. The purpose of Task 1 was to select a baseline motor for further study in the program. The information upon which the baseline motor selection was made is contained in this report. This report is being submitted to obtain formal PCO approval of the baseline motor selection.

TABLE OF CONTENTS

LIST OF TABLES

LIST OF FIGURES

LIST OF FIGURES (CONT)

I. ABSTRACT

The objective of the Task 1 work reported herein was to select a baseline motor. Each of the three candidate motors is discussed with respect to specified baseline motor selection criteria. Each motor appears to have sufficient component vibration data from static and flight tests. Also, acoustic mode analyses have been performed on each motor by the MacNeal-Schwendler Corporation. Acoustic bench tests have been performed on each motor, with the Poseidon C-3 second stage having the most comprehensive bench test results available. More significant structural dynamic analyses have been performed on the Minuteman III third stage than on either of the other two motors.

After reviewing the qualifications of each candidate motor, it was concluded that either the Minuteman III Stage III or the Poseidon C-3 second stage motor could qualify as a baseline motor. The Minuteman III Stage III motor was disqualified because the use of four separate nozzles was judged to be not typical of probable future motor designs. Hercules Incorporated selected the Poseidon C-3 second stage motor to be the baseline motor.

II. INTRODUCTION

A. Objective

The objective of this work was to select a baseline motor for further study under this program (Air Force Contract F04611-73-C-0025).

B. Approach

Existing data on component vibration spectra and internal pressure oscillation for three upper stage ballistic missile motors was surveyed. Data from the Minuteman II and III third stage motors and from the Poseidon second stage motor was included in the survey.

The following criteria were used in selecting the baseline motor:

1) Availability of component vibration and acoustic pressure oscillation data from static and flight tests.

2) Availability of acoustic mode analysis and dynamic structural analysis results.

3) Availability of acoustic bench test results.

4) Degree to which the motor configuration is representative of probable future ballistic missile motor designs.

5) Availability of an inert motor for use in the vibration testing program.

III. MINUTEMAN II STAGE III MOTOR

A. Component Vibration and Pressure Oscillation Data from Static and Flight Tests

The data required to characterize a motor for this program consists of accelerometer and pressure gage data. The accelerometer data of interest is that from accelerometers located on motor components and on the basic motor structure. Pressure oscillation data which can be correlated with accelerometer data is required to establish the desired load-response relationship. Accelerometer data should be reduced to show level of response (in g's) and frequency of response as a function of time. The reduced pressure oscillation data should indicate the oscillating pressure amplitude as a function of time.

For the Minuteman II third stage motor, the collection of representative data is complicated by the fact that motors cast from different powder lots may exhibit different pressure oscillation characteristics. The various powder lots are characterized in terms of oscillatory or nonoscillatory characteristics in Reference 1.

Another problem which must be dealt with is the dependence of the measured pressure response on the tubing-pressure gage configuration. Since the tubing which leads to the pressure gage has its own dynamic characteristics, reported pressure levels may not be accurate over the frequency range of interest. The lack of accuracy can occur when the frequency of chamber pressure oscillation is near to a resonant frequency of the pressure gage tubing. (The tubing is required to isolate the pressure gage from the hot combustion gases.) At this point, it appears that some additional work will be necessary to measure or analytically predict a transfer function for the gage tubing in order to properly interpret existing pressure data.

Minuteman Stage III oscillatory burning data have been analyzed by playing FM tapes through a Quan-Tech Model 305 Tracking Wave and Spectrum Analyzer. Use of this analysis technique results in the following determinations: (1) The frequencies present during oscillatory burning, (2) the frequency-time histories for each frequency, and (3) the amplitude-time histories for each frequency.

The Quan-Tech Model 305 Tracking Wave and Spectrum Analyzer has a frequency range of 10 Hz to 50 KHz and a selection of three constant bandwidths of 10, 100, and 1000 Hz. It has electronic tuning with the following functions:

(1) Automatic frequency control to lock onto a drifting signal and follow it over the whole or discrete portions of the tuning range (limited frequency range determined by the bandwidth).

(2) Track function to lock onto a frequency signal and follow it over the whole or discrete portions of the tuning range.

(3) Sweep function to start at a tuned frequency and scan upward in frequency over the whole or discrete portions of the tuning range as determined by a sweep increment switch.

(4) Scan (or search) as in the sweep function until a signal is found whereupon the instrument will lock onto and track the signal.

Some results from the Quan-Tech data analysis are reported in Reference 1. The data is presented in the form of pressure oscillation amplitude (A.C. component), acceleration, or strain as a function of time for various tracking frequencies. Accelerometer data obtained from three motors fired during the Safeguard program is included. Accelerometer locations are shown in Figure 1 for the Safeguard motors. Plots comparing accelerometer response data from four oscillatory static firing motors with corresponding data from three flight motors is also given in Reference 1. Accelerometer locations for the static firing/flight comparisons are shown in Figures 2 and 3. The flight data sampling rate is too low for meaningful frequency response analyses to be performed.

Perhaps the most useful data for the purposes of this program will come from static test motors VI-QA-79 through VI-QA-82. These motors were heavily instrumented with accelerometers for the purpose of measuring the vibration environment to which the various components are subjected. Accelerometer locations for motor VI-QA-82 are shown in Figures 4, 5 and 6. The extent to which the locations shown were common with VI-QA-79, -80, and -81 is indicated in Table I. Table I was extracted from Reference 2. Reduced data for motors VI-QA-79, -80, -81, and -82 are available in References 1, 2, and 3. In addition, many unpublished data plots are available in the Test Analysis section files at Hercules Incorporated.

It appears that sufficient vibration and pressure oscillation data are available to characterize the Minuteman II third stage motor.

B. Dynamic Structural Analysis Results

Significant results from dynamic structural analyses on the Minuteman II third stage motor are available from two programs:

(1) The Transportation and Handling program (Reference 4)

(2) The Pressure Oscillation Investigation program (Reference 5)

In addition, grain vibration analysis results are available in Reference 6 and structural damping of the grain is discussed in Reference 7.

In the work of Reference 4, a dynamic analysis was performed on the Stage III motor, initally using simple beam and cylinder approximations. At a later date, more refined solutions were obtained in which mathematical models, more nearly representing the geometry of the motor, were used. Finite difference type modeling techniques were used in conjunction with a direct analog computer in obtaining dynamic solutions. An investigation of the frequency content of the transportation environment experienced by the motor, based on transporter dynamic analyses and road test data, revealed essential motor resonance frequencies. The analyses were all based on two-dimensional math models and are not directly applicable in this program. However, the breathing, bending, and axial modes which were determined, having been partially verified by test data, will be useful for comparison with analysis results from this program.

A three-dimensional structural dynamic analysis of the aft dome structure, including nozzles, nozzle stacks, and nozzle control unit, was performed using the SAMIS computer program. This analysis was reported in Reference 5. Natural frequencies and mode shapes were determined separately for:

(1) The Nozzle Control Unit

(2) Nozzle

(3) The Aft Dome Including Nozzle Stacks

In addition, natural frequencies and mode shapes were determined for the entire aft dome with components and frequency response solutions were obtained for the aft dome without components. The analyses performed for the work of Reference 5 could be considered to represent analyses of a simplified model as will be required in Task 10 of this program.

The work reported in References 6 and 7 was not concerned basically with structural dynamic analyses; however, results from two-dimensional analyses giving frequency response solutions for the grain were reported. These solutions provide data which can be used to check new three-dimensional models containing the grain.

C. Acoustic Mode Analysis Results

The acoustic mode analyses which have been performed on the Minuteman II third stage motor by Hercules Incorporated are reported in References 6 and 7. The mode shape for the first longitudinal mode[6] is shown in Figure 7. The frequency was calculated to be 160 Hz for air or about 480 Hz for hot combustion gases. The plot shown in Figure 8 was taken from Reference 7. The second longitudinal mode was calculated to occur at 272 Hz. The acoustic mode analyses performed by Hercules were based on two-dimensional finite-element models and a 15-second burn time.

Additional acoustic mode analysis results are available in Reference 8. The results presented in Reference 8 were obtained with the acoustic analysis capability of the NASTRAN Level 15 computer program. Published results are shown in Table II. Mode shapes for the two lowest frequency modes for the two-inch burn time are shown in Figure 9.

D. Acoustic Bench Test Results

Acoustic testing has been performed on fullscale models of the M-57A1 motor which were constructed to represent grain cavity geometry at 3-second, 6-second, and 15-second burn times. Results of the acoustic tests were reported in References 5 and 9. Results taken from Reference 5 are shown in Figures 10, 11, and 12. The figures show the first four longitudinal mode shapes for the three different burn times. Apparently, no radial or tangential modes were established. Also of interest is the fact that no third harmonic was found for the 6-second model and the fourth harmonic was very close to the second harmonic in frequency.

IV. MINUTEMAN III STAGE III MOTOR

A. Component Vibration and Pressure Oscillation Data from Static and Flight Tests

During the "Minuteman III Third Stage Pressure Oscillation Study"[10], vibration data were collected from 24 motor firings and at 37 different locations on the motor and motor components. A standard instrumentation plan for accelerometers was developed and used in the oscillatory burning program to establish vibration envelope information of the forward dome, aft dome, and nozzle. Selected accelerometer locations were monitored during the qualification program and during some production firings. The instrumentation of flight test motors was modified to include the corresponding instrumentation from the oscillatory burning program. Accelerometer locations for the forward and aft domes are shown in Figures 13 and 14. (The figures were obtained from Reference 10.)

Vibration envelope data for many of the accelerometers shown in Figures 13 and 14 are given in Appendix A of Reference 10. The data are presented in the form of graphs showing the maximum acceleration level envelope (in g's) as a function of time after ignition. Also shown is an envelope of the predominant frequency as a function of time.

The Minuteman III third stage motor has been found to exhibit unstable acoustic pressure oscillations in two distinct modes. The general characteristics of the unstable oscillations are indicated by the pressure oscillation amplitude and frequency variation curve shown in Figure 15 (taken from Reference 10). From 0 to 4 seconds, a tangential acoustic mode causes oscillations at from 870 to 760 Hz. From

4 to 14 seconds, the fundamental longitudinal mode causes oscillations of from 350 to 200 Hz.

B. Dynamic Structural Analysis Results

Three dynamic structural analyses[10] of interest have been conducted on the Minuteman III third stage motor: 1) A modal analysis was performed on a Forward Dome model to determine mode shapes and frequencies of the dome for frequencies below 1000 Hz, 2) Frequency response analyses were performed on a model of a forward portion of the motor including a portion of the propellant, and 3) A structural dynamic analysis of the nozzle was performed simulating the configuration of the nozzle as tested in the nozzle survey. Many of the results from the analyses are given in Reference 10. However, the usefulness of these analyses in this project may depend upon the cooperation of the Aerojet analysts in making unpublished analysis details and data available.

C. Acoustic Mode Analysis Results

Acoustic analyses have been performed on the Minuteman III third stage motor using the acoustic analysis capability which is currently available in the NASTRAN Level 15 program. Results of the analyses are reported in References 8 and 10. Natural frequencies obtained from Reference 8 are given in Table III. Several plots showing pressure mode shapes are given in References 8 and 10.

D. Acoustic Bench Test Results

Acoustic bench testing was performed on a fullscale model of the Minuteman III third stage motor cavity which was constructed to represent a 3-second burn time. Details of the testing and plots of the node shapes are given in Reference 10.

V. POSEIDON C-3 SECOND STAGE MOTOR

A. Component Vibration and Pressure Oscillation Data from Static and Flight Tests

Accelerometer data are recorded from four locations on the forward dome on a routine basis for each static firing. Data from approximately 40 firings are available for the four forward dome accelerometers. Data from approximately 10 firings include two additional accelerometers; one located on the aft adapter ring, and one located on the cylindrical section near the forward dome tangent line. Accelerometer locations are shown in Figure 16.

In addition to the routine static firing data listed above, data are available from three static firing motors which were specially instrumented with from 15 to 20 accelerometers to measure component response. The three motors with special instrumentation are: SP-0115, SP-0131, and SP-0160. Accelerometer locations for SP-0160 are shown in Figures 17 and 18. The instrumentation for the two other motors was similar.

Some pressure gage and accelerometer data are available from flight tests; however, the data sampling rates used to collect the data are generally so low that valid data are obtained only for low frequencies (generally below 200 Hz). Therefore, available flight data will not be very useful for this program. (The motor exhibits acoustic oscillations at nominal frequencies of 250, 670, 750, 1300, 2000, 2600, 3300, and 4000 Hz; in addition, oscillations of generally weaker amplitude are sometimes measured at frequencies of 500, 1000, 1200, 2700, and 3900 Hz.)

A summary and analysis of Poseidon C-3 second stage vibration data is given in Reference 11. However, most of the useful data are unpublished and available only in the files of the Test Analysis Group in the Product Engineering department at Hercules' Bacchus Works. Results of a correlation study between motor parameters and oscillatory response are given in Reference 12.

B. Dynamic Structural Analysis Results

A two-dimensional model of the Poseidon C-3 second stage grain was constructed to study the structural damping characteristics of the propellant. The analysis is discussed in Section 4 of Reference 11.

C. Acoustic Mode Analysis Results

As with the two previous motors, results of acoustic analyses based on use of the NASTRAN program are given in Reference 8. Results taken from Reference 8 are shown in Table IV.

D. Acoustic Bench Test Results

A rather elaborate acoustic bench t[illegible]ng program was conducted for the Poseidon C-3 second stage motor c[illegible]. Three separate models were constructed to represent the cavity: a zero burn time model, a 4.5-second burn time model, and an 8-second burn time model. Acoustic mode shapes were mapped in detail in the fin area and in the centerbore. Some tests were repeated for different grain geometries and different igniter configurations. Results of the acoustic bench testing are reported in Volume II of Reference 11.

VI. BASELINE MOTOR SELECTION

The baseline motor selection criteria are discussed in this section one at a time as they apply to each candidate motor.

1) Availability of component vibration and acoustic pressure oscillation data from static and flight tests.

   A good deal of static firing data is available for all three motors. Flight data are not abundant, but a limited amount is available for each motor. Based on this selection criteria, all three motors are judged approximately equal.

2) Availability of acoustic mode analysis and dynamic structural analysis results.

   Acoustic mode analyses were performed on each of the three motors with the NASTRAN computer program; thus, the three motors are judged to be equal in this respect.

More extensive structural dynamic analyses have been performed on the Minuteman III motor than on either of the other two motors. Some analysis work has been conducted on the aft dome and associated hardware of the Minuteman II motor. Very little useful structural dynamic analyses have been performed on the Poseidon motor. Therefore, the motors are ranked as follows for this selection criterion:

Minuteman III Stage III

Minuteman II Stage III

Poseidon C-3 Second Stage

3) Degree to which the motor configuration is representative of probable future ballistic missile motor designs.

The Minuteman II Stage III motor is judged to be disqualified from possible selection as a baseline motor because of this selection criteria. The Minuteman II motor employs a four nozzle design which is not typical of present-day motors, nor probable future motors.

The Minuteman III Stage III motor and the Poseidon C-3 second stage motor are judged to be equal with regard to this selection criterion.

Based on the application of the stated selection criteria, it appears that either the Minuteman III Stage III motor or the Poseidon C-3 second stage motor could be selected as a baseline motor for this project. Hercules chooses to select the Poseidon C-3 second stage motor as the baseline motor for the following reasons:

1) An inert motor and some hardware are available for the acoustic testing of Task IV.

2) Hercules Incorporated has access to all unpublished analysis and static test data for this motor.

3) Hercules Incorporated is more familiar with the design features and problem areas of the Poseidon motor structure than with the Minuteman III motor.

TABLE I

ACCELEROMETER TEST RESULTS

GAGE	STATIC TEST MAXIMUM "G" LOADS (ZERO TO PEAK)			
	VI-QA-79	VI-QA-80	VI-QA-81	VI-QA-82
AC-101	100 g @ 12.4 sec	133 g @ 11.7 sec	95 g @ 11.9 sec	Invalid
AC-201	54 g @ 12.6 sec	27 g @ 12.5 sec	94 g @ 11.7 sec	Failed
AC-202	165 g (saturated)	210 g @ 12.6 sec	Invalid	43 g @ 17 sec
AC-203	121 g @ 10.6 sec	146 g @ 10.5 sec	120 g @ 12.2 sec	35 g @ 19 sec
AC-204	39 g @ 12.8 sec	128 g @ 12.9 sec	38 g @ 8.5 sec	Failed
AC-205	8 g @ 12.4 sec	Invalid	Invalid	76 g @ 13 sec 84 g @ 17 sec
AC-206	22 g @ 12.8 sec	64 g @ 9.6 sec	Invalid	79 g @ 14 sec 55 g @ 16 sec
AC-301	37 g @ 10.4 sec	14 g @ 14.6 sec*	26 g @ 12.4 sec*	150 g @ 14 sec 115 g @ 19 sec
AC-302	24 g @ 10.5 sec	47 g @ 15.0 sec*	52 g @ 10.9 sec*	81 g @ 14 sec 59 g @ 18 sec
AC-303	130 g @ 11.9 sec	Invalid*	51 g @ 12.2 sec*	100 g @ 13 sec 92 g @ 17 sec
AC-304	25 g @ 9.9 sec	Invalid*	36 g @ 12.7 sec*	23 g @ 13 sec 16 g @ 1[illegible] sec
AC-305	39 g @ 11.9 sec	10 g @ 15.0 sec*	27 g @ 11.9 sec*	16 g @ 12 sec 16 g @ 16 sec
AC-306	17 g @ 11.1 sec	11 g @ [illegible] sec*	26 g @ 12.2 sec*	20 g @ 13 sec 19 g @ 20 sec
AC-307	28 g @ 11.8 sec	1[illegible] g @ 15.1 sec	19 g @ 11.7 sec	NA
AC-308	24 g @ 12.1 sec	24 g @ 15.0 sec	Invalid	NA
AC-309	22 g @ 10.0 sec	12 g @ 13.2 sec	28 g @ 11.9 sec	NA
AC-310	Invalid	24 g @ 12.4 sec	Invalid	29 g @ 14 sec 22 g @ 18 sec
AC-401	Invalid	18 g @ 13.0 sec	18 g @ 12.9 sec	Failed

Note: The remaining gages were not installed on QA motors VI-QA-79, -80, and -81.

TABLE II

NATURAL FREQUENCIES FOR THE THIRD STAGE MINUTEMAN II MOTOR CAVITY[8]

Harmonic (n)	Mode	Frequency (Hz)			
		2-inch Burn		5-inch Burn	
		NASTRAN	Experimental	NASTRAN	Experimental
0	1	578.4	557	517.7	507
	2	982.9	939	911.7	882
	3	1,406.0		1,364.7	1340
	4	1,535.5	1432	1,621.7	1545
	5	2.007.6	1928	1,909.8	1842
	6	2,084.8			
1	1	771.4		858.7	
	2	1,449.4		1,266.9	
	3	2,004.3		1,729.1	
	4	2,294.0		1,998.0	
	5			2,290.9	
				2,493.7	

TABLE III

NATURAL FREQUENCIES FOR THE THIRD STAGE MINUTEMAN III MOTOR CAVITY[8]

Burn Time (sec)	Harmonic (n)	Mode	Frequency, Hz: This Paper	Frequency, Hz: Experimental
0.0	0	1	105.2	
		2	212.9	
		3	316.7	
		4	380.5	
		5	455.2	
	1	1	275.8	
		2	360.6	
		3	641.9	
3.0	0	1	90.1	93.0
		2	199.5	200.0
		3	310.4	312.0
		4	388.0	388.0
		5	449.1	466.0
		6	512.8	518.0
	1	1	238.9	239.0
		2	316.1	324.0
		3	541.6	
		4	567.4	

TABLE IV

NATURAL FREQUENCIES FOR THE SECOND STAGE POSEIDON MOTOR CAVITY[8]

Harmonic (n)	Mode	Frequency (Hz)			
		Zero Burn		3-inch Burn	
		NASTRAN	Experimental	NASTRAN	Experimental
0	1	388.1	398	324.0	322
	2	645.0	645	678.3	689
	3	962.0	962	1039.2	1051
	4	1422.0	1422	1430.8	1425
	5	1769.0	1728	1830.9	1831
	6	2010.8	2130	1994.4	
1	1	835.1		737.8	
	2	1313.4	1216	833.9	868
	3	1659.1	1620	1344.0	1349
	4	1832.8	1798	1558.2	1552
	5	2105.7		1812.5	
	6	2236.8		2130.1	2094

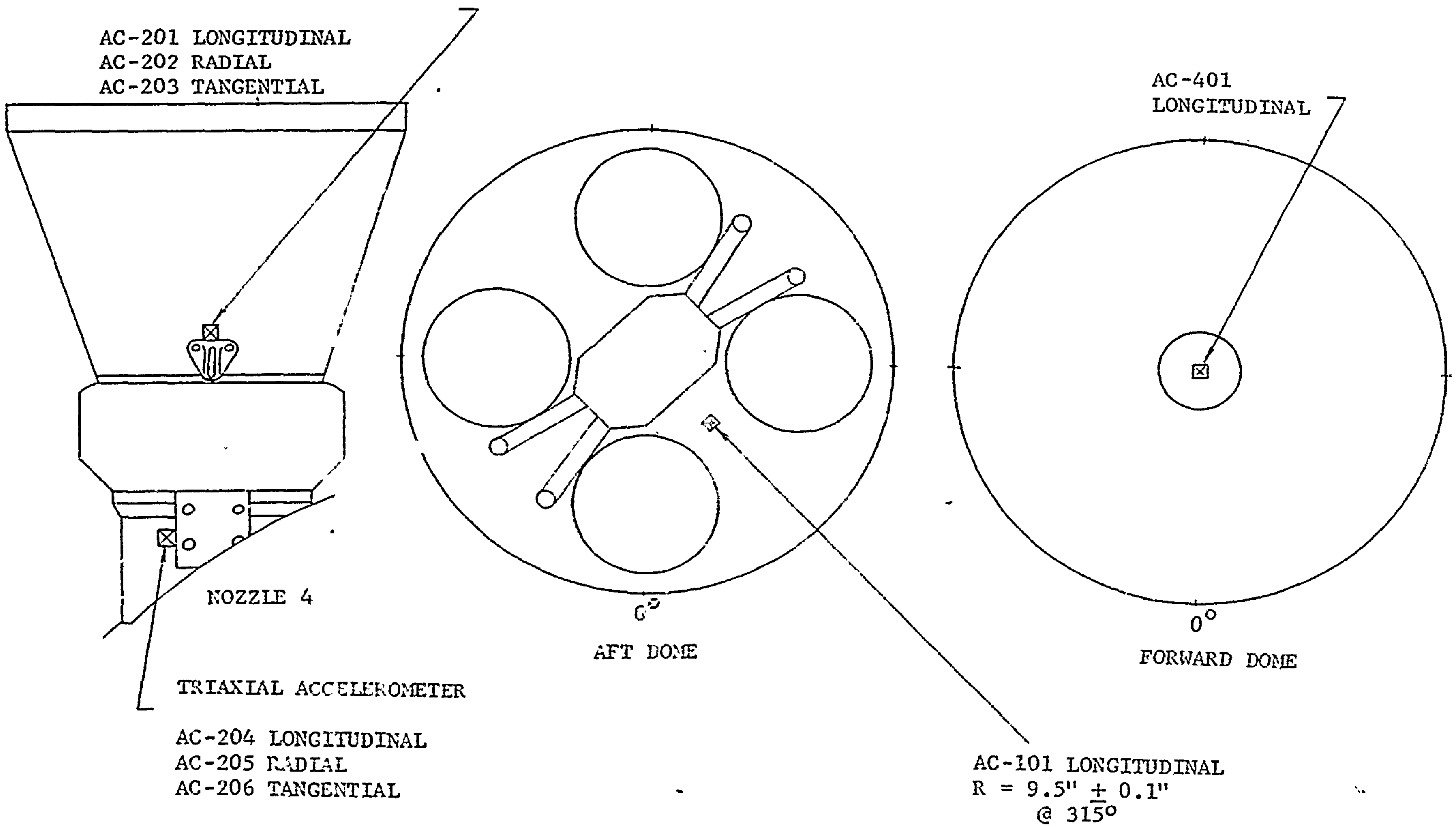

Figure 1. Safeguard Test Motor Accelerometer Locations

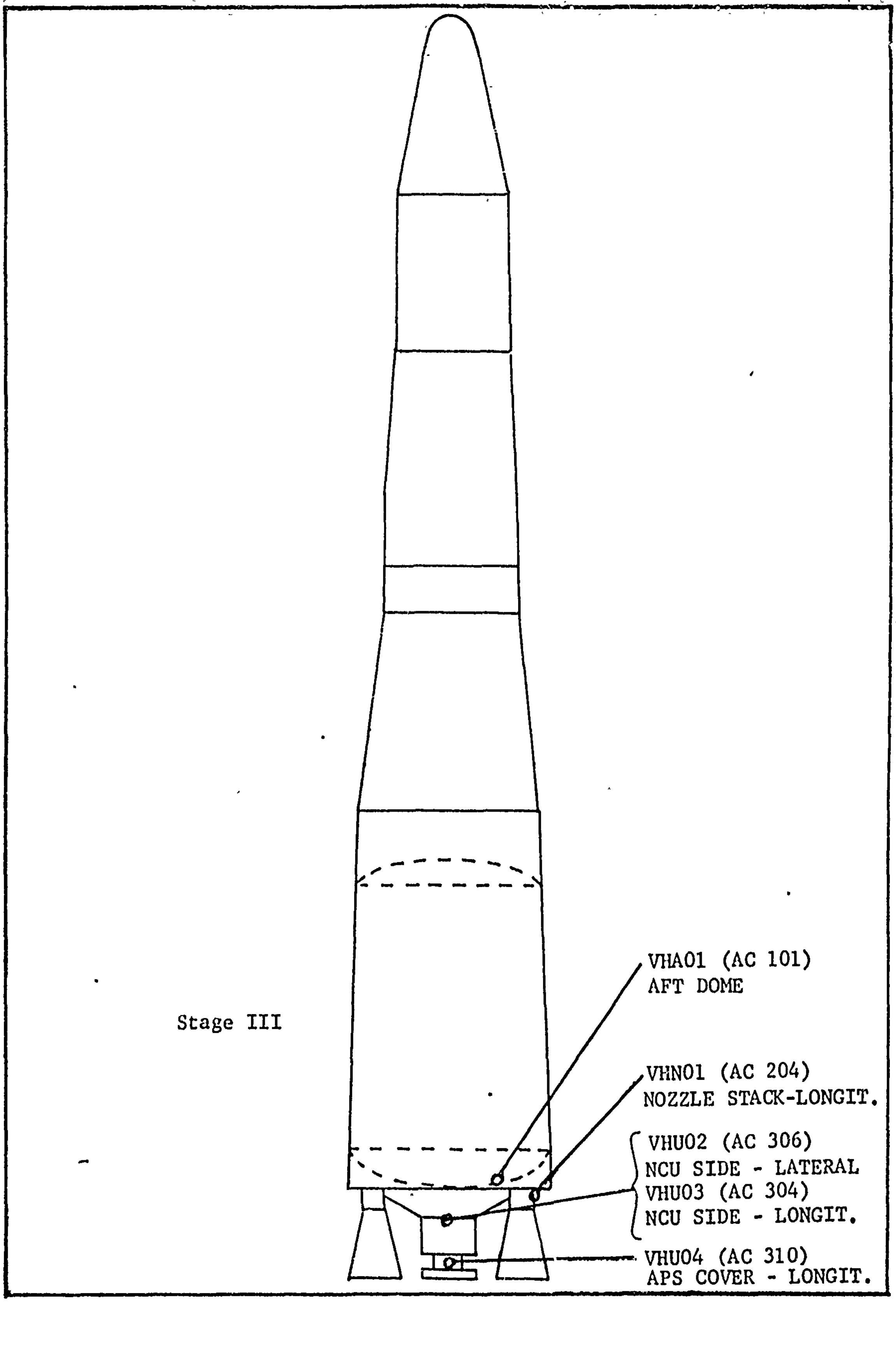

Figure 2. Flight Test Accelerometer Locations Similar to Static Test Locations

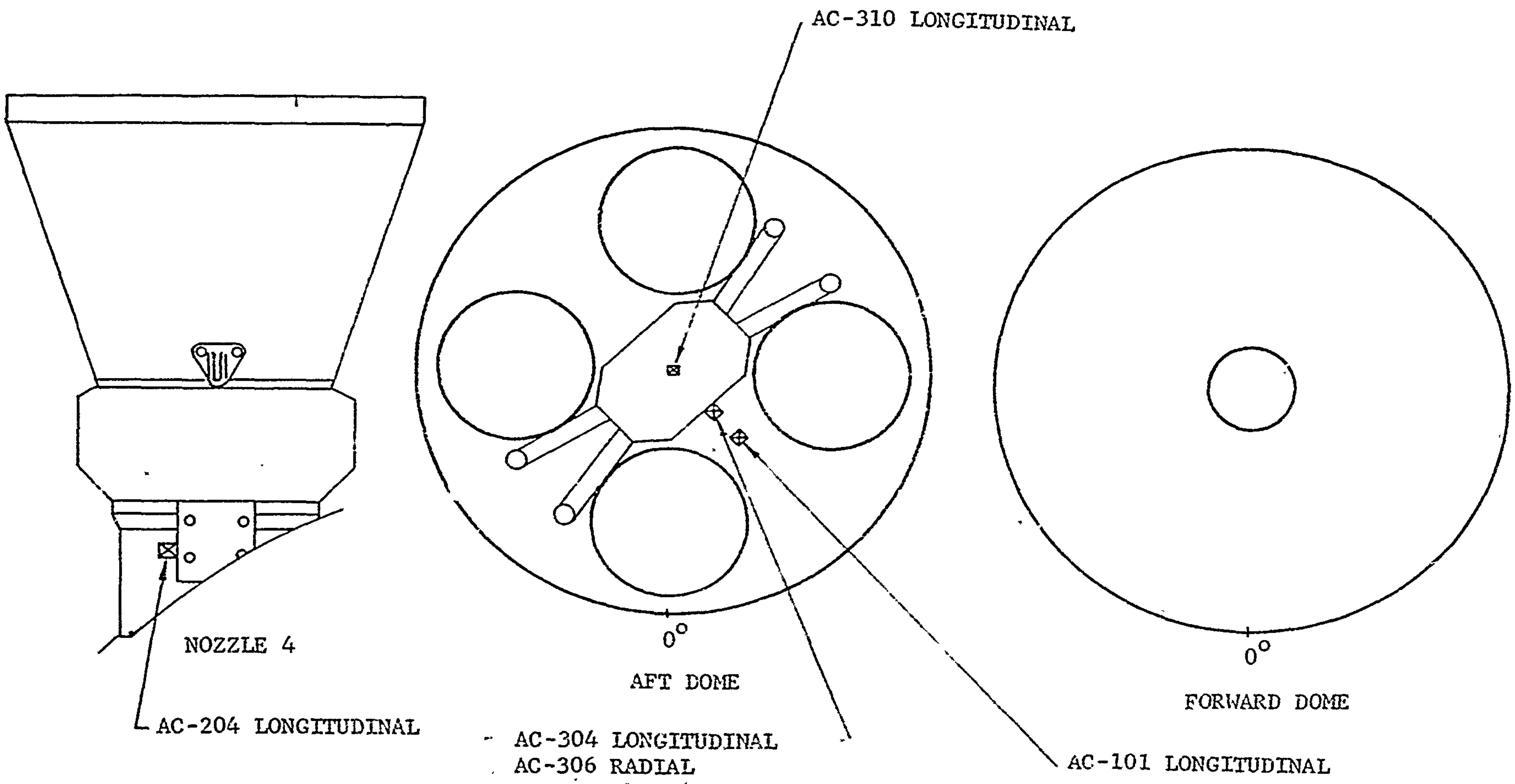

Figure 3. Static Test Motor Accelerometer Locations Similar to Flight Test Accelerometer Locations

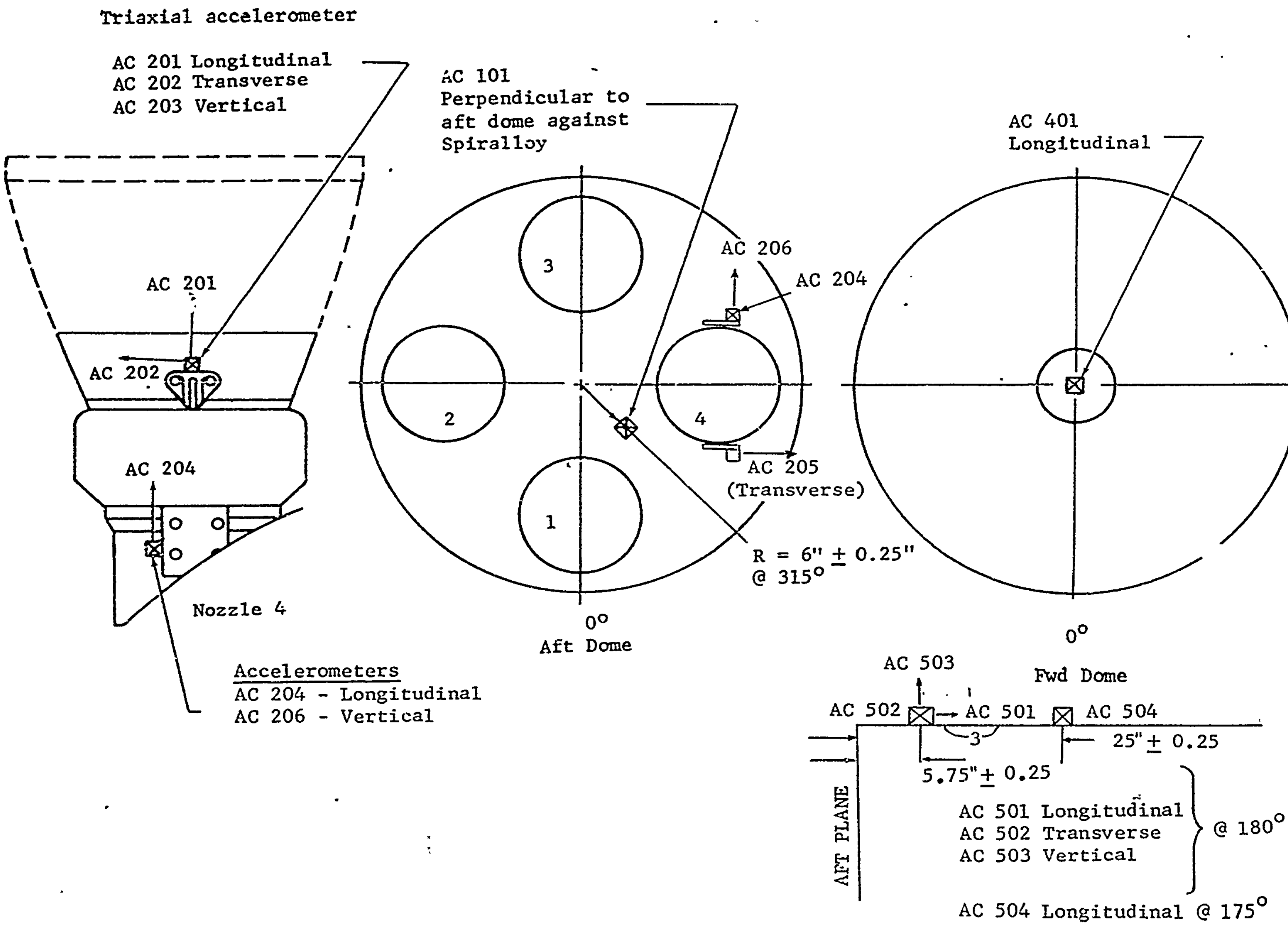

Triaxial accelerometer
AC 201 Longitudinal
AC 202 Transverse
AC 203 Vertical
AC 201
AC 202
AC 204
Nozzle 4
Accelerometers
AC 204 - Longitudinal
AC 206 - Vertical
AC 101
Perpendicular to
aft dome against
Spiralloy
3
2
4
1
AC 206
AC 204
AC 205
(Transverse)
R = 6" ± 0.25"
@ 315°
0°
Aft Dome
AC 401
Longitudinal
0°
Fwd Dome
AC 503
AC 502
AC 501
AC 504
3
25" ± 0.25
5.75" ± 0.25
AFT PLANE
AC 501 Longitudinal
AC 502 Transverse
AC 503 Vertical
@ 180°
AC 504 Longitudinal @ 175°

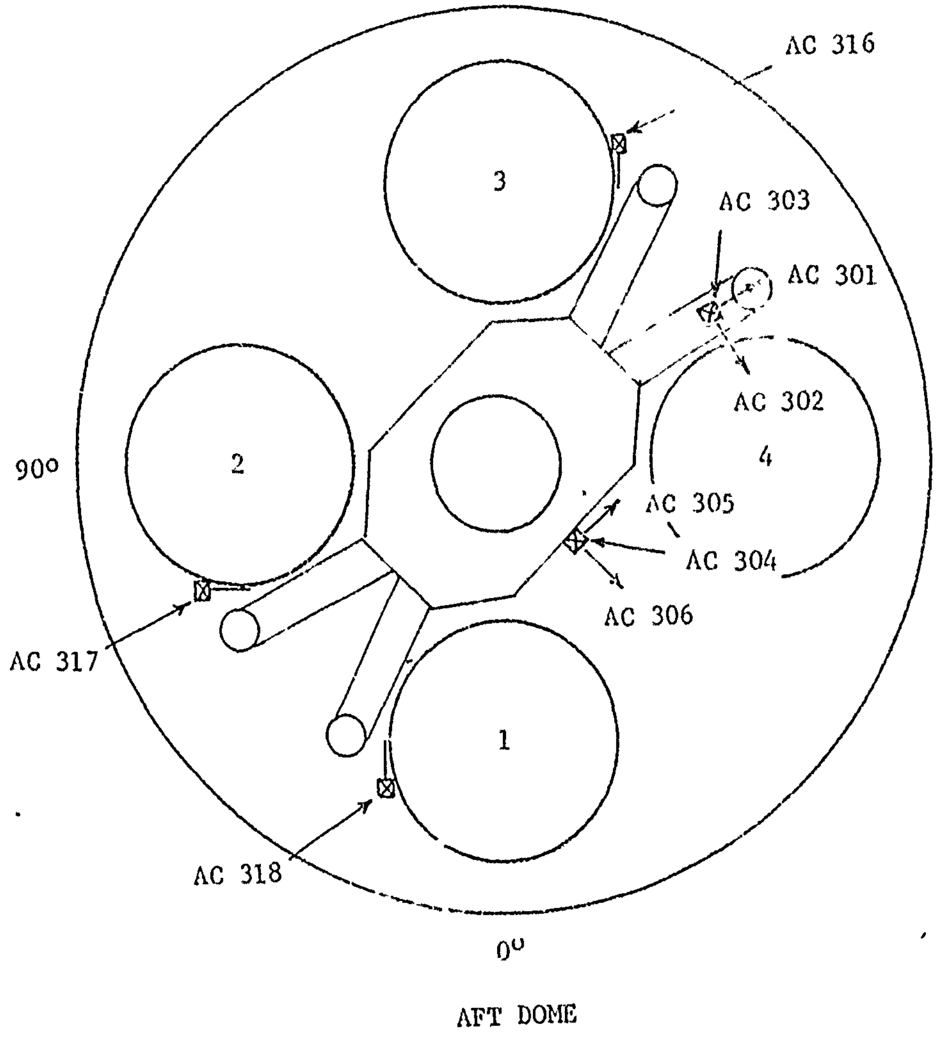

Figure 5. Nozzle and NCU Accelerometer Locations for Motor VI-QA-82

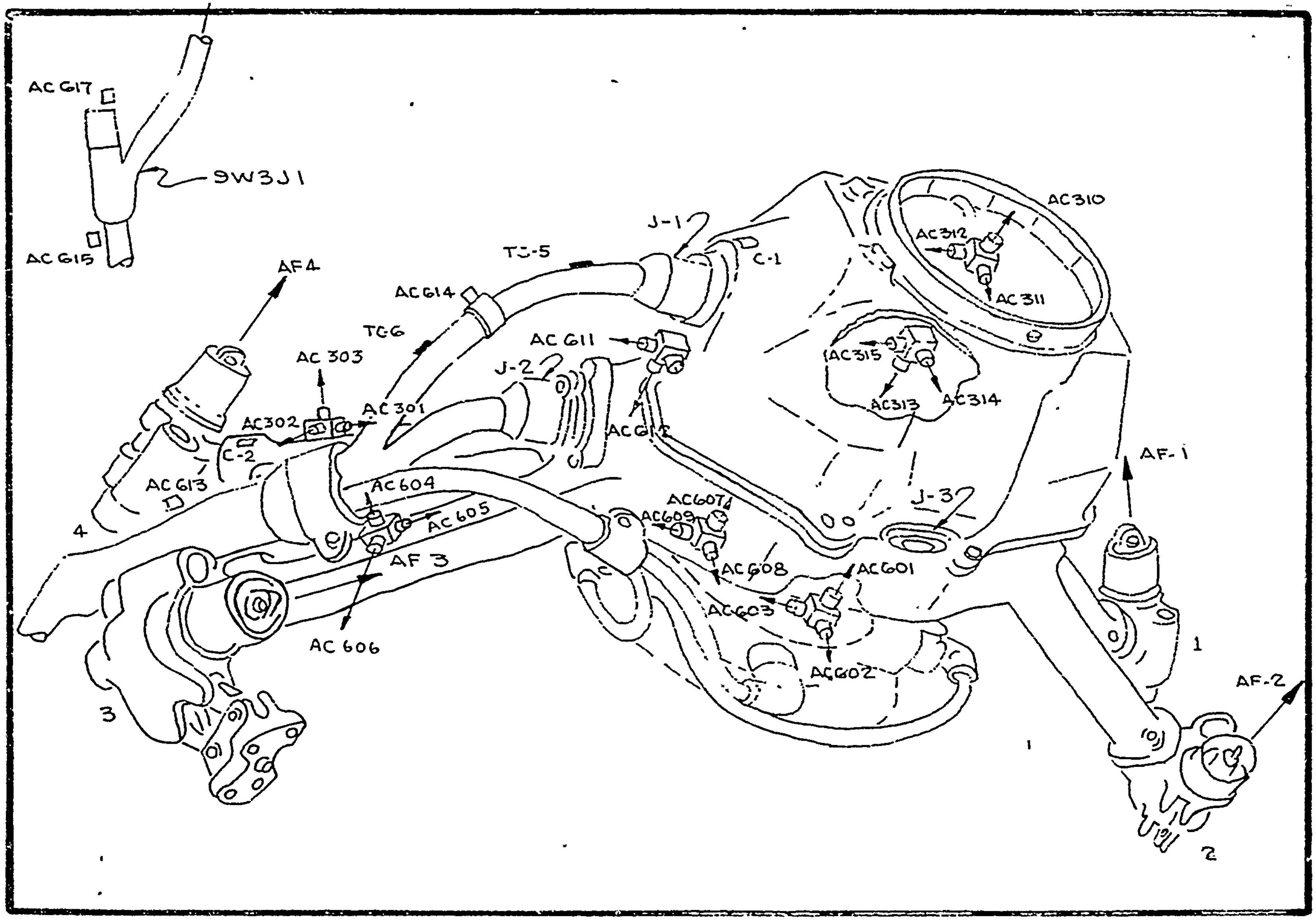

Figure 6. Nozzle Control Unit Instrumentation Locations for Motor VI-OA-82

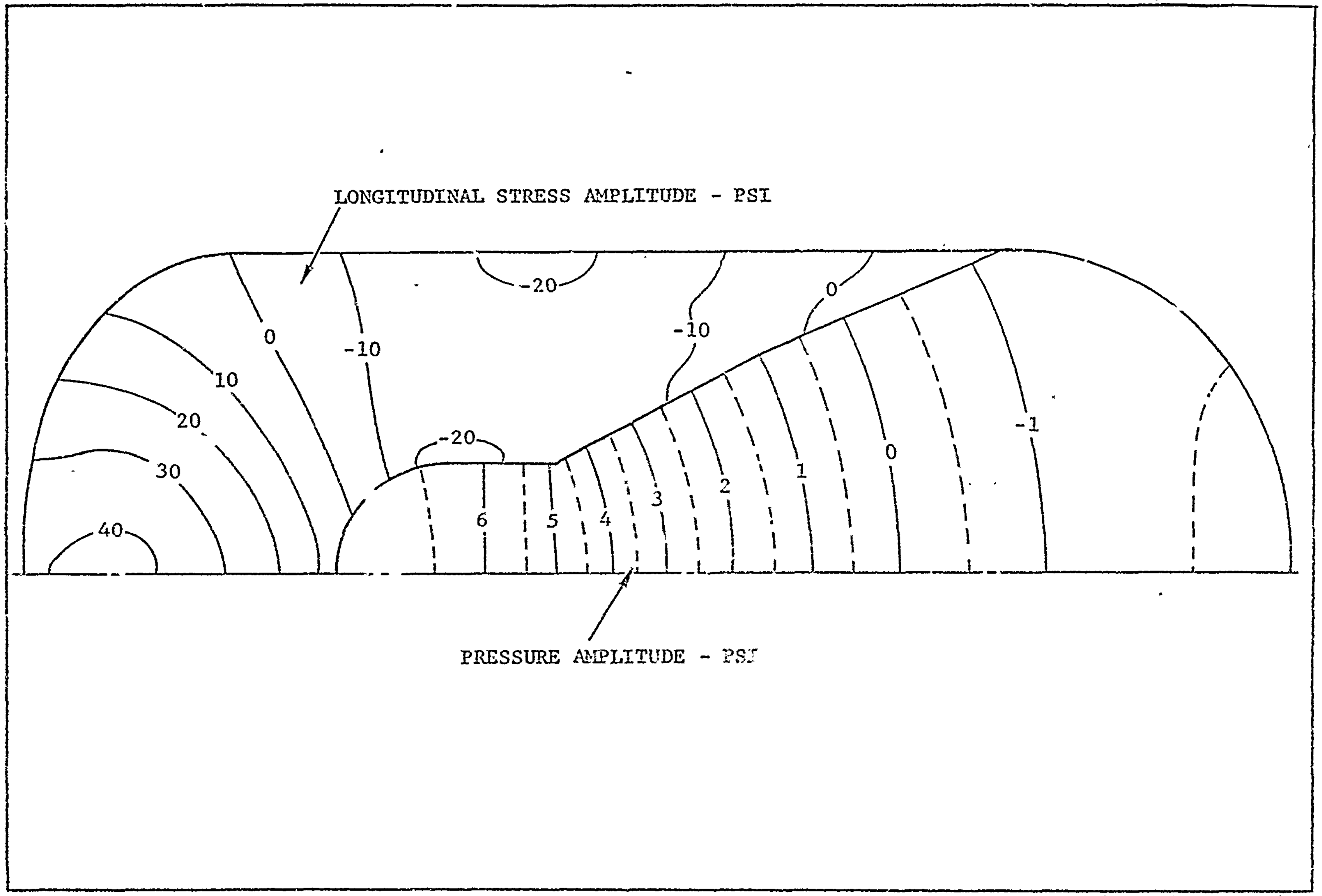

Figure 7. Isobar of Gas Pressure and Grain Stress for Coupled Vibration at 160 Hz

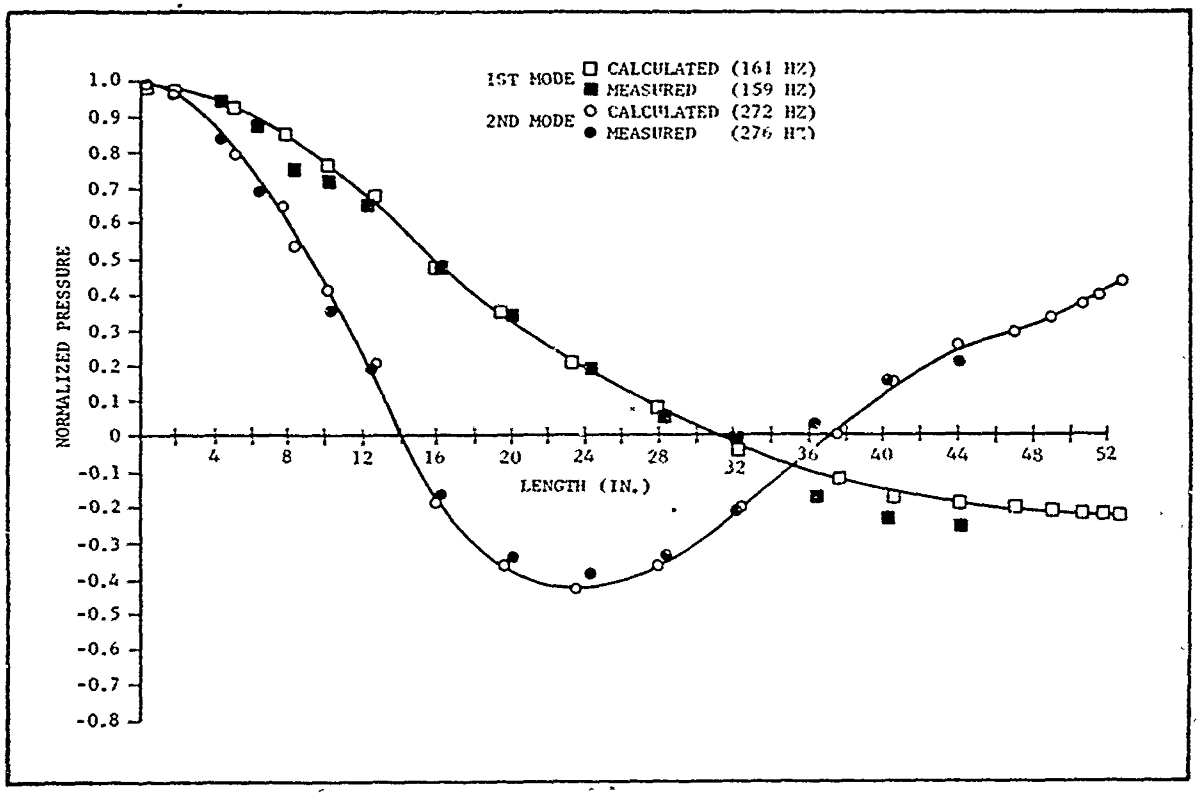

Figure 8. Comparison of Measured and Calculated Mode Shapes for Advanced Burn Configuration of M-57A1 Motor

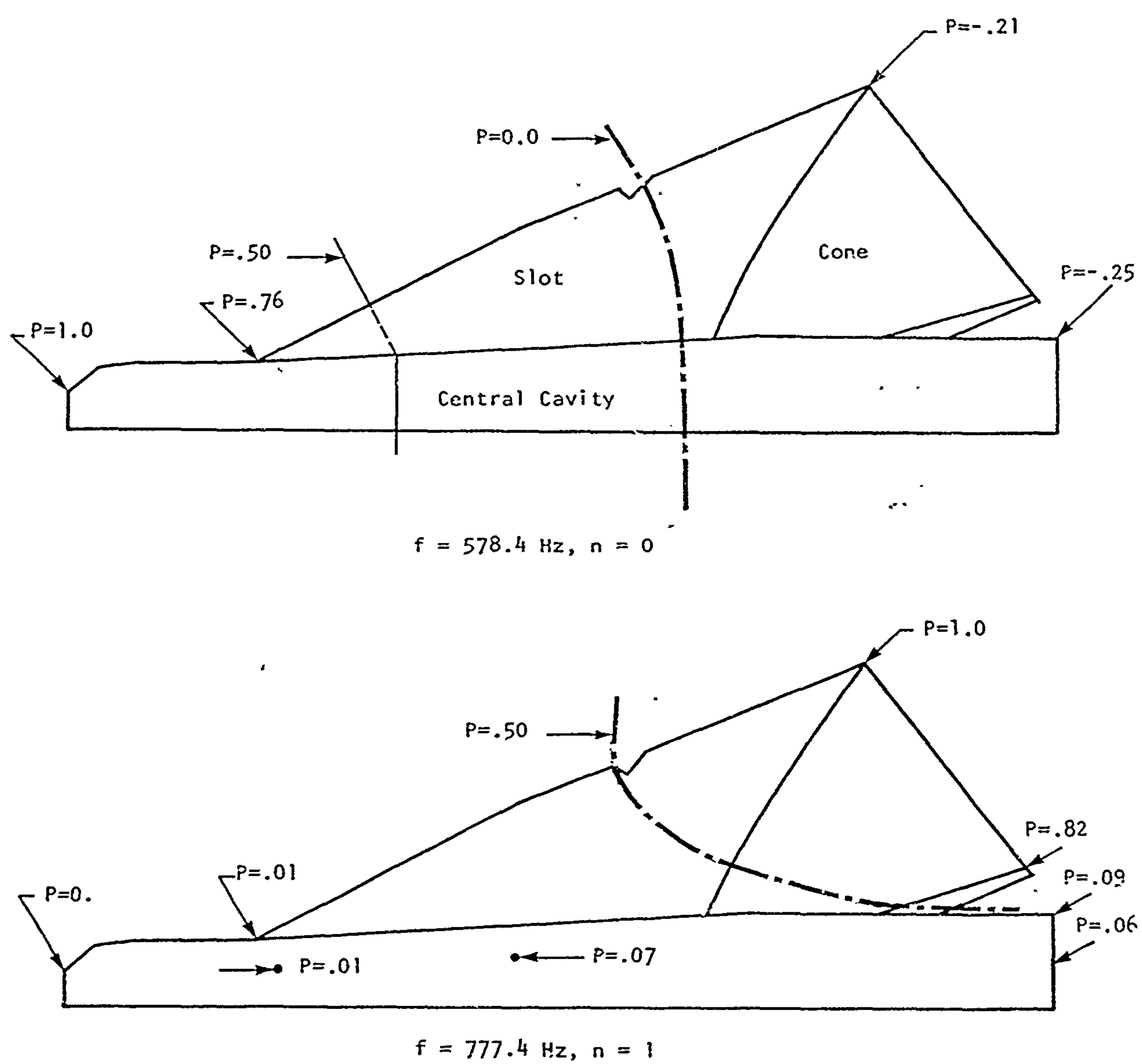

Figure 9. Minuteman II, Stage III Mode Shapes for Lowest Modes, 2-inch Burn, n = 0 and n = 1 (from Reference 8)

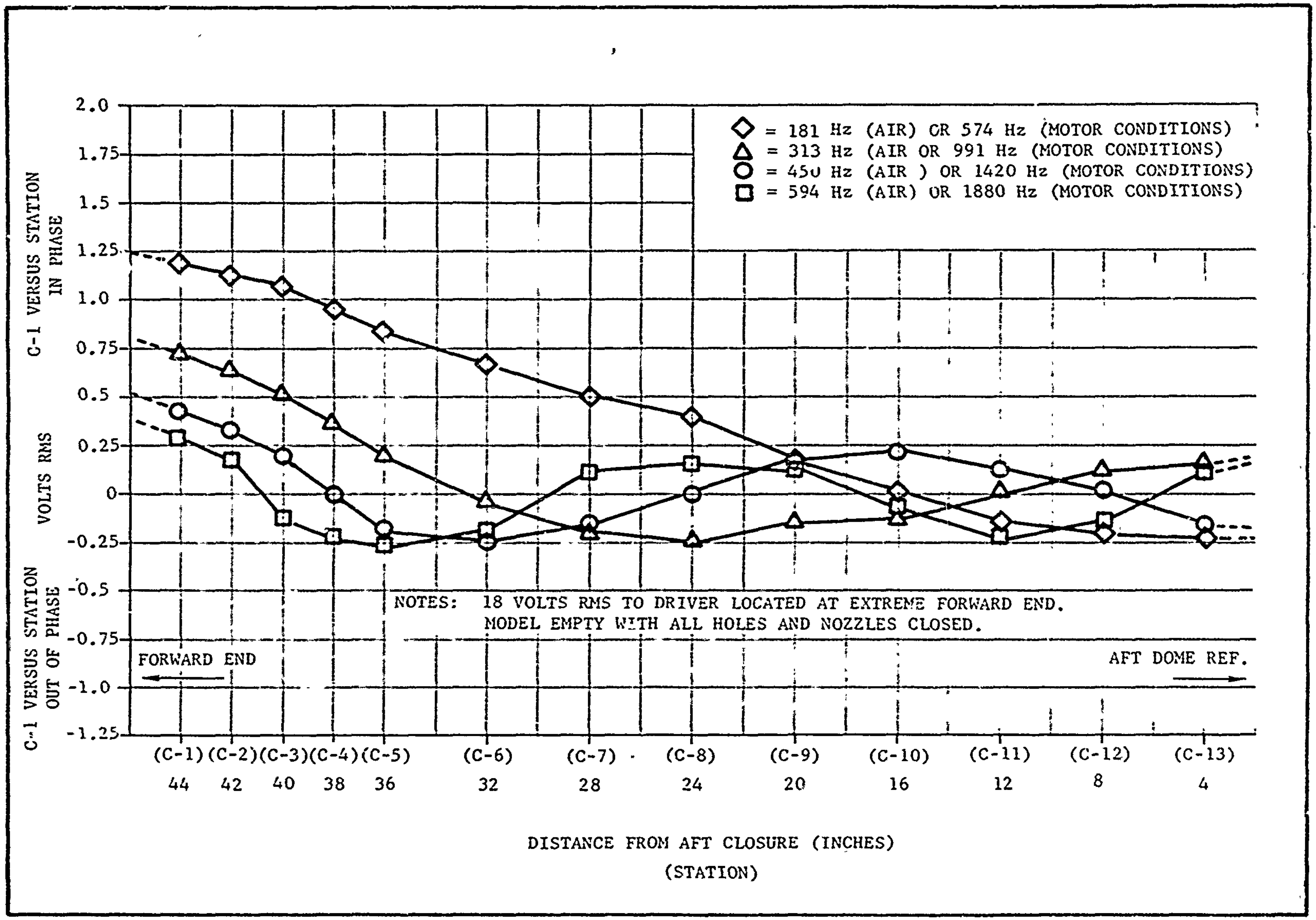

Figure 10. Acoustic Wave Shapes Along Wall Between Wing Slots of M-57A1 3-Second Burn Model

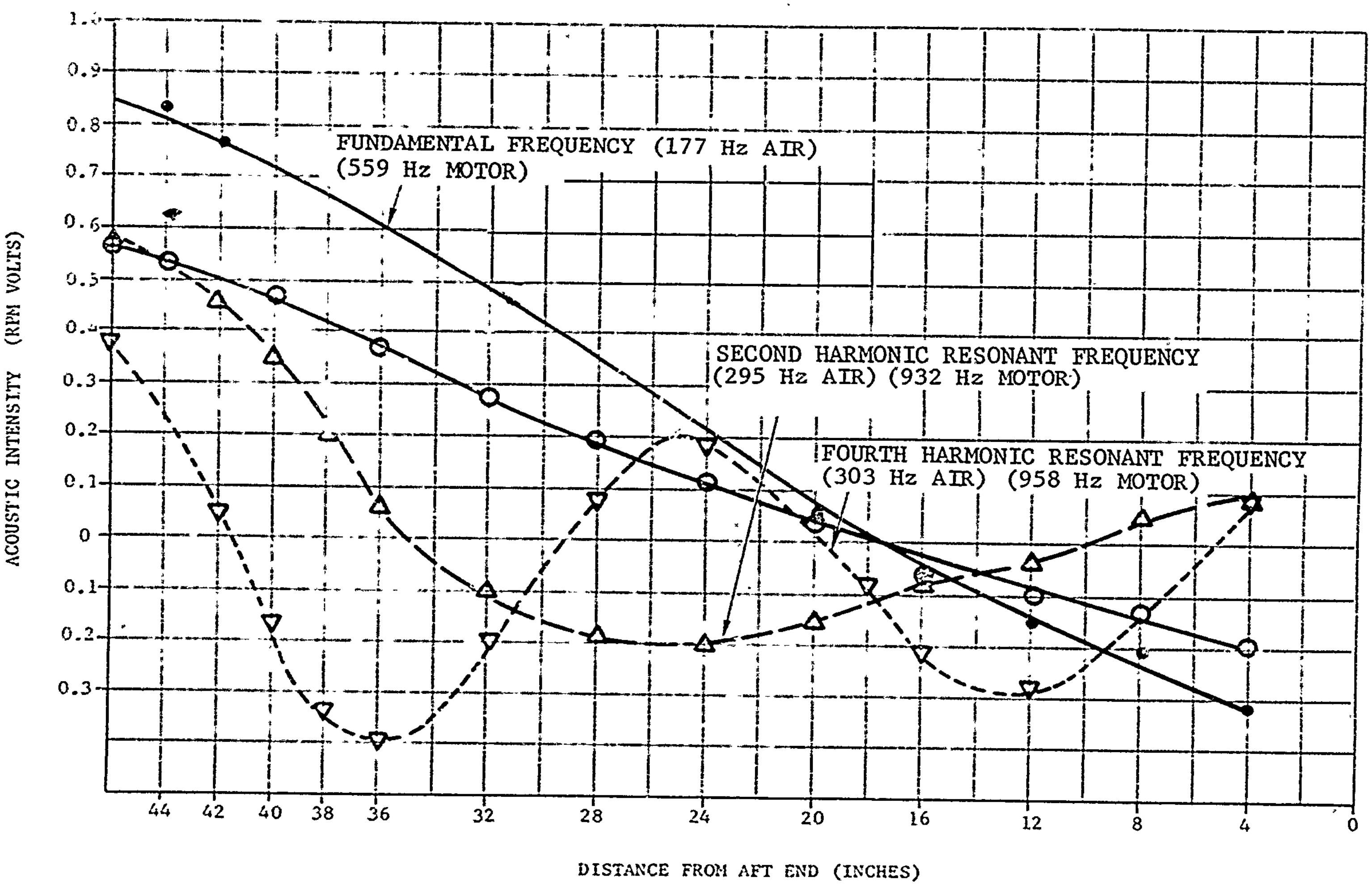

Figure 11. Acoustic Wave Forms of Fundamental and Harmonic Resonant Frequencies Near 300 Hz (6-Second Model)

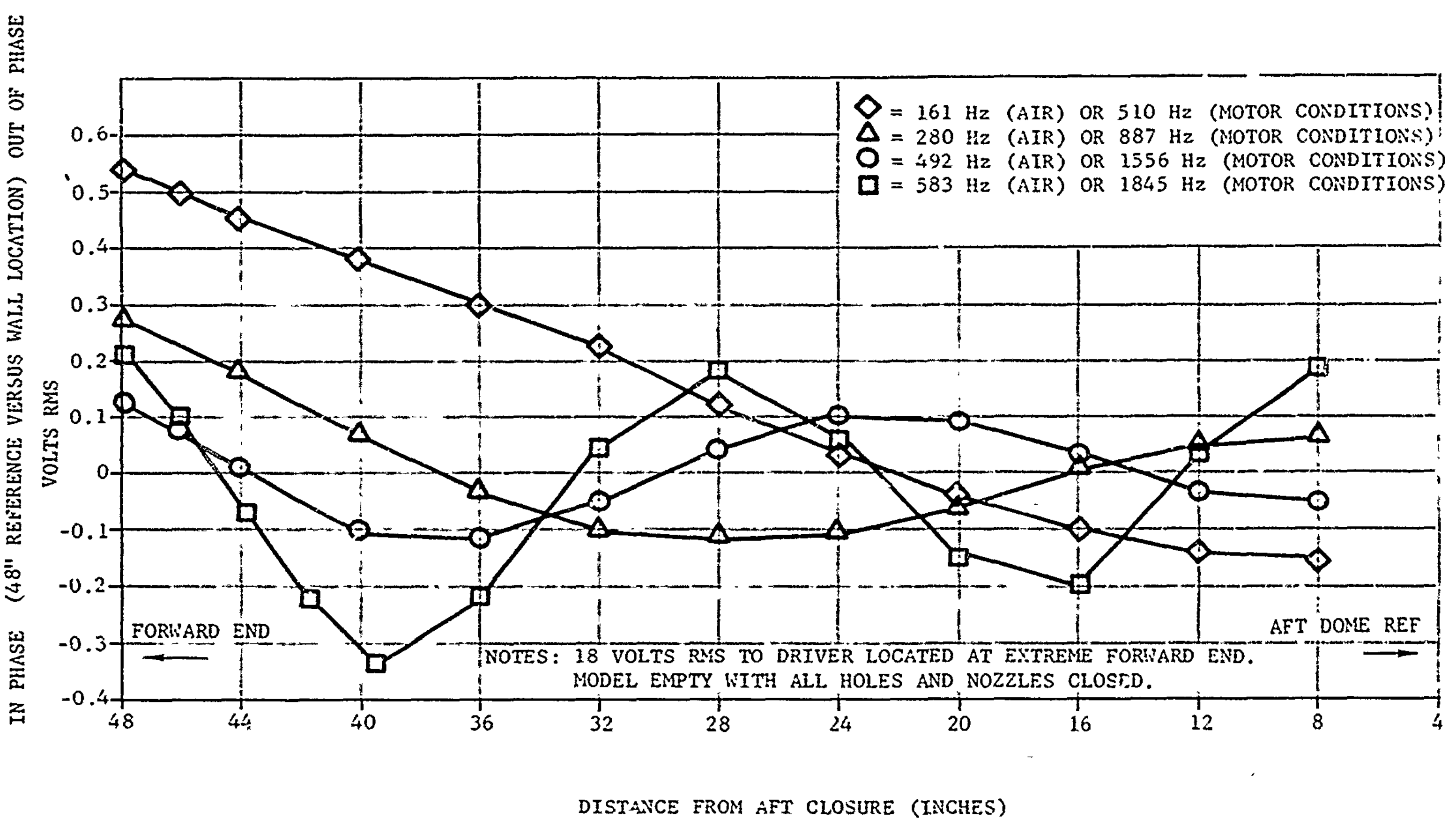

Figure 12. Acoustic Wave Shapes Along Wall Between Wing Slots of M-57A1 15-Second Burn Model

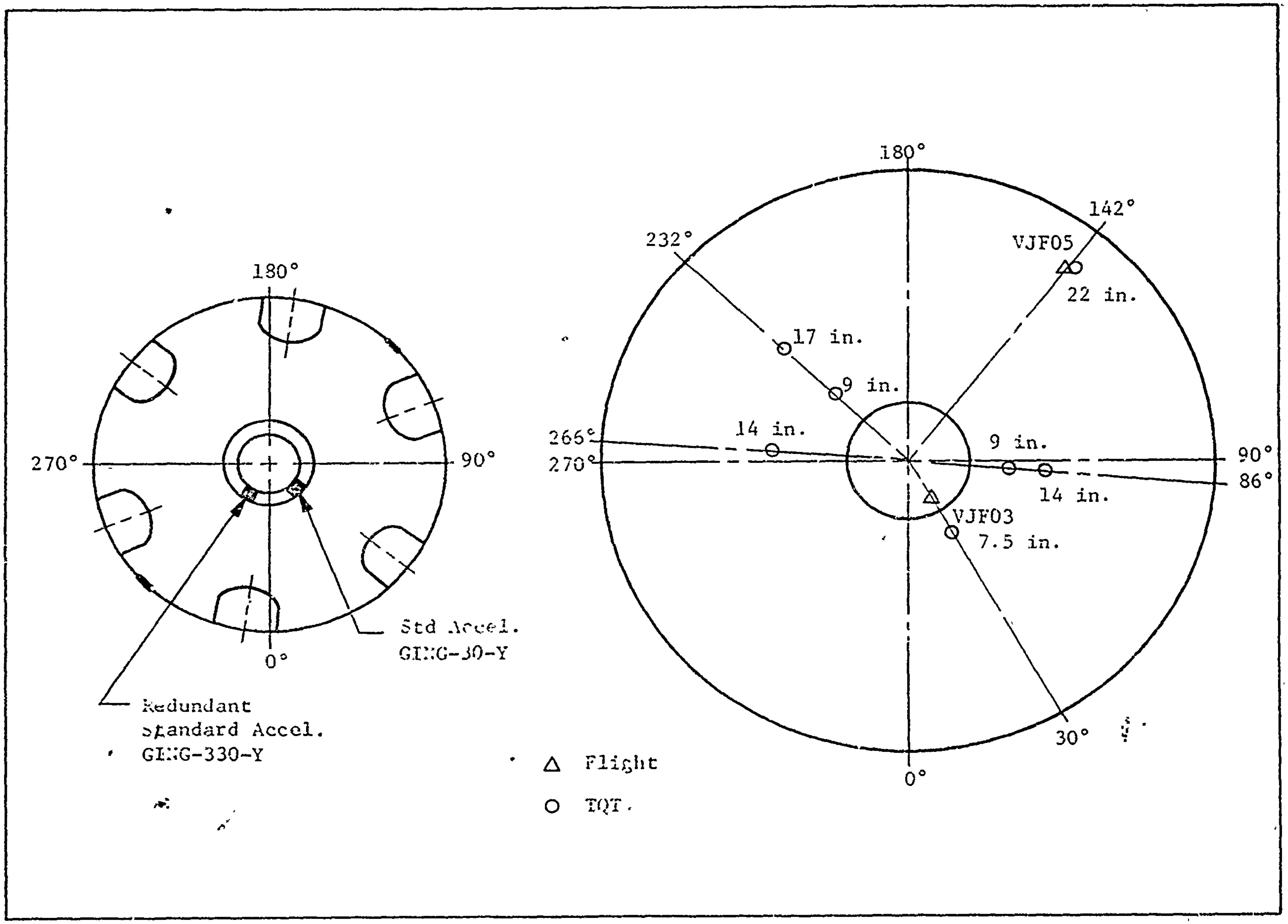

Figure 13. Forward Dome Vibration Instrumentation for the Minuteman III Stage III Motor

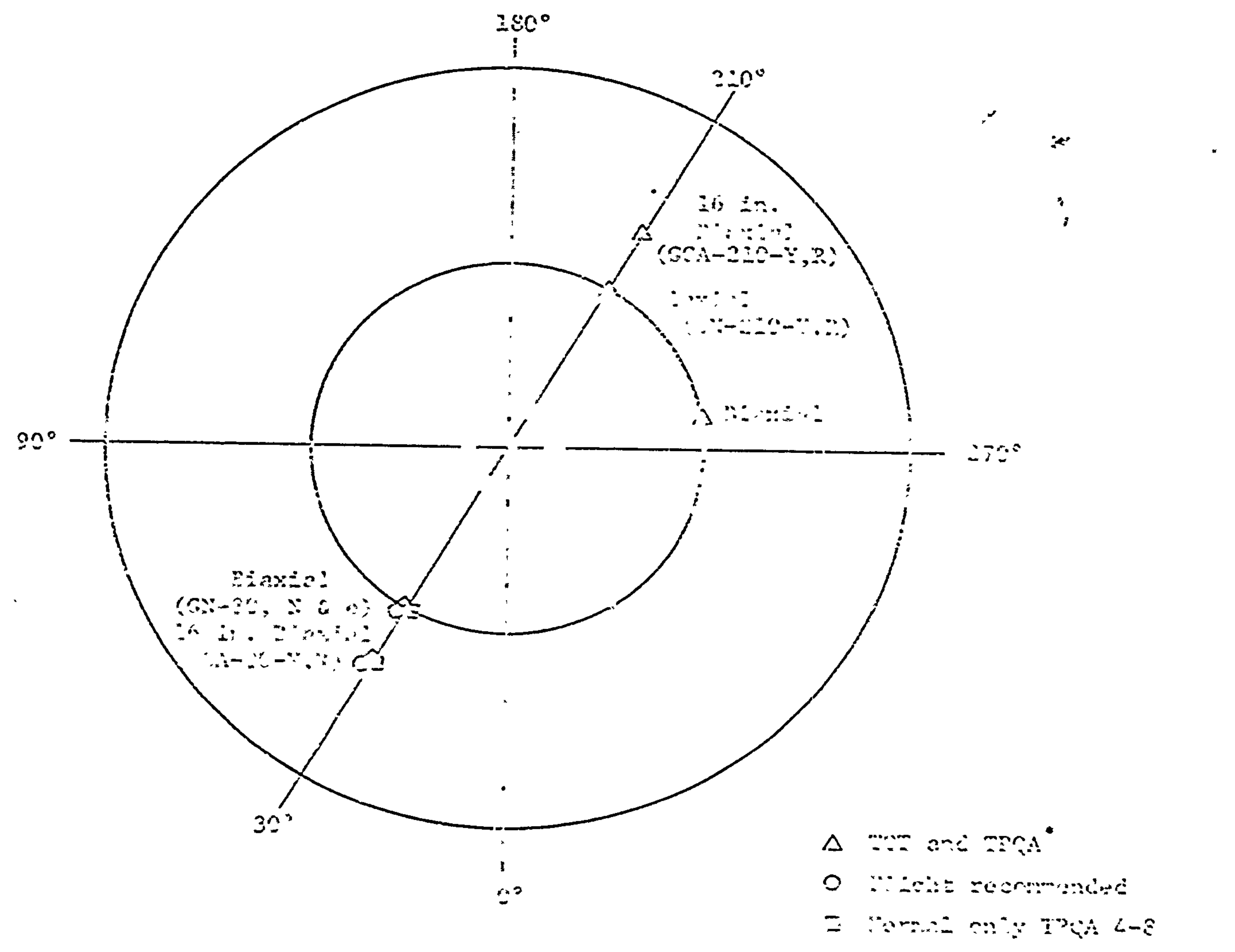

Figure 14. Aft Dome Vibration Instrumentation for the Minuteman III Stage III Motor

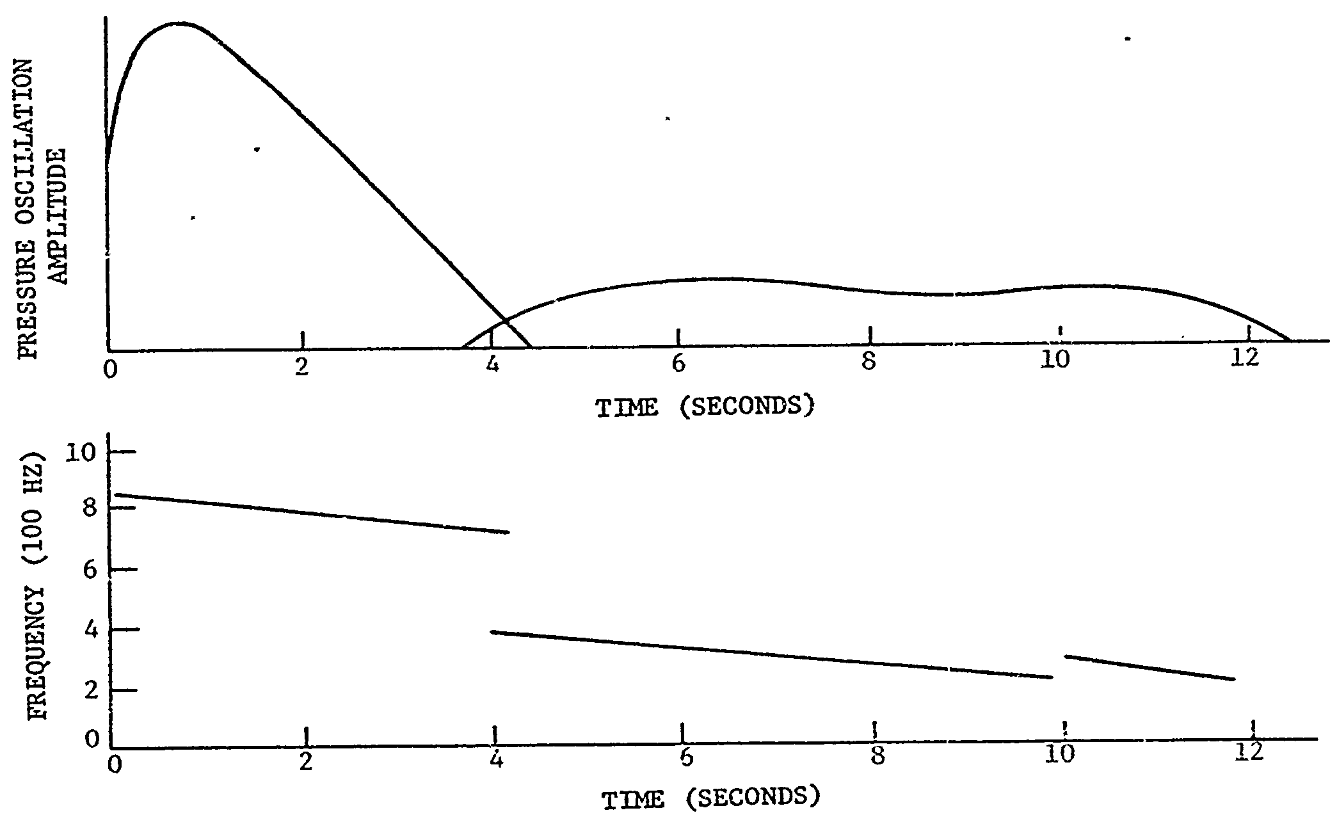

Figure 15. Unstable Pressure Oscillation Characteristics of the Minuteman III Third Stage Motor

DESCRIPTION	LOCATION	AZIMUTH	COMMENT
KISTLER PRESSURE GAGE (P5)	FORWARD ADAPTER	270°	
AC 402 (ACCELEROMETERS)	TT PORT	330°	AXIAL
AC 403 (ACCELEROMETERS)	TT PORT	30°	AXIAL
AC 404 (ACCELEROMETERS)	FORWARD ADAPTER	90°	AXIAL
AC 405 (ACCELEROMETERS)	FORWARD ADAPTER	180°	AXIAL
AC 301 (ACCELEROMETERS)	FORWARD TANGENT POINT	190°	AXIAL

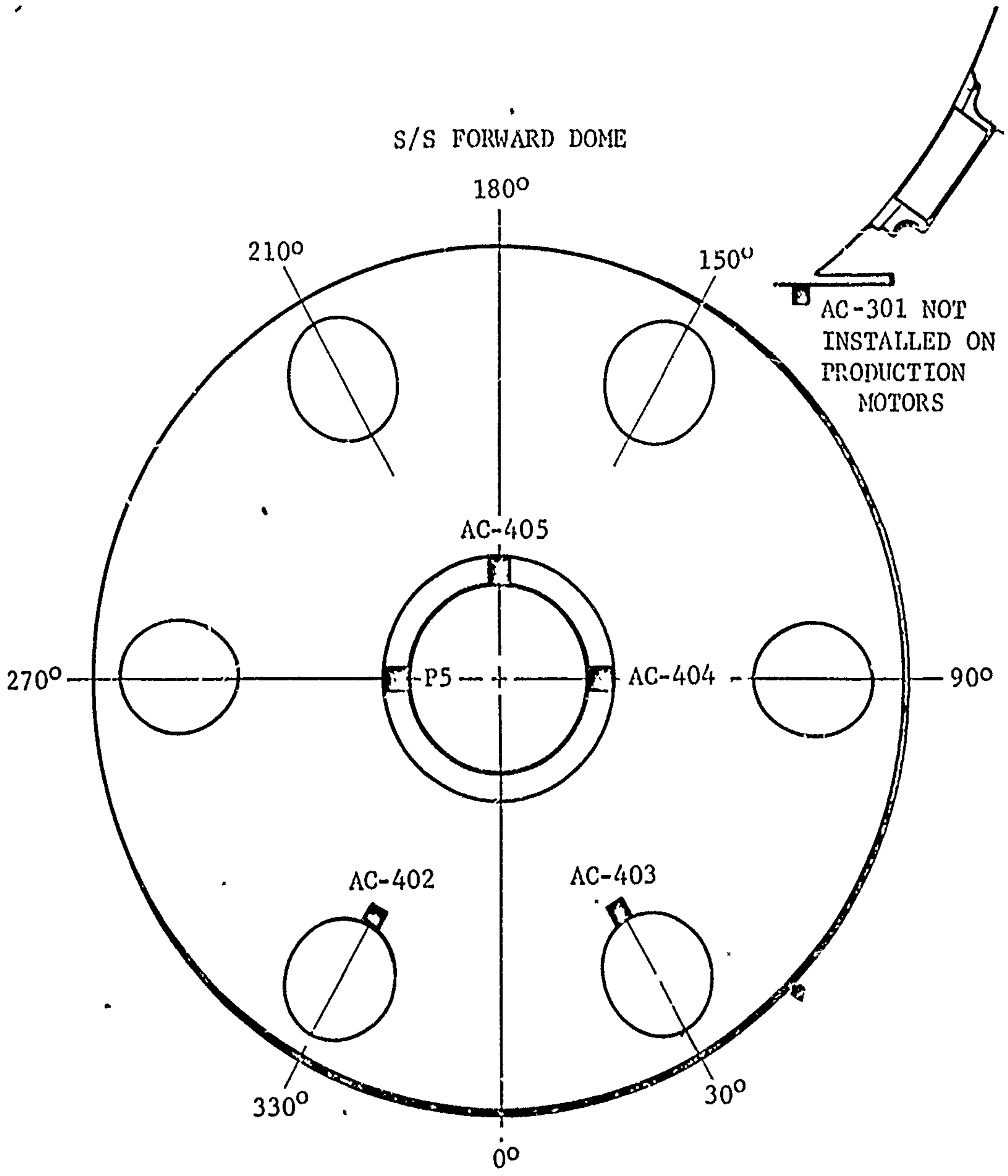

Figure 16. Poseidon Second Stage Instrumentation for Vibration Measurements

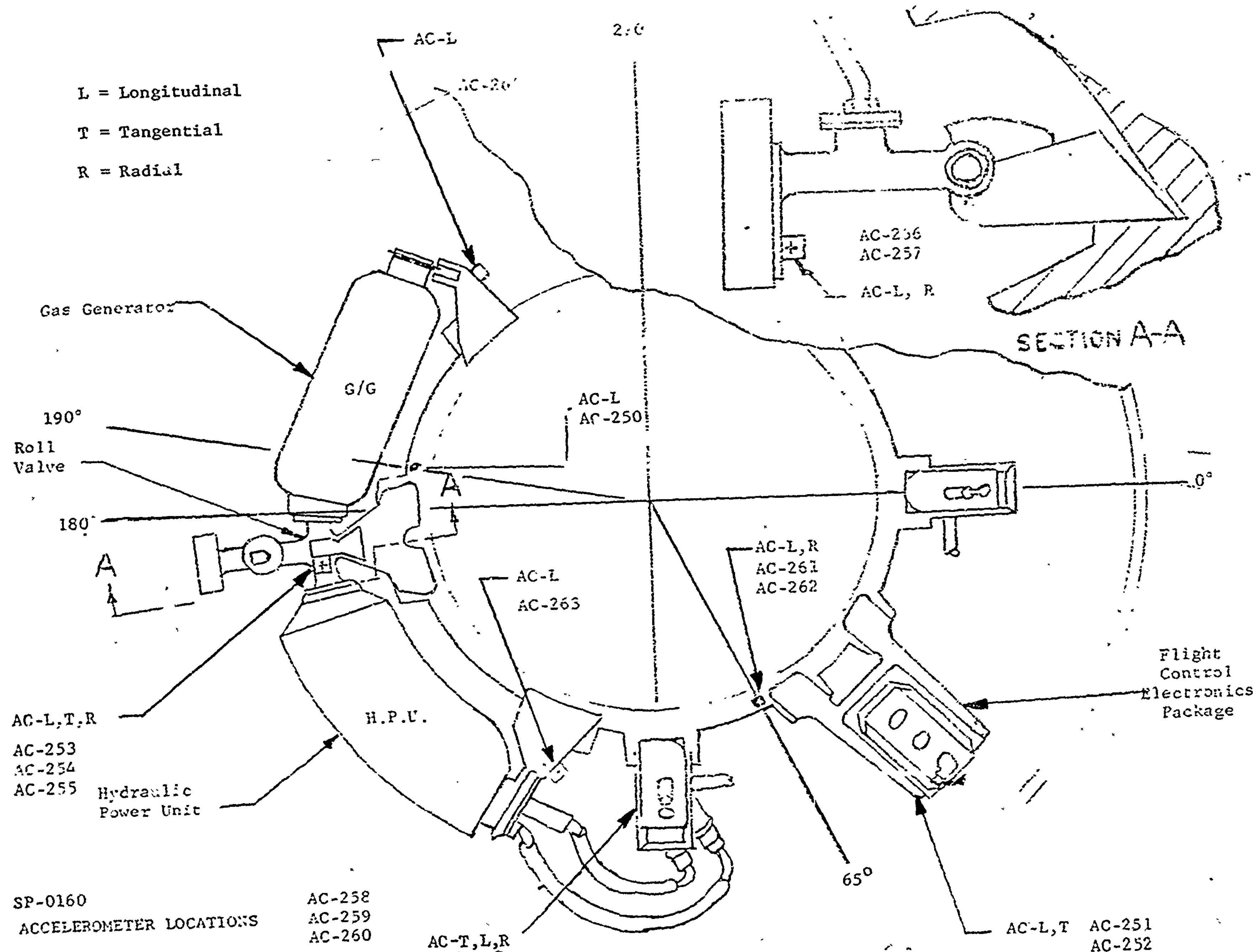

Figure 17. Special Accelerometer Locations for Static Firing of Poseidon C-3 Second Stage Motor SP-0160

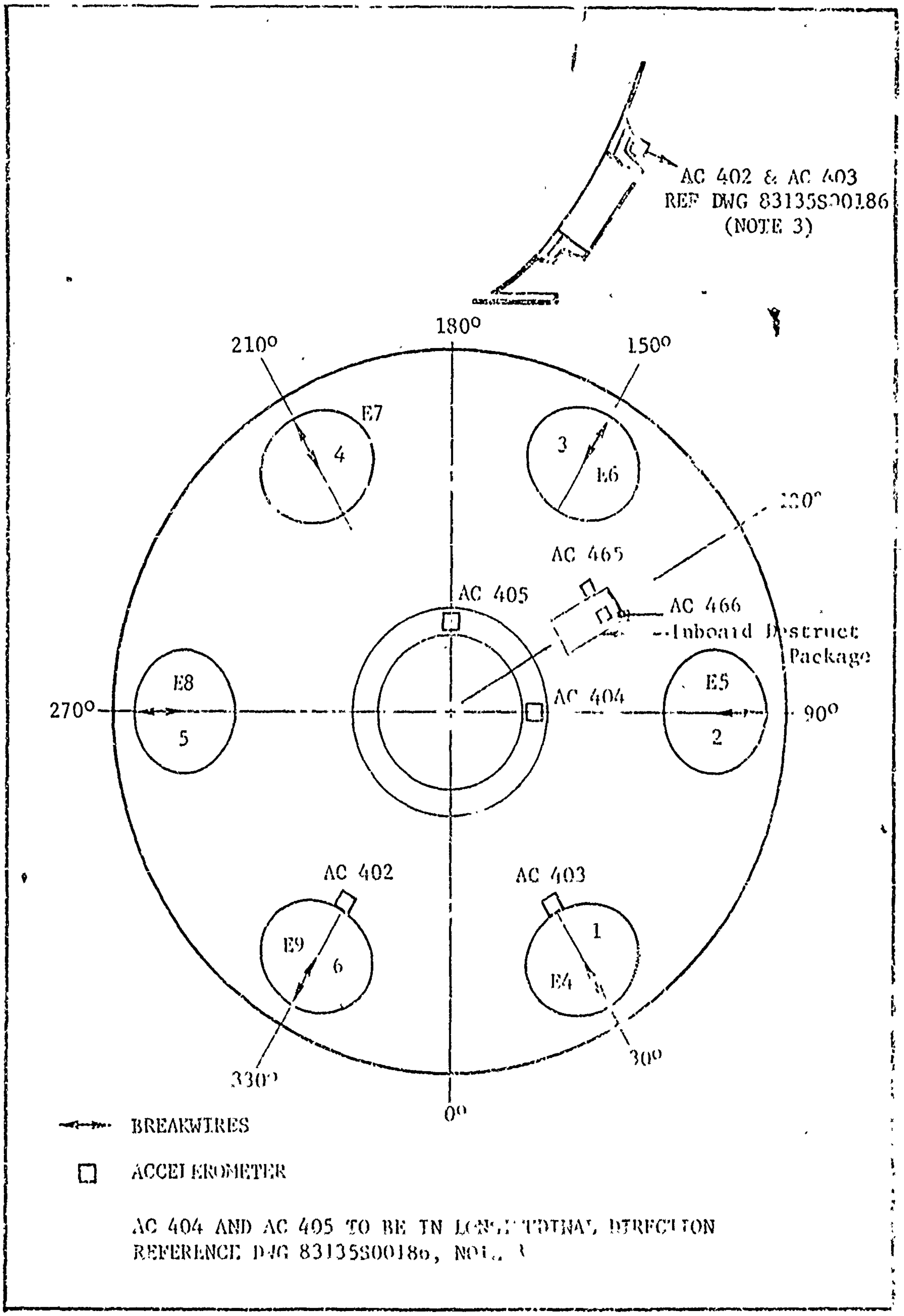

Figure 18. Forward Dome TT Port Instrumentation

LIST OF REFERENCES

1. Minuteman II Stage III Oscillatory Burning Studies and Final CYH Powder Lot Categorization Report, Weapon System 133B, AF Contract 04(694)-903, prepared by Hercules Incorporated, Magna, Utah, for Space and Missile Systems Organization, Norton AFB, San Bernardino, California, August 1970.

2. Final Report, Quality Assurance Test Number VI-QA-82, (Ground Level Test), MTO-1134-14, M57A1 Operational Rocket Motor, Weapon System 133B, AF 04(694)-903, Hercules Incorporated, Magna, Utah, 31 December 1969.

3. Oscillatory Burning and Vibration Analysis Summary, Stage III Minuteman, Weapon System 133B, AF 04(694)-903, Hercules Incorporated, Magna, Utah, 5 May 1969.

4. Final Report of the Transportation and Handling Program for the Stage III Minuteman Motor, Weapon System 133A, Contract AF 04(647)-243, MTO-21, Hercules Powder Company, Magna, Utah, 30 June 1964.

5. Final Report on the Investigation of Pressure Oscillations During Firing of the Minuteman II Stage III Motor, MTO-1124-34, Vol. III, Task II - Analysis, Contract AF 04(694)-903, Hercules Incorporated, Magna, Utah, January 1971.

6. Anderson, J. M., and Durrant, S. O., "A Finite Element Solution for Acoustic Mode Shapes and Frequencies in Rocket Motor Combustion Cavities," <u>7th JANNAF Combustion Meeting</u>, CPIA, Pub. 204, Vol. I, February 1971.

7. Anderson, J. M., "Structural Damping of Acoustic Oscillations in Solid Propellant Rocket Motors," <u>8th JANNAF Combustion Meeting</u>, CPIA, Pub. 220, Vol. I, November 1971.

8. Herting, D. N., et. al., "Acoustic Analysis of Solid Rocket Motor Cavities by a Finite Element Method," NASA TM X-2378, NASTRAN: User's Experiences, NASA, Washington, D.C., September 1971.

9. Jessen, E. C., Bangerter, C. D., and Tew, B. E., "Solid-Propellant Motor Acoustic Model Testing," <u>7th JANNAF Combustion Meeting</u>, CPIA, Pub. 204, Vol I, February 1971.

10. Final Report, Minuteman III Third Stage Pressure Oscillation Study, Report 1387-01F, Aerojet Solid Propulsion Company, Sacramento, California, August 1971.

11. Final Report on the Poseidon Second Stage Acoustics Investigation, Doc. No. SH015-B3A00HTJ-1, Contract No. N0003066C0186, Subcontract No. 17-10203, Hercules/Thiokol (A Joint Venture), Volume I, March 1971.

12. Thacher, J. H., and Dickinson, B. B., "Relationship Between Motor Parameters and Oscillatory Response in the Poseidon Second Stage Motor," <u>8th JANNAF Solid Propellant Combustion Meeting</u>, September 1971.

DISTRIBUTION LIST

Task 1 Report Only:

J. M. Anderson

M. W. Beckstead

S. C. Browning

B. A. Findley (3) for PCO

SPLB-50/D. L. Shelley

APPENDIX B

ACOUSTIC NATURAL MODE AND FREQUENCY DEFINITIONS
TASK 2 FINAL REPORT

AS PREVIOUSLY PUBLISHED

HERCULES INCORPORATED
INDUSTRIAL SYSTEMS DEPARTMENT • SYSTEMS GROUP
P. O. BOX 98, MAGNA, UTAH 84044 • TELEPHONE: 297-5911

28 September 1973

In Reply Refer To:
0025/6/40-3764

Dr. D. George/DYSC
Air Force Rocket Propulsion Laboratory
Edwards Air Force Base, California 93523

Subject: Contract No. F04611-73-C-0025, Task 2 Final Report

Dear Sir:

Forwarded are two copies of the Task 2 Final Report. This report is not a required contract data item. The report contains selected acoustic natural frequencies and mode shapes for use in Task 3 and your approval is requested.

Very truly yours,

F. R. Jensen

F. R. Jensen
Principal Investigator

FRJ/pj

Enclosures

cc: (letter only)

AFFTC/PMRB - G. M. Plock

TASK 2 FINAL REPORT

ACOUSTIC NATURAL MODE AND FREQUENCY DEFINITIONS

RPL COMPONENT VIBRATION PROGRAM

Contract No. F04611-73-C-0025

28 September 1973

Prepared for

AIR FORCE ROCKET PROPULSION LABORATORY
Edwards Air Force Base, California

Prepared by

HERCULES INCORPORATED
Bacchus Works
Magna, Utah

FOREWORD

This report was written under Task 2 of Air Force Contract No. F04611-73-C-0025. Acoustic pressure mode shapes and natural frequencies for use in Task 3 analyses are defined herein. This report is not a required contract data item. This work was performed by Hercules Incorporated, Systems Group, at the Bacchus Works, Magna, Utah. The cognizant project engineer is Dr. D. George/AFRPL, Edwards Air Force Base, California.

ABSTRACT

The purpose of Task 2 was to provide acoustic pressure mode shapes and natural frequencies for the frequency response finite-element analyses which are to be performed under Task 3. Existing data on mode shapes and frequencies from four major sources were reviewed. It was concluded that existing data could be used for definition of the mode shapes and no additional acoustic analyses were performed. Data from MSC NASTRAN analyses, NWC acoustic tests, Hercules analyses, and Hercules acoustics tests were reviewed and compared. Two longitudinal and two transverse modes were defined at each of the two selected burn times. Burn times selected for the analyses are zero and 4.0 seconds.

TABLE OF CONTENTS

LIST OF FIGURES

LIST OF FIGURES (CONT)

LIST OF TABLES

SECTION I

INTRODUCTION AND SUMMARY

A. INTRODUCTION

The work to be accomplished under Task 2 is described in the approved program plan:

> "Existing test data and analysis results will be reviewed in an effort to define acoustic pressure modes and corresponding frequencies for the baseline motor. If existing information is not sufficient, the acoustic analyses will be performed as required to supply the missing information. Two longitudinal and two transverse mode shapes are required for each of two different burn times. The particular modes will be selected on the basis of maximum hardware response. Required, but at present unavailable, acoustic analyses will be performed using the acoustic analysis capability of NASTRAN Level 15. One of the burn times considered will correspond to the zero burn condition applicable to the inert motor to be tested in Task 4. The second burn time will be selected based on maximum component response and if possible, such that both longitudinal and transverse acoustic mode excitation is present. The pressure modes will be prepared for use as input to the structural analysis of Task 3."

This report documents the work which has been accomplished under this task. Two burn times have been selected as required and mode shapes and frequencies for the pressure distributions have been defined. The pressure distribution data given in this report will be used in the analyses of Task 3.

B. SUMMARY

To make a logical selection of burn times as required in the work statement, existing data were reviewed and some additional static firing data were reduced. The zero burn time was selected for analysis so that results from the zero burn time motor configuration tested in Task 4 could be used. The second burn time of 4.0 seconds was selected based on the variety of acoustic modes which are active in the neighborhood of that burn time.

A further review of existing data was made to select particular frequencies and mode shapes for analysis. Existing frequency and mode shape data from MSC NASTRAN analyses, NWC acoustic tests, Hercules analyses, and Hercules acoustics tests were reviewed and compared. It was necessary to apply correction factors to some of the data so that comparisons could be made on a uniform basis. Two longitudinal and two tangential modes were selected for analysis at each of the two burn times as required in the work statement. All required mode shapes were defined.

SECTION II

EXISTING DATA REVIEW

The primary sources of data and information for study of acoustic modes of the C-3 Poseidon S/S motor are listed and discussed in this section. No attempt is made in this discussion of individual data sources to compare reported results. Reported data may not be directly comparable since some data correspond to cold air conditions and other data apply to hot motor firing conditions. The difference in the speed of sound in cold air compared with the speed of sound in hot combustion gas is responsible for large differences in the frequencies at which particular acoustic modes occur. An effort is made to compare results from different sources in later sections of this report by making speed-of-sound corrections. In addition, the rationale used in selecting burn times, modes, and frequencies is discussed in the following sections.

1. NASTRAN Acoustic Analysis (MSC)

An analysis was performed on the combustion cavity of the Poseidon S/S motor by the MacNeal-Schwendler Corporation using the special acoustic cavity capability which is available in NASTRAN, Level 15. Results of the analysis are reported in both References 1 and 2. Table I, extracted from Reference 1, gives the calculated natural frequencies. The pressure distribution mode shapes corresponding to the given calculated frequencies are illustrated in Figures 1a, 1b, and 1c. The figures were obtained from Reference 1.

2. Hercules Acoustics Tests

At Hercules, an effort was made to experimentally measure acoustic mode shapes and corresponding natural frequencies for the acoustic cavity. Three different fullscale models were used, including a fullscale inert motor to obtain results for three different burn times. This work is reported in Reference 3.

Three pure longitudinal modes were reported[3] to occur at frequencies of about 240, 355, and 430 Hz. Figure 2, taken from Reference 3, shows the 240 Hz mode shape.

Reference 3 is a final report on the Hercules acoustic testing program. Additional information is available in various intermediate reports. Reference 4 is an intermediate report which contains detailed mode shape plots. Figures 3 and 4, taken from Reference 4, show the mode shapes corresponding to the 355 and 430 Hz measured natural frequencies.

In Figure 2, the phase for the peak which occurs between 20 and 40 inches is indicated to be 180 degrees. Thus, this peak should be drawn down rather than up to obtain the more conventional in-phase mode shape diagram. The same reasoning must be applied to the mode shapes shown in Figures 3 and 4 where in-phase or out-of-phase is indicated by the "hash" marks along the top of the plot.

3. Naval Weapons Center Acoustics Tests

A series of acoustics tests were performed on one-quarter scale models of the Poseidon S/S combustion cavity at the Naval Weapons Center, China Lake, California. According to a recent communication with NWC, results from these tests hav not yet been published. However, some informal data on NWC tests are available in Hercules files. According to Hercules records from meetings and telephone conversations with NWC personnel, the frequencies for the first three axial modes at three different burn times are as given in Table II. A more complete listing of frequencies is given in Table III. Apparently, the axial mode frequencies given in Table III were later updated for an unknown reason to those given in Table II. Thus, Table III is apparently partially obsolete, but is presented for the sake of the tangential and radial mode frequencies which are given.

4. Hercules Finite-Element Acoustic Analysis

An axisymmetric finite-element model of the Poseidon S/S combustion cavity was analyzed with the use of Hercules program no. 62402, "Axisymmetric Vibration Potential Energy Program". A formal report on this analysis has not been issued; however, some results were given in Reference 3. The results from Reference 3 are shown in Figure 5.

Reasonable agreement between experimental and analytical mode shapes is shown in Figure 5. Note that the mode is labeled as a third mode in the figure title, but the mode shape appears to be a second mode. The mode shape shown is considered to be a third mode based on the reasoning that the pressure decreases along the grain surface in the gap between the grain and nozzle bucket, thus making the mode shape appear more like a third mode.

Although the analysis is unpublished, some results are on file at Hercules. The first three longitudinal modes were found to occur at frequencies of 126, 220, and 360 Hz. By varying the boundary conditions assumed for the axisymmetric model, the second frequency was varied from 215 Hz to 230 Hz. Another resonance was found to occur at 286 Hz, but it was not identified as a longitudinal mode. The mode shapes for the first three longitudinal modes are shown in Figures 6, 7, and 8.

5. Hercules Static Firing Data

Pressure oscillation data and accelerometer data from all Hercules static firings of Poseidon S/S motors are available from the Test Analysis Group at the Hercules Bacchus Works. These data have not been collected, analyzed, and reported as a complete set, but individual firing reports, in addition to raw data in the form of FM tapes, are available.

To isolate frequencies of interest in the firing data (accelerometer and pressure gage data), the FM tapes recorded during the firings are passed through a frequency analyzer. A Quan-Tech Model 305 Tracking Wave and Spectrum Analyzer is used. For routine firing data analysis, the usual procedure is to use the wave analyzer in the tracking mode with a 100 Hz bandwidth filter. In the tracking mode, the analyzer will track the predominant frequency in a preselected frequency range over a given time interval and output the amplitude of the signal which passes through the 100 Hz bandwidth filter.

Results from many firings[3] have been used to plot the response envelopes shown in Figure 9. The motor is said to respond generally at nominal frequencies of 250, 670, 750, 1300, 2000, and 2600 Hz and at some higher frequencies. In addition, weaker response levels are sometimes measured at frequencies of 500, 1000, 1200, 2700, and 3900 Hz. The weaker response levels are not indicated in Figure 9.

6. Task 4 Acoustic Testing Results

Acoustic vibration testing on a fullscale inert motor was conducted under Task 4 of this program. Results from the testing are reported in Reference 5. The pressure distribution along the circular portion of the centerbore was mapped at frequencies of 57, 158, 192, 265, 315, and 364 Hz. The extent of mapping conducted is not sufficient to completely define a mode shape, but it should be possible to use these data for mode shape identification by comparing with other available mode shapes. In addition, some of the accelerometer frequency response data may be useful in this Task 2 work. Plots of accelerometer output as a function of frequency are given in Reference 5.

SECTION III

BURN TIME SELECTION

One burn time has been preselected and needs no further discussion. The zero burn time is selected so that results from NASTRAN math models can be compared with test data obtained from the inert motor testing of Task 4. The inert motor had a zero burn time grain configuration.

The second burn time was to have been selected to obtain maximum component response and if possible, such that both longitudinal and transverse acoustic modes are present. To provide more information for burn time selection, accelerometer data from two static firings were analyzed in detail. An accelerometer mounted on the aft adapter ring was selected for this detailed study. The data study reported in this section was previously reported in Reference 6.

Accelerometer data from Poseidon S/S static fired motors SP-0131 and SP-0160 were analyzed. The data came from accelerometer no. AC-250, which was mounted on the aft adapter ring for both motors. The AC-250 accelerometer measured response accelerations in the motor axial direction.

The accelerometer data were analyzed by playing FM tapes through a Quan-Tech Model 305 Tracking Wave and Spectrum Analyzer. The amplitude-time response was mapped over certain frequency ranges by filtering the accelerometer signal with a 10 Hz bandwidth filter with a constant (non-tracking) center frequency. To map a particular frequency range, the filter center frequency was moved across the range of interest in 10 Hz increments with the analysis being repeated each time the filter center frequency was shifted.

As shown in Figure 9, there are four predominant frequency ranges between 0 and 2000 Hz: (1) 240 to 260 Hz, (2) 600 to 800 Hz, (3) 1200 to

1500 Hz, and (4) 1900 to 2100 Hz. To obtain a more detailed description of motor responses in these frequency ranges, each range was mapped using the procedure outlined above.

Results of the frequency mapping for the 1900 to 2100 Hz range are shown in Figures 10 and 11. Each separate curve indicates the vibration amplitude as a function of firing time. Curves for the different frequencies have been shifted on the plot so that each separate curve has a different zero reference for the vibration amplitude scale. Values for vibration amplitude are not shown, but the scales are comparable for the individual curves. Observation of Figures 10 and 11 indicates that the 2000 Hz mode begins at about one second of burn time and at a frequency of about 2020 Hz. The amplitude quickly increases to a maximum at 2 to 2-1/2 seconds as the frequency decreases slightly to between 1900 and 2000 Hz. The 2000 Hz mode has nearly disappeared by 4 seconds of burn time.

The mapping of the 1200 to 1500 Hz frequency range is shown in Figures 12 and 13. Figure 13 shows that two distinct resonances occur in the 1200 to 1500 Hz frequency range. The first begins at approximately 4 seconds and lasts until approximately 6 seconds with the frequency shifting from 1320 to 1350 Hz. From approximately 5 to 6 seconds, the amplitude of the shifting resonance subsides, as shown by the curves labeled 1360 through 1390. At approximately 6 seconds, the amplitude of the shifting resonance increases as it covers the range of 1400 to 1490 Hz. By approximately [illegible] seconds the resonance has faded away. The general trend shown by Figure 12 is similar to that shown in Figure 13, but resonant amplitudes are considerably smaller. In Figures 12 and 13 there is a small, narrow-banded resonance which occurs at 1450 Hz at approximately 3 seconds.

Results of mapping the 600 to 800 Hz frequency range are shown in Figures 14 and 15. Both figures indicate that two relatively narrow-banded resonances are present in the 600 to 800 Hz range. The first resonance occurs at approximately 3 seconds and at a frequency of 720 to 730 Hz. This resonance apparently has a strong second harmonic which occurs at 1450 Hz as discussed above (see Figure 13). The second distinct resonance occurs at 670 to 680 Hz beginning at approximately 8 seconds. The two resonances in the 600 to 800 Hz range appear to be unrelated, while the two resonances in the 1200 to 1500 Hz range could result from a frequency shift of the same mode as the burn surface advances.

Figures 16 and 17 show the results of mapping the 240 to 250 Hz range. Results are not as consistent from motor to motor as results obtained for other frequency ranges. Figure 16 shows a definite resonance in the 4 to 5 second area which begins at 250 Hz and shifts to 240 Hz. The 730 Hz response shown in Figure 14 may be a third harmonic of this 240 Hz resonance. The results shown in Figure 17 indicate that the 230 to 280 Hz range contains a relatively large amount of noise (high-level response over a broad frequency range). However, two peaks stand out from the general high noise level: (1) a peak at 3 to 4 seconds on the 260 Hz curve, and (2) a peak at 6 to 7 seconds on the 240, 250, and 260 Hz curves.

Weak responses have reportedly occurred near 500 Hz and near 1000 Hz on some motors. Both areas were mapped for motor SP-0131 and the results are shown in Figures 18 and 19. Figure 18 shows that the frequency range near 500 Hz is noisy like the 250 Hz range. However, a distinct resonance is observed at approximately 4 seconds at 530 to 540 Hz. Two other broad-banded resonances occur at approximately 6-1/2 and 10 seconds. The broad-banded resonances appear in each plot for frequencies between 450 and

490 Hz. Figure 19 indicates that no significant resonance response was measured for motor SP-0131 between the frequencies of 960 and 1200 Hz.

The data analysis reported in this section has served to display the vibration characteristics of the Poseidon S/S motor in greater detail than given in firing reports. Results given here will be used to help interpret results from finite-element models of the motor and to verify the accuracy of the models.

The accelerometer data illustrated in Figures 10 through 19 are summarized in Figure 20. Figure 20 is similar to Figure 9 in that it gives envelopes of response data from static firings. The data analysis method used to obtain Figure 20 should give improved resolution over the method used for Figure 9 (e.g., a 10 Hz bandwidth filter was used for Figure 20 compared with a 100 Hz bandwidth filter for Figure 9). However, Figure 20 is the result of analyzing only one accelerometer on each of two different firings while Figure 9 is based on many firings.

From observation of Figures 9 and 20, it can be seen that 250, 500, and 1300 Hz frequencies are present at a four second burn time. In addition, the 750 and 1450 Hz frequencies occur near to the four second burn time. A burn time of four seconds is therefore a relatively busy time for the motor and is selected as the second burn time to be analyzed in Task 3.

SECTION IV

ACOUSTIC MODE SELECTION

In Section II, acoustic frequency and mode shape data from several sources were reviewed. Some of the results were not comparable because of differences in gas properties (speeds-of-sound). In this section, the differing data are corrected for speed-of-sound differences and compared. The data are then used to select two longitudinal and two transverse modes for analysis at the two burn times.

The speed of sound in air at 20^{o} C is given as 1120 ft/sec. The speed of sound in hot gases in the combustion cavity of the motor during firing is a function of chamber pressure. Using a mean chamber pressure of 325 psi, a speed of sound of approximately 3625 ft/sec was calculated for the motor. The resulting ratio, approximately 3.2, has been used in past work[3] to convert cold air data to hot firing conditions.

Some additional consideration is necessary to study the MSC analysis data and the NWC testing data. The NWC data require application of a scale factor because the model tested was one-quarter scale. The MSC analysis data are not complete because the speed of sound used in the calculations is not specified. The following information, obtained during a telephone conversation with H. B. Mathis of the Naval Weapons Center, is applicable:

> During the time that MSC was conducting the acoustic analyses reported in Reference 1, a meeting was held at RPL between H. B. Mathis of NWC, D. N. Herting of MSC, and Robert Shoener of RPL. At this time, the NWC testing data were transmitted to D. N. Herting. The speed-of-sound employed in the MSC analysis was obtained from Aerojet. In

order to get NWC data to match MSC results, a correction factor was obtained by shifting the second mode test data frequency into exact agreement with analytical results. The same correction factor was then applied to the remainder of the NWC data to obtain the data labeled "experimental" in Table I.

To determine the factor which was used on NWC data for comparison with MSC results, the corresponding frequencies for the first three axial modes have been extracted from Tables I and II and are listed again in Table IV. The information given in Table IV shows that NWC data were multiplied by approximately 1.216 to obtain the results listed under "Experimental" in Table I.

At the present time, the speed-of-sound assumed by NWC for the data of Table II is unknown. However, Table III contains a factor of 0.822 for conversion from model to motor conditions. According to Mr. Mathis, the 0.822 contains both the scale factor (one-quarter) and a speed-of-sound conversion. It therefore appears that NWC used a conversion factor of 3.29 compared with the 3.2 used by Hercules (3.29/4.0 = 0.822).

To compare NWC results with Hercules data, a factor of 3.20/3.29 = 0.973 should be applied to NWC data. To put MSC analysis results on a comparable basis, the MSC results should be multiplied by 0.972/1.216 = 0.80. The data shown in Table V have been multiplied by the appropriate factors. The Hercules analysis and acoustic test data were multiplied by 3.2 for comparison in Table V.

In Table V there is quite good agreement between MSC results and NWC data. In addition, the Hercules analysis and test data seem to confirm the frequencies of the third and fourth longitudinal modes. To obtain this agreement, the Hercules analysis frequencies previously given for the first, second, and third modes were assumed to correspond with the second, third, and fourth modes instead. Natural frequencies were determined by the frequency response method in the Hercules analysis and a lower mode could have been overlooked. The second mode frequency (403 Hz) determined by Hercules analysis is not in good agreement with MSC and NWC data. Frequencies for the first and second tangential modes (T_1 and T_2) as determined by Hercules tests, are not in agreement with the corresponding MSC and NWC data. However, the frequencies labeled "T_1" under Hercules tests are in close agreement with the frequencies labeled "T_3" under MSC Analysis and NWC Tests. Likewise, the Hercules Test frequencies labeled "T2" appear to be in agreement with the MSC and NWC data labeled "T_6".

The MSC analysis results from Table V have been plotted in Figure 9 for three axial and three tangential modes for comparison with static firing envelopes. Based on the data comparison shown in Figure 9, the following modes are selected for use in Task 3 analyses:

A. Zero Burn Time

Since the first longitudinal mode does not occur in the static firing data at a zero burn time and the second mode response is generally weak, the third longitudinal mode at a calculated frequency of 770 Hz is selected for analysis of the zero burn time model. Response of the model to the 770 Hz mode will be used for comparison with static firing data. In addition, the fourth longitudinal mode which occurs at 365 Hz in air selected for analysis to provide results for comparison with the acoustic testing of Task 4. During the Task 4 testing, a strong response was observed at the 365 Hz frequency.

Since no static motor response is observed at the frequency of the T_2 tangential mode, the first and third modes are selected for use in the Task 3 analyses ($T1 = 668$ Hz and $T3 = 1327$ Hz). Analytical results will be compared with static firing data at the T_1 and T_3 frequencies.

B. Four Second Burn Time

The first longitudinal mode is active at the four second burn time as indicated in Figure 9. Also, frequencies near to the third mode frequency are present. Therefore, the first and third longitudinal modes are selected for Task 3 analyses. Using linear interpolation with the values given in Table V gives A_1 = 281 Hz, A_3 = 805 Hz, T_1 = 634 Hz, and T_3 = 1220 Hz for the 4.0 second burn time.

Tangentials T_1 and T_2 are selected for analysis at the 4.0 second burn time because both occur at frequencies close to the measured static firing response envelope of Figure 9. The interpolated frequencies are T_1 = 634 Hz and T_2 = 830 Hz. Mode shapes are discussed in the next section.

SECTION V

DEFINITION OF ACOUSTIC MODE SHAPES

The acoustic mode natural frequencies and the corresponding mode shapes which were selected in Section IV are summarized in Table VI. The longitudinal mode shapes, A_1, A_3, and A_4 are defined in Figure 1. The tangential mode shapes T_1, T_2, and T_3 are discussed and defined in this section.

Apparently, the only source for the tangential mode shapes is the acoustic testing performed by Hercules. Other potential sources were the NWC testing and the MSC analyses. However, no tangential mode shapes appear to be available from these other sources.

Using Hercules testing data has the disadvantage that only the higher frequency modes were studied. For example, the first tangential mode was determined to occur at 410 Hz in the model or, using the factor of 3.2 previously discussed, at 1312 Hz under hot motor conditions. As noted in Table VI, the third tangential mode was determined analytically to occur at 1327 Hz. It is therefore assumed that the mode determined by Hercules testing to occur at 1312 Hz is actually a third mode rather than a first mode. The testing program apparently missed the lower frequency modes.

The 1312 Hz tangential mode shape determined by Hercules acoustics testing is shown in Figures 21 and 22. The circumferential pressure distribution shown in Figure 22 was observed to occur all along the cylindrical section of the motor. The mode shape indicated in Figure 2. basically a first tangential mode rather than the expected third tangential mode. The longitudinal pressure distribution shown in Figure 21 indicates that the 1312 Hz mode appears to be a second longitudinal mode superimposed on a first tangential mode. The mode shapes indicated in Figures 21 and 22 will be used to define the T_3 mode shape as required in Table VI.

Since no specific information is available for definition of the T_1 and T_2 mode shapes at approximately 668 Hz and 830 Hz, it will be assumed that both are composed of the first tangential mode shape as shown in Figure 22. The second mode at 830 Hz will be assumed to consist of the first longitudinal superimposed on the first tangential and the first mode at 668 Hz will be assumed to be a pure first tangential mode distributed uniformly along the length of the combustion cavity (i.e., no superimposed longitudinal mode).

None of the mode shapes defined in this section specify a pressure distribution for the dome cavities. To account for the presence of the combustion gas in the dome cavities, scalar springs will be used in the appropriate finite-element models. The approach of using scalar springs in the dome cavities is in accordance with the approved program plan.

SECTION VI

CONCLUSIONS AND RECOMMENDATIONS

Based on the data review and discussion given in this report, it appears that the frequencies and mode shapes for the first four longitudinal modes are fairly well established. The tangential mode shapes are not as clearly defined.

It is recommended that the longitudinal and tangential acoustic mode shapes and the corresponding frequencies defined in this report be used in the analyses required in Task 3.

TABLE I

NATURAL FREQUENCIES FOR THE POSEIDON SECOND STAGE MOTOR CAVITY*

Harmonic (n)	Mode	Frequency (Hertz)			
		0 Burn		3" Burn	
		NASTRAN	Experi-mental	NASTRAN	Experi-mental
0	1	388.7	398	324.0	322
	2	645.0	645	678.3	689
	3	962.0	962	1039.2	1051
	4	1422.0	1422	1430.8	1425
	5	1769.0	1728	1830.9	1831
	6	2010.8	2130	1994.4	
1	1	835.1		737.8	
	2	1313.4	1216	833.9	868
	3	1659.1	1620	1344.0	1349
	4	1832.8	1798	1558.2	1552
	5	2105.7		1812.5	
	6	2236.8		2130.1	2094

*Taken from Reference 1

TABLE II

AXIAL ACOUSTIC MODE FREQUENCIES FROM NWC TESTS

Burn Time (sec)	Axial Mode Frequencies (Hz)		
	A_1	A_2	A_3
0	330	530	786
2.5	298	553	836
7.0	265	566	864

TABLE III

ACOUSTIC MODEL FREQUENCY CALCULATIONS
(NWC DATA)

1. Axial Frequencies (superseded by Table II)

Mode No. →	A_1	A_2	A_3	A_4	A_5	A_6
Model	378	757	1134	1513	1892	2270
Motor	311	621	932	1243	1554	1864

2. Tangential Frequencies

Mode No.	0 sec		2.5 sec		7.0 sec	
	Model	Motor	Model	Motor	Model	Motor
T_1	1630	1340	1485	1221	1250	1028
T_2	2705	2224	2463	2025	2074	1705
T_3	3720	3058	3388	2785	2853	2345
T_4	4709	3871	4288	3525	3611	2968
T_5	5679	4668	5172	4251	4356	3581
T_6	8004	6579	7290	5992	6139	5046

3. Radial Frequencies

Mode No.	0 sec		2.5 sec		7.0 sec	
	Model	Motor	Model	Motor	Model	Motor
R_1	3392	2788	3090	2540	2602	2139
R_2	6212	5106	5658	4651	4764	3916

Model to Motor Frequency Conversion Factor = 0.822

TABLE IV

COMPARISON BETWEEN NWC DATA AND MSC EXPERIMENTAL DATA

Burn	Mode	NWC	MSC "Experimental"	Ratio
0" Burn	A_1	330	398	1.206
	A_2	530	645	1.217
	A_3	786	962	1.224
3" Burn, 7.0 Sec Burn Time	A_1	265	322	1.215
	A_2	566	689	1.217
	A_3	864	1051	1.216
			Average	1.216

TABLE V

COMPARISON BETWEEN DATA FROM FOUR SOURCES WITH CORRECTION FACTORS APPLIED

Burn	Mode	Data Source: MSC Analysis	NWC Tests	Hercules Analysis	Hercules Tests
0" Burn 0 Sec Burn Time	A_1	310	321		
	A_2	516	517	403	
	A_3	770	765	736	765
	A_4	1138	1138	1152	1123
	A_5	1415	1382		1375
	A_6	1608	1704		
	T_1	668			1306
	T_2	1050	973		2180
	T_3	1327	1296		
	T_4	1466	1438		
	T_5	1685			
	T_6	1789			
3" Burn 7.0 Sec Burn Time	A_1	259	258		
	A_2	542	551		
	A_3	831	841		
	A_4	1145	1140		
	A_5	1465	1465		
	A_6	1596			
	T_1	590			1080
	T_2	667	694		1650
	T_3	1075	1079		
	T_4	1247	1242		
	T_5	1450			
	T_6	1704	1675		

TABLE VI

SELECTED ACOUSTIC MODES FOR TASK 3 ANALYSES

Burn Time (sec)	Mode	Frequency (Hz)
0	A_3	770
	A_4	365*
	T_1	668
	T_3	1327
4	A_1	281
	A_3	805
	T_1	634
	T_2	830

*In air

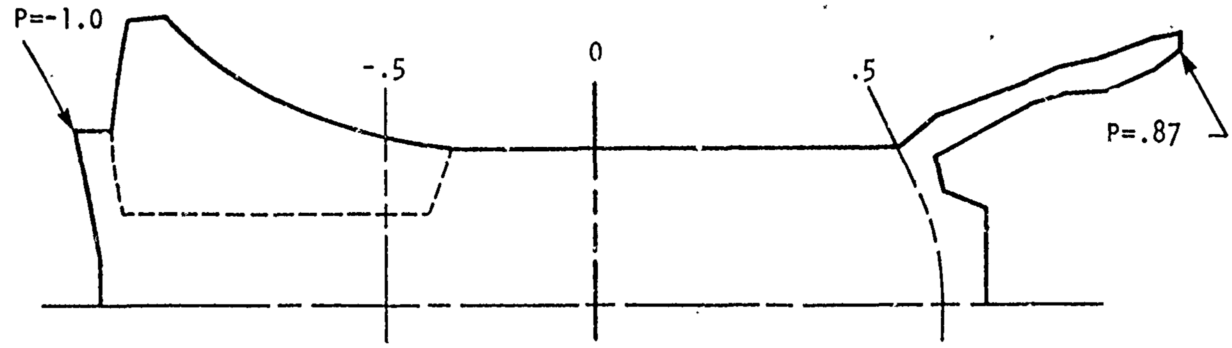

a) Mode 1. f = 388.1 Hz

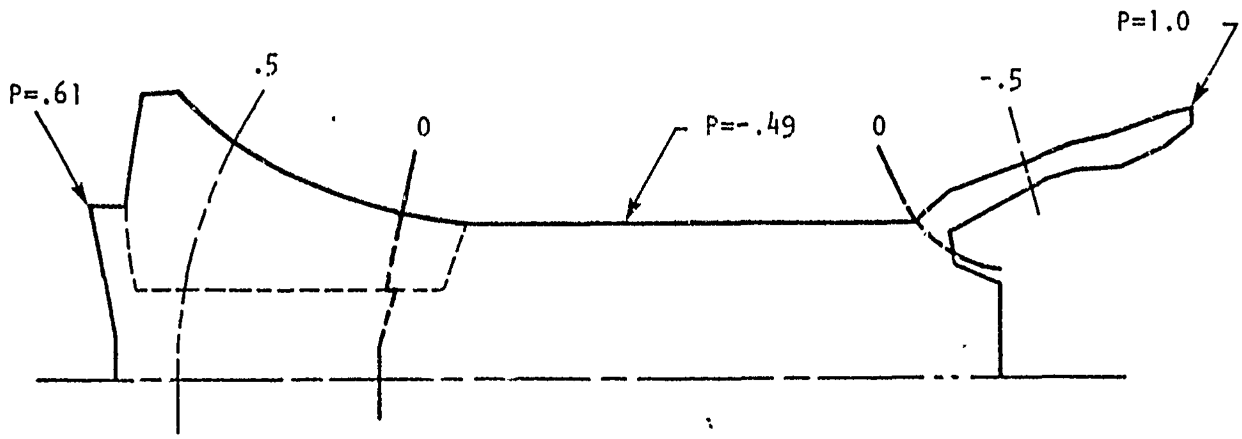

b) Mode 2. f = 645.0 Hz

Figure 1a. Poseidon Second Stage Mode Shapes, n = 0, t = 0.0 Sec

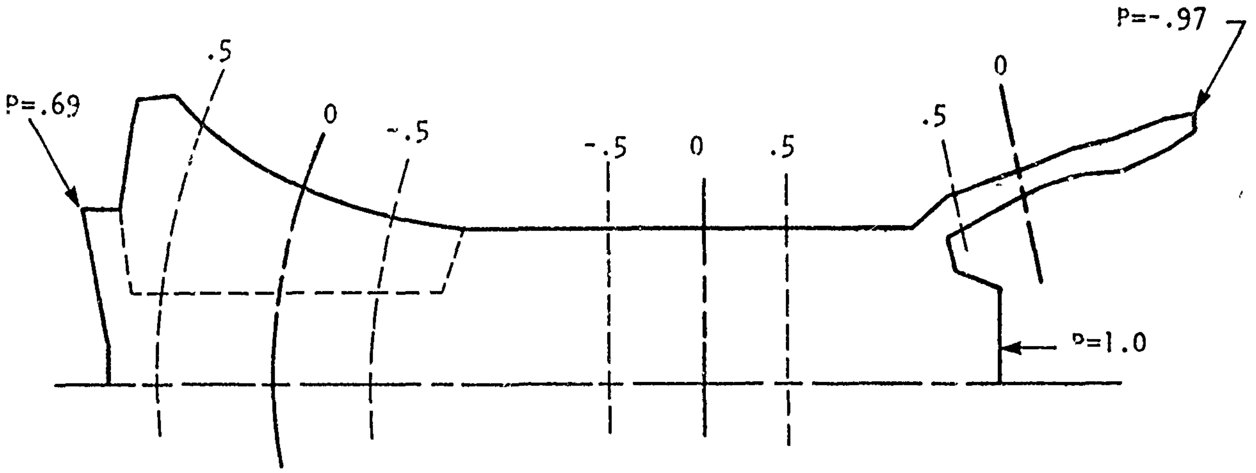

c) Mode 3. f = 962.0 Hz

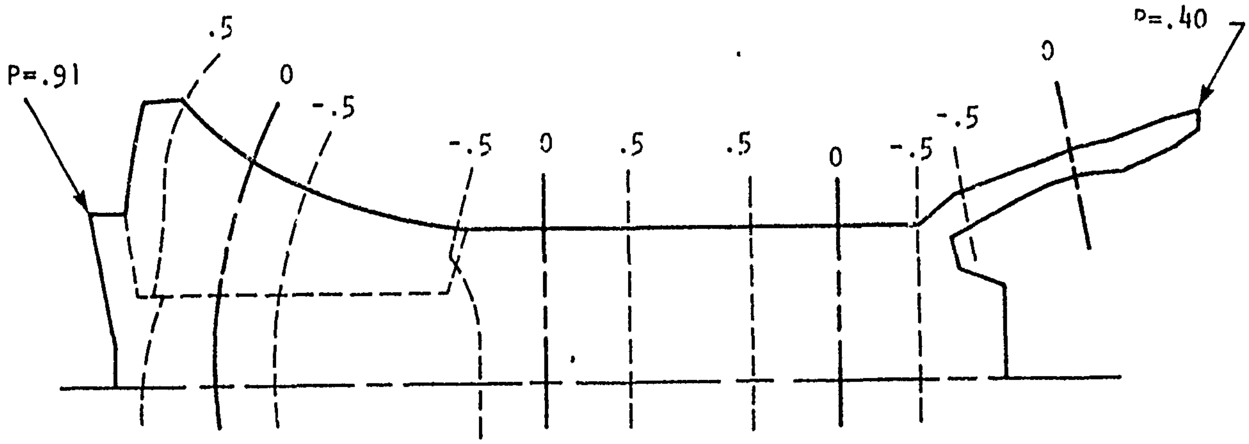

d) Mode 4. f = 1,422.0 Hz

Figure 1b. Poseidon Second Stage Mode Shapes, n = 0, t = 0.0 Sec

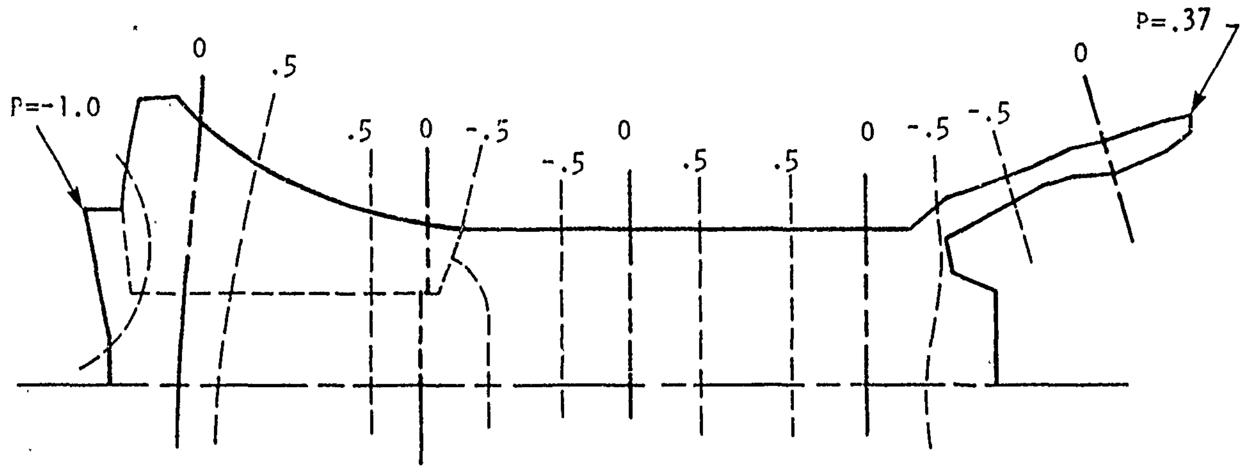

e) Mode 5. f = 1,769.0 Hz

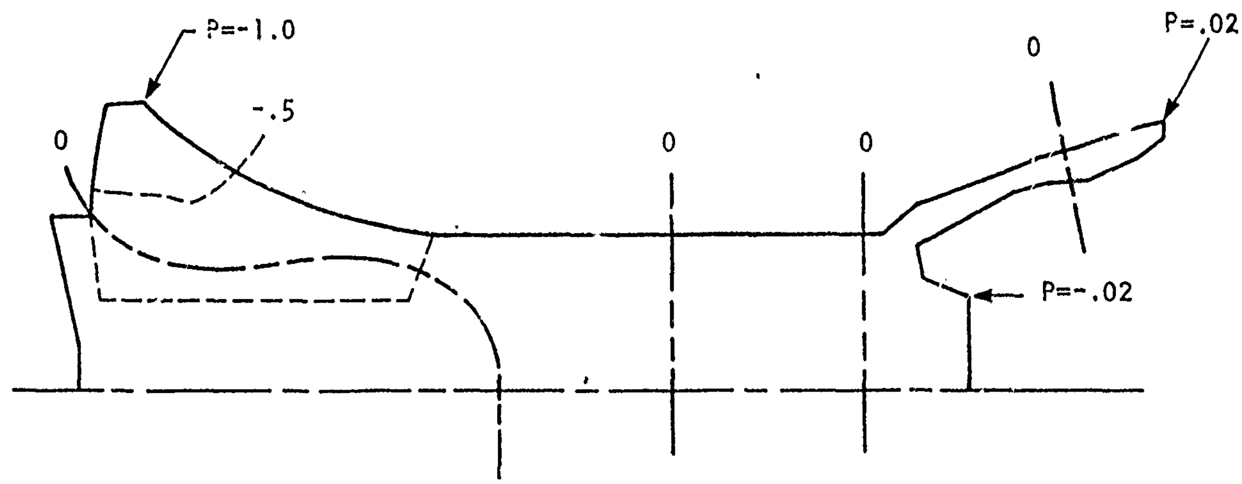

f) Mode 6. f = 2,010.8 Hz

Figure 1c. Poseidon Second Stage Mode Shapes, n = 0, t = 0.0 Sec

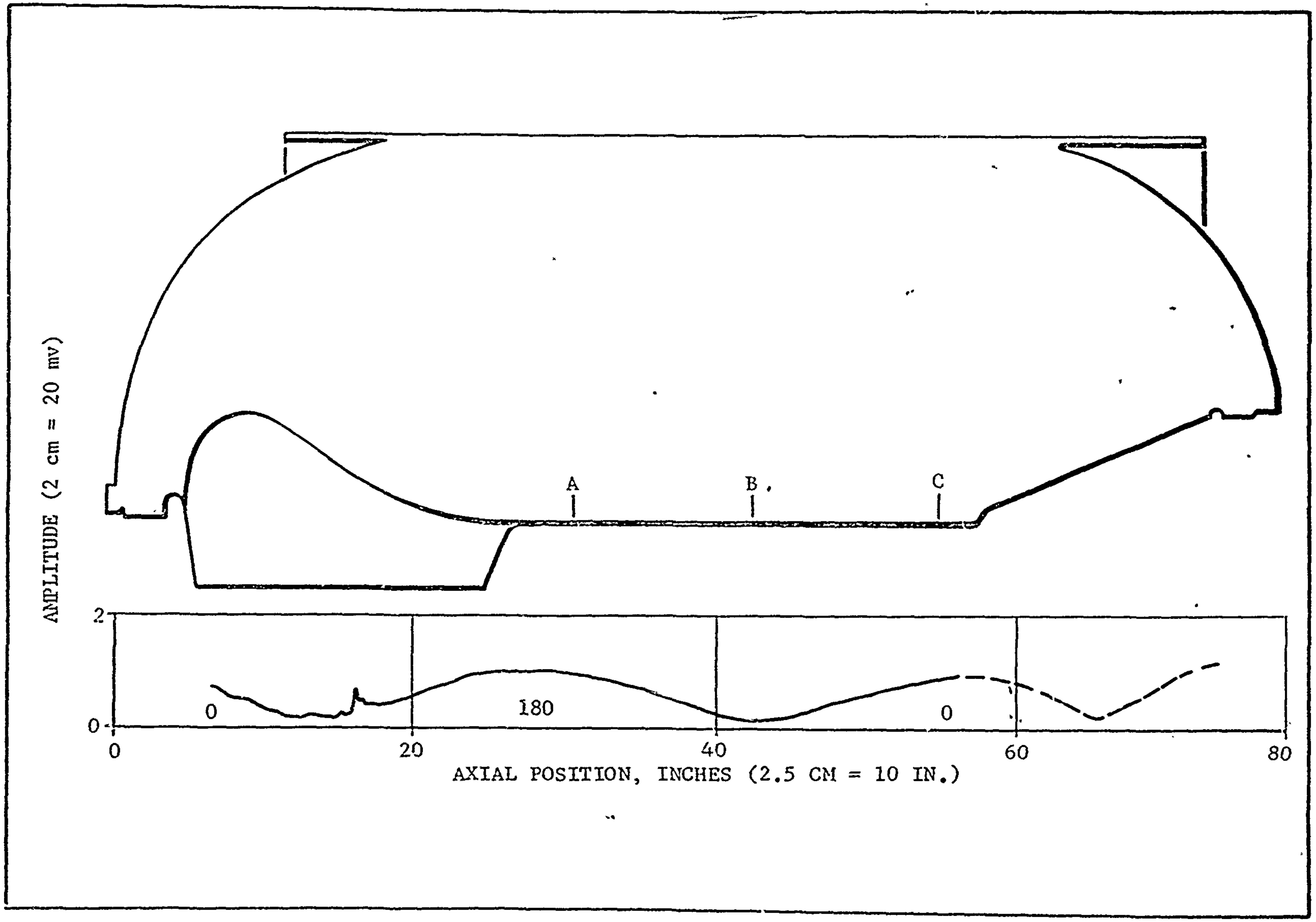

Figure 2. Longitudinal Pressure Distribution Along the Wall of the 10-1/2 L Model, 243 Hz, Driver D_2

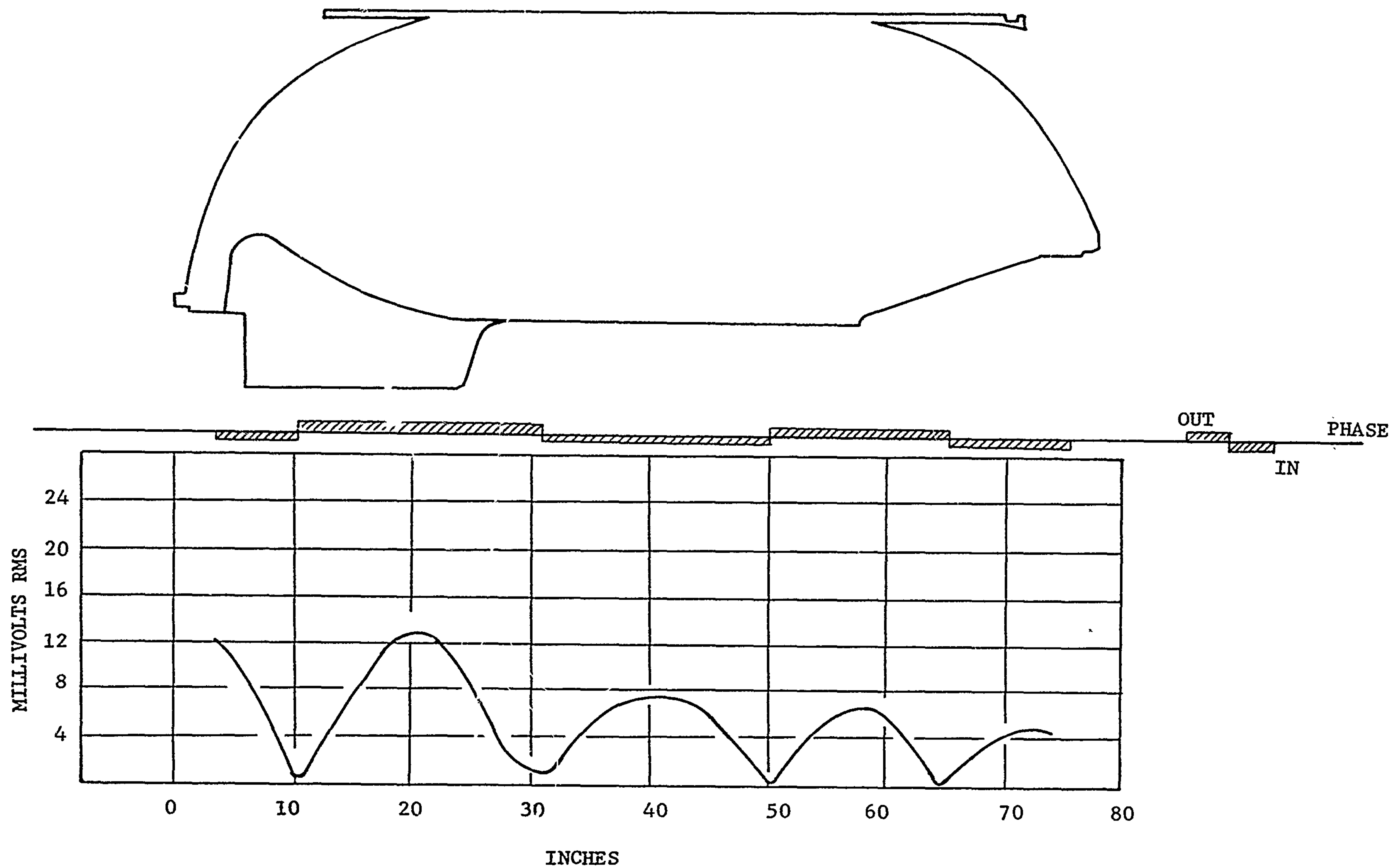

Figure 3. Longitudinal Pressure Mode Shape Measured at 354 Hz

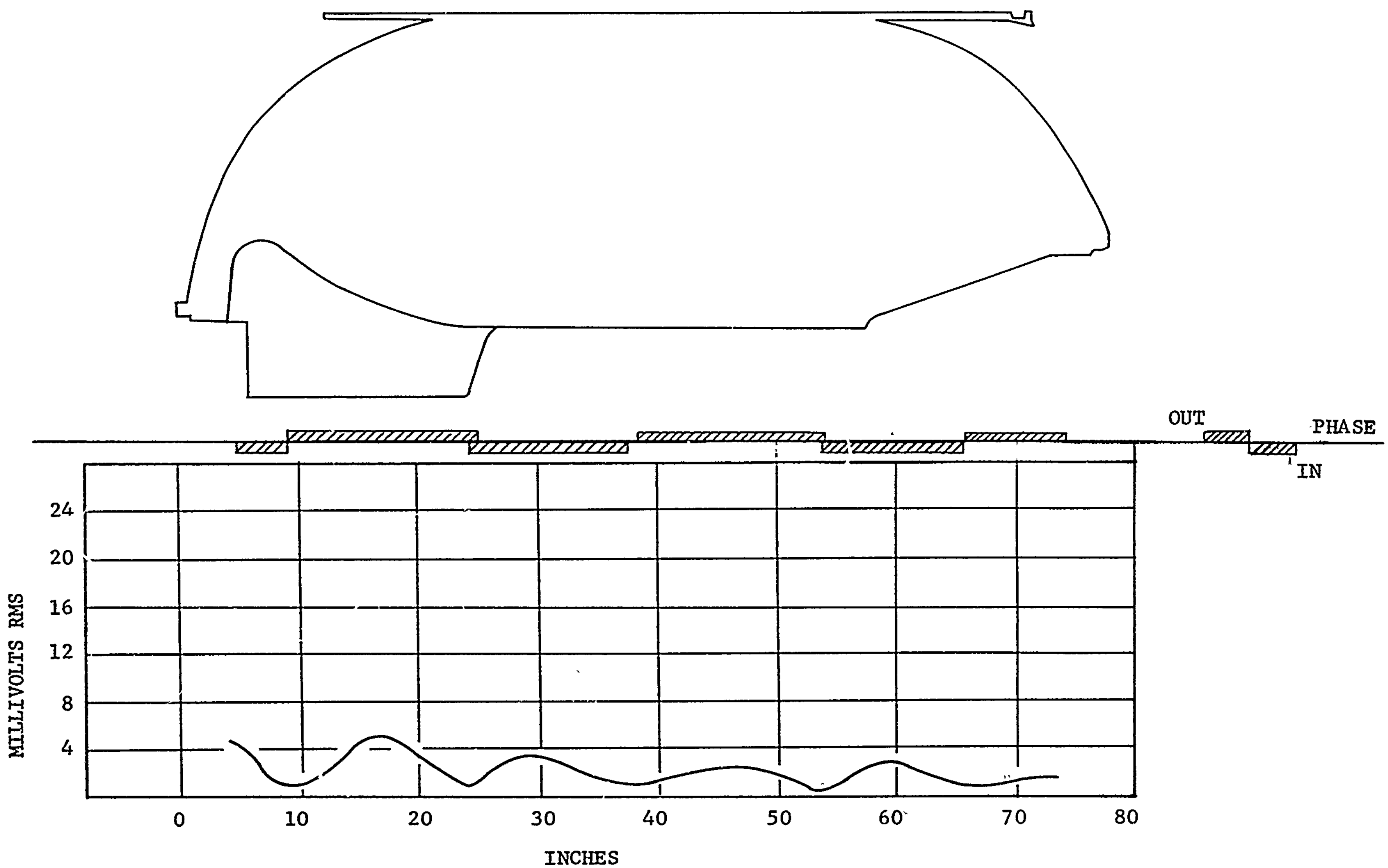

Figure 4. Longitudinal Pressure Mode Shape Measured at 427 Hz

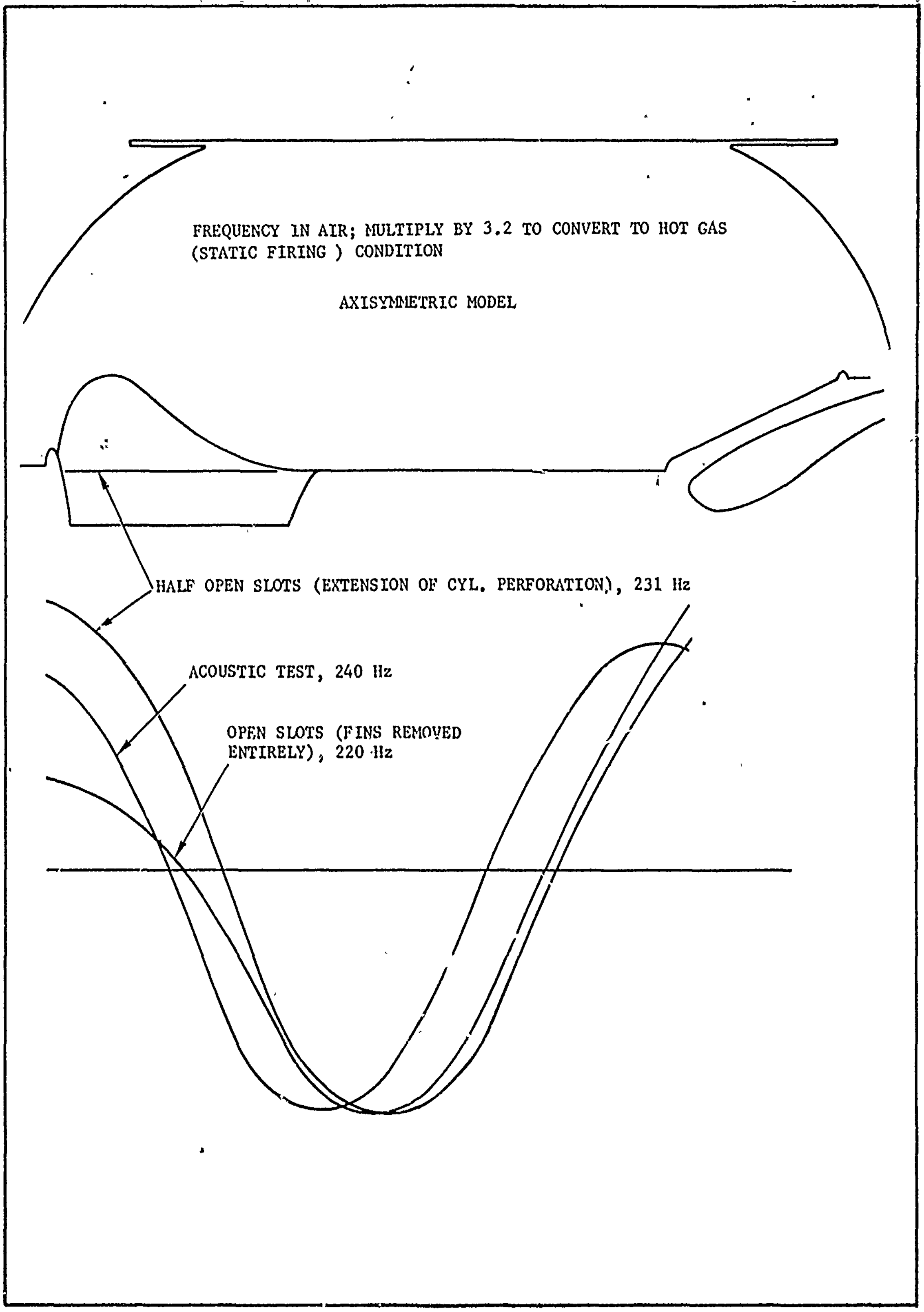

Figure 5. Comparison of Two Analytical Mode Shapes with Acoustic Bench Test Mode Shape, for Third Longitudinal Mode

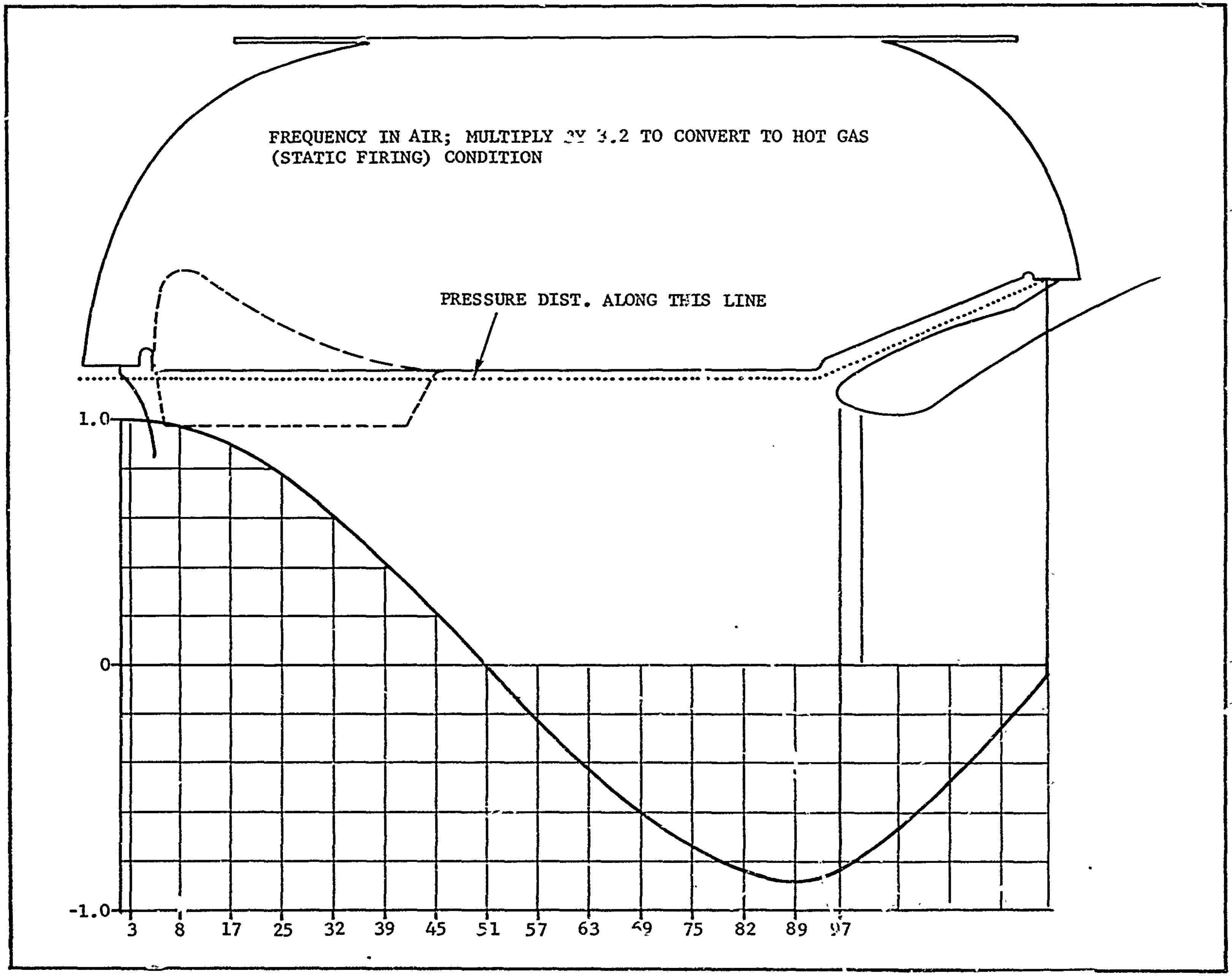

Figure 6. Acoustic Pressure Distribution for First Longitudinal Mode (126 Hz) Predicted by

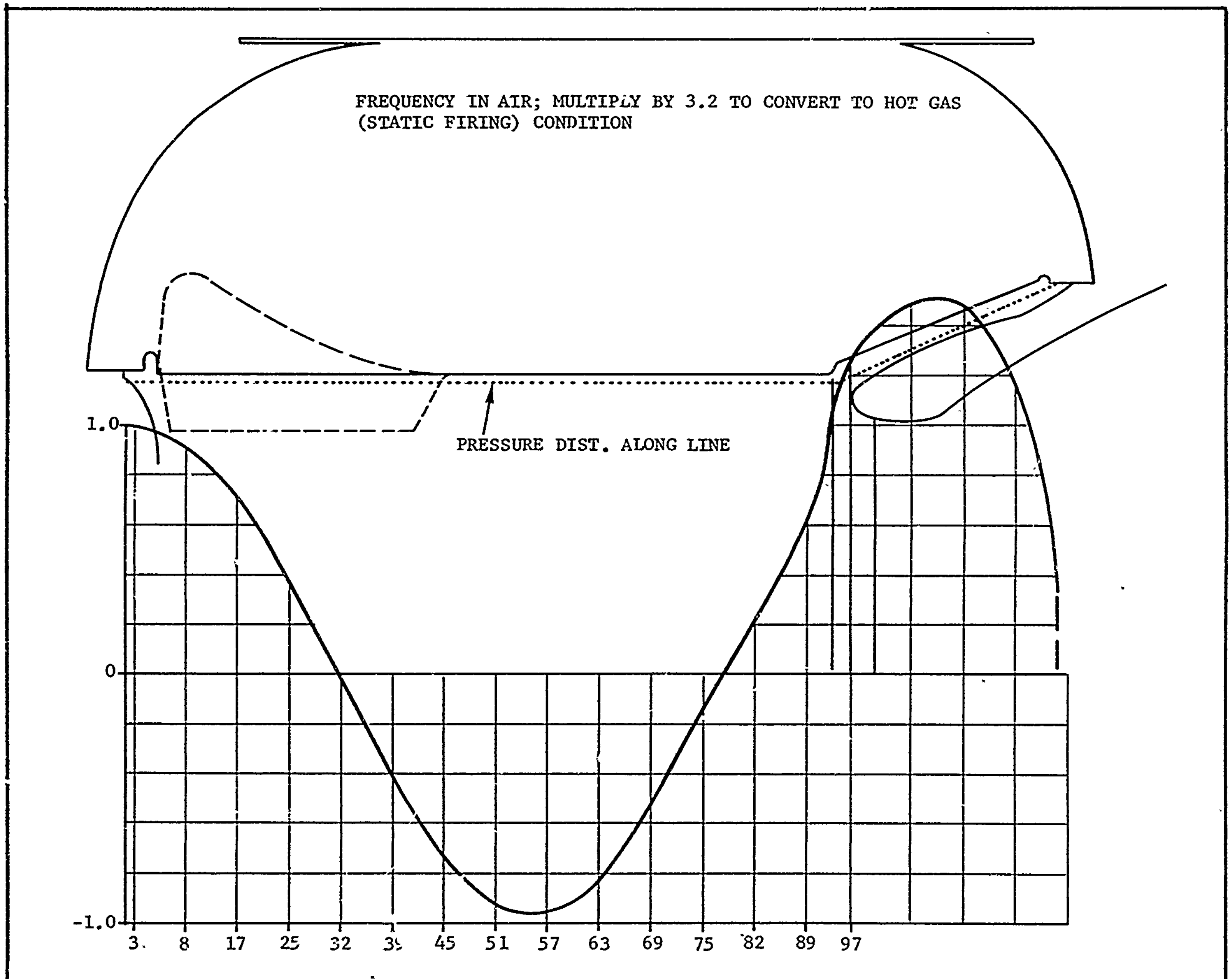

Figure 7. Acoustic Pressure Distribution for Second Longitudinal Mode (219 Hz) Predicted by Finite-Element Model with Aft Dome Cavity Open and Blocked Nozzle Throat

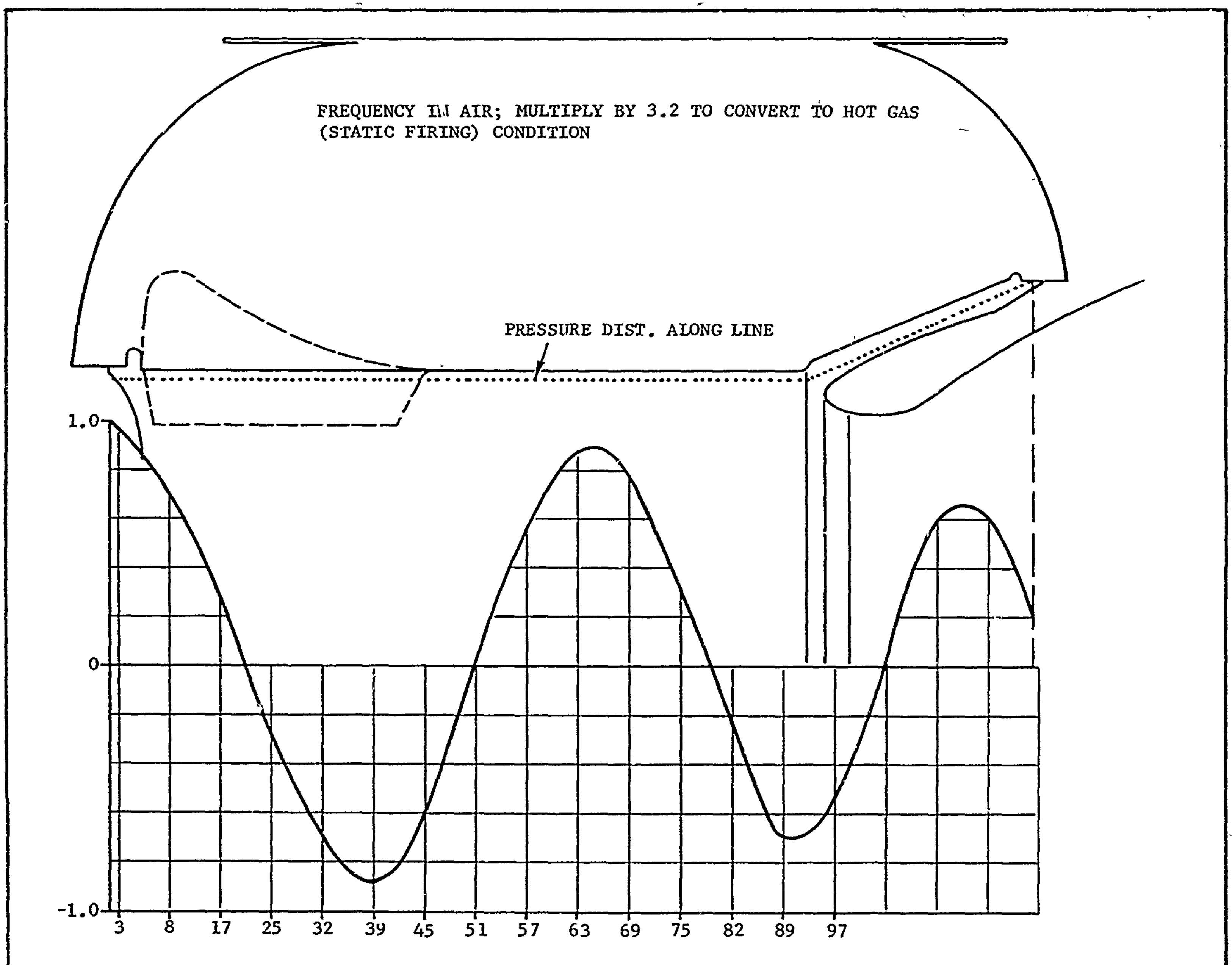

Figure 8. Acoustic Pressure Distribution for Third Longitudinal Mode (360 Hz) Predicted by

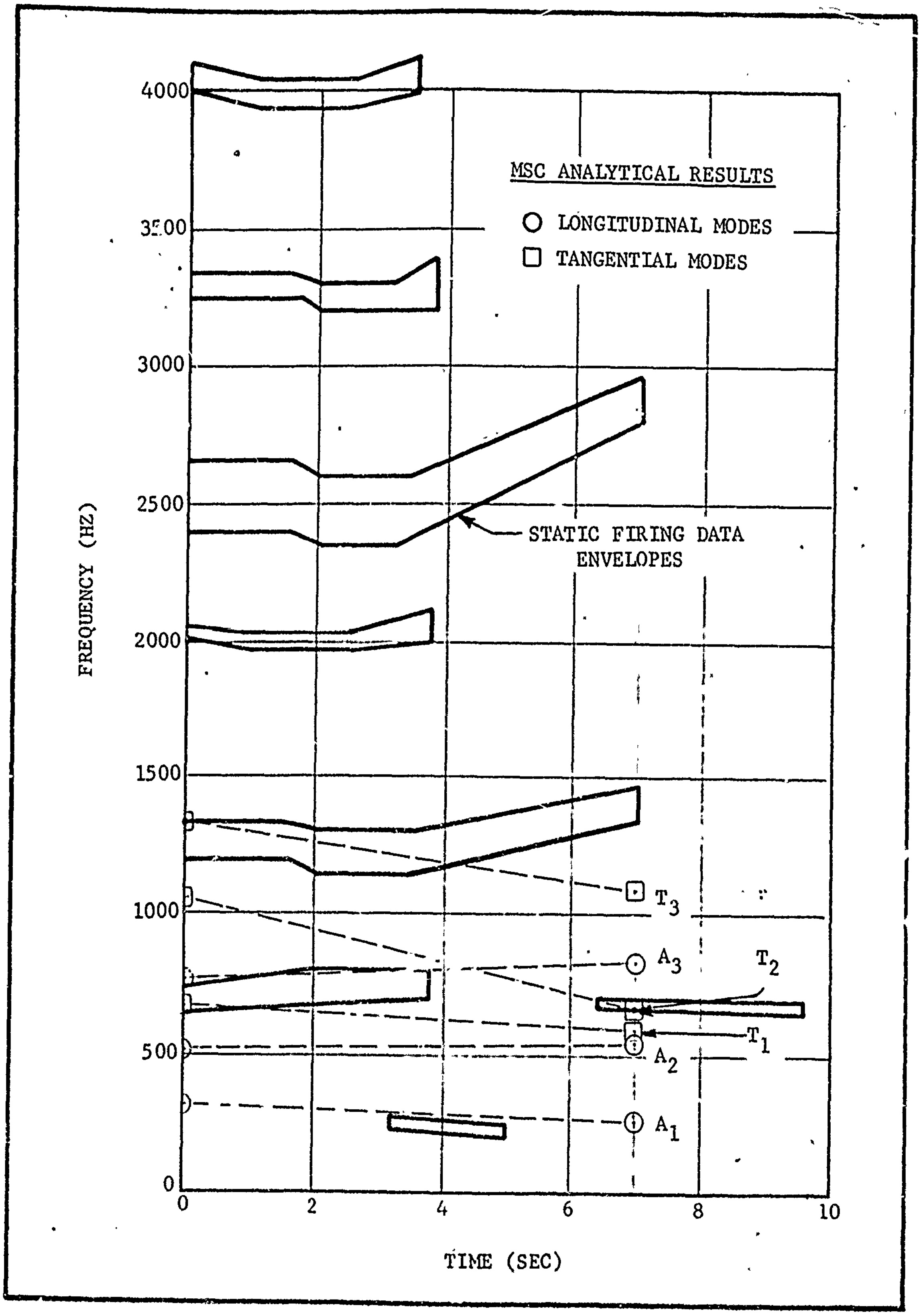

Figure 9. Envelopes of Static Firing Data (from Reference 3)

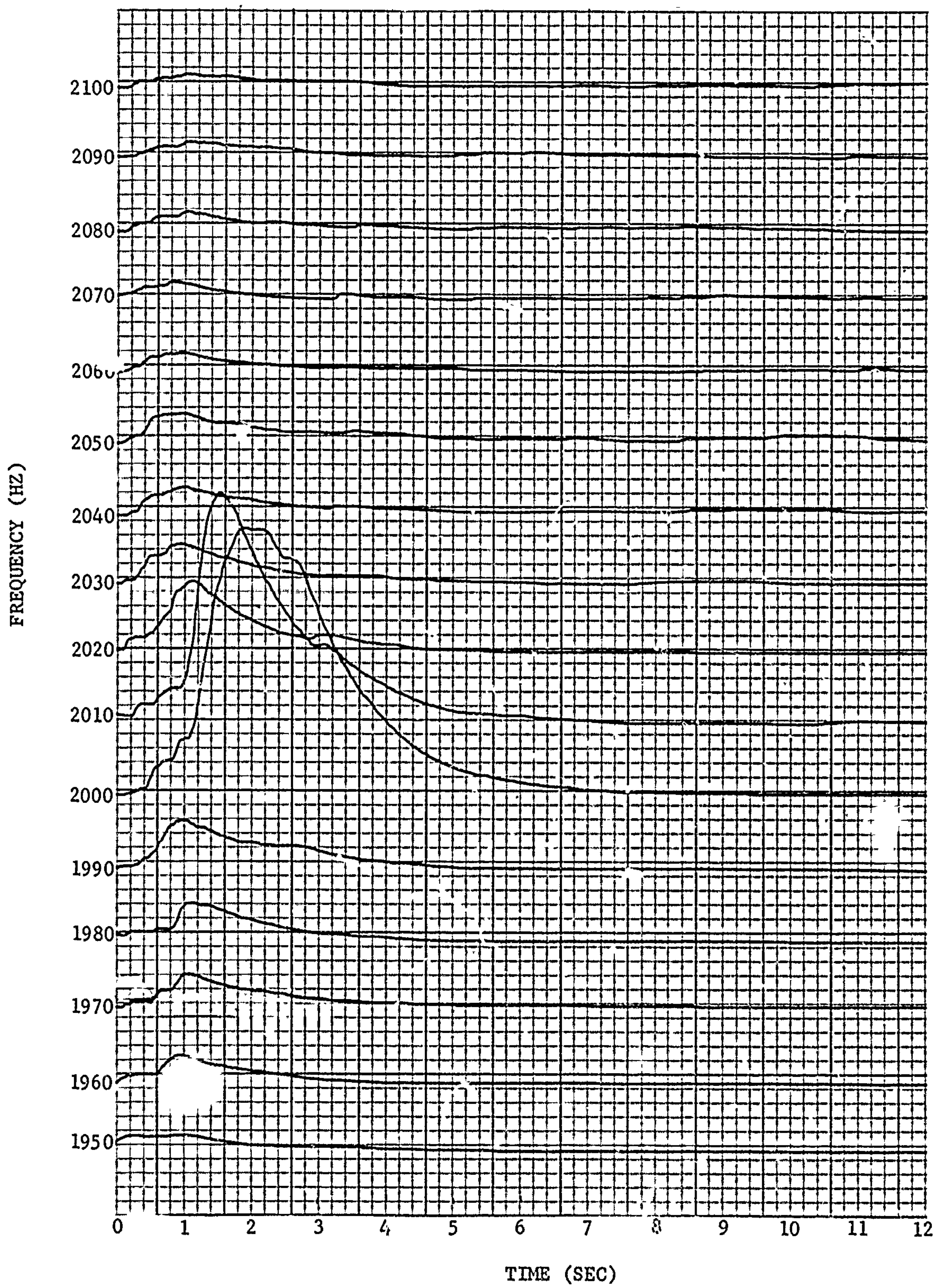

Figure 10. Frequency Mapping for Poseidon S/S Motor SP-0160, Accelerometer No. AC-250, Frequency Range 1950 Hz to 2100 Hz

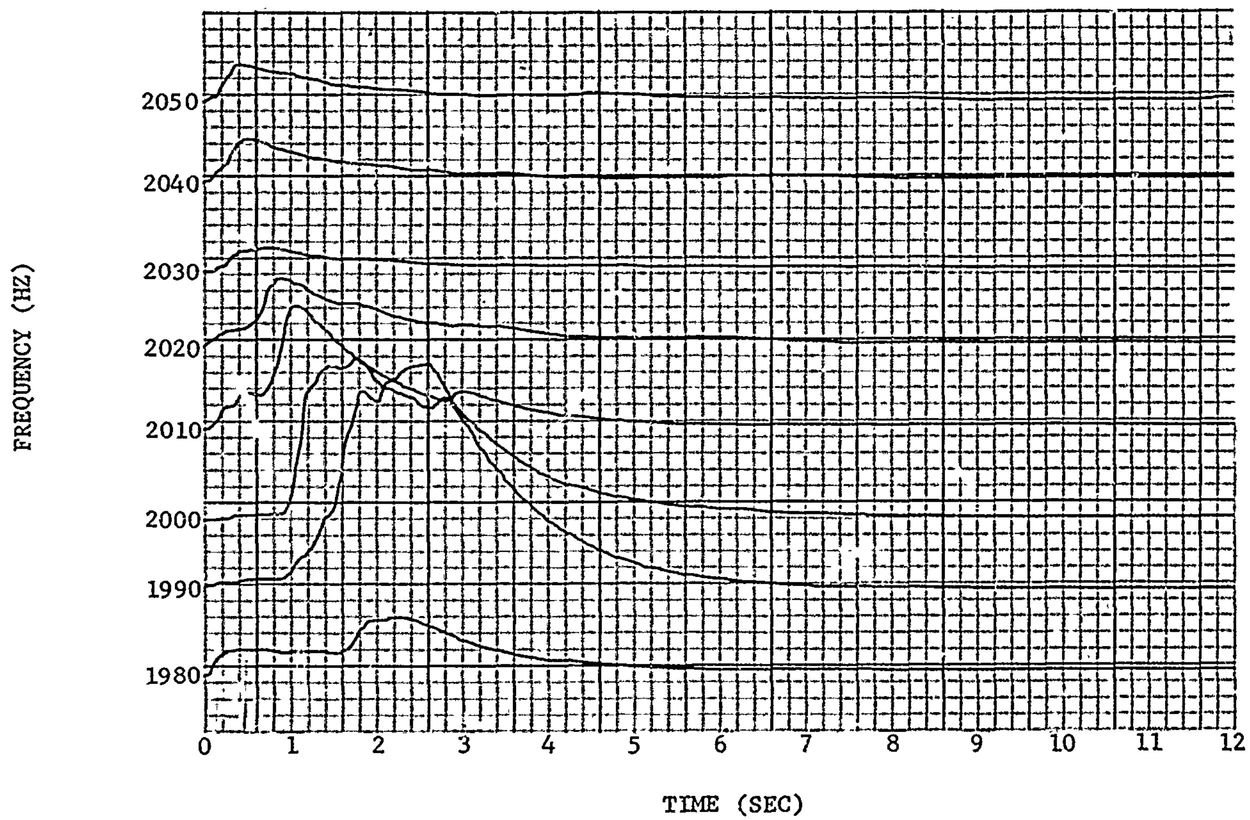

Figure 11. Frequency Mapping for Poseidon S/S Motor SP-0131, Accelerometer No. AC-250, Frequency Range 1980 Hz to 2050 Hz

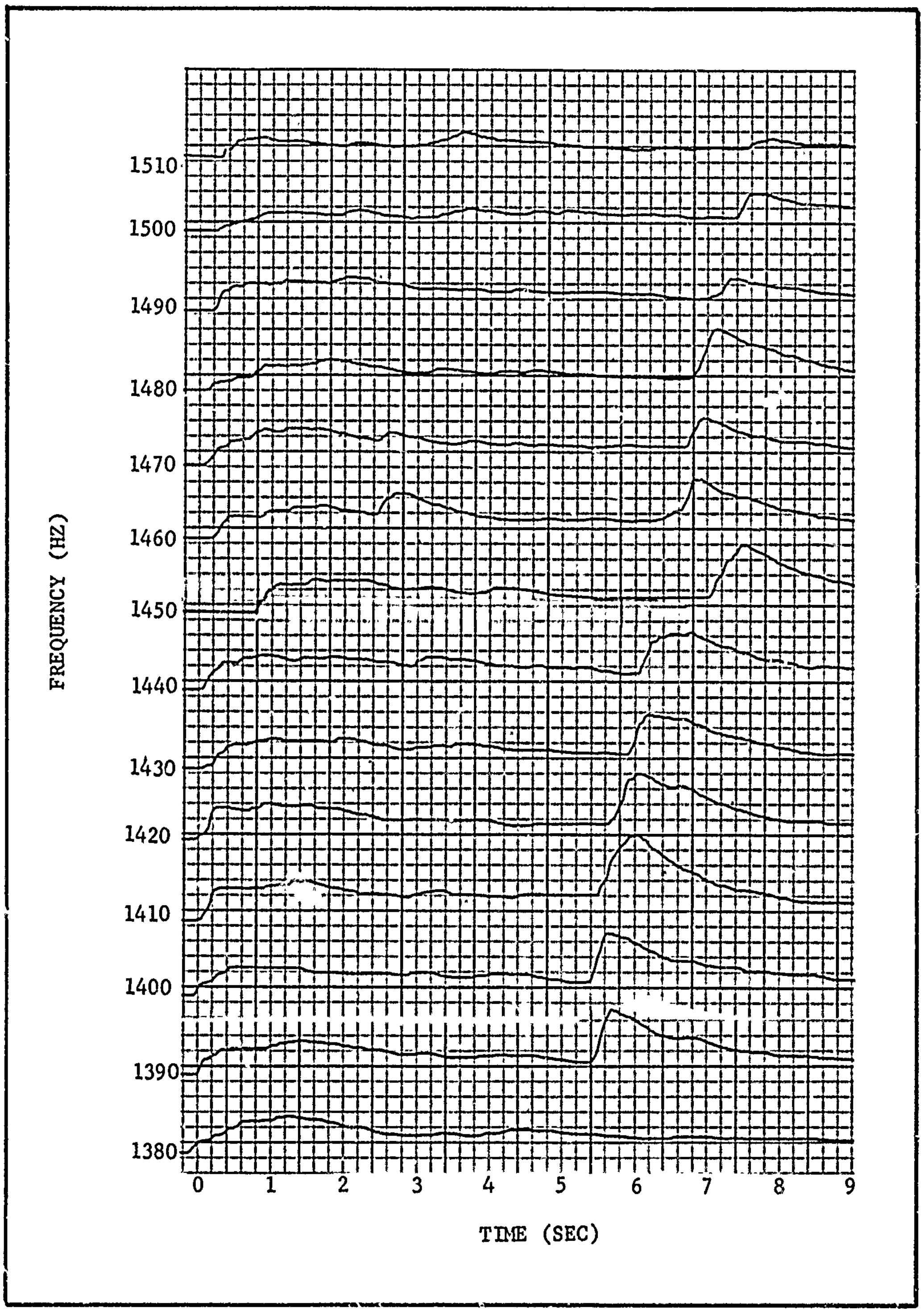

Figure 12a. Frequency Mapping for Poseidon S/S Motor SP-0160, Accelerometer No. AC-250, Frequency Range 1380 to 1510 Hz

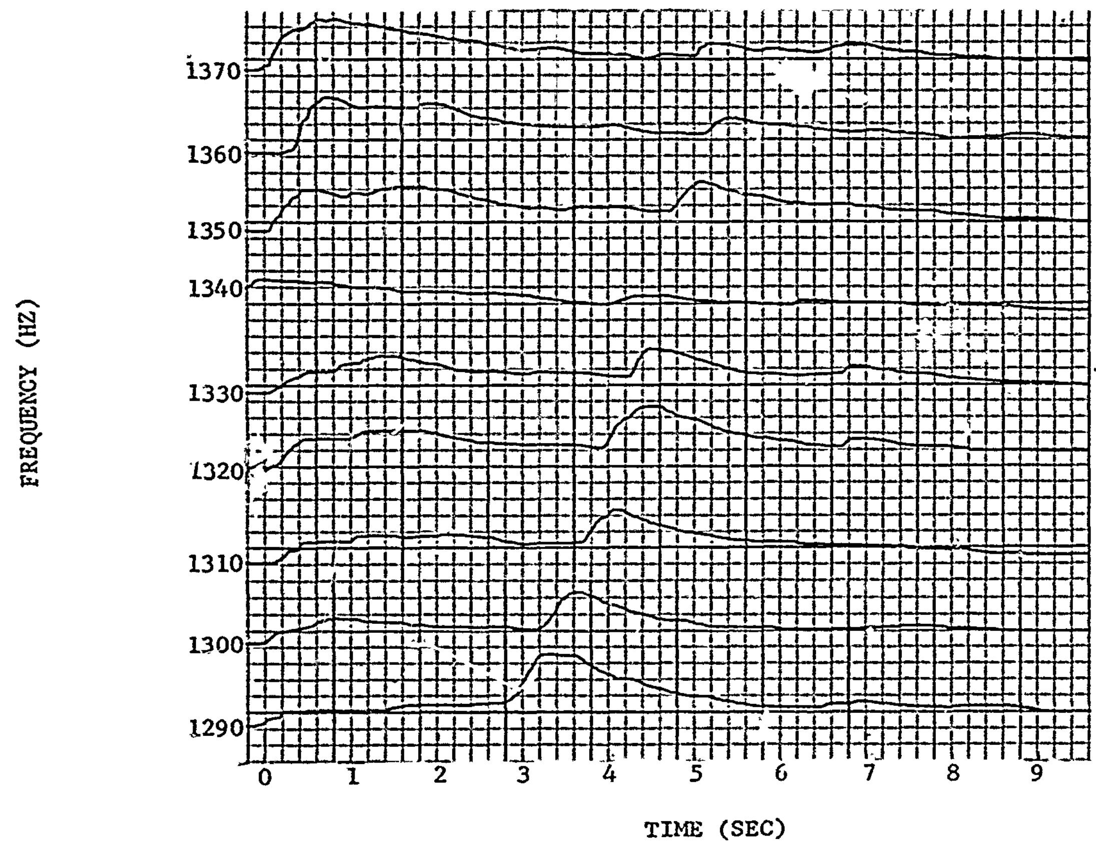

Figure 12b. Frequency Mapping for Poseidon S/S Motor SP-0160, Accelerometer No. AC-250, Frequency Range 1290 to 1370 Hz

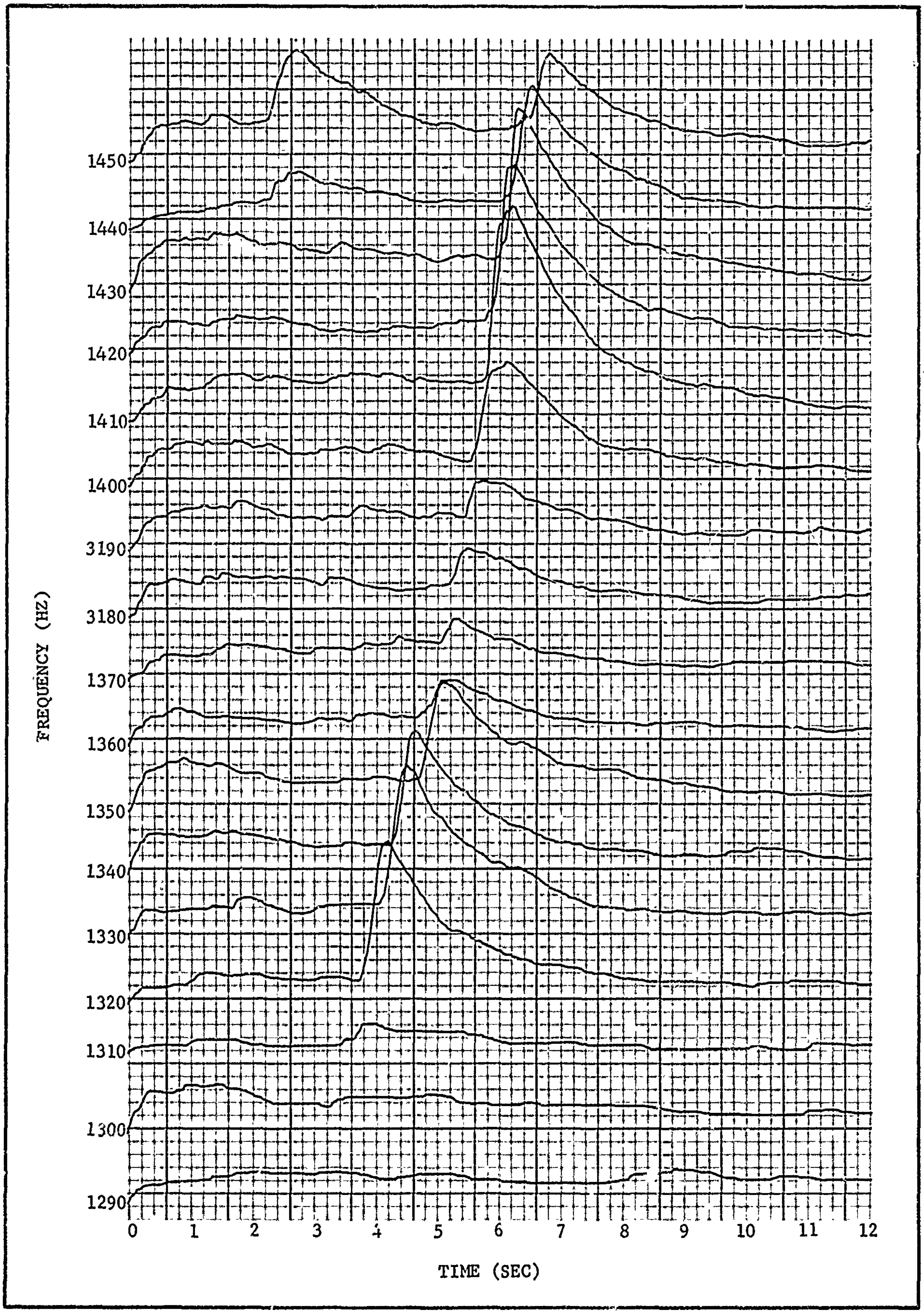

Figure 13a. Frequency Mapping for Poseidon S/S Motor SP-0131, Accelerometer No. AC-250, Frequency Range 1290 to 1450 Hz

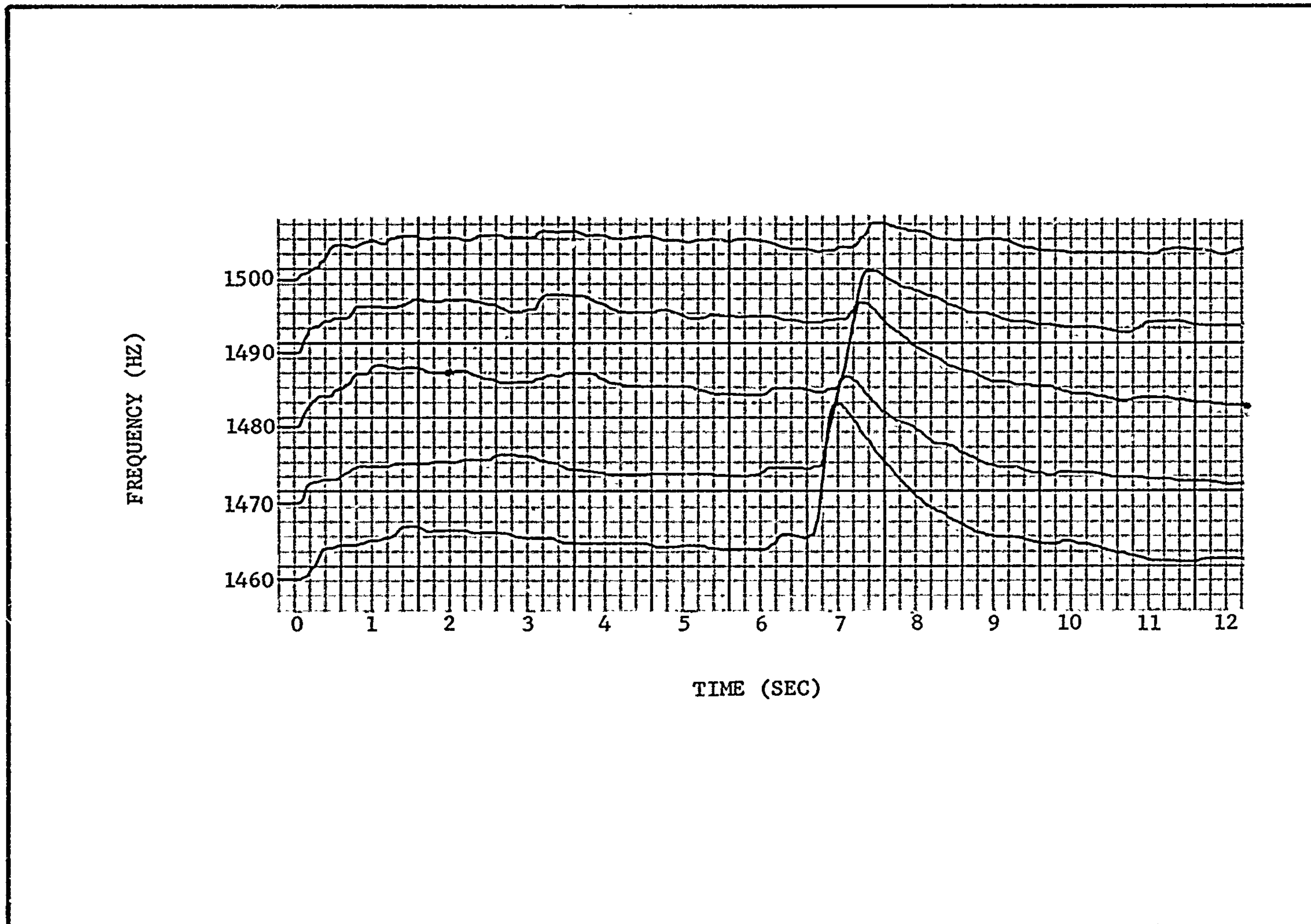

Figure 13b. Frequency Mapping for Poseidon S/S Motor SP-0131, Accelerometer No. AC-250, Frequency Range 1460 to 1500 Hz

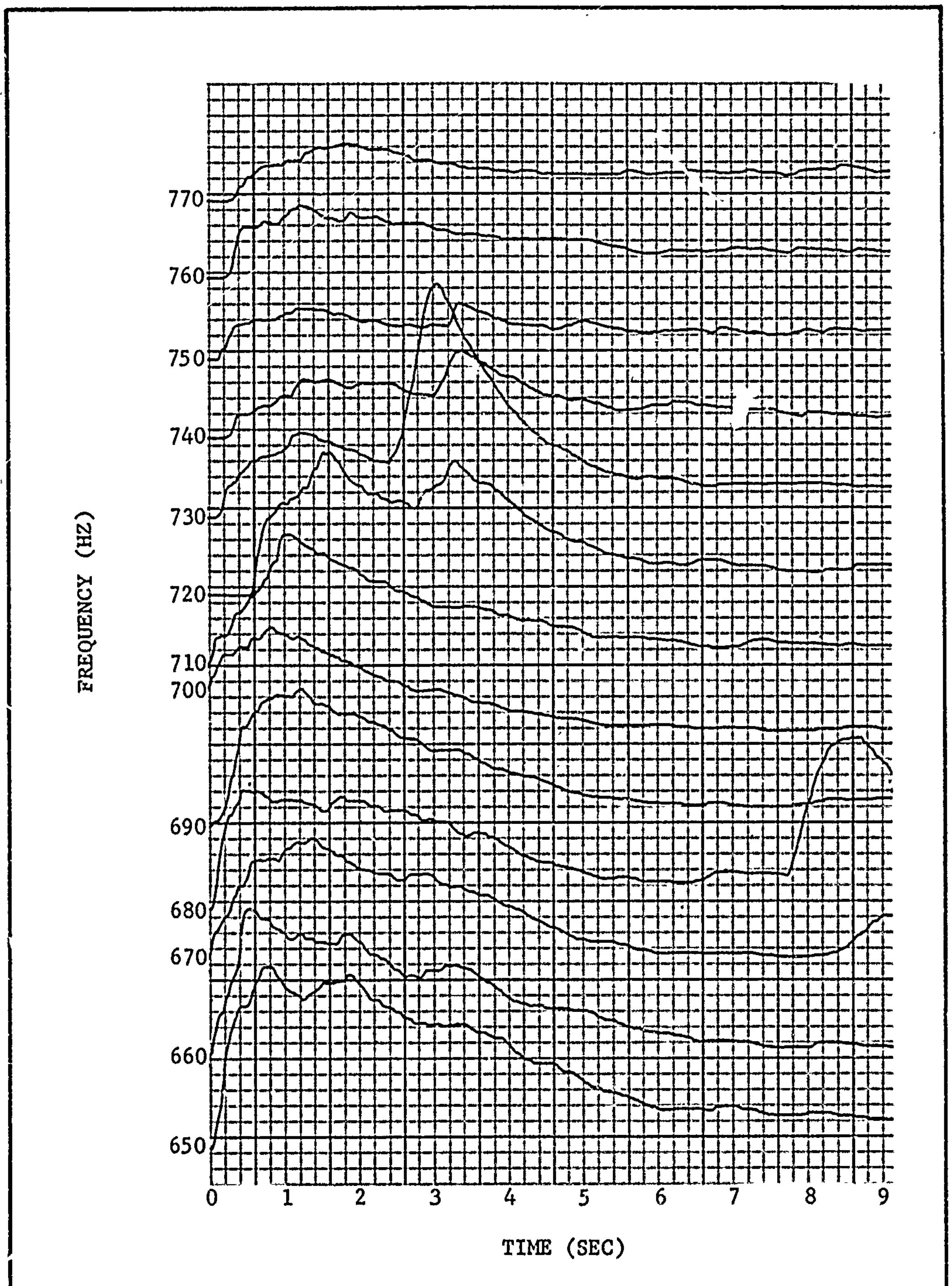

Figure 14. Frequency Mapping for Poseidon S/S Motor SP-0160, Accelerometer No. AC-250, Frequency Range 650 to 770 Hz

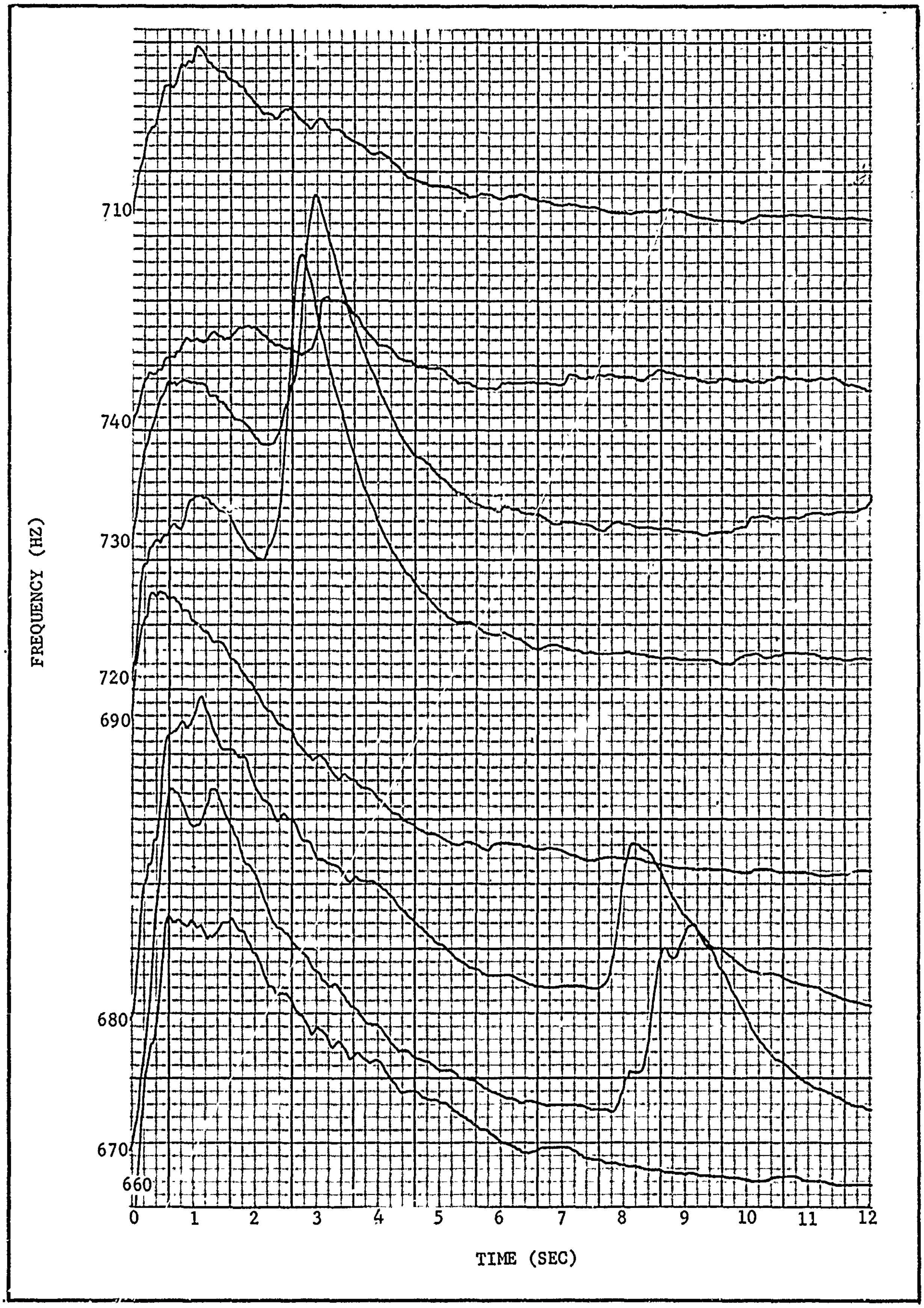

Figure 15. Frequency Mapping for Poseidon S/S Motor SP-0131, Accelerometer No. AC-250, Frequency Range 660 to 740 Hz

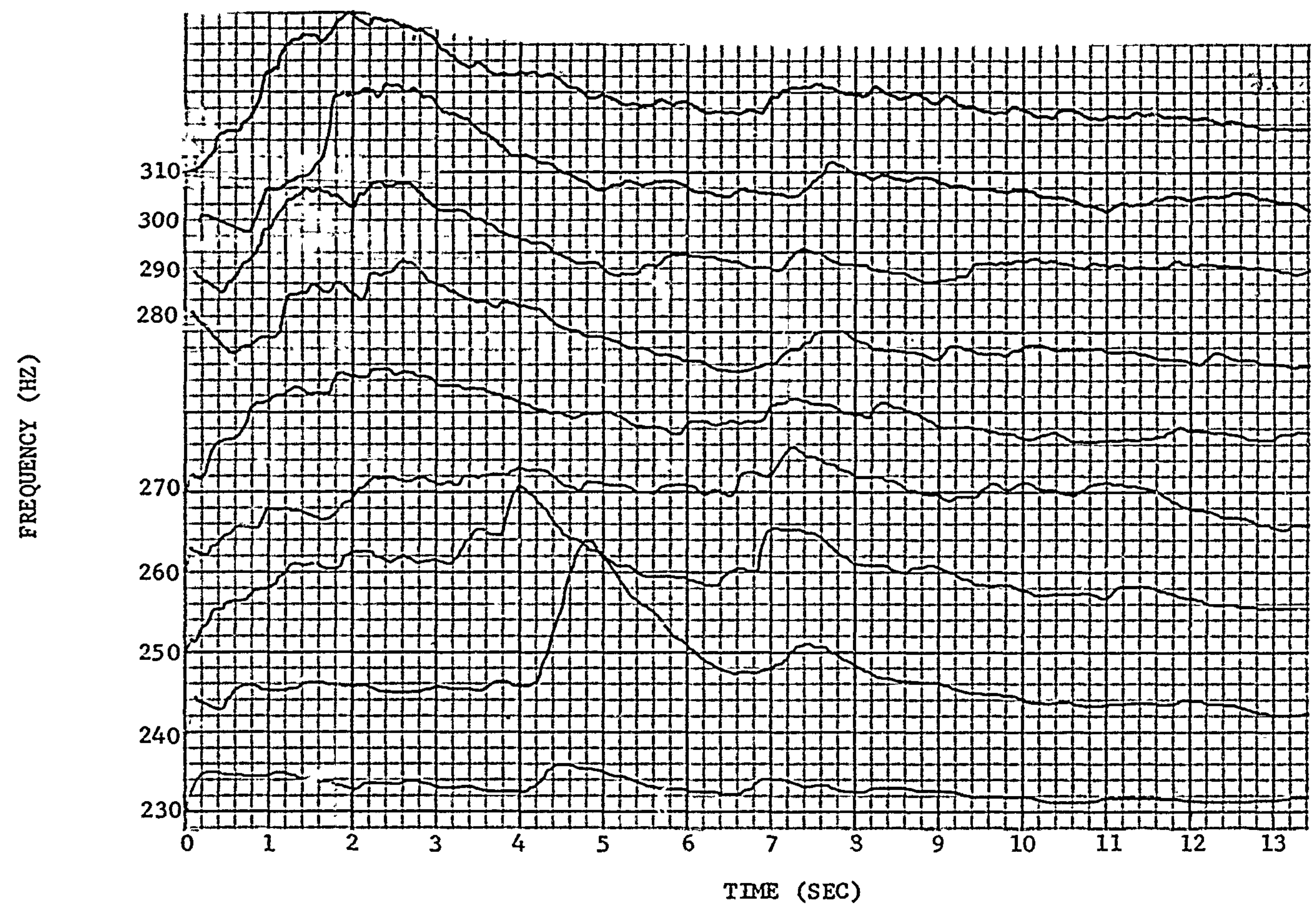

Figure 16. Frequency Mapping for Poseidon S/S Motor SP-0160, Accelerometer No. AC-250, Frequency Range 230 to 310 Hz

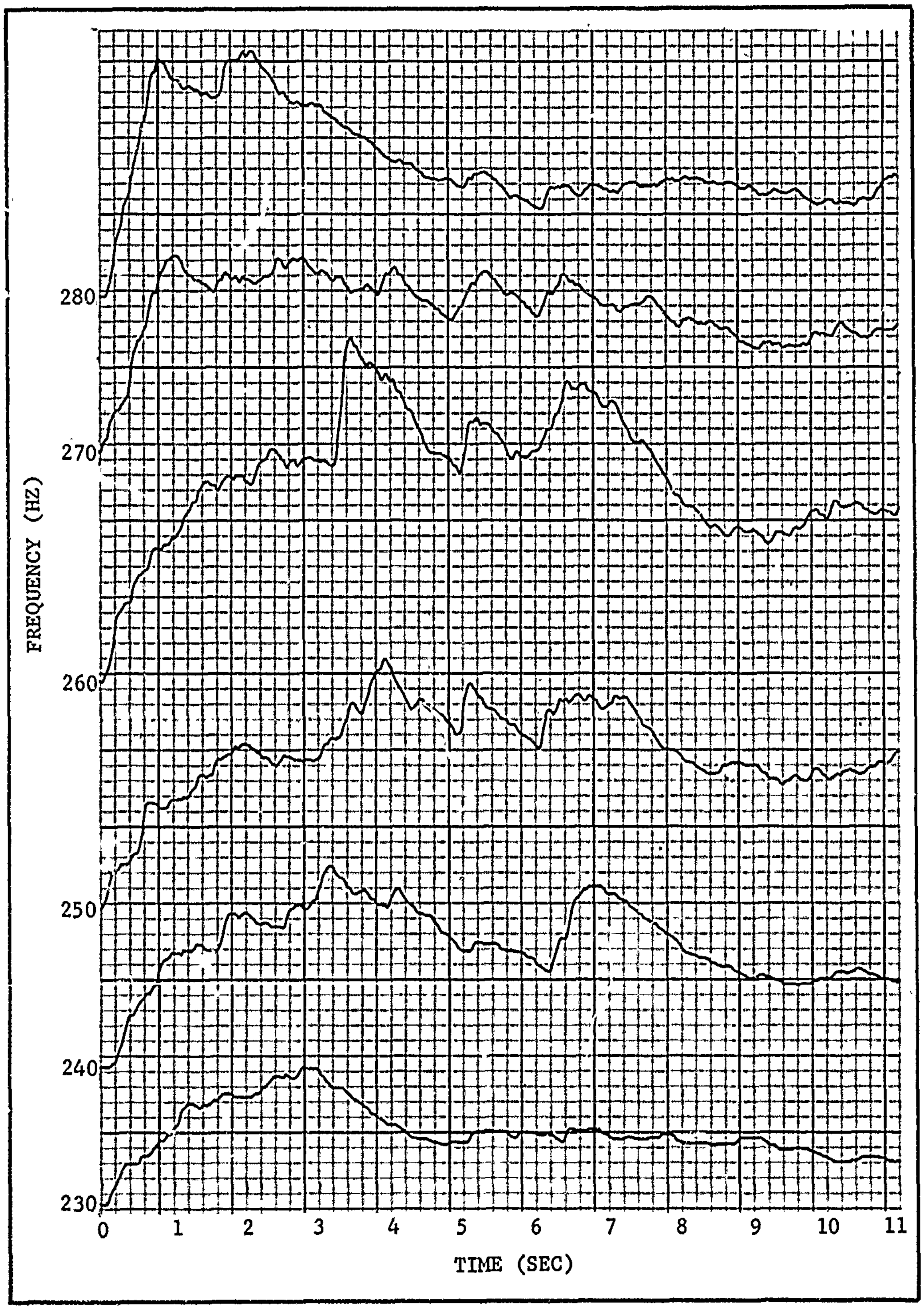

Figure 17. Frequency Mapping for Poseidon S/S Motor SP-0131, Accelerometer No. AC-250, Frequency Range 230 to 280 Hz

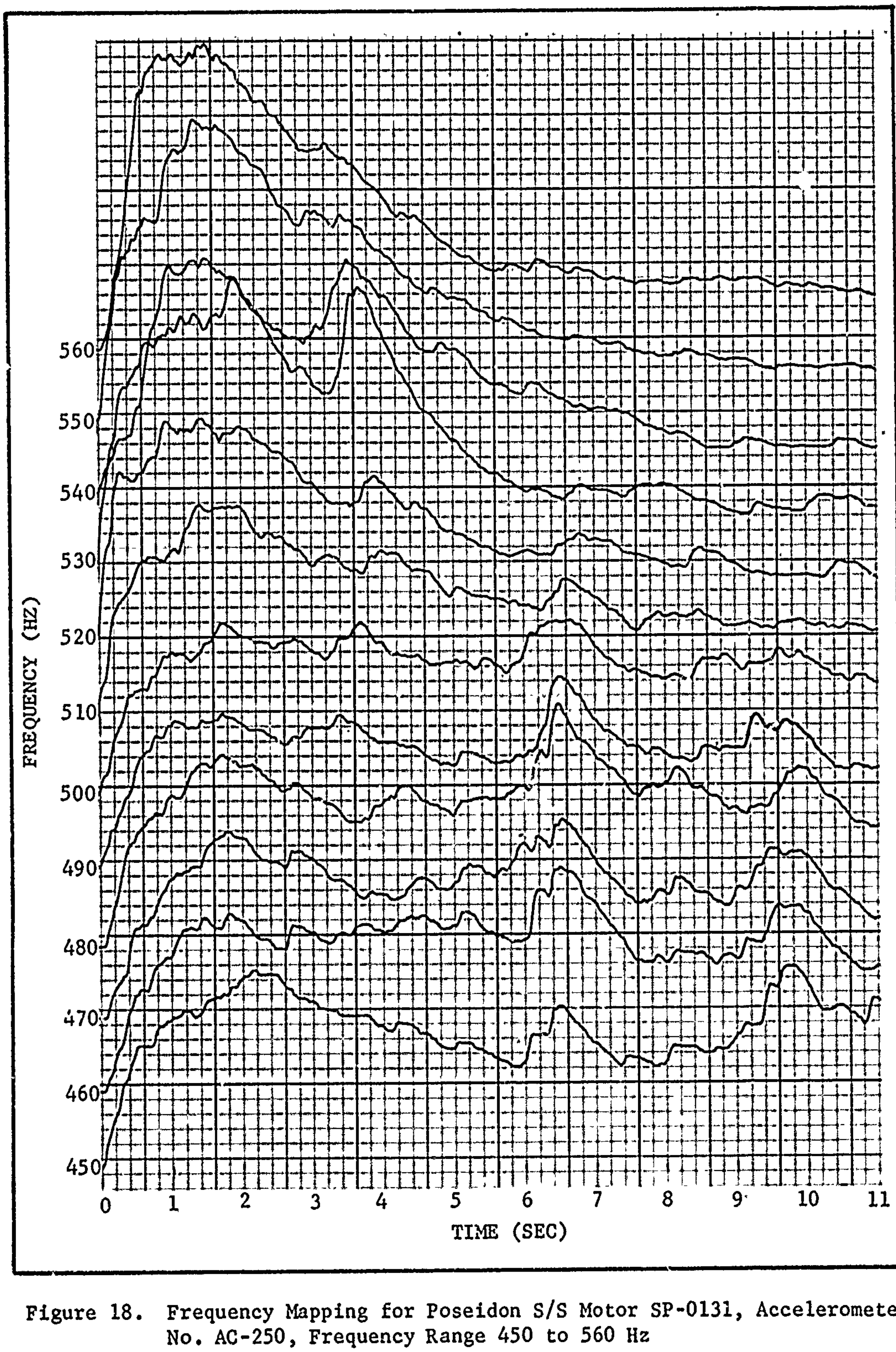

Figure 18. Frequency Mapping for Poseidon S/S Motor SP-0131, Accelerometer No. AC-250, Frequency Range 450 to 560 Hz

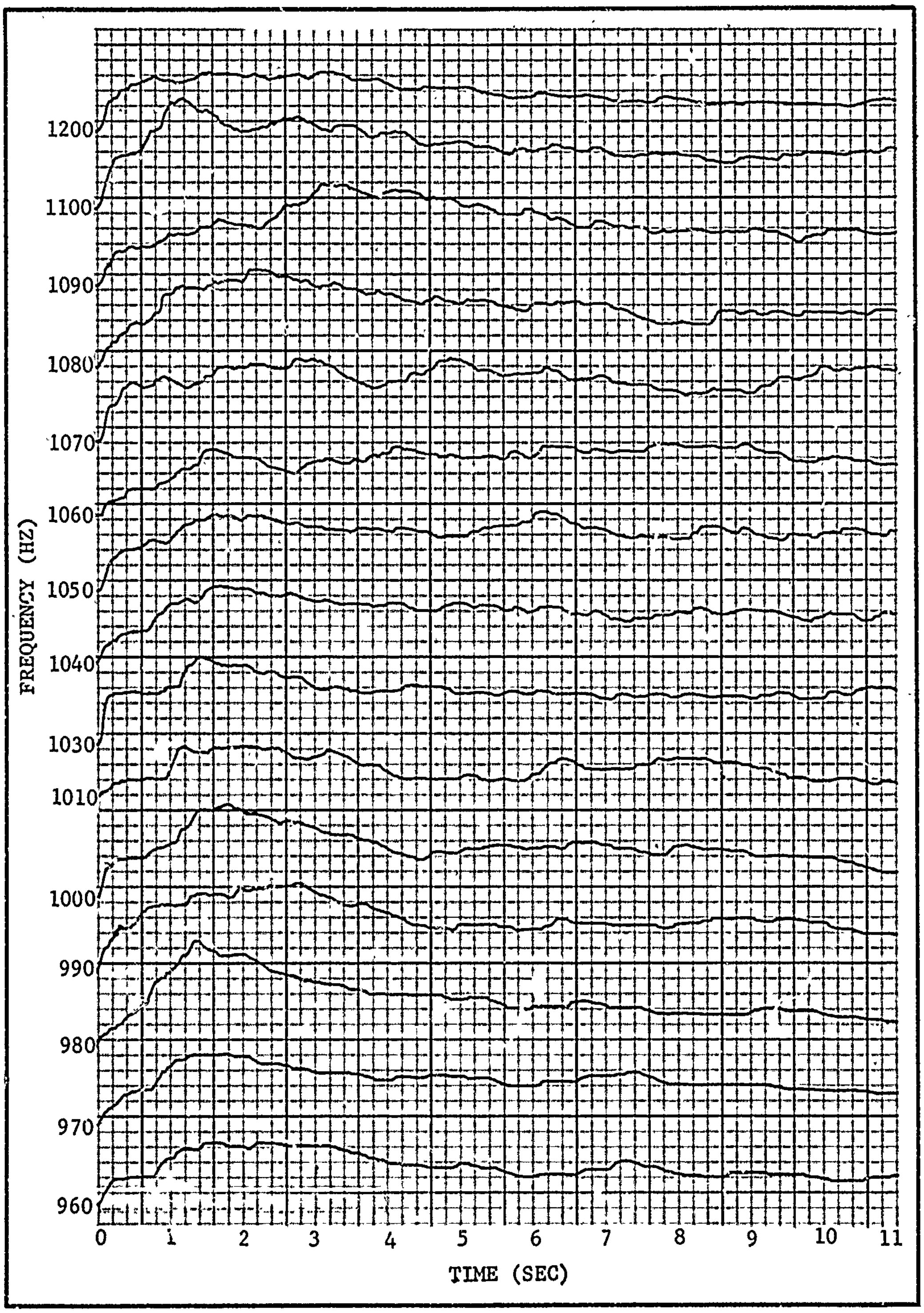

Figure 19. Frequency Mapping for Poseidon S/S Motor SP-0131, Accelerometer No. AC-250, Frequency Range 960 to 1200 Hz

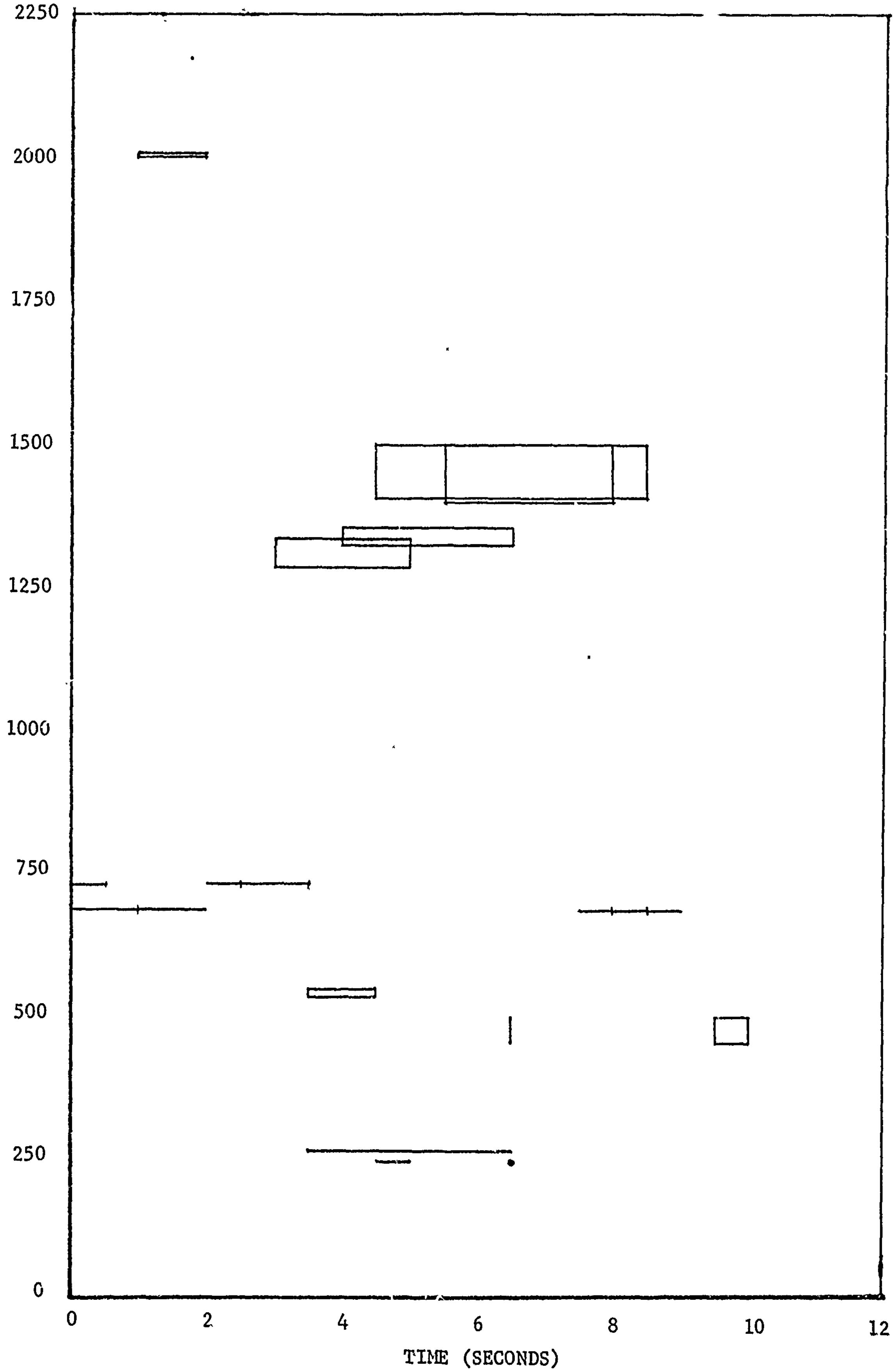

Figure 20. A Summary of the Accelerometer Data Given in Figures 10 through 19

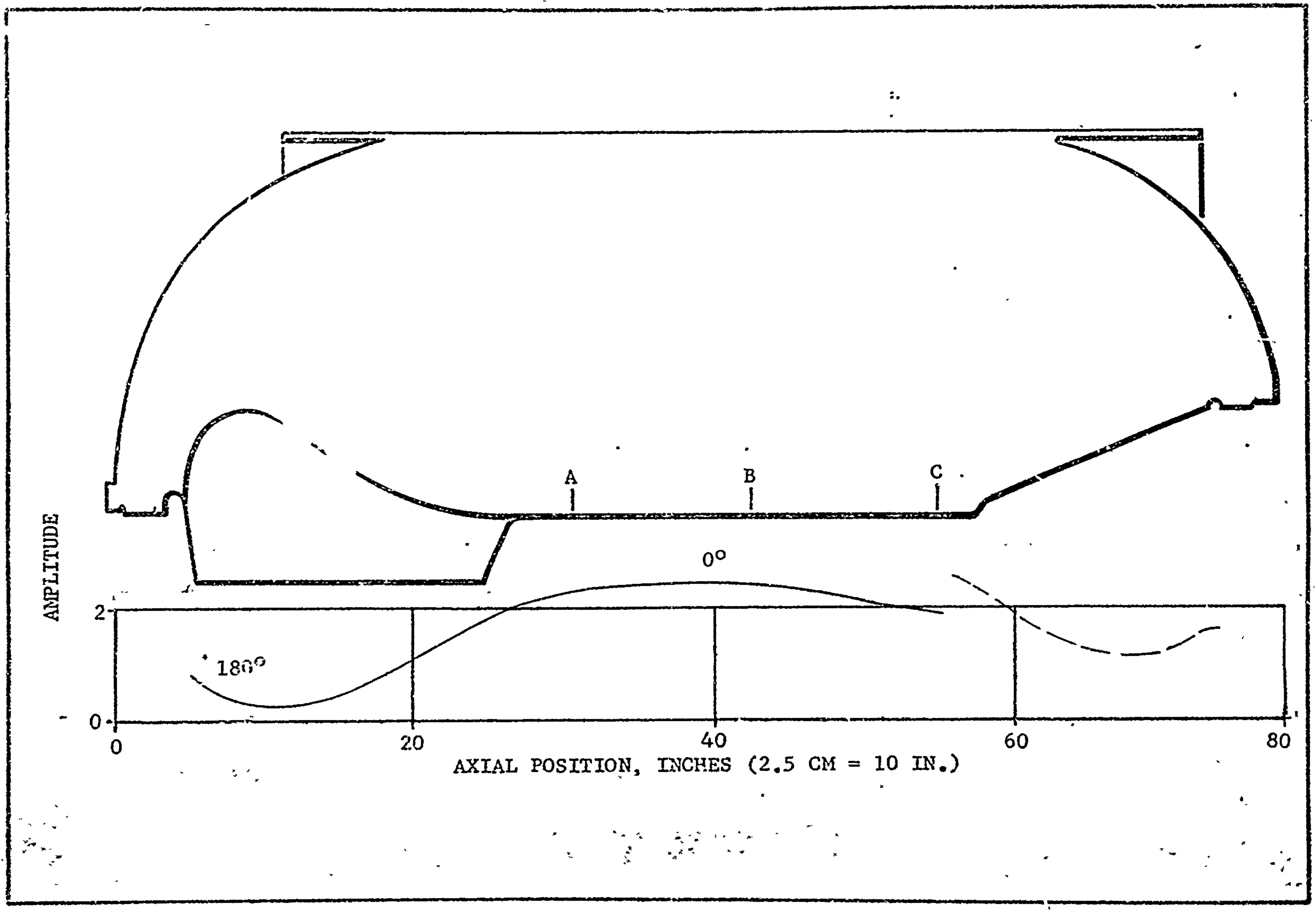

Figure 21. Longitudinal Pressur Distribution Along the Wall for the Third Tangential Mode at 1312 Hz (10·1/L Model)

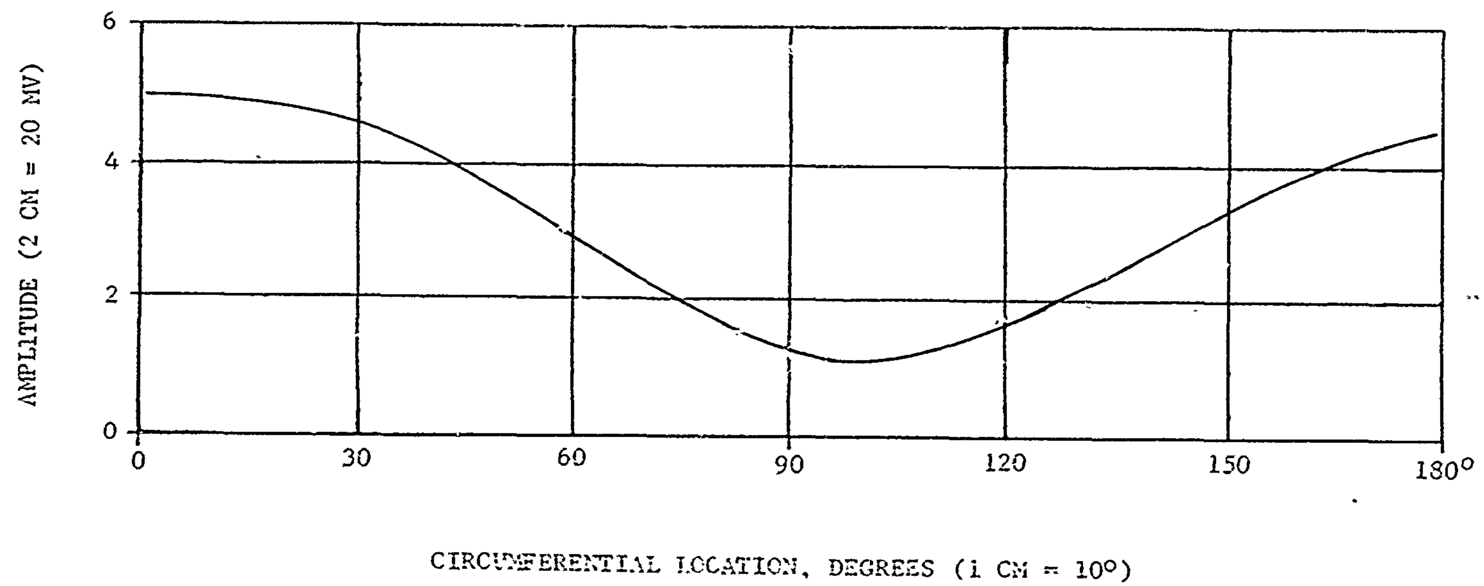

Figure 22. Circumferential Pressure Distribution, 10-1/2 L Model, 1312 Hz

LIST OF REFERENCES

1. Herting, D. N., Joseph, J. A., Kussinen, L. R., and MacNeal, R. H., "Acoustic Analysis of Solid Rocket Motor Cavities by a Finite Element Method", AFRPL-TR-71-96, for Edwards Air Force Base, Rocket Propulsion Laboratory, August 1971.

2. Herting, D. N., Joseph, J. A., Kussinen, L. R., and MacNeal, R. H., "Acoustic Analysis of Solid Rocket Motor Cavities by a Finite Element Method", NASA TM X-2378, NASTRAN: Users Experiences, Vol. 1, September 1971.

3. "Poseidon Second Stage Acoustics Investigation", Final Report, Vol. II, Resonant Conditions and Combustion Driving of Pressure Oscillations, SH015-B3A00HTJ-1, Hercules/Thiokol Joint Venture, Hercules Incorporated, Bacchus Works, Magna, Utah, March 1971.

4. Memorandum to C. D. Bangerter, from B. E. Tew, MISC/5/4-218, Hercules Incorporated, Bacchus Works, Magna, Utah, 11 February 1970.

5. "Vibration Testing of the Baseline Motor", Task 4 Final Report, RPL Component Vibration Program, Contract No. F04611-73-C-0025, Hercules Incorporated, Bacchus Works, Magna, Utah, 15 August 1973.

6. "Poseidon S/S Motor Vibrations Studies", Final Report, SA015-B3A00HTJ-23, Contract N0003073C0012, Subcontract AX10A0270M, Hercules/Thiokol Joint Venture, Hercules Incorporated, Bacchus Works, Magna, Utah, 28 June 1973.

DISTRIBUTION LIST

Recipient	Mail Stop
J. M. Anderson	100-K1-9
M. W. Beckstead	100-K1-7
S. C. Browning	100-K1-7
B. A. Findley (letter only)	100-G2-4
E. T. Hikida	100-K1-9
F. R. Jensen	100-K1-9
Library (2)	100-H

APPENDIX C

CYCLIC SYMMETRY IN DIRECT FREQUENCY RESPONSE ANALYSIS

AS PREVIOUSLY PUBLISHED BY McNEAL-SCHWENDLER CORPORATION

CYCLIC SYMMETRY IN DIRECT FREQUENCY RESPONSE ANALYSIS

EC-254 January 1974

EC-254

CYCLIC SYMMETRY IN DIRECT FREQUENCY RESPONSE ANALYSIS

for

Hercules, Inc.

January 10, 1974

The MacNeal-Schwendler Corporation
7442 North Figueroa Street
Los Angeles, California 90041

TABLE OF CONTENTS

LIST OF FIGURES

1.0 THEORY FOR ANALYSIS OF FREQUENCY DEPENDENT MATERIALS

Viscoelastic materials can be analyzed by NASTRAN in frequency response problems. The properties of viscoelastic materials (for example, a solid propellant rocket grain) include a combination of elastic and viscous phenomena. For sinusoidal response, these may be described in terms of frequency dependent material properties.

Elastic material properties available in NASTRAN are discussed in Section 4.2 of the Theoretical Manual. Section 9.3.3 shows how damping can be added to the model. These material properties are used to compute the stiffness matrix. Equation (16) of Section 9.3 is reproduced below. It shows the standard stiffness matrix for direct frequency response.

$$K_{dd} = (1+ig)\, K^1_{dd} + K^2_{dd} + iK^4_{dd} \quad , \qquad (1)$$

where

- K^1_{dd} is the stiffness matrix for structural elements. Subscript d refers to the "dynamics" degrees of freedom, e.g., set u_d.
- K^2_{dd} is the direct input matrix, which is not an "element" related matrix.
- K^4_{dd} is the element structural damping matrix.
- g is the overall structural damping.

Both K^1 and K^4 are formed by the structural matrix assembler. Their values are the sums of the element stiffness matrices. For each element, a structural damping g_e may be specified on the material property card. The K^4_{elem} matrix for each element is g_e times the K^1_{elem} matrix.

The viscoelastic properties can be described in terms of a complex shear modulus and a Poisson's ratio. The modulus

$$G(f) = G'(f) + iG''(f) \quad , \tag{2}$$

where

$G'(f)$ is the shear storage modulus.

$G''(f)/G'(f)$ is the shear loss tangent.

The Poisson's ratio is a constant, typically just less than 0.5. The element stiffness matrix is directly proportional to $G(f)$, thus if the stiffness matrix is known for a reference modulus G_{ref}, then the frequency dependent matrix is $G(f)/G_{ref}$ times the known matrix.

The model with frequency dependent materials usually contains some elements (such as the casing for the solid propellant) which do not have viscoelastic damping characteristics. The two types of materials are handled as follows:

1. All elastic material is specified with zero element damping. Thus K^4 will be zero for these elements. The value g (overall damping) is chosen to be representative for the elastic material.

2. All viscoelastic elements are specified with a material shear modulus G_{ref}, Poisson's ratio υ, and element damping g_{ref}. The values G_{ref} and g_{ref} are chosen arbitrarily, but must be nonzero. The stiffness matrix for the viscoelastic terms is not computed by (1), but rather by

$$(K_{dd})_{viscoelem} = (1+ig)\, K^1_{dd} + (TR(f)+iTI(f))\, K^4_{dd} \quad . \tag{3}$$

$$= \{(1+g_{ref}\, TR(f))+i(g+g_{ref}\, TI(f))\}\, K^1_{dd} \; .$$

TR(f) and TI(f) are tables which are used by the frequency response module to assemble the final matrix. The desired stiffness matrix for the viscoelastic elements is

$$(K_{dd})_{viscoelem} = \{(G'(f)+iG''(f))/G_{ref}\} K^1_{dd} \quad . \tag{4}$$

Comparing (3) and (4), it can be seen that the table values must be given by

$$TR(f) = ((G'/G_{ref})-1)/g_{ref} \quad , \tag{5}$$

$$TI(f) = ((G''/G_{ref})-g)/g_{ref} \quad . \tag{6}$$

In order to change the formula for the K_{dd} matrix from (1) to (3), two changes must be made. The GKAD module must not add the iK^4 to the K^1 matrix, and the FRRD1 module must add $\{TR(f)+iTI(f)\}K^4$ to K^1.

In most cases G_{ref} and g_{ref} can be chosen arbitrarily. However, it may be necessary to have an accurate value of K^1 to get good interpolation (at zero frequency). In such cases if the NASTRAN ØMIT feature is to be used, the reference modulus specified on a MATi data card should be a representative value, and equations (5) and (6) must be computed. If ØMIT's are not used, then one may choose G_{ref} such that $G_{ref} << G'$ and $G_{ref} << G''/g$. The g_{ref} can be chosen so $G_{ref}\, g_{ref} = 1$. Then

$$TR(f) \doteq G'(f) \quad .$$

$$TI(f) \doteq G''(f) \quad .$$

and no extra calculations are needed to prepare input tables.

The user must supply the following data:

1. Elastic Material - E, υ, G on MATi data card.
   g (damping) on PARAM G data card.

2. Viscoelastic Material - G_{ref}, g_{ref} on MATi data card.
   TR(f), TI(f) tables on TABLEDi data cards, selected by SDAMP in Case Control.

3. Element Geometry, Loads, Frequencies, etc., are specified in the standard manner.

4. A special ALTER is available to use the modules FRLG and FRRD1. These modules separate the functions of load generation and response calculation. The FRRD module can be used if cyclic symmetry is not involved.

2.0 THEORY FOR CYCLIC SYMMETRY FREQUENCY RESPONSE ANALYSIS

Cyclic symmetry principles can be used to solve linear frequency response problems. The theory is the same as for static analysis, which is defined in Reference 1. The two basic differences are:

1. The mass and damping (as well as the stiffness) matrices must be transformed to symmetric components for the solution.

2. The loads must be computed and transformed to symmetric components for a set of frequencies. Thus allowance must be made for several loading conditions and several frequencies.

No new theory is required, only a modification of the application. The NASTRAN frequency response module FRRD combines the functions of load generation and response calculation, and hence is unsuited to cyclic symmetry. The loads must be transformed from physical values to symmetric component solution variables, which is done by the cyclic symmetry modules. An ALTER is available for this task, which uses modules FRLG (load generator) plus FRRD1 (response calculation). Cyclic symmtery with frequency dependent material properties can be done in one execution.

2.2 MSC/NASTRAN CYCLIC SYMMETRY CAPABILITY

2.2.1 Introduction

Many structures, including pressure vessels, rotating machines, and antennas for space communications, are made up of virtually identical segments that are symmetrically arranged with respect to an axis. There are two types of cyclic symmetry as shown in Figure 1 and 2: *simple rotational symmetry*, in which the segments do not have planes of reflective symmetry; and *dihedral symmetry*, in which each segment has a plane of reflective symmetry. In both cases, it is most important for reasons of economy to be able to calculate the thermal and structural response by analyzing a subregion containing as few segments as possible.

Principles of reflective symmetry (which are not, in general, satisfied by cyclicly symmetric bodies) can reduce the analysis region to one-fourth of the whole. Principles of cyclic symmetry, on the other hand, can reduce the analysis region to a single segment in the case of dihedral symmetry and to a pair of segments in the case of simple rotational symmetry. Neither accuracy nor generality need be lost in the process, except that the treatment is limited to linear relationships between degrees of freedom.

In using NASTRAN's cyclic symmetry capability, the user supplies a model via bulk data cards for one of the identical substructures. He also supplies lists of points on the boundaries. For the case of dihedral symmetry, the *type* of coordinate system used at boundary points must also be specified. For rotational symmetry, the boundary list is a "paired" list of points on the two boundaries. There are several parameters, which must be specified, including the number of segments, the type of cyclic symmetry, the transform index, K, for vibration modes, the range of K for static analysis, and the method of sequencing the equations. Loads, temperatures, and enforced displacements may be specified in static analysis either for the physical segments or for the "transformed" segments which result from the application of symmetry principles. Output may be for either physical or transformed variables.

The use of cyclic symmetry will allow the analyst to model (i.e., make a BULK data deck for) only one of the identical substructures. There will also be a time savings for some classes of problems, such as:

a. Statics problems where the use of the ØMIT for all internal degrees of freedom will greatly reduce the solution time.

b. Statics problems with particular types of loading (such as gravity or uniform pressures) which require a limited range of symmetrical components for solution.

c. Vibration modes for a limited range of k.

2.2.2 Theory

Symmetry principles can be used to simplify the solution of linear problems with cyclic symmetric geometry. Two such types of symmetry are shown in Figures 1 and 2, where they are called *rotational* symmetry and *dihedral* symmetry. Note that dihedral symmetry is a special case of rotational symmetry. In both cases, the body is composed of identical segments, each of which obeys the same laws. The distortions (deflections or temperature changes) of the segments are not independent, but must satisfy compatibility at the boundaries between segments. Cyclic transforms will be defined, which are linear combinations of the distortions of the segments. The transformed equations of compability are such that the "transformed segments" are coupled singly or in pairs which can be solved independently.

In the theory given below, the form of the transformation is not derived, but just stated. The validity of the method is then demonstrated. The procedure follows the following steps:

a. The structure is described as a set of identical segments (substructures), each of which obeys the same physical laws. For static analysis, loads are defined for the segments. A set of intersegment compatibility relationships are written which insure continuity across the segment boundaries.

b. The Phase I transformation is introduced. Both the equations of equilibrium of the segments and the intersegment compatibility relations are transformed.

c. A set of independent variables is chosen for solution. The resulting equations are shown to be uncoupled into groups associated with a cyclic index, K. The dependent variables (constrained to satisfy compability) are determined from a Phase II transformation.

Since the transformed equations describe the same equilibrium and compatability conditions, they will produce the same results as the direct solution; no approximation is required or made.

2.2.2.1 General Rotational Symmetry

The total body consists of N identical segments, which are numbered consecutively from 1 to N. The user supplies a NASTRAN model for one segment. All quantities are given in the segment coordinate system. The boundaries must be *conformable*; i.e., when the segments are put together, the grid points and the local displacement coordinate systems of adjacent segments must coincide. This is easiest to insure if a cylindrical or spherical coordinate system is used, but such is not required. The user will also supply a paired list of grid points where connections will be made. For static analysis, the user may also supply a set of loads and/or enforced displacements for each of the N segments.

The two boundaries will be called sides 1 and 2. Side 2 of element n is connected to side 1 of element n+1, see Figure 1. Thus, the components of displacement satisfy

$$u_1^{n+1} = u_2^n \quad n = 1 \cdots N. \tag{1}$$

This applies to all degrees of freedom which are joined together. We also define $u^{N+1} = u^1$, so Equation 1 refers to all boundaries. Equation 1 is the equation of constraint between the physical segments. The notation system is discussed in Appendix A.

The rotational transformation is given by

$$u^n = \bar{u}^o + \sum_{k=1}^{k_L} [\bar{u}^{kc}\cos(n-1)ka + \bar{u}^{ks}\sin(n-1)ka] + (-1)^{n-1}\bar{u}^{N/2}, \tag{2}$$

$$a = 2\pi/N, \; n = 1, 2, \cdots, N,$$

where u^n can be any component of a displacement, force, stress, temperature, etc., in the n^{th} segment. The last term exists only when N is even. The summation limit $k_L = (N-1)/2$ if N is odd and $(N-2)/2$ if N is even. $\bar{u}^o$, $\bar{u}^{kc}$, $\bar{u}^{ks}$, and $\bar{u}^{N/2}$ are the transformed quantities which will be referred to as *symmetrical components*. Equation 2 can be displayed in the matrix form

$$\lfloor u \rfloor = \lfloor \bar{u} \rfloor \, [T] \, , \tag{3}$$

where

$$\lfloor u \rfloor = \lfloor u^1, \, u^2, \, u^3 \cdots u^N \rfloor \, ,$$

$$\lfloor \bar{u} \rfloor = \lfloor \bar{u}^o, \, \bar{u}^{1c}, \, \bar{u}^{1s}, \, \bar{u}^{2c}, \, \bar{u}^{2s} \cdots \bar{u}^{N/2} \rfloor \, ,$$

and

$$[T] = \left[\begin{array}{ccccc} 1 & 1 & 1 & \cdots & 1 \\ \hline 1 & \cos a & \cos 2a & \cdots & \cos (N-1)a \\ 0 & \sin a & \sin 2a & \cdots & \sin (N-1)a \\ \hline 1 & \cos 2a & \cos 4a & & \cos (N-1)2a \\ \cdot & \cdot & \cdot & & \cdot \\ \cdot & \cdot & \cdot & & \cdot \\ \cdot & \cdot & \cdot & & \cdot \\ 0 & \sin k_L a & \sin 2k_L a & \cdots & \sin (N-1)k_L a \\ \hline 1 & -1 & 1 & \cdots & -1 \end{array} \right] . \tag{4}$$

The last row exists only for even N. The transformation is shown as a row operation, since it involves the similar degrees of freedom of all of the segments; see Appendix A. The transformation matrix, [T], has the property,

$$[T]\ [T]^T = [D] = \begin{bmatrix} N & & & & & & & \\ & N/2 & & & & & & \\ & & N/2 & & & & & \\ & & & N/2 & & & & \\ & & & & \cdot & & & \\ & & & & & \cdot & & \\ & & & & & & \cdot & \\ & & & & & & & N \end{bmatrix}. \qquad (5)$$

i.e., the rows of T are orthogonal.

Since D is nonsingular,

$$[T]\ [T]^T\ [D]^{-1} = [I]. \qquad (6)$$

Thus, $[T]^{-1} = [T]^T\ [D]^{-1}$ and

$$\lfloor \bar{u} \rfloor = \lfloor u \rfloor\ [T]^{-1} = \lfloor u \rfloor\ [T^T D^{-1}]. \qquad (7)$$

In summation form, Equation 7 becomes

$$\bar{u}^o = (1/N) \sum_{n=1}^{N} u^n \qquad (8\text{-a})$$

$$\bar{u}^{kc} = (2/N) \sum_{n=1}^{N} u^n \cos(n-1)ka \qquad (8\text{-b})$$

$$\bar{u}^{ks} = (2/N) \sum_{n=1}^{N} u^n \sin(n-1)ka \qquad (8\text{-c})$$

$$\bar{u}^{N/2} = (1/N) \sum_{n=1}^{N} (-1)^{n-1}\ u^n \quad (N \text{ even only}) \qquad (8\text{-d})$$

It should be noted that Equations 8 apply to applied loads, and to internal forces, as well as displacement components. The validity of the symmetrical components $\lfloor \bar{u} \rfloor$ to represent the motions of the system follows from the existence of $[T]^{-1}$. It remains only to show that they are useful. The equations of motion at points interior to the segments are linear (homogenous of degree 1) in displacements, forces and temperatures, they are identical for all segments, and they are not coupled between segments. It follows that the equations for the transformed variables $\lfloor \bar{u} \rfloor$ are identical in form to those of the physical segments.

To transform the compatibility equations of constraint (1), notice that

$$u_1^{n+1} = \bar{u}_1^{o} + \sum_{k=1}^{k_L} [\bar{u}_1^{kc} \cos nka + \bar{u}_1^{ks} \sin nka] + (-1)^n \bar{u}_1^{N/2}. \qquad (9)$$

Using the identities cos nka = cos(n-1)ka·cos ka - sin(n-1)ka·sin ka and sin nka = sin(n-1)ka·cos ka + cos(n-1)ka·sin ka, Equation 9 may be written

$$u_1^{n+1} = \bar{u}_1^{o} + \sum_{k=1}^{k_L} \begin{bmatrix} (\bar{u}_1^{kc} \cos ka + \bar{u}_1^{ks} \sin ka) \cos(n-1)ka \\ + (-\bar{u}_1^{kc} \sin ka + \bar{u}_1^{ks} \cos ka) \sin(n-1)ka \end{bmatrix} - (-1)^{n-1} \bar{u}_1^{N/2}. \qquad (10)$$

Comparing Equation 10 with Equation 2 evaluated at side 2 as required by Equation 1,

$$\bar{u}_1^o = \bar{u}_2^o \tag{11-a}$$

$$\left.\begin{aligned} \bar{u}_1^{kc}\cos ka + \bar{u}_1^{ks}\sin ka &= \bar{u}_2^{kc} \qquad (11\text{-b}) \\ -\bar{u}_1^{kc}\sin ka + \bar{u}_1^{ks}\cos ka &= \bar{u}_2^{ks} \qquad (11\text{-c}) \end{aligned}\right\} \quad k = 1,\cdots,k_L$$

$$-\bar{u}_1^{N/2} = \bar{u}_2^{N/2} \; . \tag{11-d}$$

Equations 11 are the equations of constraint for the symmetrical components. The only symmetrical components coupled by the compatibility constraints are 1-c and 1-s, 2-c and 2-s, etc. Thus, there are several *uncoupled* models: the K = 0 model contains the $\bar{u}^o$ degrees of freedom; the K = 1 model, the $\bar{u}^{1c}$ and $\bar{u}^{1s}$ degrees of freedom, etc.

There is a somewhat arbitrary choice of where to transform the variables in the NASTRAN analysis. NASTRAN structural analysis can start with a structure defined with single and multipoint constraints, applied loads, thermal fields, etc., and reduce the problem to the "analysis set," $\{u_a\}$, where

$$[K_{aa}]\ \{u_a\} = \{P_a\}. \tag{12}$$

The vector $\{u_a\}$ contains only independent degrees of freedom. The decision was made to first reduce each segment individually to the "analysis" degrees of freedom, and then to rotationally transform them. This approach has several advantages, including elimination of the requirement to transform temperature vectors and single-point enforced displacements, because these quantities are first converted into equivalent loads. Also, the "ØMIT" feature can partition internal degrees of freedom, thus greatly reducing the number of degrees of freedom which must be transformed. The user specifies all constraints internal to the segments with standard NASTRAN data cards. If constraints (with MPC, SPC, or ØMIT) are applied to degrees of freedom on the boundaries, they will take precedence over the intersegment compatibility constraints; i.e., an intersegment compatibility constraint will *not* be applied to any degree of freedom which is constrained in some other way. SUPØRT data cards are forbidden because they are intended to apply to overall rigid body motions and will not, therefore, be applied to each segment. The analysis equation (Equation 12) for the segments is

$$[K] \{u\}^n = \{P\}^n , n = 1, 2 \cdots, N \tag{13}$$

The analysis equations for the symmetrical components, prior to applying the intersegment constraints, is

$$[K] \{\bar{u}\}^x = \{\bar{P}\}^x, x = 0, 1c, 1s, 2c \cdots, N/2, \tag{14}$$

where $\{\bar{P}\}^x$ is calculated using Equations 8. The matrix $[K]$ is the same for Equations 13 and 14, and is the KAA stiffness matrix of NASTRAN for one segment.

We come now to the matter of applying the intersegment compatibility constraints. We recognize that not all of the degrees of freedom in any transformed model can be independent, but it is easy to choose an independent set.

We include in the independent set, $\{\bar{u}^K\}$, all points in the interior and on boundary 1 (for both $\bar{u}^{kc}$ and $\bar{u}^{ks}$, if they exist). The values of displacement components at points on boundary 2 can then be determined from Equations 11. The transformations to independent degrees of freedom are indicated by

$$\{\bar{u}\}^{kc} = [G_{ck}]\ \{\bar{u}\}^K, \tag{15-a}$$

$$\{\bar{u}\}^{ks} = [G_{sk}]\ \{\bar{u}\}^K, \tag{15-b}$$

where each row of $[G_{ck}]$ or $[G_{sk}]$ contains only a single nonzero term if it is an interior or side 1 degree of freedom and either one or two nonzero terms if it is a degree of freedom on side 2. In arranging the order of terms in $\{\bar{u}\}^K$, the user can specify either that they be sequenced with all $\{\bar{u}\}^{kc}$ terms preceding all $\{\bar{u}\}^{ks}$ terms, or that they be sequenced with $\{\bar{u}\}^{kc}$ and $\{\bar{u}\}^{ks}$ grid points alternating. It should be emphasized that the kind of vector used in transformation Equations 3 and 15 are quite different. In Equation 3, there is one component (or column) for each segment; in Equation 15, there is one component (or row) for each degree of freedom in a segment.

Equation 15 is used to transform Equation 14 to a set of equations which satisfy the intersegment compatibility conditions

$$[\bar{K}]^K\ \{\bar{u}\}^K = \{\bar{P}\}^K, \tag{16-a}$$

where

$$[\bar{K}]^K = [G_{ck}^T\ KG_{ck} + G_{sk}^T\ KG_{sk}], \tag{16-b}$$

$$\{\bar{P}\}^K = [G_{ck}^T]\ \{\bar{P}\}^{kc} + [G_{sk}^T]\ \{\bar{P}\}^{ks}. \tag{16-c}$$

After solving Equation 16-a by decomposition and substitution, the symmetrical component variables, $\{\bar{u}\}^{kc}$ and $\{\bar{u}\}^{ks}$, are found from Equation 15. The physical segment variables, $\{u\}^{n}$, are found from Equation 3. The $\{u\}^{n}$ are NASTRAN vectors of the analysis set. They may be expanded to $\{u_g\}$ size by recovering dependent quantities. Stresses in the physical segments are then obtained via the normal stress reduction procedures.

The user may take an alternate route if he knows the transformed values for the forcing functions (loads, enforced displacements, and temperatures); i.e., $\{\bar{P}\}^{kc}$ and $\{\bar{P}\}^{ks}$. These may be input to NASTRAN, which will convert them directly to the transformed load vectors, $\{\bar{P}\}^{K}$. Data reduction may also be performed on the transformed quantities.

An approximate method for static analysis is available by merely setting

$$\{\bar{u}\}^{K} = 0 \tag{17}$$

for all $K < KMIN$ or $K > KMAX$. This is similar to truncating a Fourier series. The stiffness associated with larger K's (short azimuthal wave lengths) tends to be large, thus these components of displacement tend to be small.

The cyclic transform method can also be used for vibration analysis. The equation of motion in terms of independent degrees of freedom is

$$[K^{K} - \omega^{2}M^{K}]\{\bar{u}\}^{K} = 0, \tag{18}$$

where $[M]^{K}$ is derived by replacing [K] by [M] in Equation 16-b. The symmetrical components are recovered with Equation 15. Physical segment displacements can be recovered by Equation 3.

For frequency response, the method is the same as for statics, except that the mass and damping matrices must be transformed similar to Equation 16-b.

2.2.2.2 Dihedral Symmetry

Dihedral symmetry refers to the case when each individual segment has a plane of reflective symmetry; see Figure 2. The segments are divided about their midplanes to obtain 2N substructures. The midplane of a segment is designated as side 2. The other boundary, which must also be planar in order to be conformable, is called side 1. The two halves of the segment are called the right "R" and left "L" halves. The user prepares model information for one R half segment. He must also supply a list of points on side 1 and another list of points on side 2, and information about the orientation of the global coordinate system.

For the case of dihedral symmetry, the cyclic transformation described in Section 2.2.2.1 is used in conjunction with reflective symmetry of the segments. The physical quantities are related to the symmetric components by:

$$u^{n,R} = \sum_k (\bar{u}^{kc}+\bar{u}^{kc*})\cos(n-1)ka + (\bar{u}^{ks}+\bar{u}^{ks*})\sin(n-1)ka \qquad (19\text{-a})$$

$$u^{n,L} = \sum_k (\bar{u}^{kc}-\bar{u}^{kc*})\cos(N-n)ka + (\bar{u}^{ks}-\bar{u}^{ks*})\sin(N-n)ka \qquad (19\text{-b})$$

Here, the superscript n refers to the nth segment, R and L to the right and left halves. The superscript k for the symmetric components is an index in the range $0 \le k \le (N/2)$. The c and s refer to cosine and sine terms. Unstar and star (*) refer to symmetric and antisymmetric motion. It is to be understood that there are no sine terms, u^{os}, when k = 0 since their coefficients would be identically zero. Also, if N is even, for the maximum value of k (i.e., N/2) there will be no sine term $\bar{u}^{N/2,s}$. Equations 19-a and 19-b can be inverted in the same fashion used for rotational symmetry.

$$\left.\begin{matrix}\bar{u}^{kc}\\ \bar{u}^{kc*}\end{matrix}\right\} = \frac{\delta}{N}\sum(u^{n,R}\cos(n-1)ka \pm u^{n,L}\cos(N-n)ka) \tag{20-a}$$

$$\left.\begin{matrix}\bar{u}^{ks}\\ \bar{u}^{ks*}\end{matrix}\right\} = \frac{\delta}{N}\sum(u^{n,R}\sin(n-1)ka \pm u^{n,L}\sin(N-n)ka) \tag{20-b}$$

where the upper sign goes with the unstar term and

$$\delta = \begin{cases} 1/2 \text{ if } k=0 \text{ or } 2k=N, \\ 1 \text{ otherwise.} \end{cases}$$

For the case of reflective symmetry (or antisymmetry), the range of summation is over half of the substructures; the factor outside the equation must be multiplied by two; and only the unstar (or star) term is nonzero.

The constraints between half segments are for ensuring displacement compatibility. At each boundary, a grid point is associated with its mirror image point on an adjoining segment. Compatibility always involves a left and a right-hand coordinate system. Some components will be called "even," for which compatibility states that the components of the two points are equal. Displacements parallel to the boundary and rotations about axes normal to the boundary are even. The other components, called "odd," require that the components change sign. These conditions must be transformed to the symmetric components, resulting in:

Side 1, even

$$\begin{aligned} \bar{u}^{kc*} &= 0 \\ \bar{u}^{ks} &= 0 \end{aligned} \tag{21}$$

Side 1, odd

$$\bar{u}^{kc} = 0$$
$$\bar{u}^{ks*} = 0 \qquad (22)$$

Side 2, even

$$\bar{u}^{kc}\sin\frac{ka}{2} + \bar{u}^{ks}\cos\frac{ka}{2} = 0$$
$$\bar{u}^{kc*}\cos\frac{ka}{2} - \bar{u}^{ks*}\sin\frac{ka}{2} = 0 \qquad (23)$$

Side 2, odd

$$\bar{u}^{kc}\cos\frac{ka}{2} - \bar{u}^{ks}\sin\frac{ka}{2} = 0$$
$$\bar{u}^{kc*}\sin\frac{ka}{2} + \bar{u}^{ks*}\cos\frac{ka}{2} = 0 \qquad (24)$$

The method to satisfy the constraint is to relate each to an independent variable $\bar{u}^k$ and $\bar{u}^{k*}$, much as was done for the rotational case

$$\bar{u}^{kc} = G_{kc}\ \bar{u}^k$$
$$\bar{u}^{ks} = G_{ks}\ \bar{u}^k$$
$$\bar{u}^{kc*} = G_{kc*}\ \bar{u}^{k*} \qquad (25)$$
$$\bar{u}^{ks*} = G_{ks*}\ \bar{u}^{k*}$$

where Equations 25 will satisfy Equations 21 - 24 exactly. Note that this can be done by choosing $G_{kc*} = -G_{ks}$ and $G_{ks*} = G_{kc}$. Thus the unstar and the star equations will be identical. The stiffness matrix for the solution set variables $\bar{u}^k$ and $\bar{u}^{k*}$ are the same, and the two types can be treated as two loading conditions.

2.2.3 User Information

The cyclic symmetry modification to NASTRAN allows the solution of structures with rotational or dihedral symmetry by modeling only one of the identical segments. Special data cards and parameters are introduced to specify the method of joining the segments. In static analysis, input and output data for each individual segment are contained in separate subcases. The constrained degrees of freedom and material properties must be the same for all segments. For static analysis, the loads, the values of enforced displacements, and the temperatures may vary from element to element.

The SPCD bulk data card (Figure 3) is useful for applying enforced boundary displacements (or temperatures). These values are requested by a load set; thus, if different displacements are specified on different segments (i.e., in different subcases), the requested SPC constraint set will not change. This must be done, since looping on constraint sets is not supported in cyclic symmetry analysis.

A bulk data card, CYJØIN, (see Figure 4) is used to specify how the segments are to be connected. Existing MPC, SPC, and ØMIT constraints may be used within the segments. The SUPØRT card for free bodies is forbidden when cyclic symmetry is used, since *segment* free body modes do not necessarily imply *overall* free body modes. Constraints between segments are applied automatically to the degrees of freedom at grid points specified on CYJØIN bulk data cards which are not otherwise constrained. Grid points are not allowed to be placed on the axis of symmetry.

The user parameters are:

CTYPE — BCD. Type of problem: RØT for rotational symmetry, DIH for dihedral symmetry, DSYM and DANT for dihedral with symmetry or antisymmetry.

N — Integer. The number of segments.

K Integer. The value of the harmonic index, used only for eigenvalue analysis.

KMAX,KMIN Integers. The maximum and minimum value of K, used for static analysis. (Default is ALL)

CYCIØ Integer. +1 for physical segment representation, -1 for cyclic transform representation for input and output of data. Static analysis, default = 1.

CYCSEQ Integer. Used for method of sequencing the equations in the solution set. +1 for all cosine then all sine terms, -1 for alternating. Default = -1.

NLØAD The number of loading conditions in static analysis. Default = 1.

DMAP ALTERS are required to utilize the cyclic symmetry capability in MSC/NASTRAN. To relieve the user of the burden of the preparation and manipulation of the cards for these ALTERS, we have included the required ALTER for static analysis (RIGID FØRMAT 1) and for real eigenvalue analysis (RIGID FØRMAT 3) in the DMAP ALTER Library. The user is referred to RF1/6 and RF3/6 in Section 4 of the MSC/NASTRAN Application Manual. Complete instructions for the selection of these ALTERS from the Library are also provided in Section 4 and in Section 7.6 of the MSC/NASTRAN Application Manual.

To provide an overview of the use of the current cyclic symmetry capability in MSC/NASTRAN, the following summaries are presented.

STATICS

1. A separate subcase is defined for each segment (half segment for dihedral) and loading condition. Segments are ordered sequentially, with cosine terms before sine terms. Additional loads will appear as consecutive subcases.

2. Static loads for each subcase are specified with LØAD, TEMPERATURE (LØAD), or DEFØRM selections. Enforced deformations may be specified on SPCD (or SPC) data cards.

3. SPC's and MPC's must be selected above the subcase level.

4. If desired, the input and output may refer to symmetrical components, rather than to physical segments. In that case (CYCIØ = -1), the subcases refer to symmetrical components.

5. Output may include displacements, static loads, single point constraint forces, element forces and stresses, and undeformed and deformed plots of the substructures. Constraint forces at the joined points are not available.

6. The parameters KMAX and KMIN, which limit the range of the cyclic index K, may be specified on a PARAM bulk data card.

7. The GRDPNT (for a segment), WTMASS, IRES, and CØUPBAR parameters are operational.

NORMAL MODES

1. Constraints must be specified above the subcase level. SUPØRT is not allowed.

2. The cyclic index parameter K must be supplied by the user on a PARAM bulk data card.

3. An EIGR card is selected in case control by METHØD selection. The amplitude must be normalized on MASS or MAX.

4. The "automatic" eigenvalue summary will be printed.

5. Output may include the displacements, constraint forces, element forces and stress, all of which will be in terms of physical components. (This will result in many subcases per mode in many cases.) Undeformed and deformed plots are available.

2.2.4 Example Problems

Several examples of the application of cyclic symmetry are presented in Section 3.2 of the MSC/NASTRAN Application Manual.

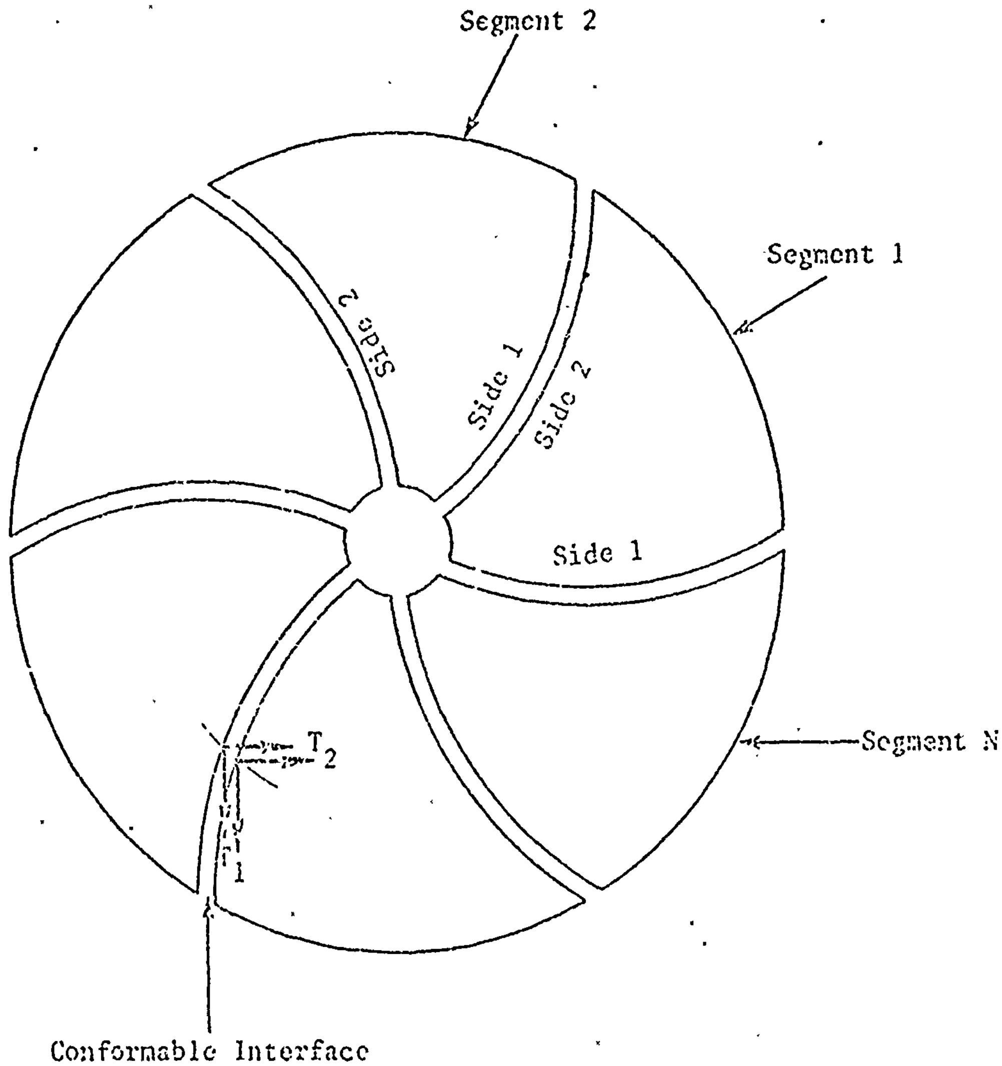

1. The user models one segment.

2. Each segment has its own coordinate system.

3. Segment boundaries may be curved. The local displacement coordinate systems (global) must conform at the joining points. The user gives a paired list of points on Side 1 and Side 2 which are to be joined.

Figure 1. Rotational Symmetry

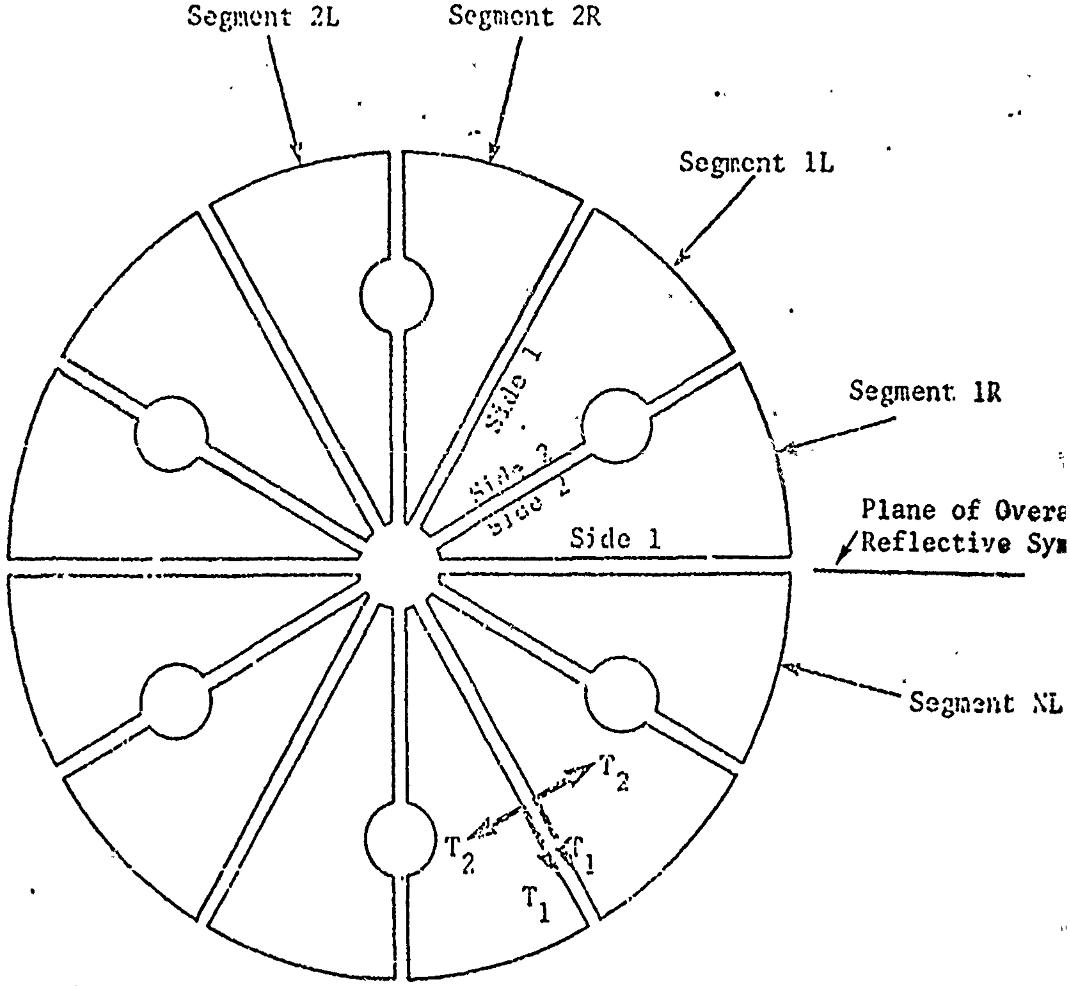

1. The user models one half segment (an R segment). The L half segments are mirror images of the R half segments.
2. Each half segment has its own coordinate system. The L halves use left hand coordinate systems.
3. Segment boundaries must be planar. Local displacement systems axes, associated with inter-segment boundaries, must be in the plane or normal to the plane. The user lists the points on Side 1 and Side 2.

Figure 2. Dihedral Symmetry

Input Data Card SPCD

Description: Defines an enforced displacement value for static analysis, which is requested as a LØAD.

Format and Example:

1	2	3	4	5	6	7	8	9	10
SPCD	SID	G	C	D	G	C	D	X	
SPCD	100	32	436	-2.6	5		+2.9		

Field	Contents
SID	Identification number of a static load set. (Integer > 0)
G	Grid or scalar point identification number (Integer > 0)
C	Component number (6 ≥ Integer ≥ 0 ; up to six unique such digits may be placed in the field with no imbedded blanks)
D	Value of enforced displacement for all coordinates designated by G and C (Real)

Remarks:

1. A coordinate referenced on this card must be referenced by a selected SPC or SPC1 data card.
2. Values of D will override to the values specified on a SPC bulk data card, if the LØAD set is requested.
3. The bulk data LØAD combination card will *not* request an SPCD.
4. At least one bulk data load card (FØRCE, SLØAD, etc.) is required in the load set selected in case control.

Figure 3. SPCD Bulk Data Card Format

Input Data Card CYJØIN

Description: Defines the boundary points of a segment in cyclic symmetry problems.

Format and Example:

1	2	3	4	5	6	7	8	9	10
CYJØIN	SIDE	C	G1	G2	G3	G4	G5	G6	abc
CYJØIN	1		7	9	16	25	33	64	ABC

+bc	G7	G8	G9	-etc.-					
+BC	72								

Alternate Form

CYJØIN	SIDE	C	GID1	"THRU"	GID2				
CYJØIN	2	S	6	THRU	32				

Field	Contents
SIDE	Side Identification (Integer 1 or 2)
C	Type of coordinate system used on boundaries of dihedral problems (BCD)
Gi,GIDi	Grid or scalar point identification numbers (Integer > 0)

Remarks:

1. CYJØIN bulk data cards are only used for cyclic symmetry problems. A parameter (CTYPE) must specify rotational or dihedral symmetry.

2. For rotational problems there must be one logical card for SIDE=1 and one for SIDE=2. The two lists specify grid points to be connected, hence both lists must have the same length.

3. For dihedral problems, side 1 refers to the boundary between segments and side 2 refers to the middle of a segment. The grid point degree of freedom which is normal to the boundary must be specified in field 3 as "T1", "T2", or "T3" ("R", rectangular, and "C", cylindrical, are the same as T2, while "S", spherical, is the same as T3). For SCALAR and EXTRA points with one degree of freedom, these should be specified as "blank", T2 or T3 if they are to have the same sign, and T1 if the two connected points are opposite in sign.

4. All components of displacement at boundary points are connected to adjacent segments, except those constrained by SPC, MPC, or ØMIT.

Figure 4. CYJØIN Bulk Data Card Format

APPENDIX A TO APPENDIX C

APPENDIX A TO APPENDIX C

NOTATION

The notation used in the text jumps back and forth between the use of matrices and vectors, and the use of explicit summation. In general NASTRAN use, the displacements are described in terms of a vector

$$\{u\} = \begin{Bmatrix} u_1 \\ u_2 \\ \cdot \\ \cdot \\ \cdot \end{Bmatrix} , \tag{1}$$

where there is one component for every degree of freedom. The components refer to displacements in the global coordinate system. Another vector with similar form is the load vector, which looks the same as Equation 1, except the letter P replaces u.

For cyclic symmetry problems, the displacements and forces will be given in terms of a matrix

$$[u] = \begin{bmatrix} u_1^1 & \cdots & u_1^N \\ u_2^1 & & u_2^N \\ \cdot & & \cdot \\ \cdot & & \cdot \\ u_M^1 & & u_M^N \end{bmatrix} , \tag{2}$$

where there is one row for each degree of freedom in a segment, and one column for each segment. All of the displacements in Equation 2 are not independent, since points on the boundaries must satisfy compatibility.

The Phase I transformation is a linear relationship between the unknowns for the "similar" degrees of freedom of the segments; thus, it involves terms in the same row of Equation 2. The operation is a post multiplication by the transformation matrix, as shown in Equation 3 of the text. The transformed degrees of freedom, called symmetric components $\bar{u}$, are also displayed in a matrix like Equation 2, only now there is one column for each symmetrical component, instead of for each segment.

Superscripts are used for segment numbers u^1, u^2, etc., and also for symmetrical components, $\bar{u}^{2c}$. The bar is used to distinguish a symmetrical component from a physical component. Subscripts are used to refer to a subset of degrees of freedom, hence u_1 and $\bar{u}_1$ are physical and symmetric components of displacement on side 1.

APPENDIX B TO APPENDIX C

THE MACNEAL-SCHWENDLER CORPORATION

7442 NO. FIGUEROA STREET · LOS ANGELES, CALIFORNIA 90041 · 254-3456

JOB NO: EC-254

MEMO NO: RLH-2

DATE: 15 October 1973

SUBJECT: Storage of Cyclic Symmetry Variables

In cyclic symmetry problems three types of variables are used. The physical components refer to displacements, loads, etc. for individual substructures. The symmetric components refer to the terms of the finite Fourier series. Both physical components and symmetric components must satisfy equations of compatibility. The symmetric components are expressed in terms of an independent set of variables called the solution set.

Rules have been imposed relating the relationship between the columns of a matrix (or a subcase ID) and the type of variable involved. Four types of transformations are to be used, called RØT, DIH, DSYMM and DANTI.

a. Rules for Subcases (loads and displacements). The identifiers for physical components are:

1. (LOAD COND). Separate subcases are needed for each loading condition. The user will supply a parameter NLOAD (default - 1) to specify a number.

2. (SEGMENT ID). Segments are identified 1, 2, ..., N, where N is a user specified parameter (no default). (An exception is given below for DSYMM and DANTI.)

3. (R,L). For the cases of DIH, DSYMM and DANTI, each segment consists of two substructures called R (right) and L (left). The user

models only one substructure. For the rotational case, there are only R substructures.

4. (FREQ), within a subcase. For frequency response problems, several frequencies are defined in each subcase. The number must be the same for all subcases.

The order for subcases (or for columns in a set of vectors) is the order specified above, with Load Cond the outer loop, Segment ID next, etc. For example,

1. DIH, N=2, NLØAD = 3, NFREQ = 2

Subcase	Load Cond	Seg ID	(R,L)	Freq
1	1	1	R	1
1	1	1	R	2
2	1	1	L	1
2	1	1	L	2
3	1	2	R	1
3	1	2	R	2
4	1	2	L	1
4	1	2	L	2

5 thru 12 repeates for loads 2 and 3 (24 total vectors)

2. RØT, N=5, NLØAD = 1, NFREQ = 1

Subcase	Load Cond	Seg ID	(R,L)	Freq
1	1	1	R	1
2	1	2	R	1
3	1	3	R	1
4	1	4	R	1
5	1	5	R	1

The following algorithm can be used to compute the number of substructures. The basic number

$$NSUB = N$$

If the type is DIH, multiply NSUB by 2. The total number of physical vectors is

NSUB x NLØAD x NFREQ .

b. Rules for storing symmetric components. The identifiers for the components are

1. K The index of the loop. The value of K must be between KMIN and KMAX where 0 .LE. KMIN .LE. KMAX .LE. (N/2).

2. (UNSTAR, STAR). The star (*) is used for unsymmetric terms, and the lack of a star for symmetric terms. This is similar to the conical shell convention. There are three cases:

TYPE	TERMS USED
RØT, DSYMM	UNSTAR only
DANTI	STAR only
DIH	UNSTAR and STAR

3. (COS, SIN). In the general case, there are both cos and sin terms. In the special cases K = 0 and 2K = N, there are only cos terms.

4. (LOAD COND). If the user is solving several loading conditions in one run, separate vectors are required for each. The number of loading conditions is specified by the parameter NLØAD.

5. (FREQ). In frequency response and eigenvalue problems there may be more than one frequency. The number of frequencies must be determined by the cyclic transformation modules, based upon the number of vectors input.

The following algorithm can be used to compute the number of symmetric components. The number of K values is KMAX - KMIN+1. The number of sin and cos types is twice this, (except if KMIN = 0, or 2KMAX = N).

$$NTERMS = 2(KMAX - KMIN+1)$$

If KMIN = 0, decrease NTERMS by 1. If 2* KMAX = N, decrease NTERMS by 1. For the case DIH, there are both unstar and star terms, thus NTERMS should be doubled. Examples are:

TYPE	N	KMIN	KMAX	NTERMS
RØT (0c, 1c, 1s, 2c, 2s)	5	0	2	5 = (2·3-1)
DIH (0c, 0c*, 1c, 1s, 1c*, 1s*, 2c, 2s, 2c*, 2s*, 3c, 3c*)	6	0	3	12 = 2(2·4-1-1)
DSYMM (1c, 1s)	3	1	1	2 = (2·1)
DANTI (0c*)	4	0	0	1 = (2·1-1)

The order shown in the above table is determined by using K in the outer loop, (UNSTAR, STAR) in the next loop, etc. The total number of vectors is equal to NTERMS * NLØAD * NFREQ.

c. <u>Rules for solution set</u>. The solution set is solved for one value of K at a time. For each K, the identifiers are

1. (UNSTAR, STAR)
2. (LOAD COND)
3. (FREQ)

The number of terms in the solution set NSSET is 1, except for DIH, when it is 2. The total number of vectors is NSSET * NLØAD * NFREQ. The order is implied by the above list, with all unstar terms before star, 1st load unstar before 2nd load unstar, etc.

APPENDIX C TO A. ÉNDIX C

THE MACNEAL-SCHWENDLER CORPORATION

7442 NO. FIGUEROA STREET • LOS ANGELES, CALIFORNIA 90041 • 254-34F6

JOB NO: EC-254

MEMO NO: RLH-3

DATE: 4 January 1974

SUBJECT: Changes Made in Cyclic Symmetry During November - December 1973

Those users who have previously used the program may be interested in what changes have been made.

1. A change has been made to allow multiple frequencies. This is the main feature needed to extend the capability to include frequency response. The same code is used for mode analysis, which allows the mode data to be output for physical quantities rather than symmetric components.

2. A change has been made in subcase order for the multiple loading conditions. In the new arrangement, all segments are defined in adjacent subcases. Thus if the user wishes to add more loads, the new subcases are added at the end.

3. The statics ALTER has been modified to break the matrix partition operation into several steps. This is recommended when CHECKPOINTing large problems due to possible long times spent in the SMP module.

4. The dihedral method has been changed to be easier to understand and more efficient. The old "DRL" and "DSA" designations were dropped, since it is believed that no users are likely to resolve the loads on left and right half segments into symmetric and antisymmetric components. The new designation DIH is equivalent to the old DRL. Two new forms DSYM and DANT are available when the results are symmtric about a plane. The theory was changed so that the plane of symmetry lies between segments 1-R and N-L,

(instead of 1-R and 1-L). Subcases are needed only for the substructures on one side of this plane, starting with 1-R. The method of specifying the global coordinate system for boundary connections on the CYJØIN data card, has been changed to allow the user to specify T1, T2, T3, whichever is the component normal to the boundary (the specification C and S for cylindrical and spherical are still allowed).

5. The parameter KMIN has been added to static analysis.

APPENDIX D TO APPENDIX C

THE MACNEAL-SCHWENDLER CORPORATION

7442 NO. FIGUEROA STREET • LOS ANGELES, CALIFORNIA 90041 • 254-3456

JOB NO: EC-254

MEMO NO: RLH-4

DATE: 3 January 1974

SUBJECT: Sample Problem

The following problem illustrates the solution for frequency dependent material properties using the methods of cyclic symmetry.

Figures 1 and 2 show the model and loading conditions. The hexagonal model consists of a frequency dependent solid (modeled with HEXA2 elements), inside of a case (modeled with QUAD2 elements). Three slots are cut into the solid. The base is fixed. Loads are applied on the inner surface. This structure has a first vibration frequency of 724 cps. It is desired to find the response at 0, 1500, and 3000 cps. for two loading conditions.

There are several choices available to model with finite elements.

Method Mneumonic	Structure Fraction Modeled	N	Comments
DIH	1/6	3	Six substructures
RØT	1/3	3	Three substructures
DIH	1/2	1	This is ordinary reflective symmetry.
DSYM	1/6	3	Requires loads symmetric about midplane.

Only the first method will be illustrated. The model, shown in Figure 3, consists of eight grid points and two structural elements. For the general problem, one-half of a symmetric substructure is modeled. Any of NASTRAN's general structural elements can be used. The NASTRAN run is shown in Figure 4.

The executive control deck requires:

1. ID card
2. APP DISP
3. SØL 8,1
4. $MERGE plus ENDALTER for the ALTER.

It is recommended that DIAG 8 be used. The sample also illustrates RESTART.

The case control deck may reference SPC's or MPC's, however they must be above the subcase level. SPC's have been used in this problem for the boundary conditions. Note that SPC's and MPC's are not used for compatibility between segments. Other required cards are:

FREQ (to select FREQ data card)

DLØAD (in subcases to select loads)

SDAMP (select table which defines viscoelastic material)

The optional cards include ØUTPUT requests, PLØT requests, TITLE's, direct input matrices (above subcase level). There is one subcase for each substructure. The first six subcases are used to define the loads and request output for the six substructures in the first loading condition. These subcases must be present even if there are no loads and no output requests. In the present examples there are two loading conditions. For each additional loading condition, extra subcases must be added to the end of the deck.

The Bulk data deck will be discussed in the sorted order (see page 8 of output).

1-2. The HEXA2 element is used for the solid.

3-4. A cylindrical coordinate system is recommended. This is the easiest way to guarantee that the inter-segment compatibility is met.

5. The QUAD2 element is used for the case.

6-7. The CYJØIN defines side 1 and side 2. Field 3 must identify the translation component normal to the boundary. If grid 201 were listed on side 1, there would be no slot.

8-10. These define the magnitude of the loads.

11-15. Not used. These are for static and vibration analysis.

16. Specifies frequency range.

17-24. Specifies the grid points. Note that the cylindrical coordinates are referenced.

25. The material property for the case. Field 9 (the element damping) should be zero. See item 31.

26. The material property for the propellant. Note that $G_{ref} = 500.$ and $g_{ref} = .50$ are arbitrarily selected values.

27. PARAM COUPMASS = 1 selects coupled mass. This is not generally recommended for frequency response problems, but was used to allow GIVIN's method for eigenvalue extraction of vibration modes.

28. This PARAM is required for cyclic symmetry problems. The options include DIH, RØT, DSYM and DANT.

29. This PARAM is defaulted to -1, the recommended value. The value used here changes the order of the equations.

30. The DECØMØPT should be set to the SYMMETRIC option (2 for IBM, 4 for CDC).

31. The PARAM G is used for overall damping. It is recommended for the damping of the case and must be entered into the calculation of the table TI (see 40-43.)

32. N is the number of segments. For the dihedral symmetry, each segment has a left and a right substructure.

33. NLØAD is required if not equal to one.

34. This parameter will cause the value of k to be printed in every loop.

35. The thickness of the case.

36-37. Assigns table 1000 for the frequency dependence of loads.

38. Removes matrix singularity since there is no stiffness for rotations associated with the solid elements.

39. Boundary condition for base.

40-43. Table for frequency dependent materials, computed by:

Frequency		0.	1500.	3000.
Data	G'	500.	860.	1180.
	G"/G'	.00	.56	.53
$TR = (G'/G_{ref}-1)/g_e$		0.	1.44	2.72
$TI = (G''/G_{ref}-g)/g_e$		0.	1.9264	2.5016

where G_{ref} = 500. g_{ref} = .5 (see 26) and g = 0. (see 31.). The table for TI is one greater than for TR. TR is selected by SDAMP in case control.

44-45. The frequency dependence of the loads is a constant.

The results are shown for displacements in the solution set. If desired, data recovery could be used for dependent displacements, element forces, constraint forces, plots, etc. For interpreting results, the user should remember that a local displacement coordinate system is used. A left hand system is used for the "L" substructures. Compare, for example, the motion of point 211 in subcase 1 and 2, which represents the same physical displacement.

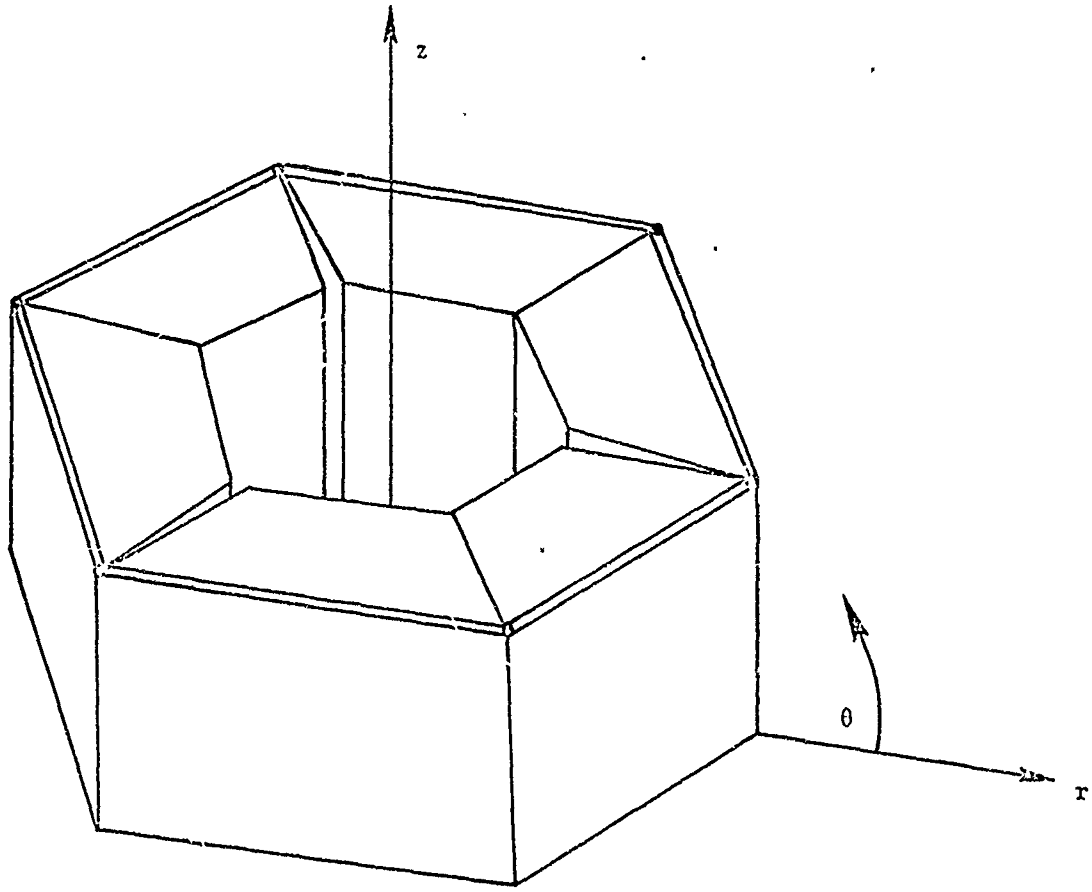

1. Elements used: plates (QUAD2) and solids (HEXA2)

2. Geometry (cylindrical coordinate system)

Inner radius	1.0
Outer Radius	3.0
Height	2.0
Plate thickness	0.1

3. Material Properties

Plate $E = 1. \times 10^7$, $\upsilon = .25$, $\rho = 2. \times 10^{-4}$, $g = 0.0$

Solid $\upsilon = .49$, $\rho = 1.66 \times 10^{-4}$

	f = 0.	1500.	3000.
Shear Storage Modulus G'	500.	860.	1180.
Shear Loss Tangent G"/G'	0.	.56	.53

4. Boundary condition. Base fixed.

5. Loads. Two conditions on inner face, see Figure 2.

Figure 1

The HEX Model

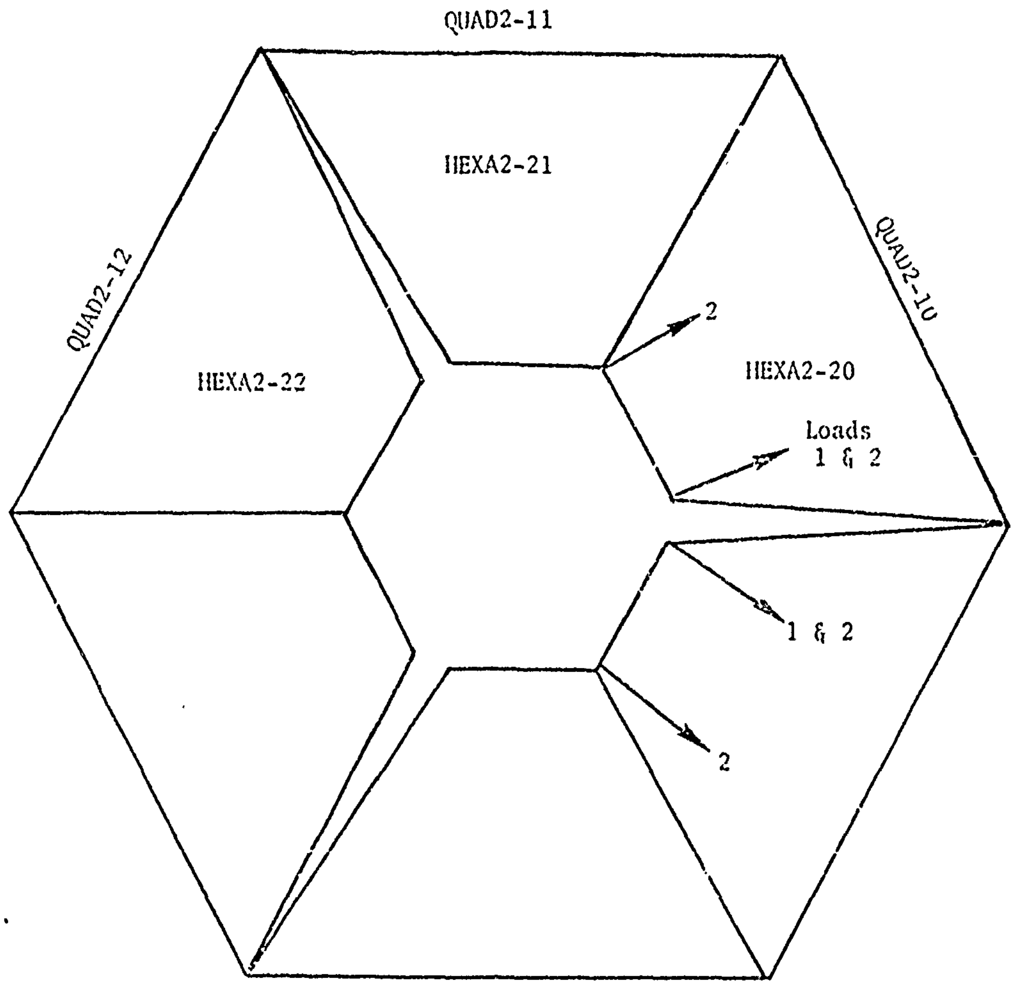

Figure 2

Top View of HEX Showing Elements and Loads

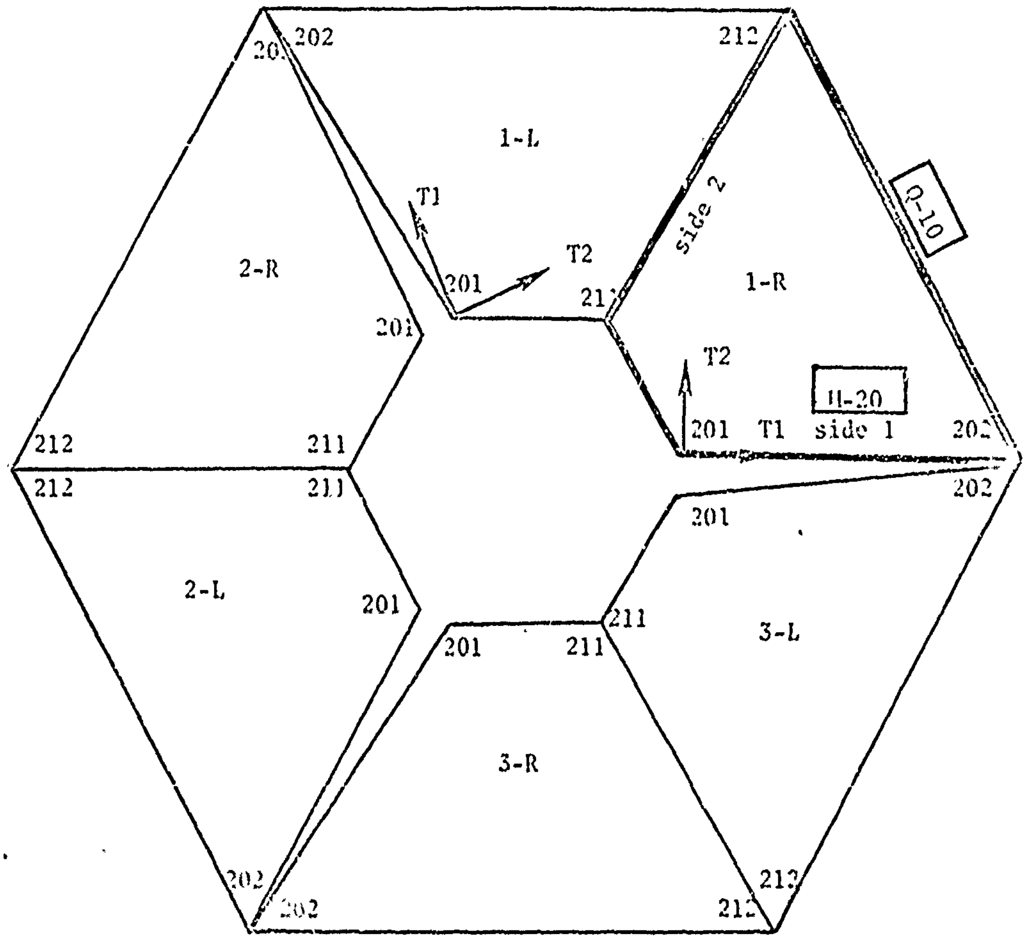

Figure 3

The dihedral (DIH) model. (Note that L-half segments have left-hand coordinate systems). The grid points on the bottom layer have ID's 100 less. Q-10 is a QUAD2 element and H-20 is a HEXA2 element. The slot has been shown with finite width for clarity. Only the 1-R substructure is modeled.

N A S T R A N E X E C U T I V E C O N T R O L D E C K E C H O

```
ID    HEXFREQ,DIH
APP   DISP
SOL   8,1  $ FREQUENCY RESPONSE
TIME 2
DIAG 8,13 $ PRINT TRAILERS AND OPEN CORE MESSAGES
DIAG 14   $ PRINT RIGID FORMAT
DIAG 2,3,4
$- CYCLIC TRANSFORMATION - FREQUENCY RESPONSE ------------------------
$     ALTER FOR FREQUENCY DEPENDENT MATERIALS    ( FRLG + FRRD1 ) R.F.=8
$                     R I G I D  F O R M A T  8  /  SERIES M
$                                                /  RLF VERSION
$  CASE CONTROL INPUT
$       A SUBCASE IS USED FOR EACH SUBSTRUCTURE AND LOADING CONDITION.
$       ALL MPC AND SPC REQUESTS MUST BE ABOVE THE SUBCASE LEVEL.
$
$  BULK DATA INPUT
$         PARAMETERS USED AR....
$      CTYPE (REQUIRED)    ROT = ROTATIONAL
$                          DIH = DIHEDRAL
$                          DSYM = DIH PLUS DEFORMATION SYMMETRY
$                          DANT = DIH PLUS DEFORMATION ANTISYMMETRY
$         N      (REQUIRED)   NUMBER OF SEGMENTS
$         KMIN   (DEFAULT 0 ) MIN RANGE OF CYCLIC INDEX K
$         KMAX   (DEFAULT -1) MAX RANGE OF CYCLIC INDEX K (-1 IMPLIES ALL)
$         CYCIO  (DEFAULT +1) INPUT/OUTPUT, +1 = PHYSICAL , -1 = SYM COMP
$         CYCSEQ(DEFAULT -1) MATRIX ELEMENT SEQUENCE, 1 = SEPARATE
$                                                -1 = ALTERNATING
$         NLOAD  (DEFAULT +1) NUMBER OF LOADING CONDITIONS
$         NOKPRT(DEFAULT -1) IF +1 K WILL BE OUTPUT AT THE TOP OF LOOP
$
$         CYJOIN BULK DATA CARDS ARE REQUIRED.
$
$       THE MODEL MUST CONTAIN K4 STRUCTURAL DAMPING (FOR FREQ DEP MATL)
$       TWO TABLEDX,TR(F) AND TI(F), ARE SELECTED IN CASE CONTROL VIA
$         SDAMP (THE ID OF TR IS SELECTED, THE ID OF TI MUST BE ONE LARGER)
$       THE STIFFNESS MATRIX (WITH STRUCTURAL DAMPING) WILL BE
$         K * ( 1. + I*G ) + K4 * ( TR(F) + I*TI(F) )
$         WHERE K = STIFFNESS MATRIX , G = PARAM OVERALL DAMPING
$
$ THE ANALYSIS WILL LOOP THRU A RANGE OF THE CYCLIC INDEX K = KMIN,KMAX
$
$-----------------------------------------------------------------------
ALTER 2
FILE     UXVF=APPEND $
ALTER 139,139  $  CHANGE FOR RESTART
GPCYC    GEOM4,EQDYN,USETD/CYCDD/V,Y,CTYPE/V,N,NOGO $  DATA FOR CYCT2
CHKPNT   CYCDD $
FRLG     CASEXX,USETD,DLT,FRL,GMD,GOD,DIT,/PPF,PSF,PDF,FOL,PHF/
         C,N,DIRECT  $  COMPUTE LOADS
```

N A S T R A N   E X E C U T I V E   C O N T R O L   D E C K   E C H O

```
CHKPNT   PPF,PSF,PDF,FOL  $
EQUIV    PPF,PDF/NOSET $
CHKPNT   PDF $
EQUIV    PDF,PXF/CYCIO $
CHKPNT   PXF $
COND     LCYC1,CYCIO $ IF (CYCIO,GE,0) TRANSFORM TO SYMMETRIC COMPONENTS
CYCT1    PDF/PXF,GCYCFF/V,Y,CTYPE/C,N,FORE/V,Y,N/V,Y,KMAX/V,Y,NLOAD/
         V,Y,KMIN $
CHKPNT   PXF $
LABEL    LCYC1 $
PARAM    //C,N,ADD/V,N,K/C,N,0/V,Y,KMIN=2 $ INITIALIZE K = KMIN
LABEL    TOPCYC $$$$$$$$$$$$$$  LOOP ON K $$$$$$$$$$$$$$$$$$$$$$$$$$$$$$
COND     NOKPRT,NOKPRT  $                                             $
PRTPARM  //C,N,0/C,N,K $                                              $
LABEL    NOKPRT $                                                     $
ALTER 140,140                                                         $
CYCT2    CYCDD,KDD,MDD,PXF,BDD,K4DD/KKKF,MKKF,PKF,BKKF,K4KKF/C,N,
         FORE,FREQ/V,Y,N=-1/V,N,K/V,Y,CYCSEQ=-1/V,Y,NLOAD=1/V,N,NOGO/
         V,Y,KMAX/V,Y,KMIN $                                          $
CHKPNT   KKKF,MKKF,PKF,BKKF,K4KKF $                                   $
FRRD1    CASEXX,DIT,KKKF,BKKF,MKKF,K4KKF,PKF,FRL,FOL/UKVF/C,N,DIRECT/
         V,N,NONCUP/C,Y,DECOMOPT=1 $                                  $
CHKPNT   UKVF $                                                       $
ALTER 141,141                                                         $
CYCT2    CYCDD,,,UKVF,,/,,UXVF,,/C,N,BACKFREQ/V,Y,N/V,N,K/V,Y,CYCSEQ/V,
         Y,NLOAD/V,N,NOGO/V,Y,KMAX/V,Y,KMIN $                         $
CHKPNT   UXVF $                                                       $
PARAM    //C,N,ADD/V,N,K/V,N,K/C,N,1 $         K = K + 1              $
PARAM    //C,N,SUB/V,N,DONE/V,Y,KMAX/V,N,K $                          $
COND     LCYC2,DONE $  IF(K.GT.KMAX) EXIT LOOP                        $
REPT     TOPCYC,100 $$$$$$$$$$$$$$$$$$$$$$$$$$$$$$$$$$$$$$$$$$$$$$$$$$$$$
JUMP     ERROR1 $
LABEL    LCYC2 $
EQUIV    UXVF,UDVF/CYCIO $
CHKPNT   UDVF $
COND     LCYC3,CYCIO $ IF (CYCIO,GE,0) TRANSFORM TO PHYSICAL VARIABLES
CYCT1    UXVF/UDVF,GCYCBF/V,Y,CTYPE/C,N,BACK/V,Y,N/V,Y,KMAX/V,Y,NLOAD/
         V,Y,KMIN $
CHKPNT   UDVF $
LABEL    LCYC3 $
$
ALTER 199
LABEL    ERROR1 $  FAILED TO SPECIFY PARAM  N,GT,0
PRTPARM  //C,N,0/C,N,N $
ENDALTER
RESTART  HEXFREQ ,DSYM    ,11/16/73,    2081,
         1,   XVPS    ,    FLAGS = 0,    REEL =   1,    FILE =      6
         2,   REENTER AT DMAP SEQUENCE NUMBER      7
         3,   GPL     ,    FLAGS = 0,    REEL =   1,    FILE =      7
         4,   EQEXIN  ,    FLAGS = 0,    REEL =   1,    FILE =      8
```

```
N A S T R A N   E X E C U T I V E   C O N T R O L   D E C K   E C H O

     5,   GPDT     ,   FLAGS = 0,   REEL = 1,   FILE =   9
     6,   CSTM     ,   FLAGS = 0,   REEL = 1,   FILE =  12
     7,   BGPDT    ,   FLAGS = 0,   REEL = 1,   FILE =  11
     8,   SIL      ,   FLAGS = 0,   REEL = 1,   FILE =  12
     9,   XVPS     ,   FLAGS = 0,   REEL = 1,   FILE =  13
    10,   USET     ,   FLAGS = 0,   REEL = 0,   FILE =   0
    11,   GM       ,   FLAGS = 0,   REEL = 0,   FILE =   0
    12,   GO       ,   FLAGS = 0,   REEL = 0,   FILE =   0
    13,   KAA      ,   FLAGS = 0,   REEL = 0,   FILE =   0
    14,   BAA      ,   FLAGS = 0,   REEL = 0,   FILE =   0
    15,   MAA      ,   FLAGS = 0,   REEL = 0,   FILE =   0
    16,   K4AA     ,   FLAGS = 0,   REEL = 0,   FILE =   0
    17,   KFS      ,   FLAGS = 0,   REEL = 0,   FILE =   0
    18,   PSF      ,   FLAGS = 0,   REEL = 0,   FILE =   0
    19,   GPC      ,   FLAGS = 0,   REEL = 0,   FILE =   0
    20,   EST      ,   FLAGS = 0,   REEL = 0,   FILE =   0
    21,   ECT      ,   FLAGS = 0,   REEL = 0,   FILE =   0
    22,   PLTSETX  ,   FLAGS = 0,   REEL = 0,   FILE =   0
    23,   PLTPAR   ,   FLAGS = 0,   REEL = 0,   FILE =   0
    24,   GPSETS   ,   FLAGS = 0,   REEL = 0,   FILE =   0
    25,   ELSETS   ,   FLAGS = 0,   REEL = 0,   FILE =   0
    26,   REENTER AT DMAP SEQUENCE NUMBER   10
    27,   ECT      ,   FLAGS = 0,   REEL = 1,   FILE =  14
    28,   XVPS     ,   FLAGS = 0    REEL = 1,   FILE =  15
    29,   REENTER AT DMAP SEQUENCE NUMBER   21
    30,   XVPS     ,   FLAGS = 0,   REEL = 1,   FILE =  16
    31,   REENTER AT DMAP SEQUENCE NUMBER   23
    32,   XVPS     ,   FLAGS = 0,   REEL = 1,   FILE =  17
    33,   GPTT     ,   FLAGS = 0,   REEL = 0,   FILE =   0
    34,   REENTER AT DMAP SEQUENCE NUMBER   27
    35,   EST      ,   FLAGS = 0,   REEL = 1,   FILE =  18
    36,   ECPT     ,   FLAGS = 0,   REEL = 1,   FILE =  19
    37,   GPCT     ,   FLAGS = 0,   REEL = 1,   FILE =  20
    38,   XVPS     ,   FLAGS = 0,   REEL = 1,   FILE =  21
    39,   GEI      ,   FLAGS = 0,   REEL = 0,   FILE =   0
    40,   K4GG     ,   FLAGS = 0,   REEL = 0,   FILE =   0
    41,   GPST     ,   FLAGS = 0,   REEL = 0,   FILE =   0
    42,   MGG      ,   FLAGS = 0,   REEL = 0,   FILE =   0
    43,   BGG      ,   FLAGS = 0,   REEL = 0,   FILE =   0
    44,   KGGX     ,   FLAGS = 0,   REEL = 0,   FILE =   0
    45,   OGPST    ,   FLAGS = 0,   REEL = 0,   FILE =   0
    46,   K4NN     ,   FLAGS = 0,   REEL = 0,   FILE =   0
    47,   K4FF     ,   FLAGS = 0,   REEL = 2,   FILE =   0
    48,   MNN      ,   FLAGS = 0,   REEL = 0,   FILE =   0
    49,   MFF      ,   FLAGS = 0,   REEL = 0,   FILE =   0
    50,   BNN      ,   FLAGS = 0,   REEL = 0,   FILE =   0
    51,   BFF      ,   FLAGS = 0,   REEL = 0,   FILE =   0
    52,   REENTER AT DMAP SEQUENCE NUMBER   32
    53,   KGGX     ,   FLAGS = 0,   REEL = 1,   FILE =  22
    54,   GPST     ,   FLAGS = 0,   REEL = 1,   FILE =  23
```

N A S T R A N   E X E C U T I V E   C O N T R O L   D E C K   E C H O

```
 55,  K4GG    ,  FLAGS = 0,  REEL = 1,  FILE =  24
 56,  XVPS    ,  FLAGS = 0,  REEL = 1,  FILE =  25
 57,  REENTER AT DMAP SEQUENCE NUMBER   36
 58,  MGG     ,  FLAGS = 0,  REEL = 1,  FILE =  26
 59,  XVPS    ,  FLAGS = 0,  REEL = 1,  FILE =  27
 60,  REENTER AT DMAP SEQUENCE NUMBER   44
 61,  KGGX    ,  FLAGS = 4,  REEL = 1,  FILE =  22
 62,  KGG     ,  FLAGS = 4,  REEL = 1,  FILE =  22
 63,  XVPS    ,  FLAGS = 0,  REEL = 1,  FILE =  28
 64,  REENTER AT DMAP SEQUENCE NUMBER   54
 65,  USET    ,  FLAGS = 0,  REEL = 1,  FILE =  29
 66,  KNN     ,  FLAGS = 4,  REEL = 1,  FILE =  22
 67,  MGG     ,  FLAGS = 4,  REEL = 1,  FILE =  26
 68,  MNN     ,  FLAGS = 4,  REEL = 1,  FILE =  26
 69,  K4GG    ,  FLAGS = 4,  REEL = 1,  FILE =  24
 70,  K4NN    ,  FLAGS = 4,  REEL = 1,  FILE =  24
 71,  XVPS    ,  FLAGS = 0,  REEL = 1,  FILE =  32
 72,  GMD     ,  FLAGS = 0,  REEL = 0,  FILE =   0
 73,  RG      ,  FLAGS = 0,  REEL = 0,  FILE =   0
 74,  GOD     ,  FLAGS = 0,  REEL = 0,  FILE =   0
 75,  REENTER AT DMAP SEQUENCE NUMBER   68
 76,  XVPS    ,  FLAGS = 0,  REEL = 1,  FILE =  31
 77,  KFF     ,  FLAGS = 0,  REEL = 0,  FILE =   0
 78,  REENTER AT DMAP SEQUENCE NUMBER   71
 79,  KFS     ,  FLAGS = 0,  REEL = 1,  FILE =  32
 80,  KFF     ,  FLAGS = 0,  REEL = 1,  FILE =  33
 81,  MFF     ,  FLAGS = 0,  REEL = 1,  FILE =  34
 82,  K4FF    ,  FLAGS = 0,  REEL = 1,  FILE =  35
 83,  XVPS    ,  FLAGS = 0,  REEL = 1,  FILE =  36
 84,  REENTER AT DMAP SEQUENCE NUMBER   74
 85,  KFF     ,  FLAGS = 4,  REEL = 1,  FILE =  33
 86,  KAA     ,  FLAGS = 4,  REEL = 1,  FILE =  33
 87,  MFF     ,  FLAGS = 4,  REEL = 1,  FILE =  34
 88,  MAA     ,  FLAGS = 4,  REEL = 1,  FILE =  34
 89,  K4FF    ,  FLAGS = 4,  REEL = 1,  FILE =  35
 90,  K4AA    ,  FLAGS = 4,  REEL = 1,  FILE =  35
 91,  XVPS    ,  FLAGS = 0,  REEL = 1,  FILE =  37
 92,  REENTER AT DMAP SEQUENCE NUMBER   93
 93,  USETD   ,  FLAGS = 0,  REEL = 1,  FILE =  38
 94,  EQDYN   ,  FLAGS = 0,  REEL = 1,  FILE =  39
 95,  DIT     ,  FLAGS = 0,  REEL = 1,  FILE =  40
 96,  FRL     ,  FLAGS = 0,  REEL = 1,  FILE =  41
 97,  SILD    ,  FLAGS = 0,  REEL = 1,  FILE =  42
 98,  GPLD    ,  FLAGS = 0,  REEL = 1,  FILE =  43
 99,  XVPS    ,  FLAGS = 0,  REEL = 1,  FILE =  44
100,  TFPOOL  ,  FLAGS = 0,  REEL = 0,  FILE =   0
101,  PSDL    ,  FLAGS = 0,  REEL = 0,  FILE =   0
102,  REENTER AT DMAP SEQUENCE NUMBER   93
103,  CYCDD   ,  FLAGS = 0,  REEL = 1,  FILE =  45
104,  XVPS    ,  FLAGS = 0,  REEL = 1,  FILE =  46
```

N A S T R A N   E X E C U T I V E   C O N T R O L   D E C K   E C H O

```
105,   REENTER AT DMAP SEQUENCE NUMBER   104
106,   XVPS    ,   FLAGS = 0,   REEL = 1,   FILE =   42
107,   ABFL    ,   FLAGS = 0,   REEL = 0,   FILE =    0
108,   KBFL    ,   FLAGS = 0,   REEL = 0,   FILE =    0
109,   REENTER AT DMAP SEQUENCE NUMBER   110
110,   CASEXX  ,   FLAGS = 0,   REEL = 1,   FILE =   48
111,   XVPS    ,   FLAGS = 0,   REEL = 1,   FILE =   49
112,   REENTER AT DMAP SEQUENCE NUMBER   132
113,   MOD     ,   FLAGS = 4,   REEL = 1,   FILE =   34
114,   XVPS    ,   FLAGS = 0,   REEL = 1,   FILE =   52
115,   K2PP    ,   FLAGS = 0,   REEL = 0,   FILE =    0
116,   M2PP    ,   FLAGS = 0,   REEL = 0,   FILE =    0
117,   B2PP    ,   FLAGS = 0,   REEL = 0,   FILE =    0
118,   K2DD    ,   FLAGS = 0,   REEL = 0,   FILE =    0
119,   M2DD    ,   FLAGS = 0,   REEL = 0,   FILE =    0
120,   B2DD    ,   FLAGS = 0,   REEL = 0,   FILE =    0
121,   BDD     ,   FLAGS = 0,   REEL = 0,   FILE =    0
122,   REENTER AT DMAP SEQUENCE NUMBER   137
123,   KDD     ,   FLAGS = 0,   REEL = 1,   FILE =   51
124,   XVPS    ,   FLAGS = 0,   REEL = 1,   FILE =   52
125,   REENTER AT DMAP SEQUENCE NUMBER   140
126,   K4DD    ,   FLAGS = 0,   REEL = 1,   FILE =   35
127,   XVPS    ,   FLAGS = 0,   REEL = 1,   FILE =   53
128,   REENTER AT DMAP SEQUENCE NUMBER   140
129,   PPF     ,   FLAGS = 0,   REEL = 1,   FILE =   54
130,   PSF     ,   FLAGS = 0,   REEL = 1,   FILE =   55
131,   PDF     ,   FLAGS = 0,   REEL = 1,   FILE =   56
132,   FOL     ,   FLAGS = 0,   REEL = 1,   FILE =   57
133,   XVPS    ,   FLAGS = 0,   REEL = 1,   FILE =   58
134,   REENTER AT DMAP SEQUENCE NUMBER   140
135,   PDF     ,   FLAGS = 0,   REEL = 1,   FILE =   59
136,   XVPS    ,   FLAGS = 0,   REEL = 1,   FILE =   60
137,   REENTER AT DMAP SEQUENCE NUMBER   140
138,   XVPS    ,   FLAGS = 0,   REEL = 1,   FILE =   61
139,   PXF     ,   FLAGS = 0,   REEL = 0,   FILE =    0
140,   REENTER AT DMAP SEQUENCE NUMBER   142
141,   PXF     ,   FLAGS = 0,   REEL = 1,   FILE =   62
142,   XVPS    ,   FLAGS = 0,   REEL = 1,   FILE =   63
$ TRUNCATED DICTIONARY
CEND
```

C A S E   C O N T R O L   D E C K   E C H O

```
CARD
COUNT
  1      TITLE = FREQUENCY RESPONSE OF HEX,  DIH METHOD, FREQ DEP MATL
  2     ECHO = BOTH
  3      SPC    = 999
  4      FREQ   = 1
  5      SDAMP  = 10
  6      SDISP  = ALL
  7     SUBCASE 1
  8      LABEL =   SEG 1-R  1ST LOAD
  9      DLOAD = 1
 10     SUBCASE 2
 11      LABEL =   SEG 1-L  1ST LOAD
 12     SUBCASE 3
 13      LABEL =   SEG 2-R  1ST LOAD
 14     SUBCASE 4
 15      LABEL =   SEG 2-L  1ST LOAD
 16     SUBCASE 5
 17      LABEL =   SEG 3-R  1ST LOAD
 18     SUBCASE 6
 19      LABEL =   SEG 3-L  1ST LOAD
 20     SUBCASE 7
 21      LABEL =   SEG 1-R  2ND LOAD
 22      DLOAD = 2
 23     SUBCASE 8
 24      LABEL =   SEG 1-L  2ND LOAD
 25     SUBCASE 9
 26      LABEL =   SEG 2-R  2ND LOAD
 27     SUBCASE 10
 28      LABEL =   SEG 2-L  2ND LOAD
 29     SUBCASE 11
 30      LABEL =   SEG 3-R  2ND LOAD
 31     SUBCASE 12
 32      LABEL =   SEG 3-L  2ND LOAD
 33      DLOAD = 2
 34     BEGIN BULK
```

S O R T E D   B U L K   D A T A   E C H O

CARD COUNT	1	2	3	4	5	6	7	8	9	10
1-	CHEXA2	20	20	101	102	112	111	201	202	+20
2-	+20	212	211							
3-	CORD2C	12		.0	.0	.0	.0	.0	1.0	+C10
4-	+C10	1.0	0.0	0.0						
5-	CQUAD2	10	10	102	112	212	222			
6-	CYJOIN	1	T2	202						
7-	CYJOIN	2	T2	211	212					
8-	DAREA	1	201	1	.8660254	201	2	.5		
9-	DAREA	2	201	1	.8660254	201	2	.5		
10-	DAREA	2	211	1	.8660254	211	2	-.5		
11-	EIGR	1	GIV	.0	1.+2		6			+E1
12-	+E1	MAX								
13-	FORCE	1	201	10	1.0	.8660254	.5			
14-	FORCE	2	201	10	1.0	.8660254	.5			
15-	FORCE	2	211	10	1.0	.8660254	-.5			
16-	FREQ1	1	.0	1500.	2					
17-	GRID	101	10	1.	0.0	2.0	10			
18-	GRID	102	10	3.	0.0	2.0	10			
19-	GRID	111	10	1.	60.	2.0	10			
20-	GRID	112	10	3.	60.	2.0	10			
21-	GRID	211	10	1.	0.0	2.	10			
22-	GRID	212	10	3.	0.0	2.	10			
23-	GRID	21	10	1.	60.	2.	10			
24-	GRID	212	10	3.	60.	2.	10			
25-	MAT1	10	1.+7		.25	2.-4				
26-	MAT1	20		500.	.49	1.66-1			.50	
27-	PARAM	COUPMASS	1							
28-	PARAM	CTYPE	DIH							
29-	PARAM	CYCSEQ	1							
30-	PARAM	DECOMOPT	2							
31-	PARAM	G	.0							
32-	PARAM	N	3							
33-	PARAM	NLOAD	2							
34-	PARAM	NOKPRT	1							
35-	PQUAD2	10	10	.1						
36-	RLOAD1	1	1			1000				
37-	RLOAD1	2	2			1000				
38-	SPC1	999	456	101	111	201	211			
39-	SPC1	999	123456	101	102	111	112			
40-	TABLED1	10								+T10
41-	+T10	0.0	0.0	1500.	1.44	3000.	2.72	ENDT		
42-	TABLED1	11								+T11
43-	+T11	0.0	0.0	1500.	1.5264	3000.	2.5016	ENDT		
44-	TABLED1	1000								+1000
45-	+1000	0.	1.0	100.	1.0	ENDT				
	ENDDATA									

FREQUENCY RESPONSE OF HEX, WITH METHOD, FREQ DE. MATL VEHL 21, .. 3 TRA 7 E.

SEG 1-R . 1ST LOAD. SUBCASE 1

FREQUENCY = 0.0

C O M P L E X   D I S P L A C E M E N T   V E C T O R (SOLUTION SET)

(REAL/IMAGINARY)

POINT ID.	TYPE	T1	T2	T3	R1	R2	R3
201	G	7.906854E-05	2.268860E-05	4.414769E-05			
		0.0	0.0	0.0			
202	G	2.681715E-06	3.479551E-07	2.891301E-08	-5.173309E-07	1.877939E-06	-7.447523E-07
		0.0	0.0	0.0	0.0	0.0	0.0
211	G	2.380324E-05	-1.790936E-05	-9.668101E-07			
		0.0	0.0	0.0			
212	G	1.329125E-06	-2.158071E-07	2.860223E-08	5.804640E-07	1.048726E-06	1.282544E-06
		0.0	0.0	0.0	0.0	0.0	0.0

SUBCASE 1

SEG 1-R 1ST LOAD
FREQUENCY = 1.500000E 03

C O M P L E X D I S P L A C E M E N T V E C T O R (SOLUTION SET)
(REAL/IMAGINARY)

POINT ID.	TYPE	T1	T2	T3	R1	R2	R3
201	G	9.068154E-06	2.454072E-06	-2.624498E-05			
		-6.082523E-05	-1.322866E-05	-4.269718E-05			
202	E	1.965920E-06	4.411733E-07	3.679962E-08	-3.907107E-07	1.156405E-06	-8.131495E-07
		-4.218735E-06	-3.834245E-07	2.997873E-08	4.610246E-07	-2.462622E-06	1.932364E-06
211	G	.797022E-06	1.011164E-05	-9.341404E-06			
		-.354938E-05	1.426342E-05	1.265377E-05			
212	G	1.395438E-05	8.594998E-08	3.767373E-08	5.299319E-08	9.621754E-07	7.571912E-07
		-1.328148E-06	6.652601E-07	-4.684941E-08	-7.628126E-07	-1.301063E-06	-2.869315E-06

ELECASE 1

SEG 1-R 1ST LOAD
FREQUENCY = 3.0000000 03

C O M P L E X D I S P L A C E M E N T V E C T O R (SOLUTION SET)
(REAL/IMAGINARY)

POINT ID.	TYPE	T1	T2	T3	R1	R2	R3
201	G	-7.813128E-26	4.622470E-20	-1.138460E-25			
		-1.592928E-25	-5.418862E-26	2.632891E-26			
202	G	-4.223620E-07	1.144183E-07	2.606644E-08	5.266494E-07	-5.681084E-08	-7.542318E-07
		-2.853302E-26	-1.734879E-07	1.628262E-07	3.432925E-07	-8.514871E-08	-5.142363E-07
211	G	-8.541496E-26	4.922089E-25	3.326428E-26			
		1.528752E-26	-2.981699E-26	-2.458830E-26			
212	G	-8.091706E-07	-3.632817E-07	-2.667632E-08	9.678822E-08	-1.065767E-07	-1.423153E-07
		9.797486E-07	1.563477E-07	-1.469223E-07	-3.297786E-26	-8.721662E-08	5.223678E-26

SEG 1-L 1ST LOAD
FREQUENCY = 0.0

SUBCASE 2

COMPLEX DISPLACEMENT VECTOR (SOLUTION SET)
(REAL/IMAGINARY)

POINT ID.	TYPE	T1	T2	T3	R1	R2	R3
201	G	-4.989852E-06	2.190788E-05	6.913927E-06			
		0.0	0.0	0.0			
202	G	-4.499242E-07	2.188970E-07	7.315919E-08	-2.360251E-07	-2.696136E-07	-4.662184E-08
		0.0	0.0	0.0	0.0	0.0	0.0
211	G	2.380324E-05	1.790946E-05	-9.668121E-07			
		0.0	0.0	0.0			
212	G	1.329125E-06	2.150071E-07	2.866382E-08	-5.804640E-07	1.048726E-06	-1.222544E-06
		0.0	0.0	0.0	0.0	0.0	0.0

SUBCASE 2

SEG 1-L 1ST LOAD
FREQUENCY = 1.500000E 03

C O M P L E X   D I S P L A C E M E N T   V E C T O R   (SOLUTION SET)
(REAL/IMAGINARY)

POINT ID.	TYPE	T1	T2	T3	R1	R2	R3
201	G	1.720640E-05	-1.544362E-05	-8.595821E-06			
		-3.647627E-06	-6.586884E-06	1.940463E-05			
202	G	7.894577E-07	1.572561E-07	2.108553E-08	-2.094551E-07	4.794206E-07	-4.576803E-07
		9.078145E-07	-4.197861E-07	-1.266425E-07	3.366883E-07	4.932598E-07	-1.118733E-07
211	G	1.797822E-06	-1.211164E-05	-9.341403E-06			
		-2.354938E-05	-1.405342E-05	1.265377E-05			
212	G	1.395436E-06	-8.594992E-08	3.767373E-08	-5.299316E-08	9.621754E-07	-7.571913E-07
		-1.928140E-06	-6.650601E-07	-4.684934E-08	7.628126E-07	-1.301884E-06	2.869632E-06

SEG 1-L 1ST LOAD SUBCASE 2
FREQUENCY = 3.000000E 03

C O M P L E X D I S P L A C E M E N T V E C T O R (SOLUTION SET)
(REAL/IMAGINARY)

POINT ID.	TYPE	T1	T2	T3	R1	R2	R3
201	G	-6.081756E-06	-3.267476E-06	3.409355E-06			
		-1.848414E-07	5.929897E-06	-2.132242E-06			
202	G	-5.213794E-07	-3.773295E-07	-2.238592E-08	7.842497E-07	-4.358807E-08	-1.123723E-06
		-1.725412E-07	2.132615E-07	9.502219E-09	-3.334867E-06	3.797527E-08	5.314445E-06
211	G	-8.541497E-06	-4.922689E-06	3.326428E-06			
		1.588758E-06	2.981699E-06	-2.458860E-06			
212	G	-8.091705E-07	-3.632016E-07	-2.667632E-08	-9.678826E-08	-1.265767E-07	1.423161E-07
		9.797486E-07	-1.563477E-07	-1.469223E-07	3.297786E-06	-8.721562E-08	-5.023678E-06

SEG 2-R 1ST LOAD   SUBCASE 3
FREQUENCY = 0.0

C O M P L E X   D I S P L A C E M E N T   V E C T O R   (SOLUTION SET)
(REAL/IMAGINARY)

POINT ID.	TYPE	T1	T2	T3	R1	R2	R3
201	G	-3.224832E-07	-3.211832E-08	-7.865359E-08			
		0.0	0.0	0.0			
222	G	-4.499242E-07	-2.188970E-07	7.315919E-08	2.360851E-07	-2.696136E-07	4.662184E-08
		0.0	0.0	0.0	0.0	0.0	0.0
211	G	-4.889141E-08	1.695723E-07	9.751028E-06			
		0.0	0.0	0.0			
212	G	2.922932E-08	8.815508E-09	2.490036E-30	-1.336151E-07	4.838029E-29	-4.775683E-07
		0.0	0.0	0.0	0.0	0.0	0.0

SEG 2-R 1ST LOAD
FREQUENCY = 1.500000E 03

SUBCASE 3

COMPLEX DISPLACEMENT VECTOR (SOLUTION SET)
(REAL/IMAGINARY)

POINT ID.	TYPE	T1	T2	T3	R1	R2	R3
201	G	1.156714E-06	1.386133E-07	1.092252E-06			
		-2.794644E-07	5.276496E-07	-4.882723E-07			
202	G	7.894577E-07	-1.572561E-07	2.108953E-08	2.094551E-07	4.794226E-07	4.576523E-07
		9.078145E-07	4.197861E-07	-1.266405E-07	-3.366883E-07	4.932598E-07	1.110733E-07
211	G	5.861637E-08	-4.013274E-07	-5.935843E-07			
		2.232464E-07	2.702725E-07	2.265855E-07			
212	G	-3.528949E-07	-1.529575E-07	4.392132E-08	1.181552E-07	-1.455113E-07	-2.796951E-07
		-4.484265E-08	-3.004133E-08	-1.456872E-09	1.241237E-07	-1.053528E-08	1.492275E-06

SUBCASE 3

SEG 2-R 1ST LOAD
FREQUENCY = 3.000000E 03

C O M P L E X D I S P L A C E M E N T V E C T O R (SOLUTION SET)
(REAL/IMAGINARY)

POINT ID.	TYPE	T1	T2	T3	R1	R2	R3
201	G	-2.581237E-08	-9.486000E-08	1.188447E-07			
		2.587822E-07	-2.615264E-07	2.240263E-07			
202	G	-5.213794E-07	3.773298E-07	-2.238652E-08	-7.642457E-07	-4.358827E-08	1.123723E-06
		-1.785412E-07	-2.132615E-07	9.582219E-09	3.334867E-06	3.797527E-08	-5.314445E-06
211	G	-1.169897E-07	1.488920E-09	-1.210830E-07			
		-1.264242E-07	-5.201442E-08	-3.811849E-09			
212	G	5.435890E-07	1.819144E-07	-7.257625E-08	9.901352E-07	6.031911E-09	-1.651763E-06
		-3.733148E-08	-5.276699E-08	2.903876E-09	4.565412E-07	-2.727322E-08	-7.447341E-07

FREQUENCY RESPONSE OF HEX, DIH METHOD, FREQ DEP MATL   NOVEMBER 24, 1973   NASTRAN 11/ 1/ 73   PAGE 8

SEG 2-L 1ST LOAD   SUBCASE 4
FREQUENCY = 0.0

C O M P L E X   D I S P L A C E M E N T   V E C T O R   (SOLUTION SET)
(REAL/IMAGINARY)

POINT ID.	TYPE	T1	T2	T3	R1	R2	R3
201	G	8.535977E-08	-1.229803E-07	-5.248346E-08			
		0.0	0.0	0.0			
202	G	-9.459573E-09	1.114570E-08	6.840043E-09	-2.378844E-07	-7.654324E-08	-7.932687E-07
		0.0	0.0	0.0	0.0	0.0	0.0
211	G	-4.289279E-26	-1.695735E-07	9.751034E-08			
		0.0	0.0	0.0			
212	G	2.922848E-08	-8.815515E-09	2.490244E-09	1.336151E-07	4.033000E-09	4.775684E-07
		0.0	0.0	0.0	0.0	0.0	0.0

SEG 2-L 1ST LOAD SUBCASE 4
FREQUENCY = 1.500000E 03

C O M P L E X D I S P L A C E M E N T V E C T O R (SOLUTION SET)
(REAL/IMAGINARY)

POINT ID.	TYPE	T1	T2	T3	R1	R2	R3
201	G	3.789983E-08	-2.299636E-08	-2.274037E-07			
		3.271853E-07	-2.819932E-07	-2.011236E-07			
202	G	1.271729E-07	1.250222E-08	7.949406E-09	-5.906917E-08	-1.684382E-08	-5.913636E-07
		-5.822007E-09	-6.119996E-08	-4.432582E-09	2.132242E-07	8.049898E-08	2.261926E-06
211	G	5.861663E-06	4.013276E-07	-5.935838E-07			
		2.232483E-07	-2.702721E-07	2.268589E-07			
212	G	-3.528950E-07	1.509575E-07	4.392131E-08	-1.181550E-07	-1.455113E-07	2.796953E-07
		-4.484271E-08	3.004137E-08	-1.456898E-09	-1.241038E-07	-1.053454E-08	-1.482275E-06

SEG 2-L 1ST LOAD SUBCASE 4
FREQUENCY = 3.000000E 03

C O M P L E X D I S P L A C E M E N T V E C T O R (SOLUTION SET)
(REAL/IMAGINARY)

POINT ID.	TYPE	T1	T2	T3	R1	R2	R3
201	G	-1.716487E-07	2.261784E-09	4.078472E-08			
		2.593518E-07	-2.658831E-07	1.842703E-07			
202	G	-2.659269E-07	-3.910579E-08	2.252346E-03	-1.432393E-07	3.744076E-08	2.877935E-07
		-2.565792E-27	-9.276209E-38	1.850856E-08	3.668431E-26	6.236957E-28	-5.779769E-06
211	G	-1.169103E-07	-1.488157E-09	-1.210837E-07			
		-1.364243E-27	5.201371E-08	-3.811675E-09			
212	G	5.435891E-27	-1.819145E-07	-7.257625E-08	-9.901341E-07	6.231912E-29	1.651783E-06
		-3.733147E-08	5.976781E-06	2.903875E-29	-4.565420E-07	-2.727322E-08	7.447345E-07

SEG 3-R 1ST LOAD SUBCASE 5
FREQUENCY = 0.0

C O M P L E X   D I S P L A C E M E N T   V E C T O R (SOLUTION SET)
(REAL/IMAGINARY)

POINT ID.	TYPE	T1	T2	T3	R1	R2	R3
201	G	-5.994031E-07	6.207279E-07	4.663484E-07			
		0.0	0.0	0.0			
202	G	-9.459573E-09	-1.114570E-08	8.640043E-09	2.378844E-07	-7.654324E-08	7.932657E-07
		0.0	0.0	0.0	0.0	0.0	0.0
211	G	-1.222418E-07	1.353236E-06	-7.723019E-07			
		0.0	0.0	0.0			
212	G	-9.236521E-07	5.129600E-07	1.132494E-07	-6.387539E-07	-5.130842E-07	-6.378262E-07
		0.0	0.0	0.0	0.0	0.0	0.0

SEG 3-R 1ST LOAD
FREQUENCY = 1.502000E 03

SUBCASE 5

C O M P L E X D I S P L A C E M E N T V E C T O R (SOLUTION SET)
(REAL/IMAGINARY)

POINT ID.	TYPE	T1	T2	T3	R1	R2	R3
201	G	1.936768E-06	-1.215941E-06	5.261499E-07			
		-5.639682E-07	1.020426E-06	5.633028E-07			
202	G	1.271729E-07	-1.250222E-08	7.949426E-09	5.906917E-08	-1.684322E-08	5.913636E-07
		-5.822007E-08	6.119996E-08	-4.432582E-09	-2.132242E-07	8.049898E-06	-2.261926E-06
211	G	3.912277E-07	-1.797137E-06	1.668128E-06			
		4.959829E-07	-1.097481E-06	2.561948E-06			
212	G	-8.218629E-07	4.435797E-07	1.076964E-07	-3.661028E-07	-3.756711E-07	-4.464459E-07
		1.627625E-06	-7.621552E-07	-1.814767E-07	7.210529E-07	7.507275E-07	1.554622E-06

SUBCASE 5

SEG 3-R 1ST LOAD
FREQUENCY = 3.000000E 03

C O M P L E X D I S P L A C E M E N T V E C T O R (SOLUTION SET)
(REAL/IMAGINARY)

POINT ID.	TYPE	T1	T2	T3	R1	R2	R3
201	G	-3.573146E-07	4.001224E-07	-1.945910E-07			
		-1.177377E-07	3.926451E-07	-1.644736E-08			
202	G	-2.659260E-07	3.910679E-08	2.252346E-08	1.432393E-07	3.744076E-08	-2.077935E-07
		-2.565792E-07	9.276209E-08	1.850896E-08	-3.668431E-06	6.236957E-08	5.779765E-06
211	G	3.336550E-07	-2.278435E-07	-4.782884E-08			
		-9.889186E-08	-7.520635E-09	-5.923675E-07			
212	G	4.377156E-07	3.193699E-08	-3.602465E-08	-1.188253E-06	-6.588547E-09	1.984081E-06
		1.408911E-06	-5.045156E-07	-1.641884E-07	2.935116E-06	-5.676421E-08	-4.417022E-06

SEG 3-L 1ST LOAD SUBCASE 6
FREQUENCY = 0.0

C O M P L E X D I S P L A C E M E N T V E C T O R (SOLUTION SET)
(REAL/IMAGINARY)

POINT ID.	TYPE	T1	T2	T3	R1	R2	R3
201	G	2.210065E-06	-5.415810E-07	5.283937E-07			
		0.0	0.0	0.0			
202	G	2.681715E-06	-3.479551E-07	2.891301E-08	5.173309E-07	1.877939E-06	7.447523E-07
		0.0	0.0	0.0	0.0	0.0	0.0
211	G	-1.222406E-07	-1.353236E-06	-7.723019E-07			
		0.0	0.0	0.0			
212	G	-9.236516E-07	-5.129600E-07	1.132497E-07	6.387538E-07	-5.130840E-07	6.376602E-07
		0.0	0.0	0.0	0.0	0.0	0.0

SEG 3-L 1ST LOAD SUBCASE 6
FREQUENCY = 1.500000E 03

C O M P L E X D I S P L A C E M E N T V E C T O R (SOLUTION SET)
(REAL/IMAGINARY)

POINT ID.	TYPE	T1	T2	T3	R1	R2	R3
201	G	-2.949034E-06	1.393903E-06	-2.635776E-06			
		-3.653979E-06	-8.101297E-07	-3.818032E-06			
202	G	1.985927E-06	-4.411733E-07	3.679962E-08	3.927107E-07	1.156405E-06	8.131495E-07
		-4.218735E-06	3.834245E-07	2.997073E-08	-4.810248E-07	-2.462622E-06	-1.932364E-06
211	G	3.912278E-07	1.797138E-06	1.668123E-06			
		4.959811E-07	1.097481E-06	2.561949E-06			
212	G	-8.218628E-07	-4.435798E-07	1.076964E-07	3.661228E-07	-3.756711E-07	4.464459E-07
		1.627625E-06	7.601552E-07	-1.814763E-07	-7.210508E-07	7.507272E-07	-1.594519E-06

SEG 3-L. 1ST LOAD
FREQUENCY = 3.000000E 03

SUBCASE 6

COMPLEX DISPLACEMENT VECTOR (SOLUTION SET)
(REAL/IMAGINARY)

POINT ID.	TYPE	T1	T2	T3	R1	R2	R3
201	G	-1.101827E-06	1.988752E-07	-3.909159E-07			
		3.013529E-07	-8.100879E-07	8.496764E-07			
202	G	-4.023520E-07	-1.144183E-07	2.606644E-08	-5.766494E-07	-5.601084E-08	7.642318E-07
		-2.853008E-06	1.734879E-07	1.622262E-07	-3.432925E-07	-8.514871E-08	5.140383E-07
211	G	3.336554E-07	2.278425E-07	-4.782020E-08			
		-9.889175E-08	7.501058E-09	-5.923677E-07			
212	G	4.377155E-07	-3.193697E-06	-3.682465E-08	1.188253E-06	-6.588554E-09	-1.984081E-06
		1.408911E-06	5.045156E-07	-1.641884E-07	-2.935115E-06	-5.676422E-08	4.417600E-06

FR.. .NCY ..SPON.. .F H.., DI. ..THOD, .REG ... MAT_ .CVE .. 2.. .973 ASTR.. .1/

SEG 1-R 2ND LOAD
FREQUENCY = 0.0

SUBCASE 7

C O M P L E X D I S P L A C E M E N T V E C T O R (SOLUTION SET)
(REAL/IMAGINARY)

POINT ID.	TYPE	T1	T2	T3	R1	R2	R3
201	G	1.208241E-04	1.193166E-05	3.797232E-05			
		0.0	0.0	0.0			
202	G	7.316174E-06	0.0	1.328916E-07	0.0	5.422378E-06	0.0
		0.0	0.0	0.0	0.0	0.0	0.0
211	G	7.096032E-05	-5.263384E-05	1.397822E-05			
		0.0	0.0	0.0			
212	G	3.226918E-06	-1.328864E-06	1.967578E-07	1.926530E-06	2.352332E-06	2.433972E-06
		0.0	0.0	0.0	0.0	0.0	0.0

SUBCASE 7

SEG 1-R 2ND LOAD
FREQUENCY = 1.500000E 03

C O M P L E X   D I S P L A C E M E N T   V E C T O R   (SOLUTION SET)
(REAL/IMAGINARY)

POINT ID.	TYPE	T1	T2	T3	R1	R2	R3
201	G	-8.442375E-07	7.826269E-06	-4.291878E-05			
		-9.083167E-05	-2.328522E-05	-4.421569E-05			
202	G	3.744367E-06	0.0	2.615618E-07	0.0	2.538532E-06	0.0
		-9.914249E-06	0.0	-1.832492E-07	0.0	-6.298958E-06	0.0
211	G	1.140870E-05	1.932581E-05	-2.276738E-05			
		-6.595108E-05	2.498452E-05	1.969858E-06			
212	G	4.114514E-06	-5.241178E-07	1.543532E-07	4.429294E-07	2.587944E-06	-1.428375E-07
		-4.972683E-06	2.273928E-06	-2.230659E-07	-2.021412E-06	-3.169968E-06	-4.636677E-06

SEG 1-R 2ND LOAD   SUBCASE 7
FREQUENCY = 3.000000E 03

C O M P L E X   D I S P L A C E M E N T   V E C T O R   (SOLUTION SET)
(REAL/IMAGINARY)

POINT ID.	TYPE	T1	T2	T3	R1	R2	R3
201	G	-1.372295E-05	1.195282E-06	-6.786059E-06			
		-1.178610E-05	-7.465294E-06	3.460747E-06			
202	G	-7.881232E-08	0.0	-2.099861E-07	0.0	-4.346513E-07	0.0
		-5.290113E-06	0.0	2.355771E-07	0.0	-4.421861E-07	0.0
211	G	-1.789123E-05	5.714282E-06	2.658349E-06			
		-2.907349E-06	-1.552738E-07	9.065695E-08			
212	G	-3.944742E-06	4.723942E-07	1.647049E-07	5.092576E-06	-2.919037E-07	-8.366974E-06
		-3.867150E-07	1.007895E-06	-1.357134E-07	-4.623113E-06	-2.627809E-07	6.665230E-06

SEG 1-L 2ND LOAD SUBCASE 8
FREQUENCY = 0.0

C O M P L E X D I S P L A C E M E N T V E C T O R (SOLUTION SET)
(REAL/IMAGINARY)

POINT ID.	TYPE	T1	T2	T3	R1	R2	R3
201	G	-1.854329E-05	6.787239E-05	2.350366E-05			
		0.0	0.0	0.0			
202	G	-1.612116E-06	6.861513E-07	2.381776E-07	-5.236377E-07	-9.916066E-07	4.468542E-07
		0.0	0.0	0.0	0.0	0.0	0.0
211	G	7.096030E-05	5.263384E-05	1.397592E-05			
		0.0	0.0	0.0			
212	G	3.026916E-06	1.[illegible]28864E-06	1.967569E-07	-1.926538E-06	2.352332E-06	-2.433969E-06
		0.0	0.0	0.0	0.0	0.0	0.0

SUBCASE 8

SEG 1-L 2ND LOAD
FREQUENCY = 1,500000E 03

C P L E X D I S P L A C E M E N T V E C T O R (SOLUTION SET)
(REAL/IMAGINARY)

POINT200.	TYBE	3,672228E-05 -1,141553E-05	-3,337326E-05 -1,969757E-05	-2,847484E-05 4,168264E-05	R1	R2	R3
202	G	1,124622E-06 2,375707E-06	6,587708E-07 -1,201045E-06	1,318126E-07 -3,434596E-07	-7,521735E-07 9,211873E-07	7,533158E-07 1,186462E-06	-2,059744E-06 -8,322396E-07
211	G	1,140678E-05 -6,595127E-05	-1,930681E-05 -2,498452E-05	-2,276788E-05 1,969867E-06			
212	G	4,114514E-06 -4,972683E-06	5,241178E-07 -2,073927E-06	1,543532E-07 -2,232659E-07	-4,429294E-07 2,021411E-06	2,587943E-06 -3,169967E-06	1,428375E-07 4,636677E-06

SEG 1-L 2ND LOAD SUBCASE 8
FREQUENCY = 3,000000E 03

COMPLEX DISPLACEMENT VECTOR (SOLUTION SET)
(REAL/IMAGINARY)

POINT ID.	TYPE	T1	T2	T3	R1	R2	R3
201	G	-7.425913E-06	-1.122834E-05	7.322799E-06			
		6.733992E-08	5.297616E-06	-9.533692E-07			
202	G	6.692784E-08	-1.080127E-06	-1.367115E-07	3.681875E-06	-1.063426E-07	-5.234848E-06
		7.462199E-07	-1.780117E-07	-1.358115E-07	-6.171569E-06	2.512069E-08	1.006372E-05
211	G	-1.789123E-05	-5.714282E-06	2.658359E-06			
		-2.987348E-06	1.552738E-07	9.065696E-08			
212	G	-3.944742E-06	-4.723942E-07	1.647069E-07	-5.092576E-06	-2.919037E-07	8.366974E-06
		-3.867158E-07	-1.007895E-06	-1.357133E-07	4.623113E-06	-2.627809E-07	-6.665229E-06

SEG 2-R 2ND LOAD
FREQUENCY = 0.0
SUBCASE 9

C O M P L E X   D I S P L A C E M E N T   V E C T O R (SOLUTION SET)
(REAL/IMAGINARY)

POINT ID.	TYPE	T1	T2	T3	R1	R2	R3
201	G	-8.592747E-07	-5.437289E-07	-4.418572E-07			
		0.0	0.0	0.0			
202	G	-1.612116E-26	-6.86[illegible]13E-07	2.381776E-07	5.236377E-07	-9.916866E-07	-4.468548E-07
		0.0	0.0	0.0	0.0	0.0	0.0
211	G	-3.002580E-07	-5.001223E-12	6.971167E-07			
		0.0	0.0	0.0			
212	G	2.249679E-07	-2.991513E-13	7.309286E-09	3.237942E-13	-5.501058E-08	-6.986362E-14
		0.0	0.0	0.0	0.0	0.0	0.0

SEG 2-R 2ND LOAD
FREQUENCY = 1,500000E 03

SUBCASE 9

C O M P L E X D I S P L A C E M E N T V E C T O R (SOLUTION SET)
(REAL/IMAGINARY)

POINT ID.	TYPE	T1	T2	T3	R1	R2	R3
201	G	2,352991E-06	2,662064E-07	2,177928E-06			
		1,167762E-06	9,189588E-07	-1,216820E-06			
202	G	1,124622E-06	-6,587728E-07	1,318105E-07	7,521735E-07	7,533158E-07	2,059744E-06
		2,375707E-06	1,221045E-06	-3,434595E-07	-9,211073E-07	1,186462E-06	8,322396E-07
211	G	4,030621E-07	3,572152E-12	-2,163363E-06			
		1,621155E-06	2,314269E-12	-7,255712E-08			
212	G	-1,400434E-06	-1,376754E-14	1,861952E-07	1,362866E-14	-7,639659E-07	-2,246736E-14
		5,489267E-08	-3,447014E-13	-3,677287E-08	6,174483E-14	3,373251E-07	-1,059945E-13

SUBCASE 9

SEG 2-R 2ND LOAD
FREQUENCY = 3.000000E 03

C O M P L E X   D I S P L A C E M E N T   V E C T O R (SOLUTION SET)
(REAL/IMAGINARY)

POINT ID.	TYPE	T1	T2	T3	R1	R2	R3
201	G	-6.231312E-08	2.788575E-07	3.592698E-08			
		3.817549E-07	-6.912587E-07	2.206915E-07			
202	G	6.692784E-08	1.060127E-06	-1.367115E-07	-3.681875E-06	-1.063426E-07	5.234848E-06
		7.462199E-07	1.782117E-07	-1.358115E-07	6.171569E-06	2.512069E-08	-1.026372E-05
211	G	-6.464557E-07	3.518437E-13	-4.053846E-07			
		-8.060090E-07	-5.825452E-15	6.767235E-07			
212	G	1.359856E-06	9.228441E-15	-2.244376E-07	3.956259E-13	1.539383E-07	-8.651695E-13
		-6.181206E-07	4.928158E-13	2.582771E-08	-1.293426E-13	5.415190E-08	-2.308239E-13

SEG 2-L ..2ND LOAD SUBCASE 10
FREQUENCY = 0.0

COMPLEX DISPLACEMENT VECTOR (SOLUTION SET)
(REAL/IMAGINARY)

POINT ID.	TYPE	T1	T2	T3	R1	R2	R3
201	G	-8.592747E-07	-5.437289E-07	-4.418572E-07			
		0.0	0.0	0.0			
202	G	-1.612116E-06	-6.861513E-07	2.381776E-07	5.236377E-07	-9.916066E-07	-4.468540E-07
		0.0	0.0	0.0	0.0	0.0	0.0
211	G	-3.002580E-07	-5.001223E-12	6.971167E-07			
		0.0	0.0	0.0			
212	G	2.249679E-07	-2.991513E-13	7.309286E-09	3.237942E-13	-5.501058E-08	-6.986362E-14
		0.0	0.0	0.0	0.0	0.0	0.0

SEG 2-L 2ND LOAD SUBCASE 10
FREQUENCY = 1.600000E 03

C O M P L E X D I S P L A C E M E N T V E C T O R (SOLUTION SET)
(REAL/IMAGINARY)

POINT ID.	TYPE	T1	T2	T3	R1	R2	R3
201	G	2.352991E-06	2.862064E-07	2.177923E-06			
		1.167780E-06	9.189588E-07	-1.216820E-06			
202	G	1.124622E-06	-6.587728E-07	1.318126E-07	7.521735E-07	7.533158E-07	2.059744E-06
		2.375727E-06	1.201045E-06	-3.434596E-07	-9.211273E-07	1.186462E-06	8.322396E-07
211	G	4.080621E-07	3.572150E-12	-2.163363E-06			
		1.601155E-06	2.314069E-12	-7.255710E-08			
212	G	-1.420434E-06	-1.376754E-14	1.861992E-07	1.362666E-14	-7.639659E-07	-2.246736E-14
		5.489267E-08	-3.447214E-13	-3.677287E-08	6.174483E-14	3.373281E-07	-1.299945E-13

SEG 2-L 2ND LOAD
FREQUENCY = 3.000000E 03

SUBCASE 10

C O M P L E X   D I S P L A C E M E N T   V E C T O R   (SOLUTION SET)
(REAL/IMAGINARY)

POINT ID.	TYPE	T1	T2	T3	R1	R2	R3
201	G	-6.231312E-08	2.786675E-07	3.592698E-08			
		3.817549E-07	-6.912887E-07	2.205916E-07			
202	G	6.692784E-08	1.080127E-06	-1.367115E-07	-3.681875E-06	-1.063426E-07	5.234846E-06
		7.462199E-07	1.780117E-07	-1.358115E-07	6.171569E-06	2.612069E-08	-1.026372E-05
211	G	-6.464557E-07	3.518437E-13	-4.253246E-07			
		-8.060298E-07	-5.825452E-15	6.767265E-07			
212	G	1.359856E-06	9.228441E-15	-2.044376E-07	3.956059E-13	1.539383E-07	-8.851695E-13
		-6.181206E-07	4.828158E-13	2.582771E-08	-1.293426E-13	5.416192E-08	-2.328239E-13

SUBCASE 11

SEG. 3-R 2ND LOAD
FREQUENCY = 0.0

C O M P L E X D I S P L A C E M E N T V E C T O R (SOLUTION SET)
(REAL/IMAGINARY)

POINT ID.	TYPE	T1	T2	T3	R1	R2	R3
201	G	-1.854329E-05	6.787239E-05	2.350356E-05			
		0.0	0.0	0.0			
202	G	-1.612116E-06	6.861513E-07	2.381776E-07	-5.236377E-07	-9.916066E-07	4.466540E-07
		0.0	0.0	0.0	0.0	0.0	0.0
211	G	7.095030E-05	5.263384E-05	1.397520E-05			
		0.0	0.0	0.0			
212	G	3.026918E-06	1.320864E-06	1.967535E-07	-1.926530E-06	2.352332E-06	-2.433969E-06
		0.0	0.0	0.0	0.0	0.0	0.0

SEG 3-R 2ND LOAD SUBCASE 11
FREQUENCY = 1,500000E 03

C O M P L E X D I S P L A C E M E N T V E C T O R (SOLUTION SET)
(REAL/IMAGINARY)

POINT ID.	TYPE	T1	T2	T3	R1	R2	R3
201	G	3,672228E-05	-3,337556E-05	-2,847494E-05			
		-1,141553E-05	-1,969757E-05	4,168264E-05			
202	G	1,124622E-06	6,587708E-07	1,318126E-07	-7,521735E-07	7,533158E-07	-2,059744E-06
		2,375707E-06	-1,201045E-06	-3,434596E-07	9,211073E-07	1,186462E-06	-8,322396E-07
211	G	1,140878E-05	-1,932681E-05	-2,076760E-05			
		-6,595107E-05	-2,498452E-05	1,969867E-06			
212	G	-4,114514E-06	6,241178E-07	1,543532E-07	-4,429294E-07	2,587943E-06	1,428375E-07
		-4,972683E-06	-2,073927E-06	-2,230659E-07	2,021411E-06	-3,169967E-06	4,636077E-06

SEG 3-R 2ND LOAD SUBCASE 11
FREQUENCY = 3.000000E 03

COMPLEX DISPLACEMENT VECTOR (SOLUTION SET)
(REAL/IMAGINARY)

POINT ID.	TYPE	T1	T2	T3	R1	R2	R3
201	G	-7.405913E-06	-1.122834E-05	7.322799E-06			
		6.733990E-08	5.297616E-06	-9.533692E-07			
202	G	6.692784E-08	-1.980127E-06	-1.367115E-07	3.681875E-06	-1.063426E-07	-5.234848E-06
		7.462199E-07	-1.760117E-07	-1.358115E-07	-8.171569E-06	2.512069E-08	1.006372E-05
211	G	-1.789123E-05	-5.714282E-05	2.658359E-06			
		-2.997348E-06	1.552738E-07	9.065695E-08			
212	G	-3.944742E-06	-4.723942E-07	1.647069E-07	-5.092576E-06	-2.919037E-07	8.366974E-06
		-3.867158E-07	-1.027895E-06	-1.357133E-07	4.623113E-06	-2.627809E-07	-6.668229E-06

SEG 3-L 2ND LOAD
FREQUENCY = 0.0

SUBCASE 12

C O M P L E X   D I S P L A C E M E N T   V E C T O R   (SOLUTION SET)
(REAL/IMAGINARY)

POINT ID.	TYPE	T1	T2	T3	R1	R2	R3
201	G	1.208241E-04	1.193166E-05	3.797282E-05			
		0.0	0.0	0.0			
202	G	7.318174E-06	0.0	1.328916E-07	0.0	5.420308E-06	0.0
		0.0	0.0	0.0	0.0	0.0	0.0
211	G	7.096032E-05	-5.263384E-05	1.397520E-05			
		0.0	0.0	0.0			
212	G	3.026918E-06	-1.320864E-06	1.967570E-07	1.926532E-06	2.352332E-06	2.433972E-06
		0.0	0.0	0.0	0.0	0.0	0.0

SUBCASE 12

SEG 3-L 2ND LOAD
FREQUENCY = 1.500000E 03

C O M P L E X   D I S P L A C E M E N T   V E C T O R   (SOLUTION SET)
(REAL/IMAGINARY)

POINT ID.	TYPE	T1	T2	T3	R1	R2	R3
201	G	-8.412375E-07	7.826269E-06	-4.091878E-05			
		-9.033167E-05	-2.328528E-05	-4.421559E-05			
202	G	3.744367E-06	0.0	2.615618E-27	0.0	2.538532E-06	0.0
		-9.914249E-06	0.0	-1.832492E-27	0.0	-6.258958E-06	0.0
211	G	1.140878E-05	1.932681E-05	-2.276768E-05			
		-6.595109E-05	2.498450E-05	1.969868E-06			
212	G	4.114514E-06	-5.241178E-07	1.543532E-07	4.429294E-07	2.587944E-06	-1.428375E-07
		-4.972663E-06	2.073928E-06	-2.232659E-07	-2.021412E-06	-3.169966E-06	-4.636677E-06

SEG 3-L 2ND LOAD
FREQUENCY = 3.000000E 03

SUBCASE 12

C O M P L E X   D I S P L A C E M E N T   V E C T O R   (SOLUTION SET)
(REAL/IMAGINARY)

POINT ID.	TYPE	T1	T2	T3	R1	R2	R3
201	G	-1.820295E-05	1.195282E-06	-8.786059E-06			
		-1.170610E-05	-7.465294E-06	3.460747E-06			
202	G	-7.881232E-08	0.0	-2.099861E-07	0.0	-4.346513E-07	0.0
		-5.290113E-06	0.0	2.355771E-07	0.0	-4.421861E-07	0.0
211	G	-1.789123E-05	5.714282E-06	2.658359E-06			
		-2.987349E-06	-1.552738E-07	9.865695E-08			
212	G	-3.944742E-06	4.723942E-07	1.647069E-07	5.092576E-06	-2.919037E-07	-8.366974E-06
		-3.867158E-07	1.007695E-06	-1.357134E-07	-4.623113E-06	-2.527809E-07	6.665230E-06

APPENDIX D

TASK 4 FINAL REPORT
VIBRATION TESTING OF THE BASELINE MOTOR
RPL COMPONENT VIBRATION PROGRAM

Because a large volume of data was produced during the test program, this report has been abridged by removing all but the most important data. The omitted data were in the original Task 4 final report which is on file at the AFRPL, Edwards, Ca.

TASK 4 FINAL REPORT

VIBRATION TESTING OF THE BASELINE MOTOR

RPL COMPONENT VIBRATION PROGRAM

CONTRACT NO. F04611-73-C-0025

15 August 1973

Prepared for

AIR FORCE ROCKET PROPULSION LABORATORY
Edwards Air Force Base, California

Prepared by

HERCULES INCORPORATED
Bacchus Works
Magna, Utah

FOREWORD

This report was written under Task 4 of Air Force Contract No. F04611-73-C-0025. Results of acoustic vibration testing on an inert Poseidon C3 S/S motor are reported herein. This report is not a required contract data item. This work was performed by Hercules Incorporated, Systems Group, at the Bacchus Works, Magna, Utah. The cognizant project engineer is Dr. D. George, AFRPL, Edwards AFB, California.

ABSTRACT

The purpose of Task 4 of Contract No. F04611-73-C-0025 was to obtain the vibration response characteristics of an inert Poseidon C3 S/S motor. A testing program was conducted on an inert motor using a loudspeaker mounted in the combustion cavity as a source of excitation. Results from this testing program will be used in Task 5 for comparison with results obtained from finite-element models.

Mode shapes of the motor structure, oscillating in response to the stimulus of the loudspeaker, were obtained by using a movable accelerometer. By using double-backed adhesive tape to mount the accelerometer, it was possible to quickly move the accelerometer from one location to another on the motor structure, recording the acceleration response magnitude and phase at each location. The mapping was carried out at several selected frequencies.

In addition to the mode shape mapping, frequency response plots were obtained at selected locations on the structure by recording the accelerometer output as a function of loudspeaker (input) frequency on an x-y recorder. The loudspeaker input frequency was swept from 50 Hz to 1000 Hz as the accelerometer output was plotted.

This report describes the test procedures and presents the testing results. All* applicable raw data are included for reference and some [illegible] mode shapes are plotted to illustrate the use of the data. No attempt i made to further interpret, evaluate, or analyze the data. The data will be studied in Task 5.

*See note on page D-1.

TABLE OF CONTENTS

LIST OF FIGURES

LIST OF FIGURES (CONT)

LIST OF FIGURES (CONT)

SECTION I

INTRODUCTION AND SUMMARY

A. INTRODUCTION

The purpose of this report is to describe the testing and document the detailed results for the acoustic vibration experiments carried out under Task 4 of AFRPL Contract No. F04611-73-C-0025. This report is not a required contract data item.

The objective of the testing program was to characterize the vibration response of the S/S Poseidon C3 motor in such a way that results could be used for verification of finite-element models that are being developed under Task 3. The testing plan contained in the appendix of the approved program plan[1] provides a general description of the testing program that has been conducted. However, details of the testing program actually conducted vary considerably from those given in the published testing plan. The actual testing program evolved through a series of check-out and evaluation tests. After preliminary tests had been conducted, an approach was formulated and an informal preliminary test report was issued. Significant details of the new approach were discussed with the project engineer at RPL, Dr. D. George, and concurrence was obtained on the general approach.

The tests were conducted on Poseidon S/S inert motor number STV-4D. The motor was obtained from the Lockheed Missiles and Space Company, Sunnyvale, California, on a six-month loan. Hardware from a Hercules lobby display motor were installed on the inert motor and the dummy training nozzle was replaced with a production full-scale nozzle furnished by the Hercules Poseidon program office. The motor, complete with hardware, was placed in Building 33 at Hercules Plant 81 where the testing was conducted.

In the following sections of this report, the test set-up is described and the test procedure is given. Then results of the testing program are presented and discussed. The final section contains the conclusions reached as a result of the testing program.

B. SUMMARY

A loudspeaker was placed in the combustion cavity to provide a source of acoustic excitation. A variable frequency oscillator was used to alter the excitation frequency. Structural response levels were recorded using a movable accelerometer. Acoustic sound pressure levels were recorded using a microphone on a probe in the combustion cavity. The motor was pressurized to 50 psi for all tests to provide separation between the chamber insulator

---

1 Program Plan for Analytical Prediction of Motor Component Vibrations Driven by Acoustic Combustion Instability, 8 January 1973, for AFFTC, Edwards AFB, California, by Hercules Incorporated, Bacchus Works, Magna, Utah

and grain shrinkage flaps in the domes. Tests on the forward dome were performed with the motor in the horizontal position. Tests on the aft dome were completed with the motor in a vertical attitude, nozzle-up.

Two different kinds of data were gathered during the testing: (1) mode shape mappings at a constant frequency, and (2) frequency sweeps with the accelerometer placed at selected locations. The mode shape mappings resulted in data that can be used to plot the mode shapes of the structure responding to an input at a particular frequency. The frequency sweep data provided the means for resonant frequency assessments.

SECTION II

TEST SET-UP DESCRIPTION

Full-scale, inert Poseidon second stage motor STV-4D was used as a test vehicle for this program. The following major hardware were on the motor:

(1) Nozzle assembly

(2) Flight control electronics package

(3) Hydraulic power unit (HPU)

(4) Inert gas generator

(5) Pitch and yaw actuators

(6) Thrust termination (TT) ports

Two separate series of tests were performed: (1) forward dome testing with the motor in the horizontal position resting on a standard handling dolly, and (2) aft dome testing with the motor in the vertical position, nozzle up. In the vertical position, the motor was supported by a special stand that was borrowed from the manufacturing department. An aluminum handling fixture (ring around aft skirt attachment area, see Figure 1) was supported and held up away from the aft skirt by a special supporting structure. Since the handling fixture was held away from the motor, it was possible for the test conductors to stand on the fixture during testing to access the aft dome accelerometer locations. The sketches shown in Figure 1 illustrate the two test configurations. The aft dome testing was performed with the motor in the vertical position because preliminary check-out tests indicated that the cantilevered nozzle in the horizontal position has a strong effect on the symmetry of some of the basic dome modes[1]. The forward dome testing was carried out before the motor was rotated to the vertical position because the forward dome is difficult to access when the motor is in the vertical position.

A block diagram showing the instrumentation used to record pressure and acceleration response is shown in Figure 2. Using the set-up shown, the frequency of a particular resonance can be determined accurately with a frequency meter. A phase meter is used to measure phase between the reference accelerometer output and the movable accelerometer output (or the microphone output). A digital voltmeter is used to measure movable accelerometer output at a particular frequency. For frequency sweeps, the movable accelerometer output was plotted as a function of frequency by an x-y plotter.

An eight-inch cone type loudspeaker was placed in the slotted region of the combustion cavity to provide the source of acoustic excitation. A special nozzle closure for containing the 50 psi chamber pressure was designed,

---

[1] Preliminary Testing Report, Acoustic Testing, Task 4, "Analytical Prediction of Motor Component Vibration Driven by Acoustic Combustion Instability" Program, Contract F04611-73-C-0025, AFRPL, by Hercules Incorporated, Magna, Utah, 12 April 1973.

constructed, and installed in the test chamber. Nitrogen gas was used to pressurize the chamber to 50 psi. An existing pressure tap in the forward closure was used to supply nitrogen to the chamber from a commercial nitrogen bottle. The pressure gage and regulator supplied with the nitrogen bottle were used to control the motor chamber pressure. Figure 3 is a sketch of the general motor testing set-up. Figures 4 and 5 are photographs showing the actual test instrumentation used and the vertical motor configuration.

SECTION III

TEST PROCEDURE

Two basic test procedures are described here, one procedure for frequency response testing and one procedure for mode shape mapping. The frequency response testing was performed first so that results could be used as a guide in choosing frequencies for mode shape mapping.

The frequency response testing was performed for a limited number of points selected on the domes and on the components. The movable accelerometer was mounted at a selected location using double-backed adhesive tape.* The power amplifier supplying the speaker was adjusted for an eight-volt output. The audio oscillator dials were then slowly turned to sweep the frequency from 50 Hz to 1000 Hz while the accelerometer output was plotted as a function of frequency on the x-y recorder. The resulting plot of acceleration amplitude versus frequency was examined to determine apparent resonant frequencies. Peaks may occur in the plot either due to acoustic cavity resonance or due to structural resonance. Significant resonance frequencies of both types were selected for mode shape mapping.

To map a mode shape, the audio oscillator was set to the selected frequency and the power amplifier output (speaker input) was adjusted to eight volts. Generally, the audio oscillator was fine-tuned to maximize the accelerometer signal from a selected location by observing the response on the oscilloscope as the oscillator frequency control was adjusted. The reference accelerometer was installed at a specified location. The movable accelerometer was moved from location to location until each point in the area being mapped was covered. For each point at which the movable accelerometer was located, the accelerometer output was read on the digital voltmeter and recorded on a data sheet. The phase angle between the response from the reference accelerometer and the response from the movable accelerometer was noted on the phase meter and recorded on the data sheet. Thus, results from a mode shape mapping were obtained in the form of a table giving acceleration amplitude and phase at a set of mapping points. Double-backed adhesive tape was used at each mapping location to allow easy and quick installation and removal of the movable accelerometer.

The accelerometer mapping locations for the forward dome are shown in Figure 6. Since there are many locations and the numbering system can be confusing, the order in which the dome layout is numbered is indicated in Figure 7. For example, the numbering system starts with 93 at the 0^{o} point on the adapter, and positions located radially outward are numbered in sequence through 108. This is indicated in Figure 7 by the " 1 " line. The numbering sequence is continued at line 2 in Figure 7, etc.

---

*Double-backed adhesive tape was shown to provide a satisfactory accelerometer mounting system, as reported in the preliminary testing report.

The accelerometer mapping locations for the aft dome structure are given in Figure 8 and the numbering sequence is shown in Figure 9. Accelerometer locations for the components are shown in Figure 10 and those for the nozzle in Figure 11. Photographs showing more precisely the locations of the accelerometers on the aft dome are given in Figures 12 through 16. It was not possible to install accelerometers at each numbered location due to interference with existing equipment. The data given in Section IV indicate which locations were used. The manufactured nozzle closure is shown in Figure 17.

Frequency response testing and acoustic mode mapping were carried out for the combustion cavity by using the microphone in place of the movable accelerometer in the procedures described above. The microphone location used in conjunction with the forward dome testing is shown in Figure 3. Frequency response data were obtained for the microphone location of Figure 3. For the aft dome testing, the microphone was mounted on a probe so that acoustic modes could be mapped in the cylinderical section between the speaker and the nozzle closure. Mapping locations for the cavity are defined in Figure 18.

SECTION IV

RESULTS

A. FORWARD DOME FREQUENCY RESPONSE TESTING

Frequency response data were obtained for different points on the forward dome. A separate graph was obtained from the x-y plotter for each point showing acceleration response as a function of frequency. One graph is given in Figure 19. The frequency response graphs are included in this report as they were received from the x-y plotter. A frequency scale and notations have been added to each graph, but no tracing or other redrawing has been done.

The notations on each graph indicate the day (date), time of day, and location of the accelerometer for each test. The vertical line near the 0 frequency mark is a calibration line showing unit acceleration response amplitude so that amplitudes on different graphs can be compared. For those graphs that have no calibration line, the line on a preceeding graph applies; the calibration line was only plotted when the gain settings were changed. For some selected peaks on the graphs, the frequency at which the peak occurred, as read on the frequency meter, has been written near the peak. In addition, the phase angle read on the phase meter is denoted after the peak frequency for some of the data. During this testing the reference accelerometer was located as position number 93; position numbers given correspond with Figure 6.

B. FORWARD DOME MODE SHAPE MAPPING

By reviewing the frequency response data, six significant frequencies were selected for detailed mode shape mapping of the forward dome. The forward dome was mapped in detail at frequencies of 100, 155, 192, 262, 320, and 367 Hz. The response was recorded at each of the points defined in Figure 6 for each of the above six frequencies. A limited mapping, usually consisting of making measurements along only one radial line, was additionally conducted at frequencies of 34, 386, 460, 517, 590, 620, 675, and 805 Hz.

The mapping data are obtained in a tabular form giving measured amplitude and phase at each mapping point. All "raw" data obtained during the forward dome mapping tests are provided in Appendix A of the original Task 4 final report.

To illustrate the use of the acquired data, consider the following example of steady state response for a system with two degrees of freedom:

At point one the amplitude, $y_1(t)$, may be expressed as a function of time as:

$$y_1(t) = Y_1 \sin (\omega t + \phi_1)$$

At point two the amplitude would then be,

$$y_2(t) = Y_2 \text{ Sin } (\omega t + \phi_2)$$

The terms ϕ_1 and ϕ_2 are the phase angles measured relative to some arbitrary reference, and Y_1 and Y_2 are the corresponding maximum (single amplitude) response amplitudes at points one and two. During the mapping process, maximum amplitudes Y_i and phase angles ϕ_i are obtained. To study the mode shape of the response oscillations, it is usual to maximize a particular response of interest; i.e., it is common to choose a time, t_o, such that $y_i(t) = Y_i$ for an i of interest. Thus a time, t_o, such that $\omega t_o + \phi_1 = 90^o$, would maximize $y_1(t)$ and the mode shape at t_o would be:

$$\begin{Bmatrix} y_1(t_o) \\ y_2(t_o) \end{Bmatrix} = \begin{Bmatrix} Y_1 \\ Y_2 \text{ Sin } (-\phi_1 + \phi_2) \end{Bmatrix}.$$

Some of the data given in Appendix A* have been reduced and the amplitudes, $y_i(t_o)$, are given on the data sheets in the column titled "amplitude". The reduced data have been plotted to show mode shapes for oscillations at 100, 155, 192, 262, and 367 Hz. Some mode shape plots are given in Figure 20 through 24.

C. ACOUSTIC CAVITY FREQUENCY RESPONSE TESTING

Frequency response plots were obtained for microphone locations 1, 8, and 15 (refer to Figure 18). The plots are presented in Figures 25, 26, and 27.

D. ACOUSTIC CAVITY MODE SHAPE MAPPING

Acoustic pressure mode shapes were recorded for the combustion cavity at frequencies of 57, 158, 192, 265, 315, and 364 Hz. Mapping locations are shown in Figure 18. The raw data are given in Appendix B for 2 frequencies. The acoustic mode shape for 364 Hz has been plotted and is shown in Figure 28.

E. MOTOR AFT-END FREQUENCY RESPONSE TESTING

Frequency response data was obtained for 15 different points on the aft end of the motor. The graphs are given in Figures 29 through 41. The location numbers given on the graphs correspond with Figures 8, 10 and 11.

F. MOTOR AFT-END MODE SHAPE MAPPING

The motor aft end was mapped in detail at frequencies of 56, 262, and 363 Hz. For the detailed mappings, data were obtained at the locations defined in Figures 8 through 11. In addition, a partial mapping was carried out on the components at several other frequencies. The Flight Electronics unit was mapped at frequencies of 104, 134, 269, 367, 409, and 685 Hz. The

*Refer to the original Task 4 final report.

HPU and Gas Generator units were mapped at frequencies of 70, 89, and 150 Hz. Some typical data obtained from these tests is given in Appendix C.

An effort was made to assure that one or two of the fundamental cantilever modes for the components would be mapped. To determine the fundamental cantilever mode of the Flight Electronics unit, an accelerometer was placed on the unit at location 585. The Flight Electronics unit was then "thumped" with the heel of a hand and the decaying response from the accelerometer was observed on an oscilloscope. An effort was then made to estimate the frequency of the decaying oscillations. Using this approach, the fundamental cantilever mode of the Flight Electronics unit was estimated to be approximately 100 Hz. To excite this mode with the speaker-driver, the response from two accelerometers, one mounted at 583 and one at 585, was viewed on a dual-beam scope while the oscillator was tuned near 100 Hz. The response ratio (585/583) peaked out at 104 Hz. Thus, it was determined that the fundamental cantilever mode for the Flight Electronics unit occurs at 104 Hz.

A similar twang or thumping test was conducted on the coupled HPU and Gas Generator assembly. For this assembly, the fundamental cantilever mode apparently occurs at 89 Hz. This mode is likely to be more complex than simple beam cantilever motion, however, due to the more complicated geometry.

G. EFFECT OF HELIUM VERSUS NITROGEN ON FREQUENCY RESPONSE RESULTS

The frequency response plots presented up to this point exhibit "peaks" at various particular frequencies. The peaks occur at resonant frequencies for the total system. It seems likely that some of the peaks occur mainly because of structural resonance while others are probably due mostly to acoustic cavity resonance. In order to identify structural resonant frequencies, a gas different from nitrogen, a helium and nitrogen mixture, was used to pressurize the chamber. The different gas has a different speed of sound than nitrogen, which results in a different frequency of oscillation for a given acoustic mode.

At the beginning of this testing, the goal was to obtain two sets of frequency response data for a selected group of accelerometer locations, with the only differences in the data being the gas used to pressurize the chamber. With this goal in mind, frequency response plots were obtained for 10 different points while nitrogen gas was used to pressurize the chamber. The data for point 93 are presented in Figure 42. During this testing, various testing system failures were experienced. The digital frequency counter was repaired, an accelerometer cable was replaced, and the speaker/driver was replaced.

In order to cancel out effects of changes in the testing system, the tests using nitrogen were repeated at three locations: 304, 585, and 594. Results from these tests are given in Figures 43, 44, and 45.

Directly following completion of the above test, where three frequency response plots were obtained using nitrogen, a gas mixture was created and three corresponding frequency response plots were obtained for comparison. The gas mixture was obtained by bleeding of the nitrogen gas until a chamber pressure of 25 psi was measured. The chamber was then repressurized to 50 psi using helium gas. The frequency response plots obtained using the nitrogen/helium mixture are shown in Figures 46, 47, and 48.

A final series of frequency response tests were run by using only helium gas to pressurize the motor to 50 psi. Data from the helium tests is presented in Figures 49 through 53.

SECTION V

CONCLUSIONS

The purpose of this report was to describe the test procedure and present the results for the acoustic vibration testing of inert motor STV-4D as required in Task 4. The tests were conducted to provide data for comparison with finite element results to verify the adequacy of the finite element models. No effort has been made to analyze or interpret the testing results obtained. The Task 4 testing appears to have been successful in providing various sets of data that can be used for verifying finite element models. However, a better judgement of the quality of the data can only be made after the data are studied in more detail and used in comparisons in the work of Task 5.

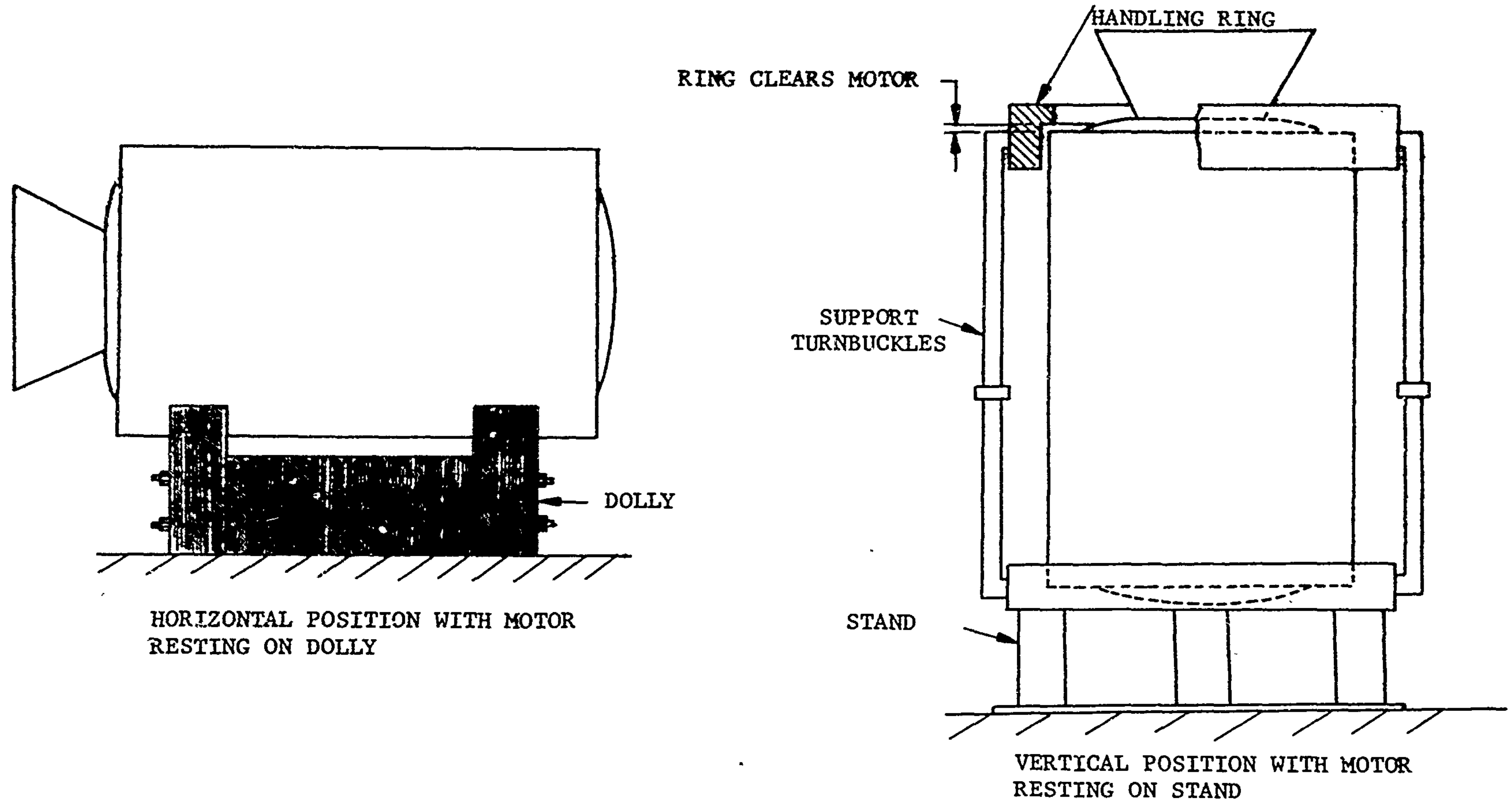

Figure 1. Motor Testing Attitudes

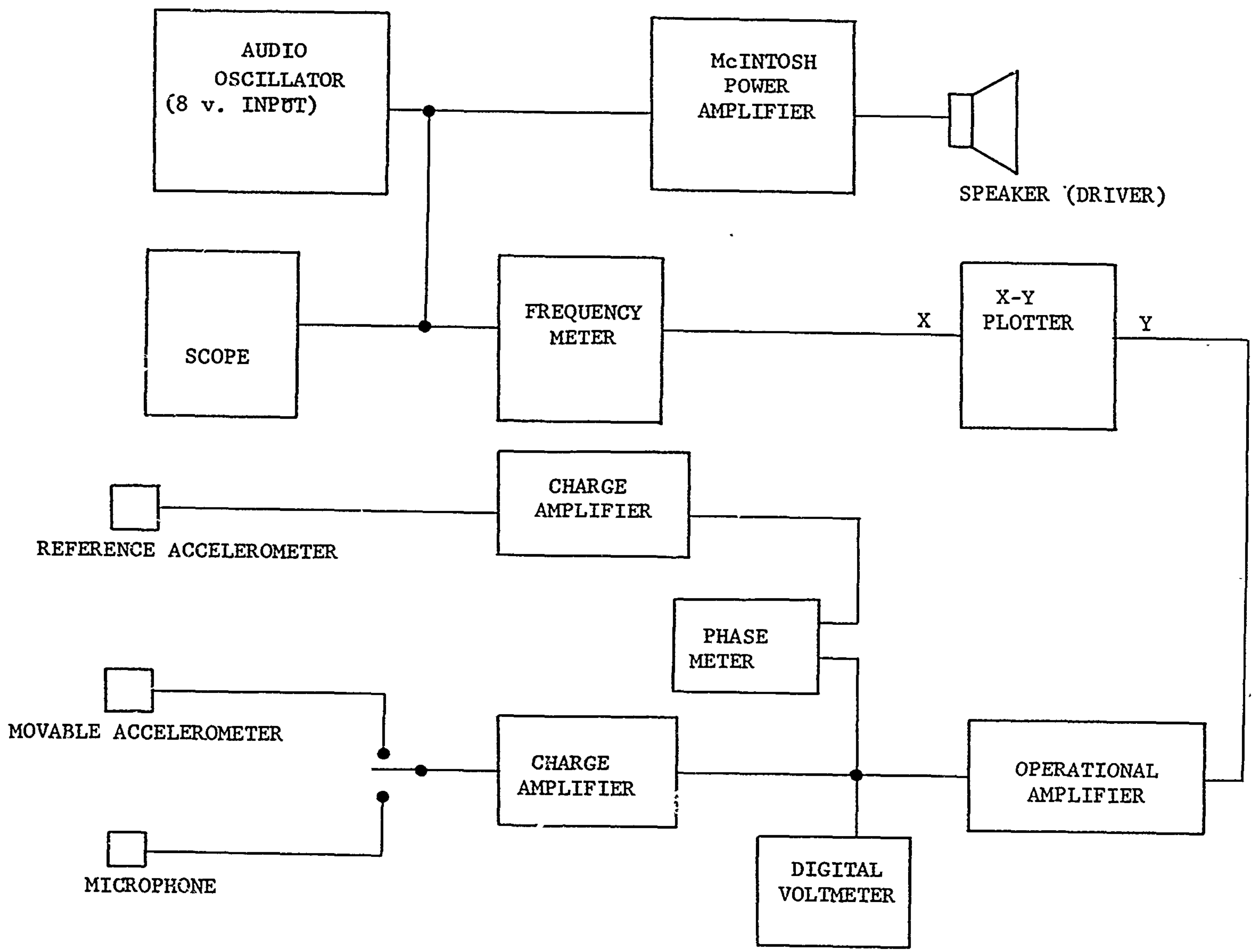

Figure 2. Electrical System for Acoustic Testing

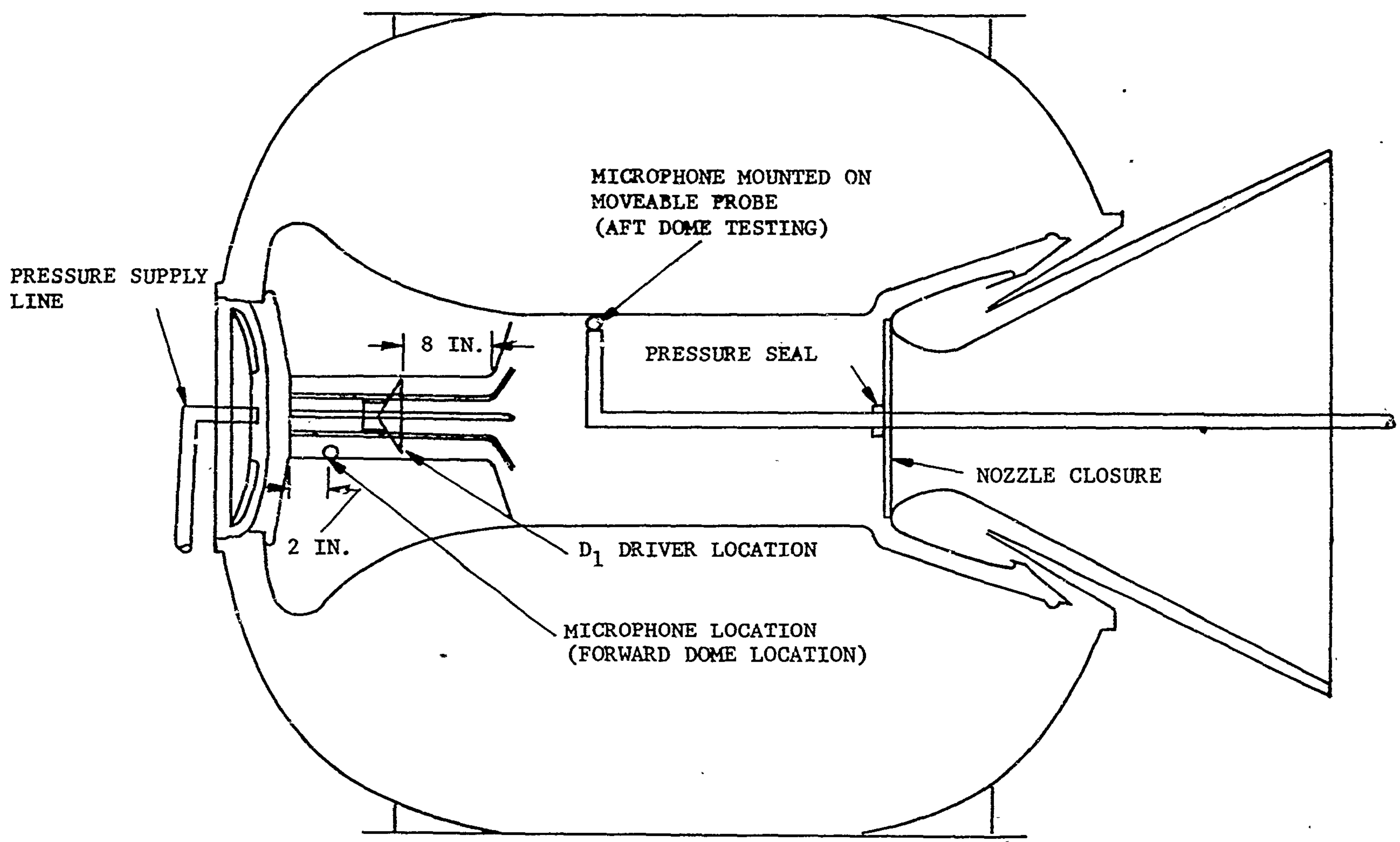

Figure 3. Driver and Microphone Locations

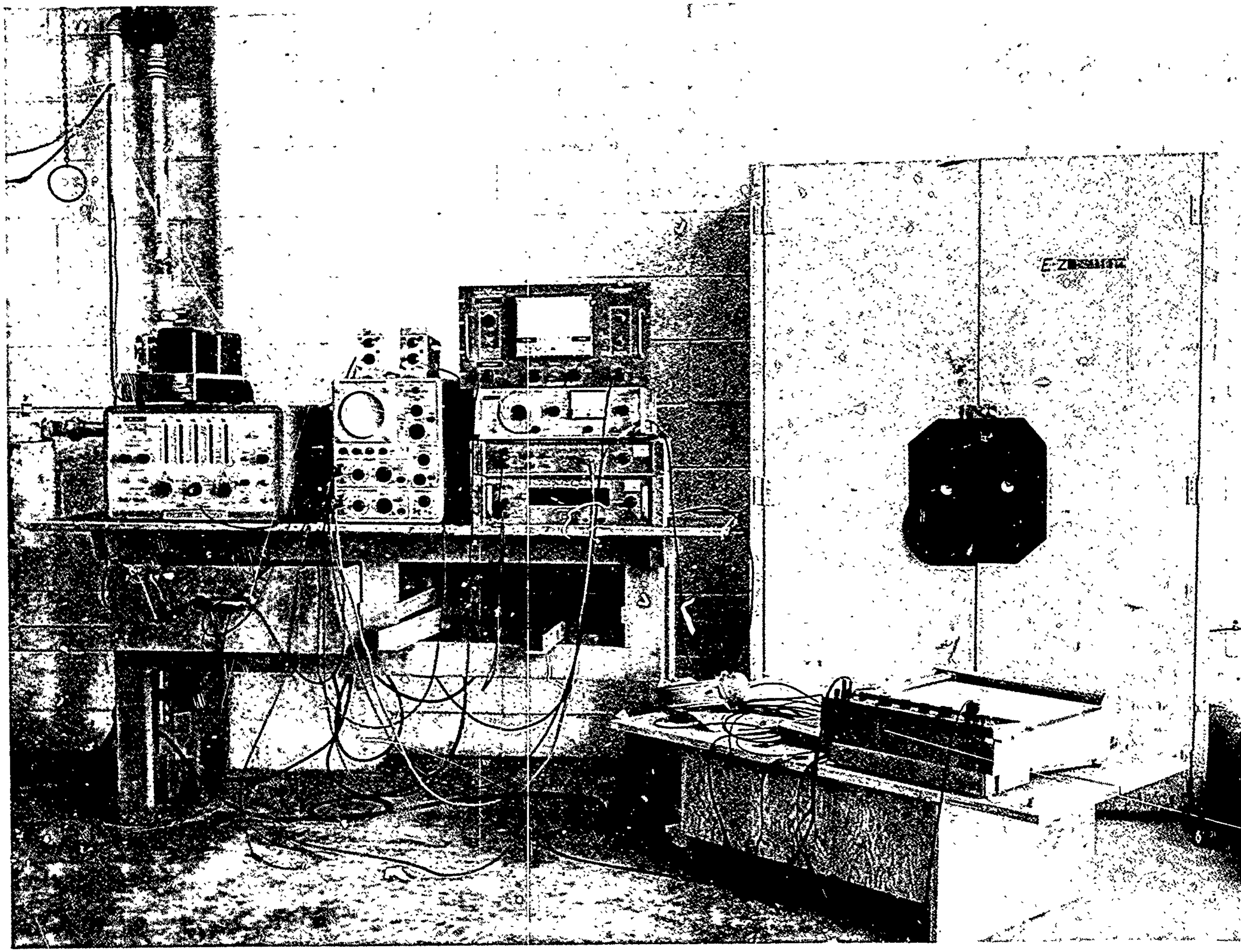

Figure 4. Test Instrumentation Set-Up

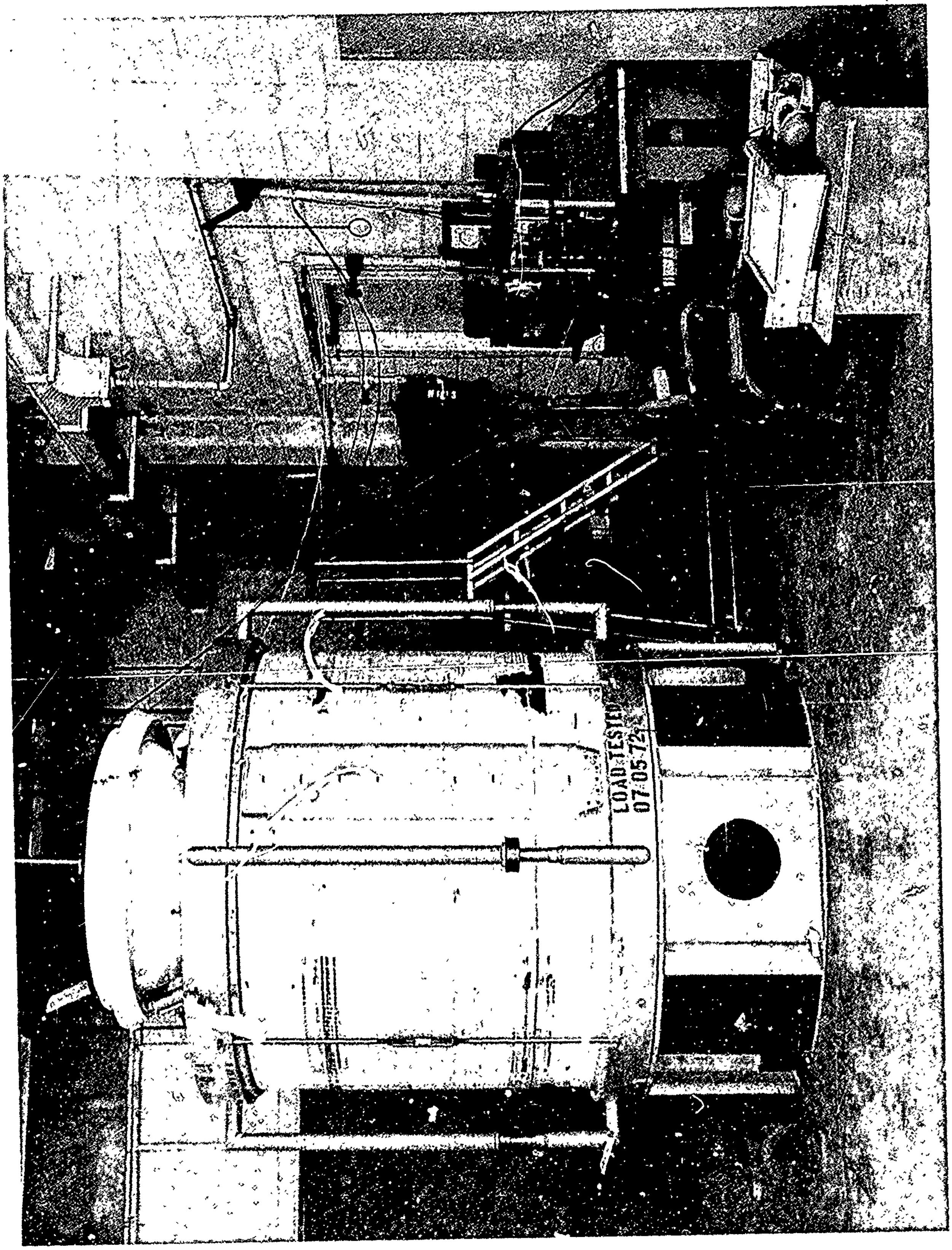

Figure 5 . Test Set-Up with Motor in Vertical Position

NOTES: 1. ALL ACCELEROMETERS ARE TO BE MOUNTED NORMAL TO THE CASE
2. ACCELEROMETERS ARE MOUNTED USING DOUBLE-BACKED TAPE
3. ACCELEROMETERS WILL BE CALIBRATED TO READ THE ACCELERA[TION] LEVEL IN g's
4. LOCATION NUMBERS BEGIN WITH [9]3 AND END AT 285

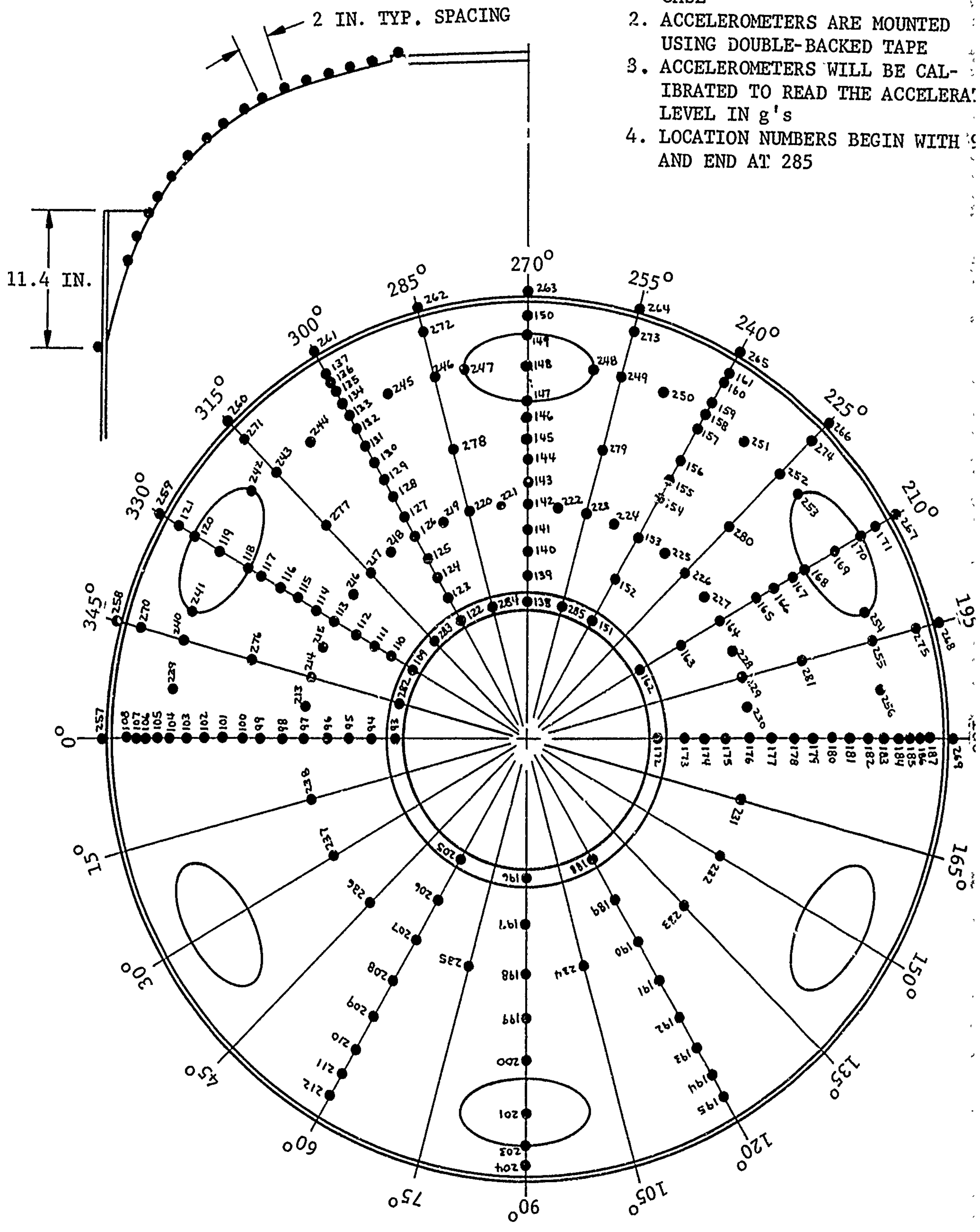

Figure 6. Accelerometer Locations for the Forward Dome

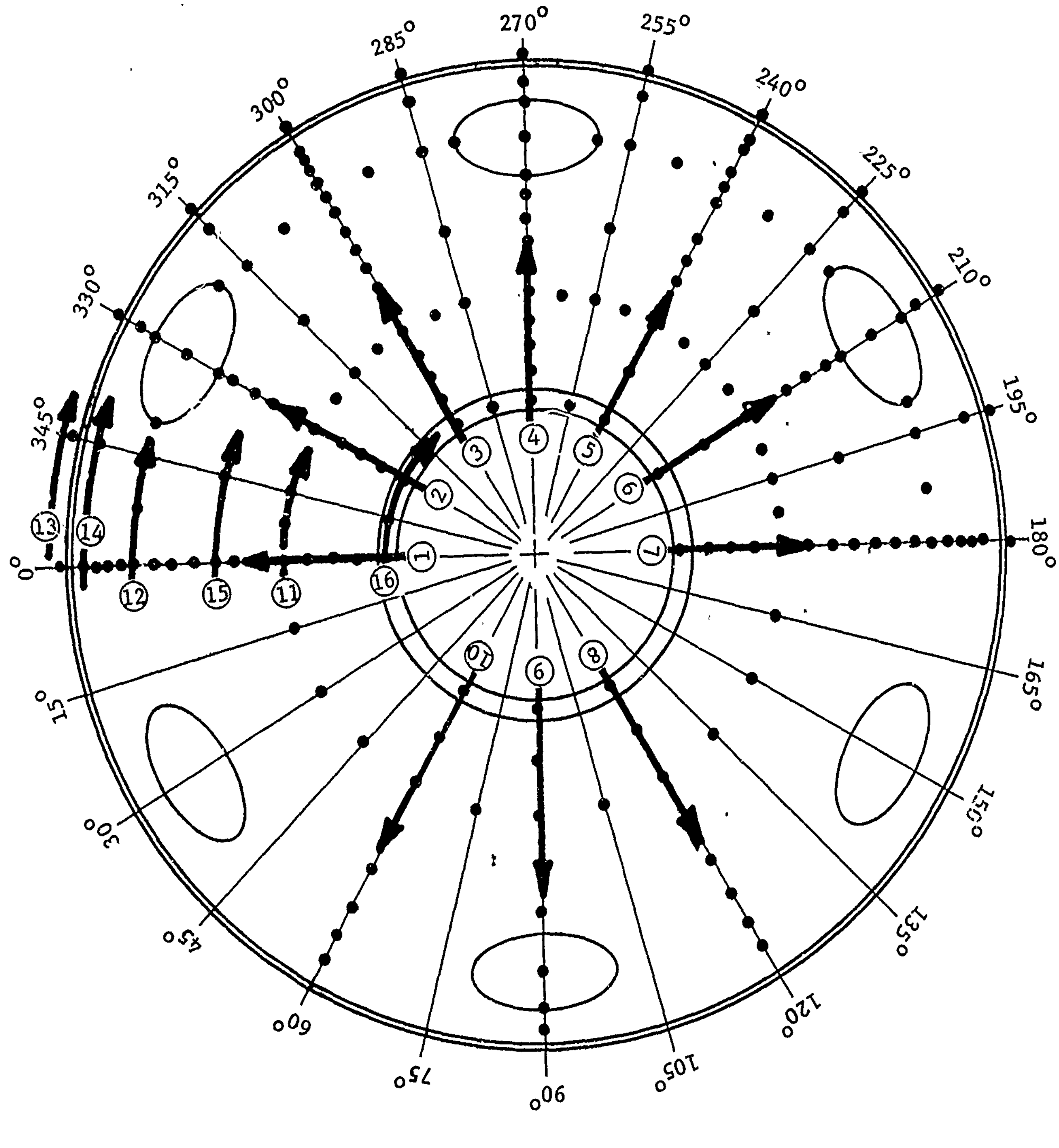

Figure 7. Numbering Sequence for Accelerometer Locations Shown in Figure 6

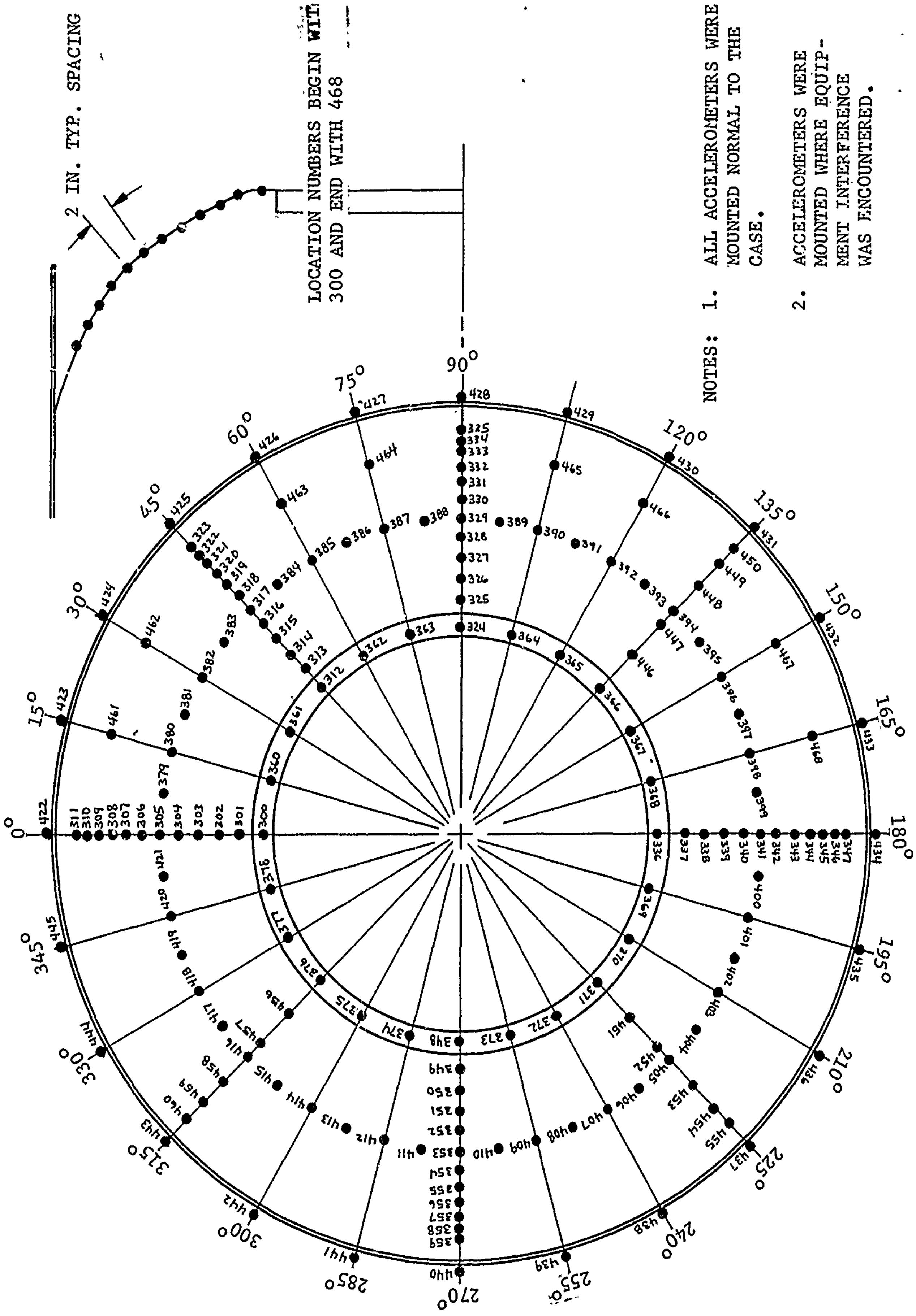

Figure 8. Accelerometer Locations for the Aft Dome

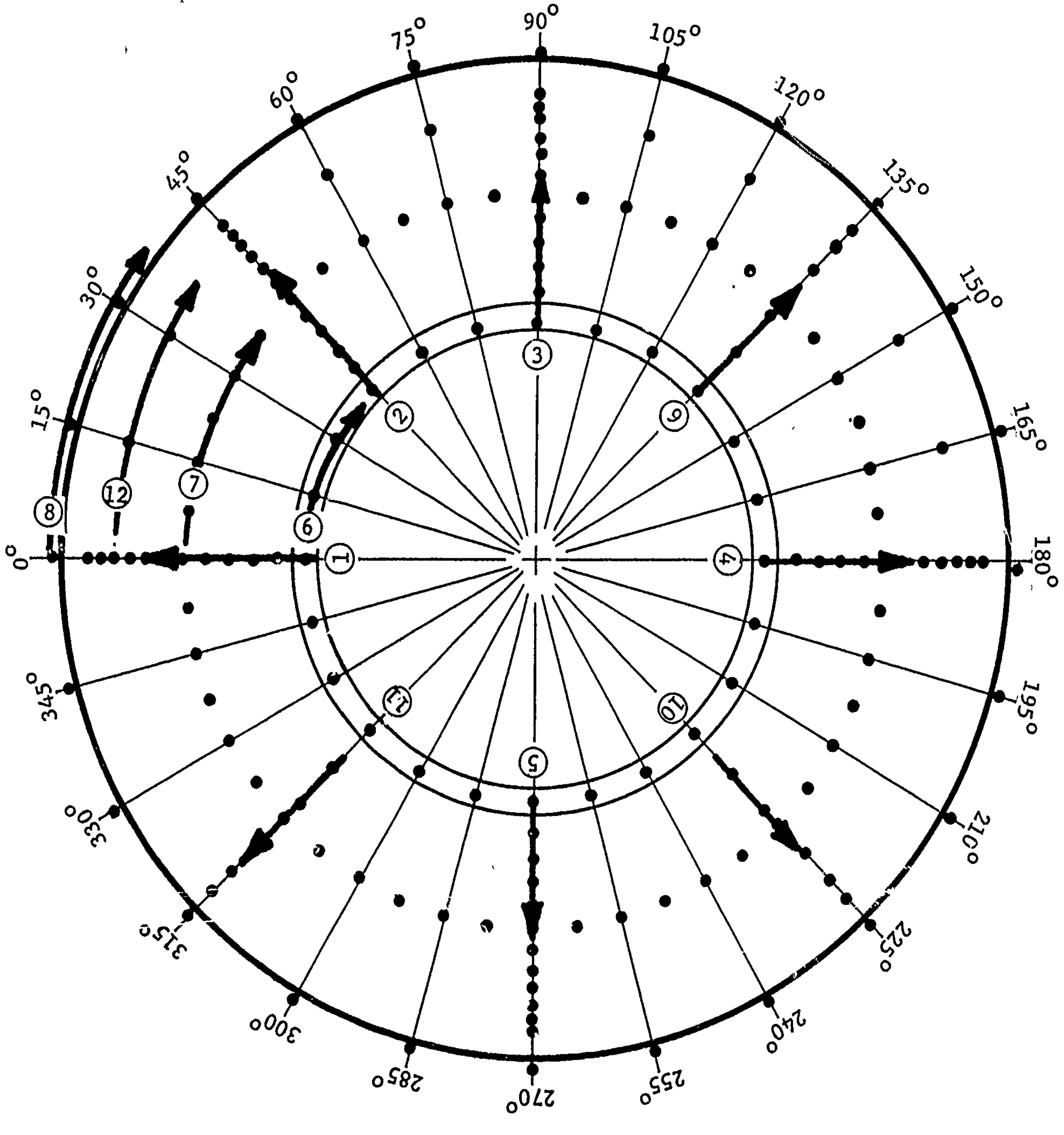

Figure 9. Numbering Sequence for Accelerometer Locations Shown in Figure 8

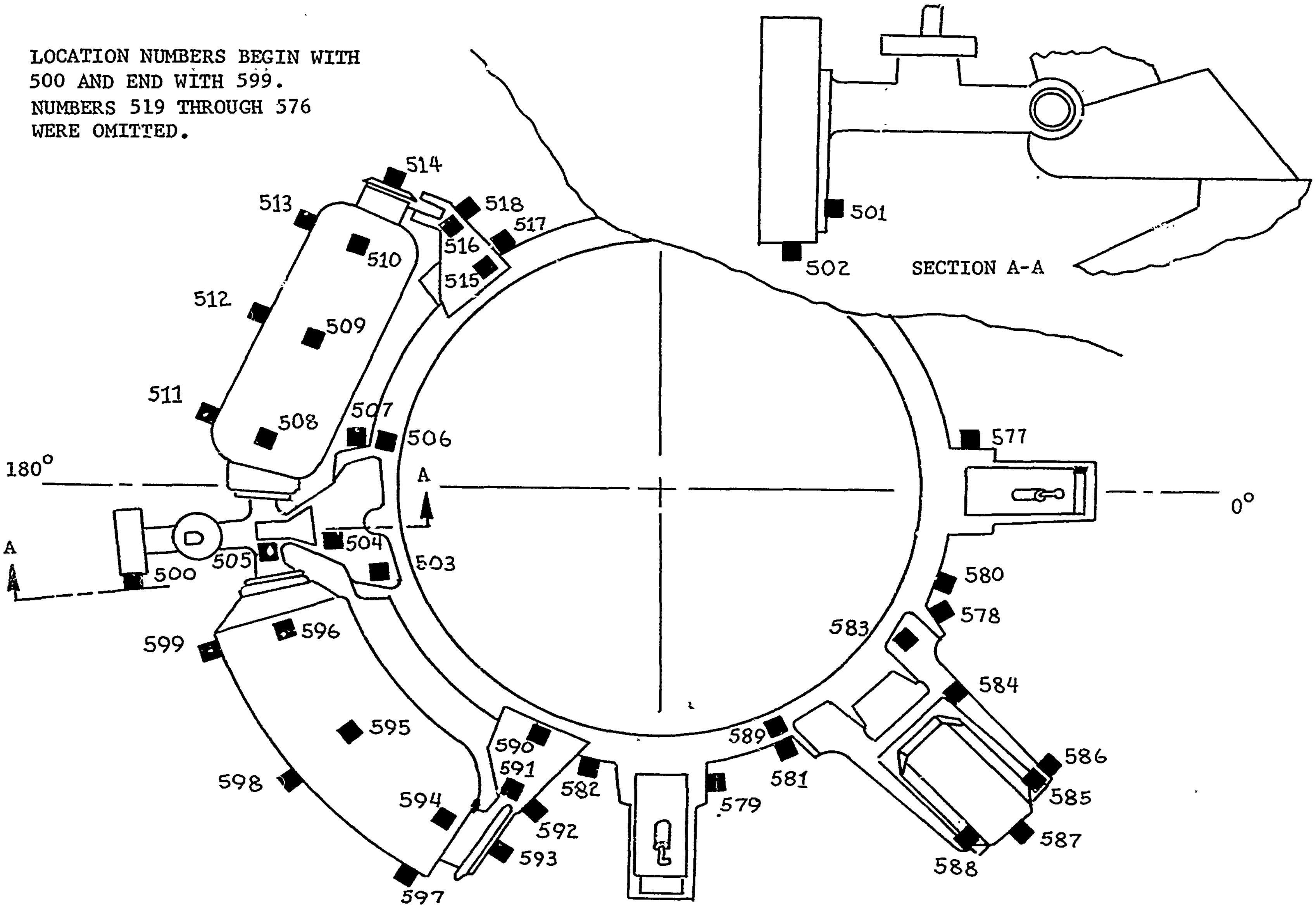

Figure 10. Component Accelerometer Locati

LOCATION NUMBERS BEGIN WITH 659
AND END WITH 676

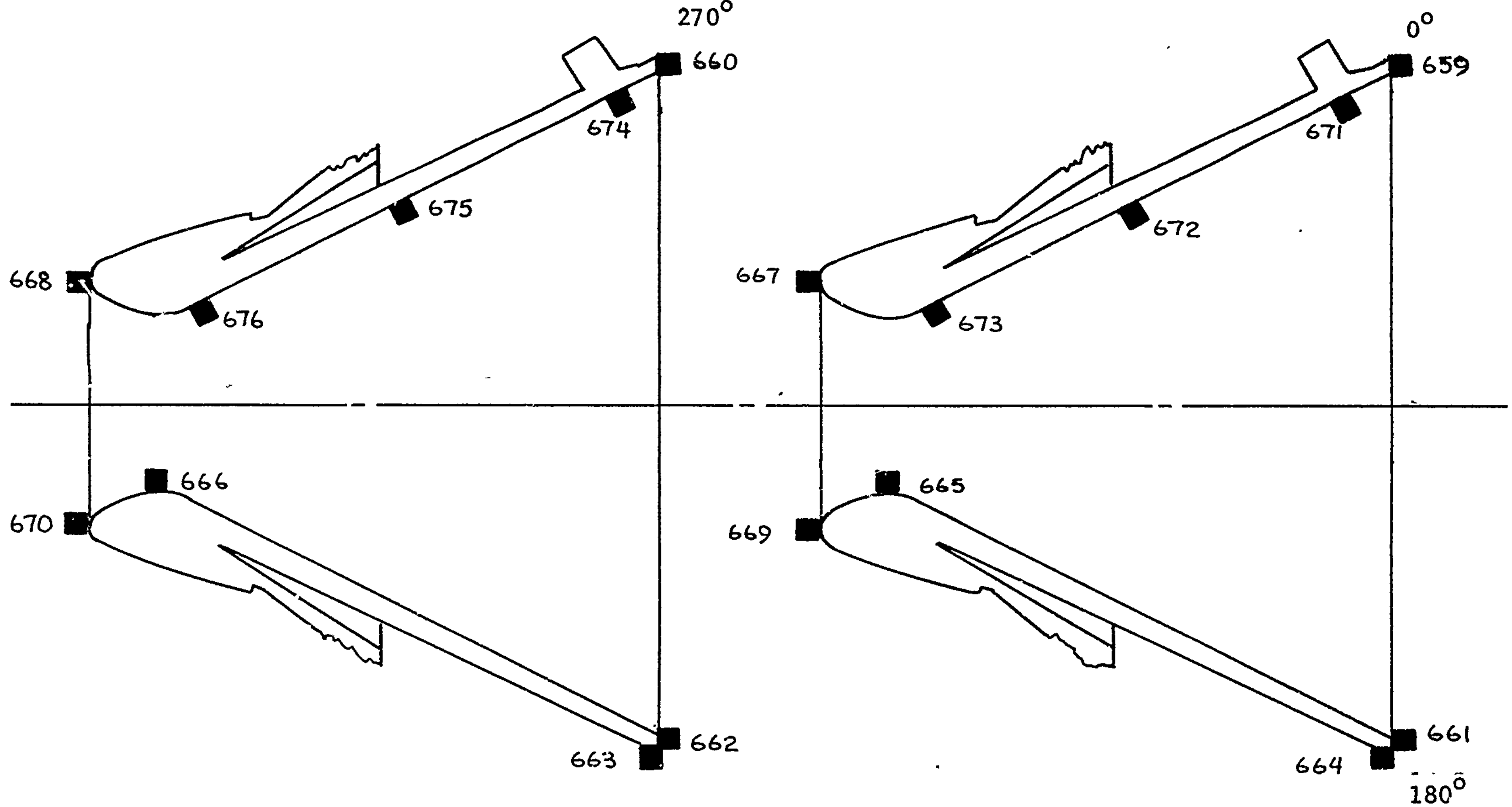

Figure 11. Nozzle Accelerometer Locations

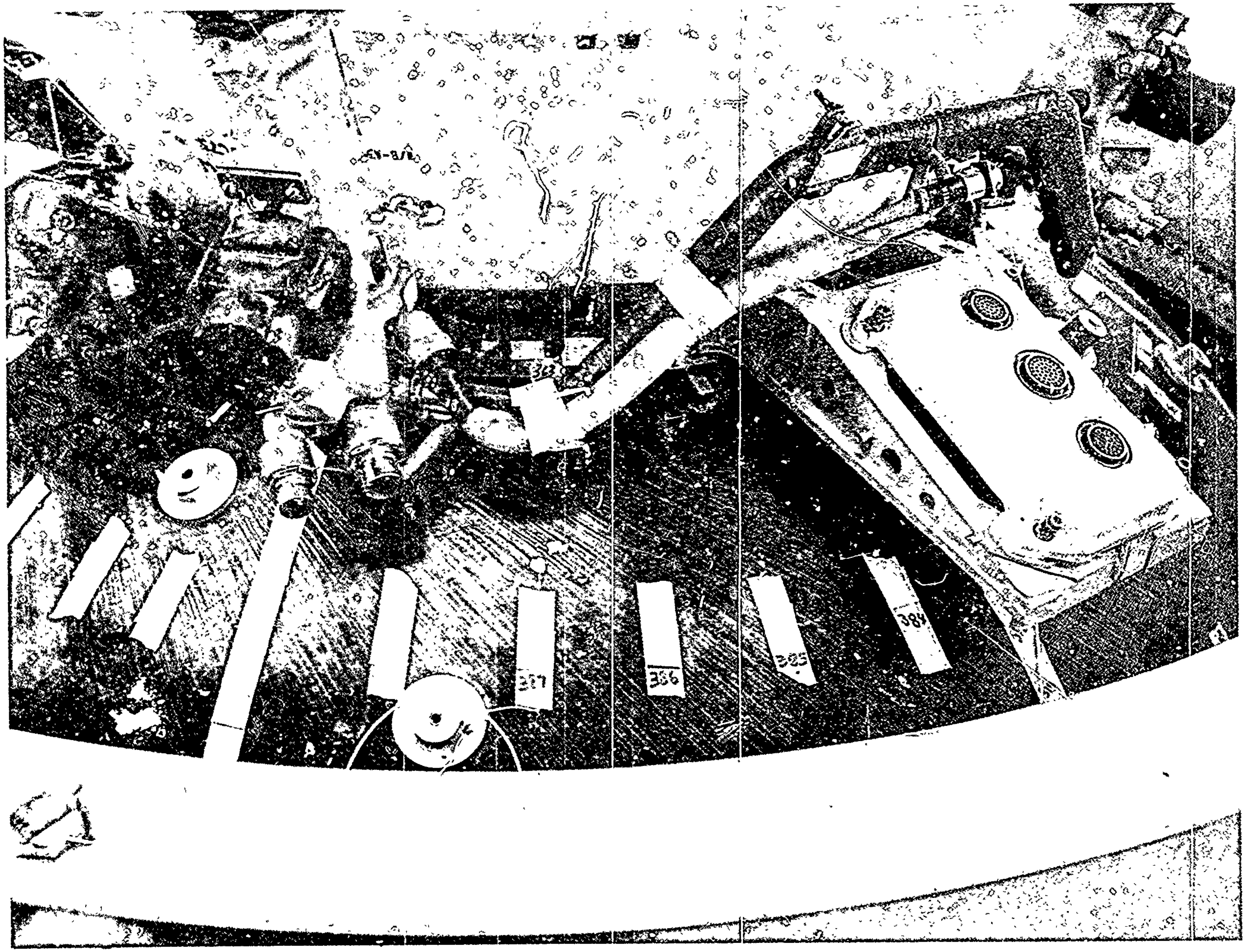

Figure 12. Aft Dome Accelerometer Locations Near 90° Actuator and Flight Electronics

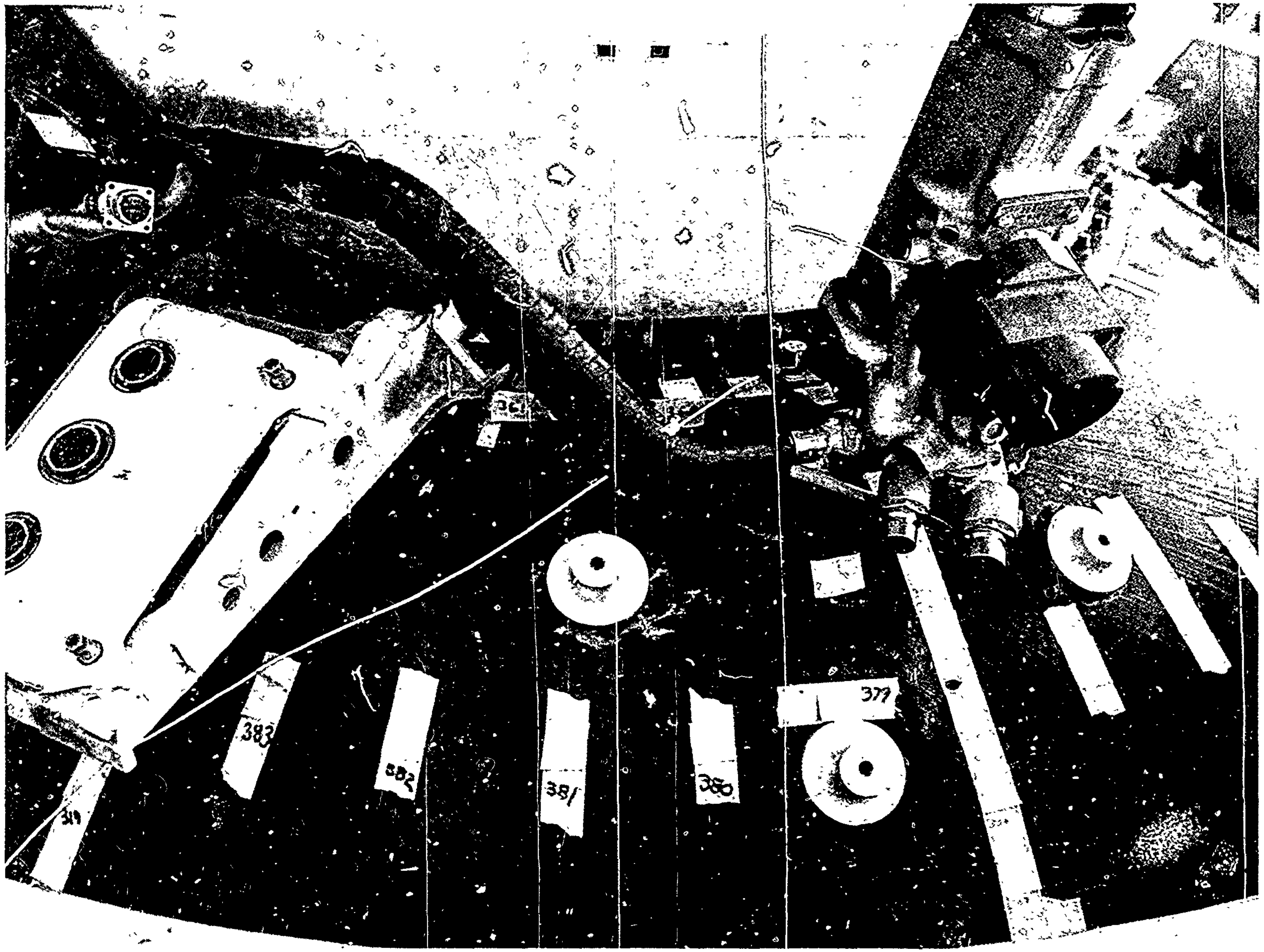

Figure 13. Aft Dome Accelerometer Locations Near 0° Actuator and Flight Electronics Package, S/S Poseidon C-3

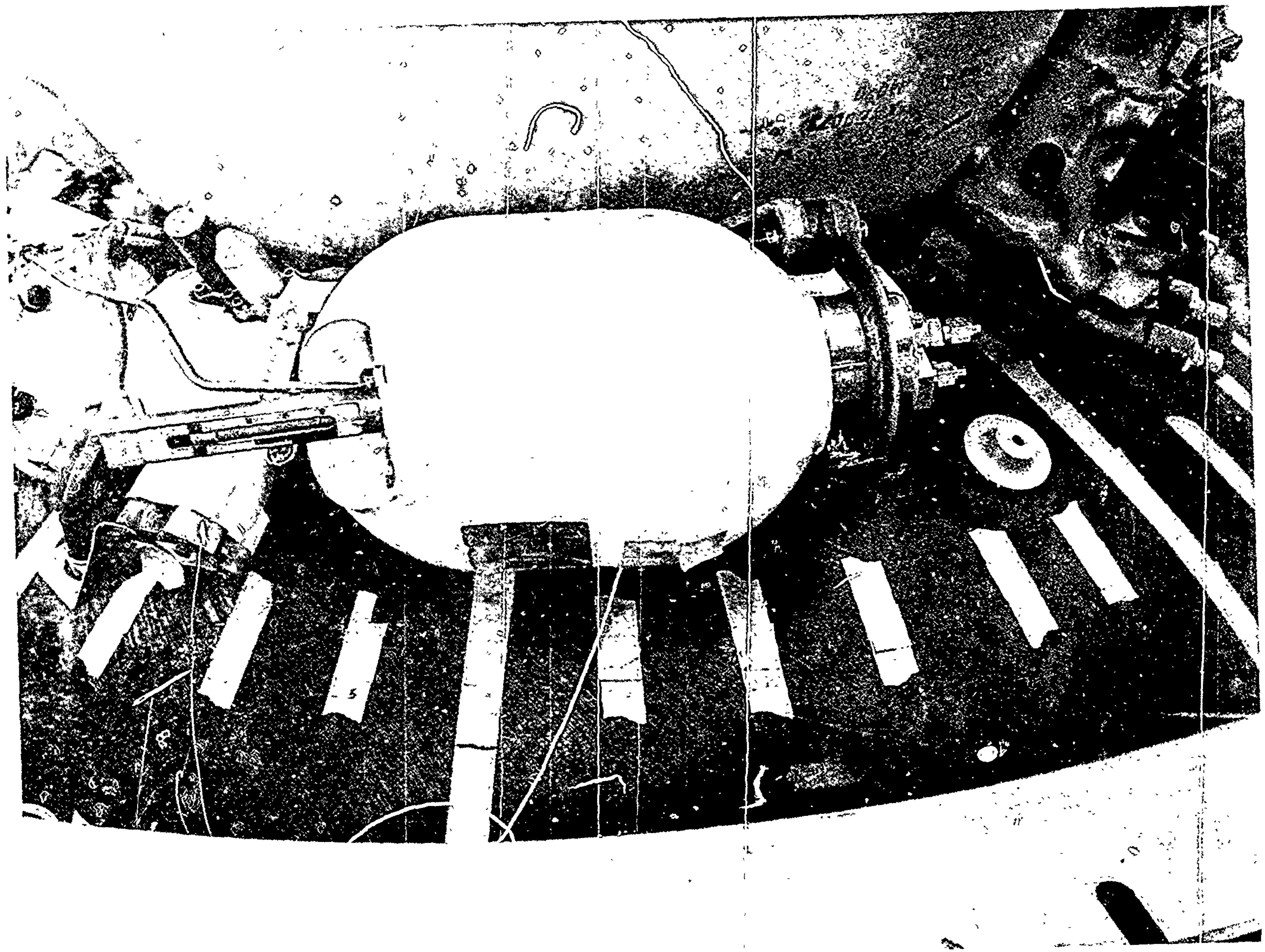

Figure 14. Aft Dome Accelerometer Locations Near the Hydraulic Power Unit, S/S Poseidon C-

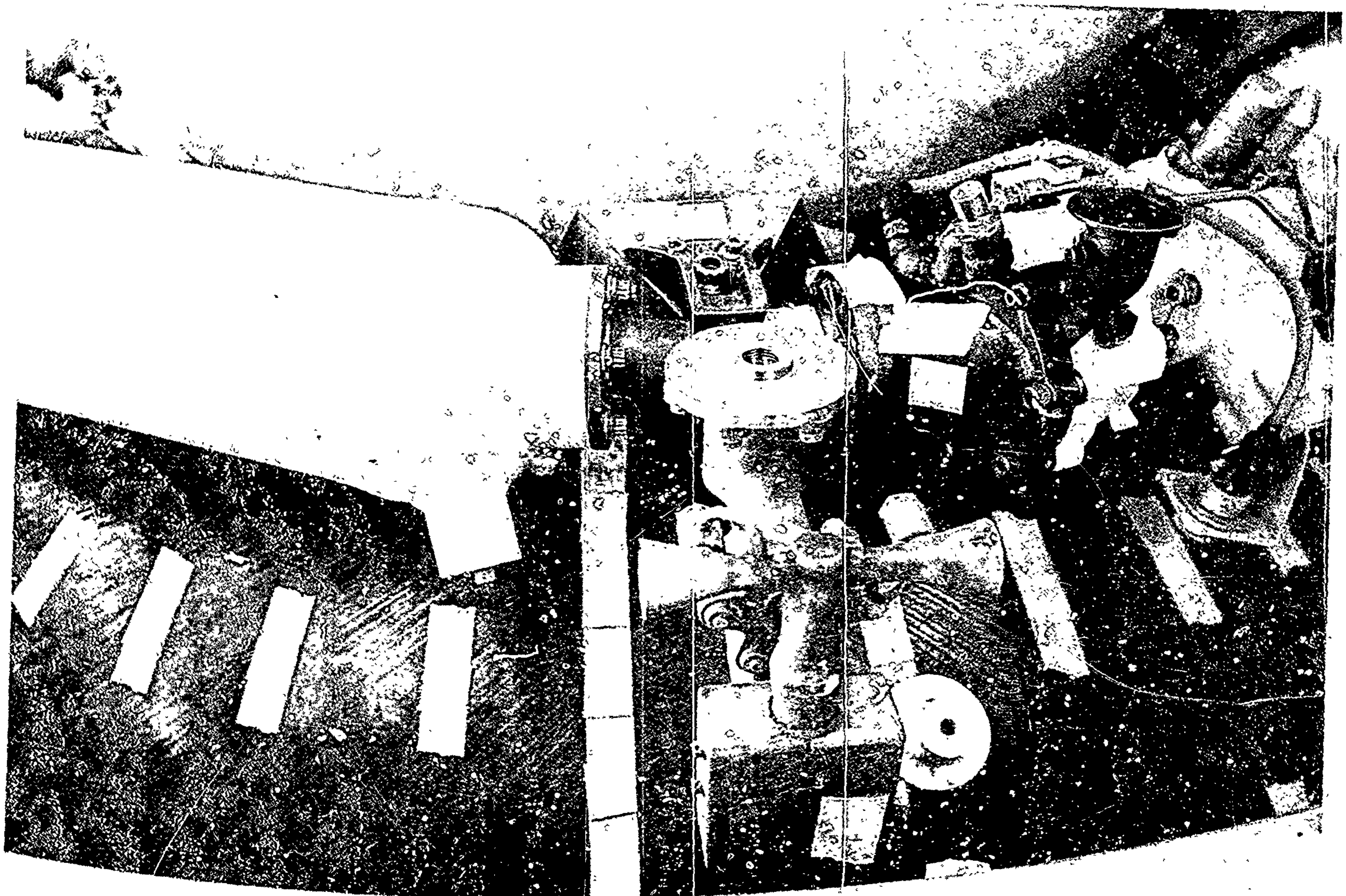

Figure 15. Aft Dome Accelerometer Locations in the Area Between the HPU and the Gas Generator, S/S Poseidon C-3

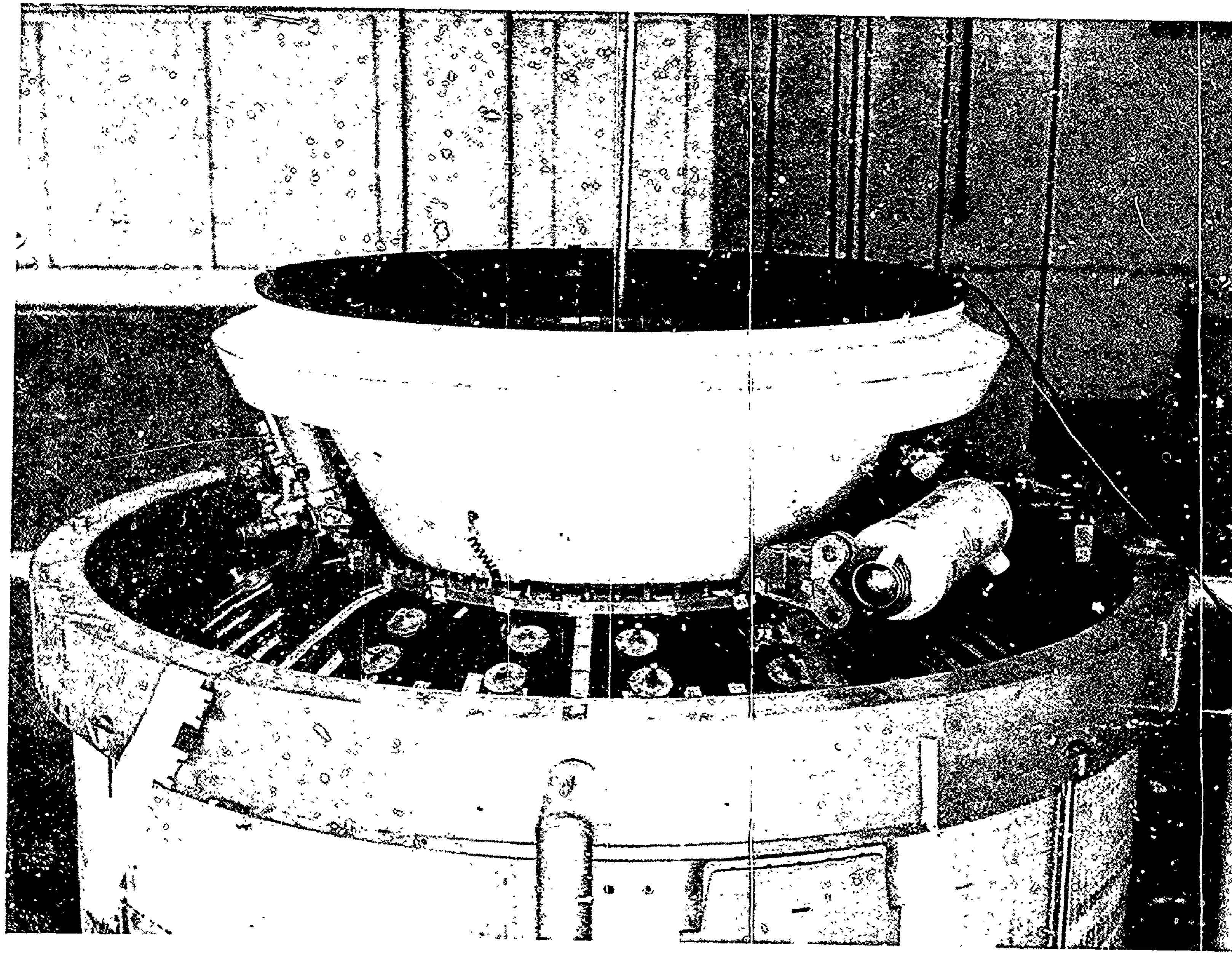

Figure 16. Aft Dome Accelerometer Locations in the Area Between the Gas Generator and the 0^{o} Actuator, S/S Poseidon C-3

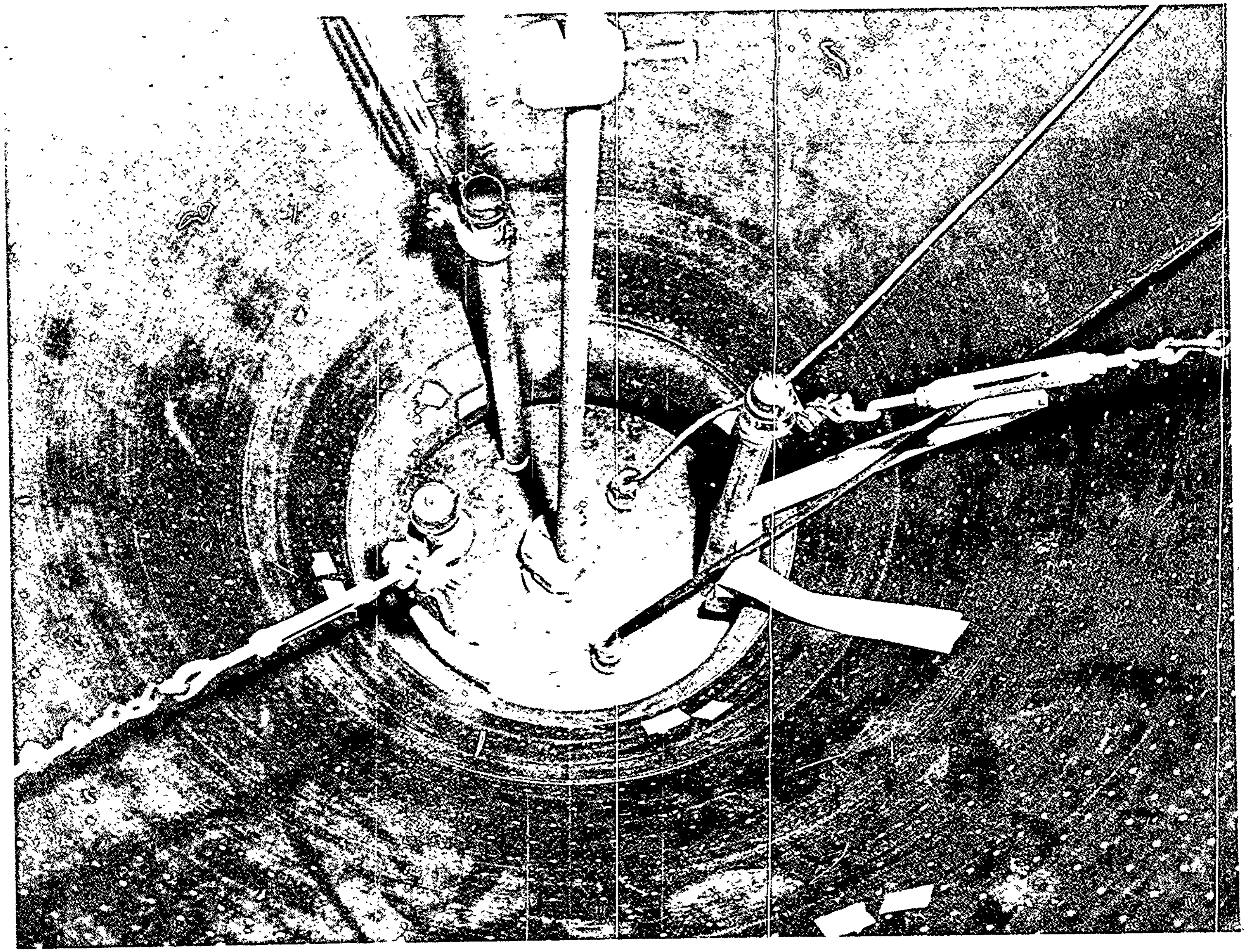

Figure 17. Nozzle Closure Showing Microphone Probe, S/S Poseidon C-3

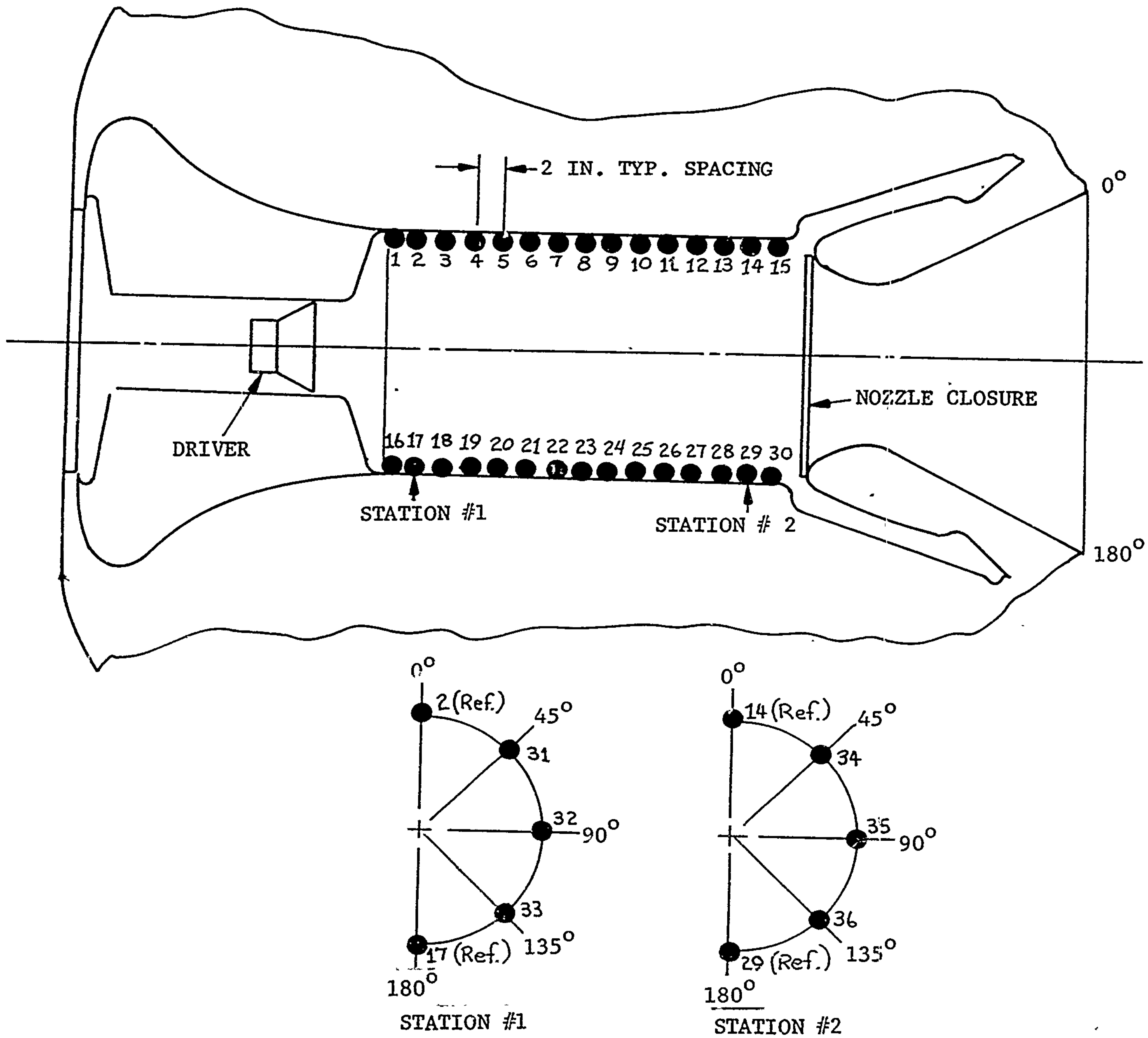

Figure 18. Microphone Locations for Mapping Acoustic Modes

NOTE: BECAUSE A LARGE VOLUME OF DATA WAS PRODUCED DURING THE TEST PROGRAM, ONLY THE MOST IMPORTANT DATA ARE INCLUDED IN THE FINAL REPORT. ALL FORWARD DOME FREQUENCY RESPONSE PLOTS EXCEPT FIGURE 19 HAVE BEEN OMITTED FROM THE FINAL REPORT. OTHER FREQUENCY RESPONSE PLOTS WERE INCLUDED IN THE TASK 4 REPORT WHICH IS ON FILE AT THE AFRPL, EDWARDS, CA.

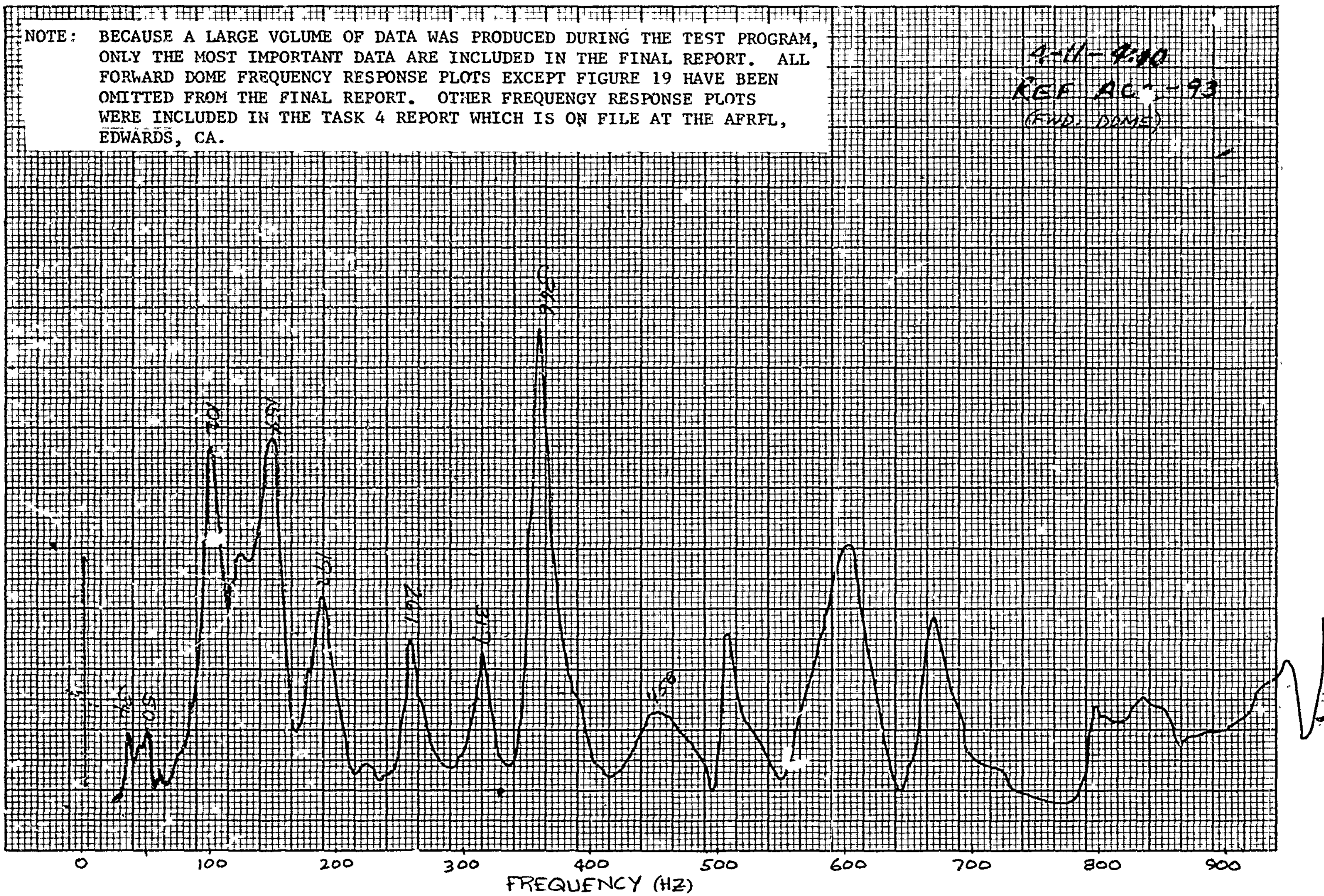

Figure 19. Frequency Response Plot for the Reference Accelerometer Located at Position No. 93 on the Forward Dome, S/S Poseidon C-3

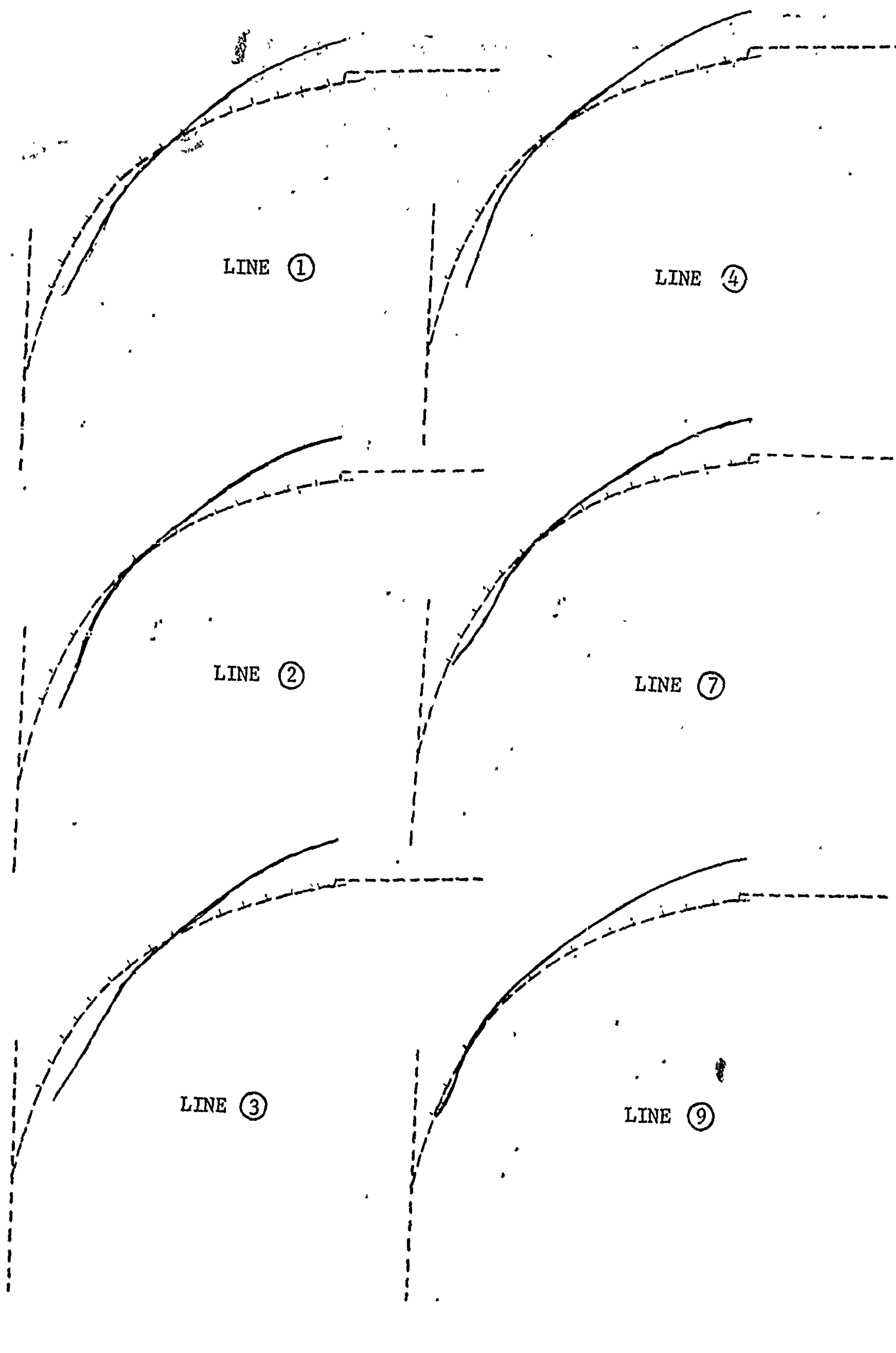

Figure 20. Forward Dome Mode Shape Plots for a 100 Hz Frequency

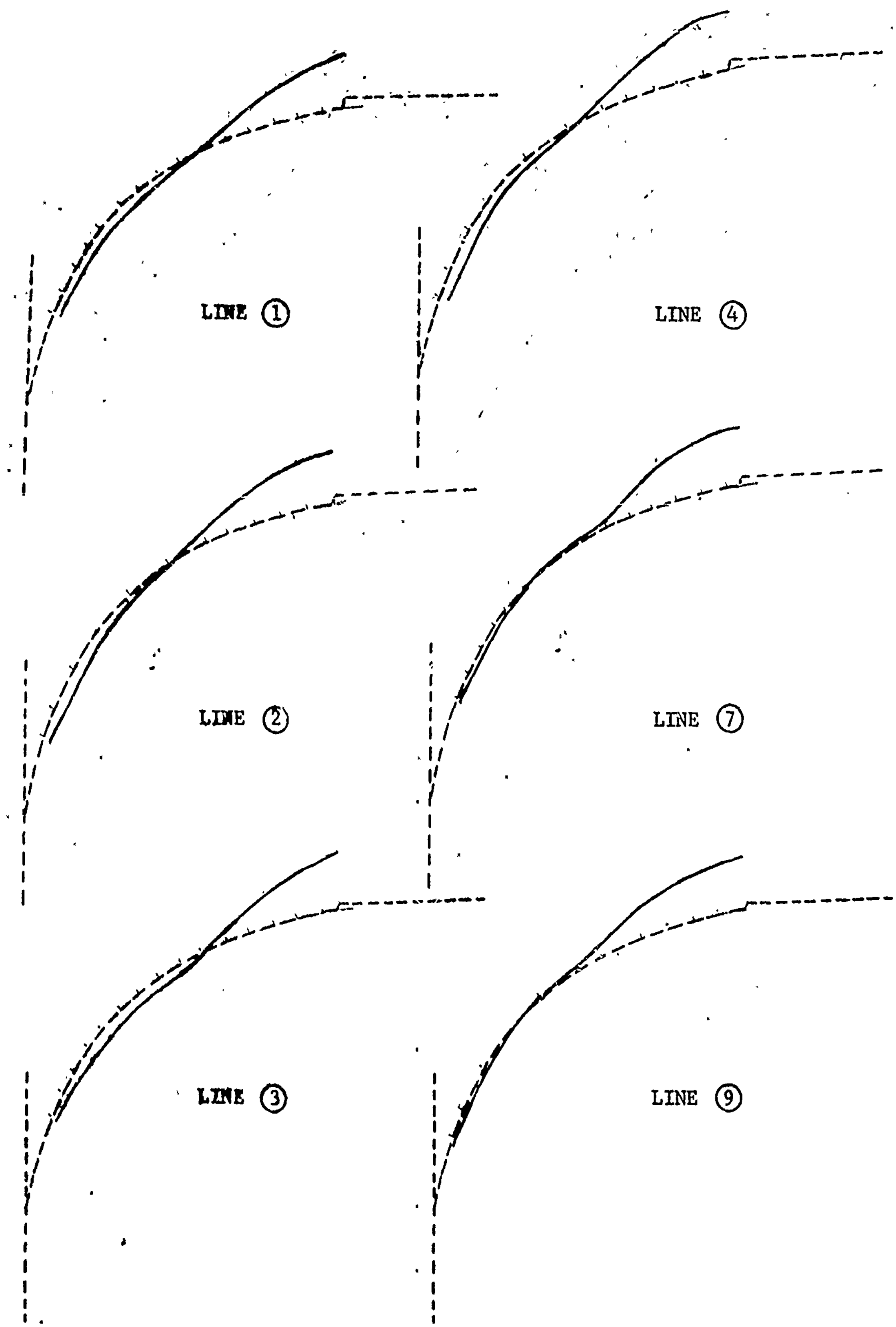

Figure 21. Forward Dome Mode Shape Plots for a 155 Hz Frequency

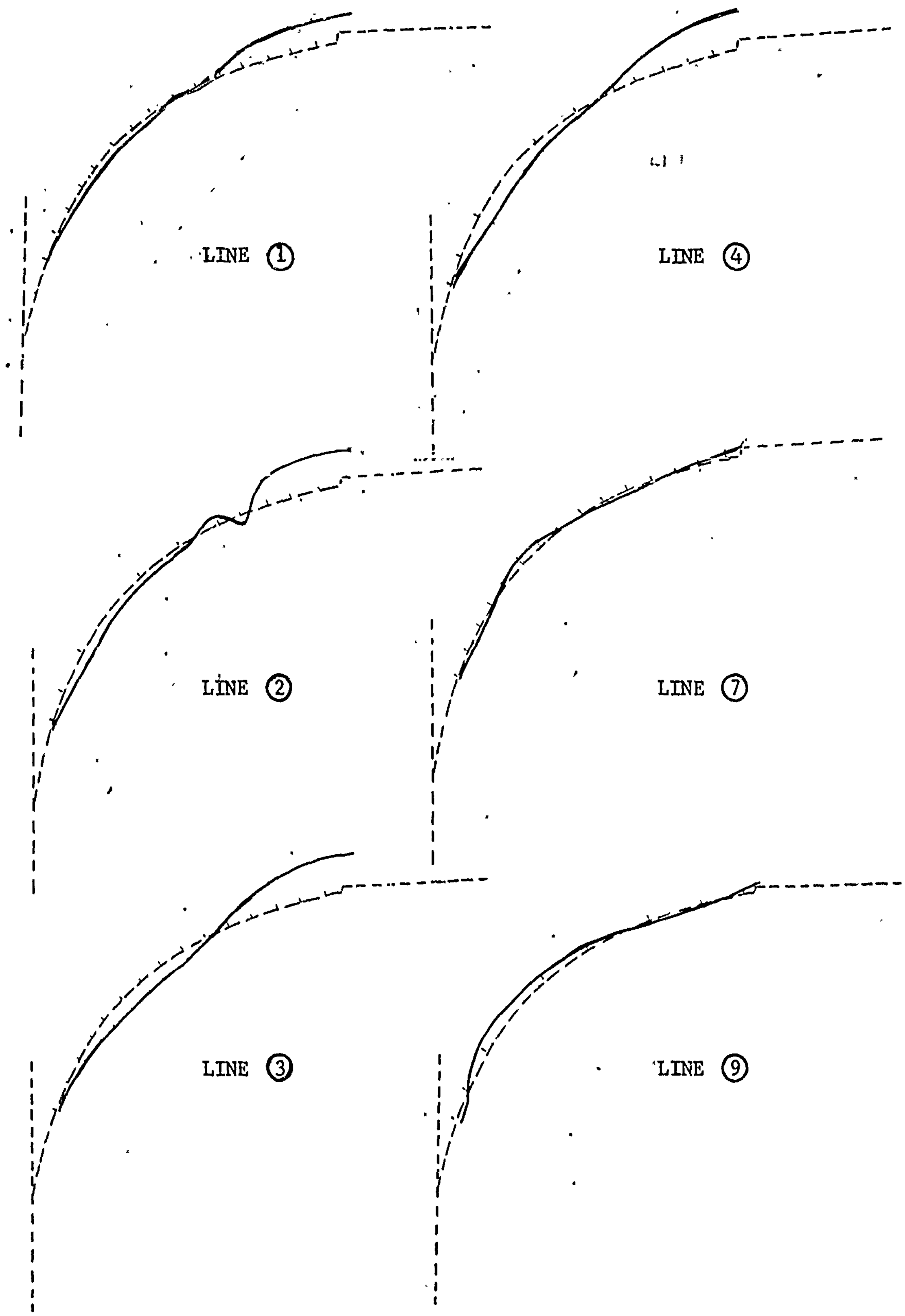

Figure 22. Forward Dome Mode Shape Plots for a 192 Hz Frequency

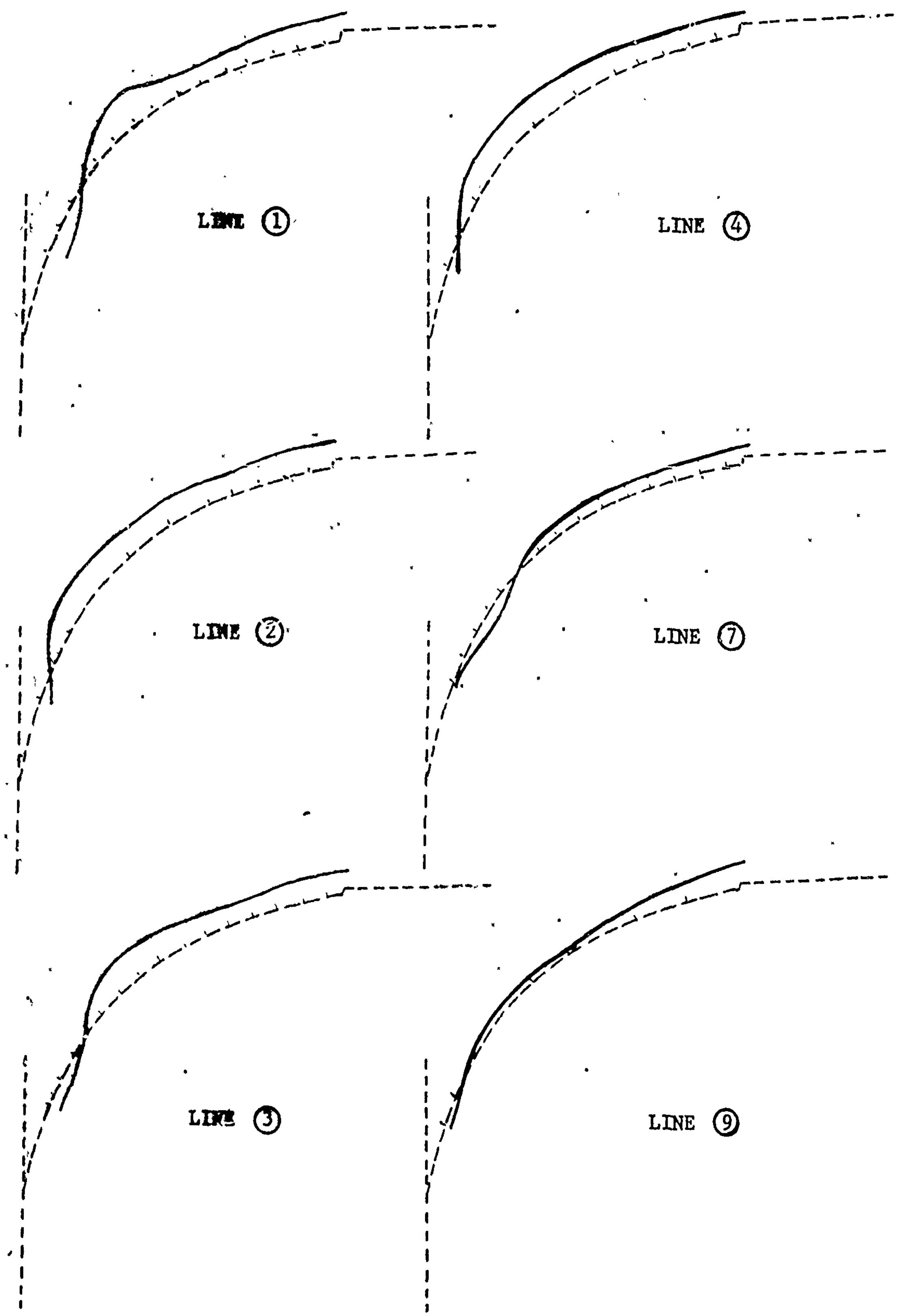

Figure 23. Forward Dome Mode Shape Plots for a 262 Hz Frequency

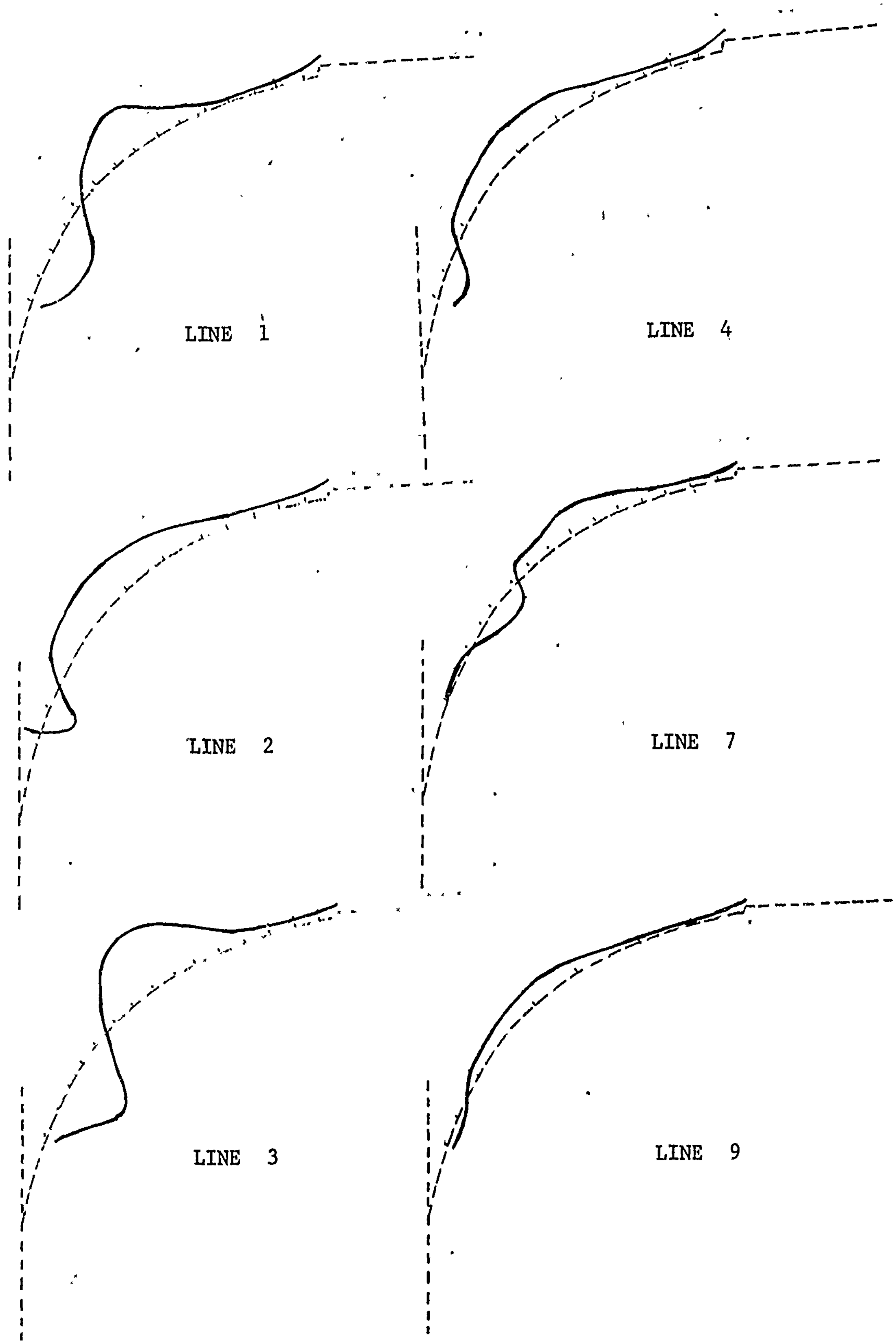

I gure 24. Forward Dome Mode Shape Plots for a 367 Hz Frequency

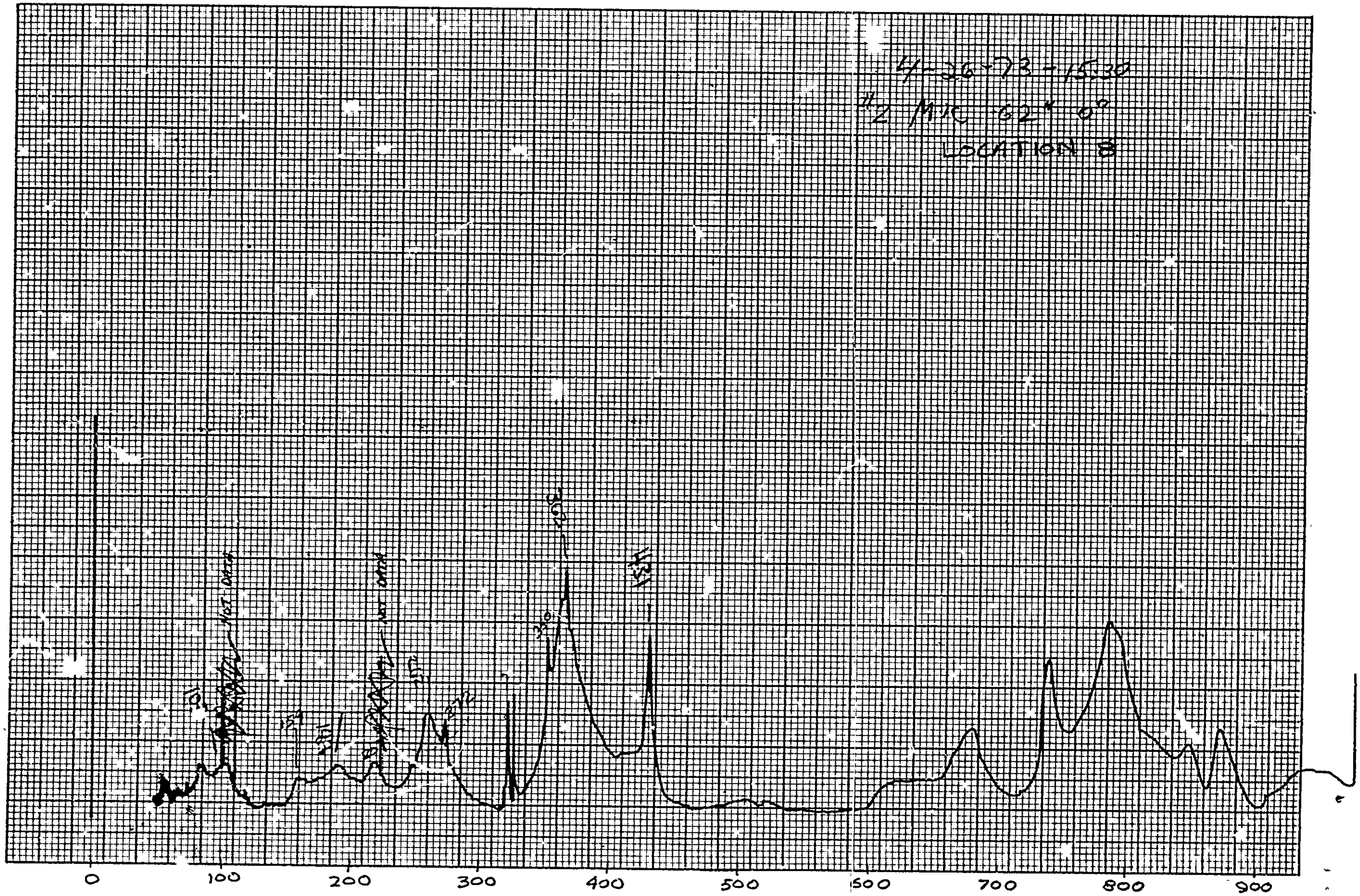

Figure 25. Acoustic Cavity Pressure as a Function of Frequency at Microphone Position No. 8

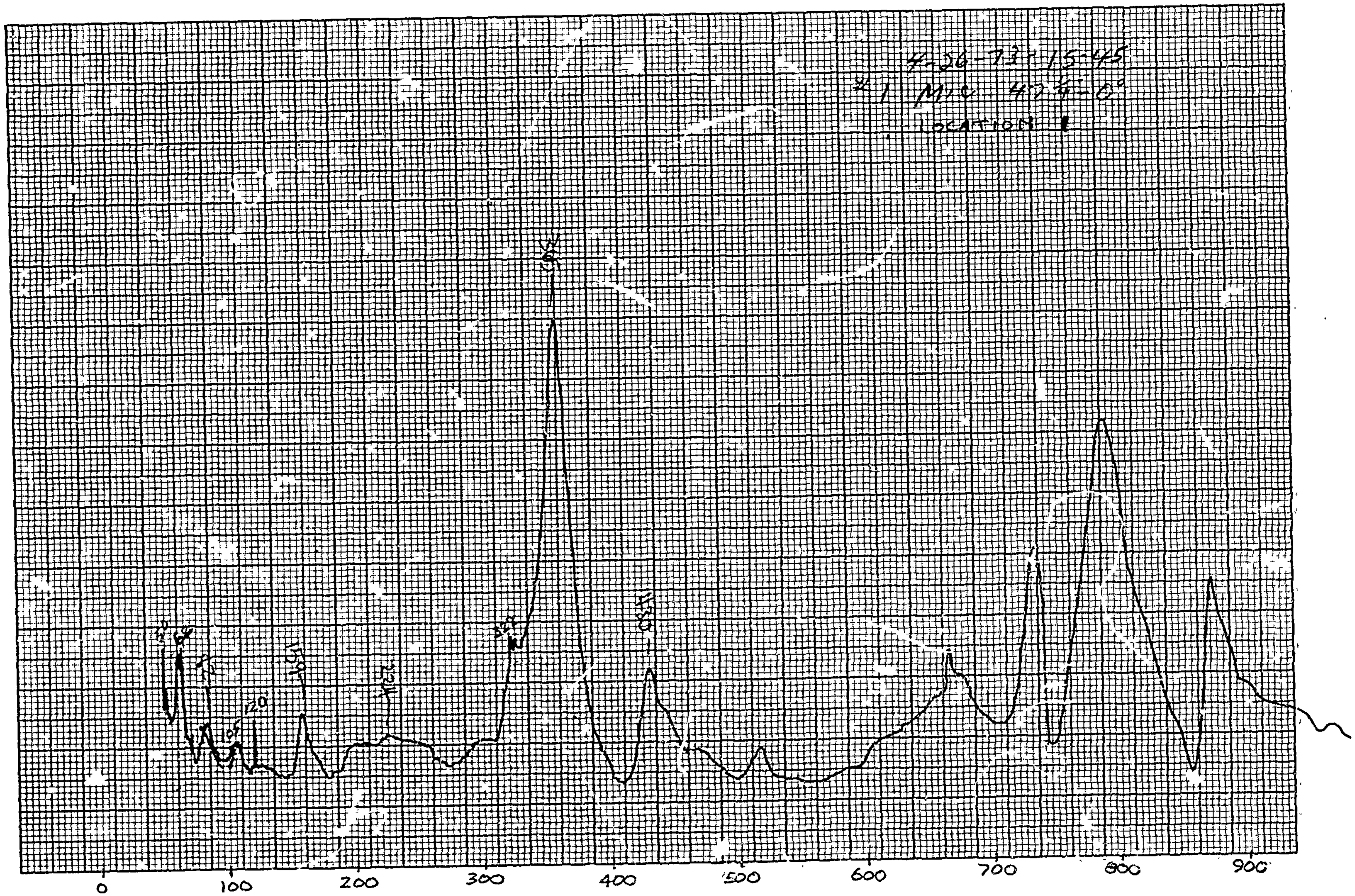

Figure 26. Acoustic Cavit · Pressure as a Function of Frequency at Microphone Position No. 1

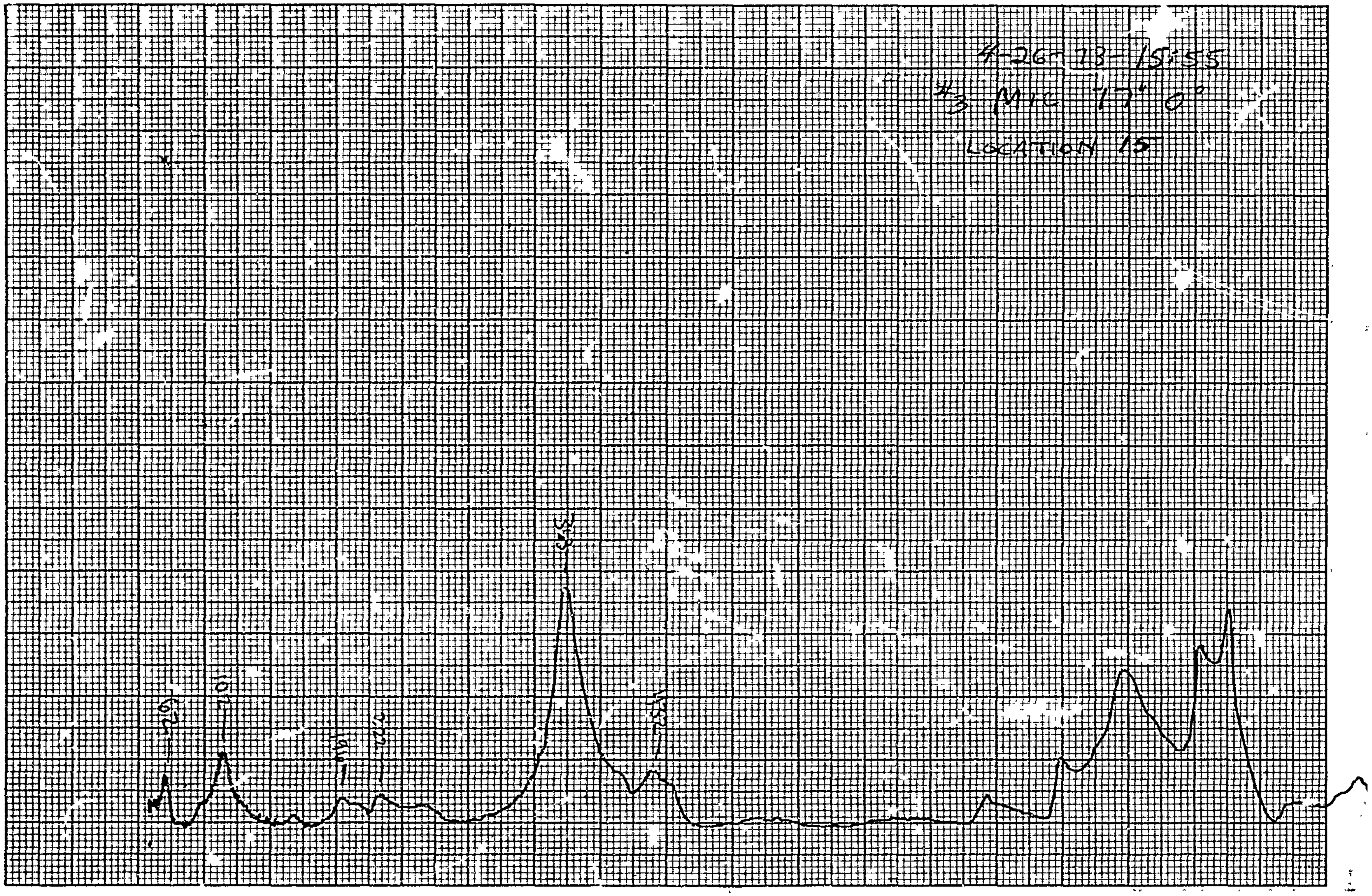

Figure 27   Acoustic Cavity Pressure as a Function of Frequency at Microphone Position No. 15

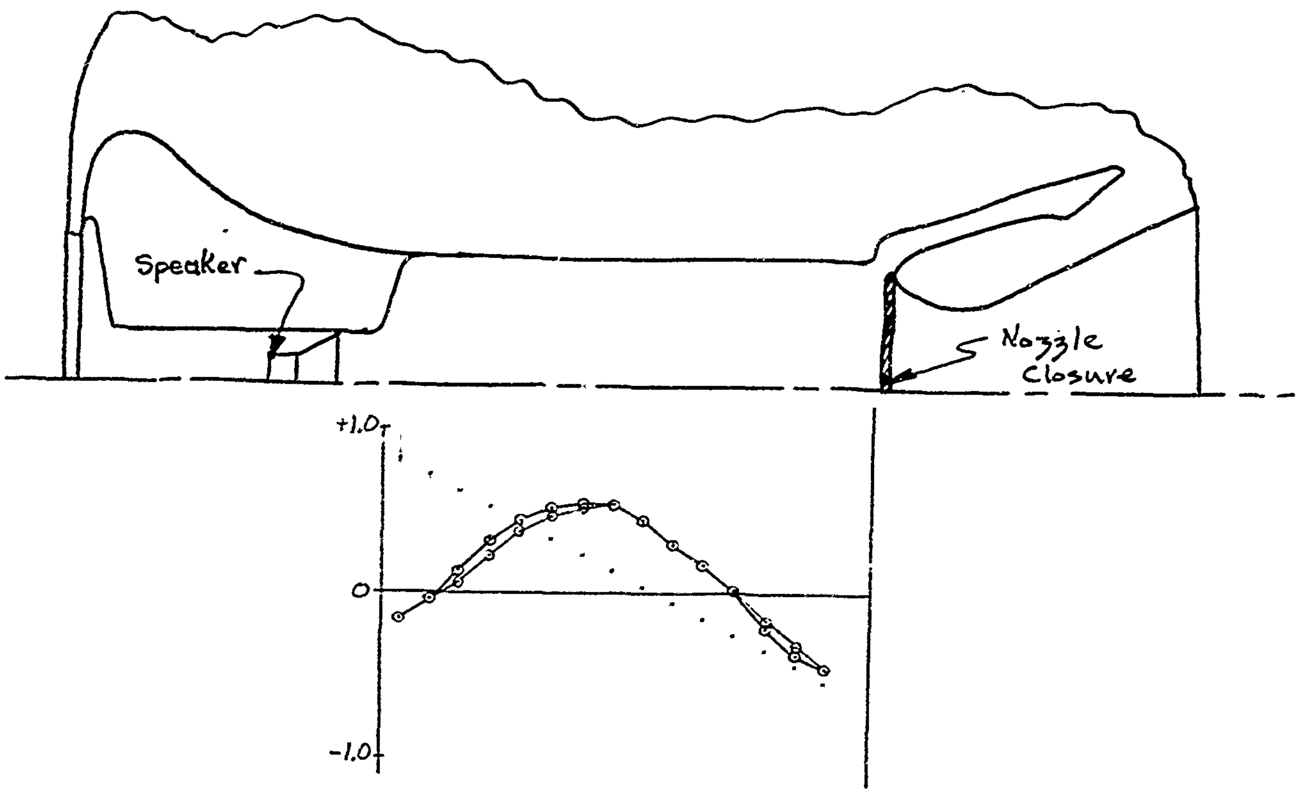

Figure 28. Mode Shape for 364 Hz Cavity Frequency

NOTE: BECAUSE A LARGE VOLUME OF DATA WAS PRODUCED DURING THE TEST PROGRAM, ONLY THE MOST IMPORTANT DATA ARE INCLUDED IN THE FINAL REPORT. ONLY SELECTED FREQUENCY RESPONSE PLOTS ARE INCLUDED FROM THE AFT DOME TESTING. OTHFR FREQUENCY RESPONSE PLOTS WERE INCLUDED IN THE TASK 4 REPORT WHICH IS ON FILE AT THE AFRPL, EDWARDS, CA.

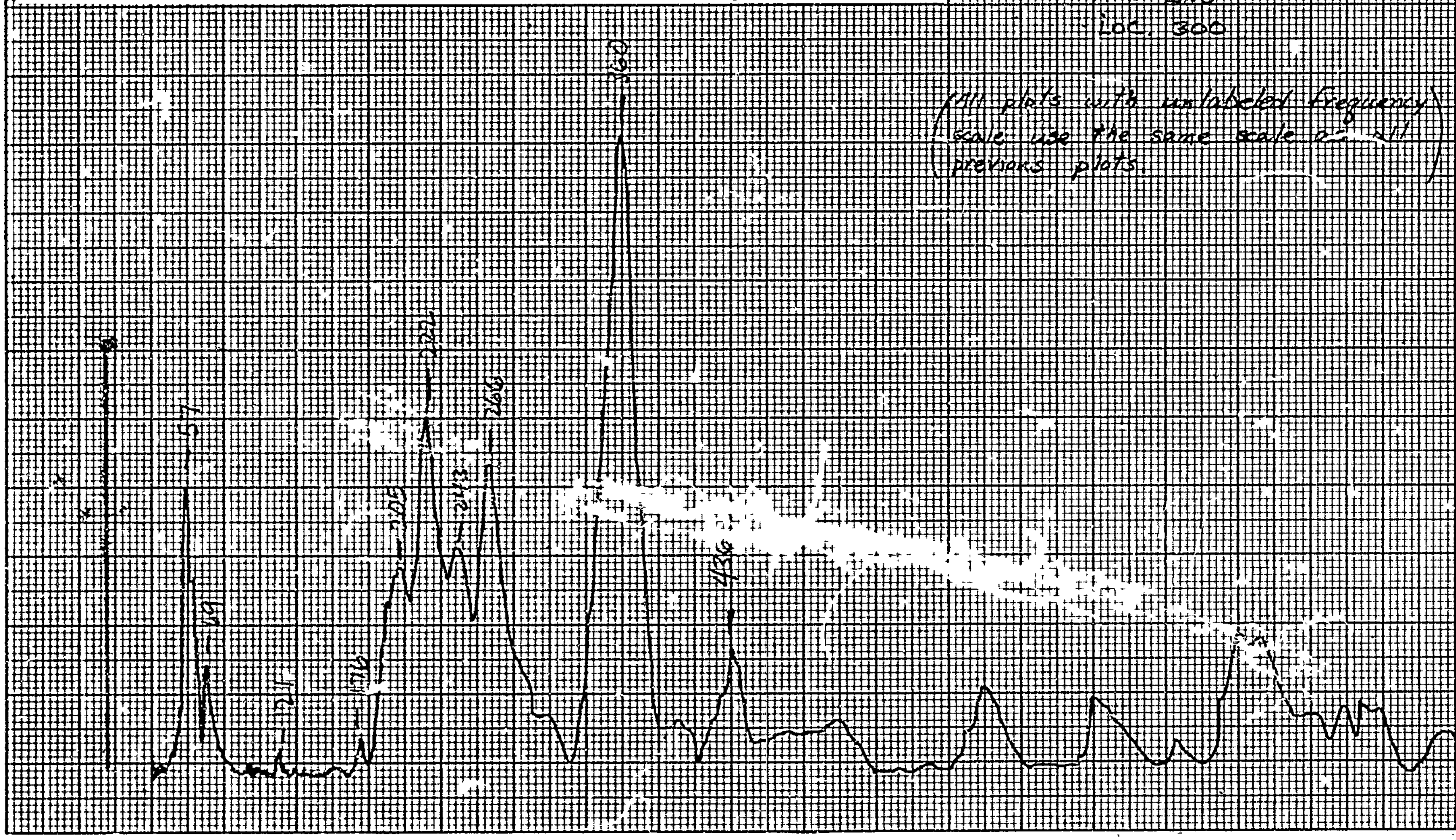

Figure 29. Frequency Response Plot for Position No. 300, Motor Aft End, S/S Poseidon C-3

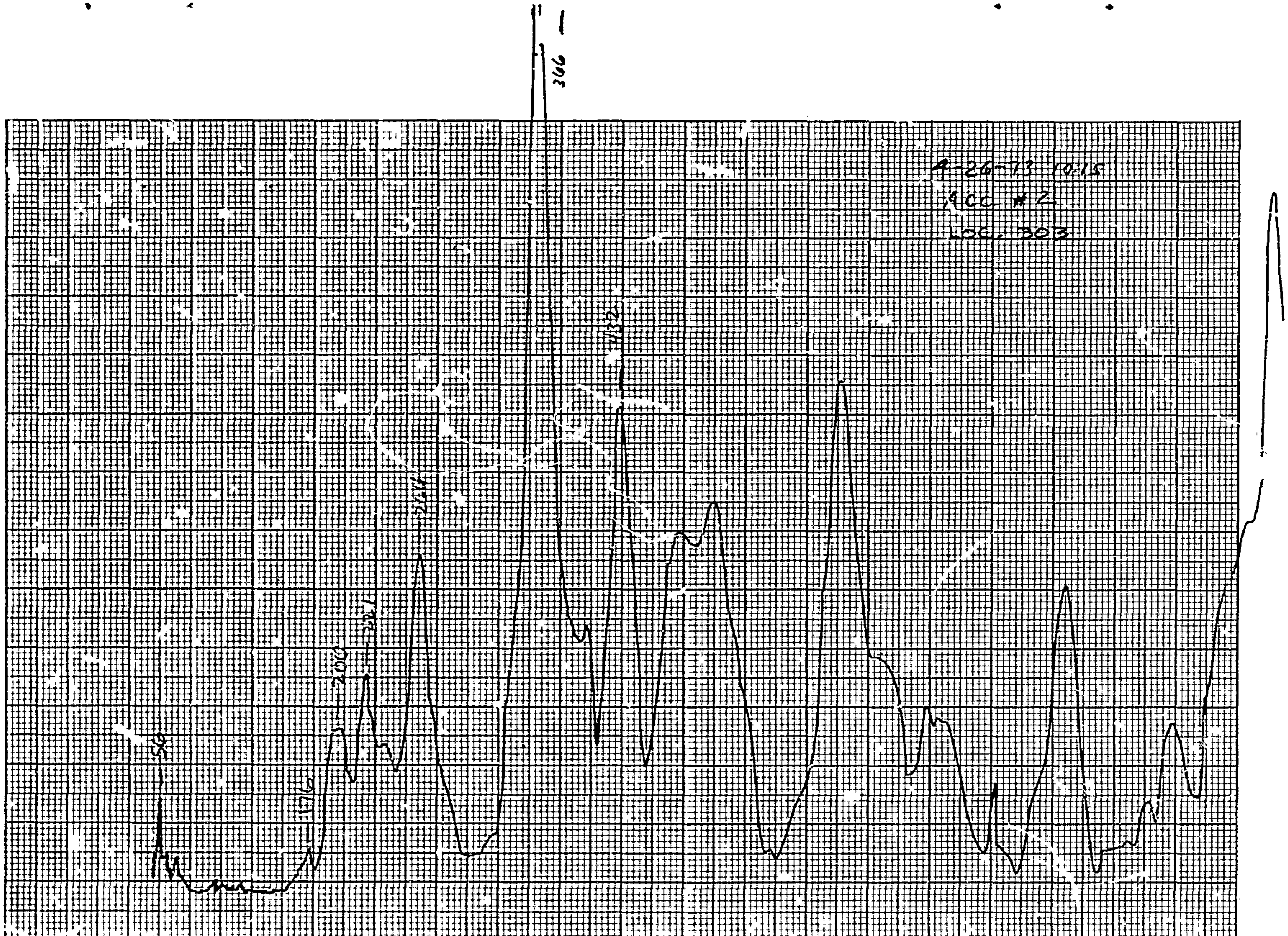

Figure 30. Freque~~y Response Plot for Position No. 303, Motor Aft End, S/S Poseidon C-3

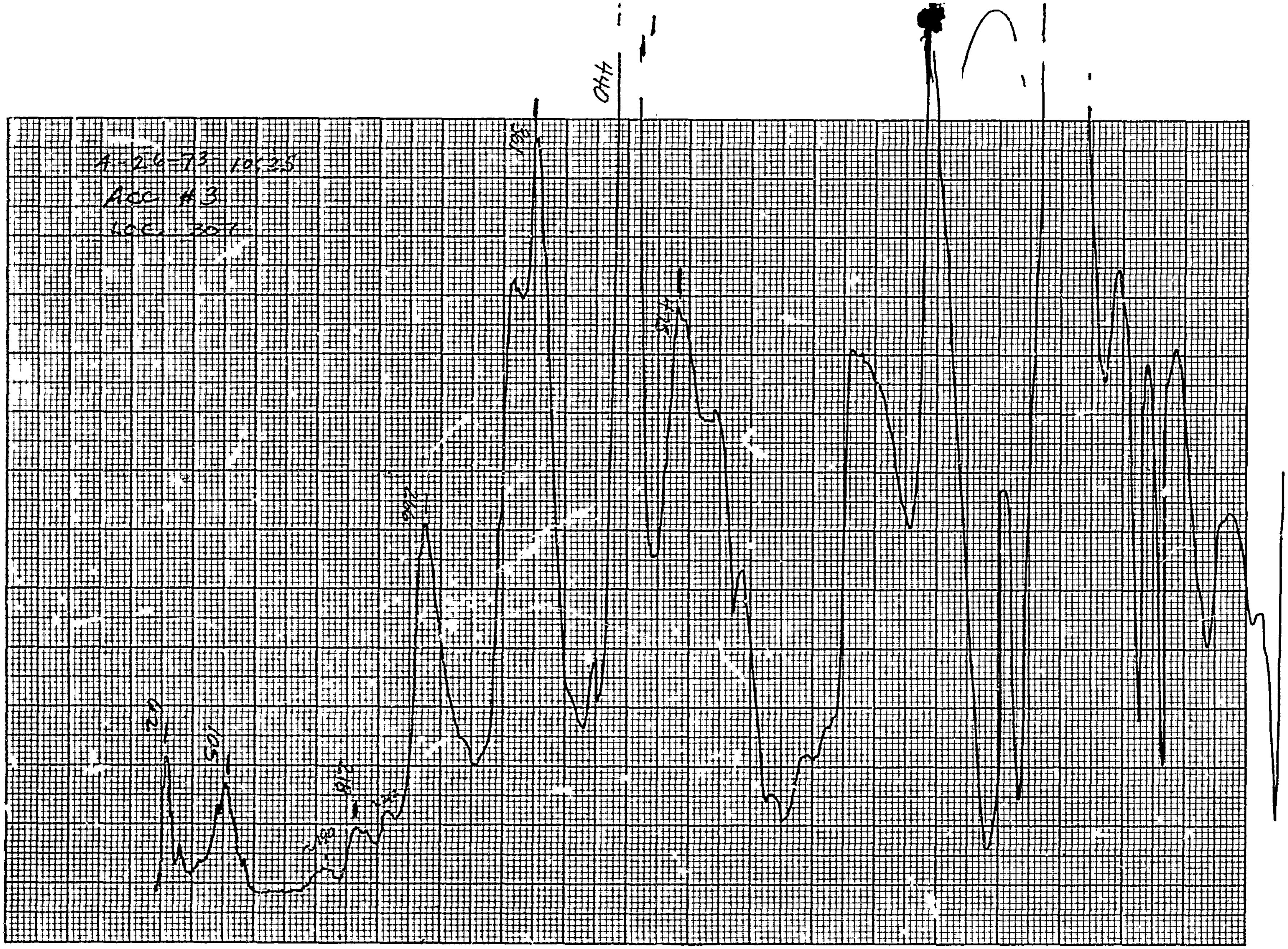

Figure 31. Frequency Response Plot for Position No. 307, Motor Aft End, S/S Poseidon C-3

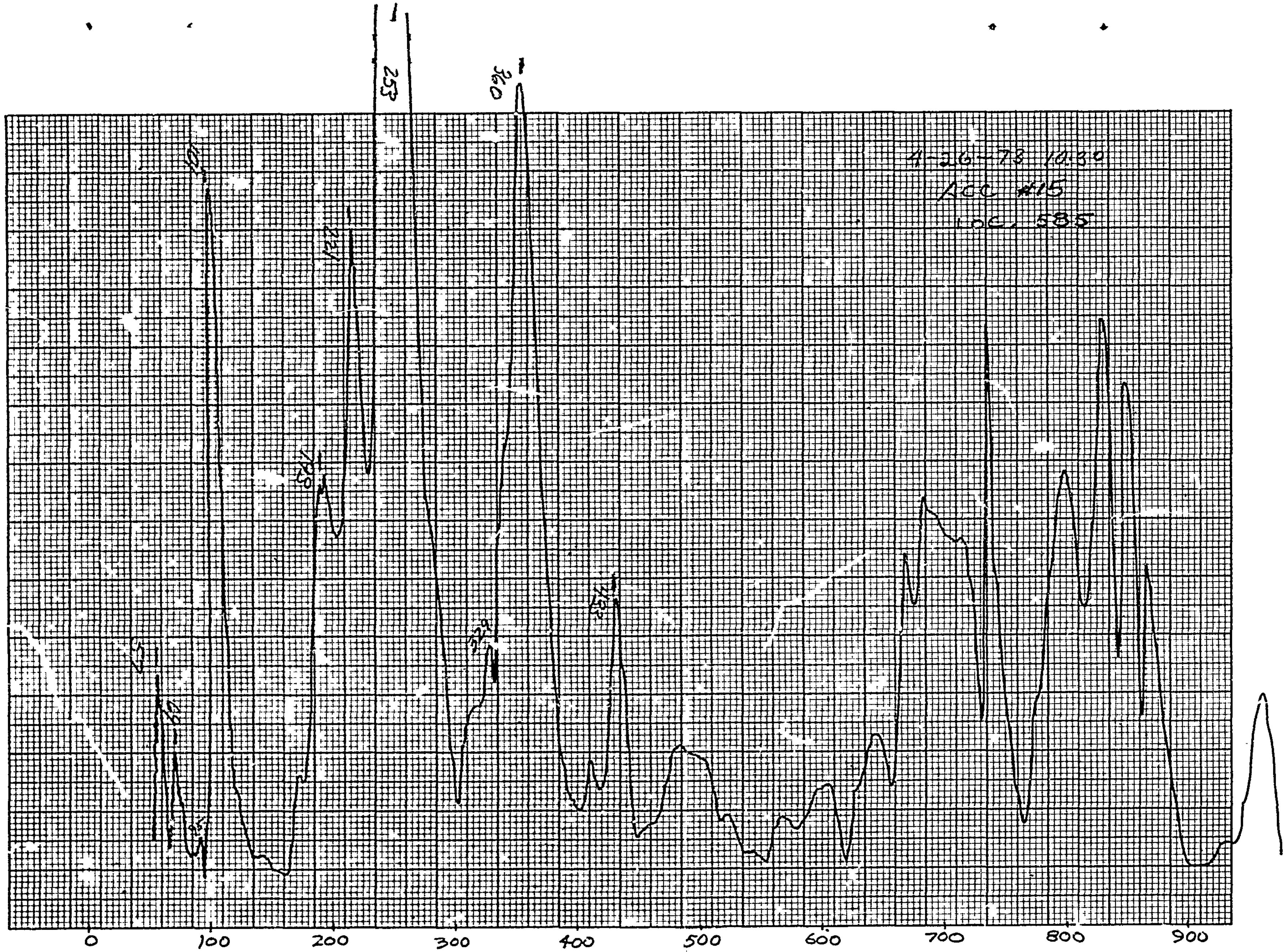

Figure 32. Frequency Response Plot for Position No. 585, Motor Aft End, S/S Poseidon C-3

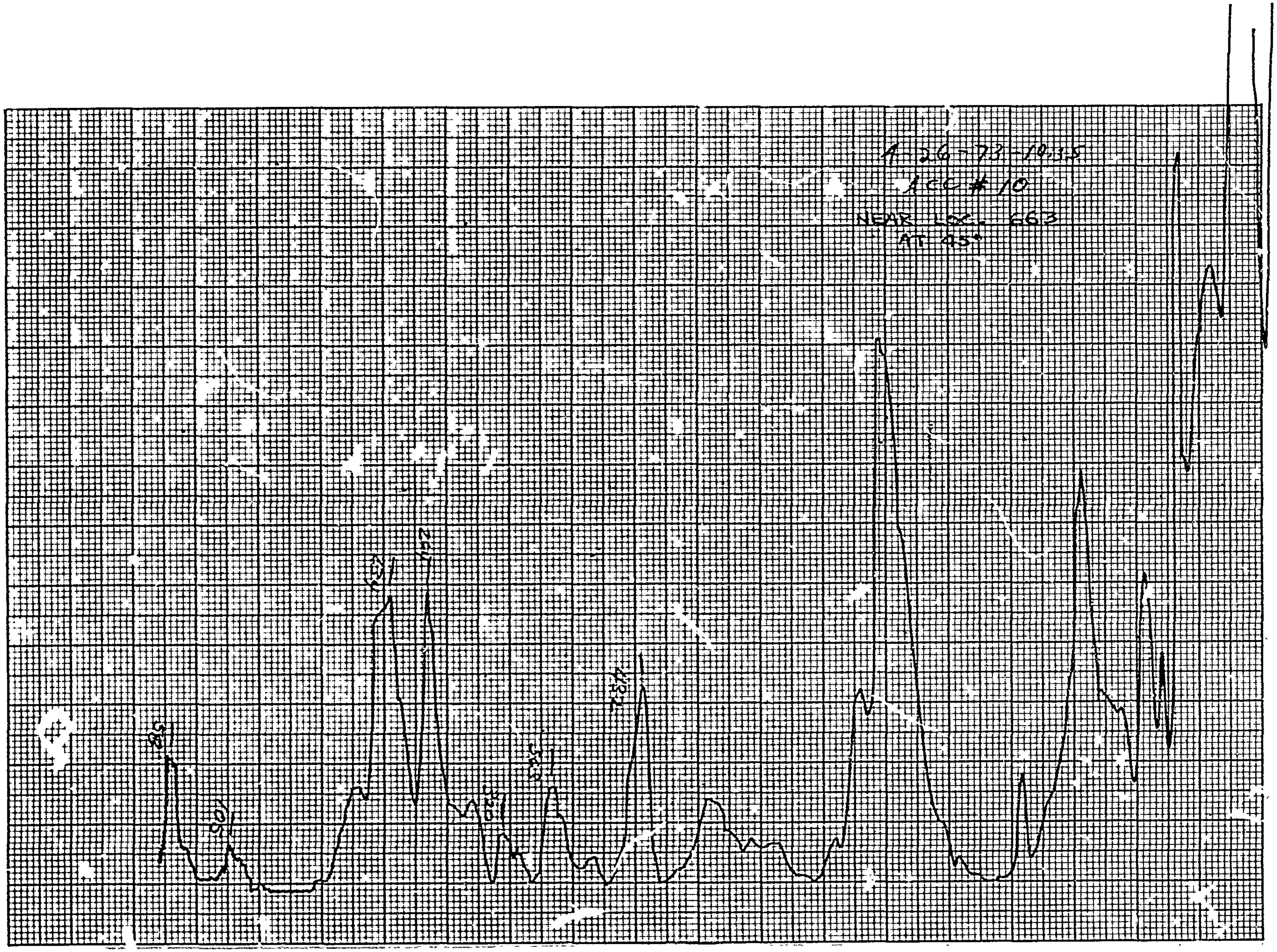

Figure 33. Frequency Response Plot for Position Near 663 at 45°, Motor Aft End, S/S Poseidon C-3

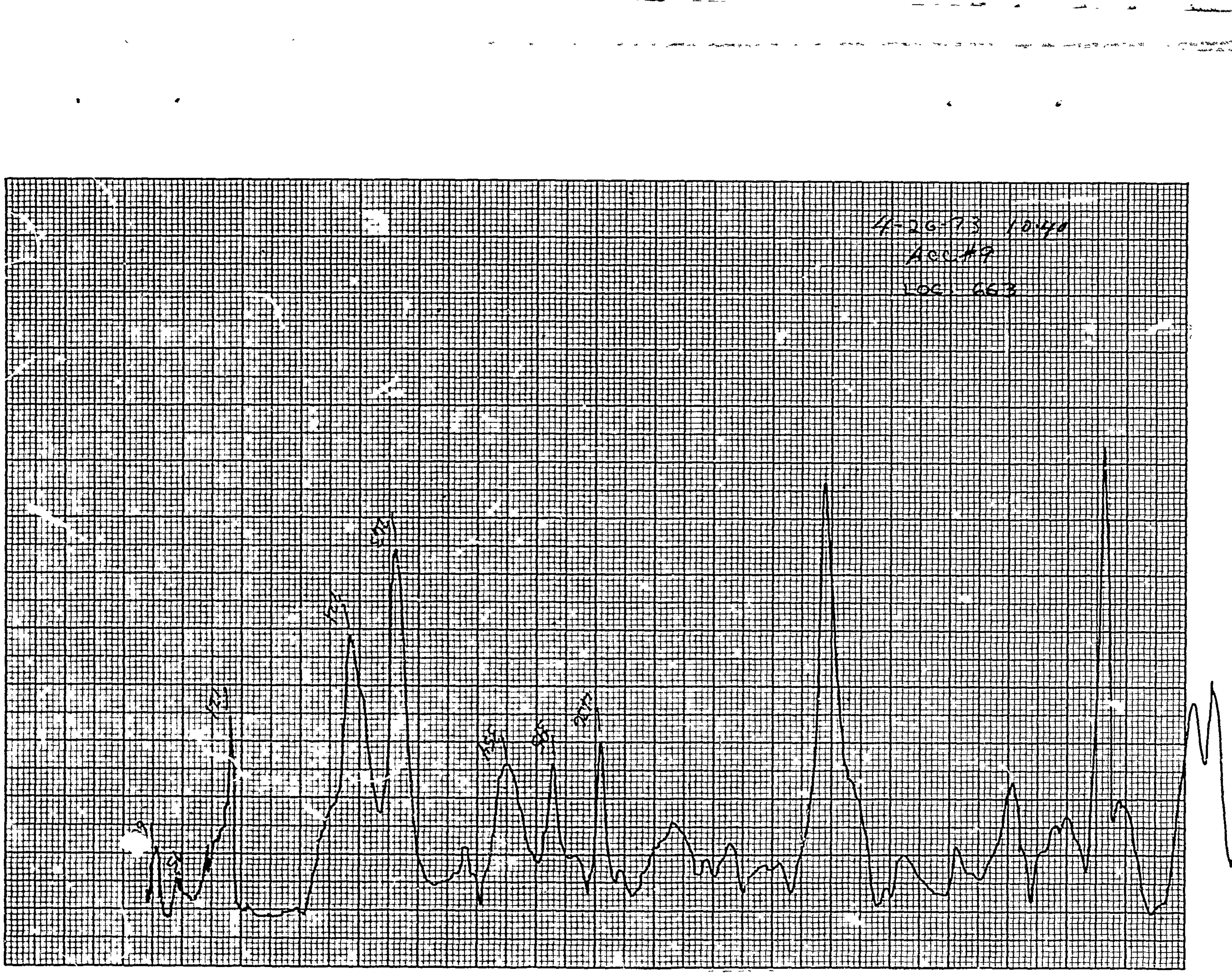

Figure 34. Frequency Response Plot for Position No. 663, Motor Aft End, S/S Poseidon C-3

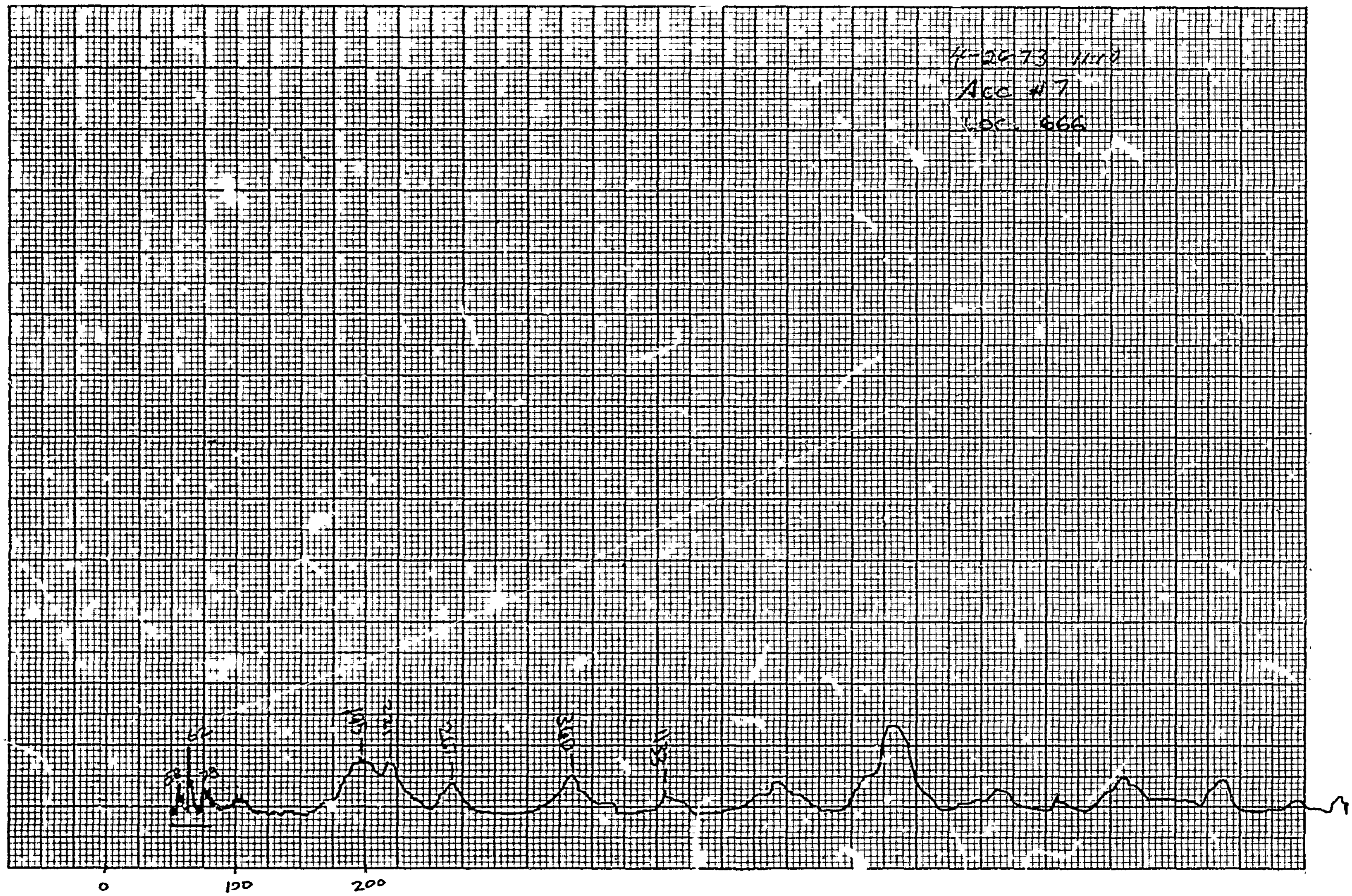

Figure 35. Frequency Response Plot for Position No. 666, Motor Aft End, S/S Poseidon C-3

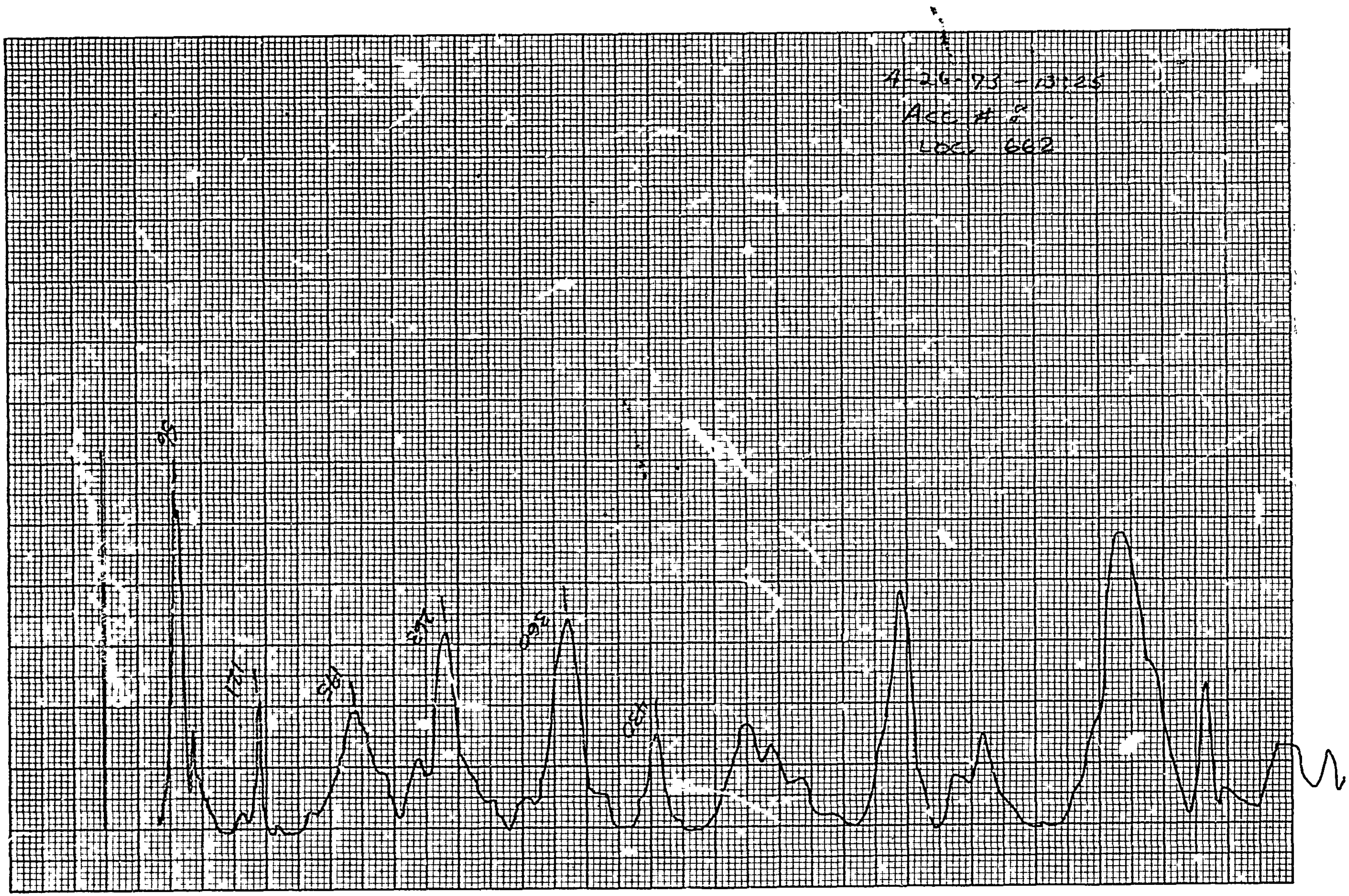

Figure 36. Frequency Response Plot for Position No. 662, Motor Aft End, S/S Poseidon C-3

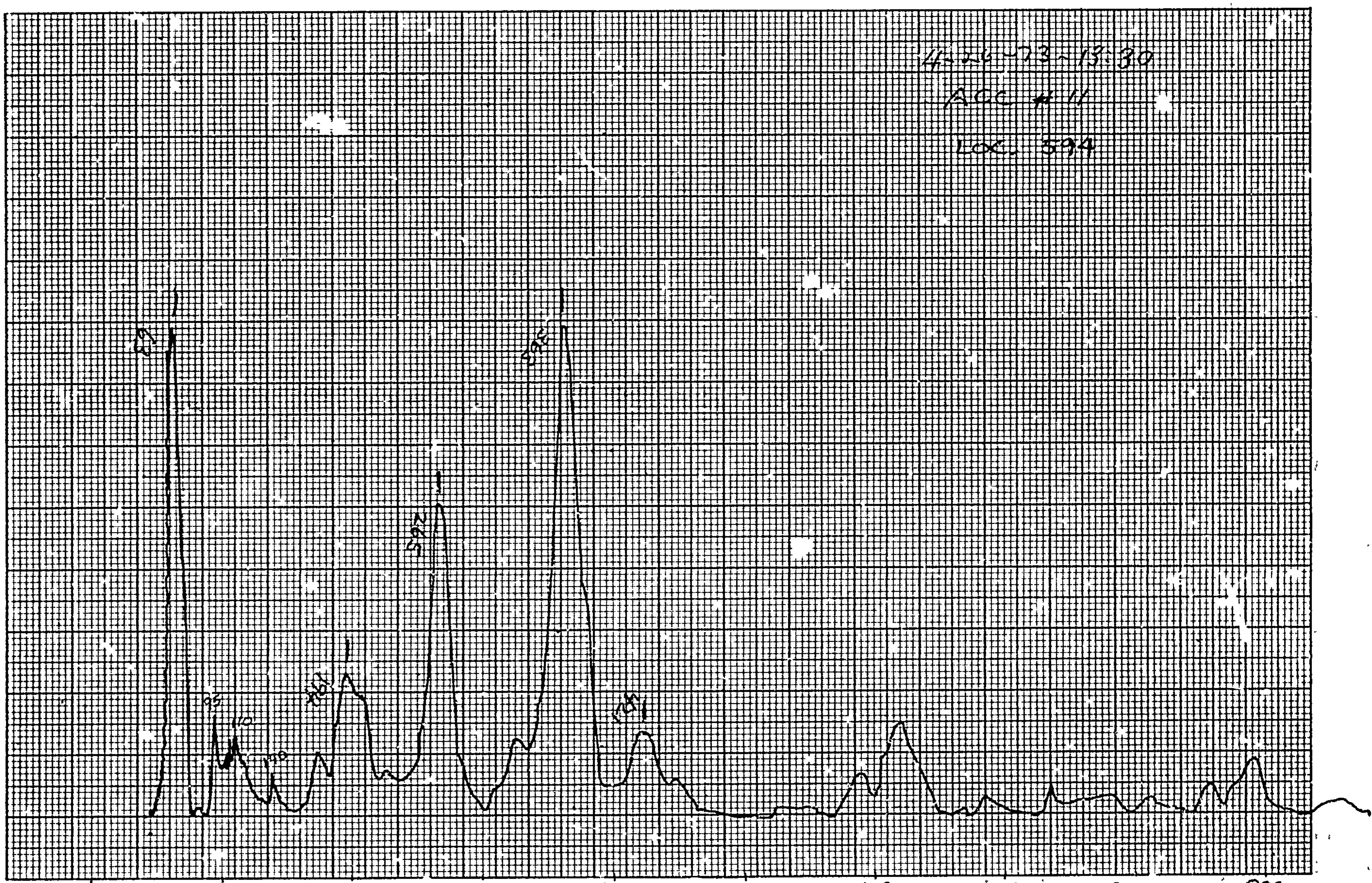

Figure 37. Frequency Response Plot for Position No. 594, Motor Aft End. S/S Poseidon C-3

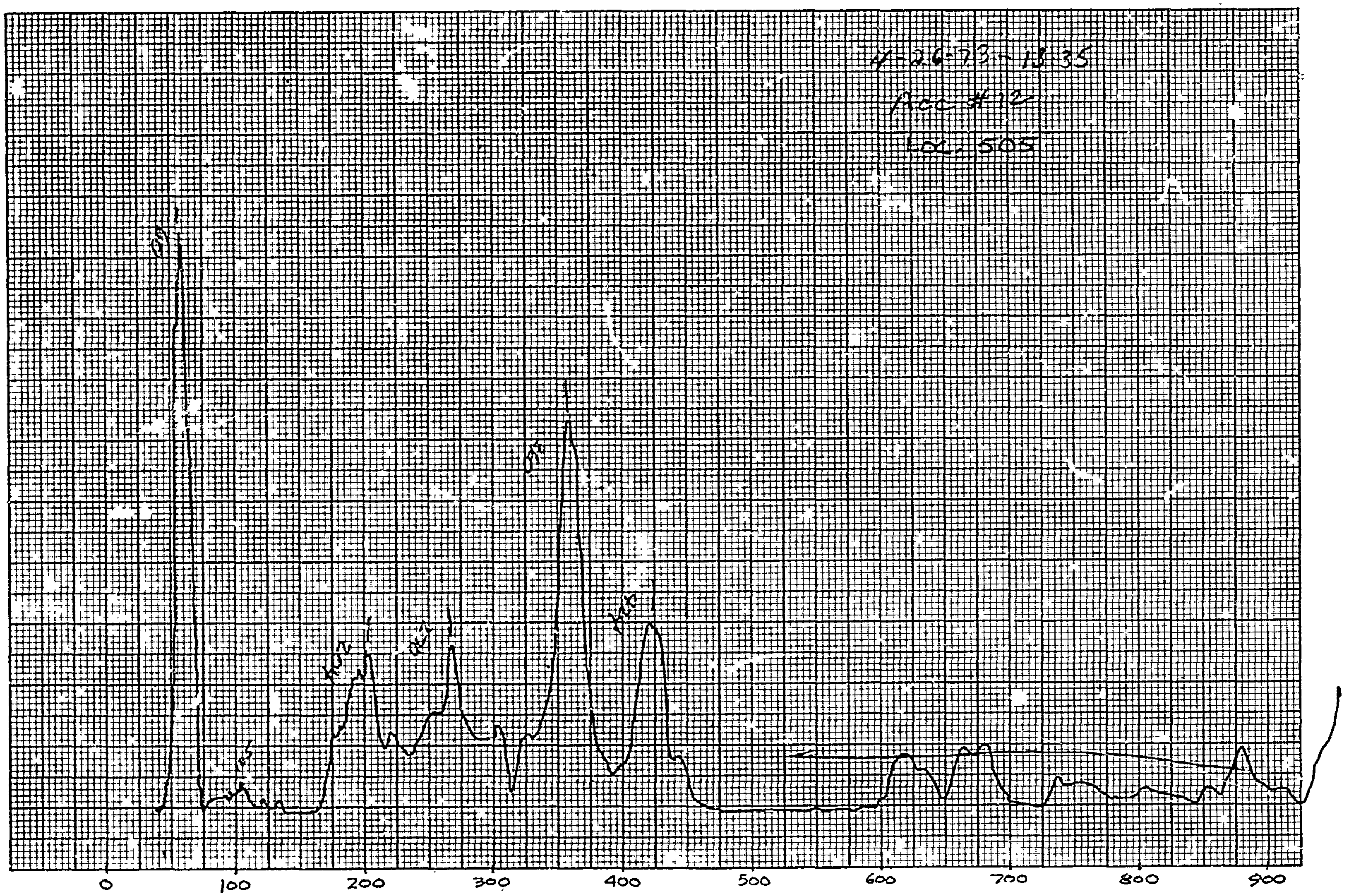

Figure 38. Frequency Response Plot for Position No. 505. Motor Aft End, S/S Poseidon C-3

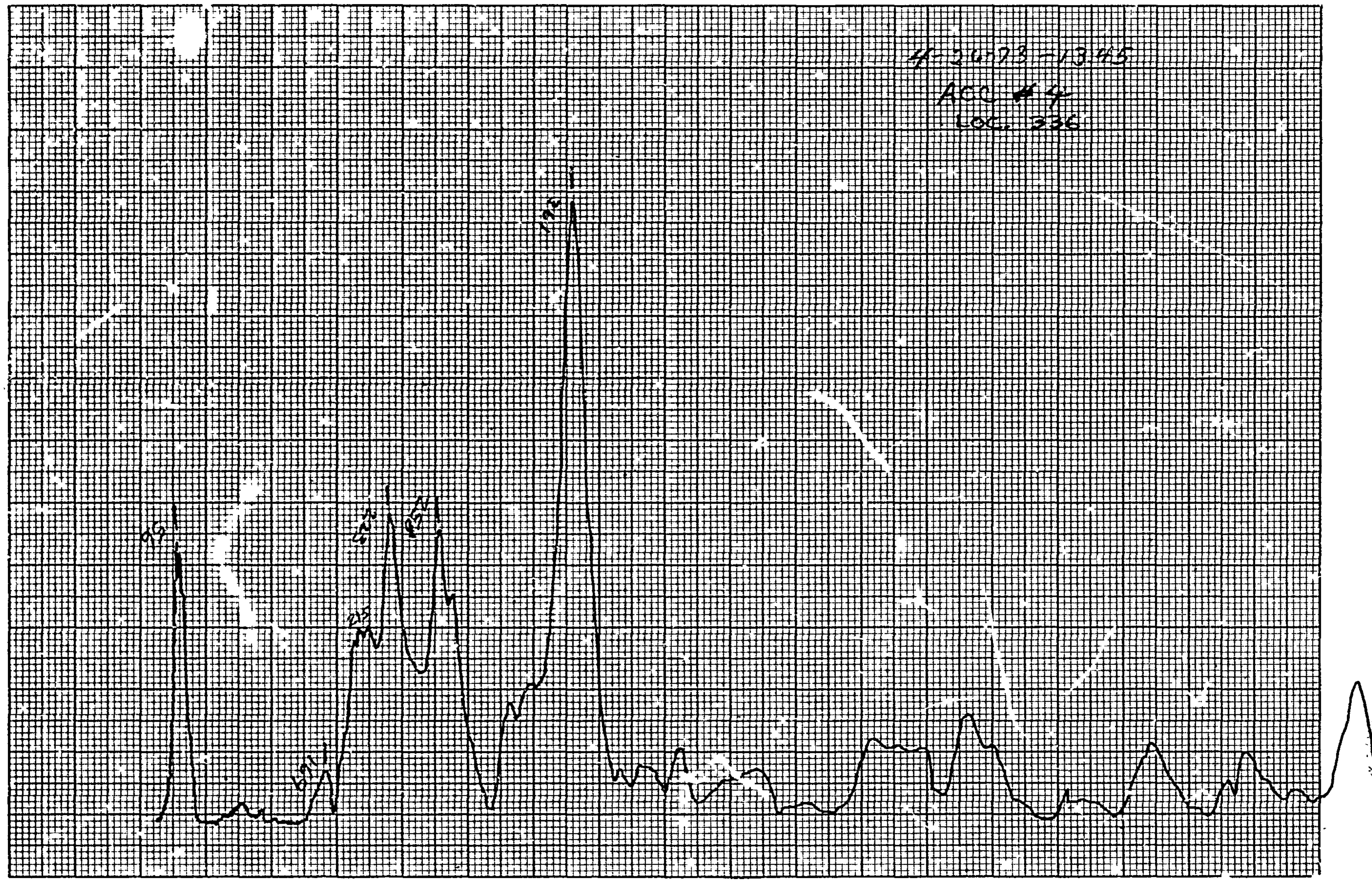

Figure 39. Frequency Response Plot for Position No. 336, Motor Aft End, S/S Poseidon C-3

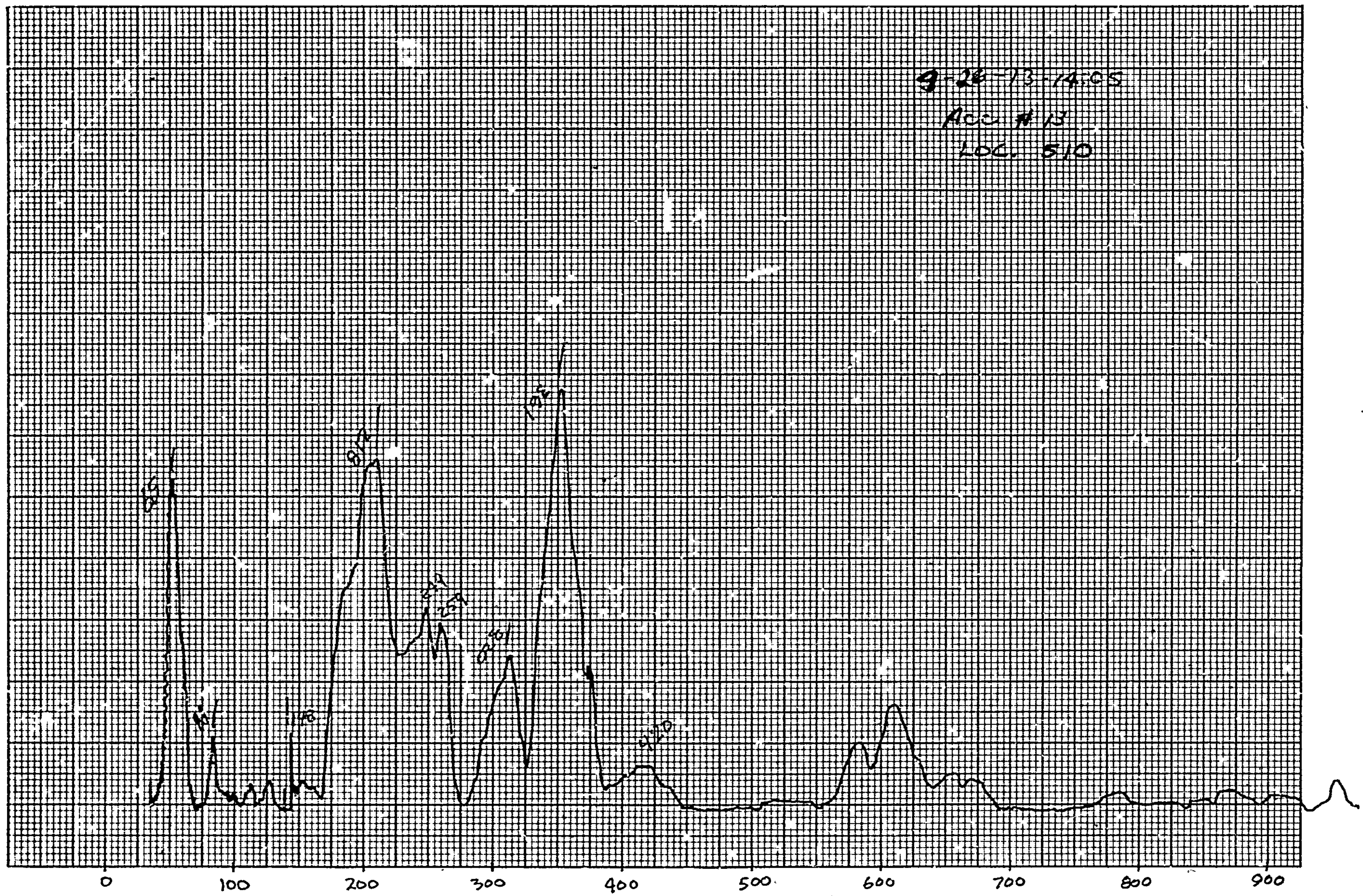

Figure 40. Frequency Response Plot for Position No. 510, Motor Aft End, S/S Poseidon C-3

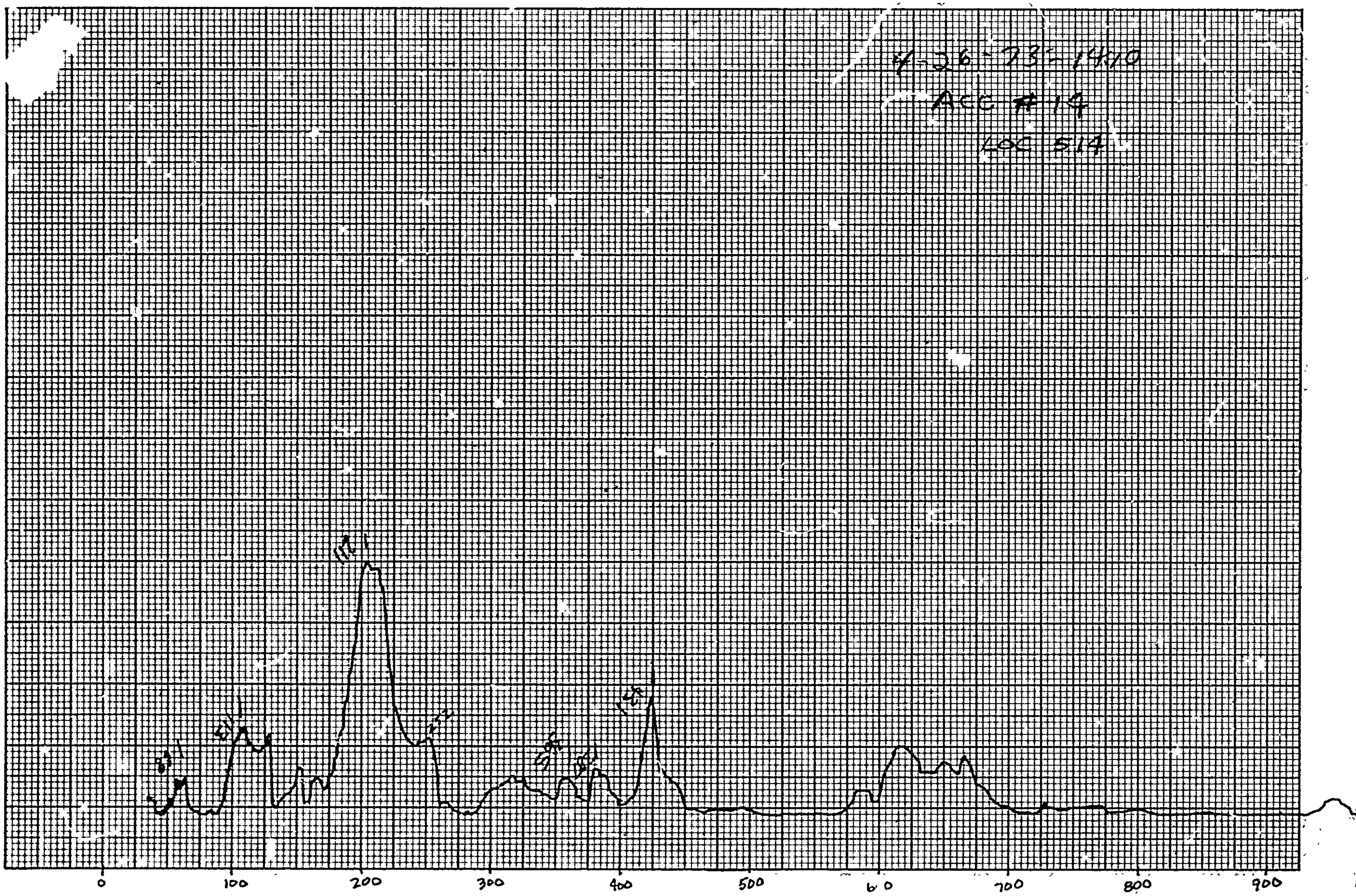

Figure 41   Frequency Response Plot for Position No. 514, Motor Aft End, S/S Poseidon C-3

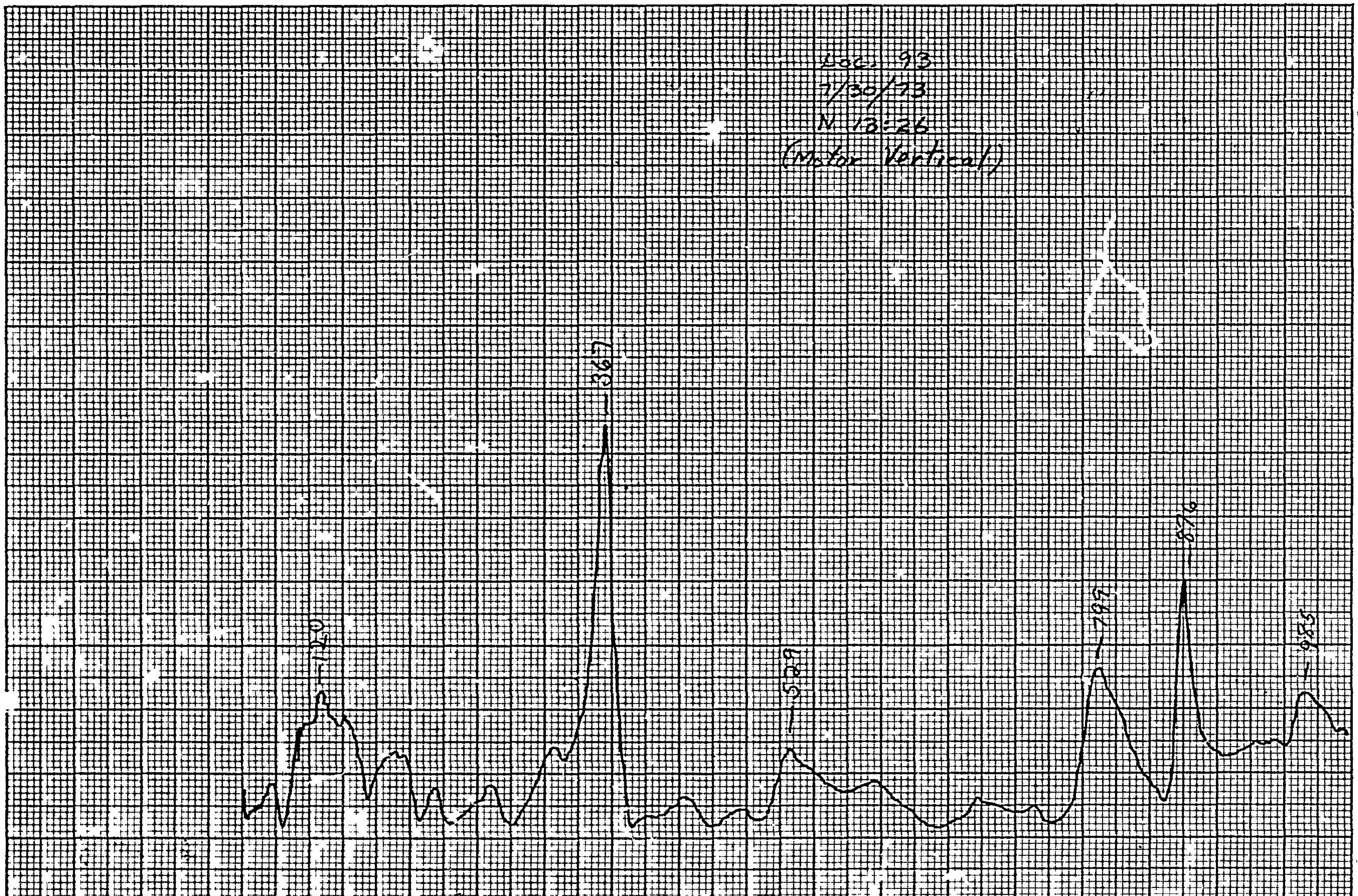

Figure 42. Frequency Response Plot for Position No. 93 Using Nitrogen Gas for Pressurization

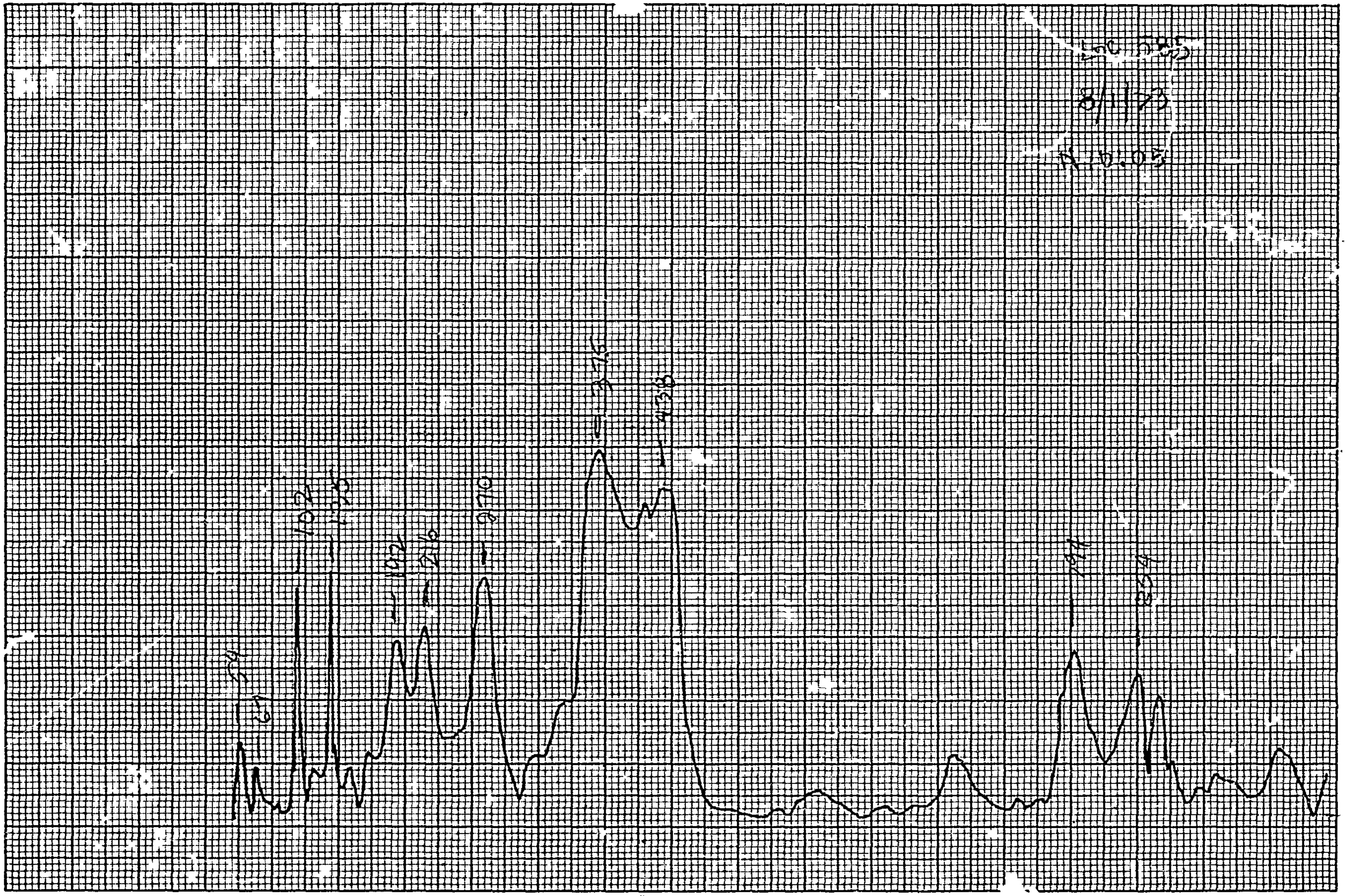

Figure 43. Baseline Frequency Response Data for Position No. 585 Using Nitrogen Gas for Chamber Pressurization

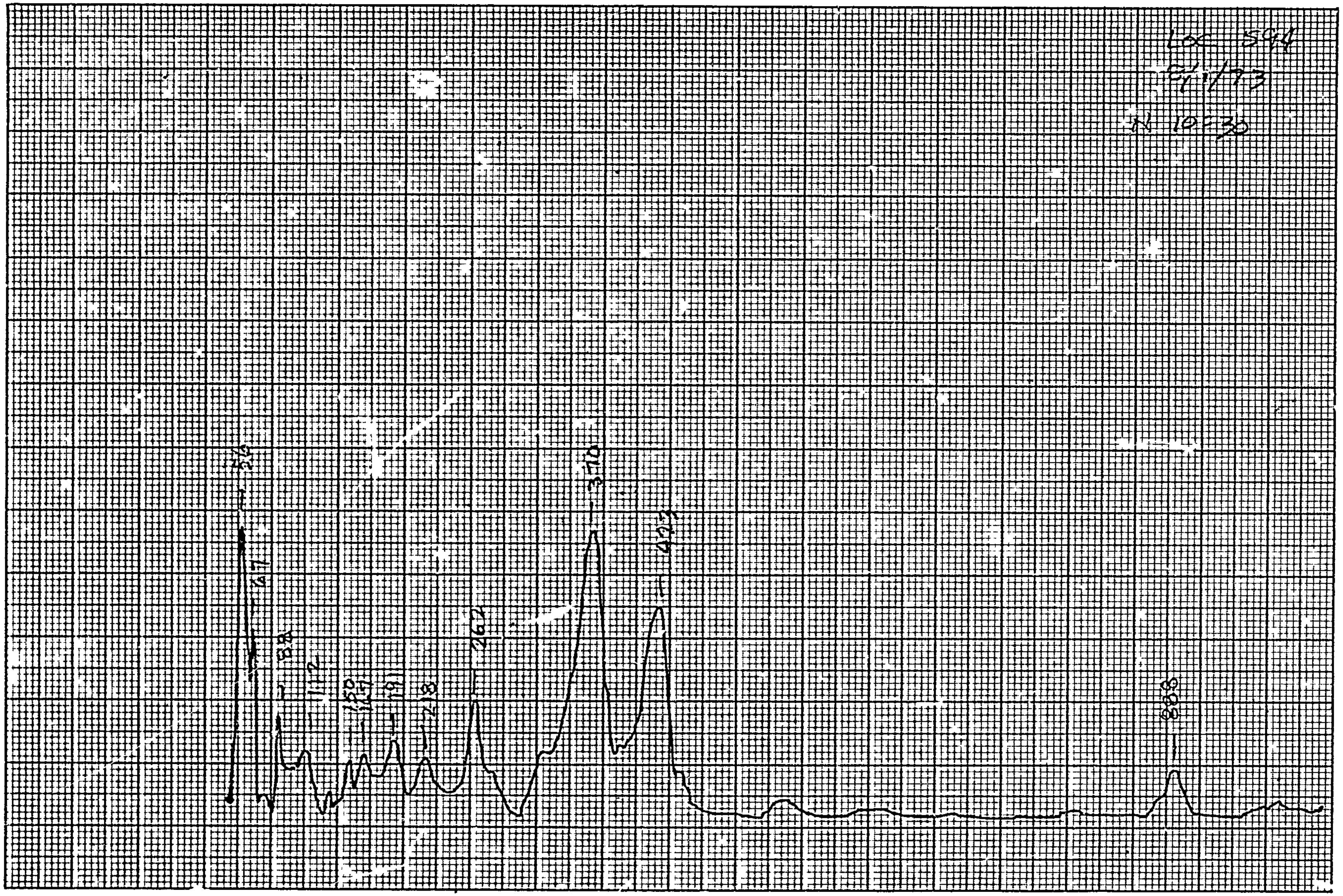

Figure 44. ‹line Frequency Response Data for Position No. 594 Using Nitrogen Gas for
‹namber Pressurization

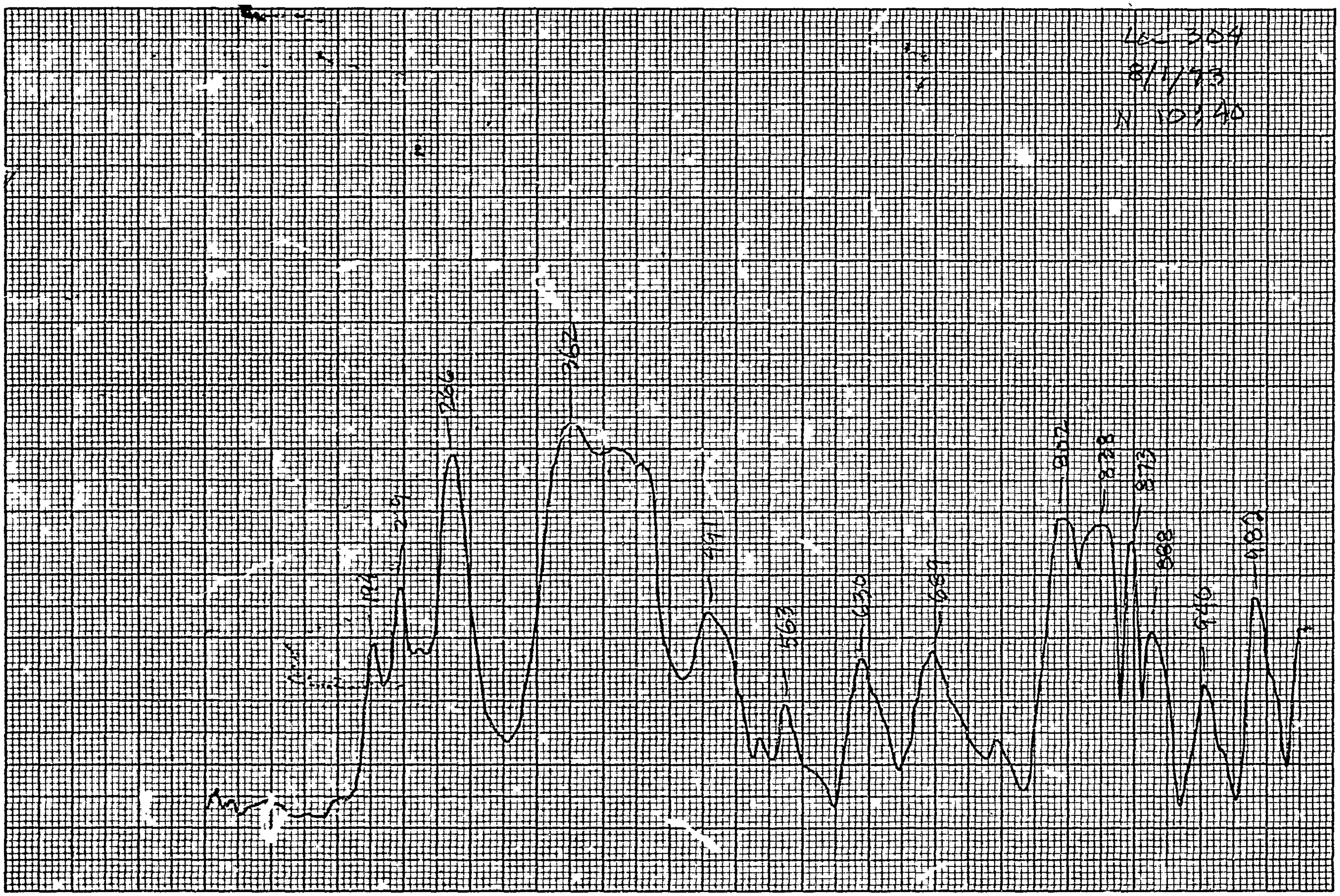

Figure 45. Baseline Frequency Response Data for Position No. 304 Using Nitrogen Gas for Chamber Pressurization

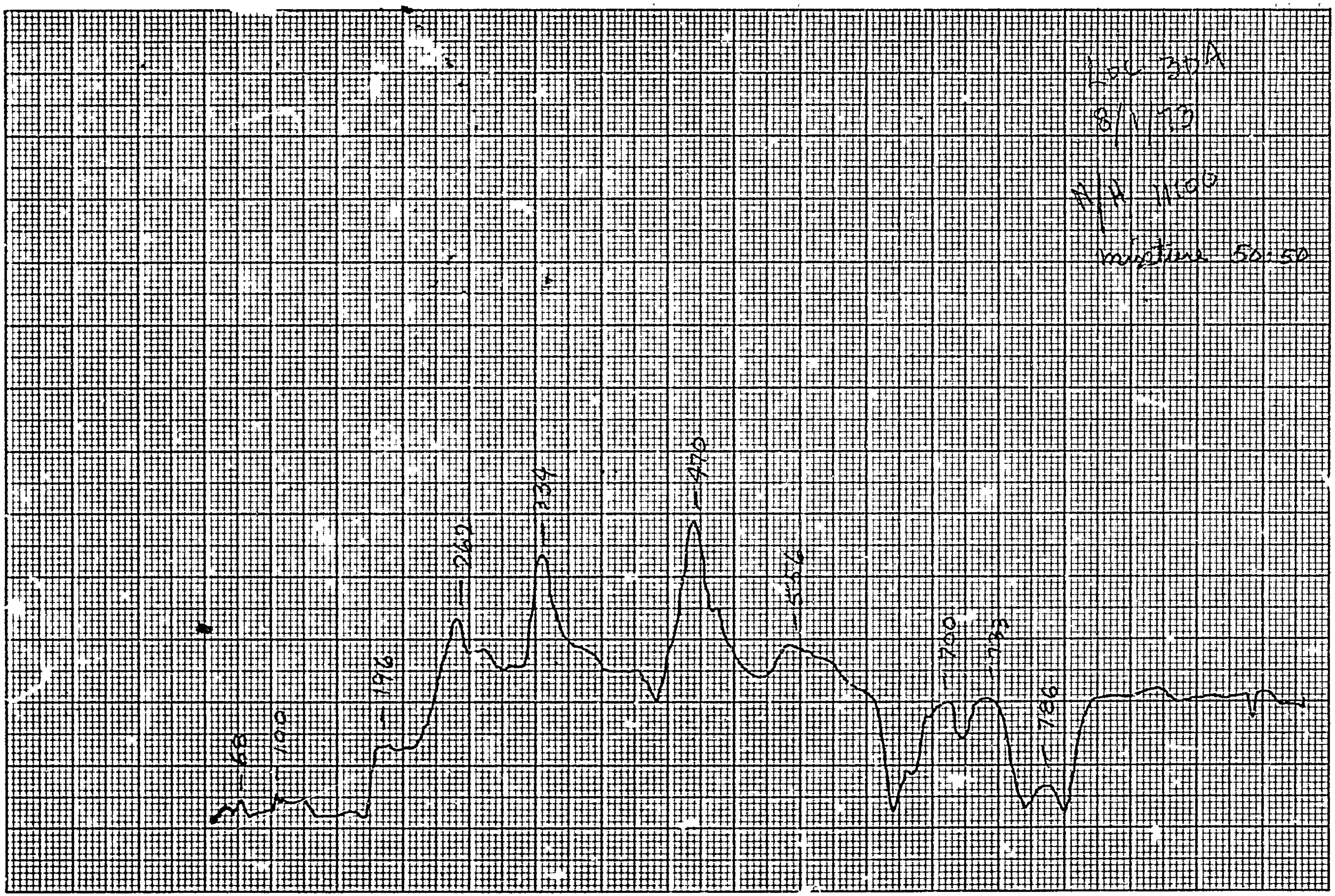

Figure 46. Frequency Response Data for Position No. 304 Using a Nitrogen/Helium Gas Mixture for Chamber Pressurization

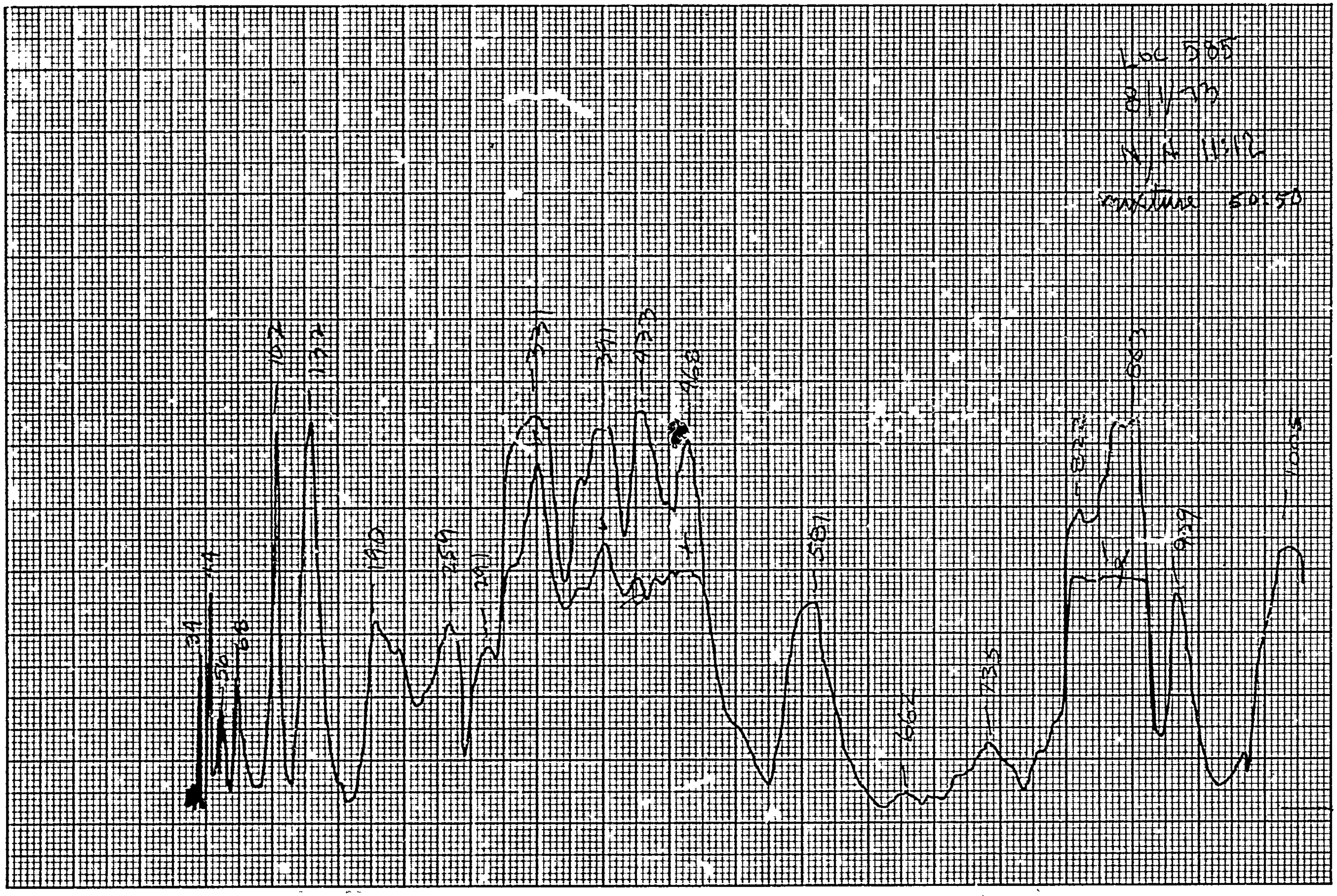

Figure 47. Frequency Response Data for Position No. 585 Using a Nitrogen/Helium Gas Mixture for Chamber Pressurization

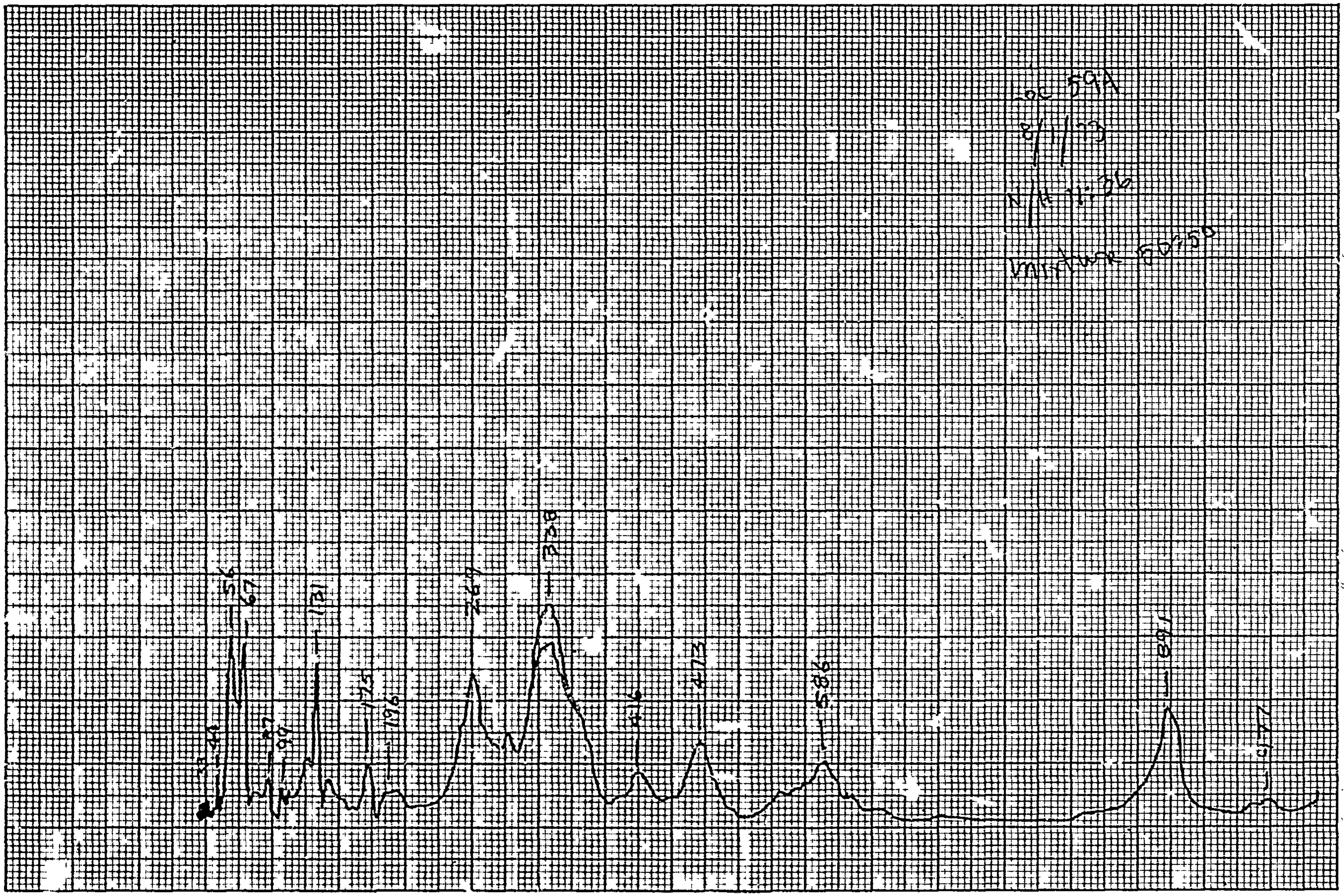

Figure 48. Frequency Response Data for Position No. 594 Using a Nitrogen/Helium Gas Mixture for Chamber Pressurization

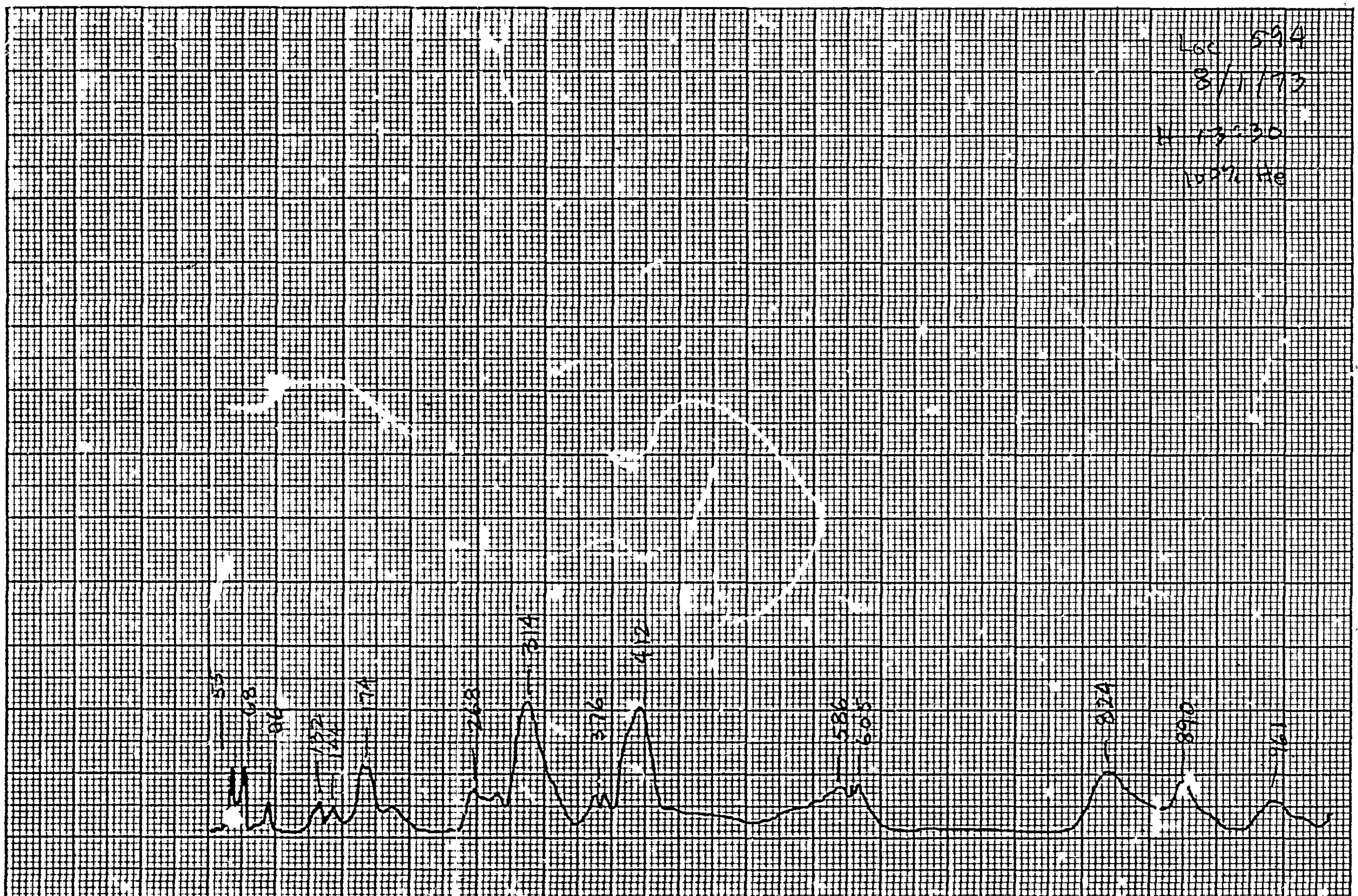

Figure 49. Frequency Response Data for Position No. 5'4 Using Helium Cas for Chamber Pressurization

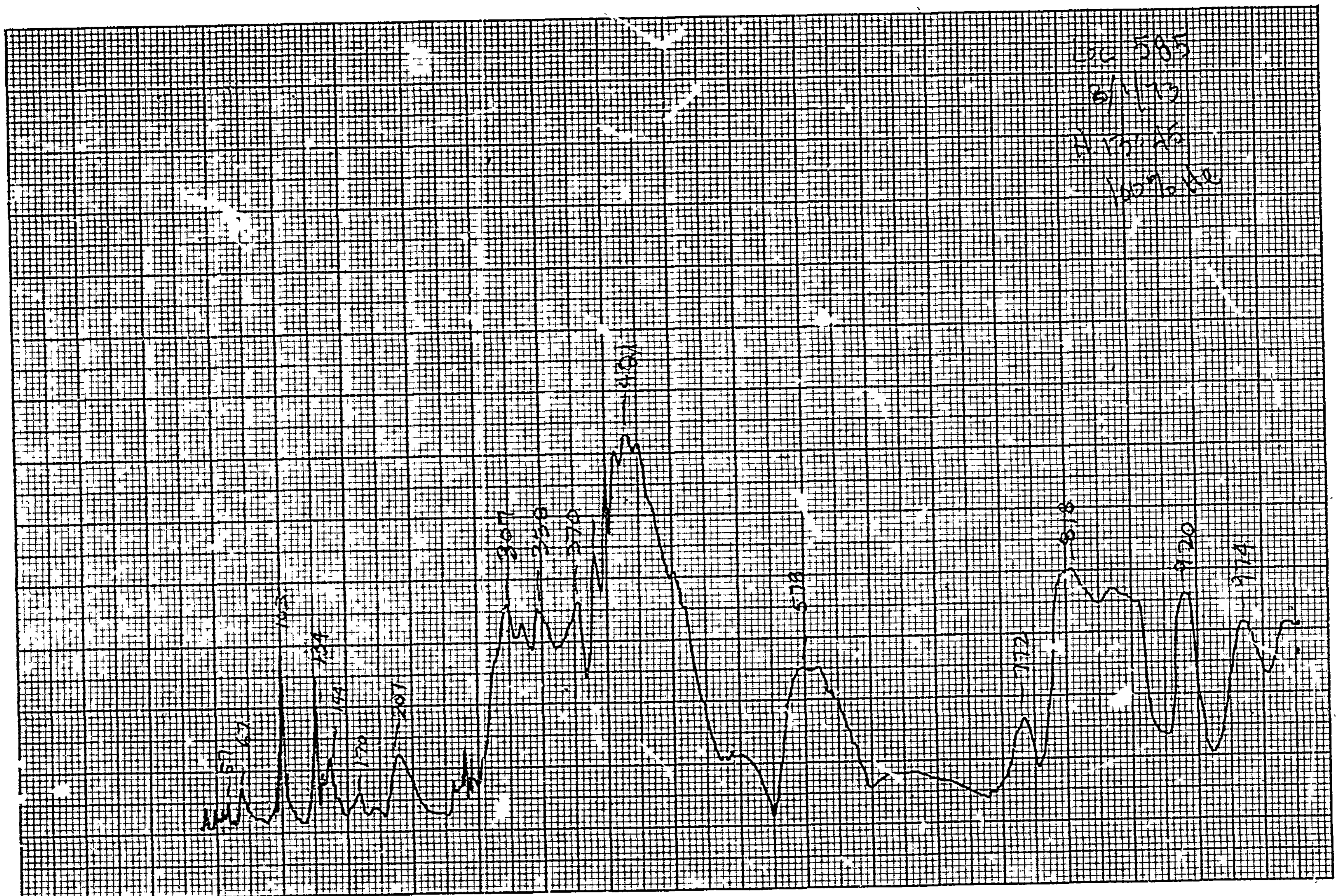

Figure 50. Frequency Response Data for Position No. 585 Using Helium Gas for Chamber Pressurization

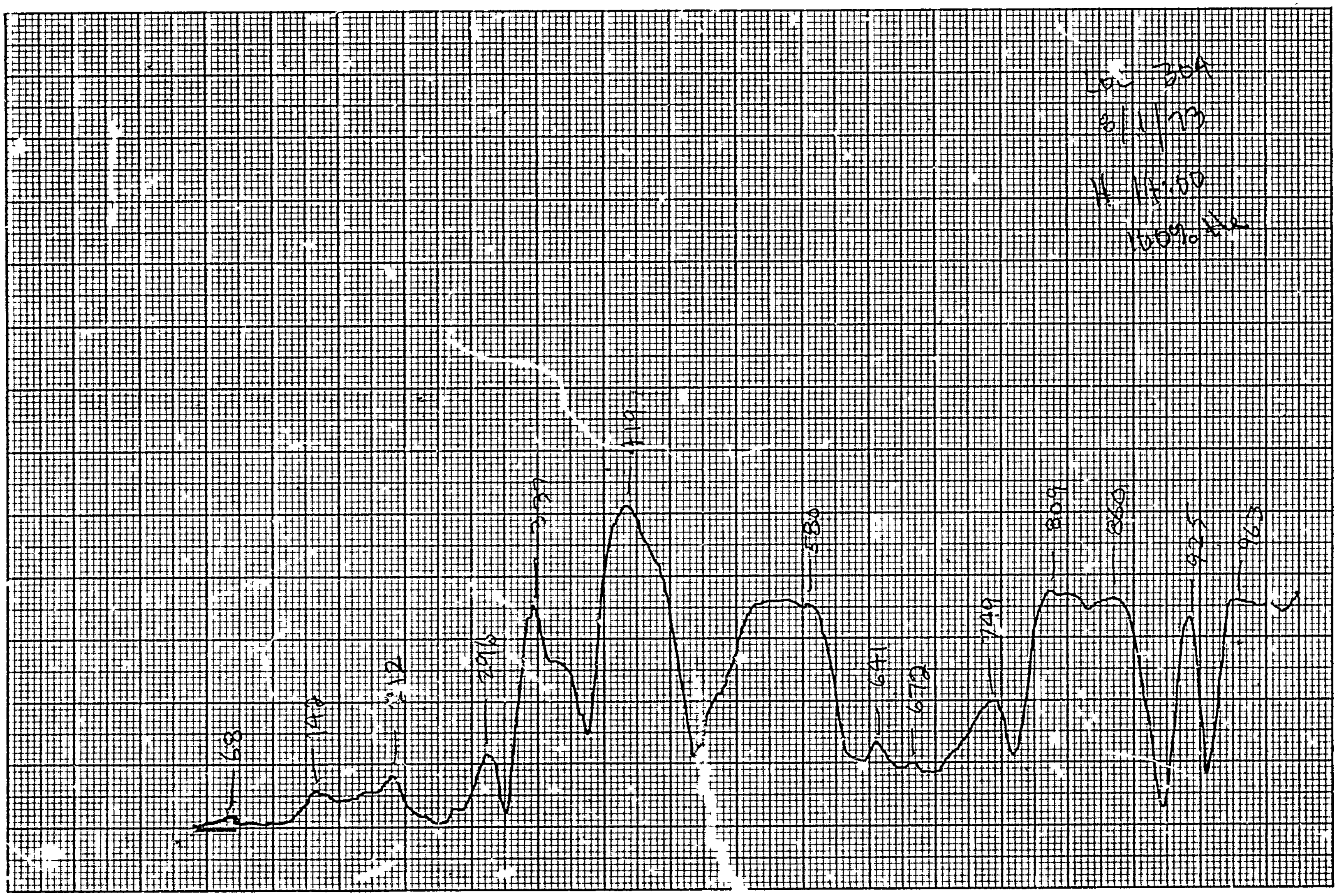

Figure 51. Frequency Response Data for Position No. 3(Using Helium Gas for Chamber Pressurization

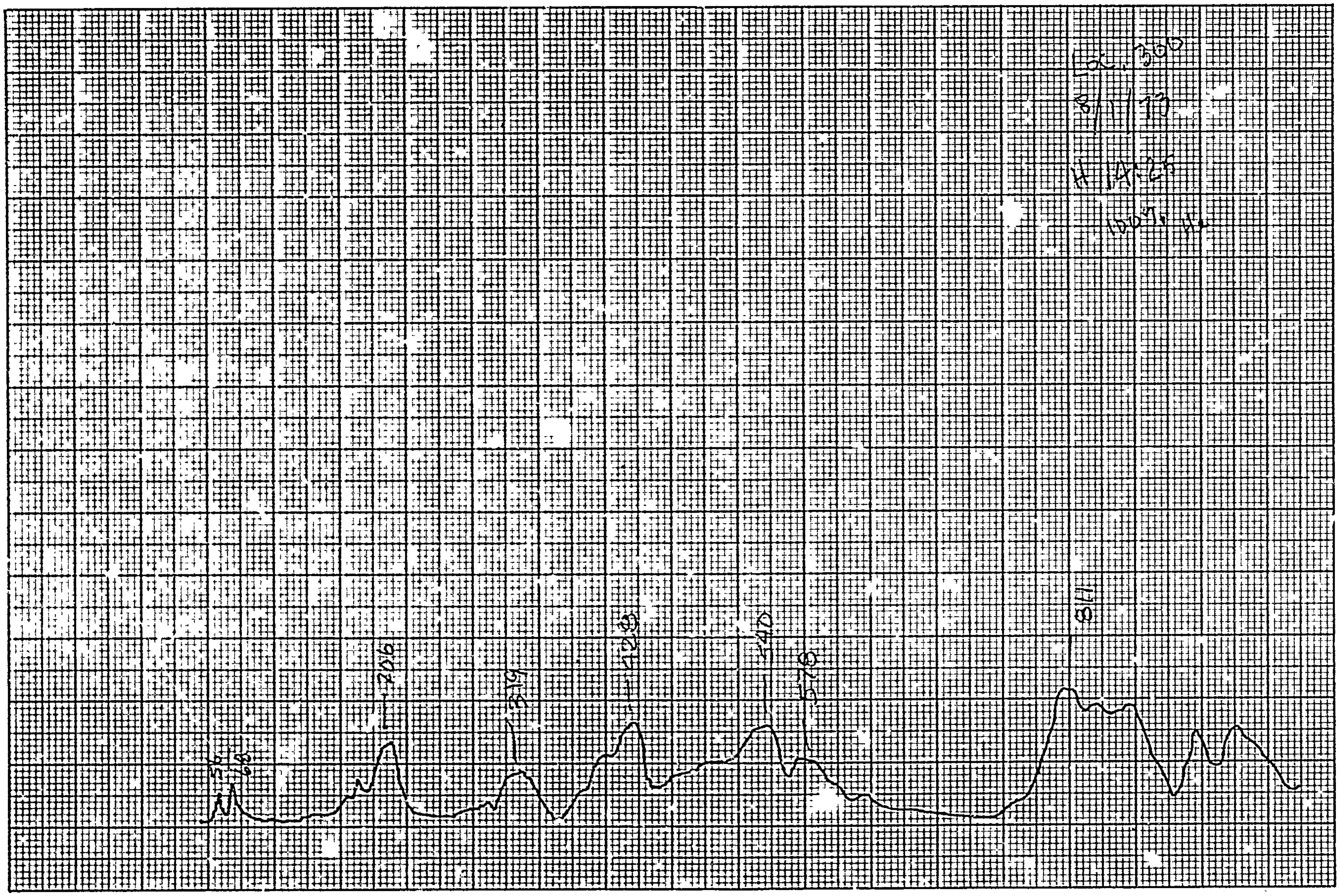

Figure 52. Frequency Response Data for Position No. 300 Using Helium Gas for Chamber Pressurization

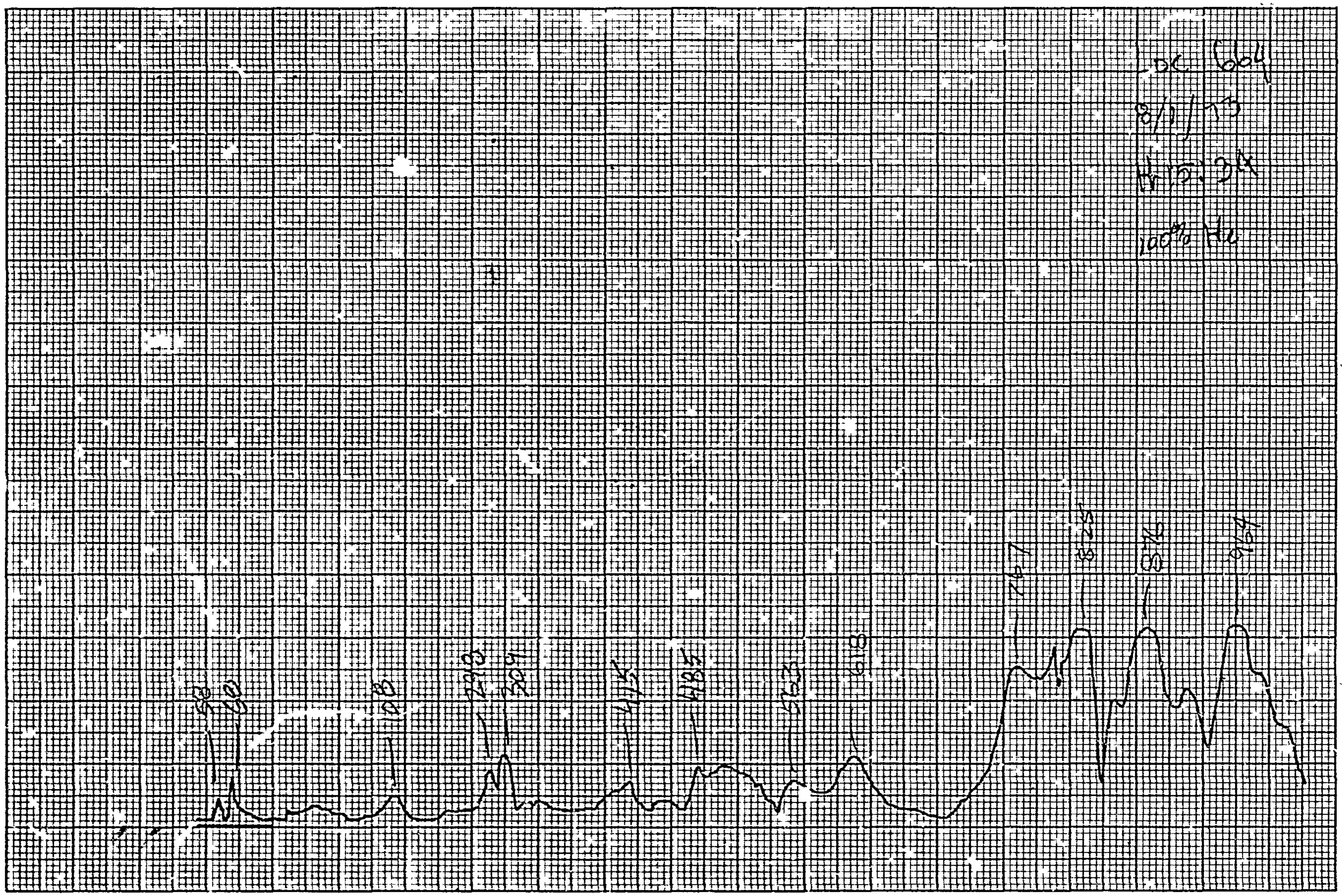

Figure 53. Frequency Response Data for Position No. 664 Using Helium Gas for Chamber Pressurization

APPENDIX A

FORWARD DOME MODE SHAPE MAPPING

(RAW TEST DATA)

Because a large volume of data was produced during the test program, only the most important raw data are included in the final report. All raw data obtained from forward dome mode mapping have been omitted. The deleted raw data are included in the original Task 4 report which is on file at the AFRPL, Edwards, California.

APPENDIX B

ACOUSTIC MODE MAPPING RESULTS

(RAW TEST DATA)

This appendix has been abridged by including only data for the 265 Hz and 364 Hz mappings.

Test Series 6-19-73

Speaker: Type Utah 8", Location Fwd Slots, Voltage 8 (RMS)

Data from Acc Mic No.

Motor Pressure 50 Phase Ret Station 300

Frequency 265 Established at Station 300

Station	Voltage (RMS) v	Phase Angle ϕ	Station	Voltage (RMS) v	Phase Angle
1	0.139	-30	21	0.069	-56
2	0.143	-30	22	0.048	-75
3	0.131	-33	23	0.036	-115
4	0.119	-38	24	0.045	-162
5	0.093	-43	25	0.070	-175
6	0.068	-54	26	0.090	-174
7	0.052	-73	27	0.107	-163
8	0.030	-130	28	0.126	+156
9	0.041	-165	29	0.129	+156
10	0.065	-175	30	0.131	+156
11	0.087	+167	2	0.139	-30
12	0.108	+162	31	0.136	-33
13	0.121	+156	32	0.143	-24
14	0.133	+151	33	0.139	-32
15	0.124	+142	17	--	--
16	0.140	-30	14	0.123	+147
17	0.139	-30	34	0.126	+149
18	0.131	-32	35	0.128	+152
19	0.115	-40	36	0.130	+156
20	0.092	-46	29	--	--

ACOUSTIC MODE MAPPING

Test Series 5-23-73

Speaker: Type Utah 8", Location Fwd Slots, Voltage 8 (RMS)

Data from Acc Mic No.

Motor Pressure 50 Phase Ret Station 300

Frequency 364 Established at Station 300

Station	Voltage (RMS) V	Phase Angle Ø	Station	Voltage (RMS) V	Phase Angle
1	0.159	-173	26	0.194	+32
2	0.086	+126	27	0.061	-75
3	0.257	+64	28	0.267	-121
4	0.458	+54	29	0.465	-127
5	0.610	+50	30	0.626	-132
6	0.691	+48	2		
7	0.718	+47	31		
8	0.665	+44	32		
9	0.544	+42	33		
10	0.331	+35	17	Couldn't read due to	
11	0.176	+21	14	open ground	
12	0.125	-80	34		
13	0.344	-120	35		
14	0.537	-126	36		
15	0.673	-125	29		
16	0.159	-165	15 - 0°	0.641	-128
17	0.104	+115	15 - 45°	0.575	-136
18	0.193	+75	15 - 90°	0.614	-136
19	0.370	+59	15 - 135°	0.629	-136
20	0.547	+54	15 - 180°	0.616	-135
21	0.651	+50	15 - 225°	0.612	-135
22	0.704	+50	15 - 45°	0.556	-133
23	0.674	+45	15 - 0°	0.633	-130
24	0.566	+46	15 - 315°	0.638	-133
25	0.408	+44	15 - 270°	0.629	-130

APPENDIX C

MOTOR AFT-END MODE SHAPE MAPPING

(RAW TEST DATA)

This appendix has been abridged by including data only for the 363 Hz mappings.

Test Series 5-2-73 0915

Speaker: Type Utah 8", Location Fwd Slots, Voltage 8 (RMS)

Data from Acc Mic No.

Motor Pressure 50 Phase Est Station 300

Frequency 363 Established at Station 300

Station	Voltage (RMS) V	Phase Angle Ø	Station	Voltage (RMS) V	Phase Angle Ø
300	0.605	+1	329	1.304	+97
301	0.569	+40	330	1.148	+41
302	0.859	+71	331	1.563	+16
303	1.535	+78	332	2.080	-31
304	2.465	+74	333	1.537	-54
305	2.974	+63	334	0.512	-84
306	2.573	+45	335	0.076	+133
307	1.672	+8	336	0.750	+3
308	1.825	-54	337	0.589	+24
309	2.446	-85	338	0.511	+61
310	2.441	-108	339	1.061	+109
311	1.691	-132	340	1.979	+121
312	0.635	+6	341	2.089	+119
317	2.084	+85	342	0.779	+88
318	1.90	+72	343	1.206	-26
319	1.256	+46	344	2.329	-40
320	0.928	+20	345	1.968	-43
321	1.349	-68	346	0.436	-37
322	1.299	-103	347	0.090	+110
323	0.844	-136	348	0.202	+13
324	0.317	+63	349	0.169	+8
325	0.312	+111	350	0.445	+74
326	0.641	+134	351	1.012	+83
327	1.10	+133	352	1.743	+73
328	1.425	+124	353	2.255	+58

Continuation of Series 5-2-73 0915

Station	Voltage (RMS) ν	Phase Angle ∅	Station	Voltage (RMS) ν	Phase Angle ∅
354	2.455	+36	383	2.230	+78
355	2.296	+10	317	2.053	+86
356	2.049	+17	384	2.059	+86
357	1.677	-48	385	1.999	+85
358	1.390	-84	386	1.914	+92
359	1.172	-120/-128	387	1.840	+93
360	0.701	+1	388	1.659	+94
361	0.727	+13	329	1.320	+102
312	0.693	+12	389	1.152	+108
362	0.494	+4	390	1.186	+122
363	0.320	+21	391	0.822	+124
324	0.295	+62	392	0.757	+131
366	0.648	+70	393	0.860	+131
367	0.674	+62	394	0.879	+131
336	0.739	+3	395	1.084	+129
369	0.804	+6	396	1.264	+127
370	0.845	+14	397	1.536	+126
372	0.666	-31	398	1.783	+123
373	0.471	-32	399	1.896	+119
348	0.216	+16	341	2.099	+115
374	0.135	+30	400	2.304	+112
375	0.226	+68	401	2.761	+108
376	0.330	+67	402	2.943	+103
377	0.393	+43	403	3.233	+98
378	0.459	+16	404	3.276	+95
300	0.674	+1	405	3.419	+90
379	3.088	+64	407	2.734	+68
380	3.029	+62	408	2.576	+68
381	2.795	+67	409	2.158	+68
382	2.518	+71	410	1.970	+61

Continuation of Series 5-2-73 0915

Station	Voltage (RMS) ν	Phase Angle ø	Station	Voltage (RMS) ν	Phase Angle ø
353	2.301	+50	441	0.562	+140
411	2.321	+42	442	0.877	+158
412	2.271	+29	443	0.872	+139
413	2.236	+32	444	0.736	+129
414	2.037	+43	445	0.622	+144
415	1.932	+51	366	0.607	+62
416	1.945	+57	446	1.017	+132
417	2.038	+56	447	1.412	+140
418	2.176	+63	394	0.884	+131
419	2.320	+65	448	2.101	-30
420	2.523	+66	449	2.225	-31
421	2.738	+64	450	0.089	+96
305	2.879	+61	451	0.596	+40
422	0.623	+142	452	2.361	+90
423	0.659	+103	405	3.279	+90
424	0.399	+88	453	1.727	+66
425	0.239	+86	454	2.305	-72
426	0.167	+93	455	0.866	-92
427	0.039	+106	376	0.310	+49
428	0.045	-173	456	0.712	+92
429	0.040	+138	457	1.849	+72
430	0.040	+134	416	2.073	+54
431	0.036	+166	458	2.651	+8
432	0.044	-178	459	2.649	-58
433	0.040	-150	460	1.395	-148
434	0.050	-136	461	2.339	-93
435	0.031	-74	462	1.929	-90
436	0.023	-97	321	1.529	-74
437	0.152	-58	463	1.819	-70
438	0.110	+36	464	2.035	-58
439	0.497	+100	333	1.724	-58
440	0.429	+98	465	1.920	-35

Continuation of Series 5-2-73 0915

Station	Voltage (RMS) V	Phase Angle ϕ	Station	Voltage (RMS) V	Phase Angle ϕ
466	2.056	-30	510	0.111	+168
449	1.802	-44	511	0.367	+176
467	1.738	-38	512	0.409	-180
468	1.973	-37	513	0.392	-168
345	2.023	-43	514	0.097	+4
454	2.320	-67	515	0.605	-24
357	1.671	-45	516	0.469	-30
459	2.619	-57	517	0.093	+30
309	2.368	-80	518	0.269	+10
659	0.104	-134	577	0.279	+2
660	0.257	-176	578	0.185	+70
661	0.245	-150	579	0.139	-26
662	0.243	+160	580	0.157	-171
663	0.169	-65	581	0.027	-97
664	0.141	+75	582	0.216	-43
665	0.058	+138	583	0.428	-29
666	0.031	-55	584	0.776	-142
671	0.227	-156	585	0.285	-108
672	0.255	+164	586	0.918	-65
673	0.084	+150	587	0.355	+1
674	0.088	-145	588	1.730	+38
675	0.242	-76	589	0.461	+13
676	0.156	-100	591	0.386	-62
500	2.412	-145	592	0.051	+147
501	5.279	-49	593	0.267	+97
502	1.013	-47	594	0.709	-32
503	0.586	+40	595	0.642	+161
504	0.533	+10	597	0.307	+55
505	0.494	-59	598	0.325	-40
506	0.775	+1	599	0.155	-127
507	0.086	+62			
508	0.313	-62			
509	0.175	-102			

FLIGHT ELECT. MODES

Test Series 5-15-73

Speaker: Type Utah 8", Location Fwd Slots, Voltage 8 (RMS)

Date from ACC No.

Motor Pressure 53 Phase Ret Station 300

Frequency Variable Established at Station 300

	Station	Voltage (RMS) v	Phase Angle ϕ
f = 104	300	0.026	+5
	578	0.086	-12
	580	0.045	-23
	581	0.02	-140
	583	0.099	-8
	584	0.21	-10
	585	0.83	-28
	586	0.135	-12
	587	0.27	-44
	588	0.65	-28
f = 134	300	0.011	+40
	578	0.01	-105
	580	0.01	-85
	581	0.011	-97
	583	0.163	-110
	584	0.67	+100
	585	1.46	+67
	586	2.50	+55
	587	0.076	+73
	588	1.31	-112
f = 269	300	0.443	+5
	578	0.265	+61
	580	0.1	-145
	581	0.216	-138
	583	0.413	+21
	584	0.168	+5
	585	0.775	-125
	586	0.031	+60
	587	0.89	-146
	588	0.147	-170

	Station	Voltage (RMS) v	Phase Angle ϕ
f = 367	300	0.446	+3
	578	0.161	+115
	580	0.137	+135
	581	0.046	-42
	583	0.86	+12
	584	0.87	+16
	585	2.659	-152
	586	0.679	+6
	587	2.93	-180
	588	0.899	+90
f = 409	300	0.176	+11
	578	0.079	+75
	580	0.055	-94
	581	0.15	-95
	583	0.126	+40
	584	0.30	+40
	585	2.5	+77
	586	0.32	-90
	587	1.25	+75
	588	1.56	-109

APPENDIX E

EVALUATION OF THE BASELINE MOTOR ANALYSIS
TASK V FINAL REPORT

AS PREVIOUSLY PUBLISHED

HERCULES INCORPORATED
INDUSTRIAL SYSTEMS DEPARTMENT • SYSTEMS GROUP
P. O. BOX 98, MAGNA, UTAH 84044 • TELEPHONE: 297-5911

8 January 1975

In Reply Refer To:
0025/6/40-4680

Mr. W. Andrepont/DYSC
Air Force Rocket Propulsion Laboratory
Edwards Air Force Base, California 93523

Subject: Contract No. F04611-73-C-0025

Dear Sir:

The Task V final report for the subject contract is enclosed. This report provides an evaluation of the Phase I work and summarizes most of the progress made to date on the component vibration program.

Very truly yours,

S. C. Browning

S. C. Browning, Manager
Product Engineering

SCB/FRJensen/pj

Enclosures

EVALUATION OF THE BASELINE MOTOR ANALYSIS
TASK 5 FINAL REPORT
RPL CONTRACT F04611-73-C-0025
COMPONENT VIBRATION PROGRAM

I. INTRODUCTION

The intent of Phase I of the Component Vibration Program was to produce a detailed full-blown dynamic structural analysis of a complete rocket motor. The analysis was to have been as detailed and as complete as present state-of-the-art techniques would allow. The purpose of the detailed analysis was to provide a baseline for judging modeling simplifications to be studied later in the program. However, as the work progressed, it was realized that even this detailed state-of-the-art model would necessarily contain some significant simplifications and modeling compromises. In the present program, the study on modeling simplifications, (Phase II), has been modified to include a study of some characteristics of the refined model, (e.g. the grain grid refinement study and the scalar spring study).

Phase I consists of five tasks. In Task 1, the Poseidon C-3 second stage motor was selected as the baseline motor to be analyzed. Acoustic modes and associated natural frequencies for the Poseidon motor were defined in Task 2. In Task 3, a detailed structural dynamics analysis was conducted on the baseline motor. Task 4 was an experimental task designed to collect data which could be used to evaluate the detailed structural analysis. Task 5 gives an evaluation of the Phase I detailed structural dynamics analysis.

At the beginning of this program, NASTRAN level 15 was specified as the state-of-the-art tool to be used in the structural analyses. The size and complexity of the finite element models required to analyze a rocket motor, complete with components, are the features that distinguish this analysis problem from routine structural dynamics analyses. Initially, the problem was to be divided into several smaller substructures and the modal synthesis method used to obtain a total structure solution. The modal synthesis approach was found to have the following three disadvantages:

a) The size of a particular substructure was limited to about 300 degrees-of-freedom by the practical limit on the size of problem that can be handled by the Given's eigenvalue extraction routine in NASTRAN.

b) A satisfactory way for handling the frequency dependent grain modulus was not available.

c) The modal synthesis approach was not automated on NASTRAN and some time would have been required for development of appropriate DMAP instructions.

At the suggestion of RPL, an alternate approach was investigated. The alternate approach consisted of using a cyclic symmetric finite element model to represent the motor proper and using the mechanical impedance method to account for the components in a frequency response analysis of the total motor. This approach was found to have the following three disadvantages:

a) The natural frequencies and mode shapes for the structure are not determined when frequency response analyses are performed.

b) A major change to the basic NASTRAN program would be required to incorporate the capability to analyze cyclic symmetric structures in the Frequency Response rigid format.

c) Some time would be required to develop DMAP instructions to implement the mechanical impedance approach on NASTRAN.

Weighing the pros and cons of each approach, the decision was made to employ the cyclic symmetry-mechanical impedance approach. The inability of modal synthesis to handle the frequency dependent grain and the more involved DMAP instructions that would be required are the major factors upon which the decision was based. The MacNeal-Schwendler Corporation was hired to make the necessary changes to NASTRAN.

The cyclic symmetry approach was used in Task 3 to analyze the complete motor at eight different frequencies. To evaluate these analyses, results have been compared with data from static motor firings. In addition, experimental results from Task 4 have been used to evaluate the structural dynamics analyses. Details of these evaluations and a discussion on the applicability of preliminary established error limits are included in this Task 5 report.

II. STRUCTURAL DYNAMICS ANALYSIS APPROACH

Two different finite element models, representing the clean motor, (no asymmetric components attached), at two different burn times, were analyzed using the NASTRAN program. The two models represent burn times of zero and 4.0 seconds. The burn times, frequencies, and mode shapes used in the analyses are shown below in Table I.

TABLE I

MOTOR CONFIGURATIONS AND CONDITIONS USED IN THE TASK III STRUCTURAL DYNAMICS ANALYSES

Analysis Identification Number	Burn Time (sec.)	Frequency (Hz)	Mode (L = Longitudinal) (T = Tangential)	Comments
1	0.0	265.	L_3	Cold gas modes selected to match Task 4 experiment conditions.
2	0.0	365.	L_4	
3	0.0	668.	T_1	Hot gas modes selected to match static firing test conditions.
4	0.0	770.	L_3	
5	0.0	1327.	$T_3 = L_2 + T_1$	
6	4.0	281.	L_1	Hot gas, advanced burn time
7	4.0	365.	L_4	Cold gas, selected for comparison with 2 above.
8	4.0	634.	T_1	Hot gas, advanced burn time

The finite element grids used for both zero and advanced burn times have been shown in previous monthly reports, (see References 1 and 2). Either grid represents a 1/24 section slice of the total motor. Therefore, using a cyclic symmetry analysis, the effective circumferential grid refinement is a longitudinal-radial plane of nodes every 15° around the motor circumference. The most important nodes in the model are the nodes where the components are attached. With a node every 15° around the circumference of the aft adapter ring, the nodes nearest to actual component connection points were selected to represent the connection points. The nodes that represent the component connection points are shown in Figure 1 together with a sketch of the aft dome components.

As indicated in Table I, some analyses were conducted with cold gas modes and others were conducted with hot gas modes. A particular mode will occur in cold gas at a different frequency than the corresponding mode in hot gas because of the difference in the speeds of sound. For example, the third longitudinal mode occurs at 265 Hz with cold gas, (room temperature Nitrogen), and at 770 Hz in the hot combustion gases during a firing. Two cold gas modes, L_3 and L_4 at 265 and 365 Hz respectively, were included in the analyses to provide results for comparison with the cold gas tests that were performed in Task 4 using an inert motor. The 365 Hz analysis using L_4 was conducted on both the zero burn time model and the advanced burn time model so that the effect of burn time on results could be assessed. The other five analyses were conducted with hot gas modes to provide results for comparison with static firing data.

Application of the Mechanical Impedance Method to this particular rocket motor analysis was discussed in References 3 and 4. The equations given in References 3 and 4 are in terms of forces, velocities, impedance matrices, and admittance matrices. As a matter of convenience, the problem was solved in terms of displacements rather than velocities. Adopting the terminology used in Reference 5, receptance matrices replace admittance matrices and inverse receptance matrices replace impedance matrices when displacements are used in place of velocities. If R_m is the receptance matrix for the motor, and R_c is the set of matrices representing component receptances, then the equation that is solved can be written:

$$\{U_T\} = [I + R_m R_c^{-1}]^{-1} \{U_o\} \tag{1}$$

The identity matrix is denoted I. The displacements at the component connection points resulting from pressure mode loading with no components attached, is denoted U_o. Then, U_T is the total displacement vector calculated to represent the response of the motor (including components) at the component connection points. For the component connection points shown in Figure 1, U_T has 42 rows.

The receptance matrices are formed by applying a unit force at one coordinate while all other forces are zero. The displacements at all component connection coordinates then form a column in the receptance matrix according to the equation:

$$\{U\} = [R] \{F\} \tag{2}$$

Solution of equation (1) results in displacements only at component connection points. Some data recovery operations are necessary if displacements at other points are desired. If displacements at U_e coordinates are desired, after U_T has been obtained, then equation (2) can be partitioned and solved for U_e:

$$\left\{\begin{array}{c} U_T \\ \hline U_e \end{array}\right\} = \left[\begin{array}{c} R \\ \hline R_e \end{array}\right] \{F\}$$

$$\{U_e\} = [R_e] \{F\} \tag{3}$$

In equation (3), R_e is part of the receptance matrix that corresponds to the extra coordinates U_e. The R_e matrix can be formed at the same time as the R matrix. The forces F must include both the pressure loading and the interconnection forces. The most convenient way to get U_e is to superimpose $(U_e)_o$ from the pressure load with $(U_e)_i$ resulting from the interconnection forces. Once the interconnection displacements, U_T, are obtained from (1), the interconnection forces can be determined from:

$$\{F_i\} = [R_c^{-1}]\{U_T\} \tag{4}$$

Then, superimposing: $$\{U_e\} = \{U_e\}_o + [R_e][R_c^{-1}]\{U_T\} \tag{5}$$

Equation (5) defines the data recovery operations required to obtain displacements at points other than the component connection points.

III. STRUCTURAL DYNAMICS ANALYSIS RESULTS

Accelerometers mounted on the aft adapter ring during static firing measure accelerations in the longitudinal direction. Nodal accelerations at the component connection points in the longitudinal direction are listed in Table II. The nodal accelerations were obtained by multiplying appropriate displacements from U_T by (ω^2/g) where ω is the circular frequency. The listed accelerations represent the response of the motor to an acoustic pressure mode with maximum pressure amplitude of $\pm$ 1.0 psi.

During static firing, the amplitude of the pressure oscillations are measured by a Kistler pressure gage with a tap through the forward closure. Therefore, it is convenient to normalize the analysis results for a pressure mode shape of unit value at the forward closure. The third longitudinal mode (L_3), for example, has a value of $\pm$ 0.69 psi at the forward closure when the maximum value along the length is $\pm$ 1.0 psi. To normalize the displacement amplitudes for a unit pressure at the forward closure, calculated values for L_3 are divided by 0.69. The list of accelerations that have been normalized for a unit value of head end pressure is given in Table III.

In order to plot mode shapes from the analysis results, data recovery calculations were performed for the 265 and 365 Hz cold gas modes. The plotted mode shapes for dome deformations have been included in previous monthly reports, (see References 2, 6, and 7). Since data recovery was not performed for hot gas modes, the only forward dome response available is from the cold gas analyses. Therefore, accelerations on the forward adapter and the forward closure have been calculated from cold gas analyses for comparison with static firing data. The forward dome accelerations are given in Table IV. Data recovery was not performed for hot gas modes because static firings do not furnish sufficient data for plotting of mode shapes.

The locations of points 9 and 21, referred to in Table IV, are shown in the mode shape plot given in Reference 7. Point 9 is near the center of the forward closure. Point (node) 21 is on the forward adapter ring.

An eigenvalue solution was obtained for the Flight Electronics Unit with connection nodes constrained to zero displacement. The first eight natural modes are plotted in Reference 7.

IV. ANALYSIS EVALUATION

The finite element models analyzed with NASTRAN have been constructed to represent a typical S/S Poseidon motor. The extent to which the models actually do represent a motor is the subject of this evaluation. A quantitative measure of the extent to which model results agree with motor results is obtained by applying previously established error limits as reported in Reference 8.

The analysis approach selected for this program consists of performing frequency response analyses on the motor. To perform an analysis, a set of in-phase steady-state forces are applied to the motor at a particular frequency. The motor structure responds at the forcing frequency. The frequencies are selected to coincide with acoustic cavity natural frequencies, not structural natural frequencies. Therefore, it is the accuracy of the response of the structure at non-resonant frequencies that is at question.

There are three main factors that effect the accuracy obtained with a finite element model: 1) the mass distribution, 2) the stiffness distribution, and 3) the damping distribution. A relatively accurate mass distribution is probably easiest to obtain because motor volume is fairly easy to model, and material densities are easily measured and well known. Obtaining an accurate stiffness distribution for a complicated structure can be difficult. Some of the factors that contribute to the difficulty in obtaining an accurate stiffness model are the following:

1) The case material is orthotropic.

2) The grain is viscoelastic.

3) The gases in the dome cavities must be considered.

4) Stiffnesses of joints such as the Y-joint and the elastomeric joint and stiffnesses at material interfaces such as between dome and adapter, are difficult to model.

5) Stiffnesses at bolted connections are difficult to model because of possible slippage and effects of bolt preload.

The damping distribution required for accurate modeling is also difficult to determine. Using NASTRAN, only equivalent viscous damping may be input. For the rocket motor model, the propellant grain provides the major damping forces. The grain damping is input as a function of frequency as determined from dynamic complex modulus material tests.

Errors or inaccuracies in the mass or stiffness modeling can result in errors in the natural frequencies and the shapes of the individual modes. Errors in the damping modeling should affect mainly the accuracy of the amplitude of response but should have a negligible effect on the natural frequencies and mode shapes. In general, a finite element model can be expected to perform best at the lower frequencies, becoming more inaccurate as the excitation frequency is increased.

When the clean motor model was constructed, the mass of the model was compared with the mass of the motor and adjustments were made until good agreement was obtained. The stiffness of the model was checked by applying a static uniform pressure in the combustion cavity and comparing dome displacements with hydrotest data. Again, adjustments were made until good agreement was obtained between the hydrotest and static pressure analysis.

Next, the L_3 and L_4 longitudinal acoustic pressure modes were applied to the motor so that mode shapes could be compared with data from the Task 4 testing program, (see References 9 and 10 for a description of the testing program and testing results). Calculated and measured mode shapes for the forward and aft domes are compared in References 2, 6, and 7. The eight mode plots in Reference 2 have been normalized so that the maximum deformation for any particular mode is unity. Figure 1 of Reference 2 shows that both calculated and measured mode shapes have a bulge along the dome for the 365 Hz L_4 excitation. However, the bulges occur at different points along the dome for the two mode shapes and the mode amplitudes at the aft adapter are significantly different. Figures 2, 3, and 4 of Reference 2 show similar agreement between measured and calculated mode shapes at different locations around the motor circumference. The conclusion is that measured and calculated mode shapes, although somewhat similar do not generally agree well. The same conclusion holds for Figures 5 through 8 of Reference 2, the mode shapes for the 265 Hz L_3 excitation, and for the forward dome mode shapes shown in Figures 1 and 2 of Reference 7. Some possible reasons why better agreement is not obtained are:

(1) The model may be responding in a similar but basically different mode than was observed in the test. A small frequency shift might excite the similar mode.

(2) The model stiffness distribution may be too inaccurate near the area of the bulge in the measured mode shape.

(3) The scalar springs used in the dome cavity of the model may not be providing the same dome excitation as the actual dome cavity pressure distribution that existed during the test.

Item (3) will be investigated in Task VII.

Some other mode shapes of interest are those for the Flight Electronics Unit shown in Figures 3 through 6 in Reference 7. Extra effort was expended in modeling the Flight Electronics Unit in an attempt to match some of the natural frequencies and mode shapes that were measured in the Task 4 testing. The basic cantilever mode shown in Figure 3 of Reference 7 occurs at 108.9 Hz in the model. The test data shown on page C25 of Reference 10 indicates a frequency of 104 Hz for the same basic mode. The model was adjusted to give this good agreement. The second mode is also in fairly good agreement. The data in Reference 10, page C25, indicates that the second mode occurs at 134 Hz and consists of a side-to-side swaying motion coupled with a twisting mode (one side up and one side down) of smaller amplitude. The side-to-side swaying mode shown in Figure 3 of Reference 7 occurs at 140.8 Hz. The next mode shown in the test data has a frequency of 269 Hz. The corresponding mode shape appears to be a twisting mode coupled with other motions. The analysis produced a third mode at 268.2 Hz and a corresponding twisting mode shape. Notice that frequencies higher than the third natural frequency have associated mode shapes that consist of local structural deformation as opposed to the general overall bending, swaying, or twisting motions of the first three modes, (see Figures 3 through 6, Reference 7). No attempt was made to accurately model the detailed package that is mounted on the basic frame structure. Such a detailed model would have required too much time. Therefore, the modes that consist of significant local structural deformation, such as mode 4, (Reference 7), cannot possibly be representative. The part that is deforming does not model, or represent, anything on the actual structure. It thus appears that 300 Hz is about the upper limit for the validity of the Flight Electronics Unit model. Time was not available to study the Hydraulic Power Unit and Gas Generator models to estimate an upper limit frequency, however, 300 Hz should be a good estimate.

The final comparisons to be made are those between analysis results and static firing data. Tables III and IV contain the significant analysis results. Table IV shows that the response to the symmetric L_3 and L_4 modes is quite symmetric around the circumference of the motor. Thus the asymmetrically mounted components on the aft dome appear to have little effect on the symmetry of response at the forward dome.

Reference 11 is a report on analysis of static firing data. Data from three motors that were static fired with components attached has been analyzed and is presented in a format selected to facilitate comparisons with analysis data.

As mentioned earlier, the analysis procedure only yields accelerations of the component connection points, all of which are located on the aft adapter, (refer to Figure 1). During the static firings, only two accelerometers were mounted on the aft adapter ring. Figures 2, 3, and 4 in Reference 11 show the locations of longitudinal aft adapter accelerometers AC-250 and AC-261. AC-250 is near component connection point $\boxed{4}$ and AC-261 is near component connection point $\boxed{8}$, (see Figure 1). The comparisons between analysis results and static firing data, at the two points that coincide, are given in Table V.

To apply the error limits that were established in Task 1, the calculated values are multiplied by a factor and compared with the static test data. For convenient reference, the table of values from Reference 8 is reproduced below:

Confidence Level	Error Limits
95%	$r \leq 1.94$ m
99%	$r \leq 2.36$ m
99.87%	$r \leq 2.71$ m

In the above table, m is the calculated response and r is the measured (accelerometer) response.

Table VI was generated using the 1.94 factor that corresponds to a confidence level of 95%. Comparing the values in Table VI, it is seen that the accelerometer data exceeds the error limits at 281 Hz and at 1327 Hz. Using the highest confidence level of 99.8% cures the problem at 1327 Hz. However, the error at 281 Hz is nearly two orders of magnitude, a calculated response of 0.29 g's/psi, compared to a measured level of 23.38 g's/psi. The possibility of an error in the static firing data was considered, however, the high response level measured at 281 Hz at three locations on the same motor (SP-0149), gives added confidence that the static firing data is valid (see Table I in Reference 11). On the other hand, no high response level was measured at 281 Hz for motors SP-0131 and SP-0160. Further investigation is needed.

V. CONCLUSIONS

Mode shape comparisons for the low frequency 265 and 365 Hz analyses showed only medium-good to medium-poor agreement. However, the agreement achieved is believed to be typical of that to be expected from an analysis of this type. Reasonable care was exercised in the construction of the model and a relatively refined grid was used. The grid had about 1000 degrees-of-freedom per slice which is equivalent to a total motor model having 12,000 degrees-of-freedom, or more if the components are included in the total.

The Flight Electronics Unit model was judged to be inaccurate above 300 Hz. But, in spite of the poor mode shape agreement and the limited capability of the component models, relatively good agreement with static firing data was achieved up to 1327 Hz. If the calculated values are multiplied by a factor of 2.0, (1.94 was used above), they apparently become reasonably good estimates of the maximum accelerometer response. However, the use of only 3 motors does not provide a good statistical evaluation of the 2.0 factor. It would be desirable to have a larger data base. One problem in obtaining more data is that motors are not routinely static fired with all components attached.

Another problem appears to be that of missing a structural mode. The difference in the model response and the motor response at 281 Hz cannot be attributed to statistical variation. There appears to be three possibilities that warrant further investigations:

1) The model may contain the mode that yields the high response, but a small shift in frequency away from 281 Hz may be necessary to excite it.

2) Due to shortcomings of the model, it may not be capable of modeling the high response mode.

3) The test data may be in error.

The work of Task VII is expected to give additional insight into the behavior of the detailed motor model. Therefore, conclusions made here will be reviewed and modified or updated, if necessary, based on Task VII results.

TABLE II

NODAL ACCELERATIONS IN THE LONGITUDINAL DIRECTION
FOR THE COMPONENT CONNECTION NODES FROM
EIGHT FINITE ELEMENT ANALYSES (Poseidon S/S C-3)

Analysis Identification Number	Frequency (Hz)	Longitudinal Nodal Accelerations (g's) Component Connection Point (See Figure 1) 1	3	4	5	6	8	9
1	265	1.024	0.921	0.949	1.342	1.140	0.691	0.685
2	365	0.605	0.695	0.657	0.676	0.708	0.726	0.665
3	668	4.529	1.231	5.102	4.080	4.049	3.213	2.706
4	770	1.737	1.095	1.338	1.129	0.531	0.846	0.636
5	1327	0.917	0.538	1.643	1.653	1.917	0.412	0.889
6	281	0.686	0.264	0.749	0.527	0.325	0.289	0.445
7	365	0.694	0.751	0.765	0.777	0.748	0.806	0.815
8	634	2.654	0.468	2.092	1.220	3.047	1.534	1.940

TABLE III

NODAL ACCELERATIONS OF TABLE II CORRECTED
FOR A UNIT VALUE OF HEAD END PRESSURE

Analysis Identification Number	Frequency (Hz)	Longitudinal Nodal Accelerations (g's) Component Connection Point (See Figure 1) 1	3	4	5	6	8	9
1	265	1.48	1.33	1.38	1.94	1.65	1.00	0.99
2	365	0.66	0.76	0.72	0.74	0.78	0.80	0.73
3	668	4.53	1.23	5.10	4.08	4.05	3.21	2.71
4	770	2.52	1.59	2.01	1.64	0.77	1.23	0.92
5	1327	1.50	0.88	2.69	2.71	3.14	0.68	1.46
6	281	0.69	0.26	0.75	0.53	0.32	0.29	0.44
7	365	0.76	0.83	0.84	0.85	0.82	0.89	0.90
8	634	2.65	0.47	2.09	1.22	3.05	1.53	1.94

TABLE IV

NODAL ACCELERATIONS FOR TWO NODES
ON THE FORWARD DOME

Node	Direction	Circumferential Location	Calculated Accelerations (g's)(f=265Hz)	Corrected* Accelerations (g's)(f=265Hz)	Calculated Accelerations (g's)(f=365Hz)	Corrected* Accelerations (g's)(f=365Hz)
9	Z	0°	9.08	13.17	9.28	10.20
9	Z	90°	9.09	13.17	9.28	10.20
9	Z	180°	9.08	13.16	9.28	10.20
9	Z	270°	9.08	13.16	9.28	10.20
21	R	0°	0.67	0.97	0.62	0.69
21	R	90°	0.61	0.89	0.63	0.69
21	R	180°	0.64	0.92	0.64	0.70
21	R	270°	0.69	1.00	0.63	0.69
21	Z	0°	6.76	9.79	6.86	7.54
21	Z	90°	6.79	9.84	6.86	7.54
21	Z	180°	6.72	9.74	6.86	7.54
21	Z	270°	6.63	9.61	6.86	7.54

*Corrected accelerations have been normalized for a unit head end pressure

TABLE V

COMPARISON BETWEEN STATIC FIRING DATA
AND NASTRAN ANALYSIS RESULTS

Frequency (Hz)	Acceleration Response (g's/psi) For Unit Head End Pressure Ampl.			
	Analysis Results For Point 4	AC-250 Static Firing Data	Analysis Results For Point 8	AC-261 Static Firing Data
281	0.75	-	0.29	23.38
634	2.09	1.45 to 3.14	1.53	1.71
668/680*	5.10	1.57 to 3.05	3.21	0.79 to 2.43
770	2.01	2.95	1.23	2.00
1327	2.69	1.86 to 5.39	0.68	1.05 to 1.87

*The NASTRAN analysis was conducted at 668 Hz. The static firing data analysis was erroneously conducted at 680 Hz.

TABLE VI

EVALUATION OF ANALYSIS RESULTS
USING ERROR LIMIT FACTOR 1.94

Frequency (Hz)	1.94 x 4	AC-250	1.94 x 8	AC-261
281	1.46	-	.56	23.38
634	4.05	3.14	2.97	1.71
668/680	9.89	3.05	6.23	2.43
770	3.90	2.95	2.39	2.00
1327	5.22	5.39	1.32	1.87

LIST OF REFERENCES

NOTICE: In the following list of references, the monthly report for this program will be referenced by date. The complete reference is: "Monthly Report for Analytical Prediction of Motor Component Vibration Driven by Acoustic Combustion Instability," Contract No. F04611-73-C-0025, for AFRPL, Edwards AFB, by Hercules Incorporated, Bacchus Works, Magna, Utah.

1. Monthly Report Dated 20 February 1974.
2. Monthly Report Dated 20 July 1974.
3. Monthly Report Dated 20 October 1973.
4. Monthly Report Dated 20 March 1974.
5. Bishop and Johnson, "The Mechanics of Vibration," Cambridge University Press, London, England, 1960.
6. Monthly Report Dated 20 May 1974.
7. Monthly Report Dated 20 August 1974.
8. Monthly Report Dated 18 May 1973, Appendix I.
9. Task 4 Preliminary Testing Report, Motor Component Vibration Program, Contract No. F04611-73-C-0025, for AFRPL, Edwards AFB, by Hercules Incorporated, Bacchus Works, Magna, Utah, April 12, 1973.
10. Task 4 Final Report, "Vibration Testing of the Baseline Motor," RPL Component Vibration Program, Contract No. F04611-73-C-0025, for AFRPL, Edwards AFB, by Hercules Inc., Bacchus Works, Magna, Utah, Aug. 15, 1973.
11. Monthly Report Dated 20 December 1974, Appendix I.

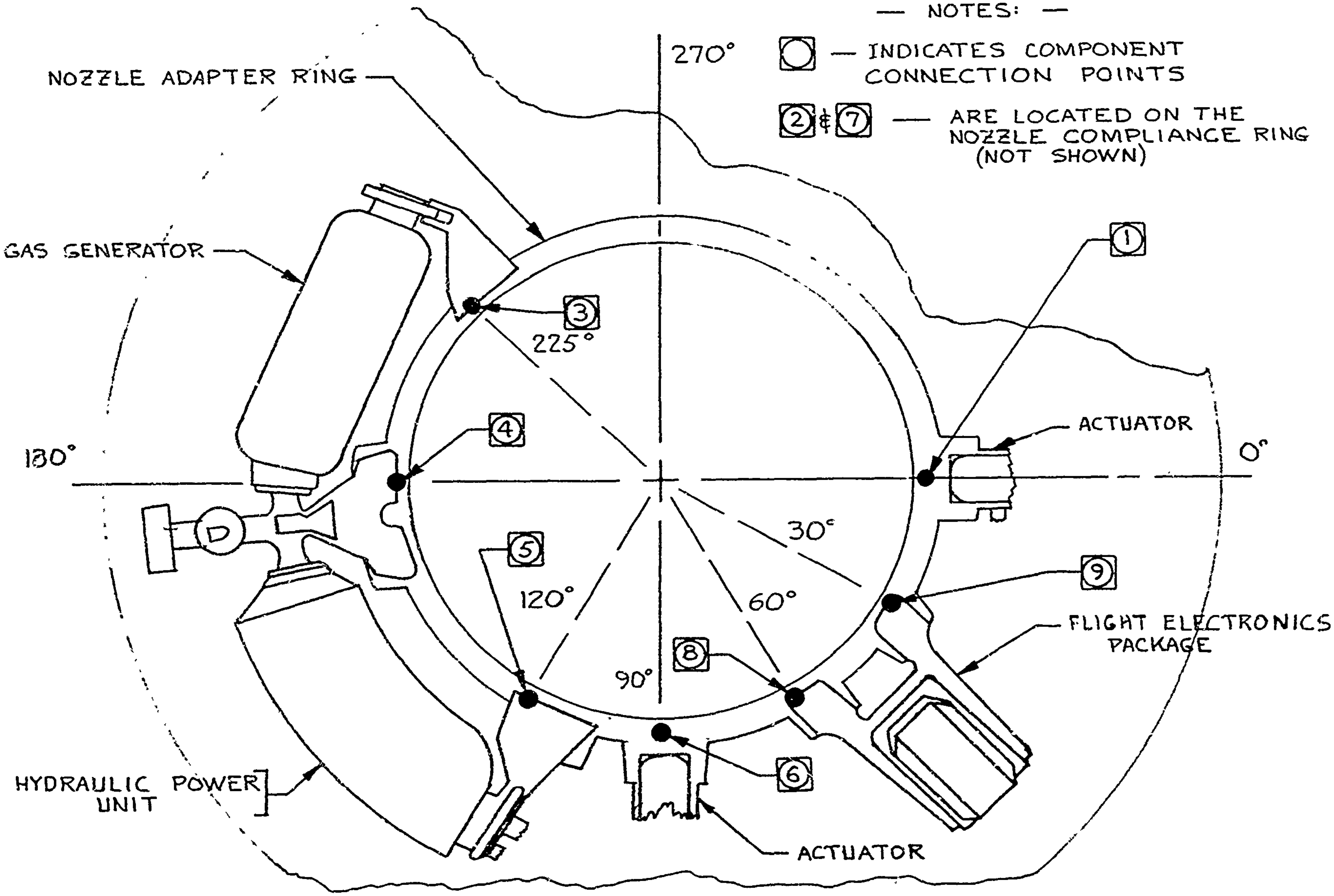

FIGURE 1 - SKETCH OF THE AFT DOME OF THE POSEIDON S/S MOTOR SHOWING LOCATIONS OF THE COMPONENT CONNECTION POINTS USED IN THE NASTRAN COMPUTER ANALYSIS.

DISTRIBUTION LIST

	Mail Stop
J. M. Anderson	100-K1-7
F. Beavers	100-K1-7
M. W. Beckstead	100-K1-6
S. C. Browning	100-K1-7
G. H. Moody	100-A
E. H. Pendergast	100-K2-6
E. D. Shank	100-C-2
E. L. Talbot	100-K1-7
Library (2)	100-H

WILMINGTON

R. Winer

ABL

W. L. Gunter/D. J. Sine

LOS ANGELES

R. Shively

APPENDIX F

MODELING TECHNIQUES EVALUATION FOR ANALYTICAL PREDICTION OF MOTOR COMPONENT VIBRATIONS DRIVEN BY ACOUSTIC COMBUSTION INSTABILITY

TASK 8 FINAL REPORT

HERCULES INCORPORATED
INDUSTRIAL SYSTEMS DEPARTMENT · SYSTEMS GROUP
P.O. BOX 98, MAGNA, UTAH 84044 · TELEPHONE: 297-5911

In Reply Refer to:
0025/6/40-5071

Mr. W. C. Andrepont, Chief
Combustion Section
Air Force Rocket Propulsion Laboratory
Edwards Air Force Base, California 93523

Subject: Contract No. F04611-73-C-0025

Dear Sir:

The Task 8 Final Report for the subject contract is enclosed. The report will be included as an Appendix in the program final report.

Very truly yours,

S. C. Browning, Manager
Product Engineering

SCB:FRJensen/pj

Enclosure

cc G. M. Pleck, AFFTC/PMRB
SPLB-50/D. L. Shelley
K. Sastch (letter only)

TASK 8 FINAL REPORT

MODELING TECHNIQUES EVALUATION FOR ANALYTICAL PREDICTION OF MOTOR COMPONENT VIBRATIONS DRIVEN BY ACOUSTIC COMBUSTION INSTABILITY

(CONTRACT F04611-73-C-0025)

July 1975

Prepared for

DEPARTMENT OF THE AIR FORCE (AFSC)
HEADQUARTERS, AIR FORCE FLIGHT TEST CENTER
Edwards Air Force Base, California

Prepared by

HERCULES INCORPORATED
SYSTEMS GROUP
Bacchus Works, Magna, Utah

TABLE OF CONTENTS

TASK 8 FINAL REPORT
MODELING TECHNIQUES EVALUATION

I. INTRODUCTION

The basic objective of the component vibration program, (contract F04611-73-C-0025), is to develop simplified techniques for structural dynamics analyses of rocket motors. The techniques are to be applicable to analyses of rocket motors performed for the purpose of calculating the response of attached components when the motor is undergoing acoustic pressure oscillations. To accomplish the program objectives, the program is subdivided into three phases.

In Phase I, a detailed structural dynamics analysis was performed on the S/S Poseidon (C3) motor. The S/S Poseidon motor was selected to provide baseline data for use in evaluation of modeling simplifications. The objective of Phase I was to provide analysis data that would serve as a standard for judging the adequacy and accuracy of the proposed modeling simplifications. Cold gas acoustics testing of an inert motor to determine structural response was included in the Phase I work. Results from the testing program were used to evaluate the detailed baseline motor analysis. The work of Phase I was reported in the Task 5 final report for this program.

Original plans for Phase II of the program called for the development of simplified modeling techniques. As the program progressed through the Phase I work, it became apparent that additional study of the characteristics of the detailed baseline model would be required before any reasonable consideration could be given to simplifications. The Phase II work thus evolved into a study of some important characteristics of the detailed model used in Phase I. The study was intended to result in improvements and simplifications, if justified, in the baseline motor model, and in a better understanding of the behavior of the model. Results from the Phase II modeling techniques studies are reported and evaluated in this Task 8 Final Report.

Phase III of the program was intended as a verification of proposed simplified modeling techniques. Present plans call for an analysis of the third stage Minuteman III motor during Phase III. Any simplifications or modeling improvements discovered in Phase II will be incorporated in the Phase III analyses.

The next section of this report contains a description of the general approach used in the Phase II simplified modeling studies. Three sections are then devoted to the three main modeling concepts which were selected by the AFRPL from a list of options given in a Hercules proposal. The selected options were incorporated into the program in a recent contract modification. The scaler spring study is Option C, the course grid study is Option E, and the half motor model study is Option G. Sections III, IV, and V of this report cover Options G, C, and E respectively. Each section contains its own figures and conclusions.

II. GENERAL APPROACH

It was necessary to acquire a good understanding of the behavior of the baseline motor model before considering any modeling simplifications. Answers to the following questions were sought:

1) How refined must the finite-element grid for the domes be in order to accurately represent mode shapes of the domes up to a particular frequency? The refinement in both the meridional and circumferential directions is at question.

2) How refined must the finite element grid for the grain be in order to accurately represent grain mode shapes over a particular frequency range?

3) Is it necessary to accurately represent grain mode shapes in the model in order to obtain accurate component response?

4) What role do the scalar springs play in the baseline motor model? (Scalar springs are used to represent combustion gases in the dome cavities so that grain motion can be transmitted through the gases to the domes.) This includes determination of how much load is transmitted through the springs and determination of how the springs restrict or modify dome motion.

5) Are response modes in the motor uncoupled to the extent that sufficiently accurate component response can be obtained by modeling only a portion of the structure such as one half of the total motor?

6) Are motor resonances generally broad enough (on a frequency basis) that a small error in frequency will not be critical, or are sharp resonances that make excitation frequency critical generally encountered?

7) Is structural response very sensitive to load distribution, or is frequency of the applied loads the predominant factor in determining response amplitudes and in determining which natural modes participate in the response?

In an attempt to provide answers to the above questions, five different models were analyzed. A full motor model, a half motor model, a half grain model, a full grain model, and an aft dome model were each analyzed separately. The NASTRAN program was used to perform static, real eigenvalue, direct frequency response, and model frequency response analyses. The aft dome model and half grain models were obtained simply by separating the half motor model at the tangent line. The half motor model was obtained from the full motor model. The grid points along the cut line, (a radial line approximately at the motor center), were repositioned so that a smooth cut plane would form one boundary of the half motor model. Other than the grid point relocations, the half motor model was exactly the same as the aft half of the full motor model. The full motor grain model was obtained by removing the domes from the full motor model. No wedge elements were used in any of the grids.

The analyses were kept as simple as possible to minimize expenses. The models were analyzed without using cyclic symmetry and without the components attached. Each model consists of a slice of the motor, (for most models the slice has an included angle of 15°). Since cyclic symmetry was not used to obtain the general three-dimensional solution, it was necessary to use symmetry boundary conditions along the faces of each slice. The use of such symmetry boundary conditions resulted in a special set of solutions that were valid only for the special boundary conditions. The models used were thus similar to axisymmetric models. The limited solutions obtained by not using cyclic symmetry are only for comparative purposes and are considered to be entirely adequate for studying certain aspects of the more general cyclic symmetry model. Omission of the components from the models is also considered to be acceptable since only comparative solutions were desired.

III. HALF MOTOR MODEL

A. Introduction

The objective of this study was to determine whether a half motor model could be used in place of a full motor model for calculation of component response. Accuracy to be expected and limitations of the half motor model were to be determined. The approach consisted of analyzing the half and full motor models under conditions that were as similar as possible. The aft half of the motor was selected for study because that is where the major motor components are mounted. Sketches of the half and full motor models used in the analyses are shown in Figures 1 and 2, respectively.

B. Dynamic Analysis Approach

When some thought was given to the problem of applying boundary conditions to the half motor model to simulate conditions of the full motor model, some of the shortcomings of a half motor model became very evident.

Consider the full motor model in Figure 3a. The motor in Figure 3a is shown with a constraint in the axial direction applied at the forward skirt. Such a constraint might be used for a motor attached to a test stand or attached to an upper stage by the forward skirt. The likely approach would be an attempt to represent the motor of Figure 3a by a half motor with symmetry boundary conditions as shown in Figure 3b. The half motor model could also be used to obtain the solution for a symmetric structure by solving with symmetric and asymmetric boundary conditions and then summing the solutions. If this were [illegible]ne, the structure being solved would appear as shown in Figure 3c. [illegible]hus becomes obvious that a half motor model cannot be used to c[illegible]rectly represent the boundary conditions shown in Figure 3a.

Another problem to be considered in using a half motor model is that of applying the load. To demonstrate this problem, assume that a solution of the full motor is desired for the pressure mode shown in Figure 3d. If half of the pressure mode as shown in Figure 3e is applied to the half motor shown in Figure 3b, the solution obtained is for a full length pressure mode that is symmetric as shown in Figure 3f. The pressure distribution of Figure 3f will likely excite quite different grain modes than the pressure mode of Figure 3d.

If a half motor model, as in Figure 3b, is analyzed just one time with half of a pressure mode, as in Figure 3e, there are three items to be considered:

a) How well does a symmetric motor represent the actual motor? (If the actual motor has a bonded dome on one end and a flapped dome on the other, poorer results might be expected.)

b) How well does a symmetric pressure mode represent the actual pressure mode?

c) How well can symmetric constraints be used to represent the actual constraints?

When the half motor model is analyzed twice, once with symmetric boundary conditions and once with asymmetric boundary conditions, and the results summed, question b) can be erased. In this case, the loads used in each solution are adjusted so that the load sum produces the desired pressure mode. Questions a) and c) always apply to half motor analyses.

The half motor model is represented by a 15° slice of the total motor as shown in Figure 1. A cylinderical coordinate system is used with T_r, T_θ, and T_z representing translational displacements in the motor radial (r), hoop (θ), and axial (z) directions respectively. Rotational displacements about the corresponding r, θ, and z axes are denoted by R_r, R_θ, and R_z. Symmetry boundary conditions were applied to the sides of the slice, (the r-z planes at $\theta = 0$ and at $\theta = 15^o$), by constraining all nodes in the side planes to have zero displacement for T_θ, R_r, and R_z. Since the slice is only one element thick, the boundary conditions were applied to all nodes. Symmetry conditions were applied to the nodes along the cut plane by setting T_z and R_θ to zero. (Note that R_r, R_θ, and R_z are constrained to zero for all nodes that appear only in CHEXA2 elements in order to remove singularities from the stiffness matrix.)

To obtain the best possible agreement between half and full motor analyses, the full motor was analyzed with an axial constraint at mid-motor like the constraint shown in Figure 3c for the symmetric motor. Frequency response analyses were conducted on both the half and full motor models by applying the third longitudiral (L_3) pressure mode at 265 Hz and the L_4 pressure mode at 365 Hz.

C. Results

The aft dome is considered to be the most important structural member of the motor model because motion of the aft dome is applied directly to the mounted components. Therefore, response of the aft dome is given major consideration throughout this report. The performance of the half motor model is compared with that of the full motor model by comparing mode shapes of the aft dome as shown in Figures 4, 5, and 6.

In frequency response analyses, the mode shapes of the structure change with time. To plot the mode shapes shown in Figures 4, 5, and 6, times for which the displacement at the nozzle adapter was a maximum were selected. To simplify comparison of the mode shapes, all modes were normalized to have unit deflection at the nozzle adapter.

The mode shapes shown in Figure 4 represent the dome response to the L_3 mode at 265 Hz. The same scalar springs (8000 lb/in.) that were used in the clean motor model analyses of Task 3 were also used for these analyses. There are three pairs of springs attached to the dome as shown in Figure 4.

Since rather poor a eement was found between the modes shown in Figure 4, the analyses were eated with no scalar springs being used. When the scalar springs were removed, the modes shown in Figure 5 were obtained. Modes resulting from the L_4 pressure mode at 365 Hz are shown in Figure 6.

The mode shape plots were normalized so that mode shape comparisons could be made without regard to magnitude. A comparison of the magnitudes between half and full motor model responses at selected nodes is given in Table I. The following general observations apply to the frequency response analysis results:

a) At node 255, located at the base of the adapter, as well as along most of the adapter and dome, the magnitude of the displacement tends to be larger in the full motor for the 265 Hz L_3 mode.

b) The phase angles in the R direction are nearly the same for the half and full motor models at 265 Hz.

c) At 365 Hz, the phase angles of the z direction displacement are approximately equal for the half and full motor.

d) Again, the magnitudes of the displacement in the z direction are slightly larger at the adapter for the full motor than for the half motor.

D. Discussion of Results

Figure 4 shows that the aft dome mode shapes are significantly different for the half and full motor models at 265 Hz when scalar springs are used. Figure 5 shows that full and half motor models produce different mode shapes even when no scalar springs are used. Figure 6 adds another data point and shows that full and half motor models also disagree at 365 Hz using the L_4 pressure mode.

The data in Table I show that the difference in the response (in the axial direction) at the aft adapter, where the components are attached, is only 0.40×10^{-5} or about 9 percent. This agreement between half and full motor models is surprising considering the poor mode shape agreement. The fact that the L_4 pressure mode is nearly symmetrical about the motor mid-plane is probably partially responsible for the good agreement between magnitudes. Another frequency, or pressure mode might be expected to produce much poorer agreement.

In the analyses discussed in this section, the difference between half and full motor models is probably due to two factors:

a) The symmetric motor model does not simulate the actual motor very well.

b) The symmetric loading distribution (represented by half motor analysis) does not represent the actual loading distribution with sufficient accuracy.

E. Conclusions and Recommendations

The limitations and approximations involved in using a half motor model to represent a full motor model have been explained. Results showing normalized response mode shapes and results showing absolute displacement magnitudes and phases have been given for comparison between half and full motor models. Results from this half motor model study should be of value to the structural analyst who is considering the use of a half motor model to represent a full motor. The analyst should keep in mind the fact that half motor model results were made to look as favorable as possible by analyzing the full motor, used for comparison, with a mid-motor axial constraint.

The case against the use of half motor models is not entirely clear cut. The results obtained in this study show that a half motor model may likewise not represent a motor attached to a test stand or bolted to other missile stages. Whenever a complete structure cannot be included in an analysis model, a decision is usually made to cut the structure at a particular location and apply boundary conditions to the model at that point to represent the effect of the omitted structure. The more that is known about the behavior of the structure, the easier it is to select a reasonable cut-off location and apply reasonable boundary conditions. The remainder of this report, covering the scalar spring study and the grid refinement study, contains considerable information on general structrual behavior of the motor.

The conclusion from this study is that significant differences between half and full motor models can exist. It is recommended that the structural analyst give careful consideration to the shortcomings of the half motor model to assure that the shortcomings do not cause problems in a particular model application. The half motor model cannot be recommended for general use because of the inaccurate representation of boundary conditions that it provides. Even a coarse grid forward motor half used with the aft motor half grid could provide the capability to represent general boundary conditions and would probably provide significantly better results. If sufficient degrees of freedom are not available to allow modeling of the entire motor, a substructure or mechanical impedance approach might be considered. The performance of two analyses, one with symmetry boundary conditions and one with asymmetry boundary conditions should provide considerably improved agreement between half and full motor models, however, no results are available to show the improved agreement. When the two analyses are performed, the load must be adjusted so that the summed loading distribution from the two analyses will match the actual applied loading distribution.

The MacNeal-Schwendler Corporation, working with the Aerojet Solid Propulsion Company (ASPC), analyzed the Minuteman III Third Stage motor using a half motor model. The analysis is reported in Reference 1. According to the report, the missing half of the motor was treated as a rigid body. Details of the boundary conditions applied to the half motor model were not made clear in the report and this study was not intended as an evaluation of the MSC-ASPC analysis.

TABLE I

DISPLACEMENT RESPONSE COMPARISON BETWEEN HALF AND FULL MOTOR MODELS USING SCALAR SPRINGS AND RESPONDING TO THE L4 PRESSURE MODE AT 365 Hz

	Half Motor Model				Full Motor Model			
	Radial (r) Direction		Axial (z) Direction		Radial (r) Direction		Axial (z) Direction	
Node	Magnitude X 10^{-6}	Phase (deg.)	Magnitude X 10^{-5}	Phase (deg.)	Magnitude X 10^{-6}	Phase (deg.)	Magnitude X 10^{-5}	Phase (deg.)
213	12.4	326.8	0.32	138.6	70.0	184.2	1.061	51.0
215	3.35	305.1	0.38	152.2	25.8	173.3	.903	59.2
217	2.48	310.0	0.39	151.8	18.94	175.1	.925	57.2
219	20.8	358.5	0.36	113.4	27.7	198.1	1.731	27.7
221	23.4	14.8	0.58	110.3	11.6	302.7	2.778	17.1
223	22.1	24.9	0.79	119.9	19.3	332.7	3.24	15.9
225	22.3	42.3	1.27	124.8	50.07	2.39	5.56	17.8
227	17.5	53.8	1.66	148.4	46.76	18.5	5.28	33.4
229	7.43	43.7	2.12	189.3	17.8	82.45	3.33	109.8
231	2.77	253.5	3.48	207.3	14.9	71.8	2.55	109.9
233	4.83	285.7	3.32	215.8	11.7	39.9	1.00	99.2
235	5.94	315.4	2.79	220.5	10.5	18.11	.118	134.0
237	6.12	336.9	2.33	216.9	8.56	4.14	.738	224.0
239	4.18	350.9	2.45	203.5	5.42	4.49	1.456	202.0
241	2.59	7.8	2.82	193.9	2.80	11.8	2.25	193.6
243	1.03	45.6	3.38	189.6	6.24	124.3	3.24	189.5
249	0.93	123.8	3.78	188.4	2.43	171.08	3.91	188.8
255	3.67	11.1	4.13	187.7	6.65	10.7	4.53	188.2

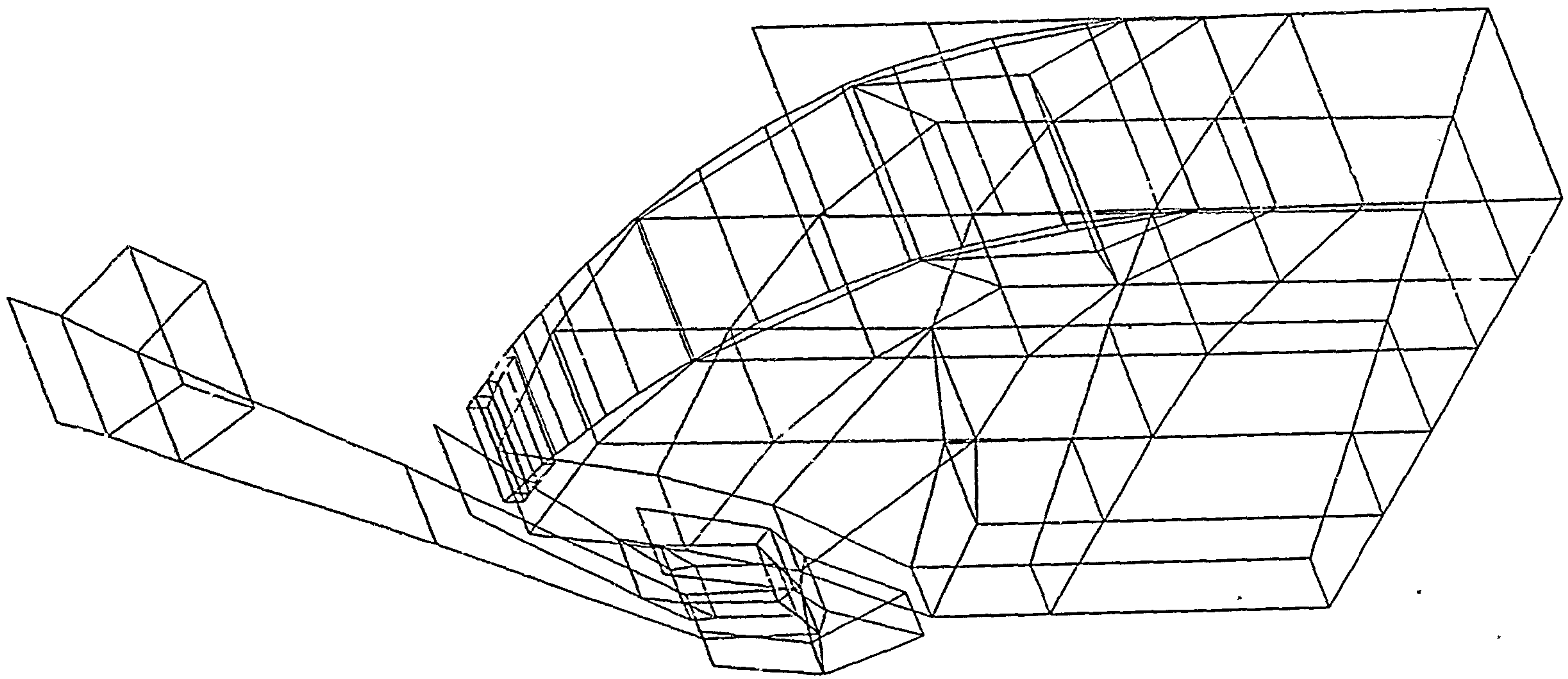

Figure 1. Half Motor Model for the Aft Half of the S/S Poseidon C-3 Motor

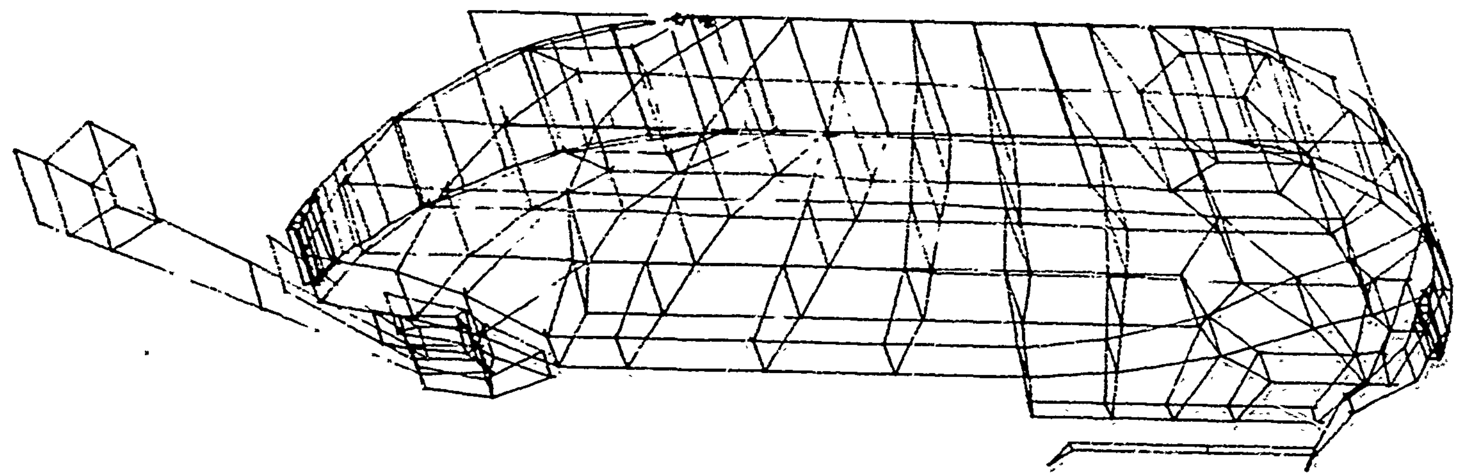

Figure 2. Full Motor Model for the S/S Poseidon C-3 Motor (Nc Wedge Elements Are Used)

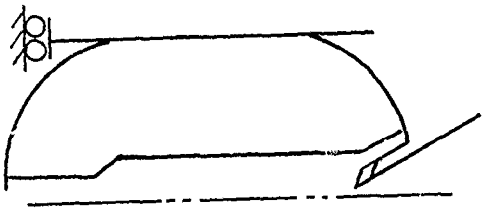

(a) TYPICAL FULL MOTOR BOUNDARY CONDITIONS

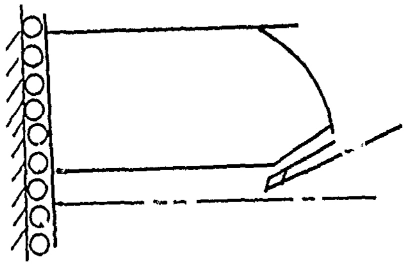

(b) MID-PLANE SYMMETRY BOUNDARY CONDITIONS APPLIED TO THE HALF MOTOR MODEL

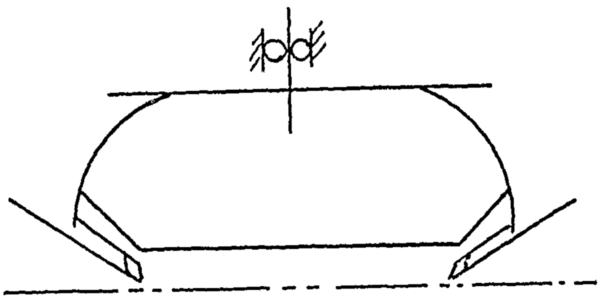

(c) SYMMETRIC MOTOR GEOMETRY REPRESENTED BY HALF MOTOR MODEL WITH SYMMETRY BOUNDARY CONDITIONS

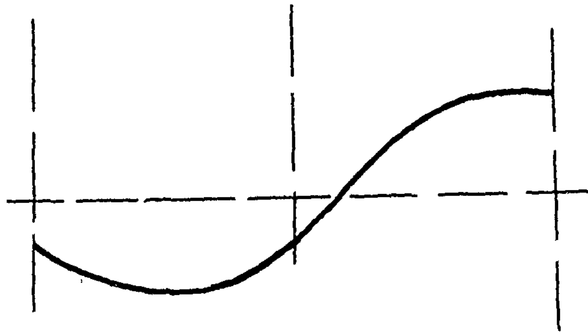

(d) TYPICAL FULL MOTOR PRESSURE MODE LOADING DISTRIBUTION

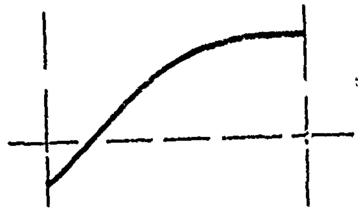

(e) PORTION OF FULL MOTOR LOADING DISTRIBUTION APPLIED TO THE HALF MOTOR MODEL

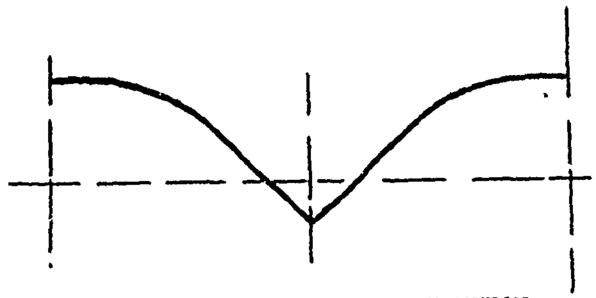

(f) SYMMETRIC LOADING DISTRIBUTION REPRESENTED BY ANALYSIS OF HALF MOTOR MODEL WITH SYMMETRY BOUNDARY CONDITIONS

Figure 3. Some Boundary Conditions and Loading Conditions Applicable to the Half Motor Model

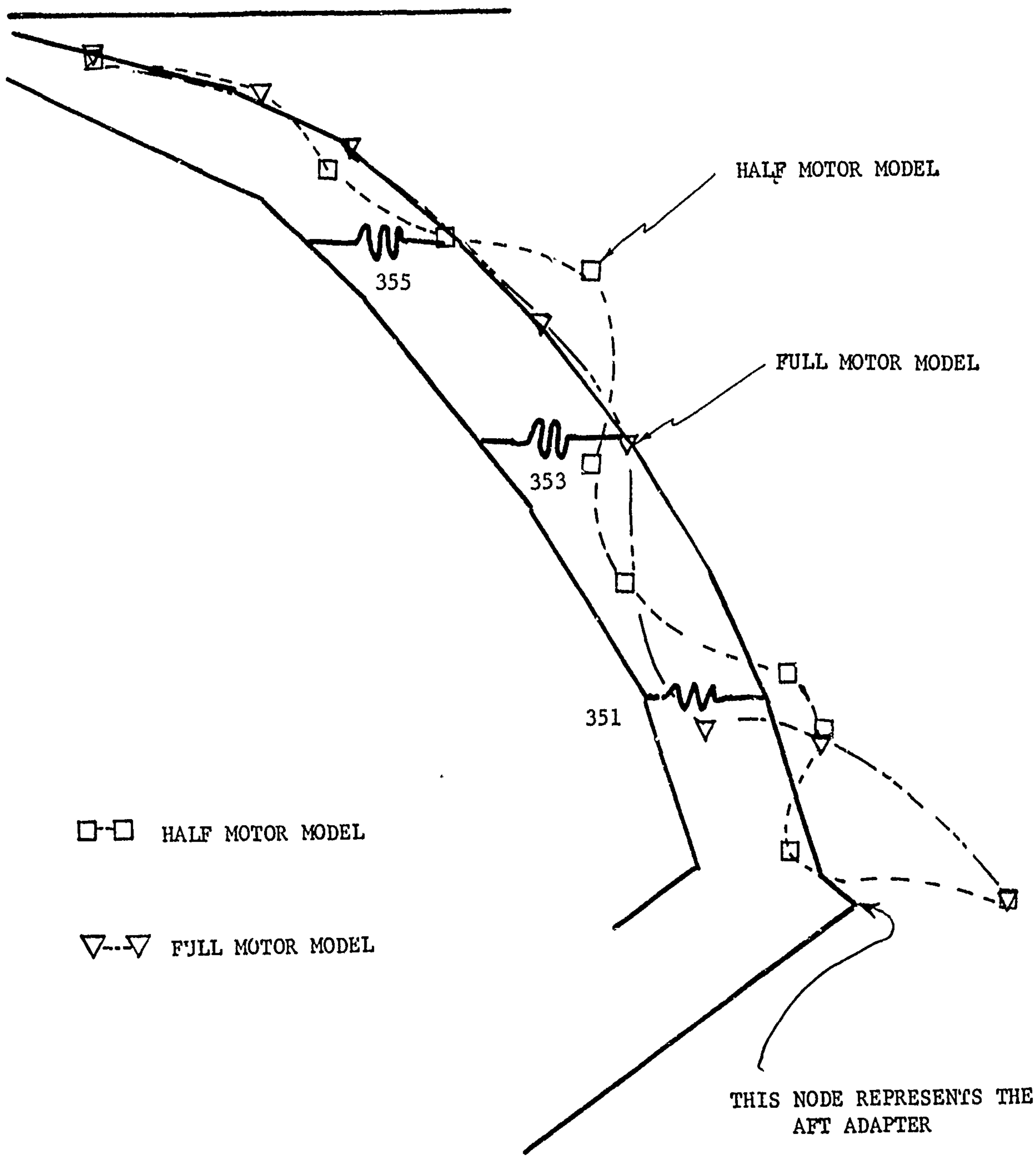

Figure 4. Aft Dome Mode Shapes for the Half and Full Motor Models with 8000 lb/in. Scalar Springs, Response to the L_3 Mode at 265 Hz

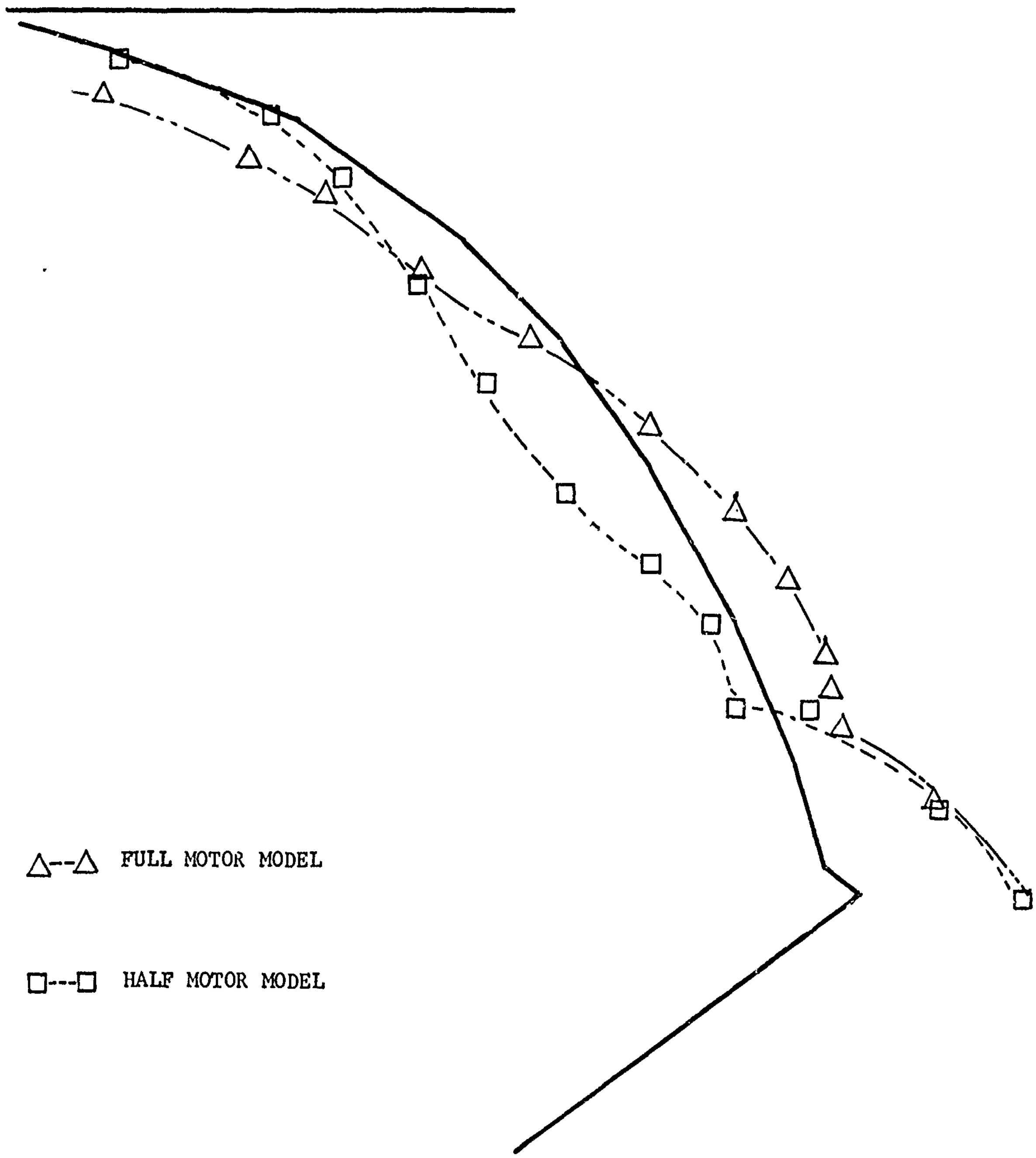

Figure 5. Aft Dome Mode Shapes for the Half and Full Motor Models Without Scalar Springs, Response to the L_3 Mode at 265 Hz

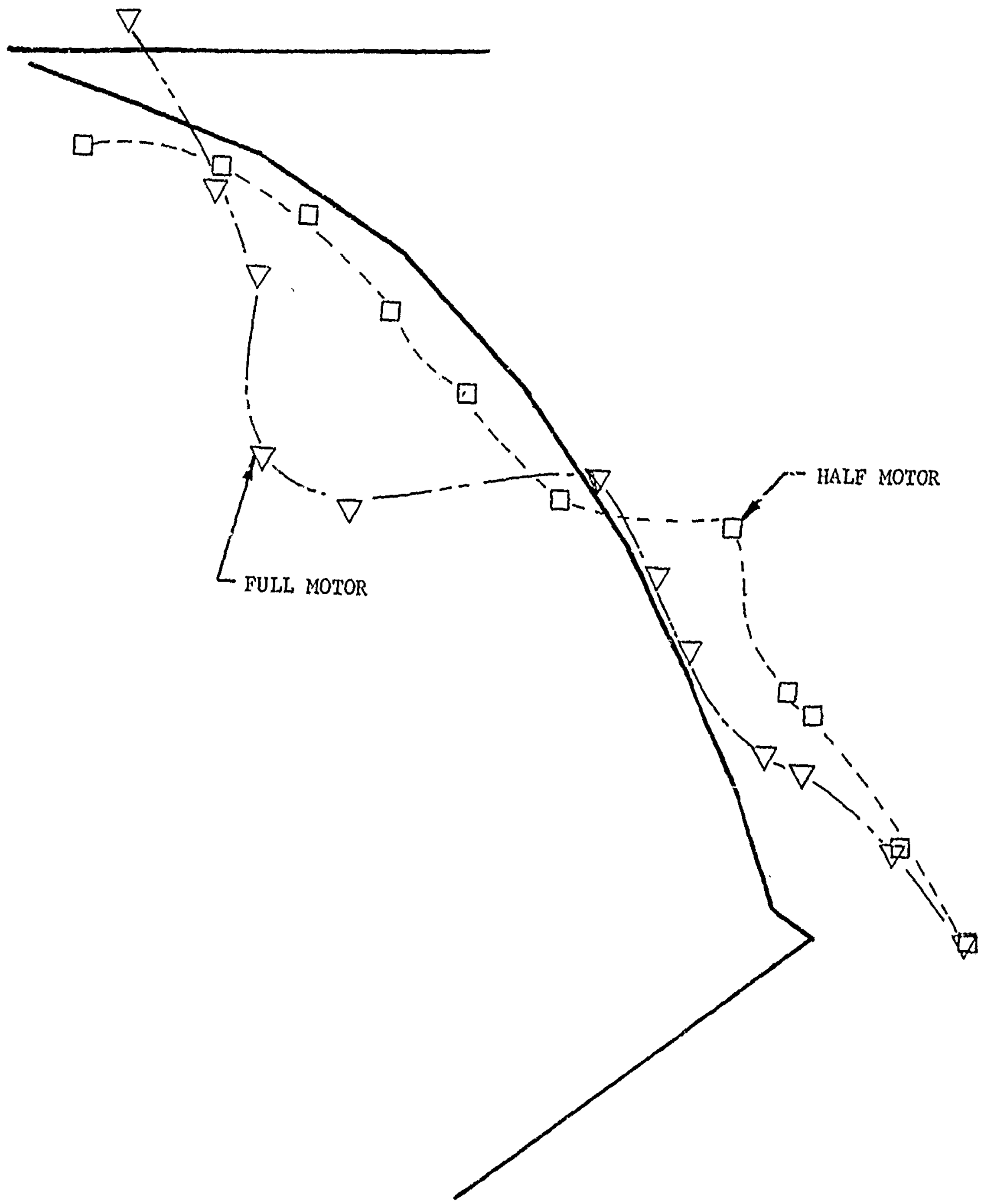

Figure 6. Aft Dome Mode Shapes for the Half and Full Motor Models with 8000 lb/in. Scalar Springs, Response to the L_4 Mode at 365 Hz

IV. SCALAR SPRING STUDY

A. Introduction

The work statement for this program specified that scalar springs be used to represent gases isolated in dome cavities. When motors with unbonded domes are pressurized, the domes can expand outward leaving gaps between the domes and the grain. When the motor is experiencing acoustic pressure oscillations, grain motion may cause the gases in the dome cavities to be repeatedly compressed and expanded. The effects of grain motion may thus be transmitted to the domes through the gases in the dome cavities. The scalar springs are intended to provide a similar load path in the finite-element model. The scalar springs are connected between the domes and the grain. This investigation was initiated to study the characteristics of the load path provided by the scalar springs.

A previous analysis[1] on the Minuteman III Third Stage motor utilized scalar springs to represent the gases in the forward dome cavity. Apparently, the grain of the Minuteman motor is forced down around the igniter, upon ignition of the motor, so that the forward dome cavity is physically sealed off from the combustion cavity until grain burning has occurred sufficient to open the seal. The Minuteman III situation is thus basically different from that of the Poseidon C-3 Second Stage motor used as a baseline motor in Task III. The Poseidon motor is unbonded at both forward and aft domes and the dome cavities open into the combustion cavity as soon as the motor is pressurized. Scalar springs were used in the model of the baseline motor for the Task III analyses. This study is based upon the baseline motor model.

B. Approach

Several different analyses were performed to study the behavior of the scalar springs. Frequency response analyses were performed on the full motor model at two different frequencies using two different modes (L_3 and L_4). The analyses were repeated both with and without the scalar springs installed. Forces in the scalar springs have been calculated as have the corresponding effective pressure distributions. One pair of scalar springs in the half motor model were released from the aft dome and given a unit deformation in the axial direction (with a static load) to determine what fraction of the unit deformation could be attributed to grain flexibility and what fraction could be attributed to spring flexibility. Frequency response analyses were performed on the half grain model with the dome end of the scalar springs constrained to zero displacement. Forces in the scalar springs were plotted as a function of frequency to show how the load transmitted to the dome could change with frequency. In addition, frequency response analyses were performed on the aft dome model using various combinations of positive and negative unit forces in place of the springs. Results from the various analyses lumped together under the heading: "Scalar Spring Study", provide insight on the general structural behavior of the motor model.

C. Static and Dynamic Analyses

1) Calculation of Scalar Spring Stiffnesses

Calculation of the spring coefficients for the scalar springs used in the baseline motor analysis was based on a simple application of

Boyle's law; $P_o V_o = P_1 V_1$. The initial pressure and volume for the gases in a segment of the dome cavity to be represented by scalar springs are denoted P_o and V_o, respectively. The volume is bounded on one side by the inside of the dome and on the other side by the propellant grain. A uniform movement of the grain tending to close the gap causes a compression of the gases to P_1 and a reduction in volume to V_1. The force required to effect the volume change is $\Delta F = (P_1 - P_o)A$, where A is the effective surface area of the grain over which the pressure acts. For a linear spring, the stiffness is defined by: $k = \Delta F/\Delta X$, where ΔX is the deflection of the grain that causes the volume to be reduced from V_o to V_1. The geometry for the assumed dome cavity is shown in Figure 7.

Solving the ΔF equation for P_1 gives:

$$P_1 = \frac{\Delta F}{A} + P_o$$

The expression for V_1 is: $V_1 = V_o - A\Delta X$

Substituting for P_1 and V_1 in Boyle's law gives:

$$P_o V_o = \left(\frac{\Delta F}{A} + P_o\right)\left(V_o - A\Delta X\right)$$

This can be reduced to:

$$k = \frac{\Delta F}{\Delta X} = \left(\frac{P_o A}{X_o - \Delta X}\right)$$

This equation shows that k is not a constant since ΔX appears on the right-hand side. The effective stiffness of the gas in this sample model is a function of displacement.

Assuming that ΔX is small compared with X_o, and using the values $P_o = 200$ psi, $A = 40$ in.^{2}, and $X_o = 0.5$ in., a value of $k = 16000$ lb/in. is calculated. Since two springs are used, one on each side of the grid slice, each spring must have a stiffness of 8000 lb/in. In the actual motor, grain deformations probably force gas from the dome cavities into the centerbore with very little increase in pressure. Therefore, this closed volume model is not likely to be very accurate.

2) <u>Motor Frequency Response Analyses</u>

Frequency response analyses were performed on both half motor and full motor models at 265 Hz and 365 Hz using the L3 and L4 modes. The analyses were performed both with and without scalar springs. Aft dome mode shapes comparing half and full motor models were shown in Figures 4 and 5. The mode shapes have been replotted to compare results with and without the use of scalar springs in Figures 8 and 9.

3) Dome Pressure Caused by Scalar Springs

In the frequency response analyses, pressure modes L3 and L4 were applied along the centerbore of the grain. Both pressure modes are normalized to have a maximum value along the centerbore of 1.0 psi. The pressure distributions applied along the centerbore of the grain cause the grain to deform and compress the scalar springs. The forces in the springs effectively apply a pressure distribution to the dome. The magnitude and distribution of the pressure applied to the dome is of interest.

Locations and identifications of the scalar springs in the aft dome cavity are shown in Figure 4. Forces in the scalar springs and corresponding equivalent pressures are shown in Table II. The full motor model had scalar springs in the aft dome only. The forward dome was left unconstrained; i.e., the grain was not attached (bonded) to the dome. Since the half motor model was analyzed with symmetry boundary conditions, results obtained are applicable to a motor loaded with a symmetric load.

4) Scalar Spring Stiffness Relative to Grain Stiffness

If the scalar springs in the dome cavities were rigid links, then any dome modes that involved motion of the spring connection points would require a corresponding motion of the grain. Since the grain is heavily damped, the use of rigid links could impose an unrealistic damping on the dome motion. On the other hand, if the scalar springs were soft in comparison with the grain, the grain damping would have little effect on the dome motion.

To determine the relative stiffness between the grain and the scalar springs, a pair of springs was disconnected from the dome of the half motor model and the disconnected ends given a unit displacement. The configuration for this static analysis is indicated in Figure 10. For a scalar spring stiffness of 8000 lb/in., and a grain shear modulus of 333 psi, a grain deformation of 0.68 inch was calculated at the spring attach points. Thus, of a 1.0 inch applied displacement, 68 percent occurs in the grain, and only 32 percent is due to stretching of the spring. When the spring stiffness was reduced to 1000 lb/in., 23 percent of the deformation was due to grain movement while 77 percent was due to spring stretch. The grain shear modulus of 333 psi represents grain stiffness only at very low frequencies (close to 1 Hz). At higher frequencies, the grain stiffness increases due to the viscoelastic behavior of the propellant. At 100 Hz, the grain stiffness is three to four times higher. Even with a stiffer grain, it appears that a significant amount of grain motion must occur when the 8000 lb/in. scalar springs are stretched or compressed.

5) Frequency Response Analyses of the Aft Dome

To determine how the dome responds to forces applied by the scalar springs, a series of frequency response analyses were performed. The three loading systems used are shown in Figure 11. Any general scalar spring force distribution can be represented by the appropriate combination of the three loading systems shown. The forces were applied at the spring attach points.

In order to efficiently calculate the dome response at many different frequencies, a real eigenvalue analysis was performed and a coordinate transformation to modal coordinates was made (NASTRAN Rigid Format No. 11). The first 40 natural modes, covering frequencies up to 2150 Hz, were used as generalized coordinates in the modal analyses. The Givens method in NASTRAN was used to calculate all 166 eigenvalues for the dome-only model. The solution required 5 to 6 minutes CPU time including recovery of 40 eigenvectors.

The frequency response analyses covered the range from 1.0 to 1000 Hz in 5 Hz increments for each of the three different loading conditions. These analyses were performed by using a restart from a previous run where eigenvalues were calculated. About 24 minutes CPU time were required to complete all frequency response analyses. Several computer-generated plots were obtained from the frequency response computer run.

Figure 11 shows the radial displacement response at node 199 as a function of frequency for the three different loading systems. The locations of the nodes are shown in Figure 11. The axial displacement responses at nodes 229 and 237 are shown in Figure 12. The axial displacement response at node 225 and the axial acceleration response at node 257 are shown in Figure 13. The axial and radial displacement responses at node 257 are shown in Figure 14. Node 257 represents the point on the adapter ring where the components are attached. The three loading systems shown in Figure 11 are denoted (plus, plus, plus), (plus, minus, plus), and (plus, plus, minus) in bottom to top order. In each of the figures showing response curves, the three curves shown are for the three corresponding loading conditions in the same bottom to top order as shown in Figure 11.

6) Radial to Axial Motion Transfer

When it was discovered that the forces in the scalar springs were very small, it became evident that the applied centerbore radial pressure loads were transmitted to the domes in some way other than through the scalar springs. The only other possible load path is through the wye joints. The possibility that dome axial motion is mainly a result of axial motion at the wye joint seems unlikely because the cylindrical case is quite stiff in the axial direction and corresponding axial displacements at the wye joints are small. Therefore, the dome axial motion must be strongly coupled to the radial motion at the wye joints.

Several computer runs were made to study the relationship between the case radial motion and the dome axial motion. First, a static unit load was applied at the wye joint (node 199) in a radial direction. As shown in Figure 15, an outward case deflection causes an inward dome deflection. The ratio between radial wye-joint deflection and axial adapter ring deflection ($199_R/257_A$), is 2.5 for a static load.

Frequency response analyses were conducted by varying the frequency of the applied unit load from 0 to 1000 Hz. The analyses are similar to those discussed above where three sets of unit loads were applied at the scalar spring attachment points. The radial displacement response and the forces required to maintain the constraints at the wye joint are plotted as a function of frequency in Figure 15. The corresponding displacement and acceleration responses for three other points along the dome and for the adapter (node 257) are shown in Figure 16. Also shown in Figure 16 is the acceleration response at node 257 in the axial direction.

D. Discussion of Results

Results from the analyses discussed above clearly show the behavior of the scalar springs used in the baseline motor analysis. In addition, results from some of the analyses give added insight into the general dynamic structural behavior of the motor model. The springs appear to be stiff compared to the grain. In spite of their apparent stiffness, the springs transmit only very small forces to the domes. The small forces transmitted to the domes by the springs do not approximate the pressure distributions in the dome cavities that are due to oscillations in the combustion cavity in a particular acoustic mode. The scalar springs were used in the finite-element model in lieu of applying a pressure distribution in the dome cavities. The scalar springs were used to allow motion of the grain to be transmitted to the domes through the combustion gases.

The apparent stiffness of the scalar springs relative to the grain is no doubt partially due to the fact that only three pairs of springs were used to represent all of the gases in the dome cavity. The three lumped springs only provide a crude approximation to the actual continuous gas distribution in the dome cavity and stress concentrations no doubt occur in the grain at the spring attach points. If a larger number of springs had been used, each spring would have a smaller stiffness value and therefore would appear less stiff relative to the grain.

1) Spring Stiffness Calculations

The use of Boyle's law to calculate scalar spring stiffnesses may seem like an oversimplification, but the use of a more refined closed volume model was not considered to be warranted since the actual dome cavity volumes are open to the combustion cavity. The fact that the dome cavities are open should reduce the effective stiffness of the gas from that calculated for a closed volume. The 8000 lb/in. spring stiffnesses used in the baseline motor analysis should apparently be considered as upper limit stiffnesses, and yet the pressures applied to the domes by the springs are very low, as shown in Table II.

2) Frequency Response of the Motor

Even though the forces in the scalar springs are small, the scalar springs can apparently cause a change in the mode shape of the response. Figure 8 shows the difference in the mode shapes calculated for the full motor model with and without using scalar springs. On the other hand, Figure 9 shows that the mode of response for the half motor model is nearly the same with or without scalar springs.

The reasons for the differences between results from the half and full motor models probably have to do with the boundary conditions used in the half motor model. The mode shapes shown in Figure 8 represent the aft dome response to the third longitudinal acoustic mode. The third mode tends to be somewhat asymmetric about the motor midplane in such a way that the pressure is positive in the forward end while it is negative in the aft end. An asymmetric type mode (such as L_3) would tend to cause more longitudinal motion of the grain than a symmetric loading (such as L_4). The spring pressures shown in Table II for the L_3 mode and the L_4 mode tend to bear out the idea that more axial grain motion is associated with the L_3 mode than with the L_4 mode. The axial grain motion would not occur in the half motor model, to a large extent, because the motor mid-plane is fixed against axial displacement. The fixed mid-plane of the half motor model is probably responsible for the low spring pressures shown in Table II for the half motor model. The maximum spring pressure in the half motor model for the L_3 mode was 0.0047 psi compared to 0.0303 psi for the full motor model. Apparently, the small spring forces in the half motor model were not sufficient, in either magnitude or distribution, to cause a significantly different aft dome response mode (as shown in Figure 9).

3) Frequency Response Analyses of the Aft Dome

The frequency response analyses were conducted to determine how the dome could be expected to respond to general loads applied through the scalar springs and to determine how sensitive the response would be to changes in load distribution. The response plots shown in Figures 11, 12, 13, and 14 show the general response behavior of the aft dome.

The response curves for the three different loading systems are strikingly different. For example, the displacement response in the radial direction at node 199, Figure 11, shows a major peak at about 320 Hz for the (plus, plus, plus) load distribution. The corresponding peak on the response curve for the (plus, minus, plus) load distribution is relatively small. The (plus, plus, plus) response curve has a minor peak at about 430 Hz which does not show up at all on the (plus, minus, plus) response curve and on the (plus, plus, minus) response curve, the 430 Hz peak is the major response peak. Similar comparisons can be made between the plots of Figures 12, 13, and 14.

The aft dome frequency response analysis results are very important because they show that realistic and accurate loading distributions must be input to the dome in order to accurately calculate the dome frequency response. The comparisons made above, between response curves for different loading distributions, indicate the magnitudes of errors that might be expected when incorrect loading distributions are used.

In the baseline motor analysis, no pressure distributions were applied to the domes. Instead, scalar springs were used to allow the grain to transmit forces to the domes. The small pressures applied by the scalar springs are no doubt inaccurate. The task of determining accurate and realistic pressure distributions is not an easy one. The extent to which dome cavities open up and the timing with which they open up during a firing are not well known. The model[2] of the acoustic cavity that was used to calculate the gas modes used in the baseline motor analysis did not include dome cavities. Recent analyses performed on an acoustic model with dome cavities indicates that pressures as high as those in the centerbore can be expected in the dome cavities. In addition, pressure mode shapes in the dome cavities appear to be extensions of the mode shapes in the main combustion cavity.

4) Radial to Axial Motion Transfer

When pressure oscillations occur in the combustion cavity, the cylindrical portion of the case is caused to expand and contract in a radial direction. The radial expansion and contraction of the cylindrical case section can cause axial dome motion as shown in Figure 15. The response of the aft adapter calculated in the baseline motor analysis is probably due mostly to radial case/grain motion. During actual motor operation, the response at the aft adapter is likely the result of both radial case/grain motion and the pressure oscillations that occur in the dome cavities.

The response plots shown in Figures 15 and 16 indicate the general dome behavior to be expected from oscillatory radial case motion. In the aft dome model analyzed, the axial displacement and the r-z plane rotation were constrained to zero. The SPC (constraint) forces required to maintain the displacement and rotation constraints are plotted as a function of frequency in Figure 15. The plots shown in Figures 15 and 16 show that most of the dome modes can be excited by the radial motion input at the wye joints. This is in contrast to the dome pressure loading where some modes were not excited at all by a particular loading distribution.

E. Conclusions and Recommendations

The behavior of the motor model with scalar springs used in the dome cavities has been studied in detail. Perhaps it may seem that too much detail was included in the study. However, the insight gained into the general structural behavior of the motor model should prove to be very worthwhile. In particular, results from the dome frequency response analyses and the radial-to-axial motion transfer should provide a better understanding of general dome behavior.

Results from this study show that the scalar springs used in the baseline motor analyses were inadequate. The springs did not apply a realistic pressure distribution in the dome cavities, and the possibility that spring coupling could result in the grain acting to damp out dome vibrations, unrealistically, was pointed out. For these reasons, the use of scalar springs in similar applications is not recommended. It is recommended that estimated (calculated) pressure distributions be applied in dome cavities to both the grain and the case in place of using scalar springs. To obtain the dome cavity pressure distributions, acoustic models with dome cavities could be analyzed or experimental data could be used.

The conclusions and recommendations given here do not apply to a previous analysis[1] which was conducted on the third stage Minuteman III motor. Apparently, the Minuteman motor has the peculiar characteristic that upon pressurization, the grain is forced down around the igniter providing a stong physical seal for the gases in the dome cavity. Since the gases in the dome cavity are in a closed volume, it is not possible for acoustic modes in the combustion cavity to affect the pressure distribution in the closed dome cavity directly. However, grain motion could cause a bulk compression of the gas entrapped in the cavity, thereby transmitting oscillatory motion to the dome. The trapped gas model used in Reference 1 utilized scalar springs, scalar masses, and multi-point constraints to model this mode of load transfer. Good results were reported for the particular trapped gas model used.

TABLE II

SCALAR SPRING FORCES AND CORRESPONDING PRESSURES FOR HALF AND FULL MOTOR MODELS

Spring No. (See Fig. 4)	FULL MOTOR MODEL			
	L_3 Mode at 265 H_z		L_4 Mode at 365 H_z	
	Force (Lbs)	Pressure (Psi)	Force (Lbs)	Pressure (Psi)
351	1.540	0.03030	0.2237	0.00383
353	-0.0938	-0.00029	-0.325	-0.00593
355	0.4181	0.00323	-0.4774	-0.00474

Spring No. (See Fig. 4)	HALF MOTOR MODEL	
	L_3 Mode at 265 H_z	
	Force (Lbs)	Pressure (Psi)
351	0.23883	0.00473
353	-0.05413	-0.00100
355	-0.27854	-0.00280

TABLE III

RELATIVE GRAIN/SPRING STIFFNESS DATA

Scalar Spring Stiffness (Lb/In)	Grain Shear Modulus (psi)	Grain Deformation (In.)	Spring Deformation (In.)
8000	333	0.68	0.32
1000	333	0.23	0.77

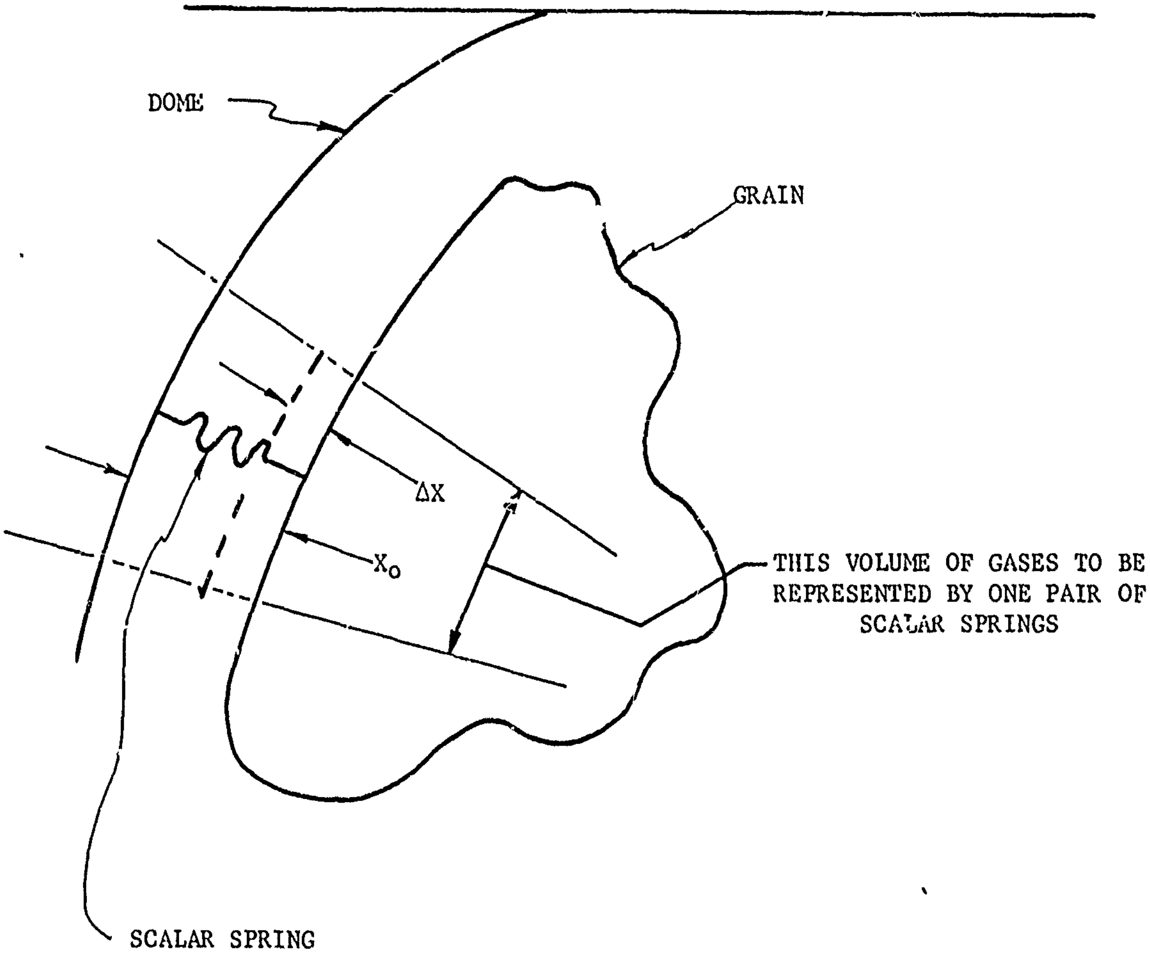

Figure 7. Sketch Showing Assumed Dome Cavity Geometry Used in Scalar Spring Stiffness Calculations

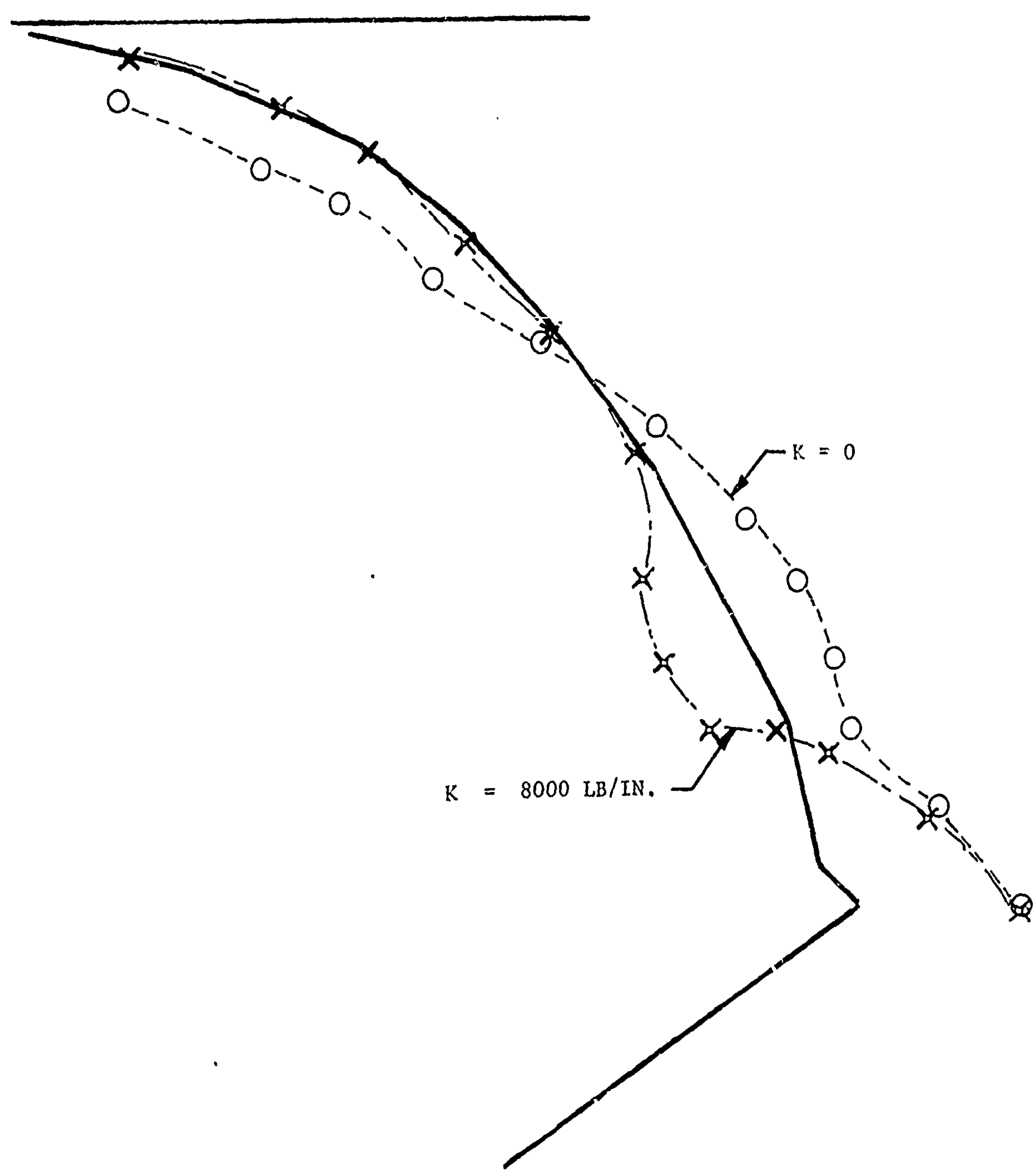

Figure 8. Full Motor Aft Dome Mode Shapes With and Without Scalar Springs for the C-3 Poseidon S/S Motor, Response to the L_3 Mode at 265 Hz

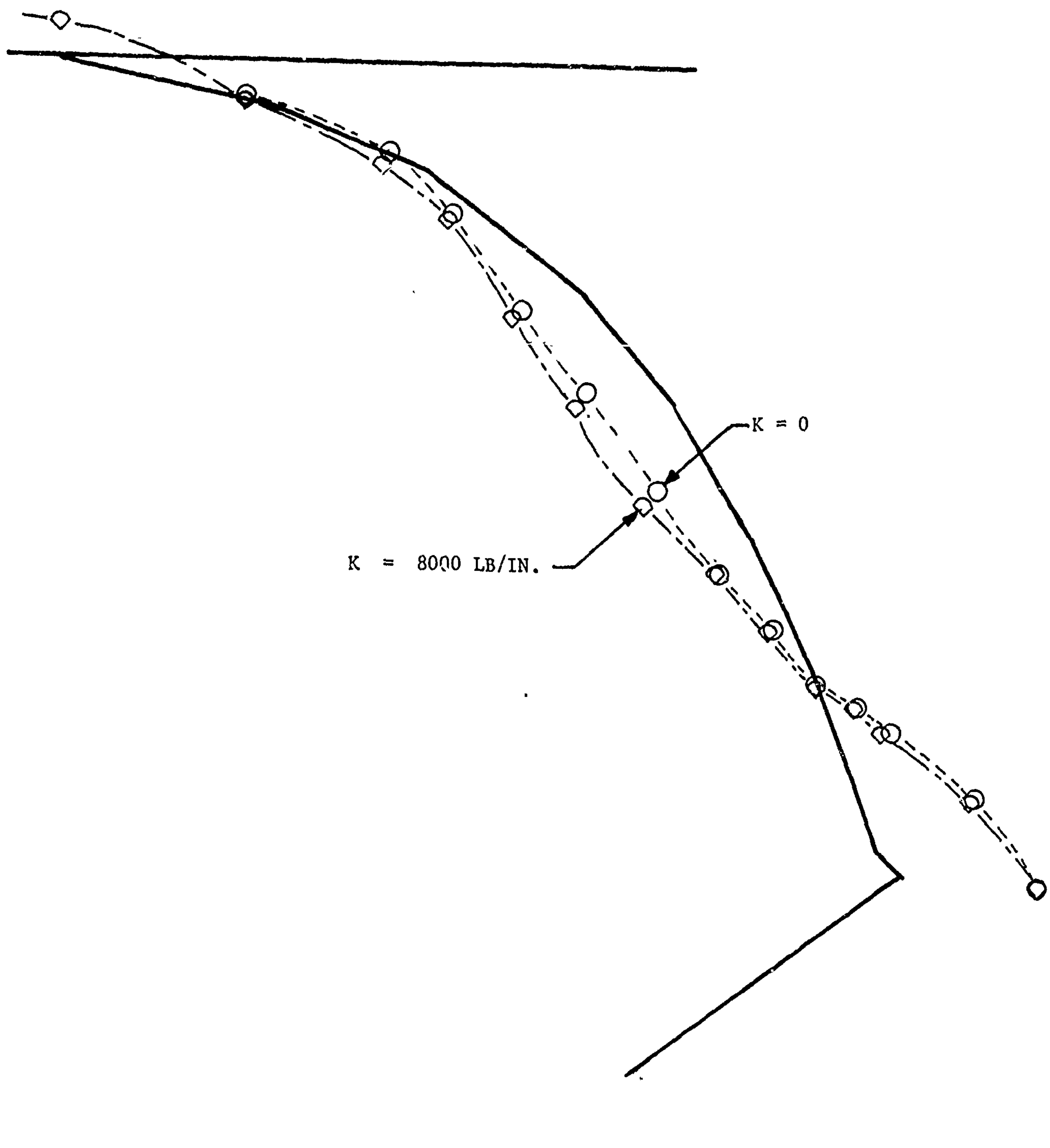

Figure 9. Half Motor Aft Dome Mode Shapes With and Without Scalar Springs for the C-3 Poseidon S/S Motor, Response to the L3 Mode at 265 Hz

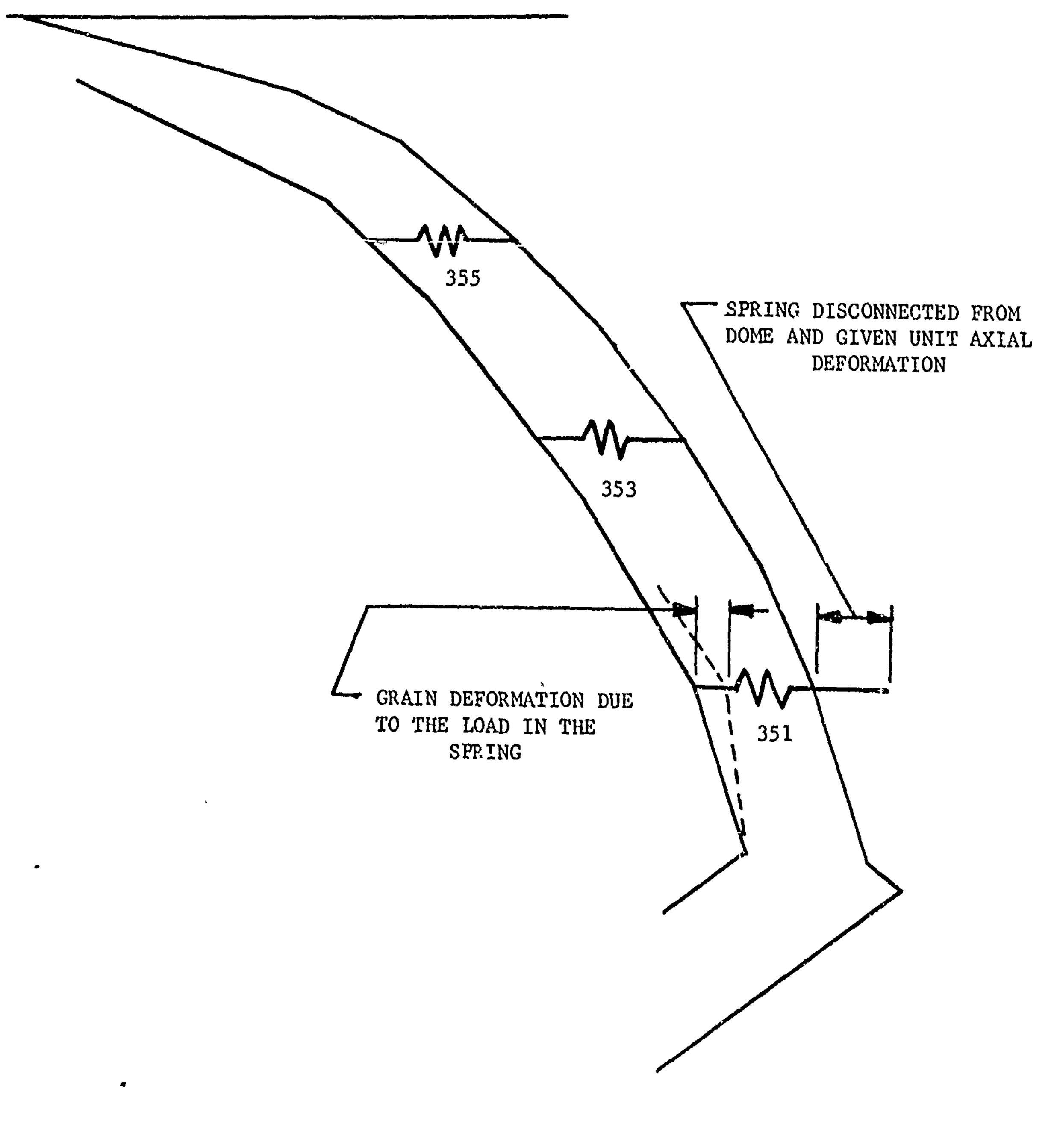

Figure 10. Static Analysis Configuration Used to Determine Relative Stiffness Between Grain and Scalar Springs

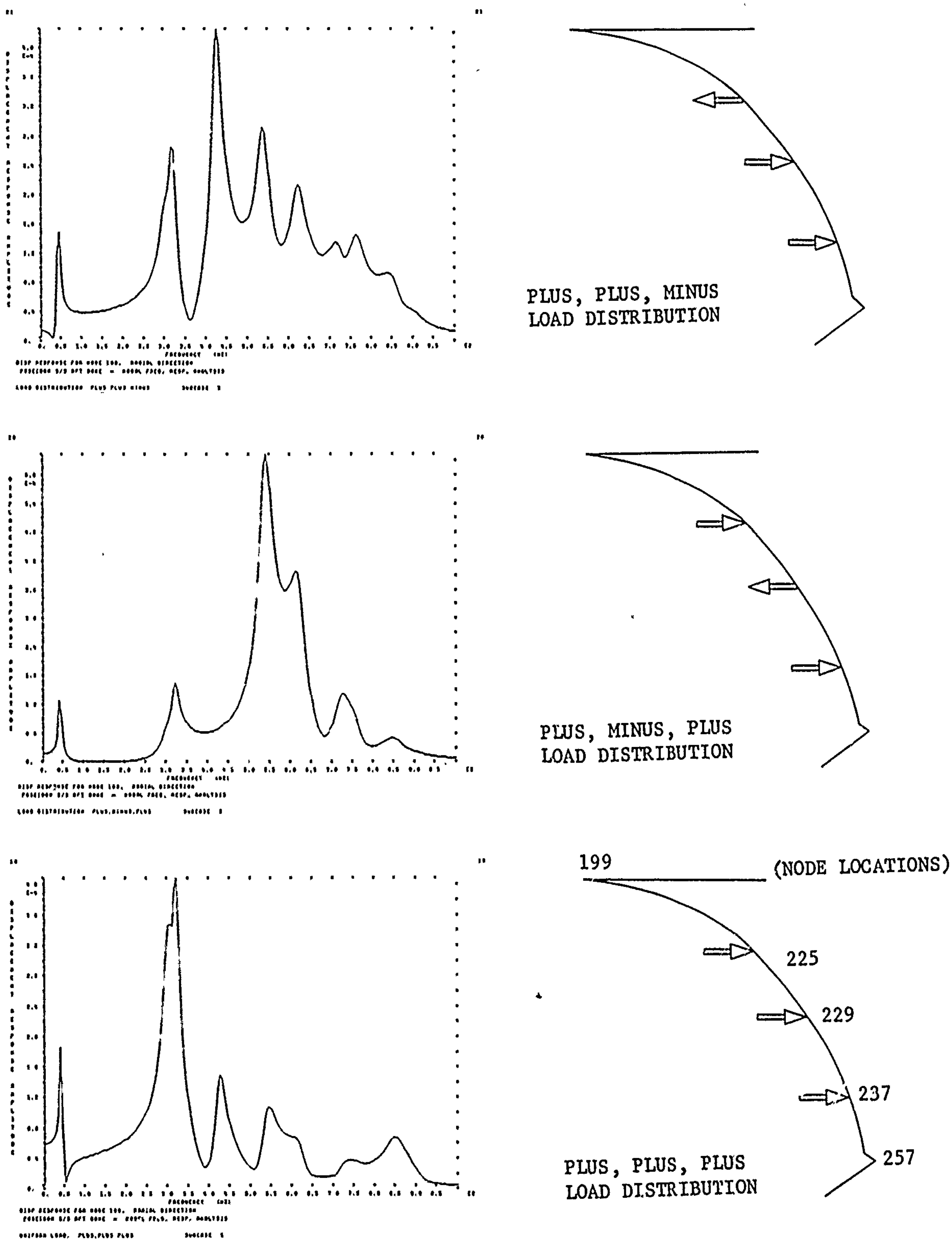

Figure 11. Aft Dome Load Distributions and Frequency Response Plots for Node 199

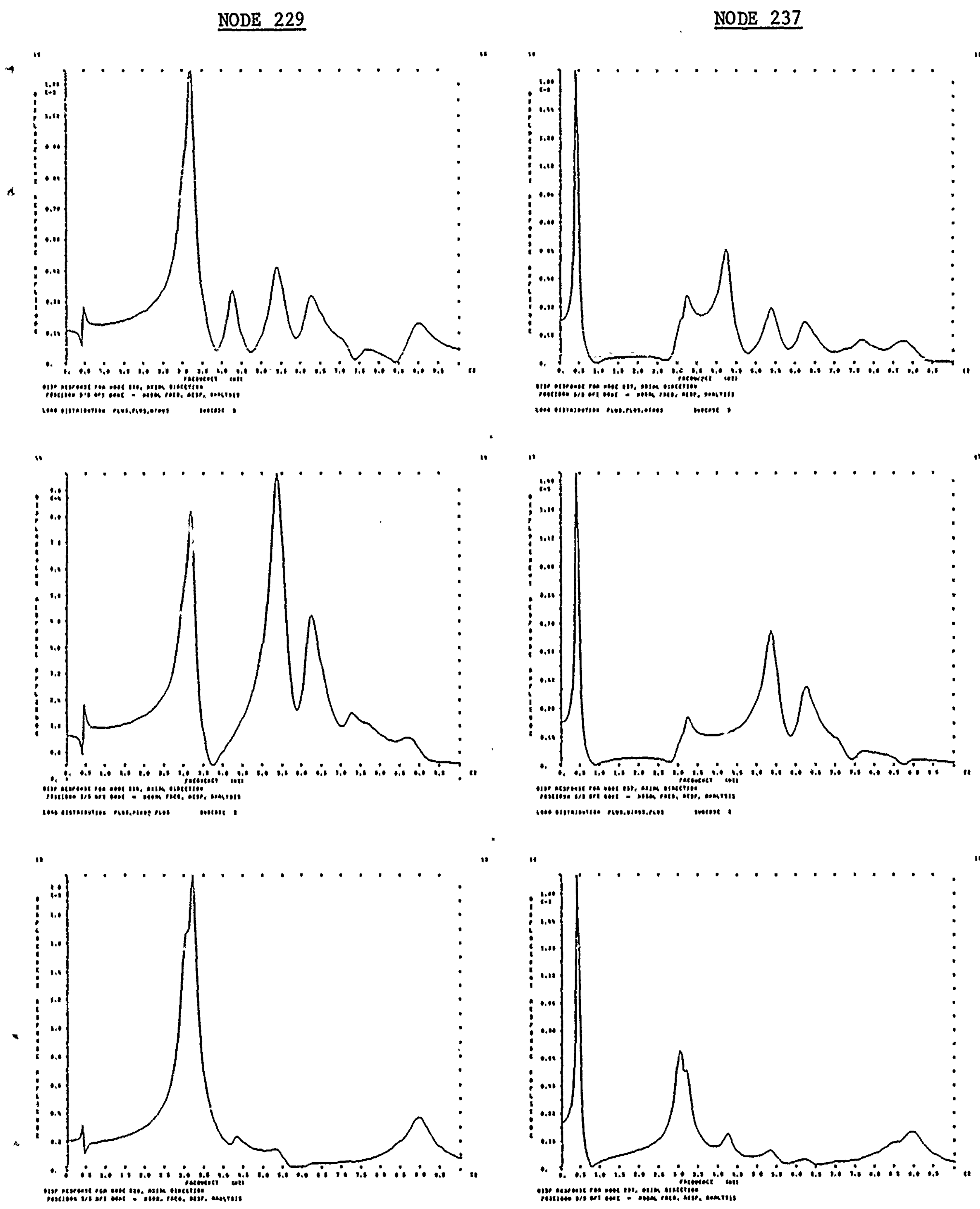

Figure 1[illegible]. Axial Displacement Frequency Response Plots for Nodes 229 and 237

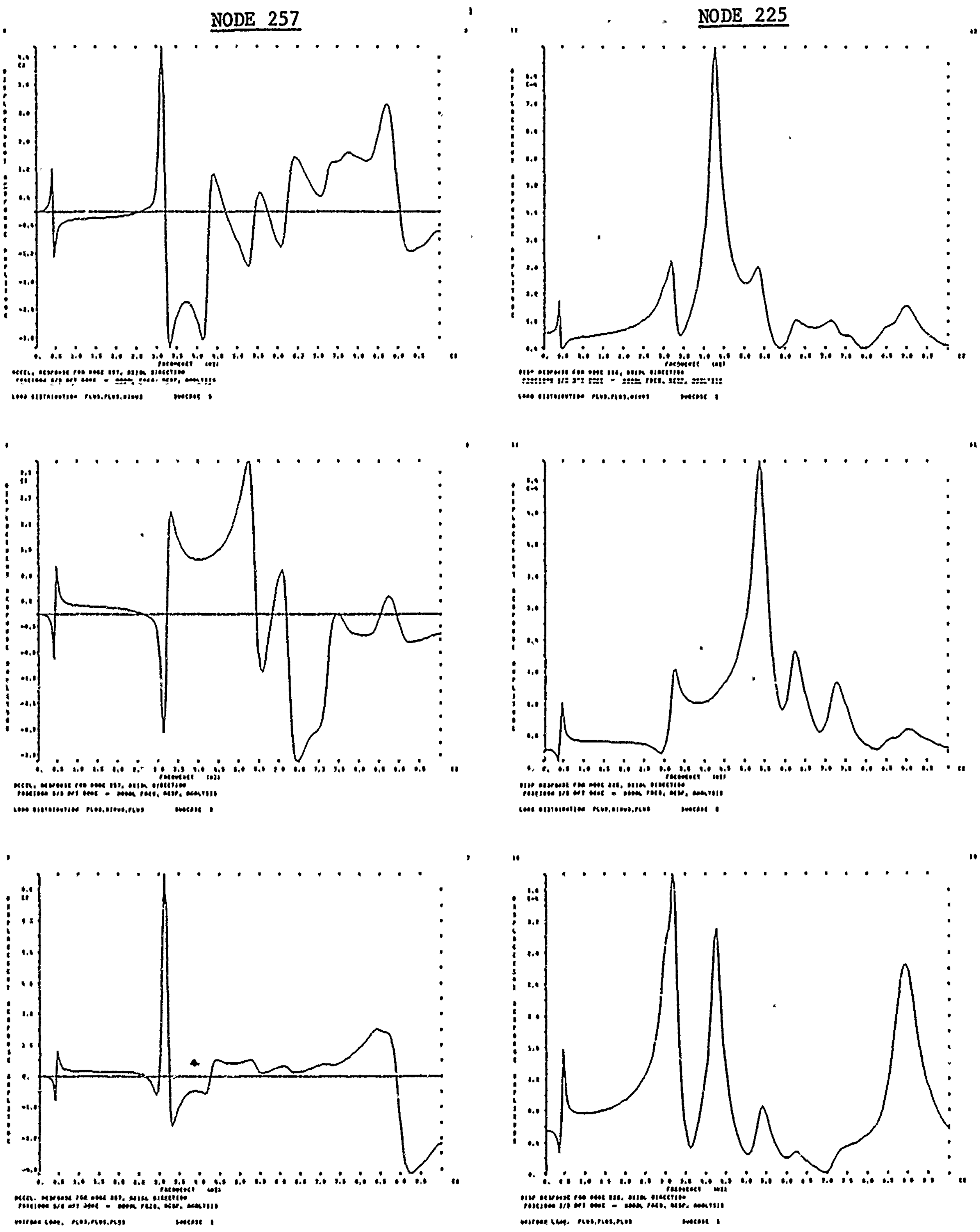

Figure 13. Axial Acceleration Frequency Response Plots for Node 257 and Axial Displacement Response Plots for Node 225

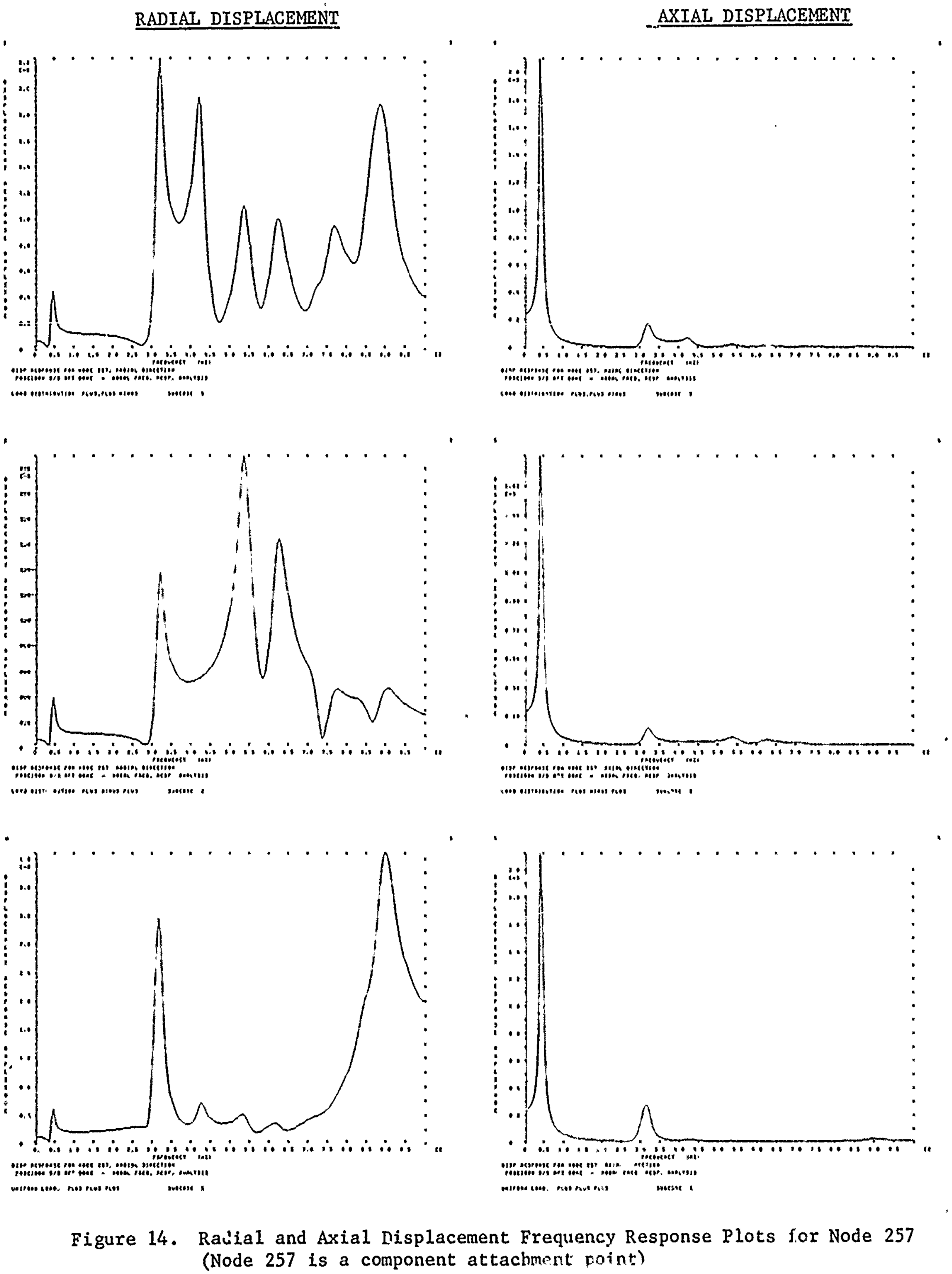

Figure 14. Radial and Axial Displacement Frequency Response Plots for Node 257
(Node 257 is a component attachment point)

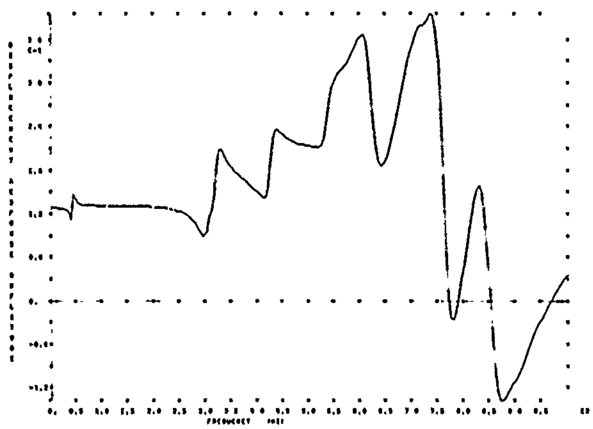

SPC FORCE FOR 199 - ROTATION CONSTRAINT

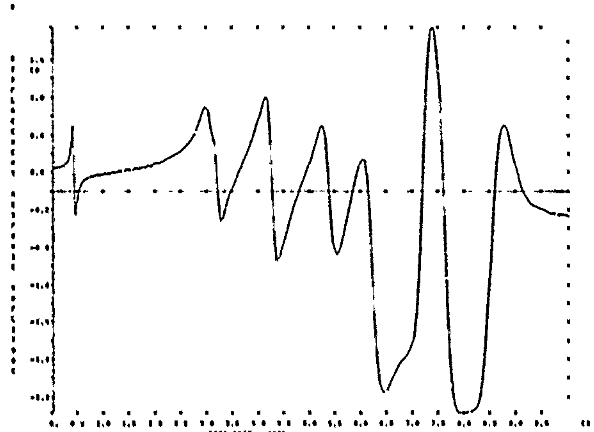

SPC FORCE FOR 199 - AXIAL DIRECTION

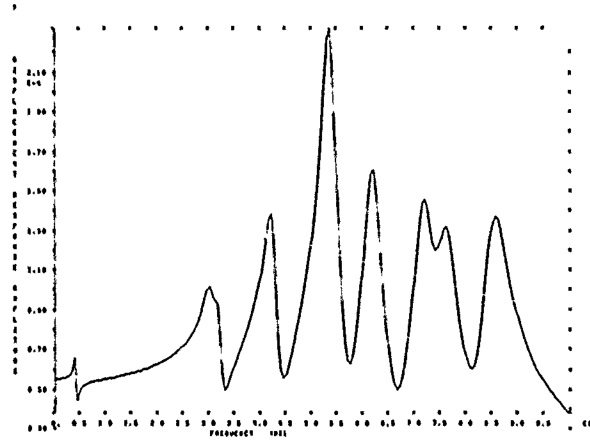

DISPLACEMENT RESPONSE FOR 199-
RADIAL DIRECTION

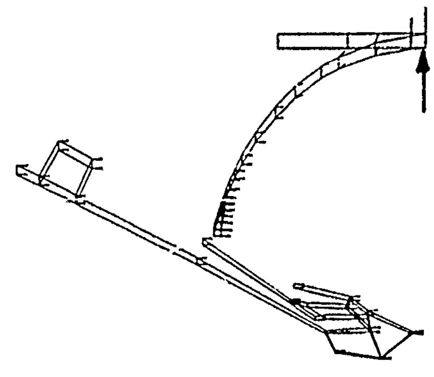

DISPLACEMENTS SHOWN BY VECTORS

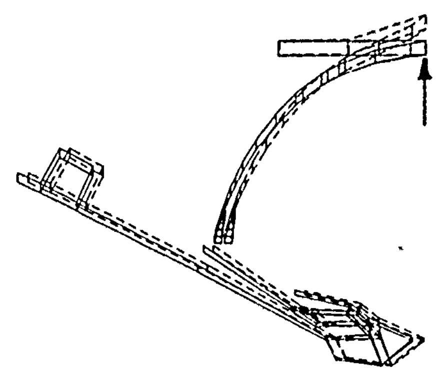

DISPLACED POSITION SHOWN BY DASHED LINES

Figure 15. Aft Dome Static Deformations for a Radial Unit Load Applied at the Wye Joint and Corresponding Response Plots for Load Frequencies Between 0 and 1000 Hz

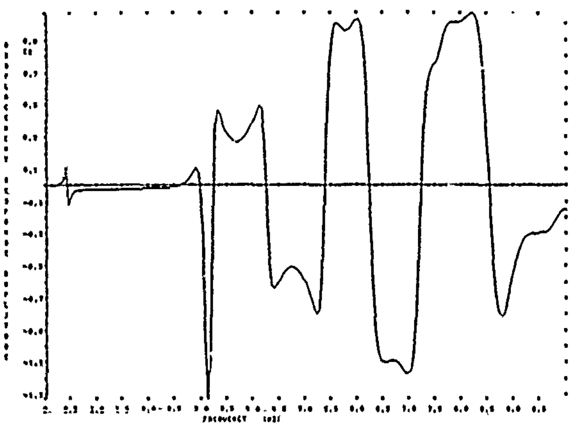

DISPLACEMENT RESPONSE FOR 257 - AXIAL DIRECTION

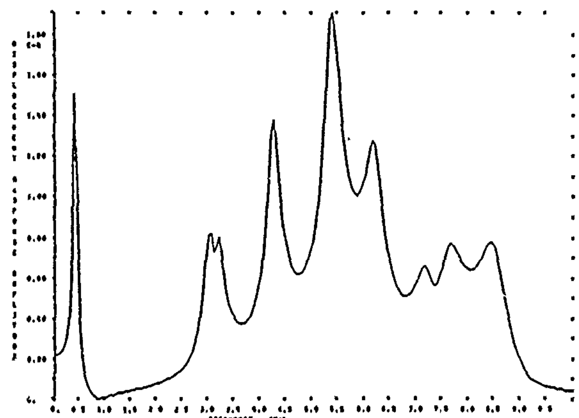

DISPLACEMENT RESPONSE FOR 237 - AXIAL DIRECTION.

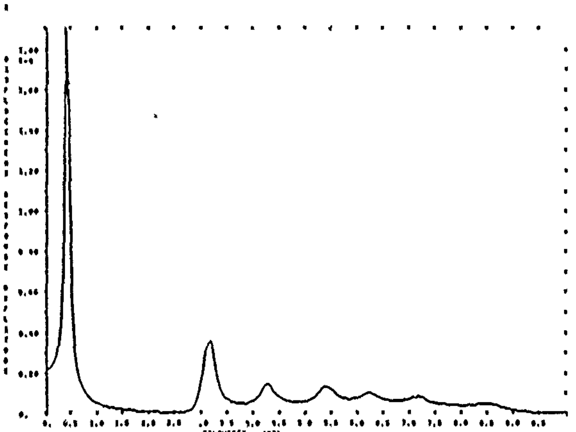

ACCELERATION RESPONSE FOR 257 - AXIAL DIRECTION

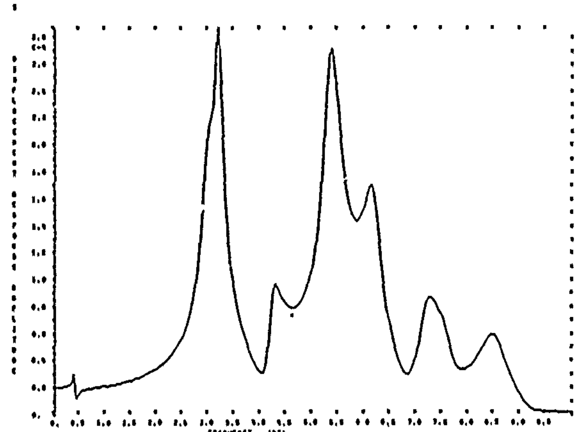

DISPLACEMENT RESPONSE FOR 229 - AXIAL DIRECTION

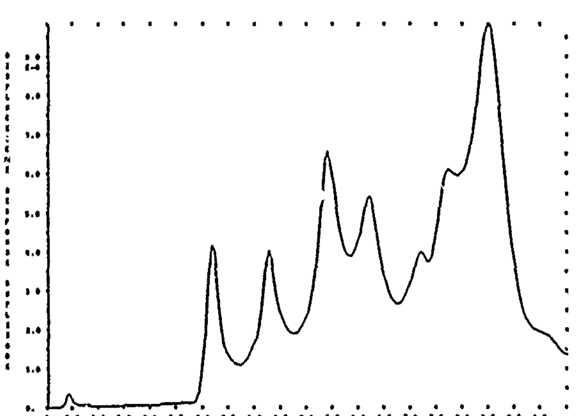

DISPLACEMENT RESPONSE FOR 257 - RADIAL DIRECTION

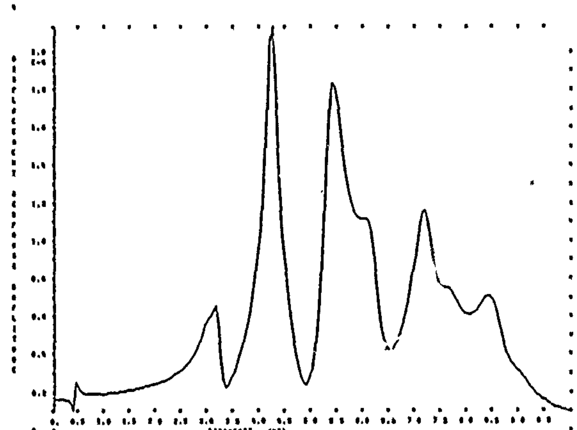

DISPLACEMENT RESPONSE FOR 225 - AXIAL DIRECTION

Figure 16. Response Plots for Nodes on the Aft Dome Responding to a Unit Radial Load at the Wye Joint

V. GRID REFINEMENT STUDY

A. Introduction

Since acoustic modes at very high frequencies are commonly observed, it would be desirable to have a finite element model that could produce accurate results at high frequencies. A rocket motor, being a continuous structure, exhibits an infinite number of natural frequencies. A finite element model, having only a finite number of degrees of freedom, can have only a finite number of natural frequencies. Each finite element model therefore has a maximum natural frequency and any natural frequency in the motor above the maximum model natural frequency is not represented by the model. As the frequency increases toward the maximum, the natural mode shapes become more complex and the accuracy of mode representation provided by the model decreases. A portion of this grid refinement study was directed at determining the frequency range over which valid (reasonably accurate) results could be obtained for the finite element model.

The question of valid frequency range cannot be answered in general because the mode of response depends to a large extent on the load distribution. The effect of load distribution on the frequency response of the aft dome was illustrated previously under the scalar spring study. A more appropriate question might therefore be: "For a particular load distribution, what is the valid frequency range for the model?" Studying the structure frequency response for a large number of load distributions would not be practical. The problem can be simplified by rephrasing the question to ask for the minimum valid frequency range; i.e., the frequency range for which the model would yield reasonably accurate results assuming the most adverse loading distribution. The problem could also be simplified by assuming a typical high frequency mode load distribution. Both simplifications have been used.

When the finite element grid for the full motor model was constructed, an attempt was made to make the grid as refined as possible while maintaining reasonable run times for a computer analysis. The grid refinement used in the dome portions of the model was selected to allow for reasonable definition of the changes in the orthotropic case properties. No guide lines were available on grid refinement required to accurately model natural mode shapes in a particular frequency range. The objective of this study was to assess the effect that grid refinement would have on the accuracy of the response of the model. The possibility of using a model with a coarser grid was to be evaluated as a possible modeling simplification.

As with the scalar spring study, the approach for the grid refinement study consisted of performing several separate analyses. Real eigenvalue solutions were obtained for the aft dome model and mode shapes were plotted over the frequency range of interest. Real eigenvalue solutions were also obtained for the half grain model. Half grain modes were plotted over the frequency range of interest. A full motor model with a very coarse grid was constructed and analyzed at 265 and 365 Hz with the L3 and L4 acoustic pressure modes. The coarse grain model was included in the study to evaluate the possibility that component response is not greatly dependent upon the accuracy with which the grain is modeled. The grain is a very massive and very heavily damped part of the rocket motor structure. The possibility that the sluggish response of the grain might cause the component response to be insensitive to locations of peaks and valleys in the grain response curve, was considered to be worth investigating.

B. Approach

One way to determine the limiting grid refinement for a particular structure, being forced at a given frequency and with a given load distribution, would be to construct a series of finite element models with decreasing degrees of grid refinement. Each model would be analyzed with the same load and at the same frequency. When displacement response results from a particular model were found to be significantly different from the results of the most refined model, the minimum acceptable grid refinement would be established. This approach was judged to be too costly and time consuming.

Another approach to the problem of establishing the degree of adequate grid refinement for a particular model is to study the natural mode shapes of the model. A rule-of-thumb that is commonly used for judging the adequacy of refinement of a particular grid is that three nodes should be used to define each half wave of the mode shape. In this study, mode shapes of the aft dome model and of the half grain model were examined in an effort to establish an upper limit frequency, above which results would possibly be in error for the particular grids being studied.

To better understand the rule-of-thumb for adequate grid refinement stated above, a uniform pinned-pinned beam was analyzed using an eight element NASTRAN model and using closed form solution. Comparisons between the theoretical and the NASTRAN models are given showing the increasing inaccuracy of the NASTRAN model with increasing mode number. Results from the beam analyses should provide a background for judging the results from the dome and grain models.

The full motor model was modified to include a very coarse grid to represent the grain. Frequency response analyses were performed using the L3 and L4 pressure modes. Comparisons are shown between results from the model with coarse grid and the original model.

C. Dynamic Analyses

1) Simply Supported Beam Analysis

A sketch of the beam model is shown in Figure 17. The equations shown on the face of Figure 17 give the closed form solutions for the beam. A NASTRAN real eigenvalue analysis was performed on the eight element model shown in the figure. A comparison between the NASTRAN calculated natural frequencies and the closed form solutions is shown in Table IV. The corresponding mode shape comparisons are shown in Figure 18. Notice that the values calculated by NASTRAN, (shown as circled points in Figure 18), are correct for all seven modes. The errors occur because sufficient nodes are not available to define a wave in the mode shape.

When a particular load distribution at a particular frequency is applied to the beam model, the response mode can be expressed in terms of a sum of fractions of each natural mode when model coordinates are used. When the applied load distribution matches exactly a natural mode the beam responds only in that mode independent of the applied frequency. The condition of the loading distribution exactly matching a natural mode shape would be rare. The response of the beam (or motor) to a similar but not exactly matching load distribution would be of more interest.

Figure 19 shows an applied load distribution and the corresponding closed form displacement response. The load distribution was arbitrarily selected to be similar to the beam second mode that occurs at 157.6 Hz. If the applied loading distribution exactly matched the second mode, then the response would be purely in the second mode. As shown, the response looks like a combination of second mode and fourth mode. The frequency of application of the applied load was exactly the same as the fourth mode natural frequency. This result shows that a high frequency mode can be excited by a low frequency-type load distribution applied at a high frequency.

2) Aft Dome Real Eigenvalue Analysis

Real eigenvalue analyses, (NASTRAN Rigid Format 3), were performed on the aft dome model. The same model used for the frequency response analyses under the scalar spring study was also used for the real eigenvalue analyses. The first 20 natural modes and corresponding natural frequencies are shown in Figures 20, 21, and 22. To simplify the problem of making reference to two typical types of mode shapes, the typical shapes will be referred to as "oil can modes" and "twisting modes". "Oil can mode" is used to describe the axisymmetric deformation of the dome that causes axisymmetric bending stresses similar to those that occur in the bottom of an oil can when the center of the can bottom is depressed with the thumb. "Twisting mode" refers to the apparent twisting of the one slice model. With reference to the total motor, lobar type modes would appear as one-slice twisting modes. Twisting modes are characterized by the two nodes opposite each other in the one slice model having equal displacements but in opposite directions. The first two twisting modes shown in Figure 20 are shown again as the two sketches at the bottom of Figure 22 to better show what is meant by "twisting mode".

The twisting modes that are calculated from any particular analysis are a function of the size of slice used in the model. A 15° angle is included between the two faces of the slice used in the model that resulted in Figures 20, 21, and 22. If a 30° slice had been used, twisting modes at different frequencies would have resulted. A possible lobar (twisting) mode for a 30° slice is shown in the center of Figure 22. Twisting modes are of very little interest in this grid refinement study.

The finite element grid refinement in the circumferential direction is of interest. A comparison between the approximation of a circle obtained by using 24 fifteen degree slices and 12 thirty degree slices is shown in the middle of Figure 22. To obtain a 30° slice model, the grid point locations for the grid points on one face of the 15° slice model were changed. The two models are thus exactly alike except for grid point locations. A real eigenvalue analysis was performed on the 30° slice model. The results are shown in Figure 23.

Because of large differences between results from the 15° and 30° slice models, one additional model was analyzed. A 5° slice model was formed by repositioning the grid points again. The mode shapes and natural frequencies obtained from the 5° slice are shown in Figure 24.

3) Half Grain Model Real Eigenvalue Analyses

Real eigenvalue analyses similar to those performed on the dome were also performed on the half grain model. Results from the analyses are shown in Figures 25, 26, and 27.

Accurate results cannot be expected from a real eigenvalue analysis of the propellant grain because the grain properties are frequency dependent. Nevertheless, the analysis is useful for identifying approximate natural frequencies and associated mode shapes so that judgements concerning the adequacy of the model over a particular frequency range can be made.

The mode shapes shown in Figures 25, 26, and 27 were obtained using a very low grain shear modulus of 333 psi. The 333 psi shear modulus corresponds to a low frequency of about 1 Hz. The natural frequencies shown in Figures 25, 26, and 27 were obtained by correcting the calculated frequency by iterating with the following equation:

$$f_n = f_{333}\sqrt{\frac{G(f_n)}{333}}$$

where: f_n - is the natural frequency estimate.

f_{333} - is the natural frequency calculated in the real eigenvalue analysis using a grain shear modulus of G = 333 psi.

$G(f_n)$ - is the grain shear modulus corresponding to frequency f_n.

It was necessary to iterate to obtain the solution because $G(f_n)$ depends on the solution, f_n.

The first 10 mode shapes and frequency estimates for the grain model with symmetry boundary conditions at the mid plane are shown in Figure 25. The corresponding first 10 modes and frequencies for asymmetric boundary conditions at the midplane are shown in Figure 26. Figure 27 was included to show some mode shapes at higher natural frequencies. The 30th through the 39th mode shape and corresponding frequencies are shown in Figure 27. Scalar springs were attached to the grain for all analyses as they were for the baseline motor analyses. The case (dome) ends of the scalar springs were constrained to have zero displacement for these real eigenvalue analyses.

4) Coarse Grain Grid Model Analyses

A clean motor model with an extra coarse grid to represent the grain was constructed. A comparison between the regular and coarse grid models is shown in Figure 28. The coarse grid analysis was intended to be identical to the regular grid analysis in every way except for the grid refinement. However, it was discovered that the same load distribution could not be applied to the coarse grid model because fewer grain nodes were available at which to apply the loads.

Both coarse and regular grid models were analyzed using the L3 pressure mode at 265 Hz. The load distributions used on each were not exactly the same because of differences in node spacing. To keep the net effect of each load the same as nearly as possible, the total positive or negative forces in each half wave of the mode shape were made equivalent. The displacement response of the coarse and regular grid models is compared at several selected points in Table 5.

D. Discussion of Results

1) Simply Supported Beam

Results from analyses on a simple beam model cannot be applied on a one-to-one basis to results from the more complicated motor models. However, having a knowledge of the performance of a beam model should be of value in making qualitative judgements on the adequacy of the motor models.

The degradation of the mode shapes supplied by the beam finite element model with increasing natural frequency is shown in Figure 18. The rule-of-thumb that 3 nodes should be available to define each half wave of a mode can be justified by the results shown in Figure 18. The second mode has 3 nodes per half wave and the comparison between closed form solution and NASTRAN solution shows very good agreement. The corresponding frequency comparison as shown in Table IV indicates that NASTRAN and theoretical frequencies are within .032 percent, surprisingly good agreement. When only two nodes are available to define a half wave of the mode shape, as in the third mode of Figure 18, the errors, (differences between theoretical and NASTRAN solutions), become more evident.

It is interesting to note that the correct displacement amplitude is calculated by NASTRAN at each node even up to the 7th mode. That is, the calculated points, shown in Figure 18 as circled points, all fall on the theoretical mode shape. The errors in mode shape prediction occur because the node density and spacing are not sufficient to define the deformed mode shape.

Based on evaluation of results from the beam analyses, it appears that the three node per half wave rule-of-thumb may be too restrictive. It is recommended that each calculated mode be judged individually without using a rigid "go" or "no-go" criteria. The curves of Figure 18 can be used as a guide. The possibility of errors should be considered when fewer than three nodes are available to define a half wave of the mode shape.

Experiments with closed form frequency response solutions for the beam model showed that in many cases the mode of the beam response followed quite closely the general shape of the load distribution. The result shown in Figure 19 is an exception because the response appears to contain higher frequency harmonics than the input load distribution. The response is a distorted fourth natural mode while the load distribution is most similar to a second mode shape. To relate these results to the beam finite element model, we conclude that the finite element model would have to be sufficiently refined to represent the fourth beam bending mode in order to provide a sufficiently accurate solution for the loading distribution shown in Figure 19 when the loading frequency is 630 Hz.

To generalize these results, we conclude that a model should be capable of representing natural mode shapes over a frequency range that includes the frequency range of the applied loading systems. In addition, the model should be capable of representing response mode shapes that are likely to be excited by the particular load distribution being applied.

2) Aft Dome Real Eigenvalue Analysis

A study of the real eigenvalue analysis results shown in Figures 20 through 24 should provide valuable insight into the structural dynamic behavior of the aft dome model. In the first mode, (f_1), as shown in Figure 20, the dome and nozzle move in and out together. The f_4 mode in the same figure shows the dome and nozzle moving in opposite directions causing deformation of the nozzle flex-seal. In some of the higher frequency modes the dome forms various waves while the nozzle is relatively quiet.

The peaks and valleys on some of the frequency response plots shown in Figures 11 through 16 can be correlated with these real eigenvalue analysis results. For example, consider the response at node 229 shown in Figure 12 for the three different loading distributions. The response plot for the plus-plus-plus loading distribution, shown in Figure 12, contains one major peak near 300 Hz. The peak is apparently a combination of response in the f_4 and f_5 modes shown in Figure 20 since both modes would likely be excited by the plus-plus-plus load distribution and the frequencies, 304 to 319 Hz, correspond with the response plot. The plus-minus-plus load distribution response plot in Figure 12 shows major response at about 320 Hz and 540 Hz. Apparently this non-uniform load distribution causes a large response in both the f_5 and the f_7 modes. An examination of the plus-minus-plus character of the f_7 mode shape shows clearly why a large response in this mode could be expected from a plus-minus-plus load distribution.

A main purpose in obtaining the real eigenvalue solution plots shown in Figures 20, 21, and 22, was to show the performance of the particular finite element grid as a function of frequency. For the f_8 mode at 620 Hz shown in Figure 20, only two nodes are available to represent half waves at two different places along the dome. Based on the experience with the beam analysis, we might judge the model to be adequate at 620 Hz but also realize that the quality (accuracy) of mode shapes for higher frequencies will decrease as the frequency increases.

The original dome model was constructed to represent a 1/24 section (15° slice) of the motor. The 1/24 section was selected because the total motor could be represented by such a section in a cyclic symmetry analysis. The motor has 12 slots in the propellant grain. An r-z plane through the middle of a slot and another half way between the slots forms a 15° slice. For a motor with fewer slots, similar reasoning would produce a large slice. A motor modeled with sections larger than 15° would have less grid refinement in the circumferential direction. To study the effects of more or less grid refinement in the circumferential direction, 5° and 30° slices were analyzed.

The results from analysis of the 30° slice are shown in Figure 23. The mode shapes and natural frequencies do not compare well with those obtained for the 15° slice shown in Figure 20. The first natural mode for the 30° slice occurs at a frequency 24% higher than the 43.3 Hz calculated for the 15° slice. The nozzle-dome mode (f_3 for the 30° slice) occurs at a frequency of 335 Hz which is 10% higher than the corresponding 304 Hz mode in the 15° slice model. Other modes in the 30° slice model have similarly large errors when compared to results from the 15° slice model.

The results from analysis of the 5° slice model as shown in Figure 24 can be compared with the results from the 15° slice model in Figure 20. The first natural frequency of the 15° slice model is in error by 11% when compared to the 5° slice results. No twisting modes were found among the first 8 modes in the 5° slice model.

A peculiar difference between the 5° slice and the 15° slice is seen by comparing the nozzle-dome modes for each model, (the "nozzle-dome mode" refers to the mode where the nozzle and dome move in opposite directions). In the 15° slice model, the nozzle-dome mode occurs with the dome in a first-oil-can type mode at 304 Hz. In the 5° slice model, a dome mode occurs at 251 Hz without any significant nozzle participation. Then, two modes involving the nozzle occur along with higher order dome modes at 299 Hz and 310 Hz, (f_3 and f_4 in Figure 24). Based on this analysis, it appears that even a 15° slice may not be providing sufficient grid refinement in the circumferential direction.

3) Half Grain Model Real Eigenvalue Analysis

The three-node-per-half-wave rule discussed above can be applied to results from the half grain analyses. The f_{10} mode shown in Figure 25 has the following sequence of radial displacements for nodes along the center bore starting at the motor mid-plane and moving aft: positive, positive, negative, negative, positive, negative. For the 203 Hz f_{10} mode, only one or two nodes define each half wave of the mode shape along the center bore. Since less than three nodes per half wave are available to define the mode shape, we conclude that the mode shape accuracy provided by the half grain model deteriorates above approximately 200 Hz. The mode shapes for the asymmetric boundary conditions shown in Figure 26 appear to be of approximately equal quality with those shown in Figure 25. The higher frequency mode shapes shown in Figure 27 are definitely of inferior quality. Several twisting modes are shown and many of the uniform modes have only one node to define a half wave of the deformed shape.

The conclusion that the accuracy of results obtained from the half grain model deteriorates for frequencies above 200 Hz needs to be clarified. Obviously the mode shapes obtained from real eigenvalue analyses of the model will be inaccurate for natural frequencies above about 200 Hz. However, the main use of a grain model is for frequency response analysis. For frequency response analyses, the 200 Hz frequency limitation would apply only if the loading distribution were such that modes like f_{10} in Figure 25 would be excited. For frequency response analyses, it is recommended that response modes be examined and judged for each different loading distribution and each different frequency. To estimate the grid refinement required for the grain before the model is constructed, the response modes must be estimated. The loading distributions to be applied and the natural mode shapes shown in Figures 25, 26, and 27 can be used as a guide. To provide one additional result to guide estimation of response modes, the response of the grain surface along the center bore, to the L3 acoustic mode at 770 Hz, is plotted in Figure 29.

4) Coarse Grain Grid Model

The response of the coarse grid model compares quite well with the response of the regular grid model considering that the grain representations are very different between the two models (see Figure 28). As shown in Table 5, the radial displacement at the wye joint was underestimated by the coarse grid model by about 21%. The axial displacement at the aft adapter where the components are mounted was underestimated by the coarse grid model by about 17%. The largest percentage error for the data shown in Table 5 occurs at node 145 where the coarse grid underestimates the deflection by 86%. For the particular frequency and load distribution used in these comparison analyses, the coarse grid generally underestimates the response. With a different loading distribution and a different frequency, the coarse grid might be found to over-estimate the response.

The data shown in Table 5 were provided to assist the analyst in making decisions about the use of coarse grids. The degree of grid refinement to be used in the grain model must be selected based on the following considerations: (1) the shape of the loading function, (2) the frequency range to be covered, and (3) the limited degrees of freedom available to maintain reasonable computer run times and analysis costs. The coarse grid versus regular grid comparisons were obtained by analyzing single slice models with symmetry boundary conditions, (cyclic symmetry was not used). The coarse grid analysis required about 9 minutes CPU time while the regular grid required about 15 minutes CPU time. The difference would be considerably larger for a full cyclic symmetry analysis.

E. Conclusions and Recommendations

Results presented from this grid refinement study have provided a valuable insight into the structural dynamic behavior of the motor model. The results should also be valuable for reference when decisions must be made regarding degree-of-grid-refinement to be used in a particular finite element model.

Based on the results of the grid refinement study as well as other experience gained during the coarse of the Component Vibration program, the following recommendations are made regarding selection of grid refinement:

1) Consider the loading distribution with the shortest half wave length, (usually the highest frequency acoustic mode). Plan to use 6 nodes along each half wave length of the loading distribution. The loading distribution may cause a response of modes with higher harmonics. If the response mode has a half wave length one-half that of the loading distribution half wave length, then 3 nodes will be available for each half wave of the response.

2) Concentrate first on getting adequate grid refinement for the domes where the components are attached. The domes are the most important parts of the model when component response is desired.

3) If sufficient degrees of freedom are not available, a more coarse grain representation should be considered. If a coarse grain model is found to be desirable, an attempt should be made to use more nodes around the grain boundaries and fewer nodes in the grain center. This will provide more nodes for a better definition of the loading function and more nodes for interfacing between the grain and case. Figure 30 shows some recommended configurations for concentrating the nodes around the boundaries. No results are available for the recommended grid configurations.

4) Results from the aft dome model analyses indicated that a slice smaller than 15° would be desirable. In a cyclic symmetry analysis, the size of the slice is usually determined by the number of slots in the grain. It is recommended that extra slots be introduced in the model if necessary to obtain a single slice smaller than 15°. For example, a motor with 6 slots could be analyzed as though it had 12 slots so that a 15° slice could be used as a model, or 24 slots could be used to obtain a $7\frac{1}{2}^{\circ}$ slice model.

The recommendations made here are based on experience gained in analyzing the C-3 Second Stage Poseidon motor. The Poseidon motor has unbonded domes. For a motor with bonded domes or other major differences, different modeling procedures may be desirable. The modeling recommendations given here are only intended to provide guidelines that must be modified or tailored to fit a specific different situation.

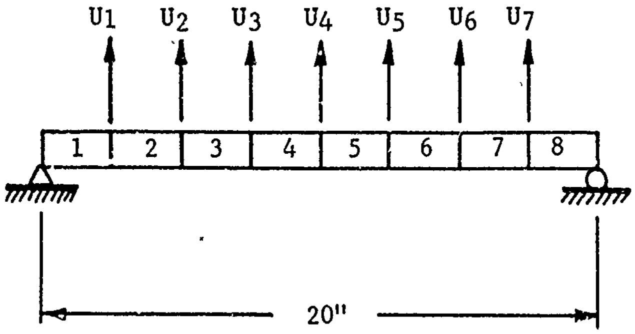

FINITE ELEMENT BEAM MODEL

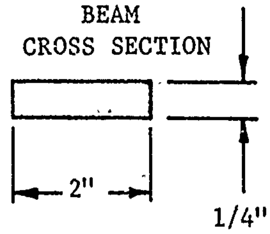

$I = 0.002604$ IN.^{4}
$E = 5 \times 10^6$ PSI
$\rho = 2.58799 \times 10^{-4}$

$$f_n = \frac{n^2 \pi}{2 \ell^2} \sqrt{\frac{EI}{m}} = (39.3911)\, n^2$$

f_n = NATURAL FREQUENCY OF NTH MODE

$$\varphi_n (X) = \sin \frac{n \pi X}{\ell}$$

φ_n = NATURAL MODE SHAPE

Figure 17. Beam Model Used to Study Mode Shapes

TABLE IV

COMPARISON BETWEEN FINITE ELEMENT AND CLOSED-FORM NATURAL FREQUENCIES

n	f_n (NASTRAN) (Hz)	f_n (Theory) (Hz)	Error (%)
1	39.39	39.39	0.0
2	157.52	157.57	0.032
3	353.87	354.53	0.186
4	625.68	630.28	0.730
5	962.04	984.81	2.312
6	1328.46	1418.13	6.323
7	1641.03	1930.23	14.983

TABLE 5 - DISPLACEMENT RESPONSE COMPARISON
BETWEEN REGULAR GRID AND COARSE GRID MODELS.

Node No.	Location	Displacement Responses (Magnitude . 10^5, Phase in deg.)					
		Ur/Phase		Uz/Phase		θ/Phase	
		Reg.	Coarse	Reg.	Coarse	Reg.	Coarse
145	Case Near Mid-cylinder	7.70/352	1.07/92	0.0	0.0	1.50/132	1.94/308
199	Case At Wye-joint	5.91/38	4.65/33	0.36/206	0.96/246	4.71/343	2.75/259
223	Aft Dome At 34" Radius	11.3/345	6.33/340	1.83/264	2.15/254	0.71/301	0.50/289
229	Aft Dome At 27½" Radius	5.34/325	3.90/314	9.23/184	5.43/198	2.52/156	1.27/145
257	Aft Dome Adapter - Component Attachment Point	6.23/345	5.18/346	35.6/163	25.6/161	4.86/164	3.99/164
281	Nozzle - Throat	3.02/165	2.30/165	62.4/344	50.9/345	0.0	0.0
299	Nozzle - Exit Plane	3.11/160	2.55/161	69.9/344	57.4/344	0.16/339	0.13/340
155	Grain - Center Bore, Near Mid-cylinder	4.05/21	4.20/4	19.6/41	9.78/298	0.0	0.0
181	Grain - Center Bore, Near Forward Edge Of Nozzle	26.2/205	21.2/194	7.17/215	15.7/128	0.0	0.0
211	Grain - Center Bore, Near Aft Dome Adapter	36.3/355	18.9/25	34.4/31	7.59/36	0.0	0.0

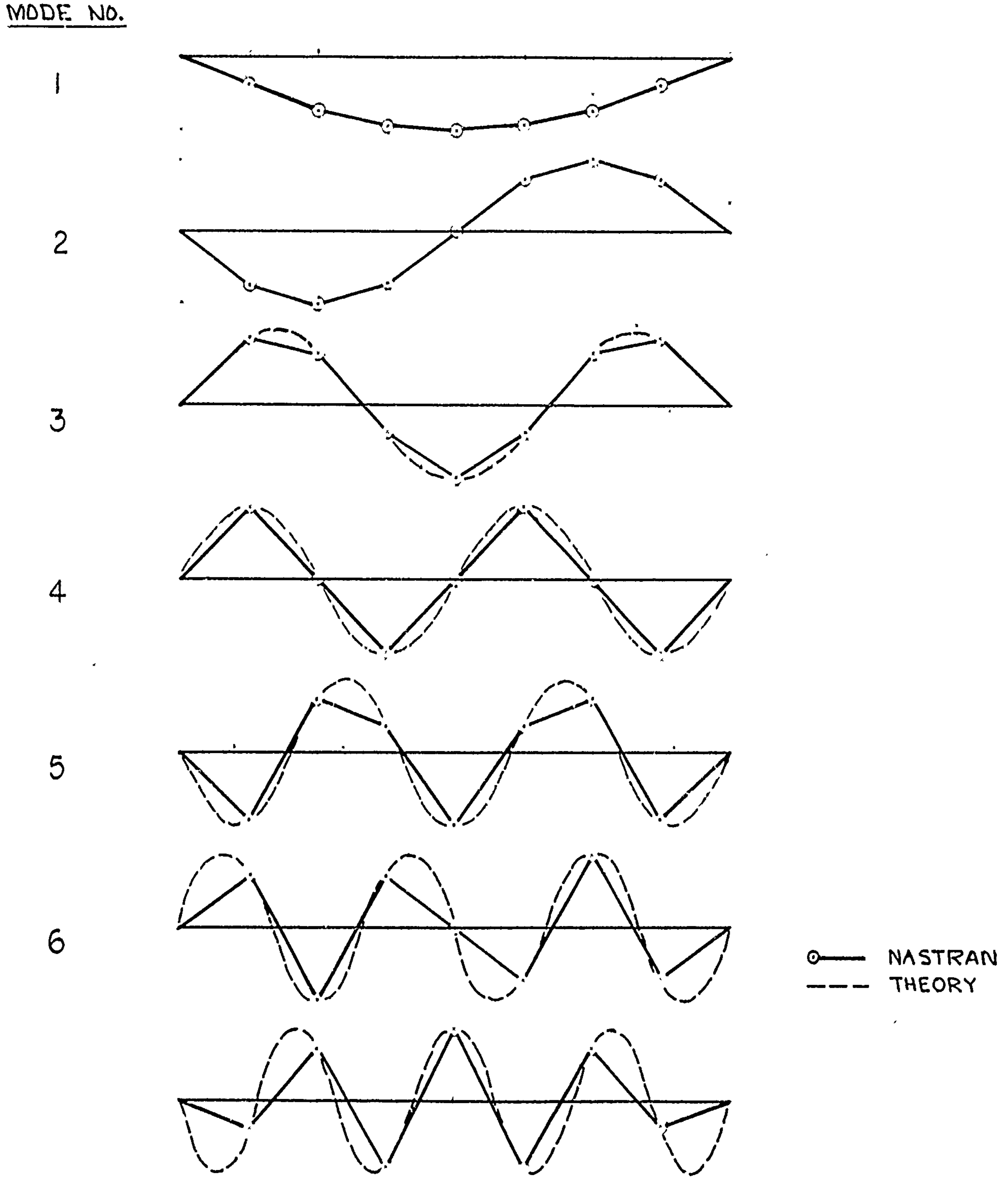

Figure 18. Comparison Between NASTRAN Calculated Mode Shapes and Theoretical Mode Shapes

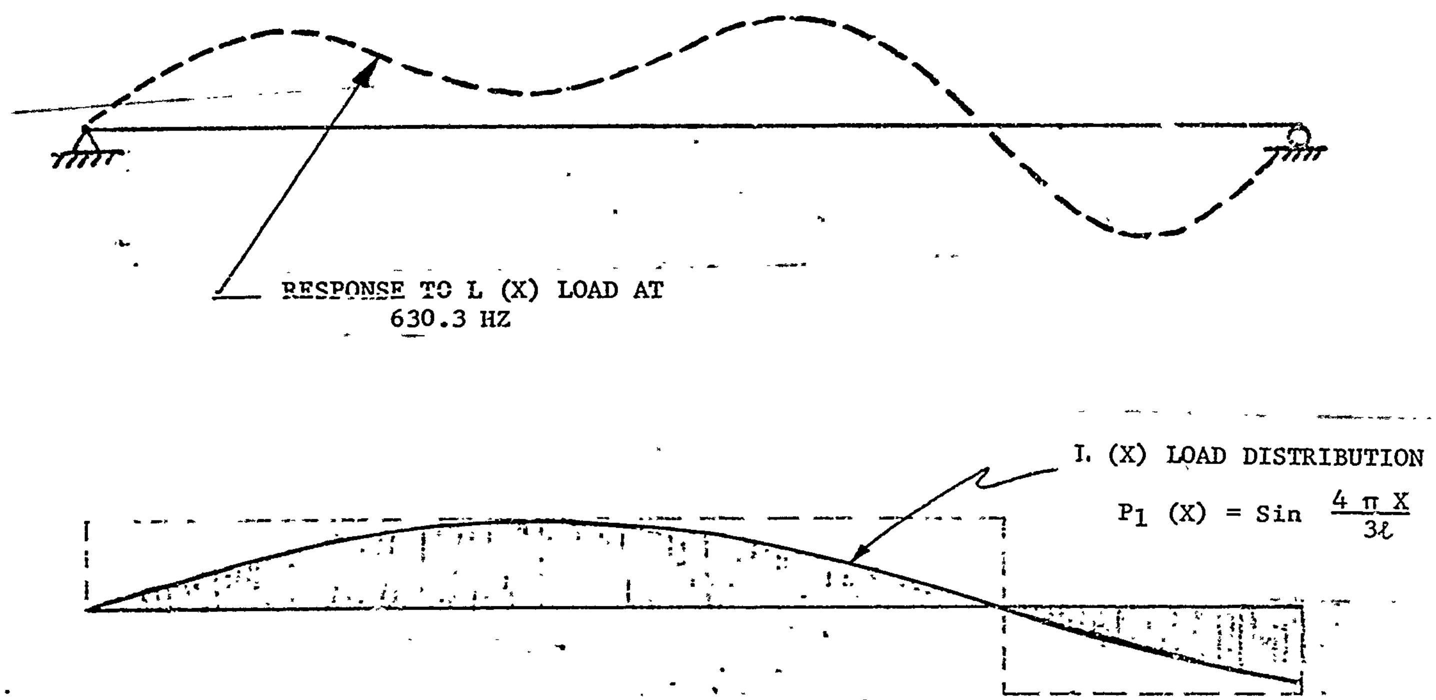

Figure 19. Response of Beam to Arbitrary Smooth Loading Distribution

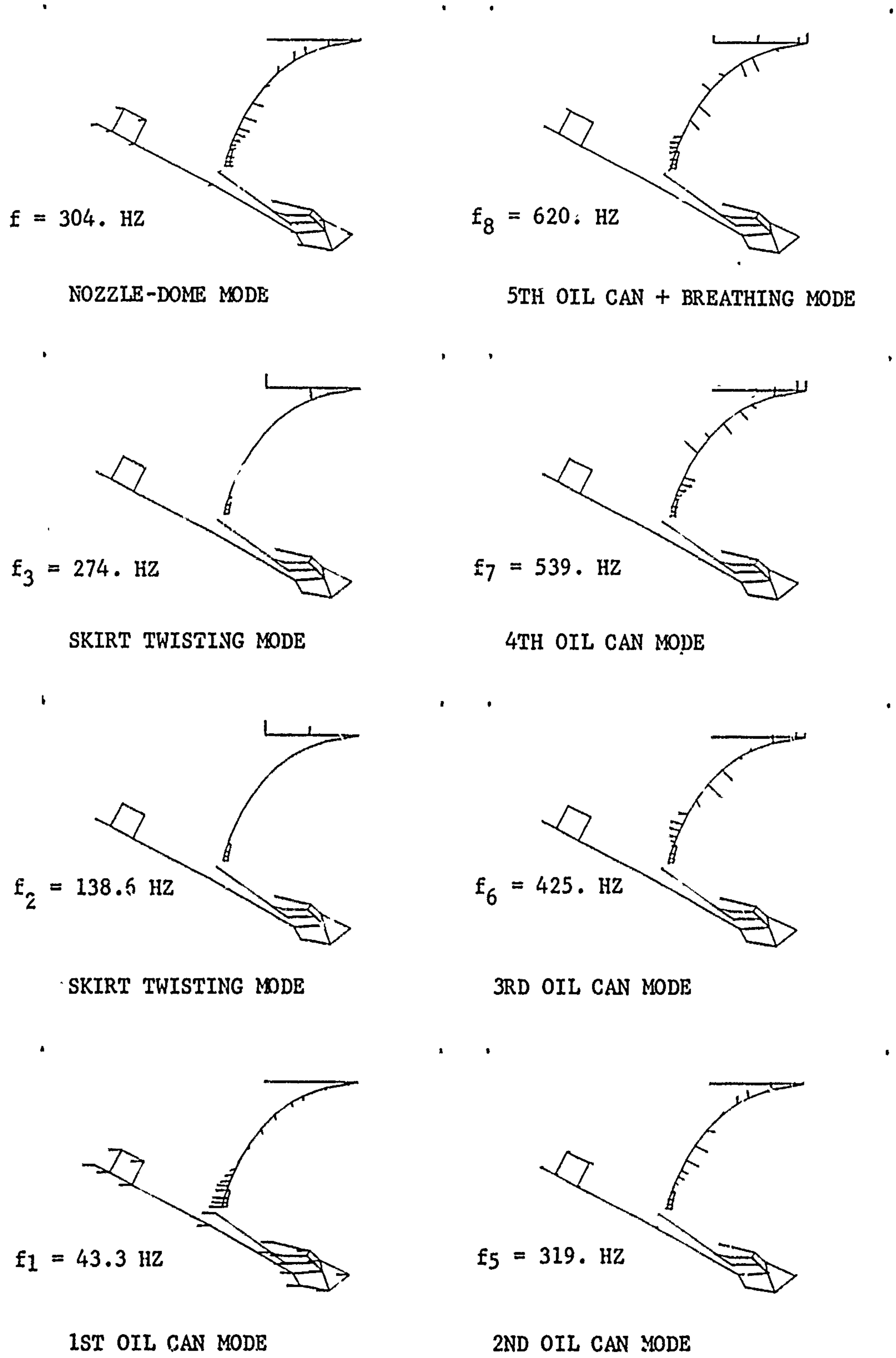

Figure 20. Poseidon C-3 Second Stage Aft Dome Mode Shapes for the First Eight Natural Modes

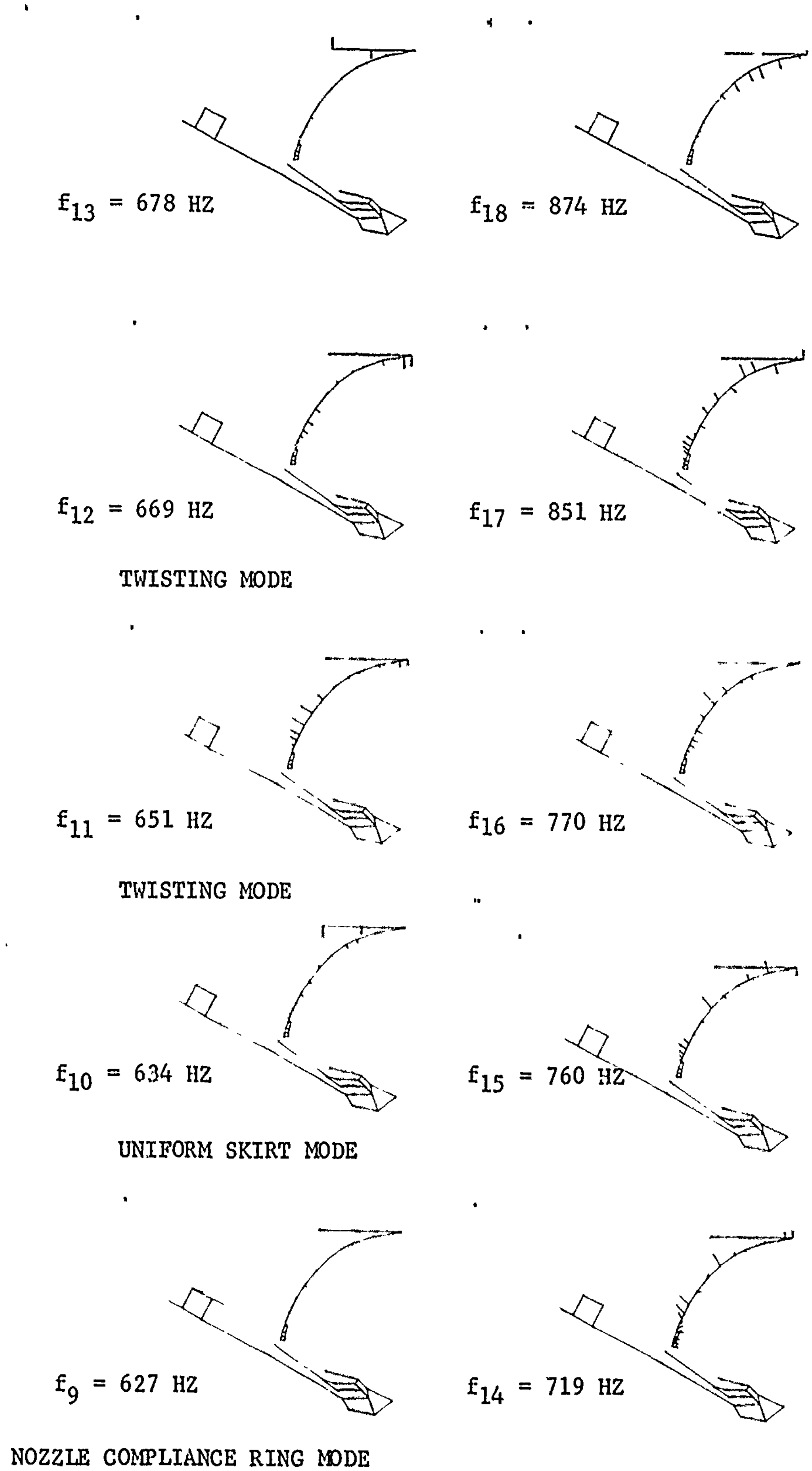

Figure 21. Poseidon C-3 Second Stage Aft Dome Mode Shapes for the Ninth through Eighteenth Natural Modes

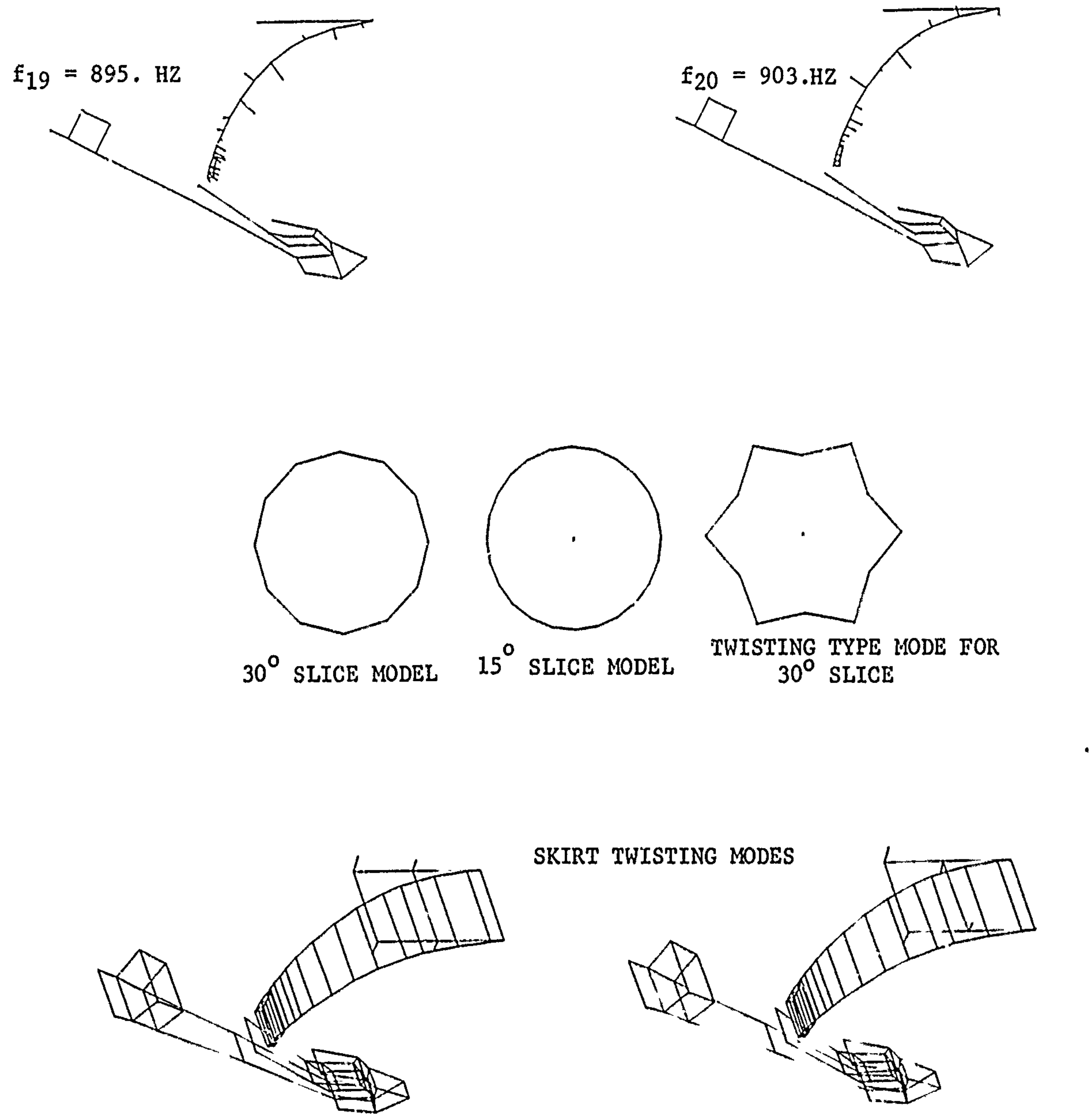

Figure 22. Poseidon C-3 Second Stage Aft Dome Mode Shapes with Sketches Showing Twisting Type Modes

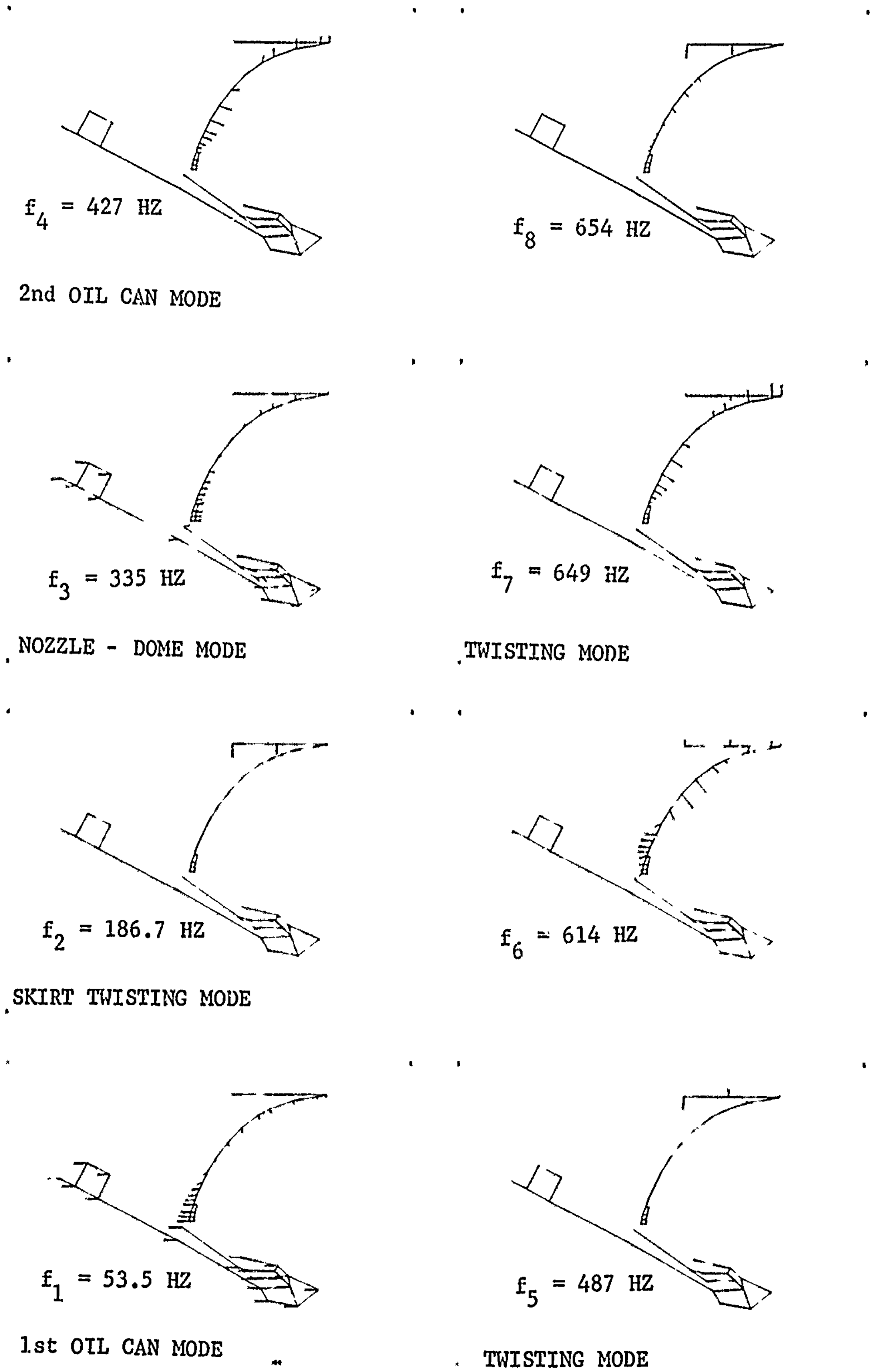

Figure 23. Poseidon C-3 Second Stage Aft Dome Mode Shapes Using a 30° Slice Finite Element Model.

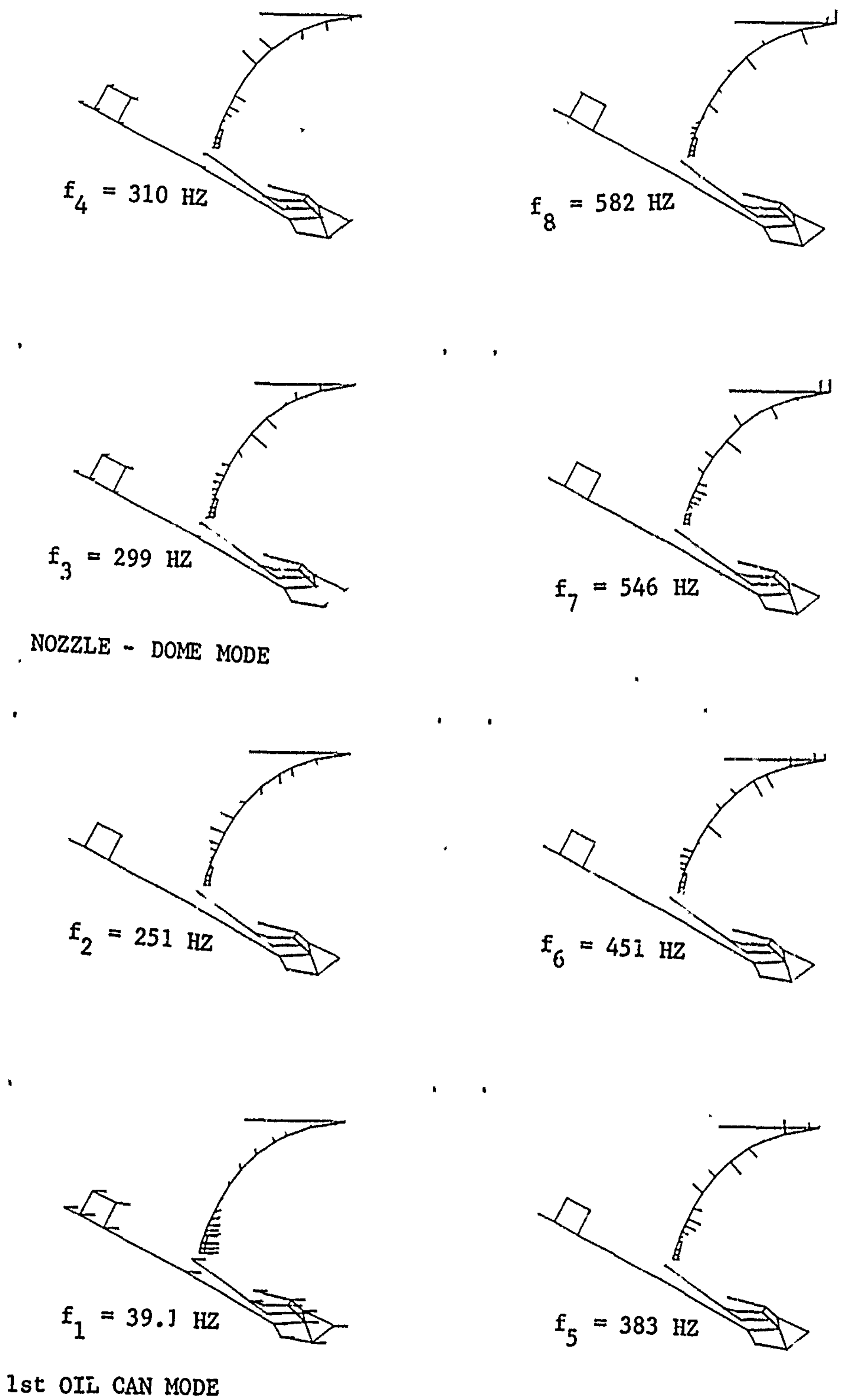

Figure 24. Poseidon C-3 Second Stage Aft Dome Mode Shapes Using a 5° Slice Finite Element Model.

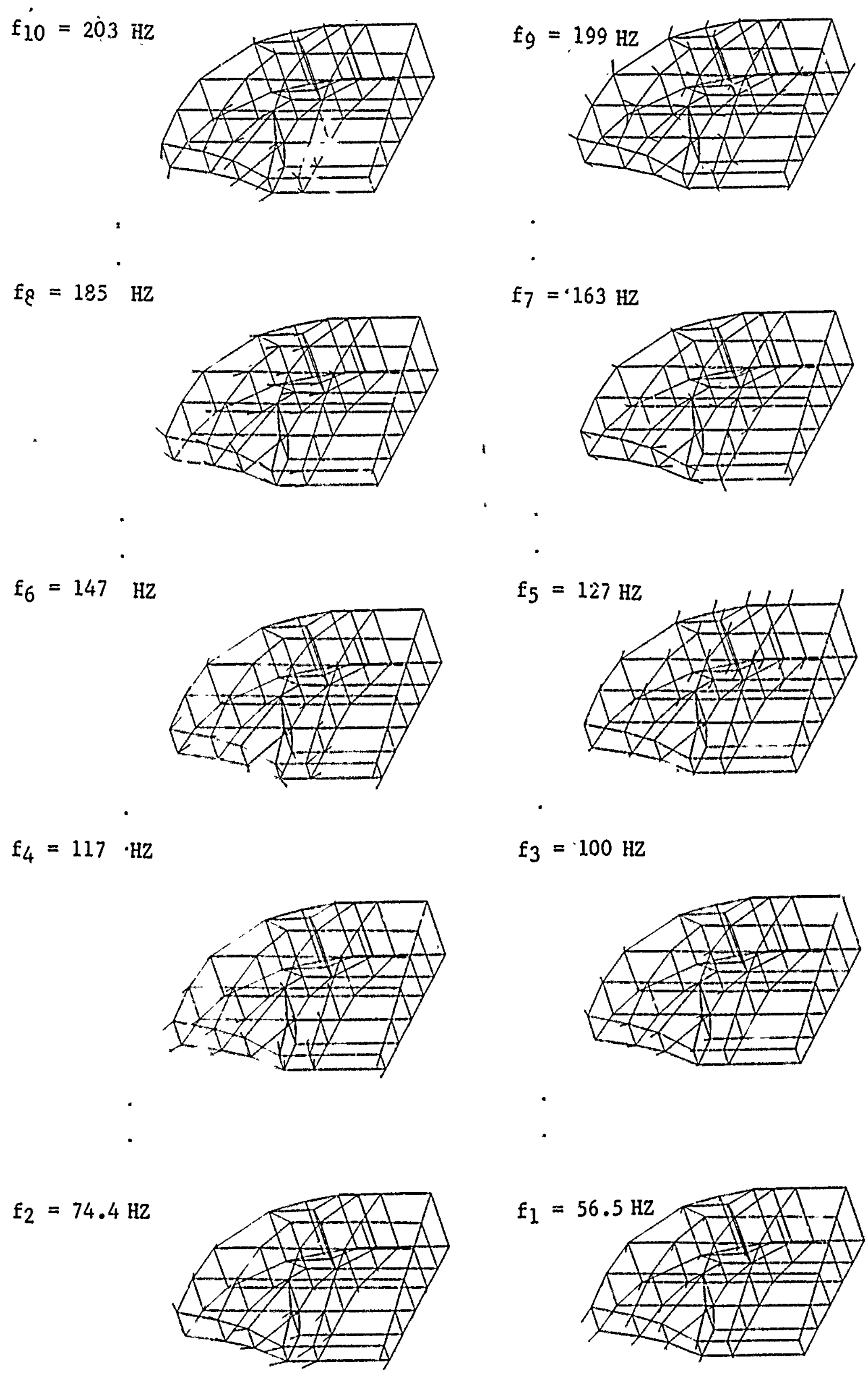

Figure 25. Poseidon C3 Second Stage Aft Half Grain Model Natural Modes for Symmetry Boundary Conditions.

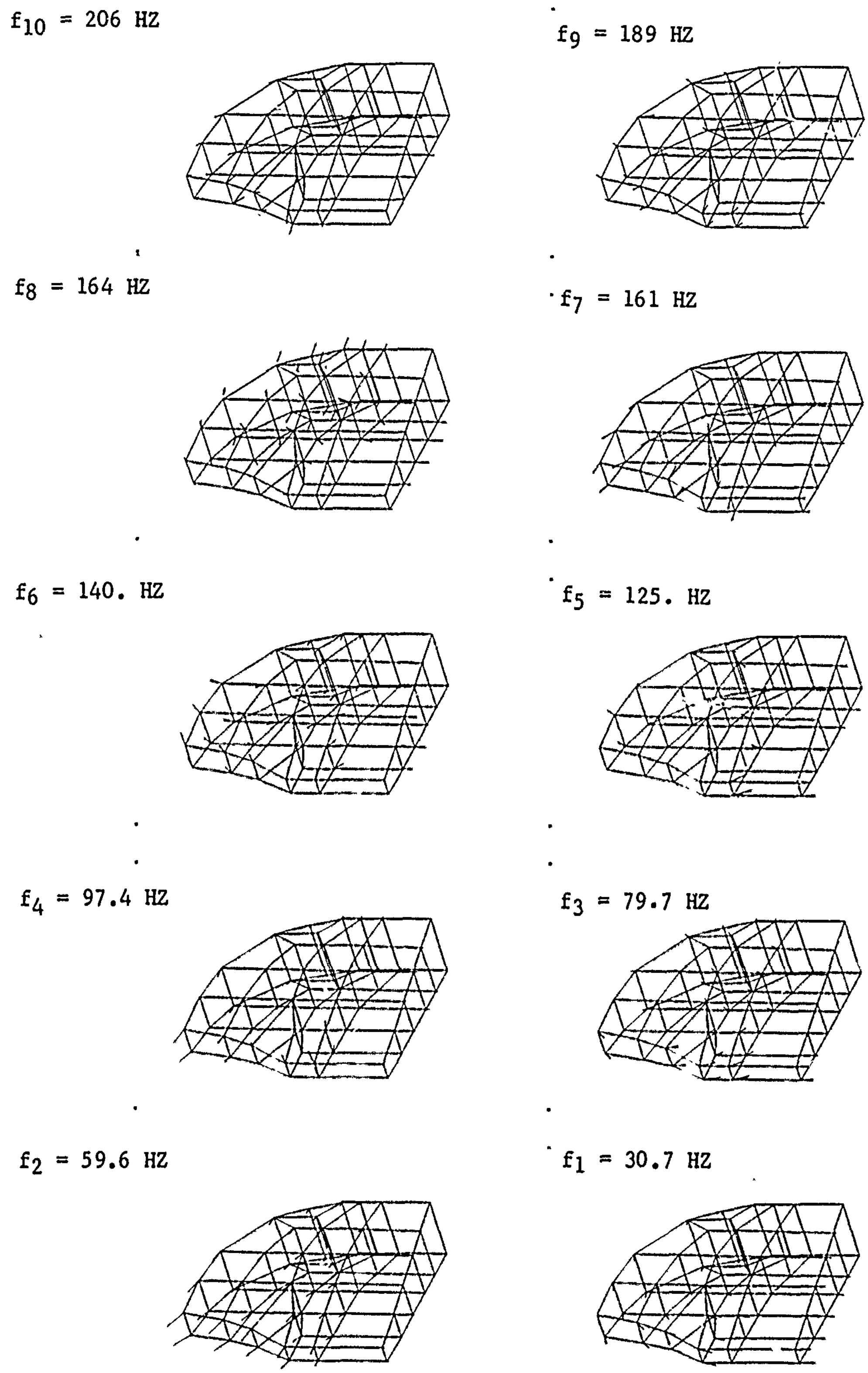

Figure 26. Poseidon C3 Second Stage Aft Half Grain Model Natural Modes for Asymmetric Boundary Conditions

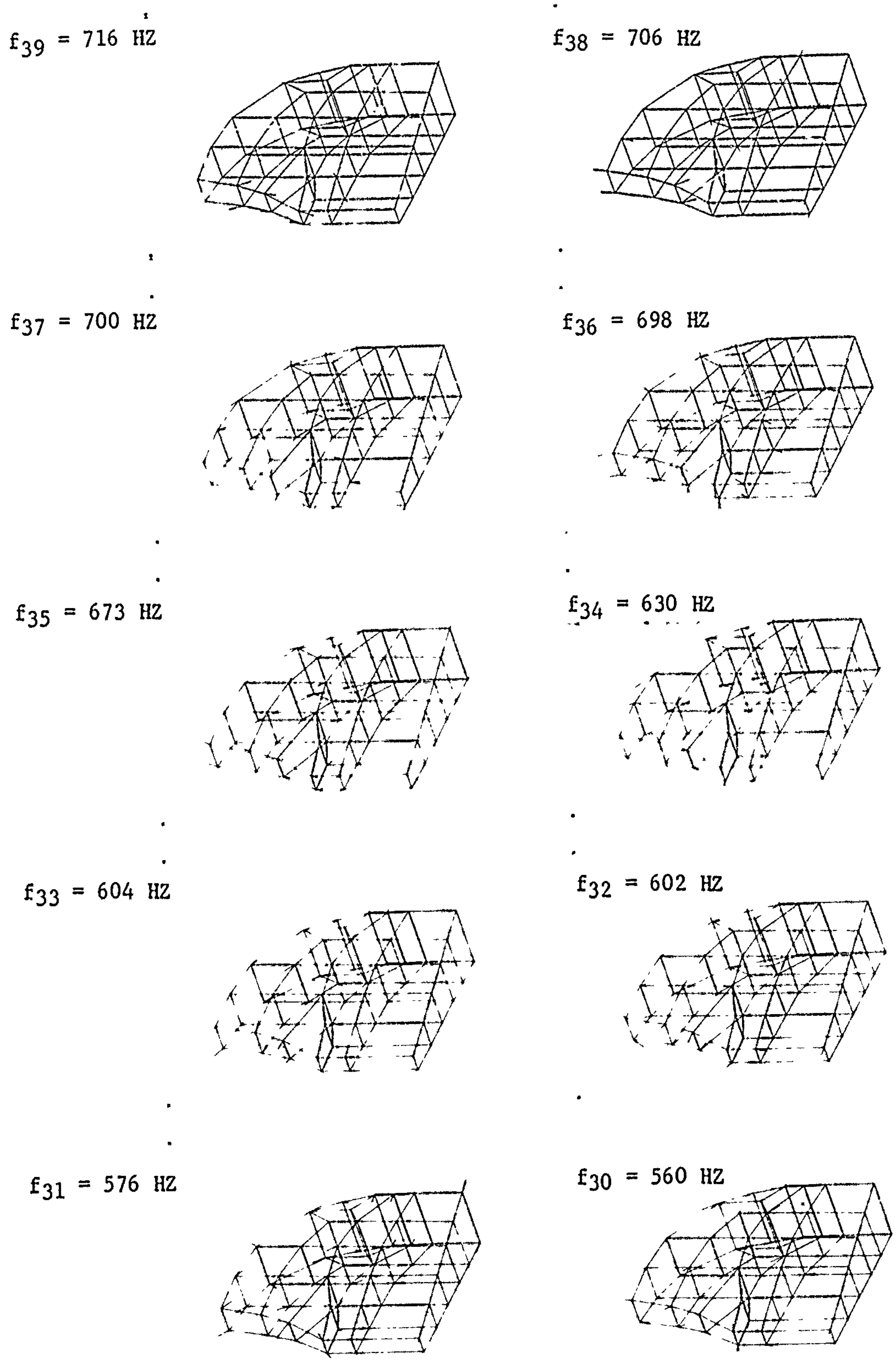

Figure 27. Poseidon C3 Second Stage Aft Half Grain Model Natural Modes for Symmetry Boundary Conditions.

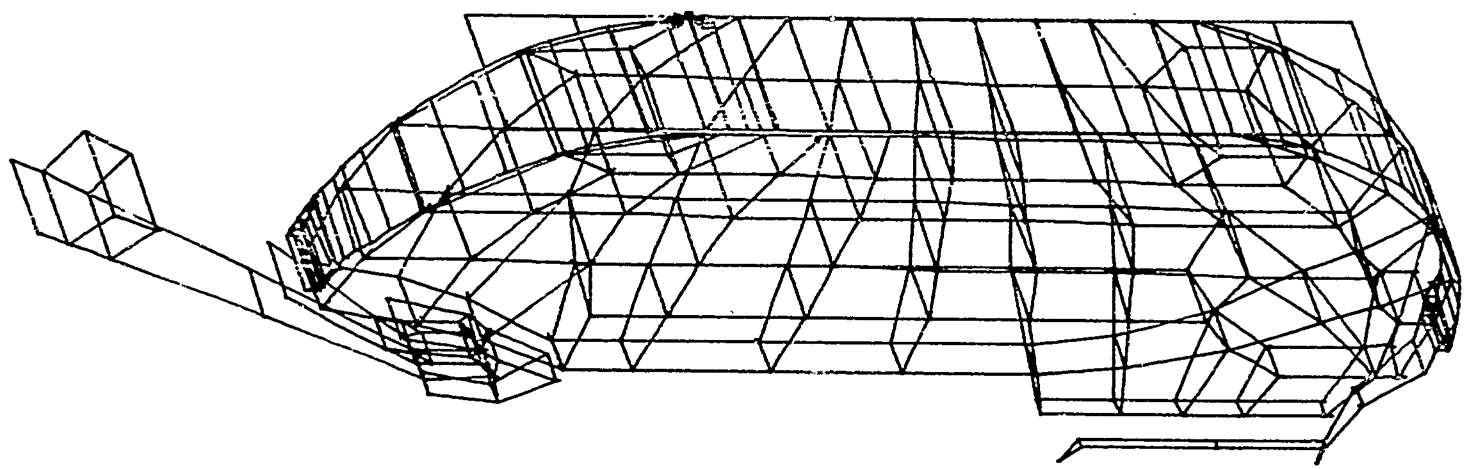

GRID FOR THE POSEIDON SS MOTOR CONTAINING NO WEDGE ELEMENTS

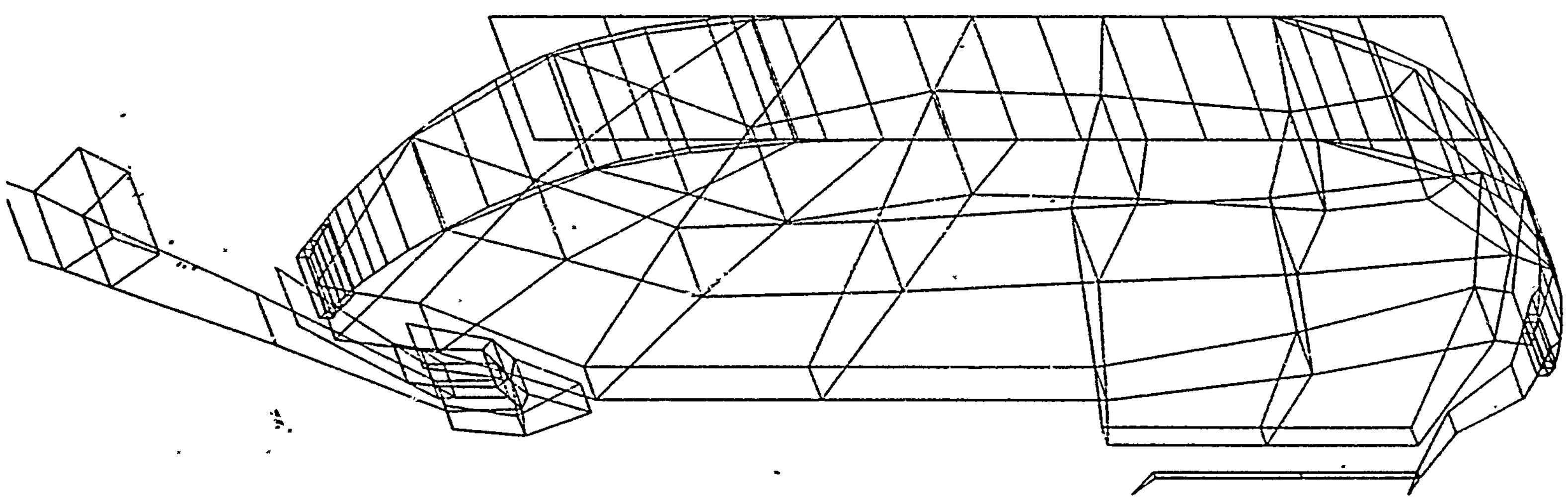

FULL MOTOR MODEL WITH COARSE GRAIN

Figure 7 Comparison Between Regular and Coarse Grain Grid Models of the C-3 Second Stage Poseidon Motor

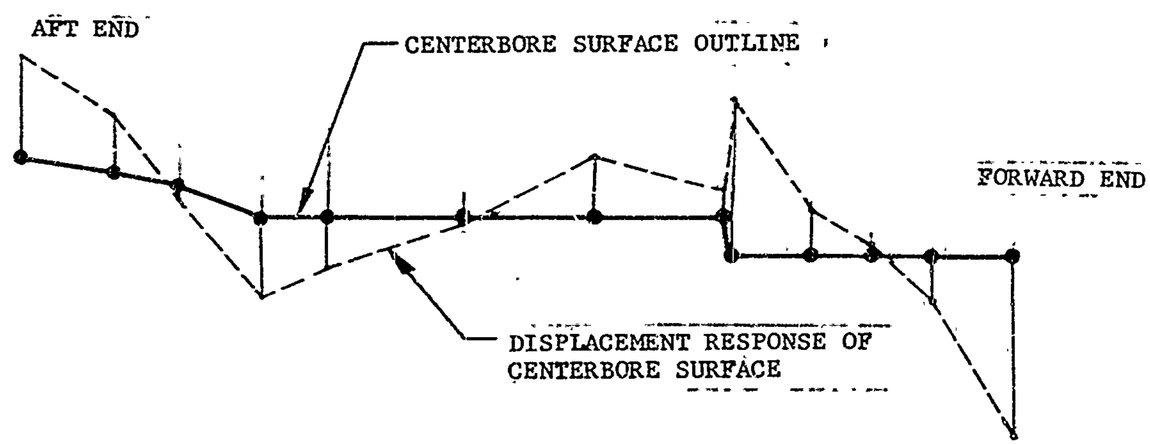

Figure 29. Response of the Poseidon S/S Grain Along the Centerbore to the 770 Hz L_3 Acoustic Mode

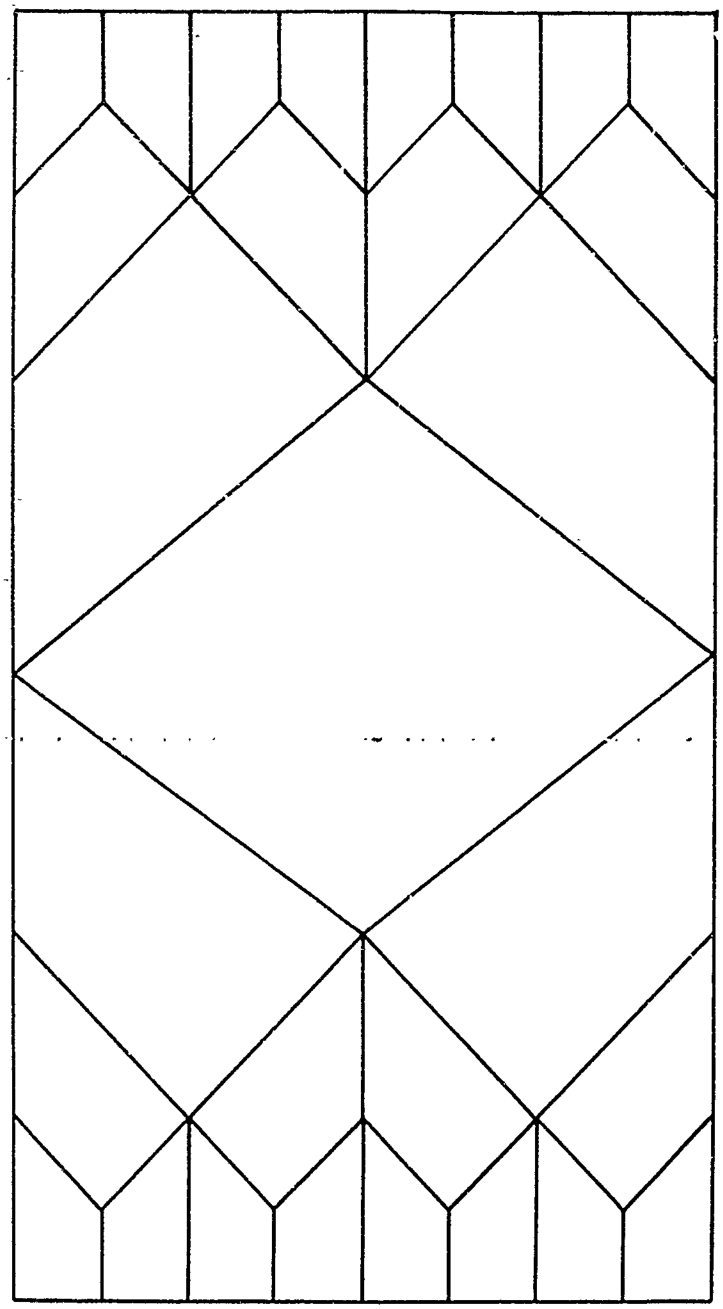

Figure 30. An Example of a Finite Element Grid with Refined Boundaries Top and Bottom

LIST OF REFERENCES

1. Final Report, Minuteman III Third Stage Pressure Oscillation Study, Report 1387-01F, August 1971, Aerojet Solid Propulsion Company, Sacramento, California.

2. "Acoustic Analysis of Solid Rocket Motor Cavities by a Finite Element Method", D. N. Herting, et al., by MacNeal-Schwendler Corporation, Los Angeles, California, for Department of the Air Force, Edwards Air Force Base, RPL (AFRPL-TR-71-96), August 1971.

APPENDIX G

EXTRACTS FROM R&D MONTHLY STATUS REPORTS

1. Extracted from 20 December 1975 Monthly R&D Status Report
2. Extracted from 18 May 1973 Monthly R&D Status Report
3. Extracted from 20 January 1975 Monthly R&D Status Report
4. Extracted from 20 July 1975 Monthly R&D Status Report
5. Extracted from 20 May 1975 Monthly R&D Status Report
6. Extracted from 20 August 1975 Monthly R&D Status Report
7. Extracted from 20 November 1974 Monthly R&D Status Report
8. Extracted from 30 March 1974 Monthly R&D Status Report
9. Extracted from 20 April 1974 Monthly R&D Status Report
10. Extracted from 20 September 1974 Monthly R&D Status Report

EXTRACTED FROM 20 DECEMBER 1974
MONTHLY R&D STATUS REPORT

TASK 5 REPORT

ANALYSIS OF ACCELEROMETER AND PRESSURE GAGE DATA FROM THREE S/S POSEIDON STATIC FIRINGS

Contract No. F04611-73-C-0025

Air Force Rocket Propulsion Laboratory
Edwards Air Force Base, California

December 20, 1974

Prepared by

Hercules Incorporated
Bacchus Works
Magna, Utah

ANALYSIS OF ACCELEROMETER AND PRESSURE GAGE DATA FROM THREE S/S POSEIDON STATIC FIRINGS

I. INTRODUCTION

Data recorded during static firings and stored on FM magnetic tapes for motors SP-0131, SP-0149, and SP-0160 were analyzed through the Quan Tech wave analyzer. Data from these motors was selected for analysis because each firing was conducted with several accelerometers mounted on the motor structure and the flight hardware at various points. The objective of this data analysis work was to characterize the response of the structure with respect to the amplitudes of the acoustic pressure modes. A special Kistler pressure gage was used in each firing to measure the amplitude of the pressure oscillations. Data from the Kistler pressure gage were reduced for motor SP-0115. However, since significant pressure oscillations were not evident at most frequencies of interest, the corresponding accelerometer data were not reduced for motor SP-0115.

Finite element models are analyzed to determine how a rocket motor structure responds to pressure oscillations that occur in the motor's combustion cavity. To assess the validity of the structural analyses, calculated results can be compared with data from actual static firings. This report presents a compilation of static firing data that were reduced especially for the purpose of making such comparisons. The static firing data were reduced for use in the RPL Component Vibration Program, AF contract F04611-73-C-0025.

The computer analysis of finite element models yields accelerations at nodal points. The nodal accelerations represent the structural response to a particular pressure distribution loading function, (i.e., a particular acoustic mode), at a particular frequency. By contrast, the accelerometer data from a static firing represents the response of the actual motor structure to a number of different loading systems. The loading systems include the harmonic acoustic pressure oscillations that are due to resonance of the gas column in the combustion cavity, (i.e., a particular acoustic mode as discussed above), as well as several ill-defined loading systems. The loading systems that are not well defined include noise excitation (i.e., broad frequency band excitation) due to flow in the motor proper and especially due to flow through the nozzle and reflections of acoustic noise from the ground and other surfaces in the static firing bay. Also, igniter operation during the first 1/2 second of burn time is a source of structural excitation.

In addition to the fact that response data includes various sources of excitation, one factor that must be considered in comparing analysis results with firing data is the shifting frequency characteristic of most acoustic modes. As the burning surface in a rocket motor advances into the grain, the geometry of the combustion cavity changes sufficiently to cause a gradual change in the frequency for a particular mode. The routine data analysis procedure used by Hercules, calls for use of the Quan Tech wave analyzer in the tracking mode to follow the peak response amplitude for a particular mode as the frequency shifts throughout the firing. For reasons discussed below, the analyses reported here used a fixed rather than tracking filter mode.

To obtain data for comparison with analysis results, the FM tapes containing accelerometer and pressure gage information were played through the Hercules Quan Tech wave analyzer. Only the first 10 seconds of the firing were analyzed since past experience has shown that most acoustic pressure oscillation activity occurs during that time. Filter bandwidths of both 10 and 100 Hz were used since both proved to be useful at different times. The filter was set at a particular frequency and the rms output from the filter was plotted as a function of time. A constant frequency was used because the structural analysis technique (NASTRAN), is only capable of producing steady state response at a particular frequency. The analysis could be repeated for a series of frequencies to represent the shifting frequency but this procedure would be too expensive.

II. TRANSDUCER LOCATIONS

Locations of accelerometers on the forward dome were the same for all four motors as shown in Figure 1. Accelerometers AC-404 and AC-405 were mounted on the forward closure adapter ring as shown in the figure. The Kistler pressure gage tap was through the forward closure. The Kistler pressure gage is denoted as PT-5. Locations of accelerometers on the aft dome are indicated in Figures 2, 3, and 4 for motors SP-0131, SP-0149, and SP-0160, respectively.

III. DATA ANALYSIS APPROACH

Data from each of the three firings were analyzed at frequencies of 281, 634, 680, 770, and 1327 Hz. These frequencies were selected because they correspond to frequencies for which the motor has been analyzed using NASTRAN. The selected frequencies also correspond to acoustic modes that were previously[1] determined to commonly occur in the motor.

Results from the Quan Tech analyses are shown in Figures 5 through 22. An x-y plotter was used to plot the rms pressure and acceleration levels from the Quan Tech analyzer. The rms values have been converted to zero-to-peak values. The peak values are denoted on each plot at points of interest. Each figure (except Figure 22) shows the results from using both 10 Hz and 100 Hz filter bandwidths. An averaging time constant of 0.1 seconds was used in all analyses.

For each analysis, three accelerometer channels were plotted directly above the corresponding pressure gage response. Thus it is easy to see when the accelerometers respond at the same time and in the same way as the pressure gage responds. Each analysis was limited to one pressure plot and three accelerometer plots to avoid crowding or overlapping of the curves on a single plot. The total number of plots or analyses performed was limited by the time and budget allotted for this data analysis task. For each motor, the three accelerometers judged to be most useful for making comparisons with the finite element model were selected for analysis. The accelerometers selected were those mounted on the forward or aft adapters measuring longitudinal structural response. An extra set of three accelerometers was selected on motor SP-0160 to measure component* response. The component accelerometers were analyzed at frequencies of 281, 680, 770, and 1327 Hz.

It may seem odd that more attention was not paid to analysis of component response. However, it is prediction of motor structural response with components attached that is of prime interest rather than response of the components themselves.

IV. DATA ANALYSIS RESULTS

The results from the Quan Tech analyses are displayed in Figures 5 through 22. Nearly all of the curves, regardless of location or frequency represented, exhibit an initial peak near the zero to one second time range. These initial peaks are probably caused by igniter operation (duration is about 1/2 second) and by events that occur during motor ignition. Even though peaks in the pressure trace occur, it is believed that no distinct particular acoustic modes occur in the combustion cavity during the ignition interval. Therefore, the initial response peaks have been ignored in the following data analyses.

The following observations have been made regarding the data plotted in Figures 5 through 22.

(a) Some records did not show any significant response for the 10 second interval plotted other than during the ignition interval.

(b) Accelerometers mounted on the aft dome are generally significantly more noisy than forward dome accelerometers. The noise is probably due to the high velocity flow of hot gases through the nozzle.

(c) Peaks in the response curves plotted for the 100 Hz filter are often missed entirely in the corresponding analysis using the 10 Hz filter. (For example, see Figure 15).

(d) When a relatively "clean" accelerometer response is shown for a clean peak in the pressure trace for the 10 Hz analysis, the corresponding 100 Hz analysis may indicate a noisy or irregular response indicating that the 100 Hz bandwidth filter is passing response data for excitation other than the acoustic pressure oscillation. (An example is shown in Figure 19).

(e) At times, peak responses are shown on the accelerometer plots when no corresponding peak occurs in the pressure plot. This indicates that the structure is responding, at the analysis frequency, to excitation other than acoustic pressure oscillations. (See Figure 15 between 6.0 and 7.0 seconds).

*The components of interest on the S/S Poseidon motor are the Flight Electronics Package, the Hydraulic Power Unit, and the Gas Generator.

(f) Forward dome accelerometers seem to be more sensitive to the pressure oscillations than aft dome accelerometers. Some response peaks detected on the forward dome were not present in the aft dome response data. (See Figures 10 and 15).

It is evident from the above observations that either the 10 Hz or the 100 Hz filter can provide the more appropriate data depending on the particular situation. Therefore, results from both filters were used in the data analyses.

Many of the curves in Figures 5 through 22 appear to show nicely how the accelerometers respond to an acoustic mode. For example, the 100 Hz analysis shown in Figure 6 shows a $\pm$ 0.16 psi pressure oscillation for PT-5 at about 3.7 seconds. The accelerometers AC-261, AC-404, and AC-405 respond with $\pm$ 3.74 g's, $\pm$ 5.00 g's, and $\pm$ 3.29 g's respectively. The shapes of the accelerometer response plots between 3.5 and 4.5 seconds are similar to the shape of the PT-5 pressure curve over the same time interval. The similarity of curve shapes gives us added confidence that the transducers are all responding to the same excitation. The peak in the pressure trace at about 3.7 seconds is assumed to occur because of an acoustic pressure oscillation in the first natural mode for the cavity. A review of Reference 2 and the Quan Tech analysis results shown therein, would show that peaks in the response curves similar to those discussed, (Figure 6), would be expected to result from acoustic pressure oscillations.

To obtain response data that can be compared with analysis data, the accelerometer peak g levels were divided by the peak pressure levels. The ratio is called a "transfer number" with units of (g's/psi). The transfer number thus indicates the accelerometer response that would correspond to a pressure oscillation of unit magnitude. All transfer numbers that appeared to be reasonably representative have been calculated and are listed in Table I.

V. CONCLUSIONS

There is considerable variation in the transfer numbers shown in Table I. For example, six different values for TN_2 for the 680 Hz mode cover the range from 1.22 to 13.28 g's/psi. Large variations were not unexpected. Rather, large variations are typical of vibration data from rocket motors.

The transfer numbers shown in Table I will be useful for evaluating results from the NASTRAN finite element analyses.

List of References

1. Acoustic Natural Mode and Frequency Definitions, RPL Component Vibration Program, Task 2 Final Report, Hercules Incorporated, (Contract No. F04611-73-C-0025), 28 September 1973.

TABLE I

SUMMARY OF TRANSFER NUMBERS CALCULATED FROM THE DATA SHOWN IN FIGURES 5 THROUGH 22

Frequency/ Bandwidth (Hz/Hz)	Approx. Time (sec)	TN_1 = (AC-261)/(PT-5) SP-0131	SP-0149	SP-0160	TN_2 = (AC-404)/(PT-5) SP-0131	SP-0149	SP-0160	TN_3 = (AC-405)/(PT-5) SP-0149	TN_4 = (AC-250(/(PT-5) SP-0131	SP-0160	TN_5 = (AC-253)/(PT-5) SP-0160	TN_6 = (AC-263)/(PT-5) SP-0160	TN_7 = (AC-264)/(PT-5) SP-0160
281/100	3.7	-	23.38	-	-	31.25	-	20.56	-	-	-	-	-
634/100	8.0	-	1.71	-	10.74	9.27	2.43	3.27	1.45	3.14	-	-	-
680/10	8.0	0.80	1.55	1.90	11.68	7.52	1.22	3.06	2.01	2.85	0.95	4.05	1.85
680/100	2.5	-	2.03	2.43	7.53	5.17	4.01	4.50	2.70	2.30	0.85	2.90	2.44
	8.0	0.79	1.83	2.14	13.28	9.23	2.21	3.17	1.57	3.05	1.10	4.44	2.23
770/100	2.5	-	2.00	-	9.03	5.03	3.97	4.62	2.95	-	0.85	3.08	2.65
	8.0	-	-	-	27.50	-	-	-	-	-	-	-	-
1327/10	5	1.87	1.60	1.05	19.17	2.87	4.14	1.33	5.39	1.86	1.47	3.40	2.77
1377/100		-	-	-	-	7.28	-	3.88	-	-	-	-	-

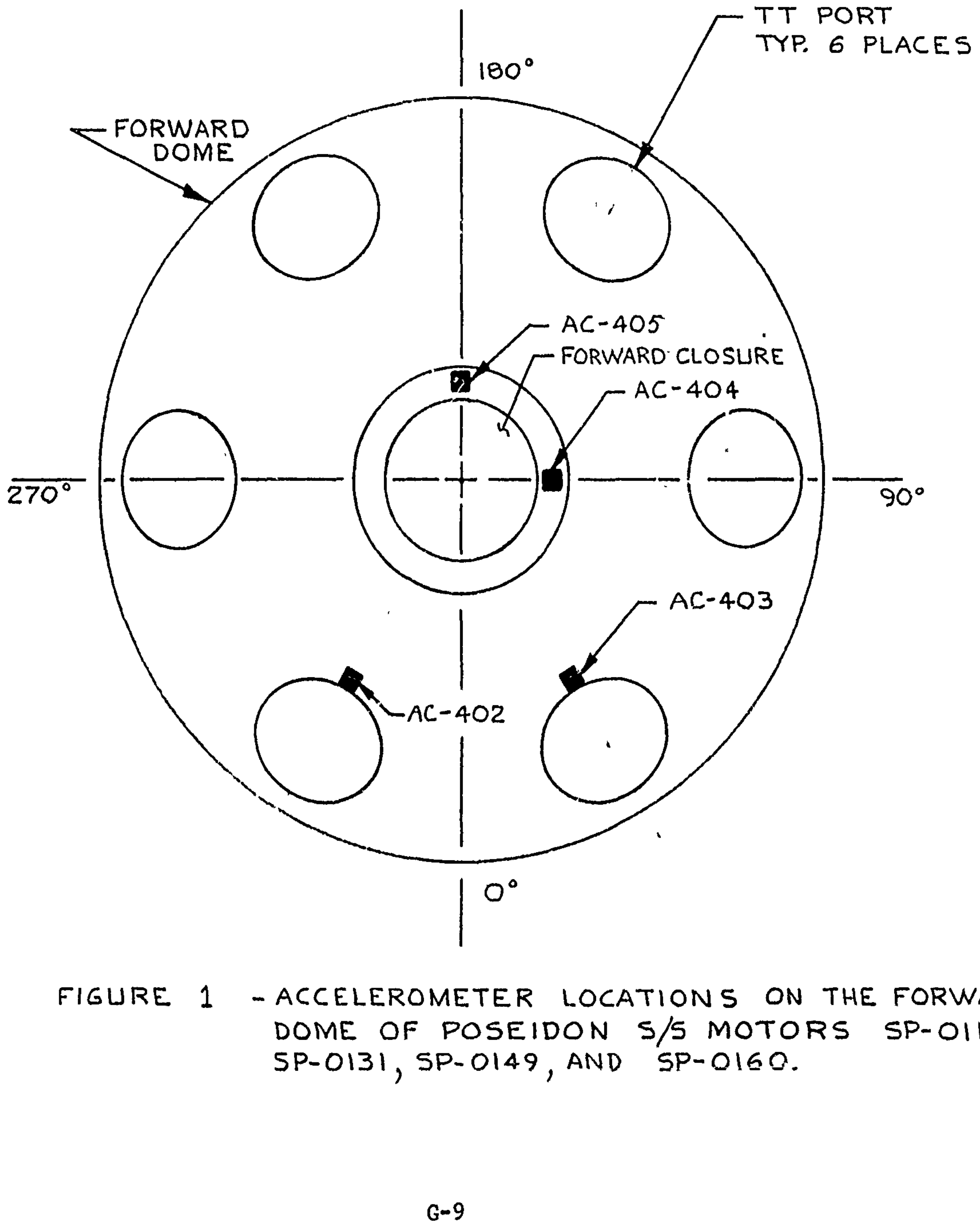

FIGURE 1 - ACCELEROMETER LOCATIONS ON THE FORWARD DOME OF POSEIDON S/S MOTORS SP-0115, SP-0131, SP-0149, AND SP-0160.

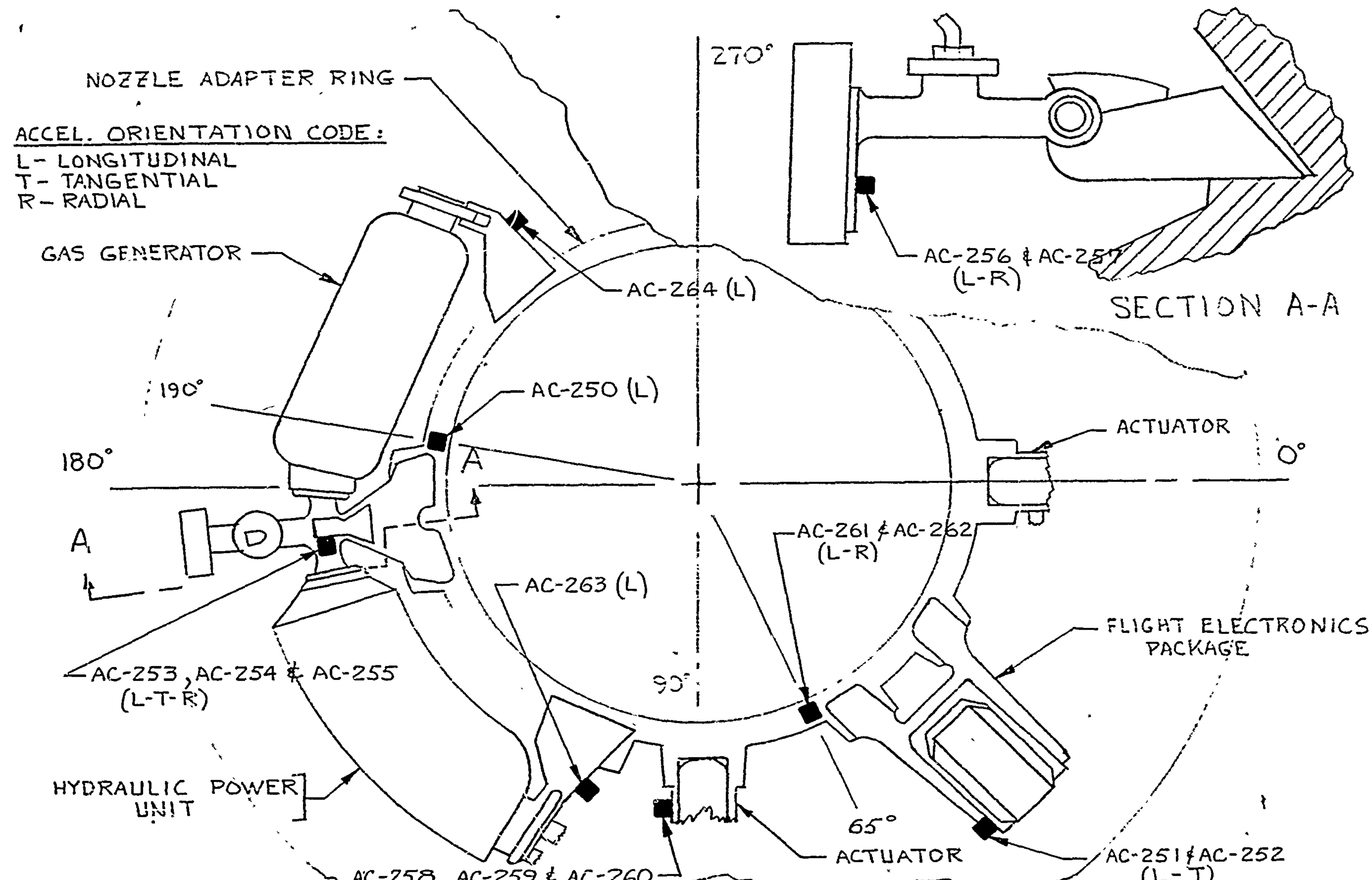

FIGURE 2 - AFT DOME ACCELEROMETER LOCATIONS FOR THE STATIC TEST FIRING OF POSEIDON S/S MOTOR SP-0131.

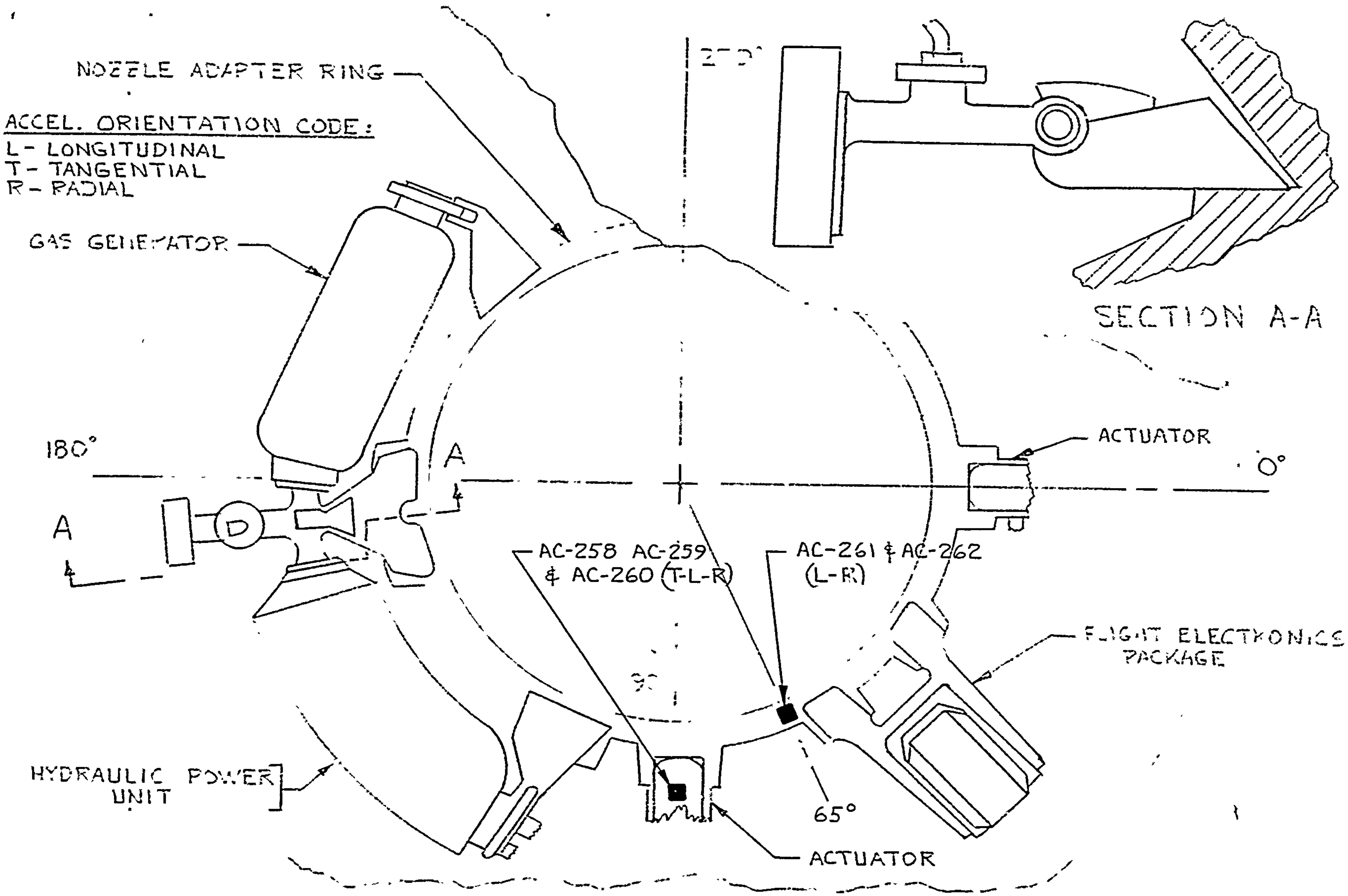

FIGURE 3 - AFT DOME ACCELEROMETER LOCATIONS FOR THE STATIC TEST FIRING OF POSEIDON S/S MOTOR SP-0149.

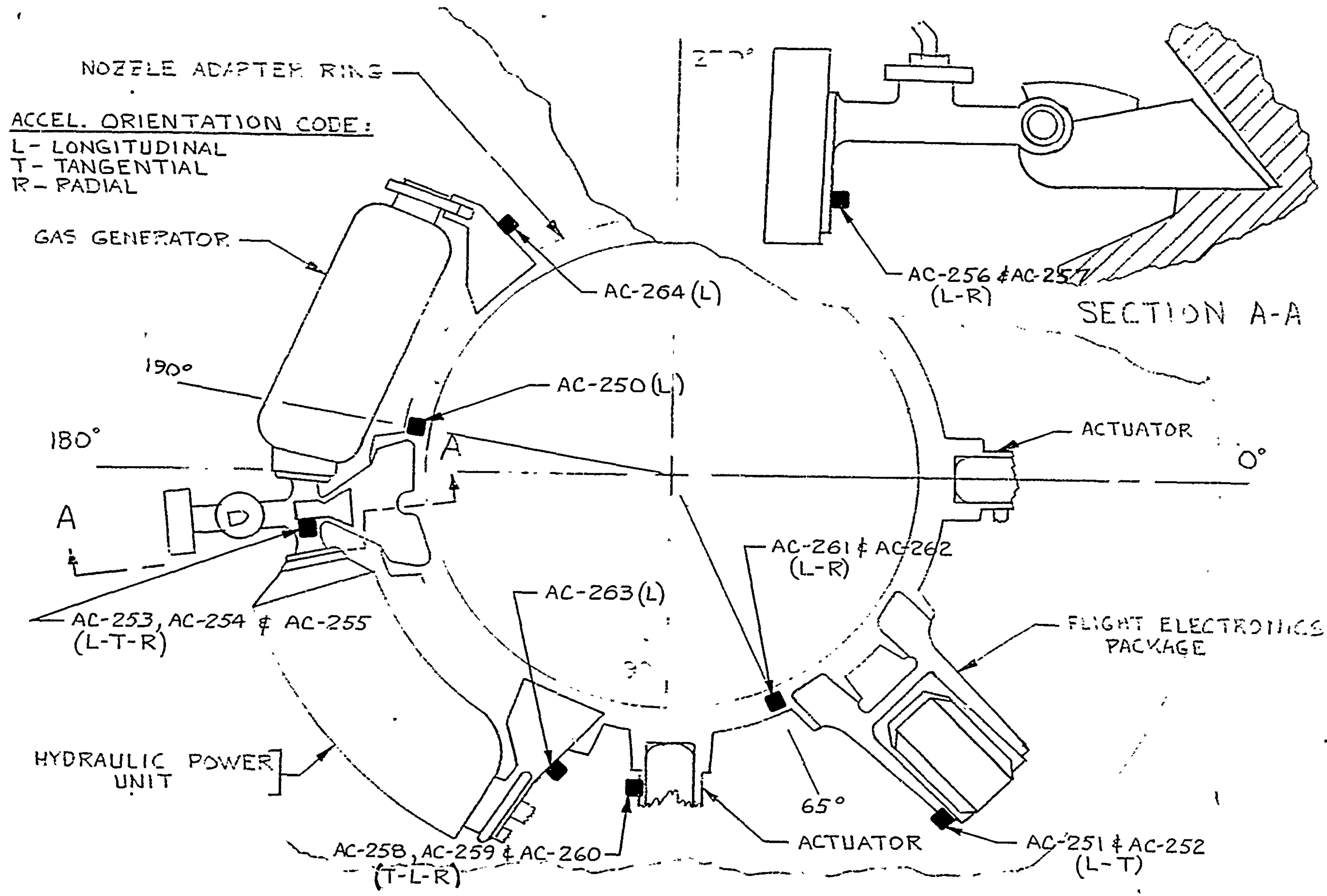

FIGURE 4 - AFT DOME ACCELEROMETER LOCATIONS FOR THE STATIC TEST FIRING OF POSEIDON S/S MOTOR SP-0160.

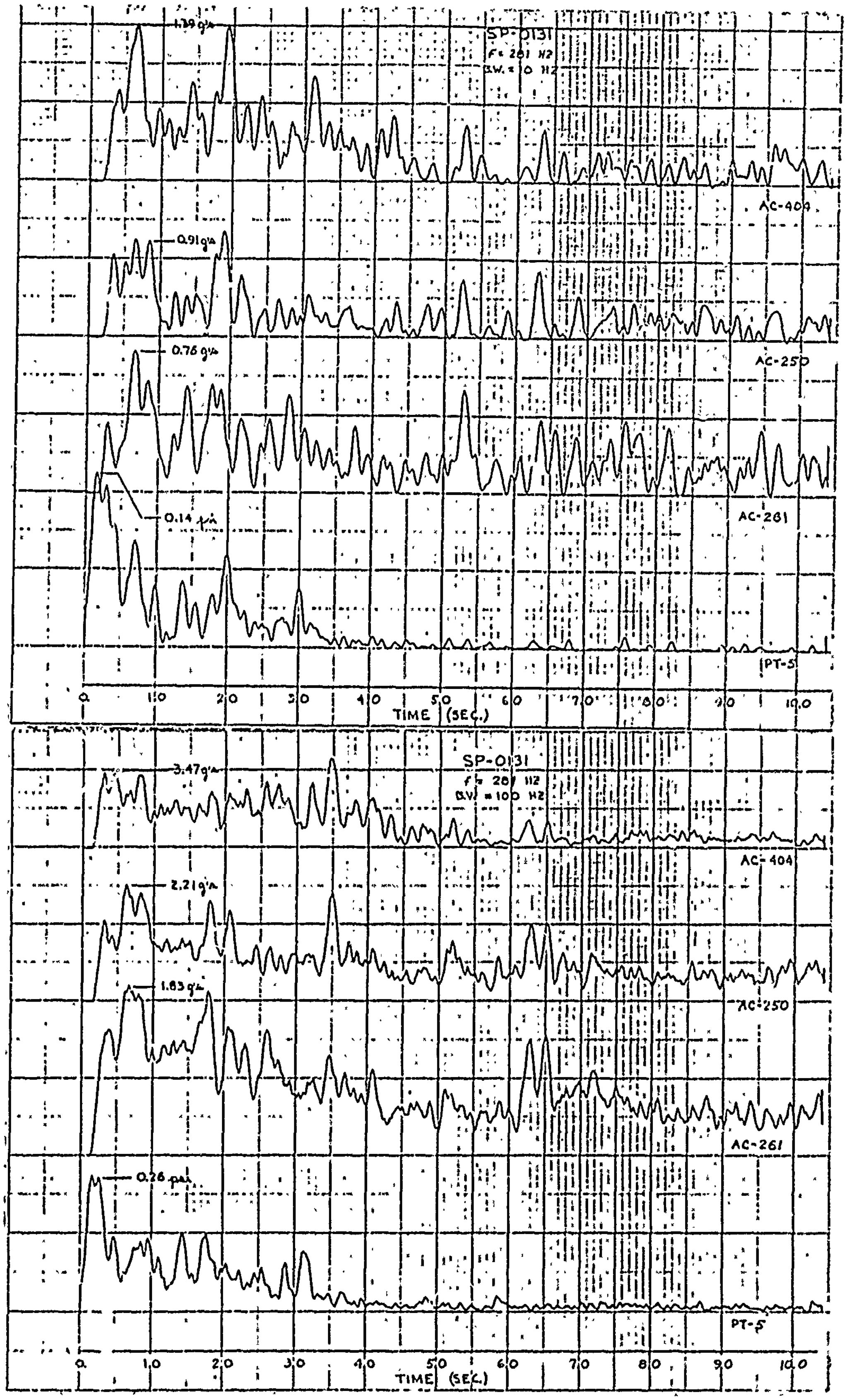

Figure 5. Filtered Pressure Gage and Accelerometer Response for Poseidon S/S Motor SP-0131. (Quan Tech Analyses at F = 281 Hz with Filter Bandwidths of 10 and 100 Hz)

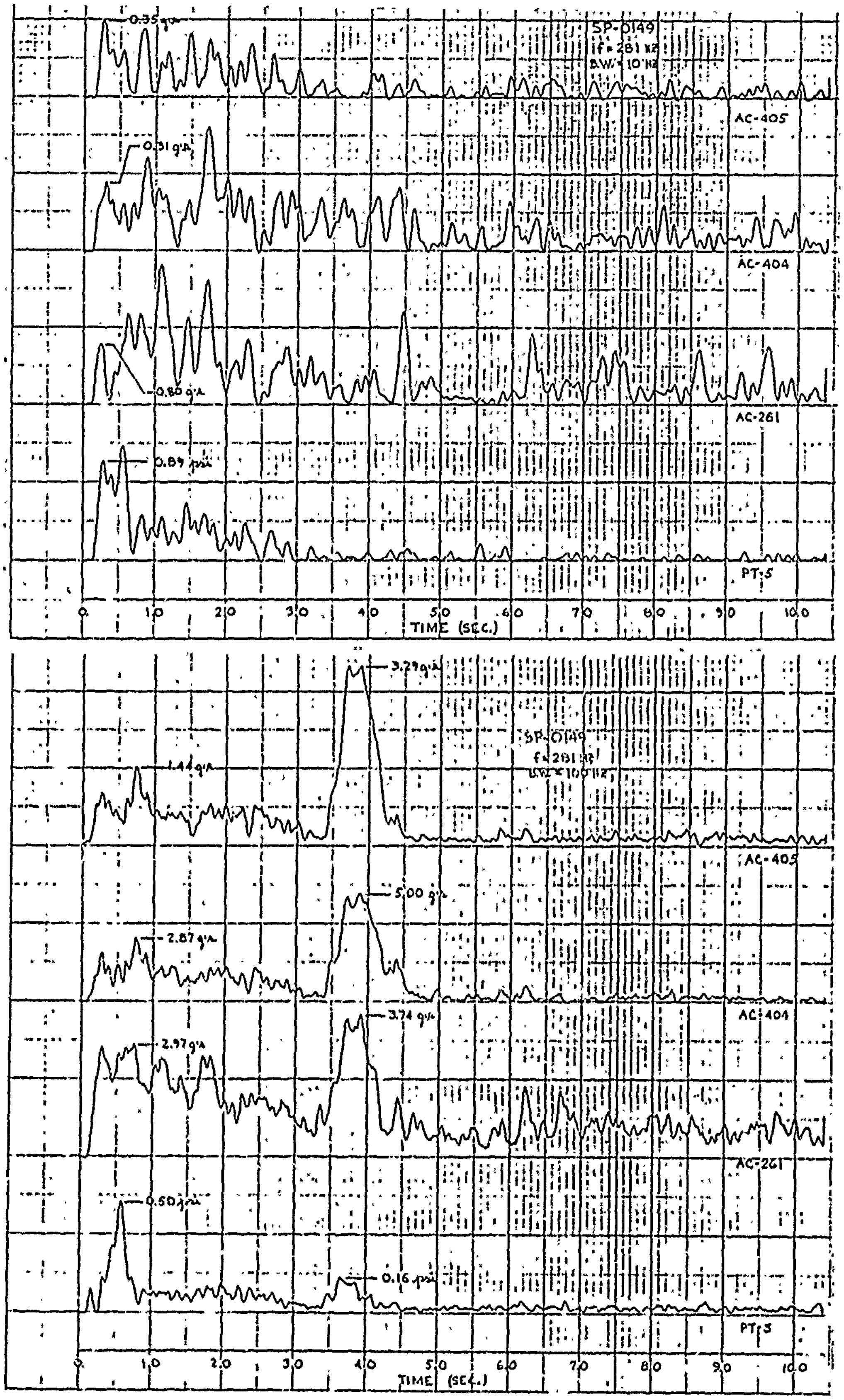

Figure 6. Filtered Pressure Gage and Accelerometer Response for Poseidon S/S Motor SP-0149. (Quan Tech Analyses at F = 281 Hz with Filter Bandwidths of 10 and 100 Hz)

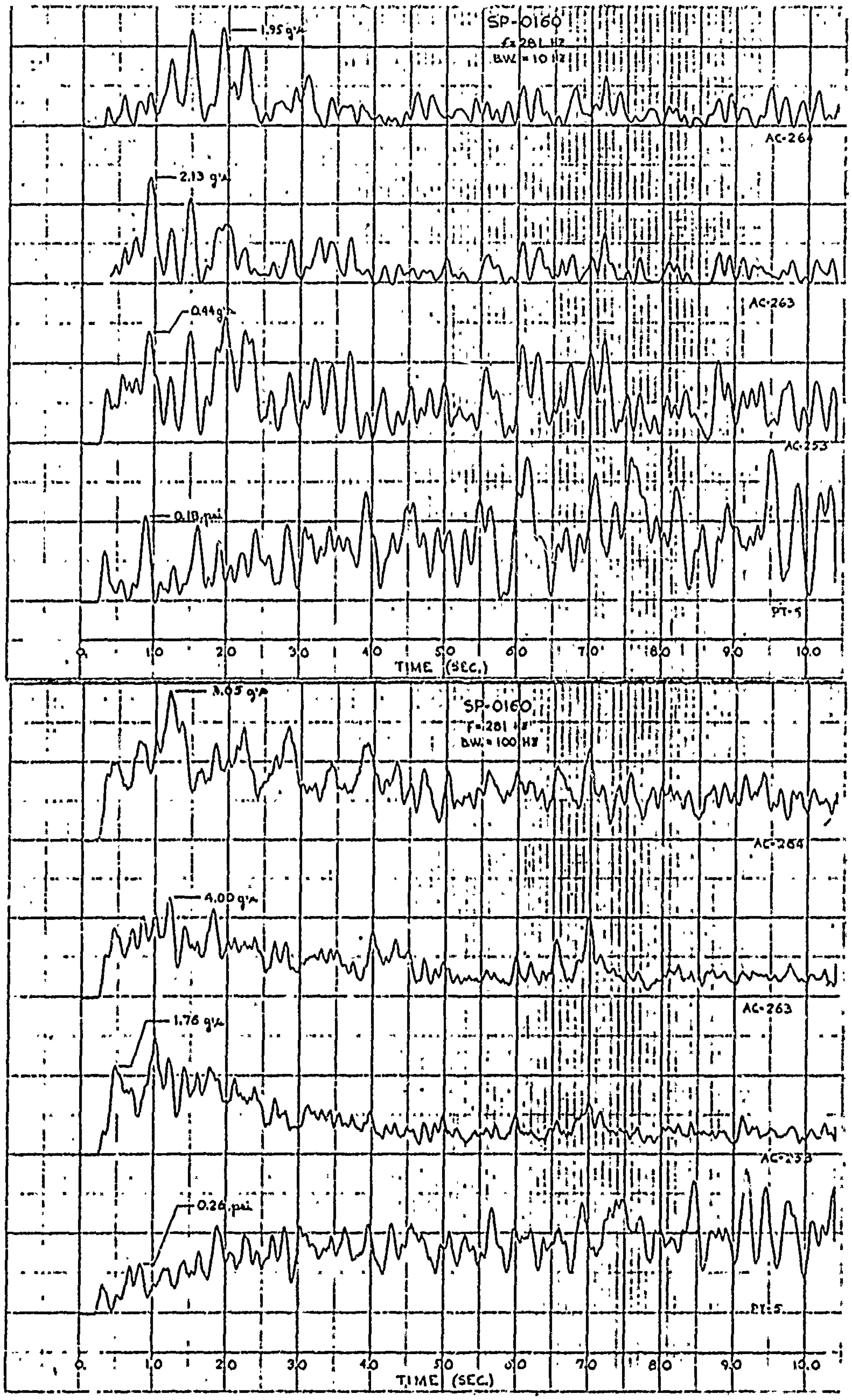

Figure 7. Filtered Pressure Gage and Accelerometer Response for Poseidon S/S Motor SP-0160. (Quan Tech Analyses at F = 281 Hz with Filter Bandwidths of 10 and 100 Hz)

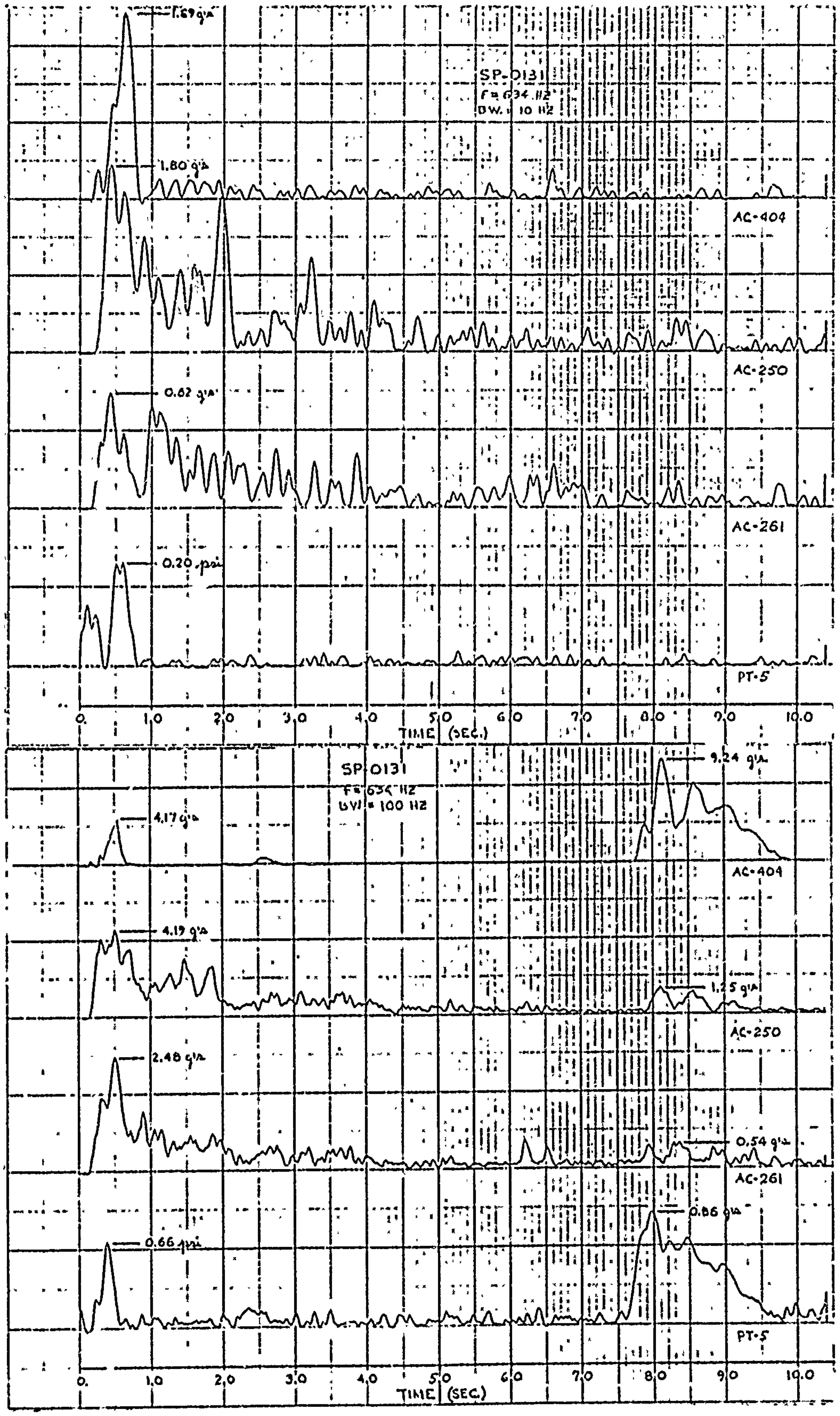

Figure 8. Filtered Pressure Gage and Accelerometer Response for Poseidon S/S Motor SP-0131. (Quan Tech Analyses at F = 634 Hz with Filter Bandwidths of 10 and 100 Hz)

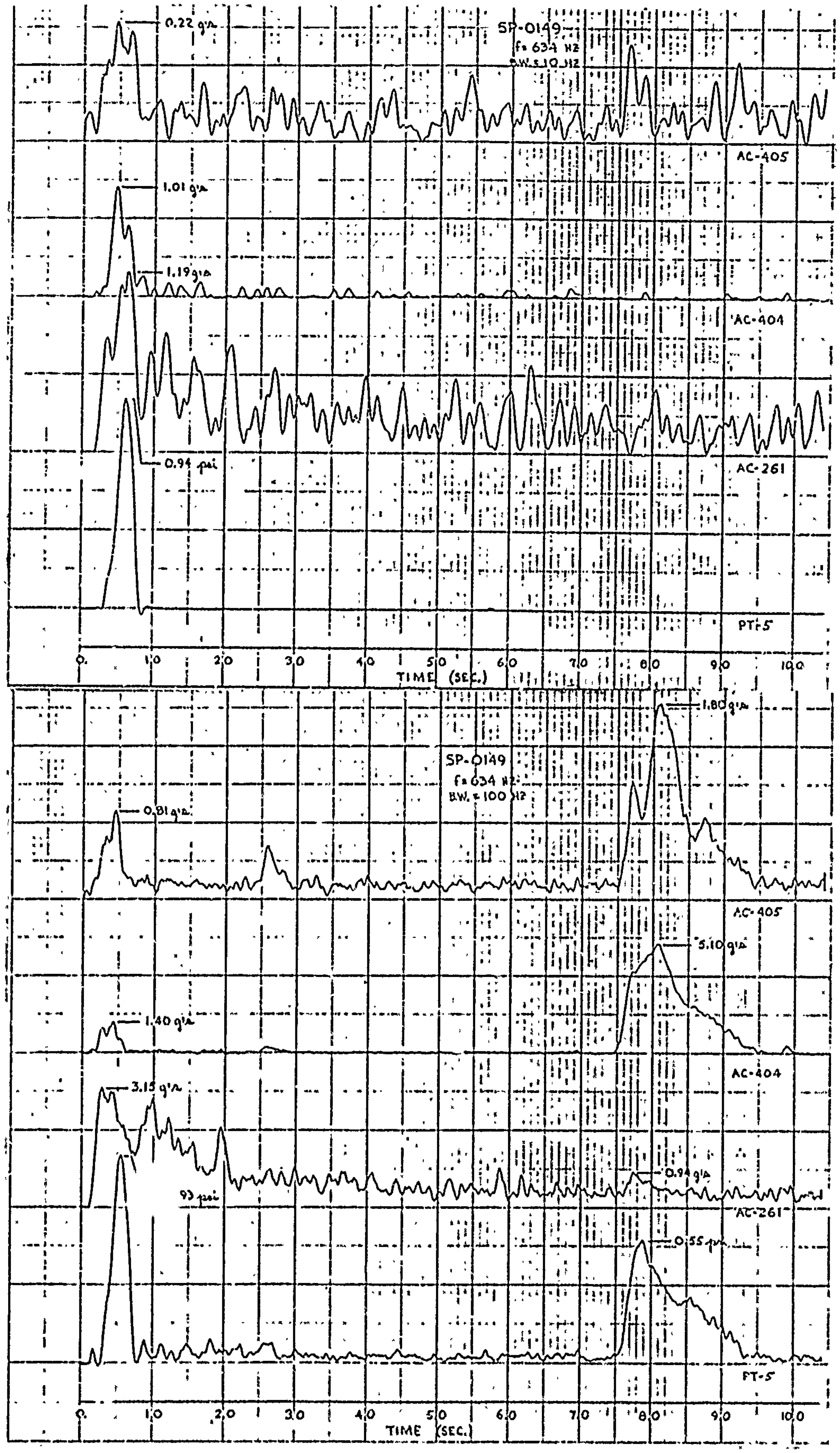

Figure 9. Filtered Pressure Gage and Accelerometer Response for Poseidon S/S Motor SP-0149. (Quan Tech Analyses at F = 634 Hz with Filter Bandwidths of 10 and 100 Hz)

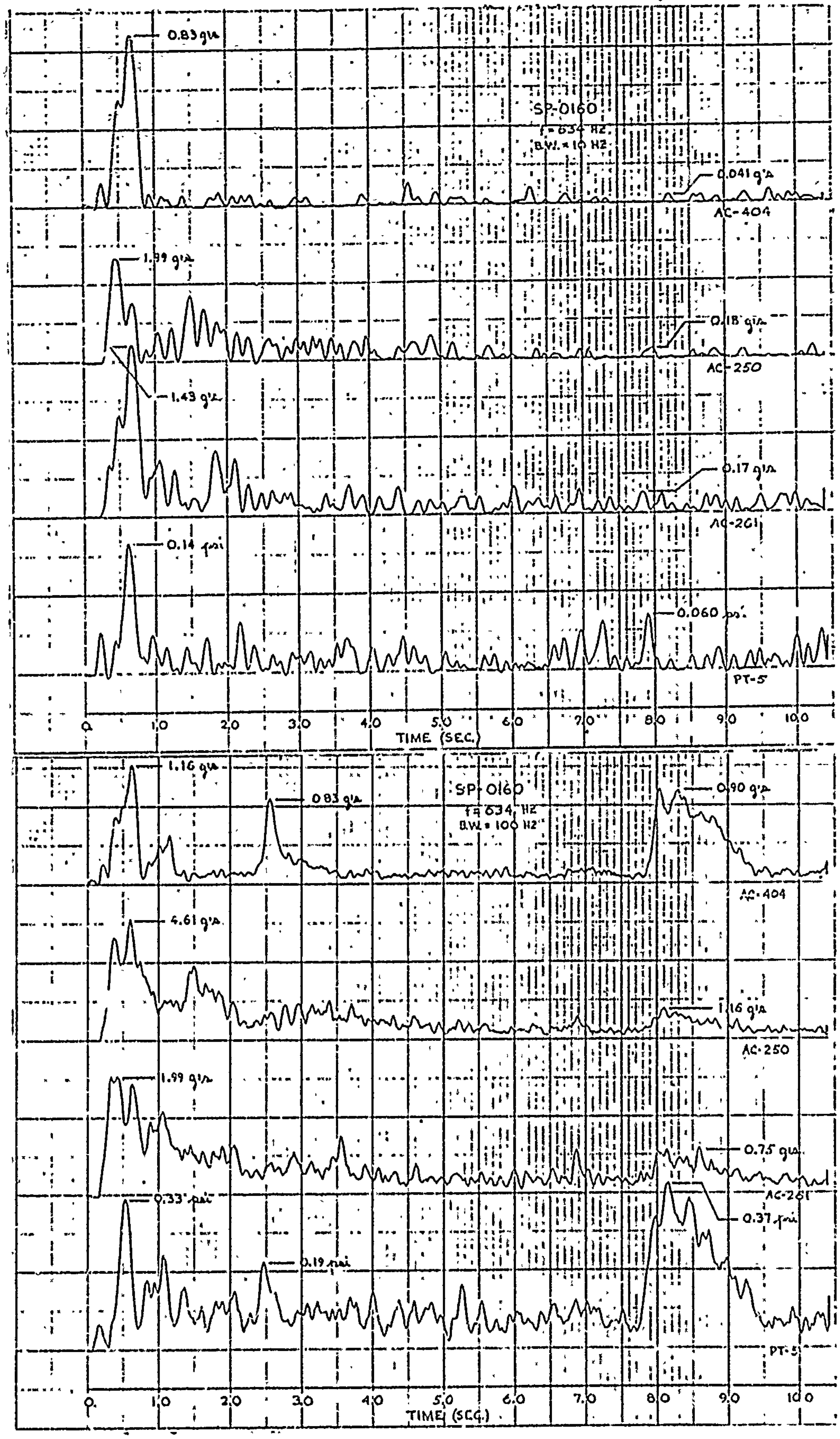

Figure 10. Filtered Pressure Gage and Accelerometer Response for Poseidon S/S Motor SP-016C. (Quan Tech Analyses at F = 634 Hz with Filter Bandwidths of 10 and 100 Hz)

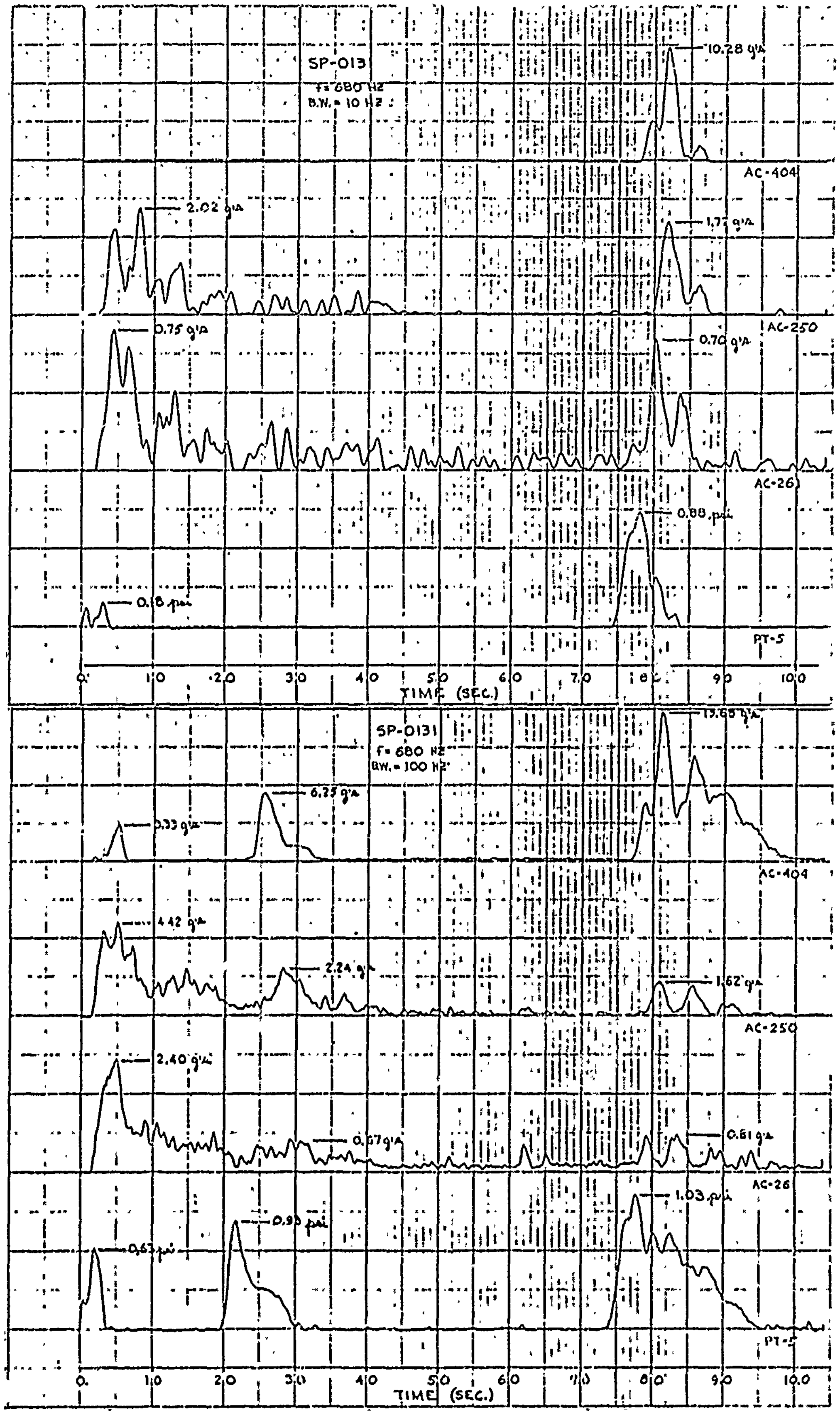

Figure 11. Filtered Pressure Gage and Accelerometer Response for Poseidon S/S Motor SP-0131. (Quan Tech Analyses at F = 680 Hz with Filter Bandwidths of 10 and 100 Hz)

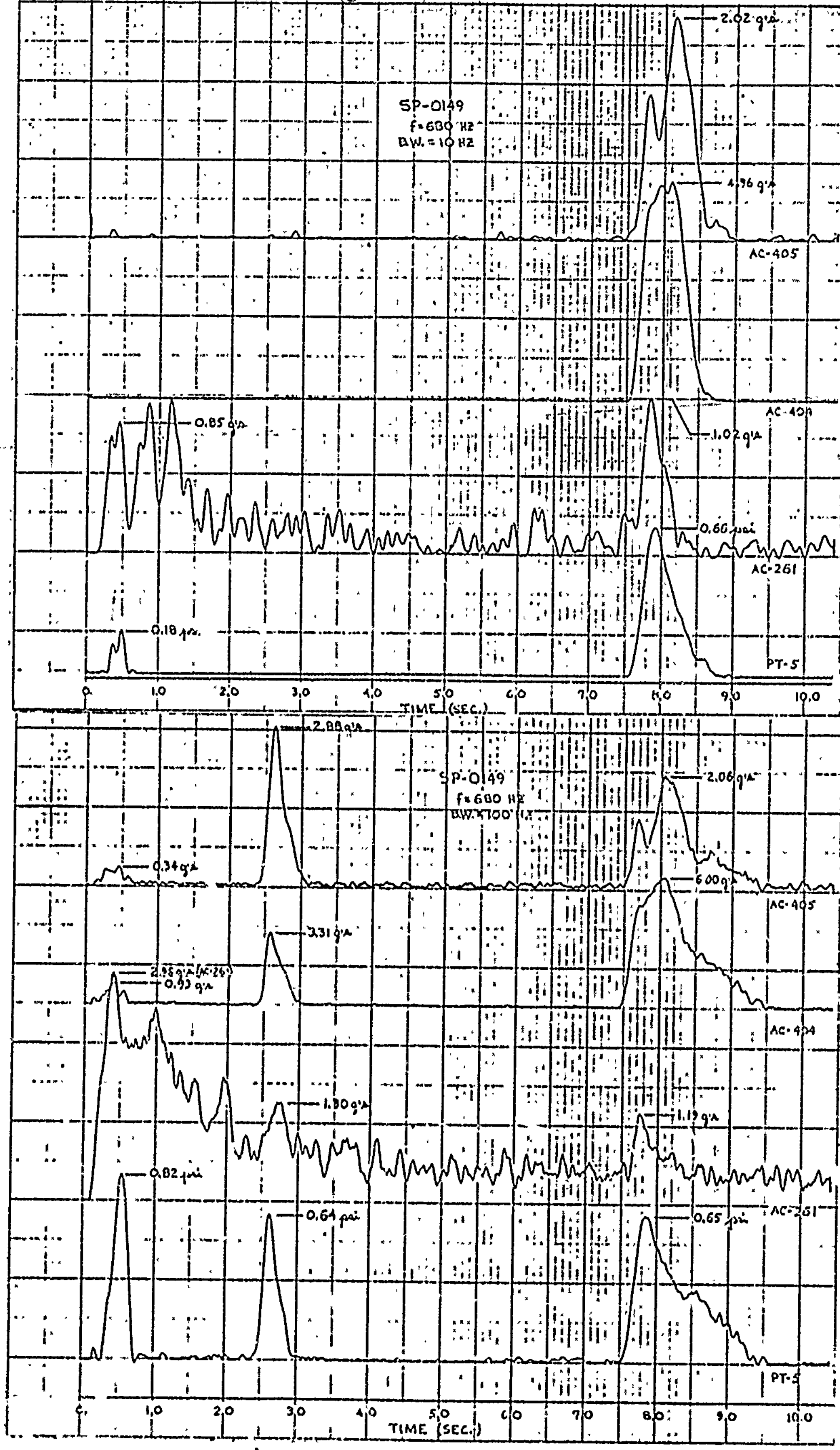

Figure 12. Filtered Pressure Gage and Accelerometer Response for Poseidon S/S Motor SP-0149. (Quan Tech Analyses at F = 680 Hz with Filter Bandwidths of 10 and 100 Hz)

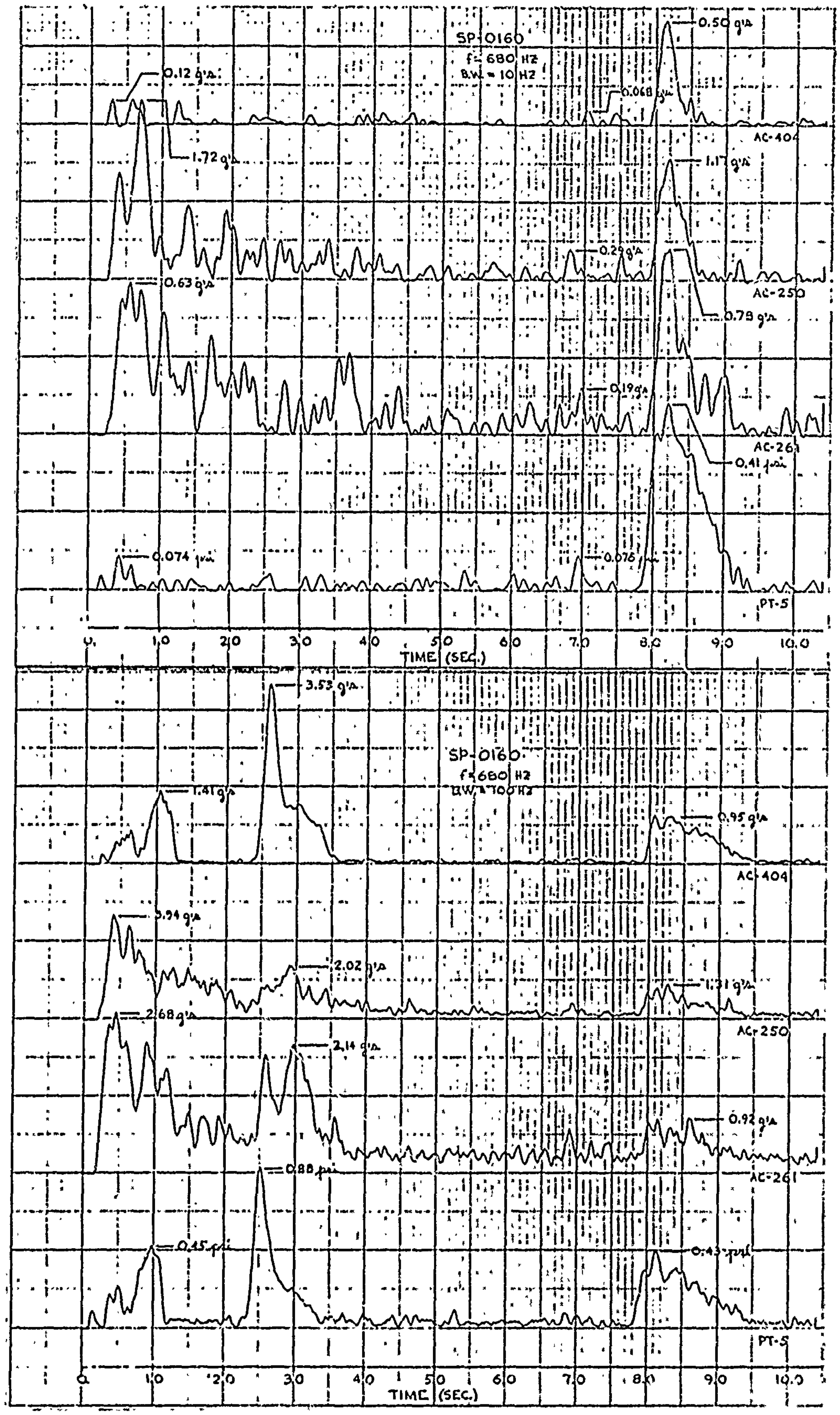

Figure 13. Filtered Pressure Gage and Accelerometer Response for Poseidon S/S Motor SP-0160. (Quan Tech Analyses at F = 680 Hz with Filter Bandwidths of 10 and 100 Hz)

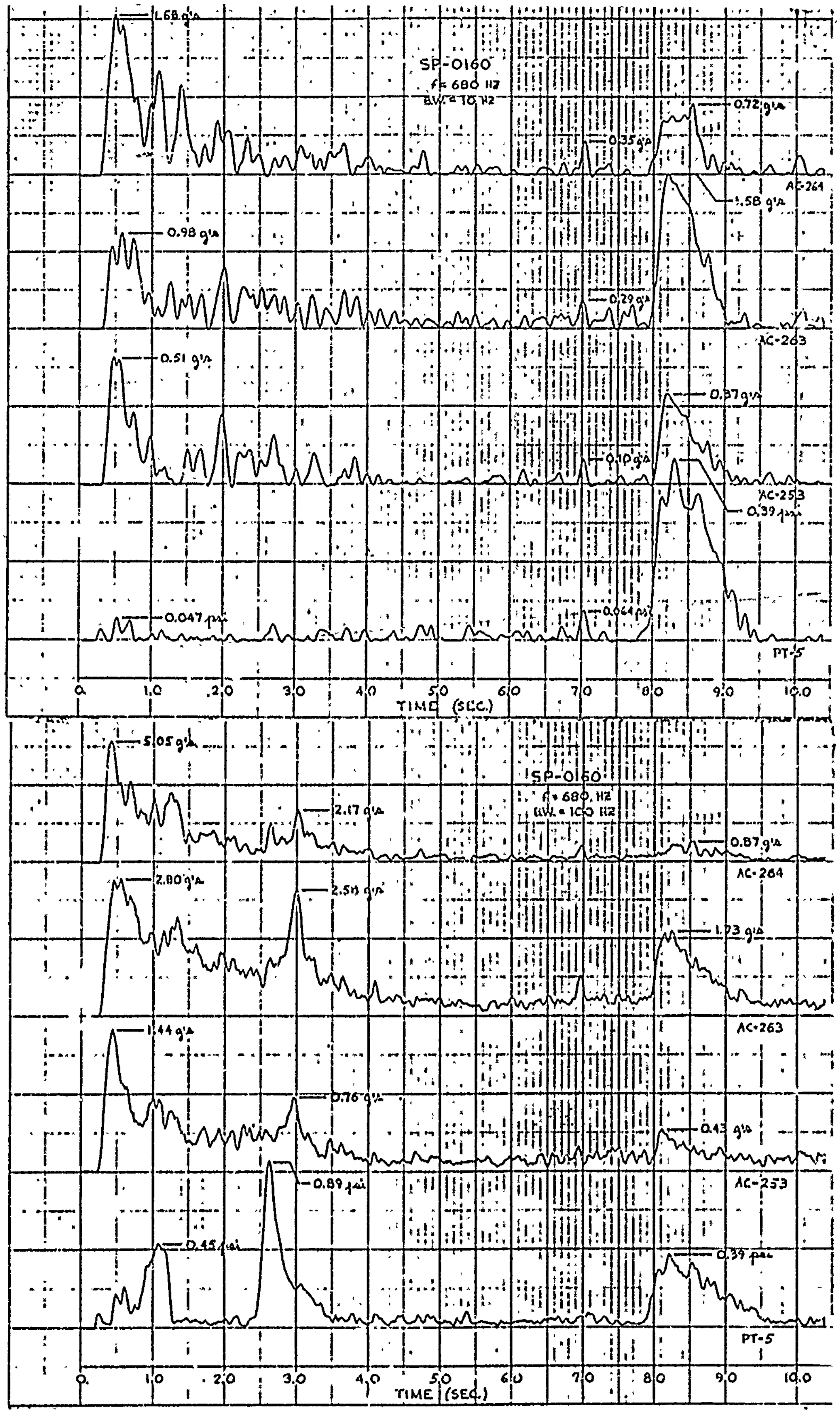

Figure 14. Filtered Pressure Gage and Accelerometer Response for Poseidon S/S Motor SP-0160. (Quan Tech Analyses at F = 680 Hz with Filter Bandwidths of 10 and 100 Hz)

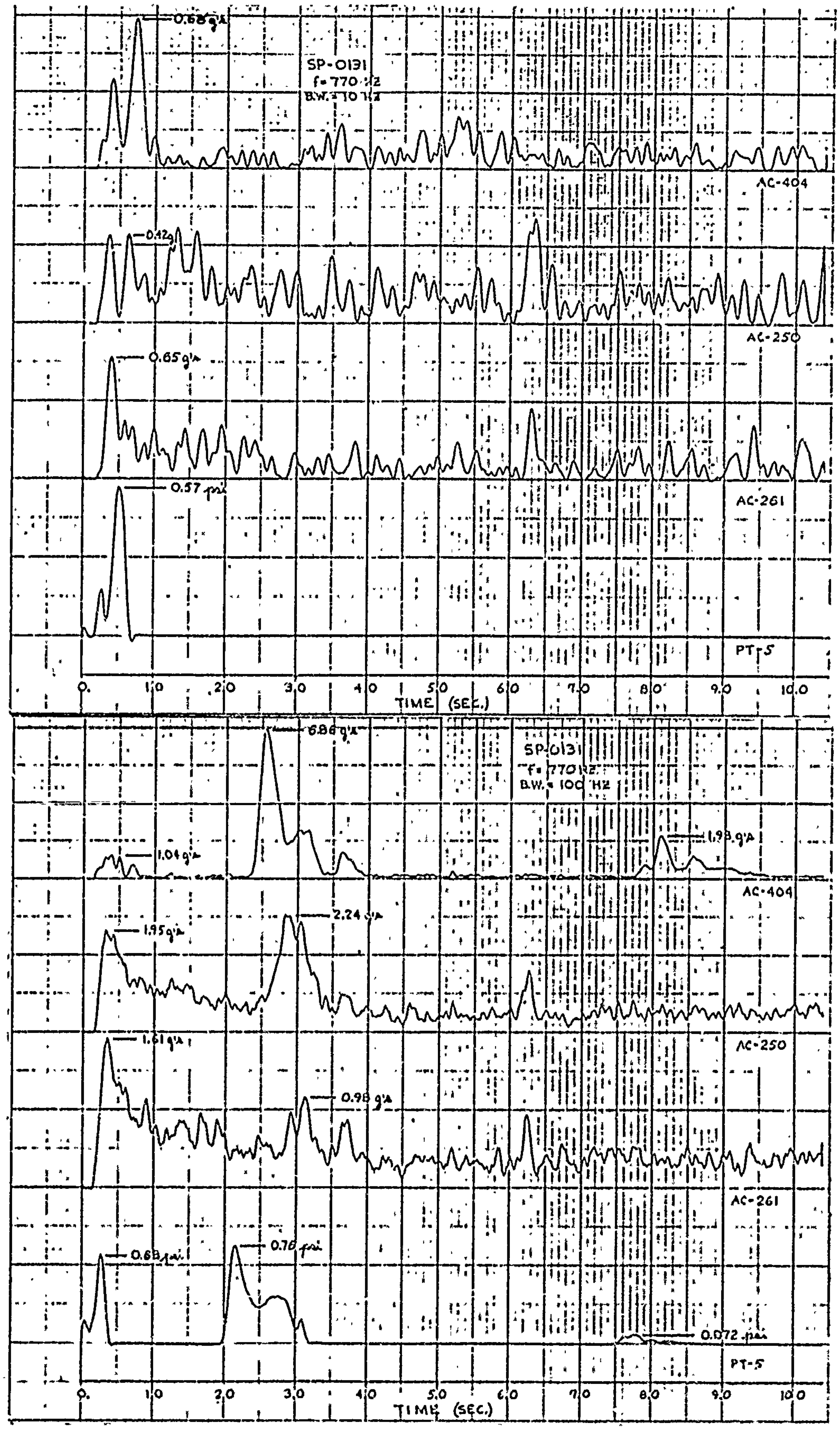

Figure 15. Filtered Pressure Gage and Accelerometer Response for Poseidon S/S Motor SP-0131. (Quan Tech Analyses at F = 770 Hz with Filter Bandwidths of 10 and 100 Hz)

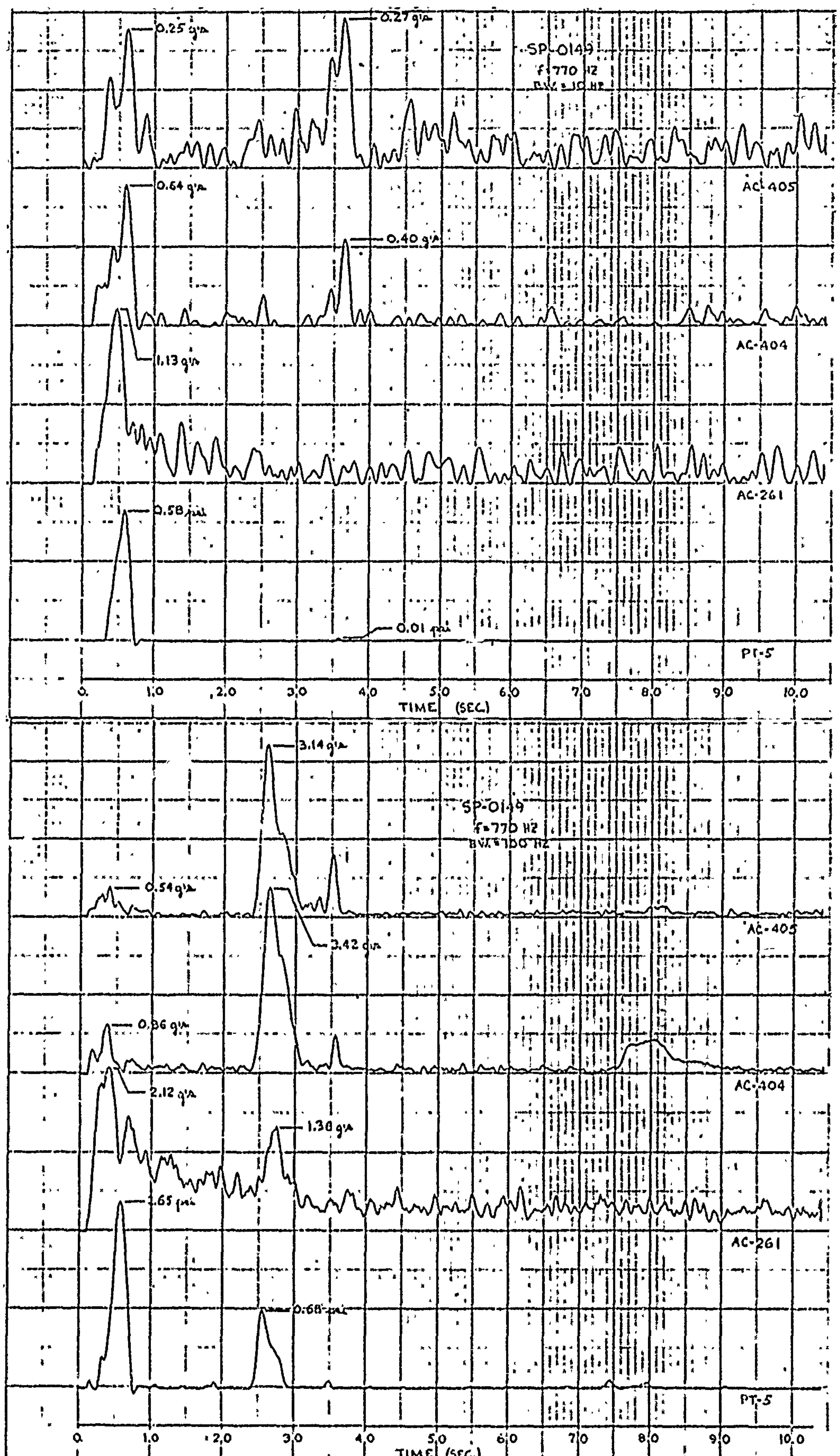

Figure 16. Filtered Pressure Gage and Accelerometer Response for Poseidon S/S Motor SP-0149. (Quan Tech Analyses at F = 770 Hz with Filter Bandwidths of 10 and 100 Hz)

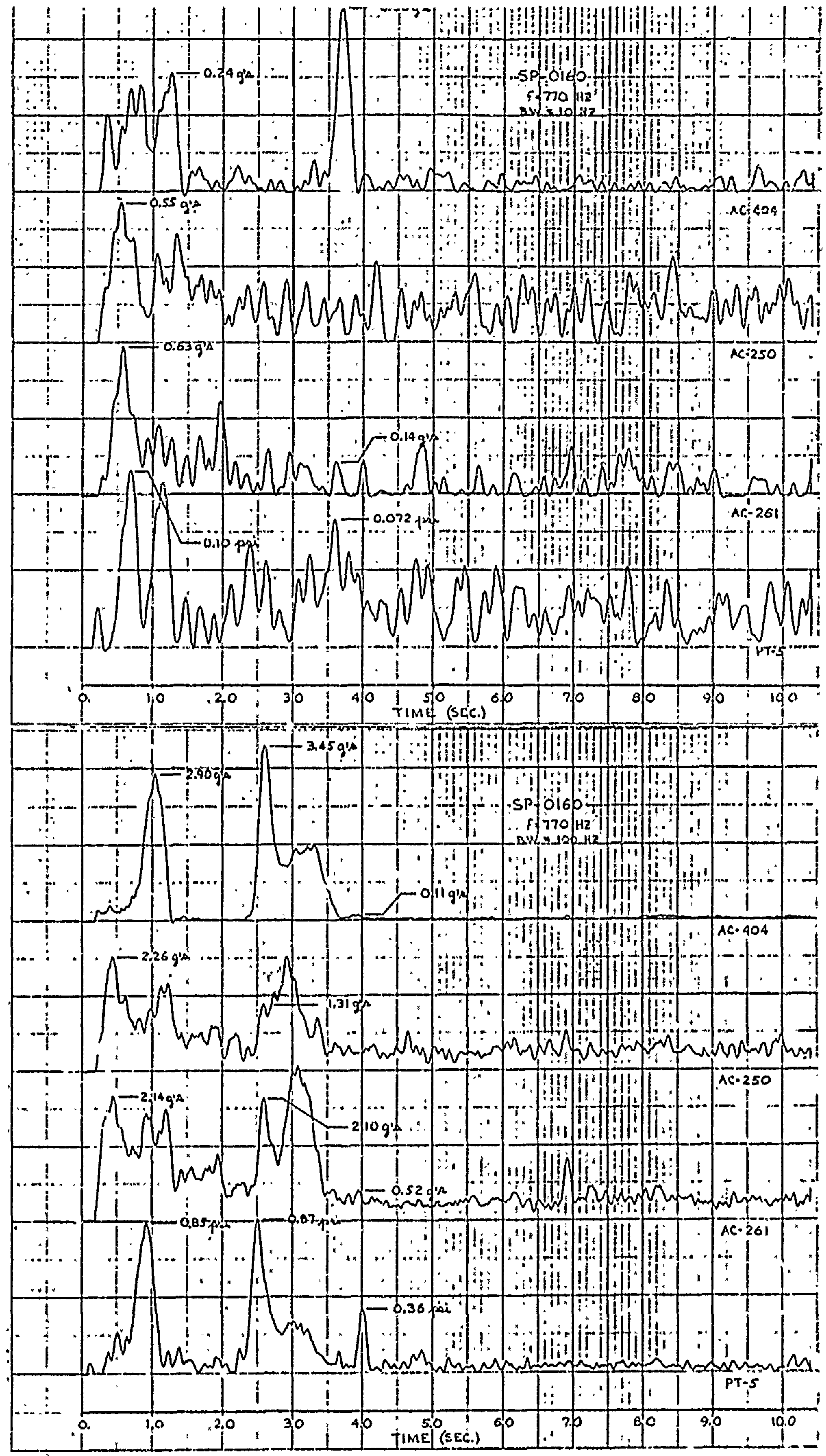

Figure 17. Filtered Pressure Gage and Accelerometer Response for Poseidon S/S Motor SP-0160. (Quan Tech Analyses at F = 770 Hz with Filter Bandwidths of 10 and 100 Hz)

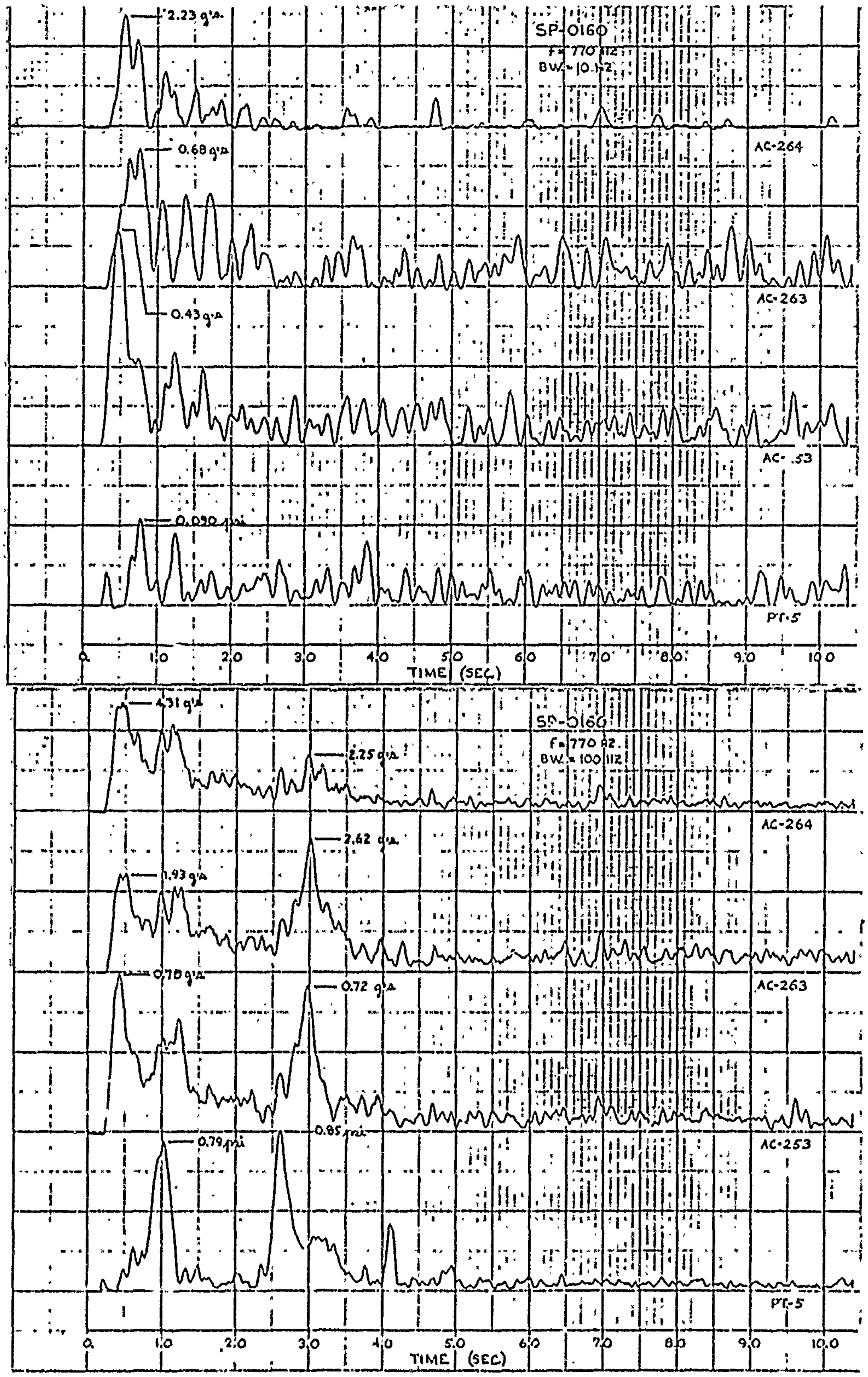

Figure 18. Filtered Pressure Gage and Accelerometer Response for Poseidon S/S Motor SP-0160. (Quan Tech Analyses at F = 770 Hz with Filter Bandwidths of 10 and 100 Hz)

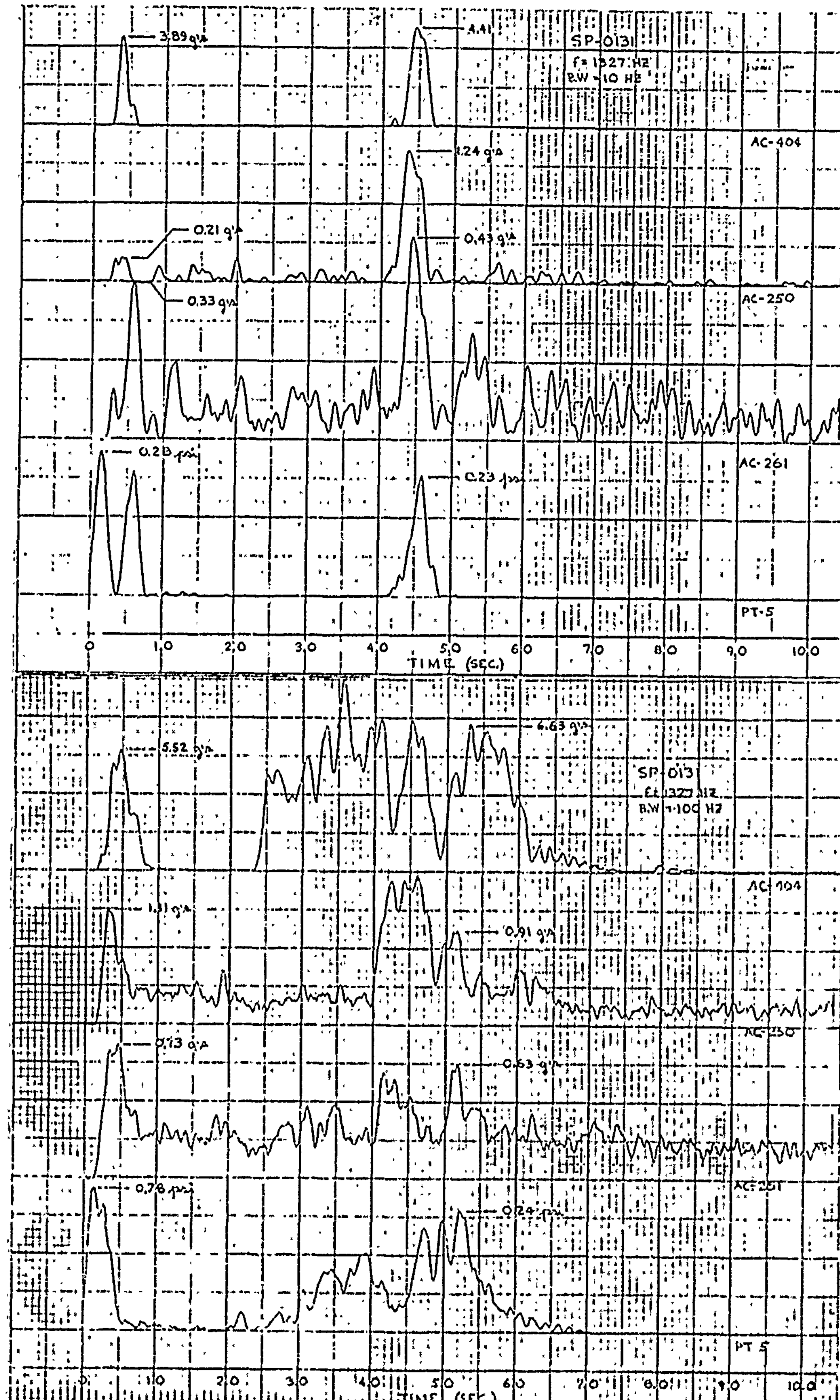

Figure 19. Filtered Pressure Gage and Accelerometer Response for Poseidon S/S Motor SP-0131. (Quan Tech Analyses at F = 1327 Hz with Filter Bandwidths of 10 and 100 Hz)

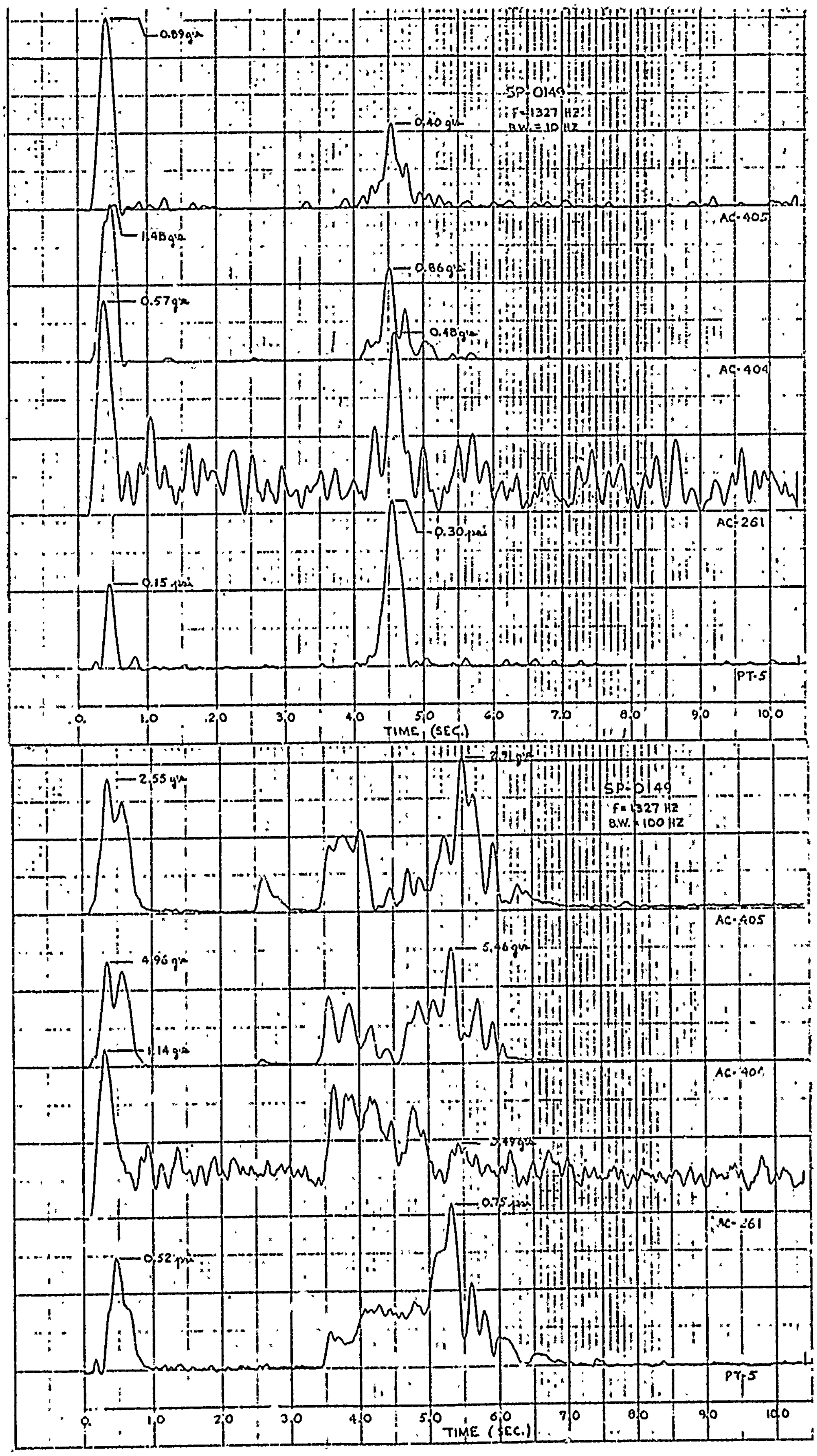

Figure 20. Filtered Pressure Gage and Accelerometer Response for Poseidon S/S Motor SP-0149. (Quan Tech Analyses at F = 1327 Hz with Filter Bandwidths of 10 and 100 Hz)

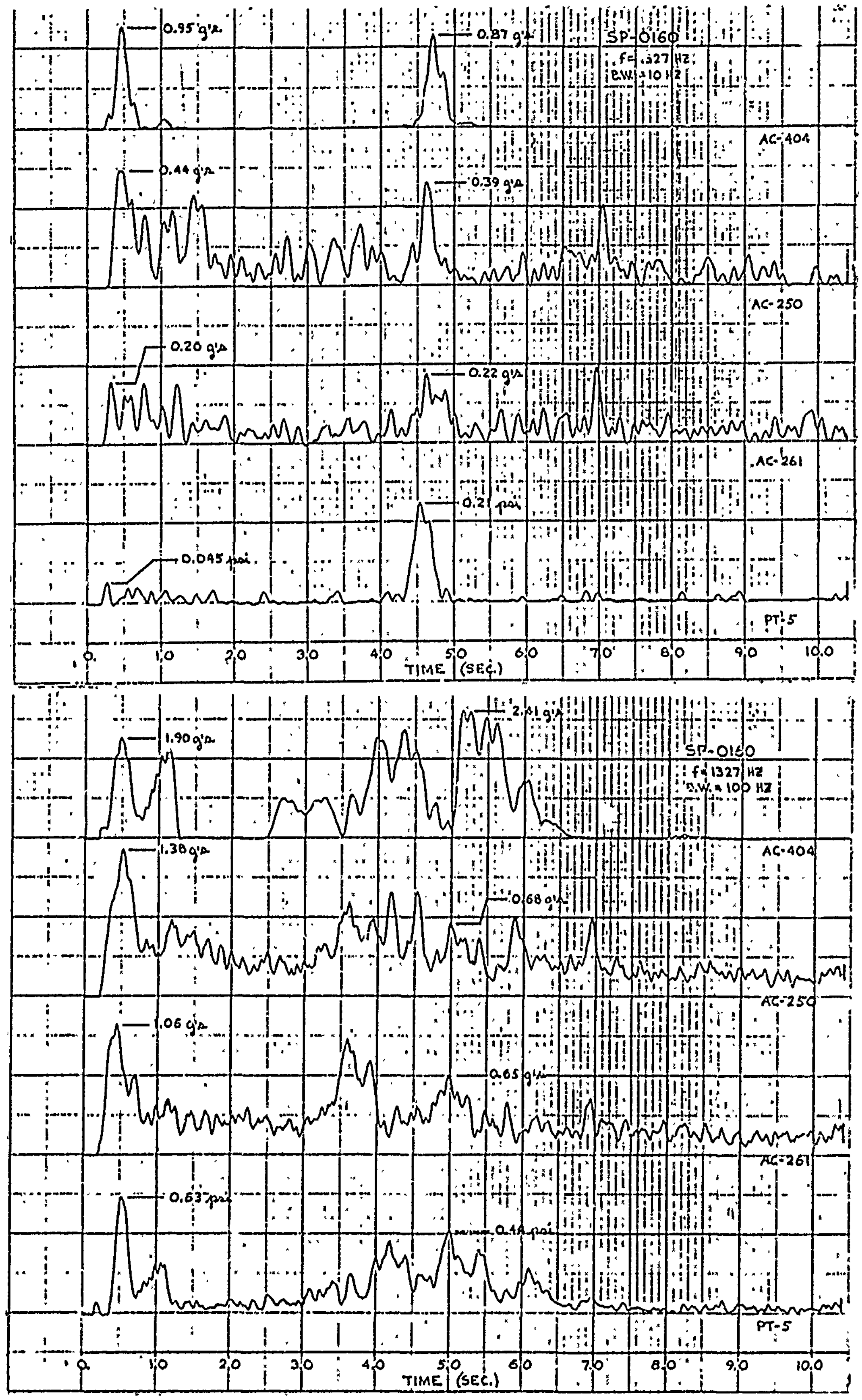

Figure 21. Filtered Pressure Gage and Accelerometer Response for Poseidon S/S Motor SP-0160. (Quan Tech Analyses at F = 1327 Hz with Filter Bandwidths of 10 and 100 Hz)

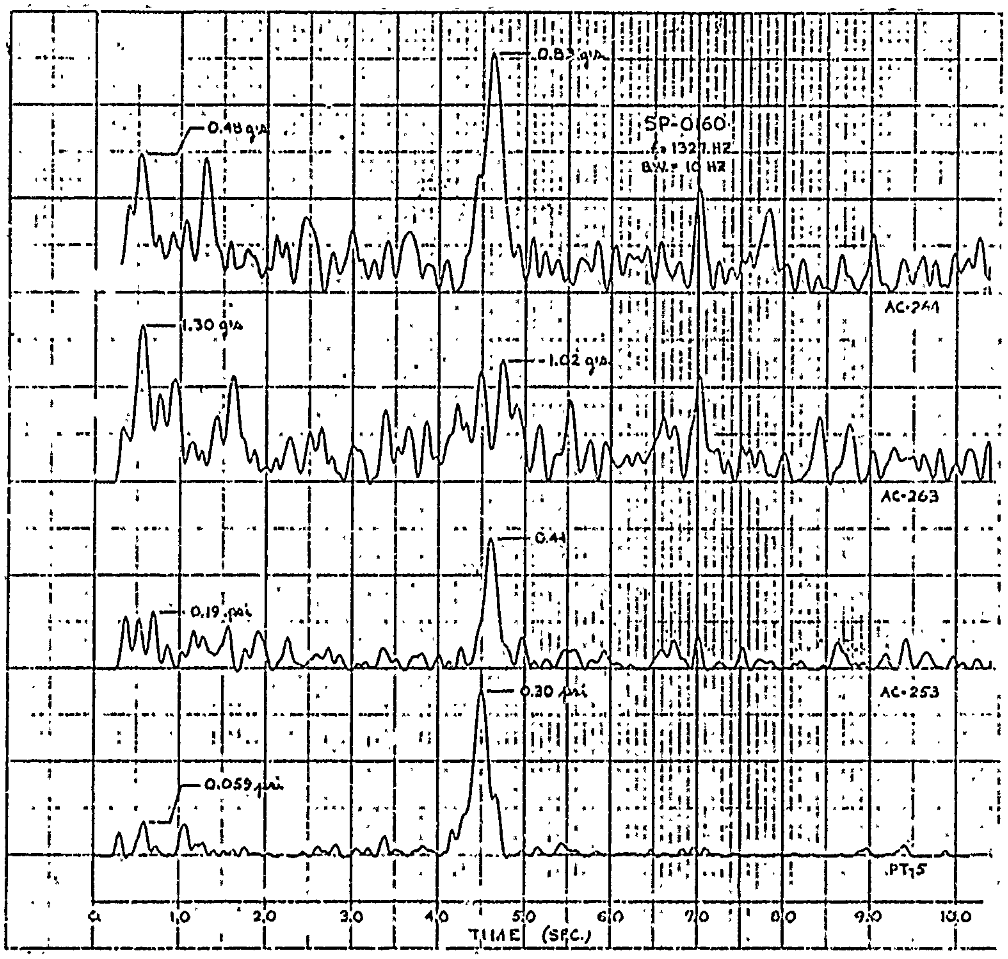

Figure 22. Filtered Pressure Gage and Accelerometer Response for Poseidon S/S Motor SP-0160. (Quan Tech Analyses at F = 1327 Hz with Filter Bandwidth of 10 Hz)

EXTRACTED FROM THE 18 MAY 1973
MONTHLY R&D STATUS REPORT

TASK 1 REPORT

ESTABLISHMENT OF ERROR LIMITS

Contract No. F04611-73-C-0025

AIR FORCE ROCKET PROPULSION LABORATORY
Edwards Air Force Base, California

18 May 1973

HERCULES INCORPORATED
Bacchus Works
Magna, Utah

I. INTRODUCTION

Acceptable error limits for component vibration levels predicted by dynamic structural analyses must be established. The error limits will be used to judge the accuracy of analysis results when compared with accelerometer data from static firings. The error limits established in this task will be re-evaluated in Task 5 and modified if necessary. Finally, the error limits will be used in Task 8 to judge the quality of various simplified models. This report covers the rationale and the data analysis upon which the established error limits are based and presents numerical values for the proposed error limits.

II. ERROR LIMIT RATIONALE

Due to the nature of this problem, the established error limits must be based on a statistical approach. There are two aspects to the problem which can be considered separately:

a. Given a population of similar rocket motors, the acceleration response at a particular location on a motor selected at random will have a particular statistical distribution. A knowledge of the distribution would be useful to answer questions such as, "How close to the mean would 95% of the samples from such a population lie?"

b. A finite element model constructed to represent an actual motor must always be based on certain simplifying assumptions. In the model, geometry, material properties, and loads are all idealized. The accuracy with which a mathematical model can represent a physical motor must be considered in comparing analytical results with data obtained from the physical motor.

In this report, contributions to the error limits due to item no. b., listed above, are ignored. This is equivalent to assuming that the finite element model provides an exact representation of the physical motor. The fact that error limits based on item no. b. tend to be very broad is offered as partial justification for ignoring item no. b. at this time. Effects of item no. b. will be estimated and incorporated in the error limits in Task 5 if deemed necessary.

Since item no. b. is being ignored, results from the finite element models are assumed to represent mean values, m. Error limits about m are then based on results from statistical analyses of static firing data. The statistical analyses yield an estimate of the standard deviation, s, for a given acceleration response. Assuming a normal distribution, 95% of the response, r, values obtained by choosing a static firing motor at random, would fall in the range:

$$m - 1.96s \leq r \leq m + 1.96s$$

However, the lower side of the range is of little interest since we are mainly concerned with exceeding allowable values. Therefore, we can establish one-sided ranges:

Percentage of Values in Range	Range (error limits)
95%	$r \leq m + 1.65s$
99%	$r \leq m + 2.4s$
99.87%	$r \leq m + 3.0s$

To use the error limits given above, a value for m is obtained from a finite element analysis and a value of s is obtained from a statistical analysis. The error limits then state that, for example, 95% of the response levels (r), measured during static firing tests should fall below m + 1.65s. Results from statistical analyses providing recommended values for s are given in the next section.

III. STATISTICAL ANALYSIS OF STATIC FIRING DATA

Most static firings of Poseidon C3 S/S motors have been conducted with at least two "standard location" accelerometers and a Kistler pressure gage set up to measure pressure oscillation amplitude. The two "standard locations" are: 1) the forward adapter ring, and 2) a TT port.

For each static firing, a Quan-Tech analysis is performed on the pressure and accelerometer data by setting the Quan-Tech analyzer to track at a certain frequency. An oscillograph record is thus made showing amplitude versus firing time for the portion of the signal near the pre-set tracking frequency. Tracking frequencies of interest used are 250, 670, 750, 1300 and 2000 Hz. The tracking filter bandwidth is 100 Hz. To reduce the data for firing reports, the maximum values recorded during a firing are listed in tabular form and are included in each firing report. An example of a firing report data table is given in Table I. The statistical analysis discussed in this section is based on all data available from static firing reports. From 18 to 44 data points were available per condition.

To detect and document the correlation between acceleration response amplitude and pressure oscillation amplitude, linear regression analyses were performed on the static firing data. The estimated regression equation of acceleration (y) on pressure (x) is:

$$y = \bar{y} + b\,(x - \bar{x})$$

TABLE I

EXAMPLE OF FIRING REPORT DATA TABLE
(FREQUENCY-AMPLITUDE DATA)

Channel	AC-402	AC-403		AC-404	AC-405		P-5 (Kistler)	
Location	TT Port	TT Port	Average TT Port	Forward Adapter	Forward Adapter	Average Forward Adapter	Forward Closure	
Azimuth	330°	30°		90°	180°		270°	
Orientation	Axial	Axial		Axial	Axial		Maximum Zero-to-Peak Pressure Oscillations (psi)	Time of Occurrence (sec)
Mode (Hz)	MAXIMUM ZERO-TO-PEAK ACCELEROMETER AMPLITUDE (G)							
250	5	5	5.0	3	3	3.0	Note 2	---
670	24	25	24.5	1	2	1.5	Note 2	---
750	51	31	41.0	4	7	5.5	0.9	2.4
1300	29	37	33.0	13	11	12.0	0.9	7.2
2000	33	18	25.5	7	15	11.0	0.9	1.7
2600	30	50	40.0	15	16	15.5	1.8	2.4
2700	15	27	21.0	7	7	7.0	0.5	2.4
3300	77	43	60.0	14	37	25.5	1.8	2.5
4000	33	83	58.0	11	15	13.0	1.4	2.0

UNCLASSIFIED

Note 1: Maximum zero-to-peak 250 Hz thrust oscillation equals 230 lb_f.

Note 2: The 250 Hz and 670 Hz modes could not be evaluated on the Kistler pressure gage due to noise.

Values of the coefficient b were calculated for each location and frequency as shown on Table II. The F statistic was then used to test the hypothesis that the real b is not significantly different from zero. Values for the calculated F and critical values of F_c are shown on Table II. The critical F_c values shown are for significance at the 5% level. The F-ratio test indicates that significant correlation between pressure oscillation amplitudes and acceleration response amplitudes exists only for conditions A, B, F, and I ($F > F_c$). The correlation is particularly significant at either location at the 250 Hz oscillation frequency.

The variance about the regression line, s^2, was also calculated for each condition and is given in Table II. The large variance of 1414 obtained for condition I appears to be unreasonably large compared to the other values in Table II. Therefore, data from three questionable firings including the high and the low were deleted and another analysis was performed. Results based on the corrected data are shown in parentheses in Table II. The new analysis resulted in a variance of 543.

The mean values for the pressure oscillation amplitude ($\bar{x}$), the mean acceleration amplitude ($\bar{y}$), and the standard deviation (s) are shown in Table II. There is considerable variation in the s values shown. To display the data on a more uniform basis, the coefficient of variation (c.o.v.) was calculated (c.o.v. = $s/\bar{y}$), for each condition as shown in Table II. Using the values for n and c.o.v. given in Table II, a weighted ave› :ge for the c.o.v. was calculated $(\text{c.o.v.})_{avg}$ = 0.569.

IV. ESTABLISHMENT OF ERROR LIMITS

To define error limits for different confidence levels, the error limits given in Section II can be rewritten in terms of the coefficient of variation:

Confidence Level	Range
95%	$r \le (1. + 1.65\ \text{c.o.v.})\ m$
99%	$r \le (1. + 2.40\ \text{c.o.v.})\ m$
99.87%	$r \le (1. + 3.00\ \text{c.o.v.})\ m$

Using the average value of 0.569 for the c.o.v., the following error limits are established:

Confidence Level	Error Limits
95%	$r \le 1.94\ m$
99%	$r \le 2.36\ m$
99.87%	$r \le 2.71\ m.$

TABLE II

STATISTICAL ANALYSIS DATA AND RESULTS

(Condition) Location/Frequency (Hz)	n	b	F	F_c (5%)	s^2
A. Forward Adapter/250	20	40.4	20.3	4.41	262.
B. Forward Adapter/670	27	6.33	15.0	4.24	5.84
C. Forward Adapter/750	36	1.36	1.15	4.10	10.3
D. Forward Adapter/1300	42	1.42	.287	4.08	80.1
E. Forward Adapter/2000	44	1.10	.146	4.06	40.2
F. TT Port/250	18	18.9	30.8	4.49	42.2
G. TT Port/670	24	2.02	.043	4.30	260.
H. TT Port/750	34	-5.47	.474	4.15	403.
I. TT Port/1300	41 (40)	29.5 (20.6)	6.97 (8.40)	4.08 (4.08)	1414 (543.)
J. TT Port/2000	41	19.5	3.11	4.08	684.

Condition	$\bar{x}$ (Mean Pressure)	$\bar{y}$ (Mean Acceleration) (g's)	s	c.o.v.
A.	.480	16.45	16.2	.985
B.	.547	3.44	2.42	.703
C.	.764	4.51	3.21	.711
D.	.957	13.31	8.95	.672
E.	1.104	15.30	6.34	.414
F.	.574	13.39	6.50	.485
G.	.477	38.21	16.1	.421
H.	.763	40.26	20.1	.500
I.	.862 (.864)	50.93 (48.40)	37.6 (23.3)	.738 (.481)
J.	1.110	54.32	26.2	.482

The error limits are to be used as follows in judging the accuracy of the finite element models:

a. Calculate a response acceleration using a finite element model. For example, suppose a response of $m = 10$ g's is calculated for a point of interest on the model.

b. Compare available data with the calculated m value by using the error limits. To continue the example, suppose that the following (fictitious) data are available from five different static firings:

$$r_1 = 12 \text{ g's}$$

$$r_2 = 7 \text{ g's}$$

$$r_3 = 13 \text{ g's}$$

$$r_4 = 19 \text{ g's}$$

$$r_5 = 16 \text{ g's}$$

If the model provides a reasonably accurate representation of the motor, then 95% of the observed response (r) values should satisfy the inequality:

$$r \leq 1.94\ m = 19.4 \text{ g's}$$

In our example, all five available test data points satisfy the inequality, so we conclude that the finite element model is satisfactory.

V. CONCLUSIONS

The complete statistical characterization of a rocket motor with regard to vibration response and pressure oscillation amplitude is a difficult and complicated task. The response of the motor is affected by many variables which are difficult to identify and quantify, and the characterization is complicated by the fact that many variables and responses of interest are functions of time. In the present program, the establishment of error limits is a small part of the total effort and can therefore only be allotted a small part of the total time. Therefore, the problem has been simplified and error limits have been proposed that appear to be reasonable based on presently available data.

EXTRACTED FROM 20 JANUARY 1975
MONTHLY R&D STATUS REPORT

STUDY ON EFFECTS OF USING NASTRAN

WEDGE ELEMENTS IN A

FINITE ELEMENT MODEL

STUDY ON EFFECTS OF USING NASTRAN WEDGE ELEMENTS IN A FINITE-ELEMENT MODEL OF THE S/S POSEIDON MOTOR

I. INTRODUCTION

Wedge elements have been used in several previous analyses. Aerojet Corporation has utilized NASTRAN wedge elements in its modeling of a T/S Minuteman motor. Hercules, also, has implemented wedge elements in the cyclic symmetry modeling of a S/S Poseidon motor.

During the evaluation of one of the models of the S/S Poseidon motor, it was observed that symmetric loading conditions produced asymmetric deformations. A thorough examination of boundary and loading conditions produced no explanation. As a natural progression of the investigation, a study was initiated to isolate the cause-effect relationship of symmetric loading and asymmetric deformations problem. The investigation started with the examination of various NASTRAN elements.

II. CHARACTERISTIC OF THE INDIVIDUAL WEDGE ELEMENTS

A. Problem Definition

The evaluation of the various types of elements proceeded with the investigation of isolated elements with symmetric loading. Using MSC/NASTRAN cyclic symmetry, several models were created of a simple cylinder (see Figure 1). Each cylinder was one-inch in thickness and one-inch in width. Each cylinder with a 5-inch internal radius, had a unit force of one-pound placed on the internal corners of the element. Figure 2 displays the node numbering scheme used in the analyses.

Four types of elements were investigated, as designated by the cylinders labeled A, B, C, and D (see Figure 1). Cylinder A was composed of a CHEXA1 element, cylinder B was composed of CHEXA2, cylinder C was created from two wedge elements and cylinder D was composed of 12 overlapping wedge elements.

B. Results

The results of the analysis showed that the cylinder composed of two symmetrically-loaded wedge elements, case C, produced an asymmetric deformation. In addition, case A, as well as the case D, the CHEXA1 element, and the overlapping wedge elements, respectively, produced asymmetric deformations. These results are reflected in Table I. Because the elements were symmetric with symmetric loading, it was expected that nodes 5, 6, 7, 8; nodes 13, 14, 15, 16; nodes 21, 22, 23, 24; and nodes 29, 30, 31, 32 would have identical deformations in all directions. This was not observed in the ring composed of CHEXA1, the two wedge elements, or the 12 overlapping wedge elements.

It can be concluded that the cylinders composed of the two wedge elements and the 12 overlapping wedge elements were unsatisfactory for use in modeling of asymmetrically loaded rocket motors. The wedge elements produced deformations which were not physically accurate representations. The two wedge elements produced deformations which were as much as 478% greater than cylinders composed of the CHEXA2 element. In addition, the deformations were not uniform around a boundary. The 12 overlapping wedge elements were formed similarly to the CHEXA2 element. The cylinder composed of the 12 overlapping wedge elements produced deformations which were as much as

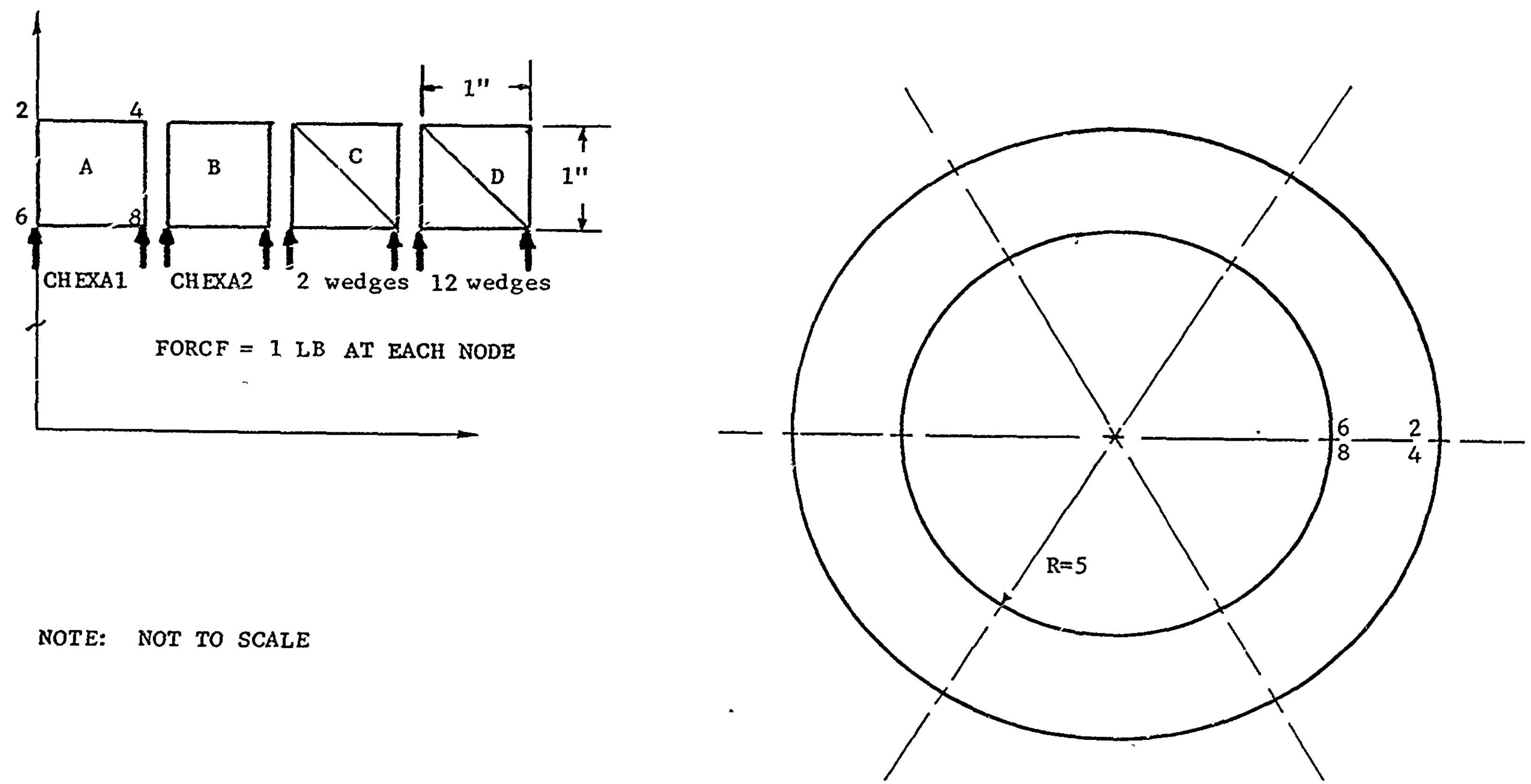

Figure 1. Views of Cylinders Used in Element Evaluation

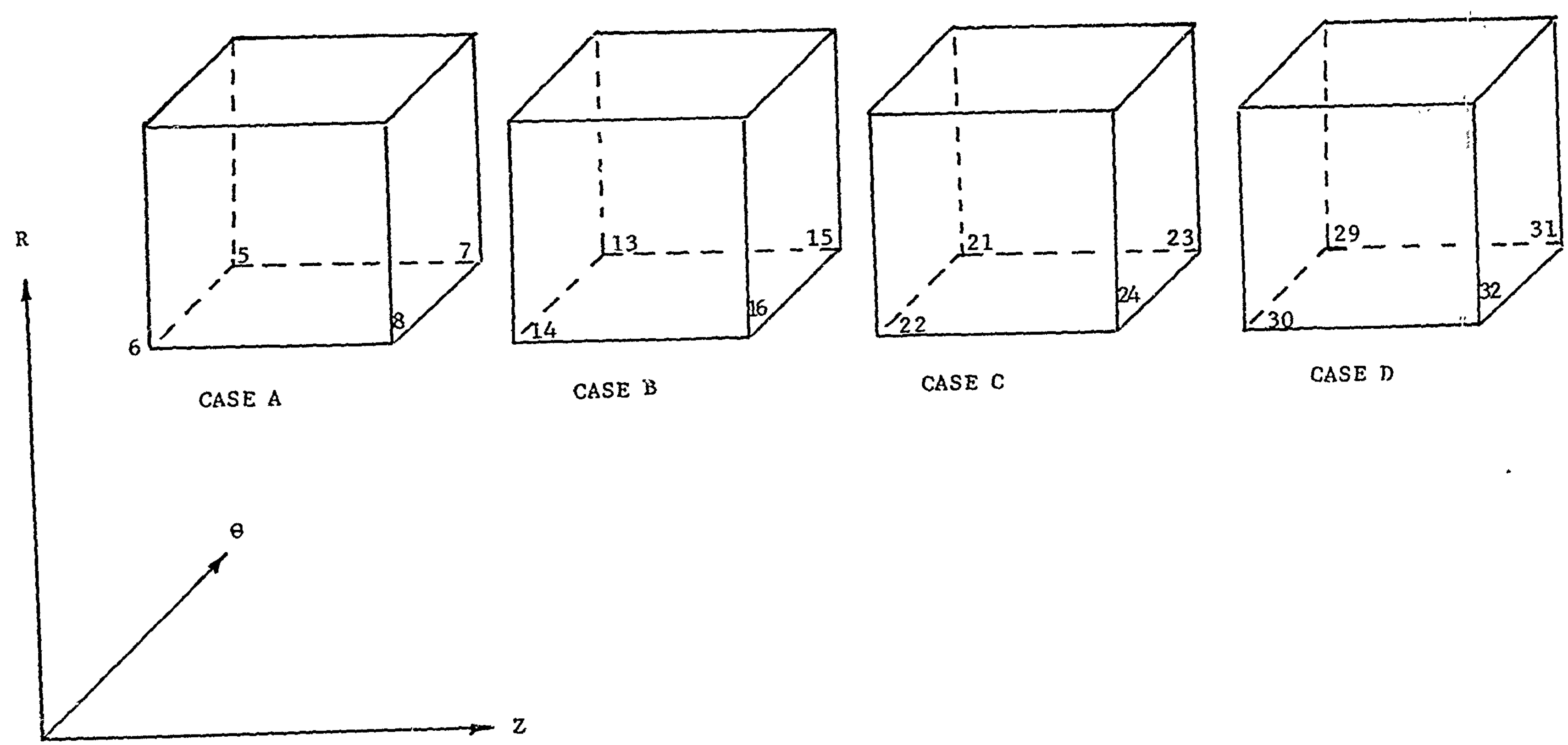

Figure 2. Numbering Techniques Used in Test Cases

TABLE I

COMPARISON OF DISPLACEMENT FOR VARIOUS NASTRAN ELEMENTS

Node Number	r-Direction	Type Element
5	1.251360×10^{-6}	CHEXA1
6	1.361747×10^{-5}	
7	1.361748×10^{-5}	
8	1.251368×10^{-6}	
13	1.73782×10^{-6}	CHEXA2
14	1.73782×10^{-6}	
15	1.73782×10^{-6}	
16	1.73782×10^{-6}	
21	9.996527×10^{-6}	Two Wedge Elements
22	8.981884×10^{-6}	
23	1.122589×10^{-6}	
24	1.117386×10^{-6}	
29	9.09438×10^{-6}	12 Overlapping Wedge Elements
30	9.09438×10^{-6}	
31	9.39799×10^{-7}	
32	9.39799×10^{-7}	

440% greater than the CHEXA2 element.

Because of the magnitude of the error discovered, it became necessary to evaluate the significance of wedge elements used in the modeling of full-sized motors.

III. EFFECTS OF WEDGE ELEMENTS ON FULL MOTOR MODEL SOLUTIONS

A. Problem Definition and Approach

The evaluation of the effects of the wedge elements on full motor model solutions required the generation of an additional model which contained no wedge elements. In order to facilitate a comparison of results, a full motor model was created by altering an existing model by the removal of wedge elements. For the purposes of identification, the full motor model which contained wedge elements shall be referenced as full motor w/wedges. The full motor model which contained no wedge elements shall be referenced as full motor w/o wedges.

The full motor w/o wedge model was created from an existing model. This was accomplished by several slight modifications including the redefinition of two wedge elements as a CHEXA2 element and movement of two nodes located on the interior of the grain. Another grain modification required the deletion of two nodes at one location and the addition of two nodes at another location. All the exterior surfaces of the case and propellant remained the same. Finally, wedge elements were removed from the bucket by their replacement with CHEXA2 elements with modified properties. Every effort was made to minimize differences between the two models. Figure 3 shows the full motor model w/o wedges which was created.

Figure 4 shows the full motor model with wedges, discussed in previous reports. It consists of CHEXA2, CQUAD1, and CWEDGE elements. The model is a 15 degree slice of a motor. All solutions utilize SDAMP in the characterization of the viscoelastic properties of the propellant. The full motor w/o wedges has identical boundary conditions and solution techniques to the full motor w/wedges model.

B. Results

A series of comparative runs were made to determine the effects on deformation of wedge elements for a variety of loading conditions. Both static and dynamic solutions were obtained. Static solutions were completed for one pressure distribution. Dynamic solutions were obtained for the third longitudinal mode at frequencies of 10, 265, 500, 770, and 1000 Hz. Dynamic solutions were also obtained for the fourth longitudinal mode at 365 Hz. These solutions will also be used in a study on the effects of scalar springs.

The static analysis solutions were obtained for one set of loading and boundary conditions. The pressure distribution used to load the propellant core was third longitudinal acoustic mode at one instant in time. Symmetry boundary conditions were applied to both the 0 degree face and 15 degree face.

For the static analysis, comparisons were made at various locations in the propellant, case, and bucket. It was observed that the deformations of the full motor w/o wedges produced symmetric deformations and rotations; this was not observed in the full motor w/wedges. Comparisons of the two models at various locations were shown in Table II.

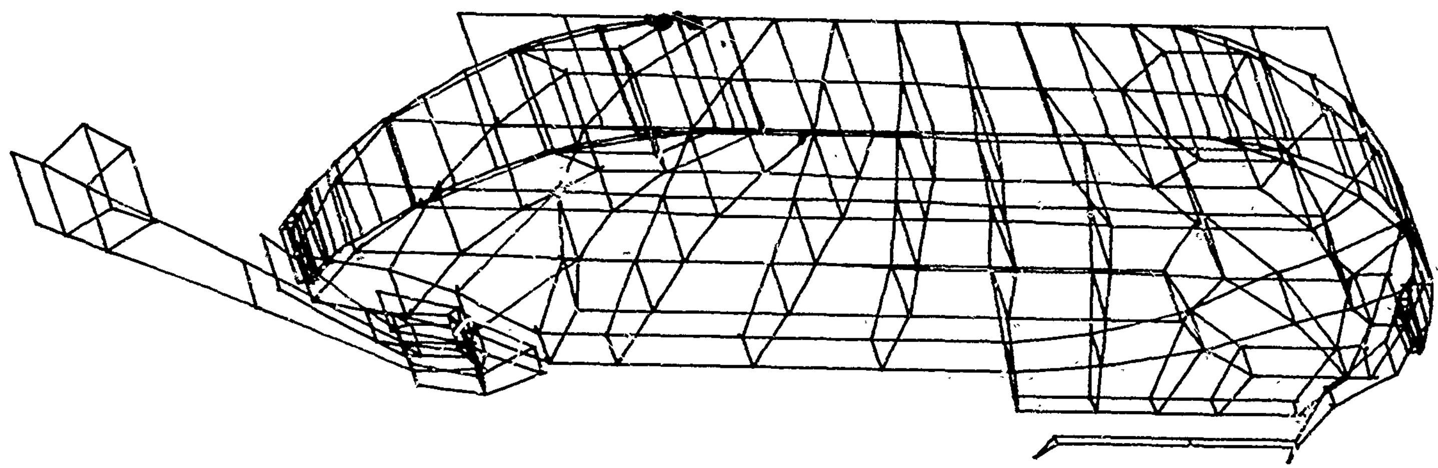

Figure 3. Modified Grid for the S/S Poseidon Motor Containing No Wedge Elements

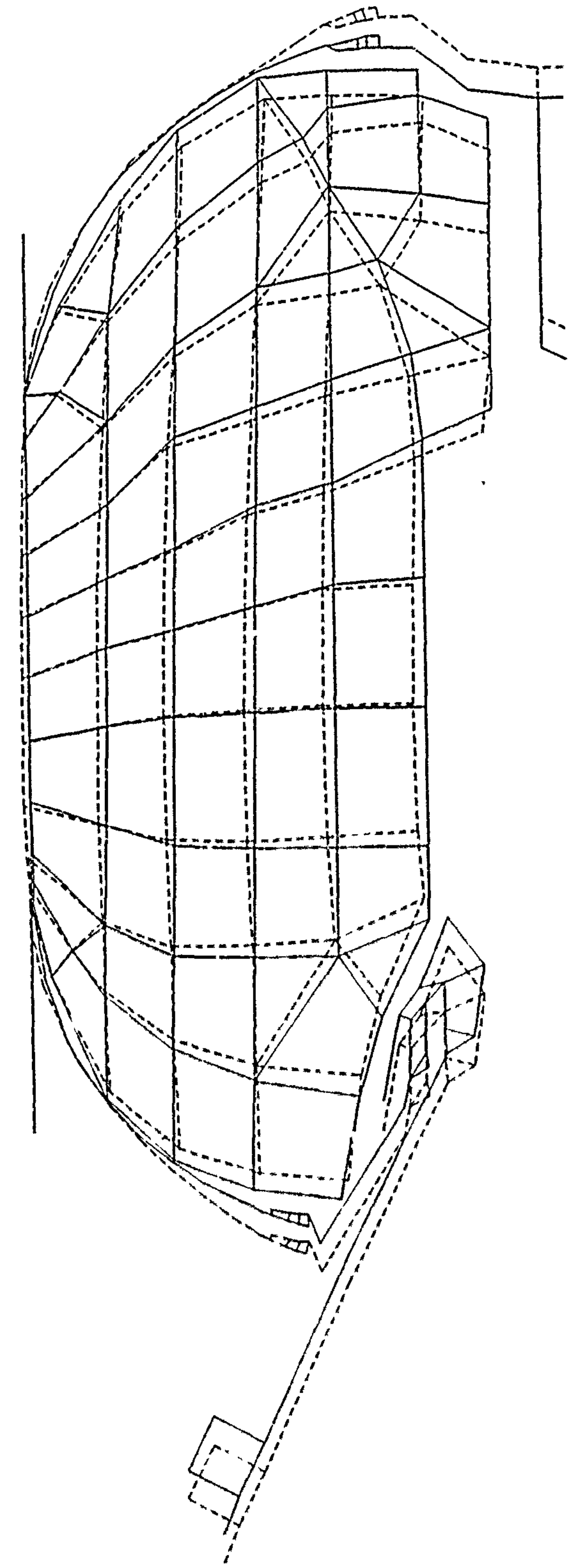

Figure 4. S/S Poseidon Motor W/Wedges and Deformed Shape

TABLE II

COMPARISON OF STATIC SOLUTIONS OF FULL MOTOR WITH WEDGES TO FULL MOTOR WITHOUT WEDGES MODELS

Location	Node No.	Full Motor w/wedges		Full Motor w/o wedges		% Difference	
		r-direction ($x10^{-4}$)	z-direction ($x10^{-3}$)	r-direction ($x10^{-4}$)	z-direction ($x10^{-3}$)	Δr	Δz
Fwd Case	18	1.3922	-3.3539	1.3922	-3.332	0.0	1.0
	46	-3.5526	.022653	-3.3579	.029932	5.8	23.3
Propellant	94	3.0227	.270515	3.3493	.38855	9.6	30.5
	112	-4.1742	-.080864	-1.4664	.11761	71.4	31.2
	126	-3.6531	-.206986	-4.0442	-.17809	9.7	16.1
Case Mid Cyl.	146	.97338	0.0	1.1953	0.0	18.6	0.0
Aft Dome	226	2.00489	.080297	2.3166	.075352	13.6	6.5
Aft Dome	254	-.47573	-.71325	-.7543	-.75828	0.0	5.9
		The maximum difference between models in the aft dome was				240	80

Several conclusions can be made from the comparison of static solutions of the full motor models with and without wedges. First, the wedge elements produce non-symmetric deformations. The asymmetry is slightly greater on the 0 degree face than the 15 degree face, which is consistent with observation of the single wedge element. Secondly, the percent difference in the models is a function of distance from the wedge element, as the distance becomes greater the difference becomes less. Next, because of the case stiffness, the effect of wedge elements is less severe in the aft and forward domes than in the propellant. The maximum difference between models in the case is 240% in the radial direction and 80% in the z-direction. Note, however, that the 240% difference for the r-direction is for a small displacement magnitude when compared to the z-direction displacement. The conclusion is that the wedge element has a significant effect upon the static solutions. Because of the differences, it became necessary to evaluate the effects of the wedge elements upon dynamic solutions.

The dynamic solutions were performed for several conditions. Symmetry boundary conditions were applied along both 0 and 15 degree faces of the models. The fourth longitudinal mode, L-4, was analyzed at 365Hz. Analyses were performed at frequencies of 10, 265, 500, 770 and 1000 Hz with the third longitudinal mode, L-3, pressure distribution.

Several general observations were made pertaining to the dynamic solutions. These are listed below:

1. For both the third and fourth longitudinal modes, the full motor w/o wedges produced displacement amplitudes which were less than the full motor w/wedges. This was consistent with observation of the individual wedge elements described in the previous section.

2. For the full motor w/wedges model, the 0 degree face of the slice generally produced larger displacement amplitude than the 15 degree slice. This observation was consistent with observations made on the characteristics of the wedge element, discussed previously. It was seen from Table I, that wedge element predicted greater deformation on the front surface than the back surface.

3. For the full motor w/wedges model, the difference in magnitude of displacement of corresponding points on 0 and 15 degree planes became less severe in the case than in the propellant. This implies that the case was sufficiently stiff to assist in damping the warping between the 0 and 15 degree faces. For the propellant, the differences (up to 100%) in displacement of the 0 and 15 degree faces were most severe at the corners of the wedge elements. The difference reduced to 25% one CHEXA2 element away from the wedge element.

4. For the full motor w/wedges model, it appeared that the differences between the 0 and 15 degree faces were frequency dependent. The greatest percent difference appeared to be at 500 Hz.

Dynamic solutions were compared for all the conditions analyzed. Tables III and IV demostrate some of the differences. Table III showed the magnitude and phase angle of displacement at various locations throughout the aft case for the full motor model with wedges at 265 Hz. Table IV displayed the magnitude and phase angle of displacement at 265 Hz for the full motor model w/o wedges at various locations.

Direct comparison of displacements of dynamic solution requires additional interpretation. Because of dome curvature and phase angle of the oscillating displacement, the mode shape must be normalized to a datum reference. For illustrative purposes, the datum reference is the base of the adapter-bucket connection on the aft dome. Using the adapter-bucket datum reference, the mode shapes of the full motor w/o wedges and the 0 degree slice of the full motor w/wedges are shown in Figure 5 for 265 Hz at one instant. Because of the wedge element the mode shapes are substantially different. Figure 6 shows the calculated mode shapes at 365 Hz of the full motor model w/o wedges as well as the 0 and 15 degree faces of the full motor w/wedges model. It can be seen that the full motor w/wedges model predicts a warping of the case, which cannot be an accurate representation of a symmetrically loaded structure. Also, it appears that the full motor model w/o wedges approximately averages the mode shapes of the 0 and 15 faces of the full motor w/wedges.

IV. CONCLUSIONS AND RECOMMENDATIONS

The study has shown that substantial error can be induced through the use of the wedge elements. For the individual wedge elements, the error can be in excess of 400%. When the wedge elements are an integral part of a model of a full motor, the error is a function of the distance from the wedge element. In the propellant, the error at the corners of the wedges can be in excess of 100%; however, within one panel length, the error reduces to 25%. The error is less severe in the case because of its greater stiffness than the propellant. It is also important to note that mode shape of models which do not contain wedge elements are substantially different from those which do contain wedges. The wedges seem to couple symmetric deformation patterns with warping deformation patterns.

Because of wedge element induced errors, it is suggested that all further analyses do not use wedge elements.

TABLE III

FULL MOTOR WITH WEDGES

	Node No.	r-Direction Magnitude ($x10^{-4}$)	r-Direction Phase	z-Direction Magnitude ($x10^{-4}$)	z-Direction Phase
	219	.3835	318.62	.2061	197.4
	220	.3499	313.07	.2054	196.6
	223	.08040	260.49	.3135	173.3
	224	.06858	261.5	.3041	170.1
	229	1.953	306.5	1.8431	300.1
	230	2.0267	307.1	1.9495	301.3
	235	1.2166	349.8	1.2519	63.9
	236	1.197	350.6	1.2739	66.2
	237	.9526	354.6	1.4329	94.1
	238	.9363	355.6	1.4693	95.5
	239	.61235	351.4	1.7259	124.4
Aft Dome	240	.60478	352.0	1.7560	124.5
	243	.1206	327.8	3.0167	149.4
	244	0.1205	328.0	3.0191	149.4
	249	.05855	208.0	3.5196	151.9
	250	.058001	208.3	3.5200	151.9
	253	.16963	179.3	3.96099	153.5
	254	.16886	179.4	3.9604	153.5

TABLE IV

FULL MOTOR WITHOUT WEDGES

	Node No.*	r-Direction		z-Direction	
		Magnitude ($x10^{-5}$)	Phase	Magnitude ($x10^{-4}$)	Phase
Aft Dome	219	1.8912	17.84	.086014	237.2
	223	1.5999	341.0	.11522	244.3
	224	1.5999	341.0	.11522	244.3
	229	4.6133	330.24	.302878	323.6
	230				
	231	7.3245	340.50	.66831	345.0
	232				
	233	8.9399	345.23	.902308	353.0
	234				
	235	9.2204	347.29	.8923	357.7
	236				
	237	7.8355	348.34	.526342	9.1
	238				
	239	5.3202	348.030	.239555	118.7
	240				
	241	3.2972	347.53	.817504	155.6
	242				
	243	1.1386	349.29	1.520619	160.7
	244				
	249	.26136	148.88	1.9775	161.8
	250				
	253	1.3156	162.16	2.3738	162.42
	254				

* Missing nodes have magnitudes and phase angles identical to preceding node.

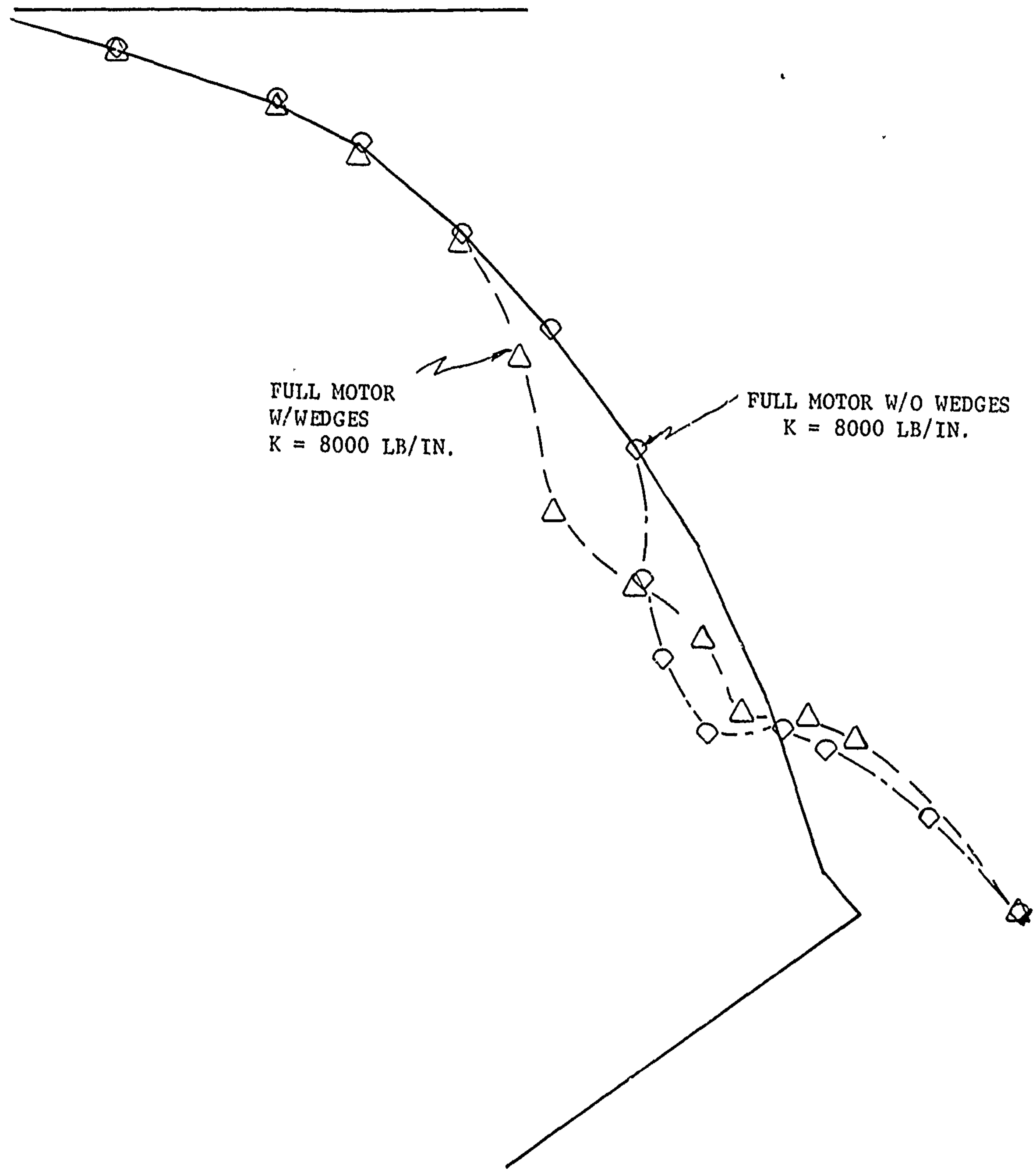

Figure 5. Comparison of Mode Shape at One Time for C-3 Motor at a Frequency of 265 Hz

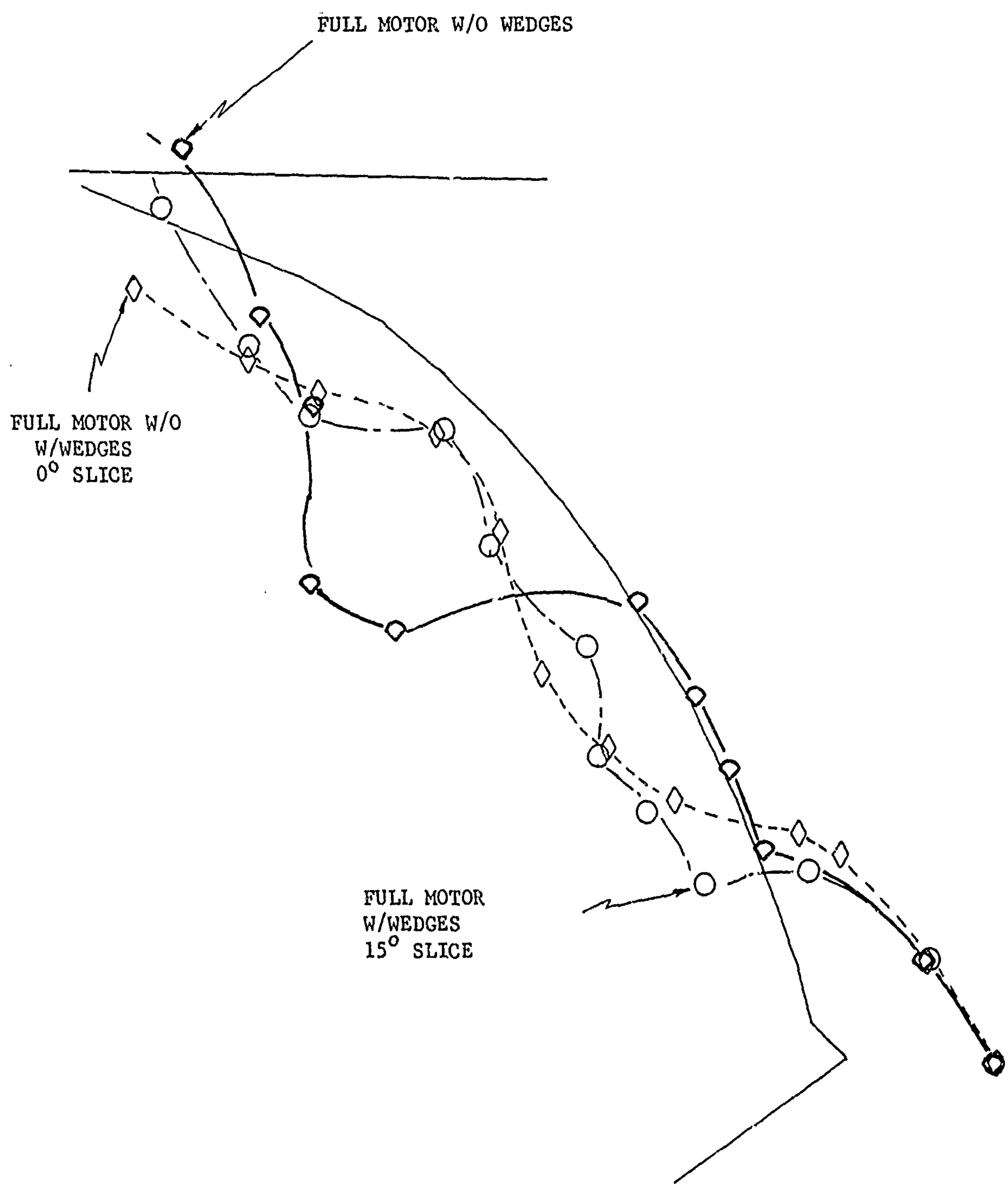

Figure 6. Mode Shape for 365 Hz C-4 Motor

EXTRACTED FROM THE 20 JULY 1974
R&D MONTHLY STATUS REPORT
FOR THE
COMPONENT VIBRATION PROGRAM

(Contract F04611-73-C-0025)

EXTRACTS FROM 20 JULY 1974 MONTHLY STATUS REPORT

To evaluate the baseline motor analysis, the mode shapes calculated for the aft dome at 265 Hz have been compared with corresponding test data from Task IV. The r-z components of displacement were resolved into a direction normal to the dome surface and plotted at four sections through the motor. Locations of the sections used for mode shape plotting are shown in Figure 2.

Calculated mode shapes (Task III) are compared with measured mode shapes (Task IV) in Figures 3 through 10. The plot in Figure 3 was given in a previous report (dated 20 May 1974). In the May monthly report, the data were normalized to obtain phase and amplitude agreement at node 255 (measurement point 300). This approach applied to the data plotted in this report yielded rather large deformations in the measured mode data. Therefore, the measured modes plotted in Figures 3 through 10 have been normalized to produce a unit deformation at the point of maximum deformation for the four sections. The calculated modes are normalized to produce a unit deformation at measurement point 300 (a point on the aft adapter at 0^{o} with measurement in the axial direction). The modes shown in Figures 3 through 10 are not natural modes but represent the forced response of the dome to a particular excitation.

Most of the measured data show a bulge in the mode shape about halfway along the dome between the adapter and the Y-joint. The bulge does not show in Figures 9 and 10. The calculated mode shapes for 365 Hz exhibit only a slight bulge at a location closer to the adapter than the bulge in the measured modes. The dip in the measured mode shapes near the adapter, as shown in Figures 5 and 6, is also followed by a small dip in the calculated mode shapes. The comparison between measured and calculated modes at 365 Hz is encouraging as the general shapes are similar. However, the amplitudes and locations of maximums are not in good agreement. The same comments generally apply to the 265 Hz mode shapes.

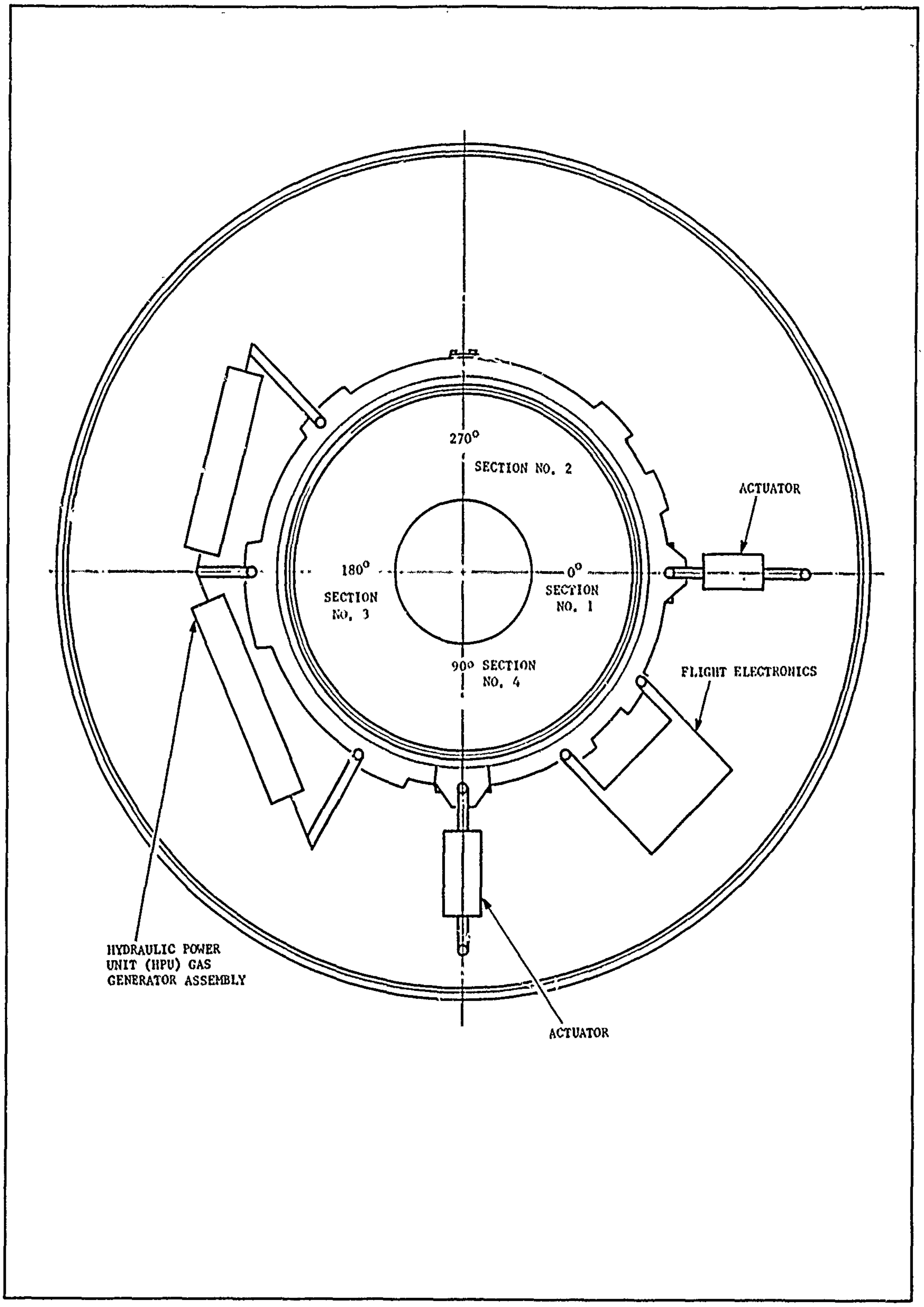

Figure 2. Sections Used for Plotting Aft Dome Mode Shapes

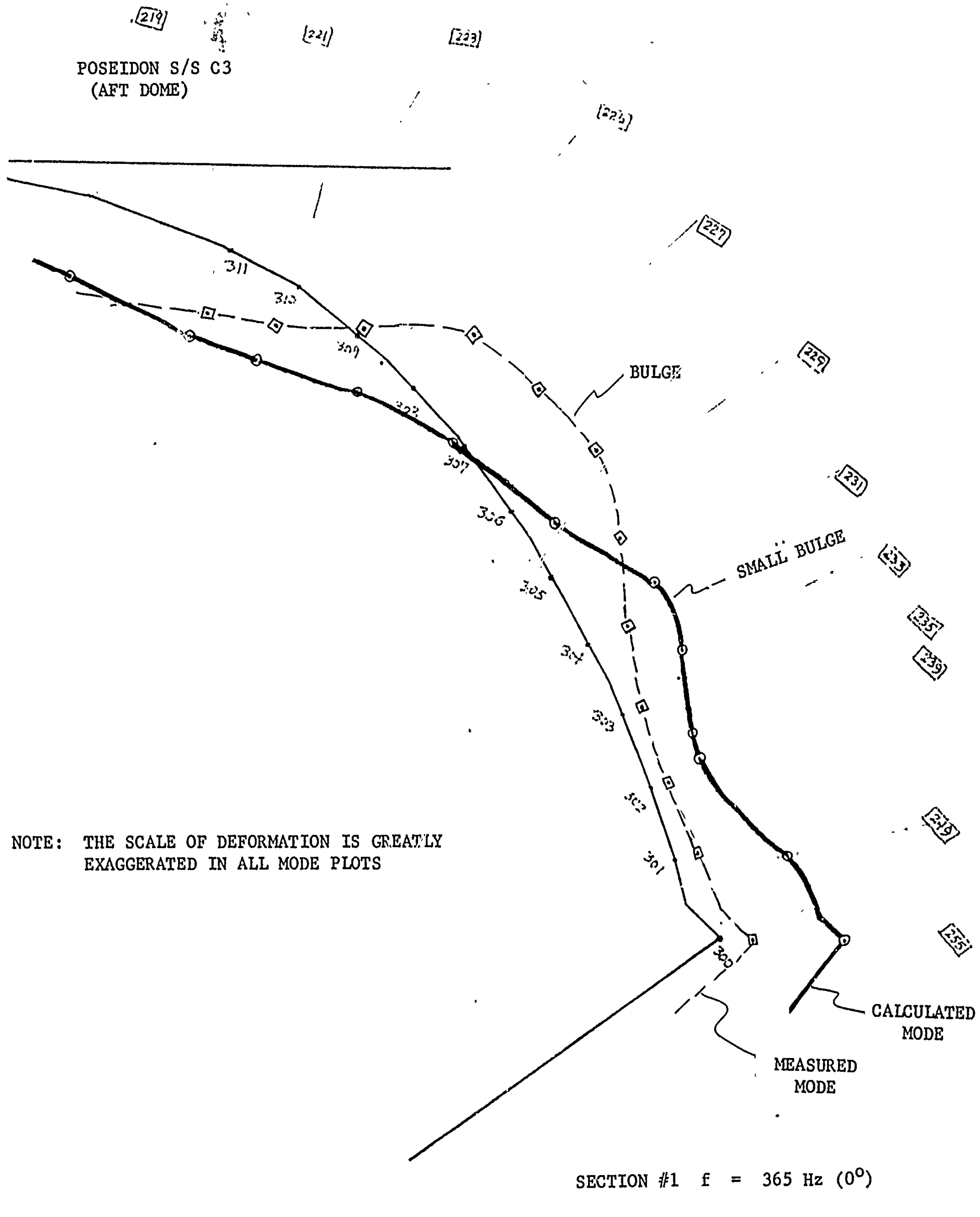

Figure 3. Mode Shape Comparisons for Section #1 at 365 Hz

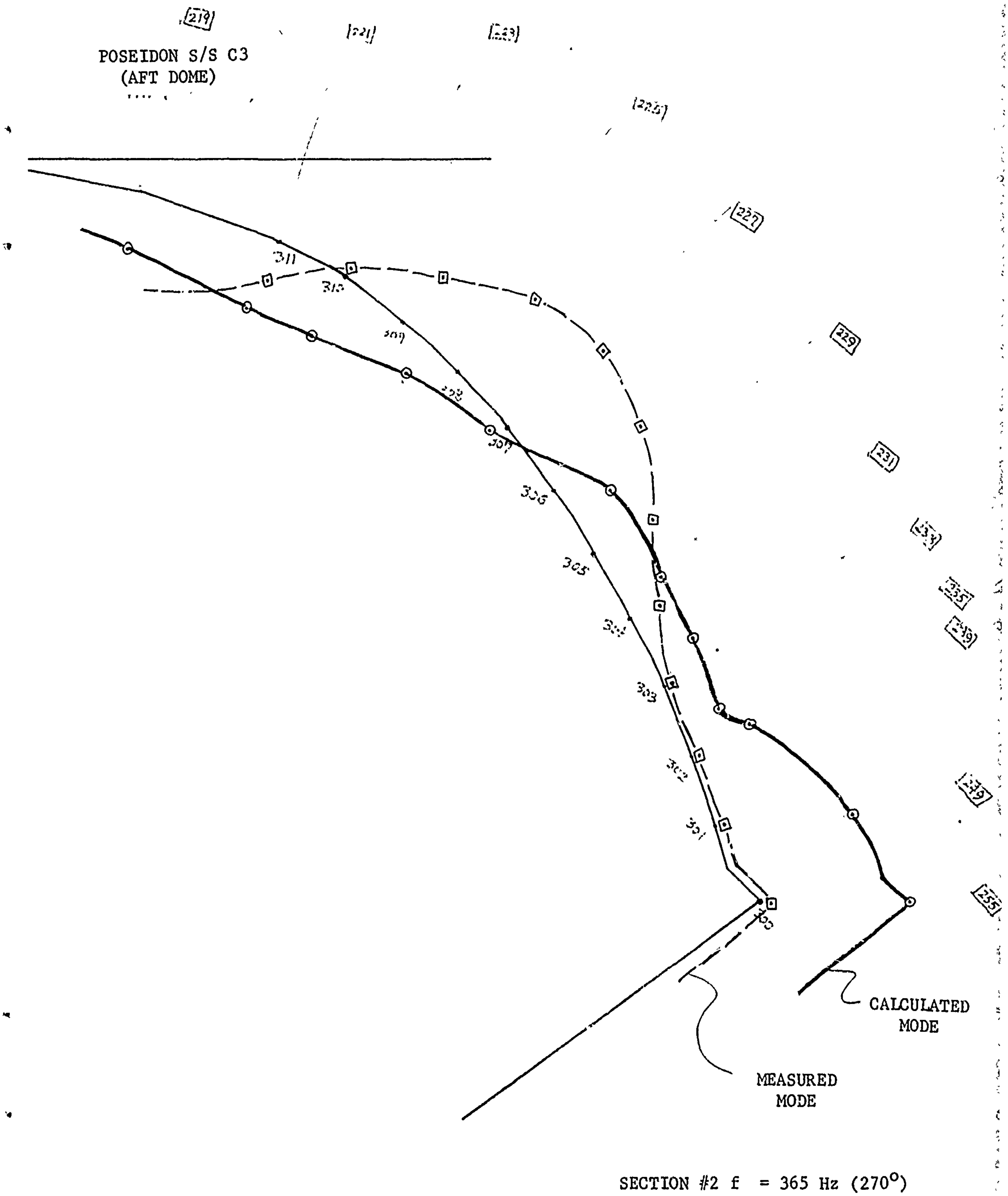

Figure 4. Mode Shape Comparisons for Section #2 at 365 Hz

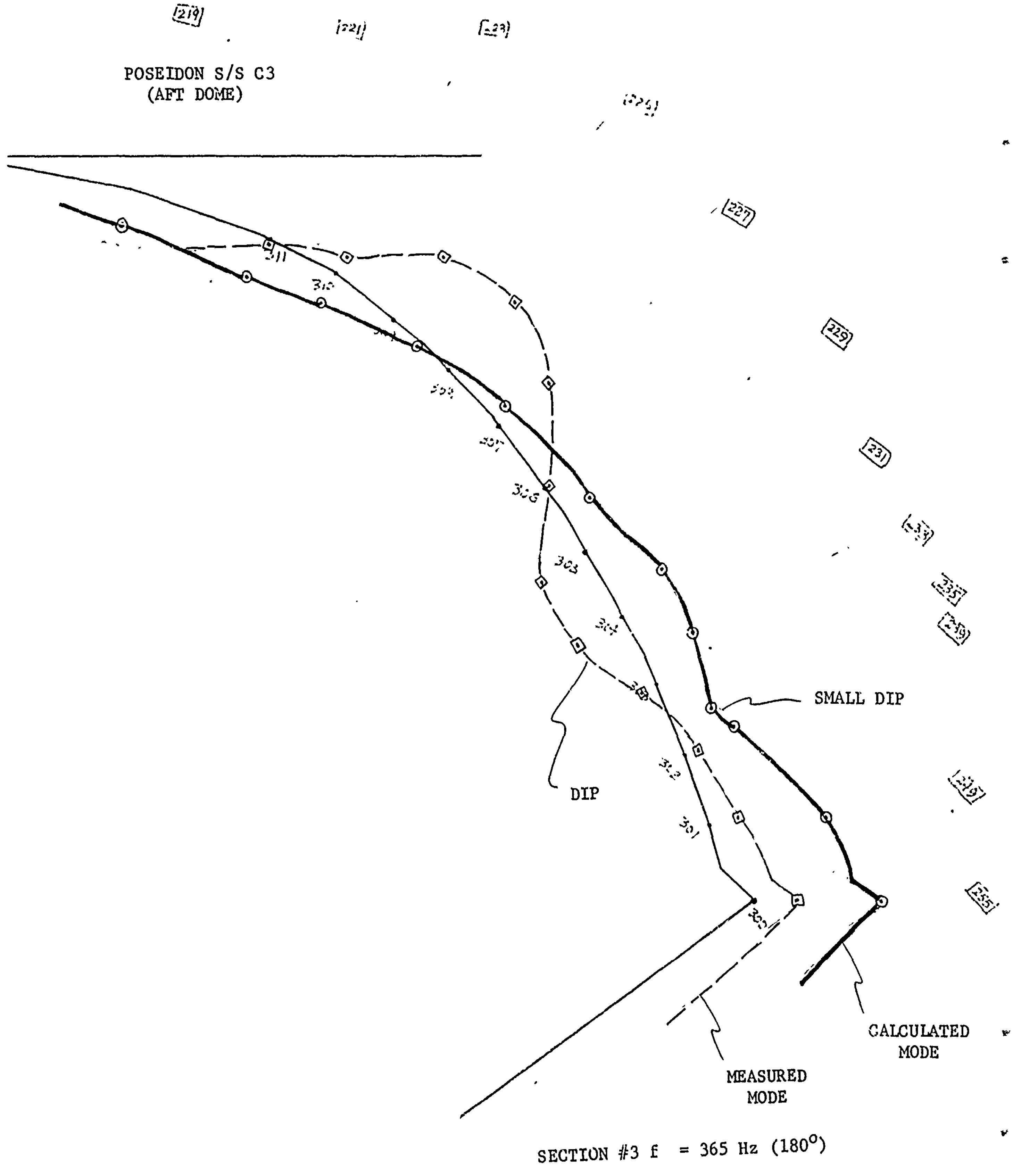

Figure 5. Mode Shape Comparisons for Section #3 at 365 Hz

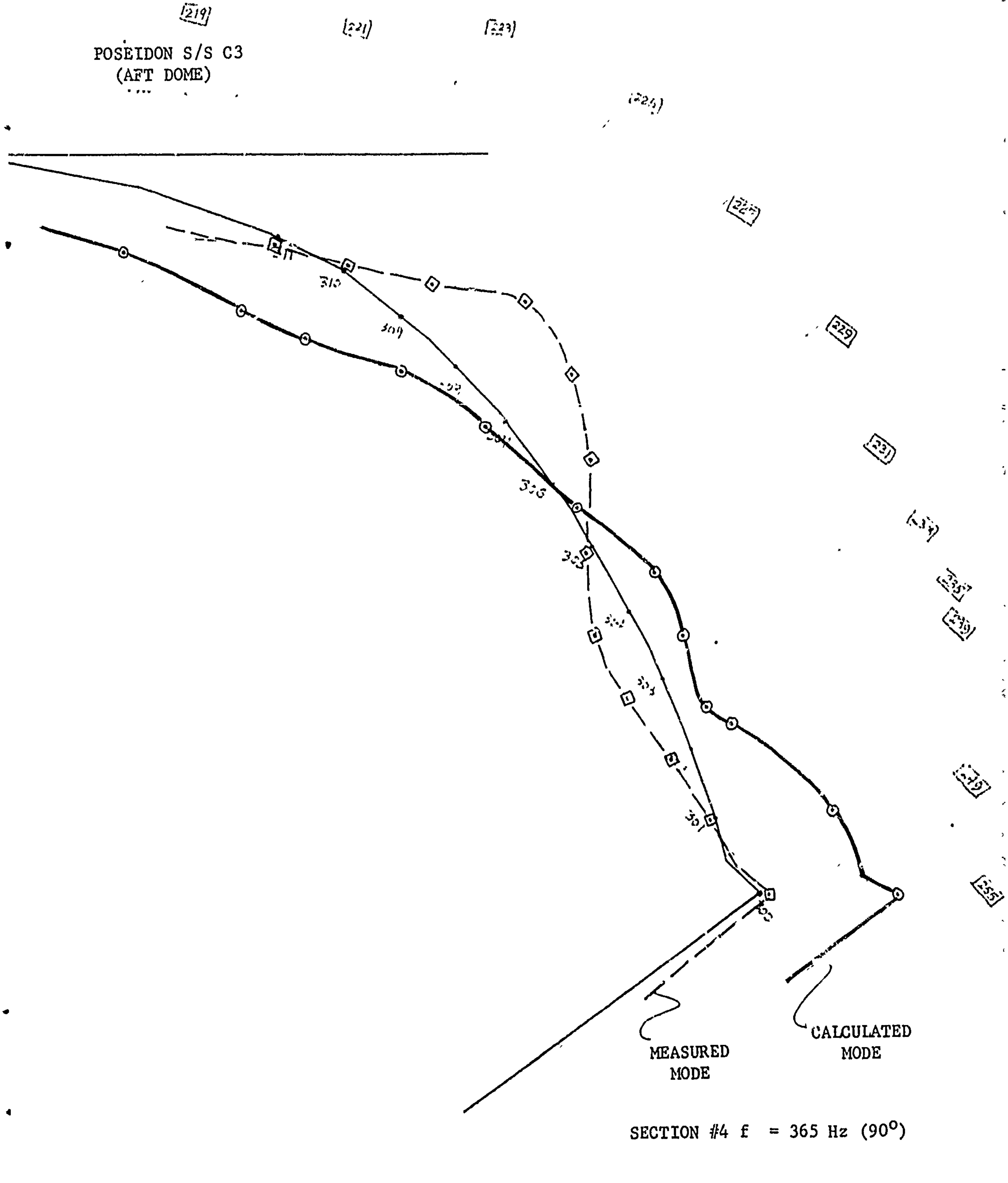

Figure 6. Mode Shape Comparisons for Section #4 at 365 Hz

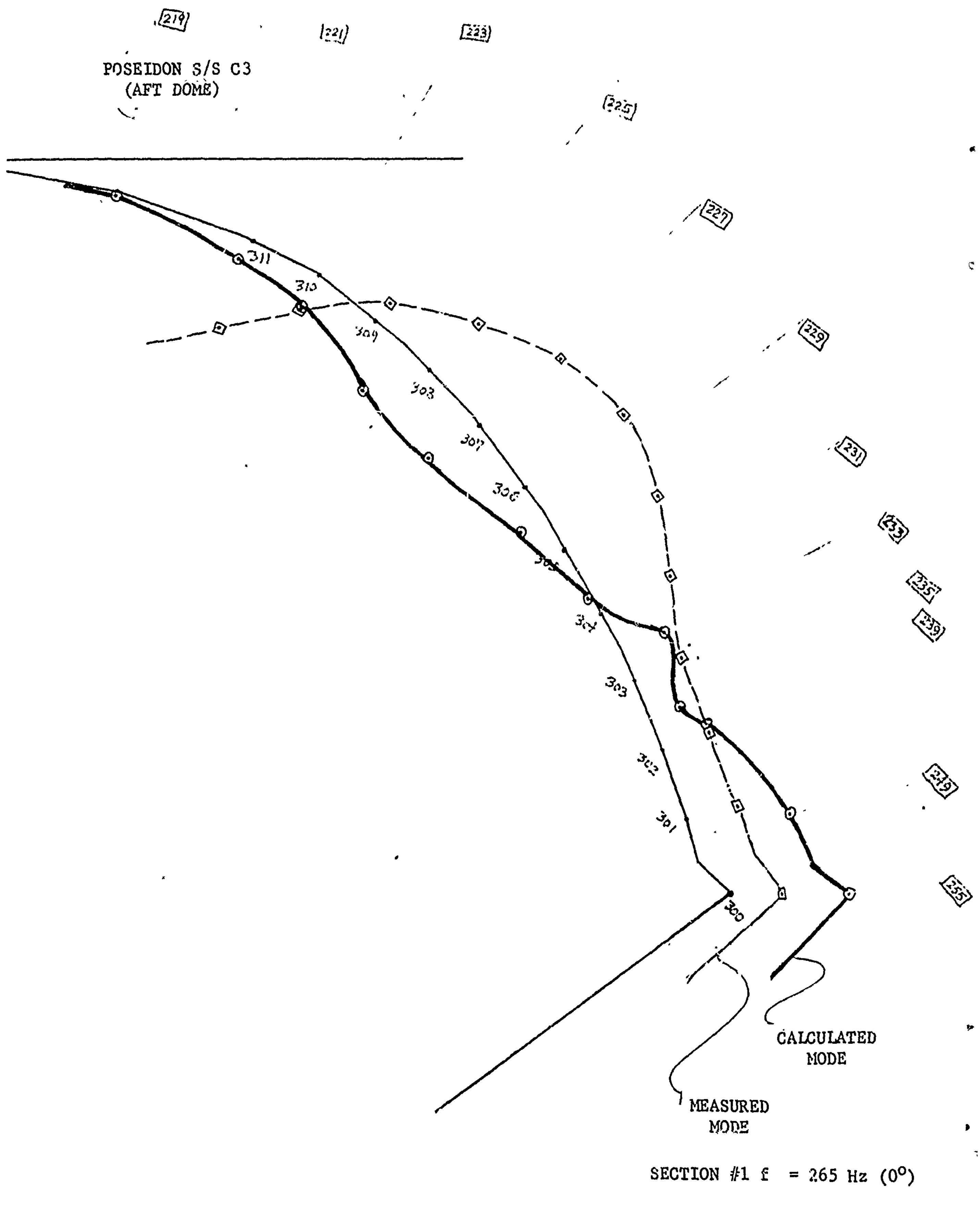

Figure 7. Mode Shape Comparisons for Section #1 at 265 Hz

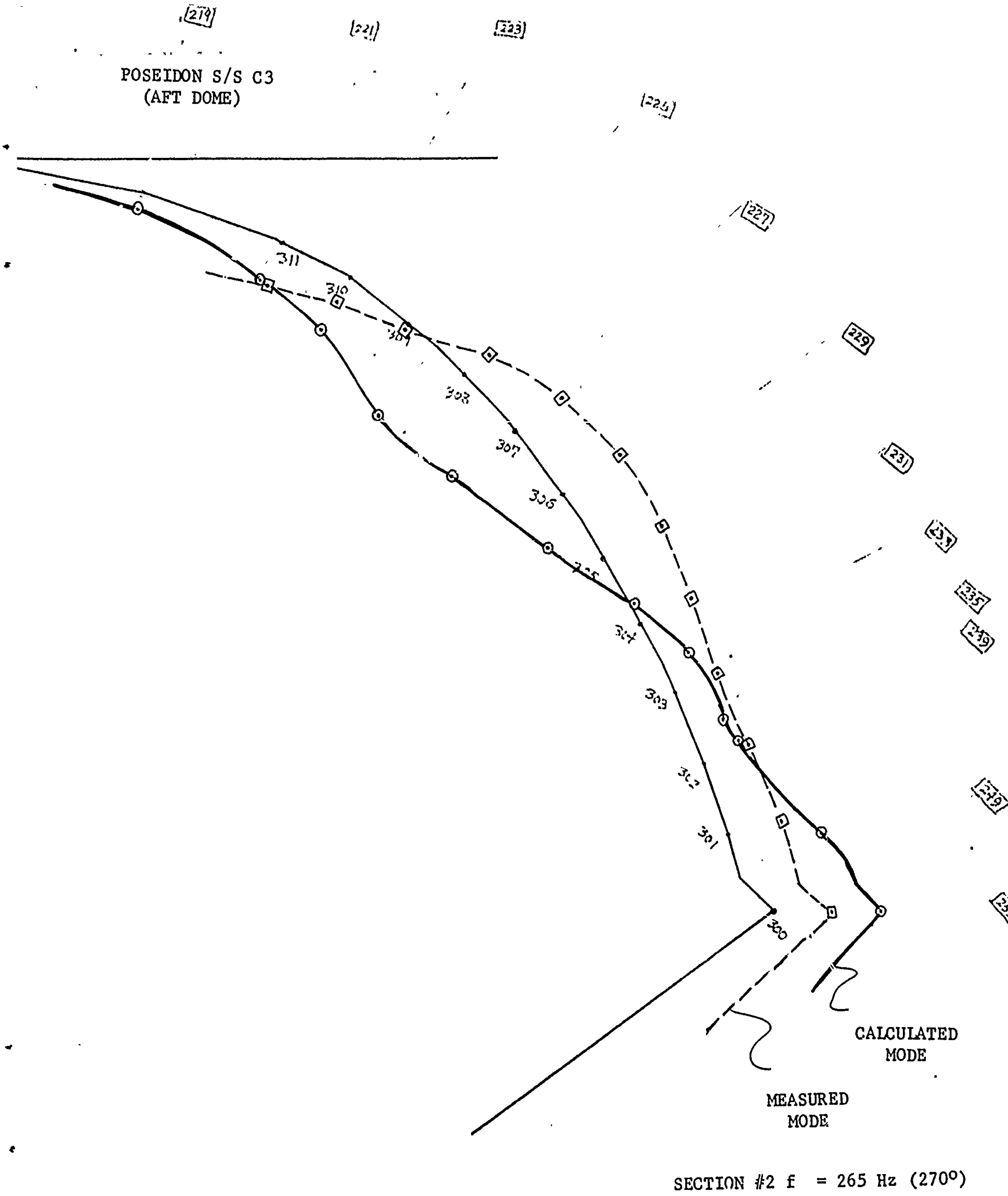

Figure 8. Mode Shape Comparisons for Section #2 at 265 Hz

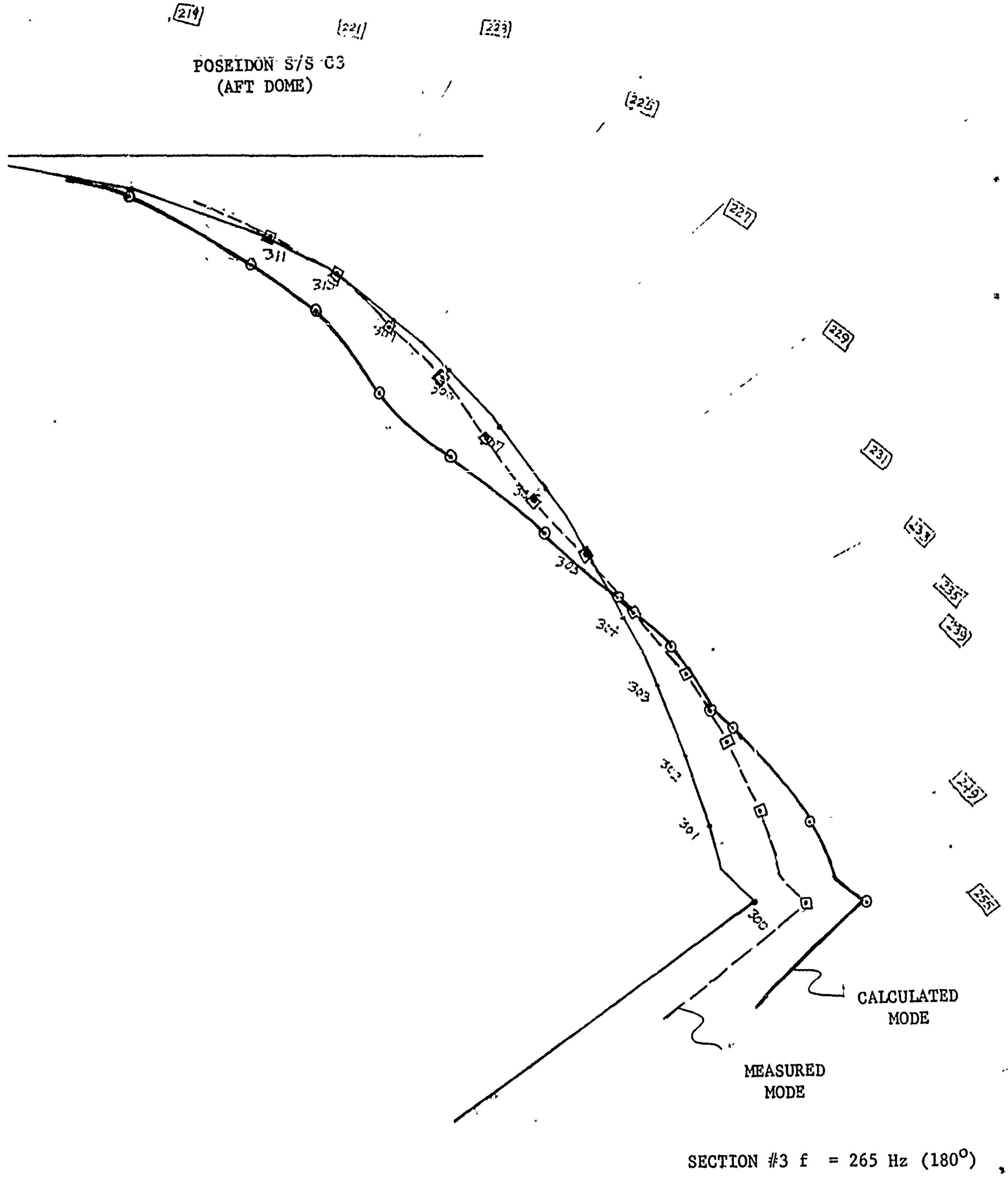

Figure 9. Mode Shape Comparisons for Section #3 at 265 Hz

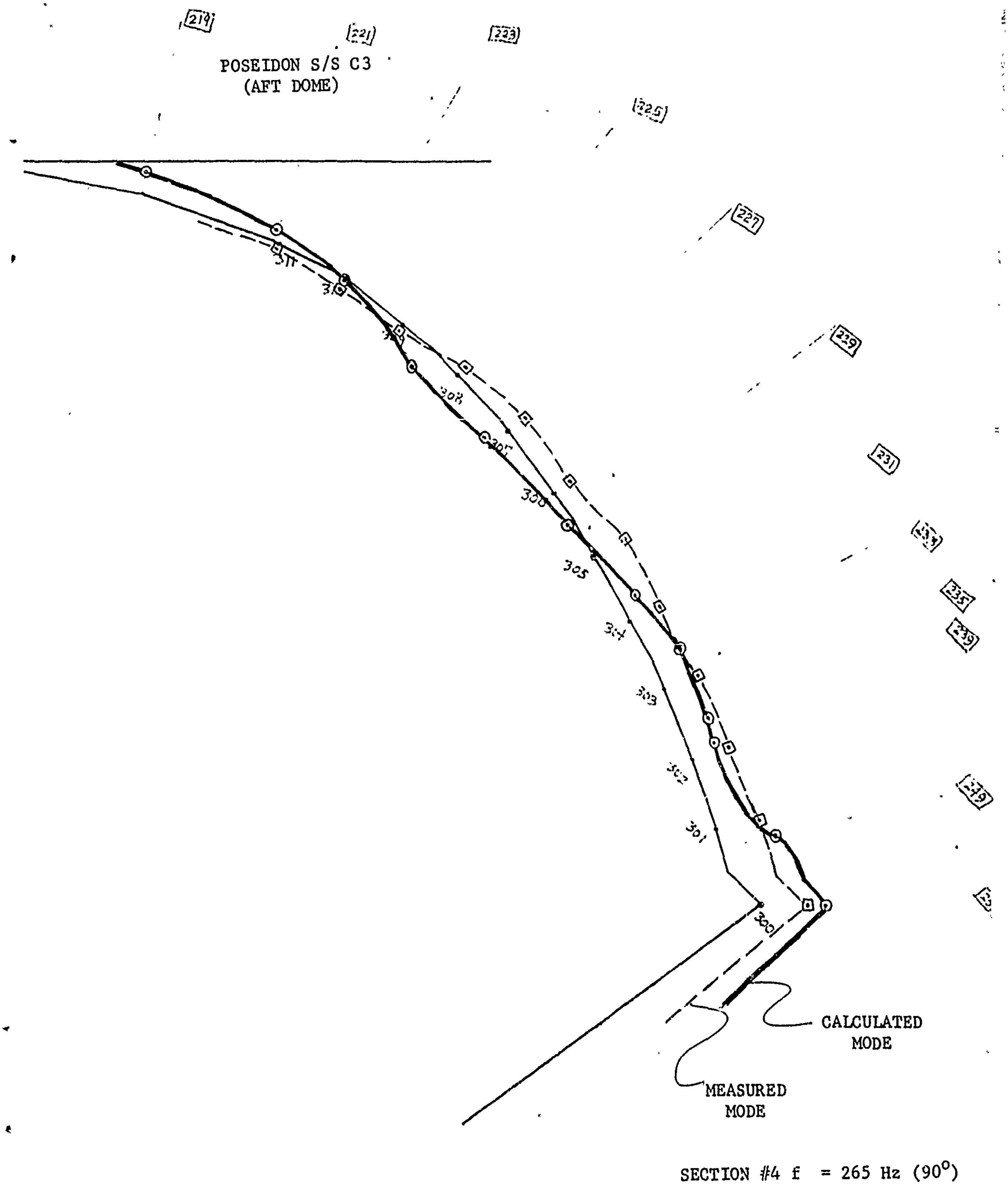

Figure 10. Mode Shape Comparisons for Section #4 at 265 Hz

EXTRACTED FROM THE 20 MAY 1974
R&D MONTHLY STATUS REPORT
FOR THE
COMPONENT VIBRATION PROGRAM

(Contract F04611-73-C-0025)

EXTRACTS FROM 20 MAY 1974 MONTHLY STATUS REPORT

Measured responses have been compared with calculated responses for the 365 Hz mode at all points where accelerometers were mounted on the Flight Electronics unit. For each accelerometer, the node in the finite element model nearest the accelerometer location was selected for comparison. In some cases, the location match-ups are only approximate, with as much as two or three inches separating locations of corresponding calculated and measured responses. The comparative data are given in Table I. The calculated data were normalized to obtain magnitude and phase agreement at point 300. The response at the component connection points is measured approximately by accelerometers 361, 362, 583, and 589. The points 361, 362, and 589 are located on the adapter ring, 583 is on the mounting bracket. See the Task IV report for location definitions.

The comparisons given in Table I show much better agreement at some points than at others. There does not appear to be a trend in the data; the calculated response is higher than the measured response only about 50 percent of the time. The agreement between calculated and measured response data shown in Table I is generally worse than that obtained for the attach points.

Calculated dome displacements are compared with dome measurements for the 365 Hz mode in Figure 1. The dome section shown in the figure was taken at the 0^{o} motor location. To obtain the mode shapes shown, the data were normalized to obtain agreement at the aft adapter. The accelerometer data from Task IV were plotted normal to the dome. The out-of-phase r and z displacement components obtained from the analysis were resolved into a direction normal to the dome to obtain the plot labeled: "Calculated mode shape".

The measured and calculated dome mode shapes shown in Figure 1 are similar in that each has a positive and a negative displacement region along the dome with only one zero crossover. However, the crossover does not occur at quite the same place for both modes. Even though the mode shapes are similar, the bulge in the measured mode indicates a definite difference. Some possibilities for the difference are:

(1) The model may be responding in a similar but basically different mode than was observed in the test. A small frequency shift might excite the similar mode.

(2) The model may be too stiff near the area of the bulge in the measured mode shape.

(3) The scalar springs used in the dome cavity of the model may not be providing the same dome excitation as the actual dome cavity pressure distribution that existed during the test.

TABLE I

COMPARISONS BETWEEN CALCULATED AND MEASURED
RESPONSE OF THE FLIGHT ELECTRONICS UNIT
AT 365 Hz

Measurement Point (Refer to Task IV Report)	Measured Response (Magnitude/Phase)	Calculated Response (Magnitude/Phase)
578	.185 / + 70	.0129 / + 117
580	.157 / - 171	.0925 / + 149
583	.438 / - 29	.7022 / 0
(361)	(.711 / + 13)	(.7022 / 0)
584	.776 / - 142	.4202 / - 1
585	.285 / - 108	1.1712 / + 168
586	.918 / - 65	.1630 / - 158
587	.355 / + 1	.7322 / + 169
588	1.730 / + 38	.9285 / + 159
581	.027 / - 97	.1987 / - 157
589	.461 / + 13	.7674 / + 7
(362)	(.493 / + 4)	(.7674 / + 7)

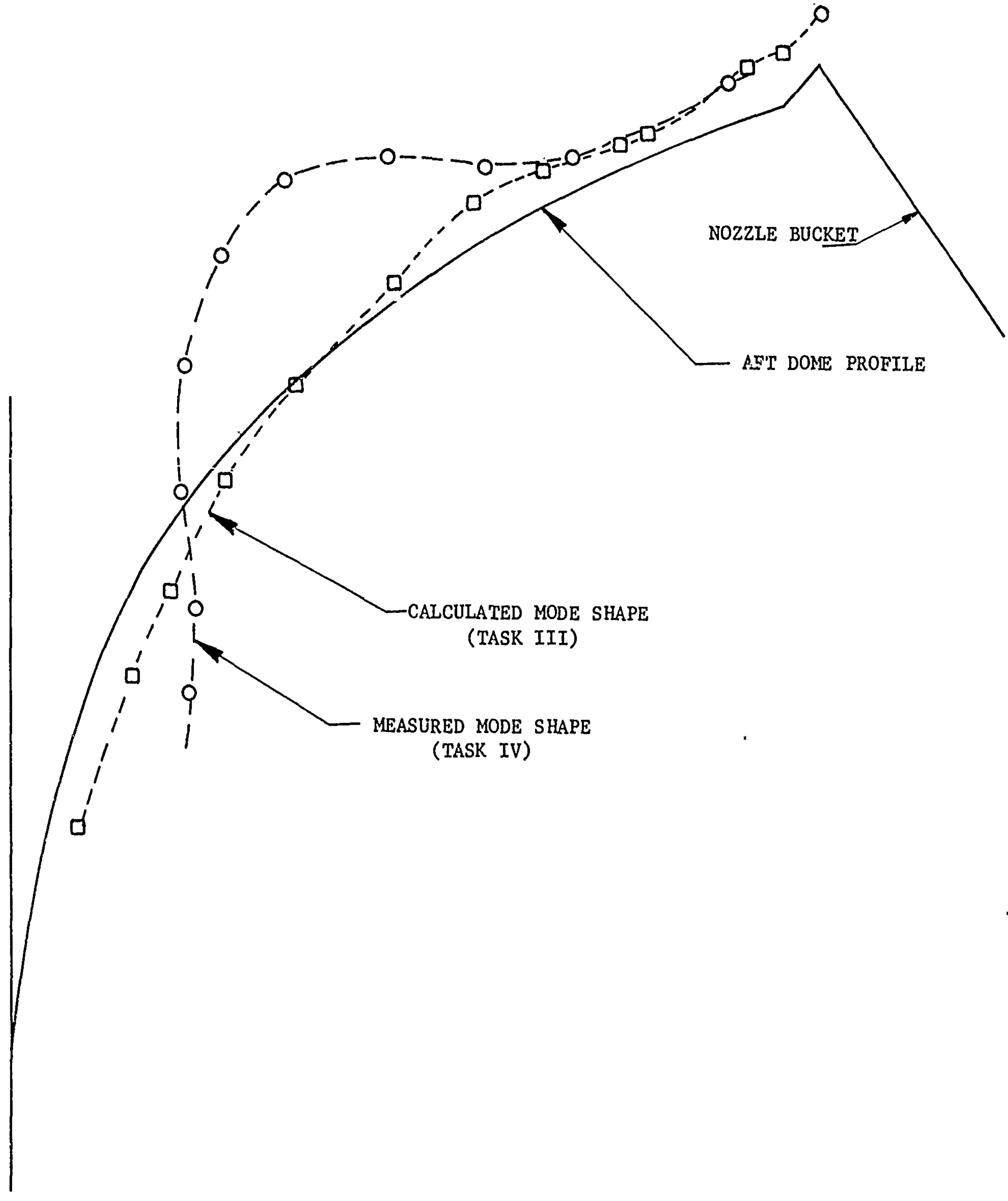

Figure 1 - Comparison of Calculated and Measured Aft Dome Mode Shapes at 365 Hz.

EXTRACTED FROM THE 20 AUGUST 1974
R&D MONTHLY STATUS REPORT
FOR THE
COMPONENT VIBRATION PROGRAM

(Contract F04611-73-C-0025)

EXTRACTS FROM 20 AUGUST 1974 MONTHLY STATUS REPORT

Mode shapes were plotted comparing measured and calculated responses for the forward dome. The comparative plots are shown in Figures 1 and 2. The agreement between calculated and measured modes for the forward dome is poor. Notice that the two calculated modes are similar (one for 365 Hz and one for 265 Hz), and the two measured mode shapes are similar. Reasons for the discrepancies between measured and calculated modes are unknown at the present time. Hopefully, future experimentation with the model will help uncover reasons for the poor agreement between calculated and measured modes of the forward dome.

Mode shapes of the Flight Electronics Unit were studied in an effort to estimate the quality of the high frequency response of this model. NASTRAN plots of the mode shapes for the first eight natural modes are shown in Figures 3 through 6. The first natural mode is basically up and down cantilever beam-type deformation (Figure 3). The second mode is a side-to-side swaying of the structure at 140.8 Hz. The third mode is a twisting mode where one side of the frame is up while the other side is down (Figure 4). The first three modes are, thus, general over-all structural modes involving bending, swaying, and twisting. The fourth mode, and higher modes, all involve local structural deformation (see Figures 4, 5, and 6). For example, the fourth mode consists of bending of the plate that is used to simulate the electronics package which bolts to the frame. In construction of the model, no attempt was made to model the bending stiffness of the bolted-on package. Therefore, the fourth mode, and each higher mode that involves significant local deformation, is likely to be very inaccurate. It, thus, appears that the upper frequency limit for which this particular model can provide an accurate model of the structure is 150 to 200 Hz; i.e., between the third and fourth modes. Considerable additional detail would be required in the component models to provide accuracy at higher frequencies.

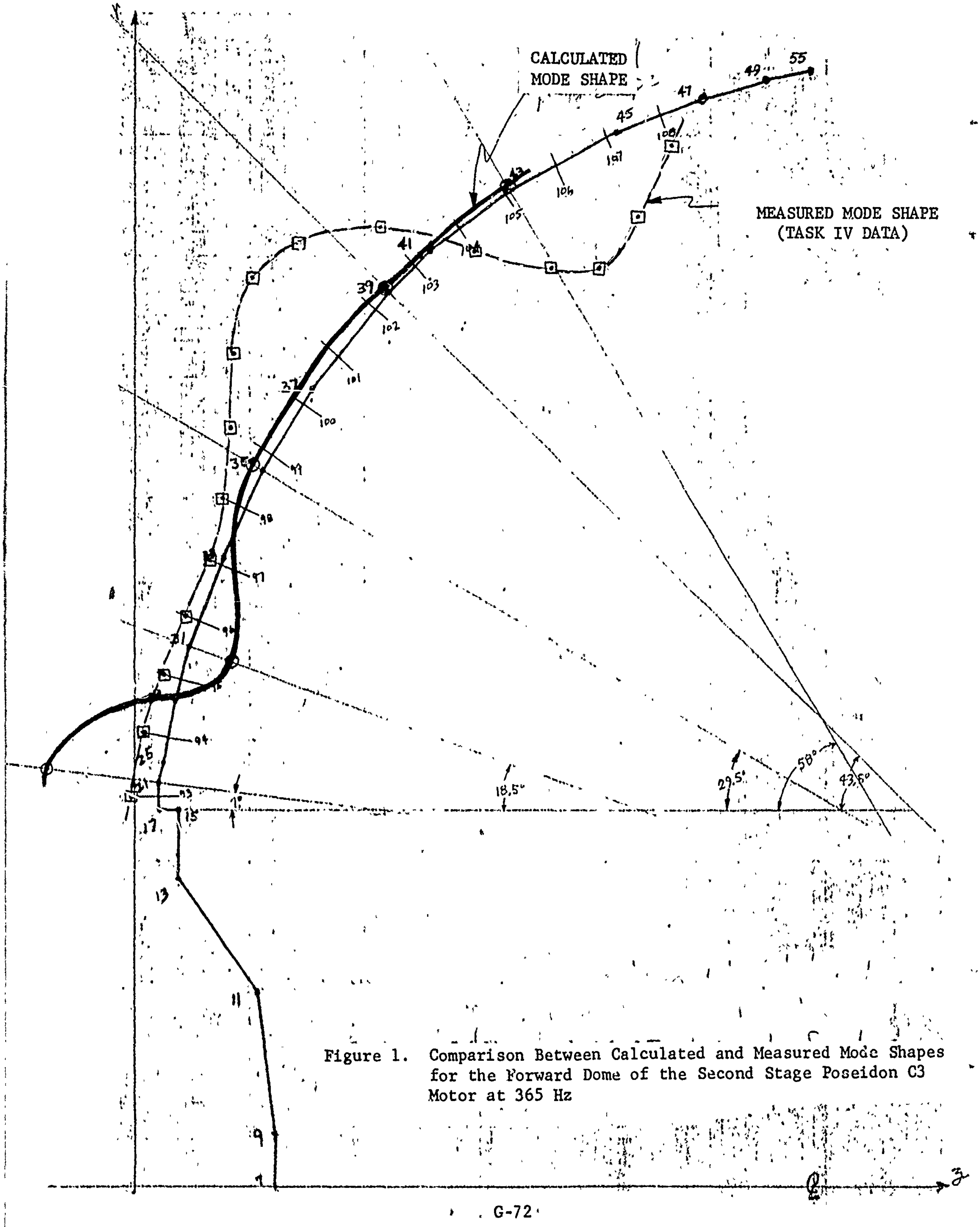

Figure 1. Comparison Between Calculated and Measured Mode Shapes for the Forward Dome of the Second Stage Poseidon C3 Motor at 365 Hz

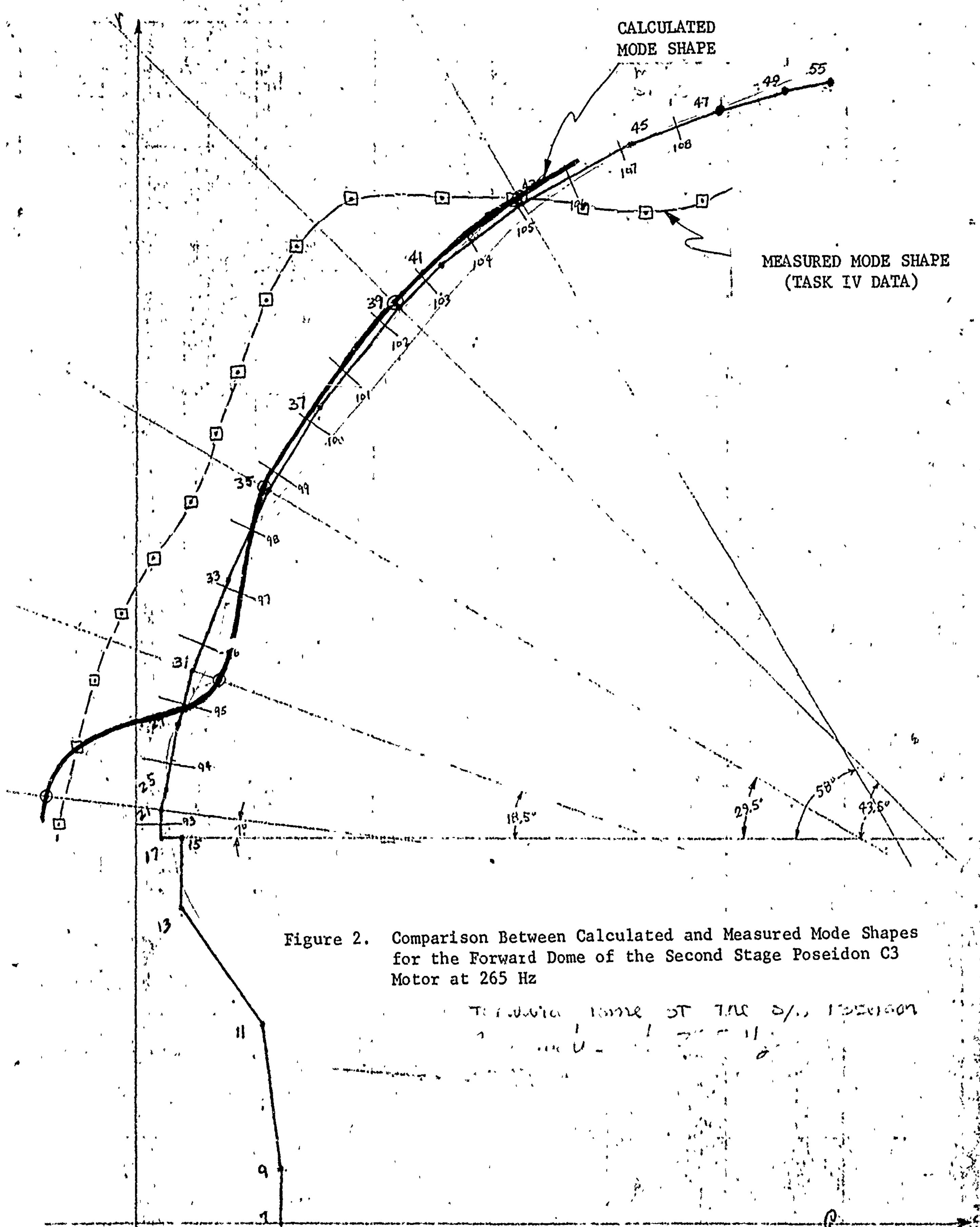

Figure 2. Comparison Between Calculated and Measured Mode Shapes for the Forward Dome of the Second Stage Poseidon C3 Motor at 265 Hz

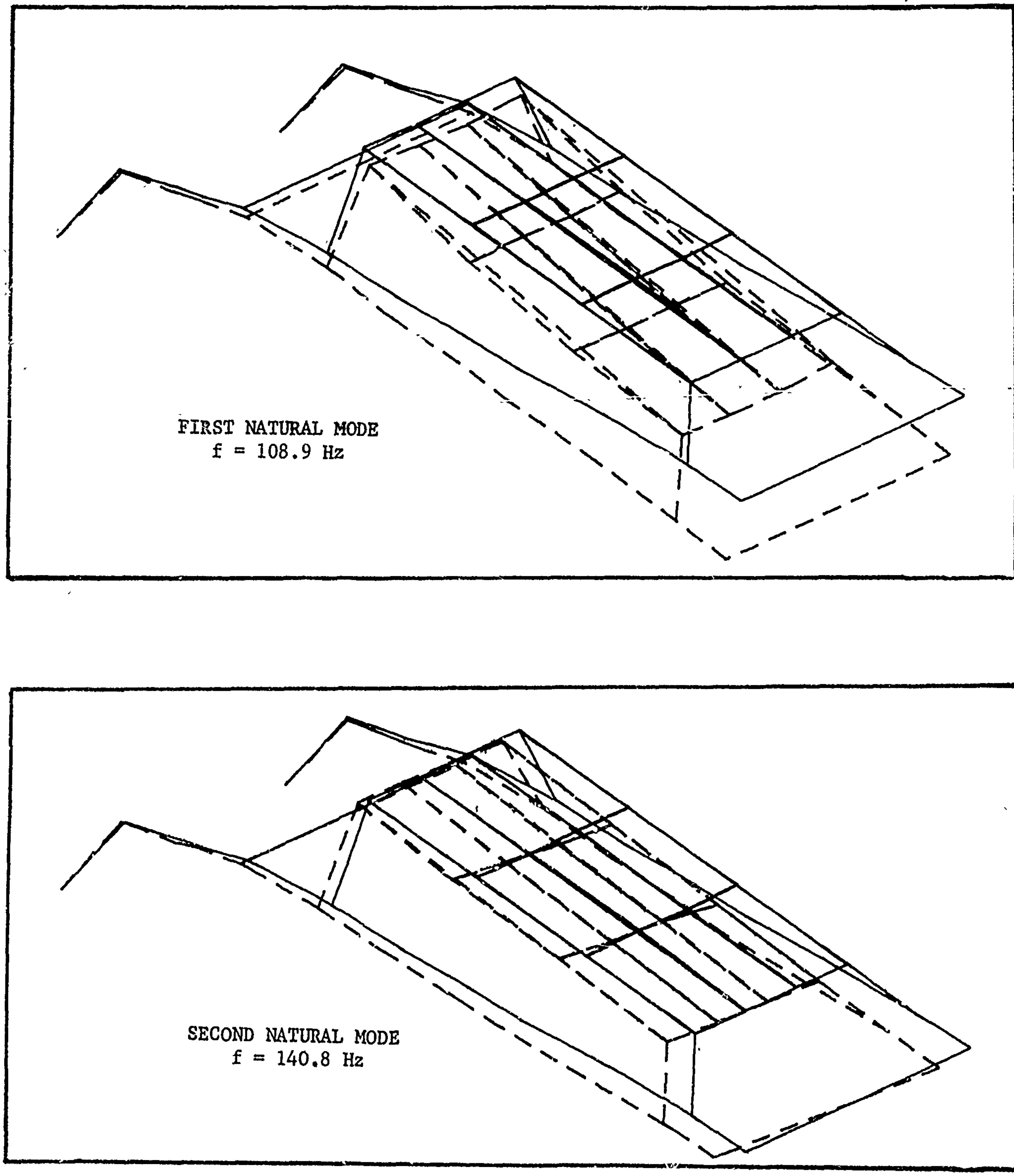

Figure 3. First and Second Natural Modes for the Flight Electronics Unit (Solid Lines show Undeformed Position)

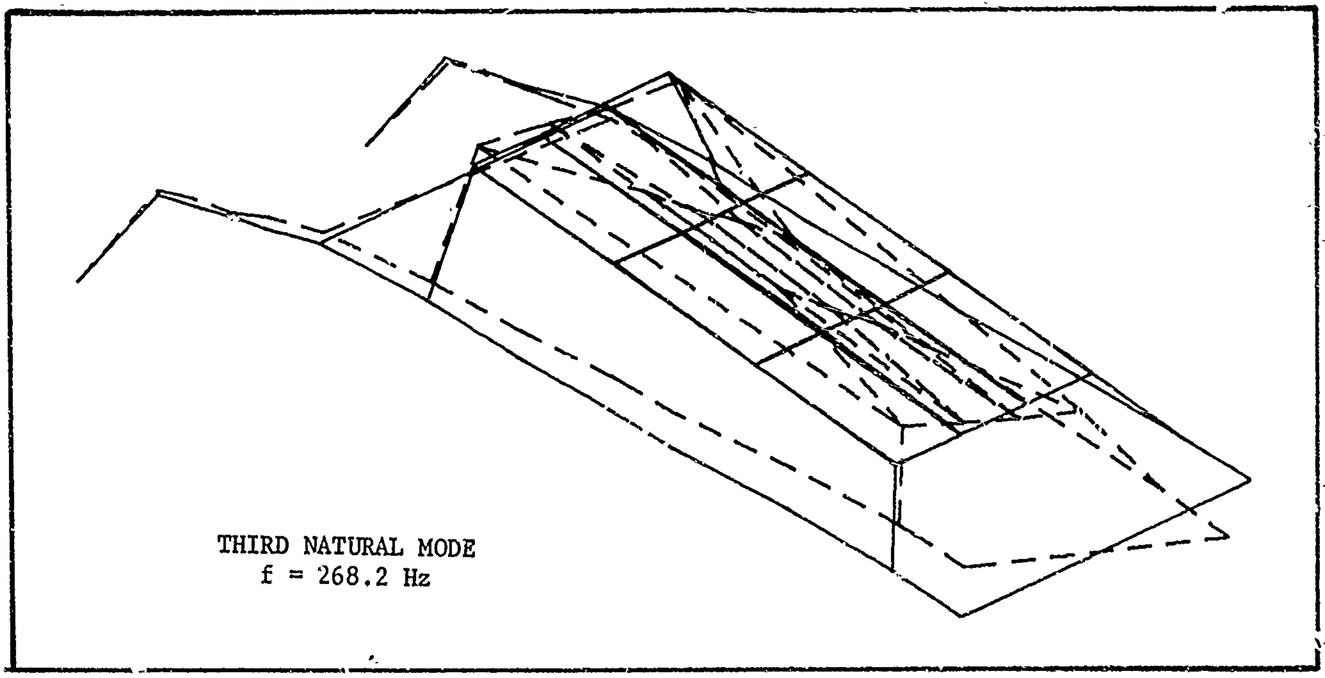

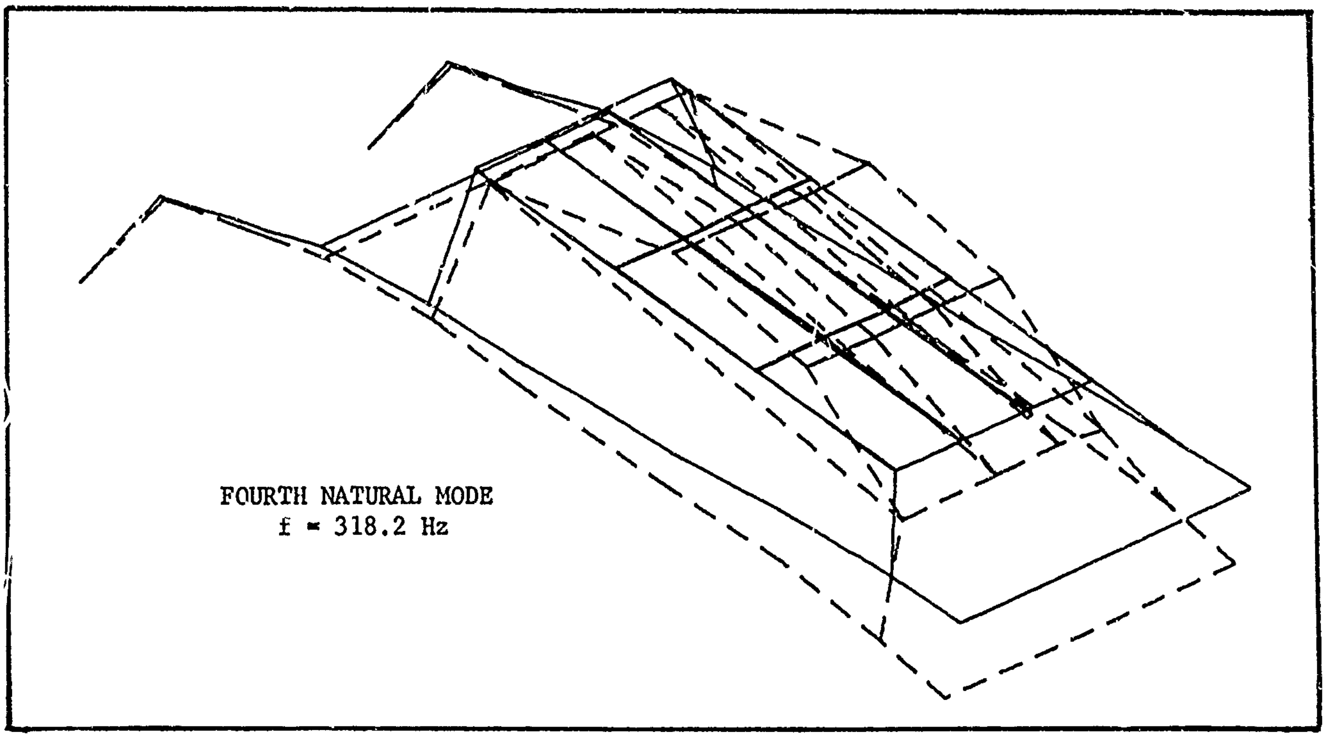

Figure 4. Third and Fourth Natural Modes for the Flight Electronics Unit (Solid Lines Show Undeformed Position)

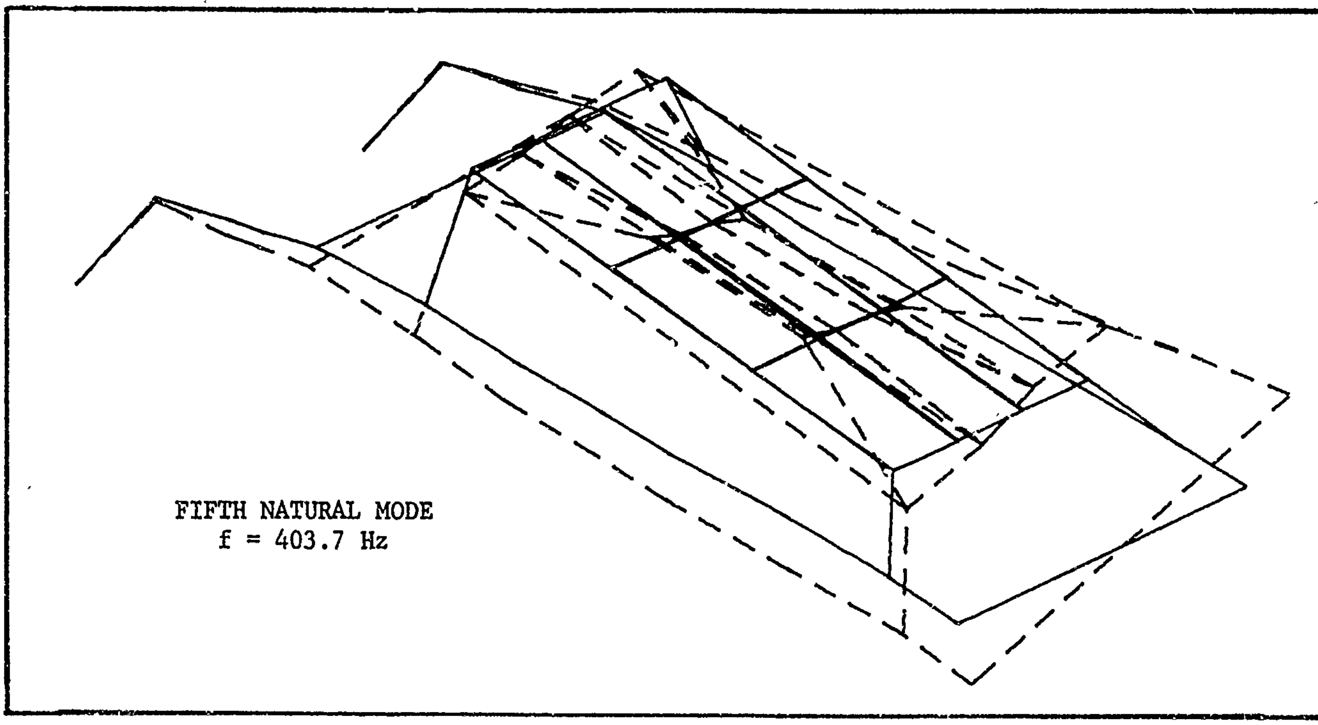

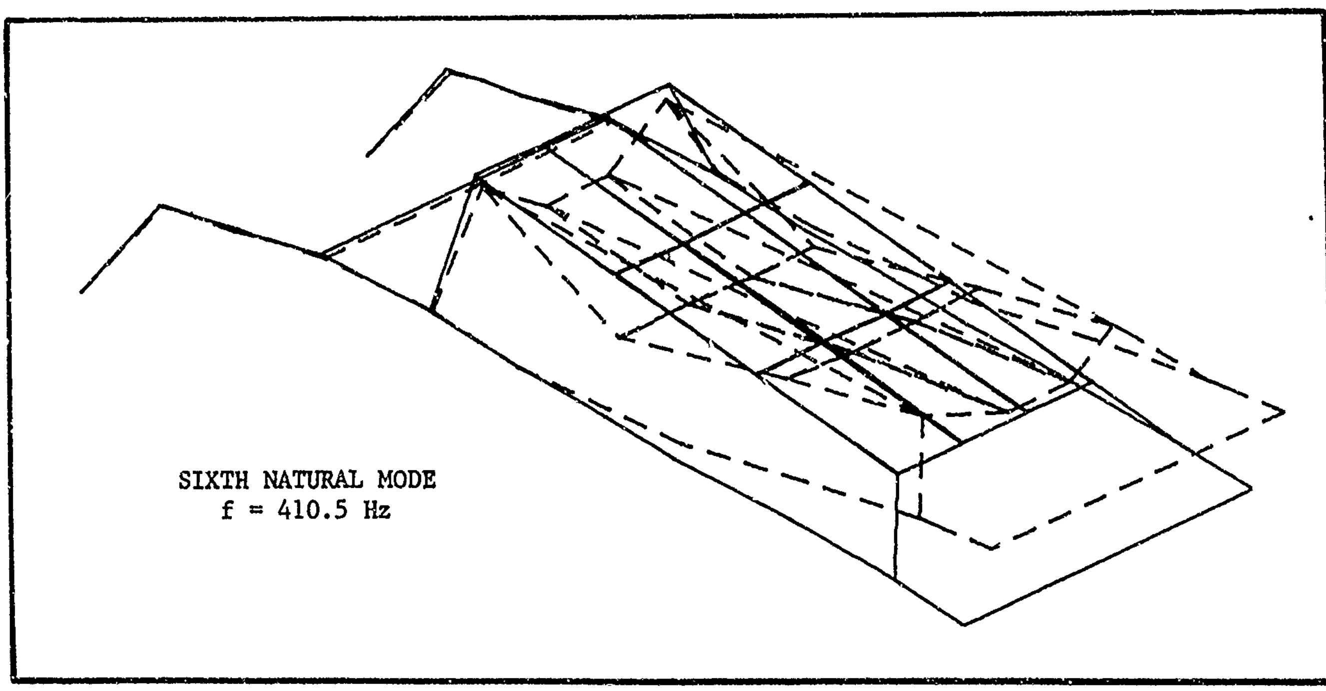

Figure 5. Fifth and Sixth Natural Modes for the Flight Electronics Unit (Solid Lines Show Undeformed Position)

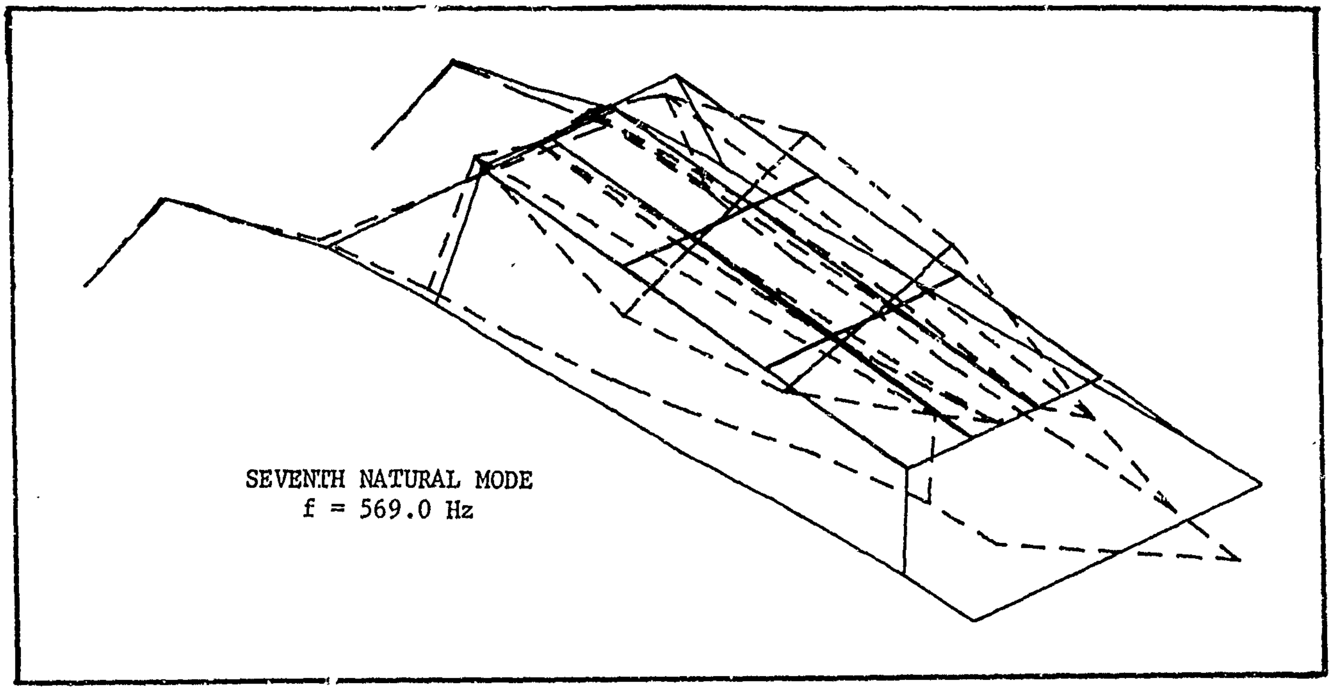

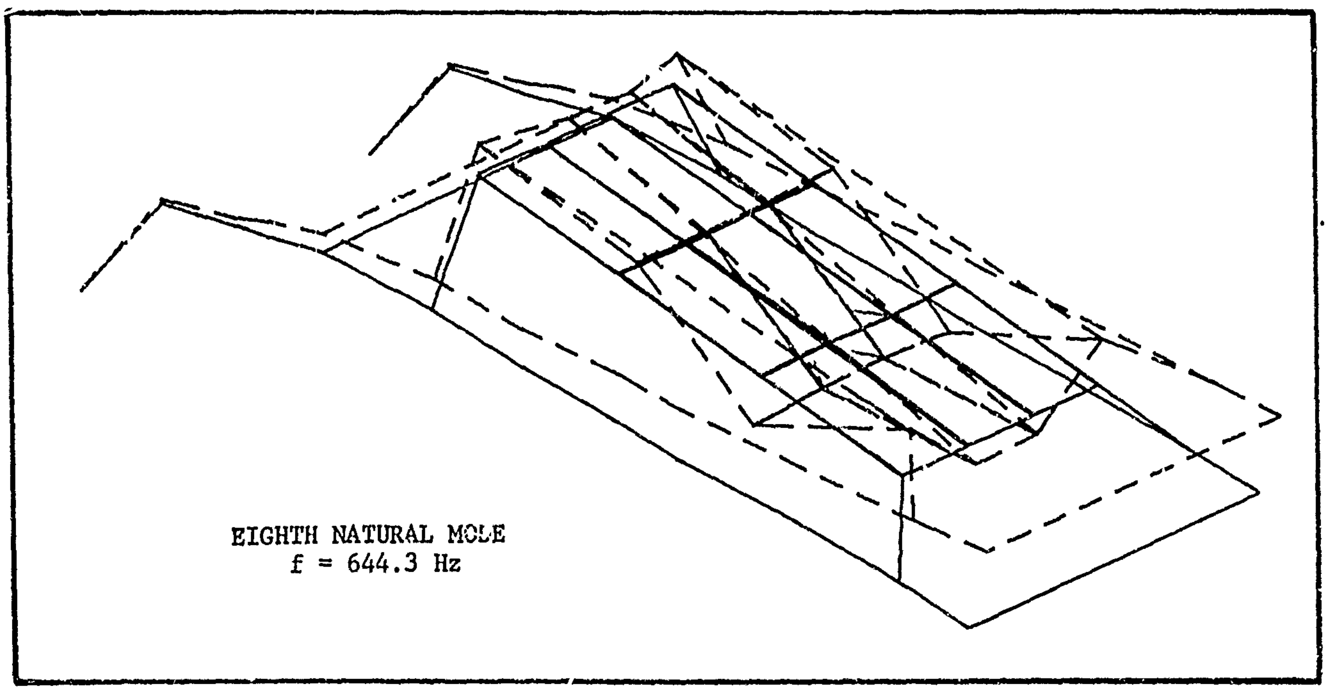

Figure 6. Seventh and Eighth Natural Modes for the Flight Electronics Unit (Solid Lines Show Undeformed Position)

EXTRACTED FROM THE 20 NOVEMBER 1974
R&D MONTHLY STATUS REPORT
FOR THE
COMPONENT VIBRATION PROGRAM

(Contract F04611-73-C-0025)

EXTRACTS FROM 20 NOVEMBER 1974 MONTHLY STATUS REPORT

The transfer numbers shown in Table I indicate that a $\pm$ 1.0 psi pressure oscillation can cause a response on the aft dome in the longitudinal direction (AC-261) between 0.65 g's and 23.38 g's. The 23 g maximum is not typical and a more representative number would be four to five g's.

For comparison with the static firing data, analysis results are given in Table II. The analysis results consist of response accelerations in the longitudinal direction at the component connection points. Data are shown only for the component connection points on the aft adapter ring in the longitudinal direction.

The most direct comparison possible with the data shown in Tables I and II would be between AC-261 from Table I and component connection point number 8 in Table II (AC-261 is mounted very near to point 8). Table II shows a response of 3.21 g's at 668 Hz. Table I has corresponding numbers of 1.71, 1.55, 2.03, and 1.83 g's for the 634 and 680 Hz frequencies and for filter bandwidths of 10 Hz and 100 Hz. (Notice that transfer numbers between 0 and 1 0 second have been ignored.) Apparently the zero-burn time calculated value is only about 50 percent too high. The advanced burn analysis at 634 Hz gives 1.53 g's for point 8.

TABLE I

SP-0149 TRANSFER NUMBERS

Frequency/ Bandwidth (Hz/Hz)	Approximate Time (Sec)	TN_1* (AC-261/PT-5)	TN_2* (AC-404/PT-5)	TN_3* (AC-405/PT-5)
281/10	0.25	0.90	0.35	0.39
281/100	0.60	5.94	5.74	2.88
	3.70	23.38	31.25	20.56
634/10	0.50	1.27	1.07	0.23
634/100	0.50	3.39	1.51	0.87
	7.90	1.71	9.27	3.27
680/10	0.50	4.72	--	--
	7.90	1.55	7.52	3.06
680/100	0.50	4.48	1.41	0.52
	2.60	2.03	5.17	4.50
	7.90	1.83	9.23	3.17
770/10	0.60	1.95	1.10	0.43
	3.60	--	40.00	27.00
770/100	0.50	1.28	0.52	0.33
	2.60	2.00	5.03	4.62
1327/10	0.40	3.80	9.87	5.93
	4.55	1.60	2.87	1.33
1327/100	0.40	2.19	9.54	4.90
	5.30	0.65	7.28	3.88

*The units are (g's/psi) for the transfer numbers

TABLE II

CALCULATED RESPONSE AT THE AFT ADAPTER COMPONENT ATTACH POINTS FOR THE SECOND STAGE POSEIDON MOTOR

Component Connection Point Identification	Motor Circumferential Location (Degree)	Response to 668 Hz Mode (g's)	Response to 770 Hz Mode (g's)	Response to 1327 Hz Mode (g's)
1	0	4.53	1.74	0.92
3	225	1.23	1.10	0.54
4	180	5.10	1.39	1.64
5	120	4.08	1.13	1.65
6	90	4.05	0.53	1.92
8	60	3.21	0.85	0.41
9	30	2.71	0.64	0.89

EXTRACTED FROM THE 30 MARCH 1974
R&D MONTHLY STATUS REPORT
FOR THE
COMPONENT VIBRATION PROGRAM

(Contract F04611-73-C-0025)

EXTRACTS FROM 20 MARCH 1974 MONTHLY STATUS REPORT

The available accelerometer data can be compared with analysis results. The comparison is shown in Table I.

TABLE I

COMPARISONS BETWEEN CALCULATED AND MEASURED MOTOR RESPONSE

Measurement Point (Refer to Task IV Report)	Measured Response (Magnitude/Phase)	Calculated Response (Magnitude/Phase)
300	0.6395/ + 1	0.6395/ + 1
659	0.0735/ - 134	0.3985/ + 170
515	0.548 / - 24	0.734 / + 4
336	0.743 / + 3	0.694 / + 1
324	0.149 / + 63	0.748 / + 13
662	0.227 / + 160	0.357 / + 165
362	0.493 / + 4	0.767 / + 7
361	0.711 / + 13	0.702 / + 0

It was necessary to normalize the calculated response data to obtain the comparisons shown. Point 300 was arbitrarily selected as a reference point and both magnitude and phase were normalized to agree with test data at that point, making comparisons of relative phase and magnitudes possible. The agreement between measured and calculated response data shown in Table I is somewhat encouraging, considering the amount of computation that was required to obtain the calculated response. The magnitude and phase are in very poor agreement at points 659 and 324. However, agreement appears to be reasonable at other points, and the calculated results are conservative where the larger differences occur.

Normally, a motor analysis would be considered to be complete at this point since the desired input motion to the components has been calculated. However, present plans for this analysis include additional data recovery so that additional comparisons can be made with test data.

EXTRACTED FROM THE 20 APRIL 1974
R&D MONTHLY STATUS REPORT
FOR THE
COMPONENT VIBRATION PROGRAM

(Contract F04611-73-C-0025)

EXTRACTED FROM THE 20 APRIL 1974 MONTHLY STATUS REPORT

The effect of the components, collectively, on the response at the connection points can be seen by comparing the response at the points for the clean motor model, V_O, with the total components-attached response V_T. The comparison is given in Table II. Only the first 20 points of 42 are shown.

TABLE II

COMPARISON BETWEEN CALCULATED RESPONSE AT
THE CONNECTION POINTS WITH AND WITHOUT COMPONENTS ATTACHED
(10^{-6} Multiplier Omitted from Given Values)

	Components Not Attached V_O	Components Attached V_T
1.	0.0 + 0.0i	1.3225 + 1.5296 i
2.	3.4384 + .09298i	2.7481 - 2.3885 i
3.	-46.344 - 7.1156 i	-44.331 - 3.5167 i
4.	19.079 - 3.8172 i	-83.366 - 3.3677 i
5.	0.0 + 0.0 i	2.8381 + 0.8148 i
6.	170.51 + 16.414 i	27.547 - 3.0133 i
7.	0.0 + 0.0 i	- 2.4769 - 5.0205 i
8.	3.4452 + .09512i	- 0.1633 - 2.0433 i
9.	-46.336 - 7.1107 i	-50.549 - 7.0926 i
10.	0.0 + 0.0 i	0.10709 + 0.20723i
11.	- 5.0783 + 0.8280 i	- 6.7356 - 0.4462 i
12.	0.0 + 0.0 i	0.3759 + 0.6260 i
13.	0.0 + 0.0 i	2.883 + 0.56498i
14.	3.4384 + .09298i	4.1318 - 3.0646 i
15.	-46.344 - 7.1156 i	-48.078 - 4.0287 i
16.	0.0 + 0.0 i	0.1488 - 0.03966i
17.	- 5.0711 + 0.8308 i	- 7.3551 - 0.3976 i
18.	0.0 + 0.0 i	- 0.01026 - 0.01982i
19.	0.0 + 0.0 i	7.2448 + 6.4114 i
20.	3.4384 + .09298i	7.6046 + 4.7589 i

The V_o column in Table II indicates the response of the cyclic symmetric clean motor model to the axisymmetric fourth longitudinal acoustic mode. Because of the symmetry, some response motions are uncoupled from the loading system; thus, several null rows appear in V_o. When the components are attached, the structural symmetry no longer exists and the motion becomes coupled as indicated in the V_T column in Table II.

The data shown in Table II indicate that the components have a very marked effect on the response at the connection points for this particular motor at a frequency of 365 Hz. This analysis thus provides an example where the proposed low-order simplified model described above would be inadequate. Based on the data shown in Table II, the component-only simplified model concept is thus rejected and will not be further evaluated.

EXTRACTED FROM THE 20 SEPTEMBER 1974
R&D MONTHLY STATUS REPORT
FOR THE
COMPONENT VIBRATION PROGRAM
(Contract F04611-73-C-0025)

EXTRACTS FROM 20 SEPTEMBER 1974 MONTHLY STATUS REPORT

Both the zero burn and the advanced burn clean motor models have been analyzed at 365 Hz using the fourth longitudinal acoustic mode to define the pressure loading distribution. In each case the acoustic mode was normalized so that the maximum pressure applied was 1.0 psi. Therefore, a comparison of the results from the two models shows the effect of removing a portion of the grain to obtain the advanced burn geometry. This comparison is made to study the possibility that the component response is not very sensitive to exact grain geometry. The U_0 displacement vectors for both computer runs were converted to accelerations which are shown in Table I. The 42 coordinates represent the nine component connection points on the aft dome adapter ring and nozzle compliance ring. For example, coordinates 1, 2, and 3 represent the θ, r, and z coordinates respectively at an attach point for the 0^o actuator on the adapter ring. The accelerations shown for comparison in Table I apply to the clean motor model with no components attached. Apparently changing the burn configuration of the clean motor model from zero seconds to 4.0 seconds burn time does not cause drastic changes in the response but the changes are significant. The maximum acceleration of 2.33 g's for the zero burn time model becomes 1.67 g's for the advanced burn model, a reduction of 28 percent due to the burn time change.

For further use of the information in Table I, the response at other pressure oscillation levels can be obtained by using the appropriate ratio on the given accelerations. For example, a maximum acceleration of 2.33 g's occurs in response to the fourth longitudinal mode at a pressure oscillation level of $\pm$ 1 psi. For a $\pm$ 2 psi pressure oscillation, the maximum response would be 4.66 g's.

Another possibility that seemed to be worthy of further investigation is that the component response may not be very sensitive to the exact form of the pressure distribution used in the solution. In Table II, accelerations for the first longitudinal mode and the third longitudinal are compared In addition to the differences due to using a different acoustic mode, the data shown in Table II contain differences due to different burn times (0.0 second versus 4.0 seconds and due to slightly different frequencies, (265 Hz versus 281 Hz). In spite of these differences, the response data are not drastically different for the two different solutions shown. The maximum response of 8.25 g's for the third mode response compares to the maximum response of 6.24 g's for the first mode response, a reduction of 24 percent.

Comparing the maximum response of 8.25 g's for the 265 Hz analysis with the maximum of 2.33 g's given in Table I for a 365 Hz analysis, it appears that the response is more sensitive to large changes in frequency than to changes in burn time or acoustic mode shape. However, sufficient data are not available to justify any firm conclusions.

TABLE I

COMPARISON OF ACCELERATIONS FOR THE
ZERO BURN MODEL AND THE ADVANCED BURN MODEL

Coordinate No.	U_{zero} For 365 Hz Zero Burn Model		U_{zero} For 365 Hz Adv. Burn Model	
	Phase (deg.)	Accel. (g's)	Accel. (g's)	Phase (deg.)
1	0.0	0.0	-*	--
2	1.55	.0468	.0241	4.42
3	-171.3	.6382	.5571	-172.4
4	-11.3	.2648	.1872	-10.41
5	0.0	0.0	--	--
6	5.50	2.33	1.67	5.72
7	0.0	0.0	--	--
8	1.58	.0469	.0245	4.48
9	-171.3	.6381	.5570	-172.5
10	0.0	0.0	--	--
11	170.7	.0700	.0537	171.0
12	0.0	0.0	--	--
13	0.0	0.0	--	--
14	1.55	.0468	.0241	4.42
15	-171.3	.6382	.5571	-172.4
16	0.0	0.0	--	--
17	170.7	.0699	.0536	171.0
18	0.0	0.0	--	--
19	0.0	0.0	--	--
20	1.55	.0468	.0241	4.42
21	-171.3	.6382	.5571	-172.4
22	0.0	0.0	--	--
23	170.7	.0699	.0536	171.0
24	0.0	--	--	
25	0.0	0.0	--	--
26	1.55	.0468	.0241	4.42
27	-171.3	.6382	.5571	-172.4
28	-11.3	.2648	.1872	-10.41
29	0.0	0.0	--	--
30	5.50	2.33	1.67	5.72
31	0.0	0.0	--	--
32	1.55	.0468	.0241	4.42
33	-171.3	.6382	.5571	-172.4
34	0.0	0.0	--	--
35	170.7	.0699	.0536	171.0
36	0.0	0.0	--	--
37	0.0	0.0	--	--
38	1.55	.0468	.0241	4.42
39	-171.3	.6382	.5571	-172.4
40	0.0	0.0	--	--
41	170.7	.0699	.0536	171.0
42	0.0	0.0	--	--

*The dashes (-) indicate that corresponding numbers are small enough to be ignored, i.e. 10^{-20} compared with 10^{-5}.

TABLE II

COMPARISON OF ACCELERATIONS FOR TWO ANALYSES AT
SIMILAR FREQUENCIES BUT WITH DIFFERENT ACOUSTIC MODES AND DIFFERNT BURN TIMES

Coordinate No.	U_{zero} for 265 Hz, Zero Burn Cold Gas Third Long. Mode		U_{zero} for 281 Hz, Adv. Burn Hot Gas First Long. Mode	
	Phase (deg.)	Accel. (g's)	Accel. (g's)	Phase (deg.)
1	84.4	.0968	--*	--
2	-39.3	1.45	.368	134.6
3	150.7	3.56	1.75	-83.0
4	-23.8	.316	.346	125.4
5	-173.4	.0305	--	--
6	-24.3	8.25	6.24	129.1
7	-52.9	.432	--	--
8	-32.2	.715	.368	134.5
9	-40.4	1.42	1.75	-83.0
10	128.4	.0673	--	--
11	160.5	.426	.292	-50.8
12	130.4	.0704	--	--
13	151.9	.182	--	--
14	-40.4	1.42	.368	134.6
15	150.4	3.54	1.75	-83.0
16	-37.5	.0223	-	-
17	160.4	.416	.292	-50.8
18	-46.0	.0199	--	--
19	133.0	.339	--	--
20	73.7	.393	.368	134.6
21	162.2	2.48	1.75	-83.0
22	-49.2	.0508	--	--
23	159.9	.425	.292	-50.8
24	-52.0	.0496	--	--
25	-46.8	.123	--	--
26	94.5	.581	.368	134.6
27	165.0	2.34	1.75	-83.0
28	-32.8	.434	.345	125.4
29	160.2	.0034	--	--
30	-22.8	7.89	6.24	129.1
31	-46.0	.468	--	--
32	5.21	.394	.368	134.6
33	158.5	2.78	1.75	-83.0
34	131.4	.0696	--	--
35	160.0	.421	.292	-50.8
36	128.4	.0679	--	--
37	-41.0	.374	--	--
38	-36.5	1.19	.368	134.6
39	152.3	3.41	1.75	-83.0
40	[illegible].1	.0532	--	--
41	[illegible]2	.414	.292	-50.8
42	[illegible].9	.0511	--	--

* Values are very small and may be ignored.

APPENDIX H

SEALED ENVELOPE PREDICTIONS

MINUTEMAN III THIRD STAGE MOTOR

COMPONENT VIBRATION ANALYSIS RESULTS

SEALED ENVELOPE PREDICTIONS

(Contract F04611-73-C-0025)

31 July 1975

Prepared For

Department of the Air Force (AFSC)
Headquarters, Air Force Flight Test Center
Edwards Air Force Base, California

Prepared By

Hercules Incorporated
Systems Group
Bacchus Works, Magna, Utah

I. INTRODUCTION

Contract number F04611-73-C-0025 calls for submittal of "sealed envelope" predictions to the AFRPL Commander at the close of the Phase III work, (analysis of the verification motor). This report contains the sealed envelope predictions. The Minuteman III third stage motor has been designated as the verification motor. The response of the motor to the first longitudinal and the first tangential acoustic modes has been predicted.

The motor was analyzed at frequencies of 200, 240, and 300 Hz with a 6 sec. burn configuration to obtain response to the first longitudinal mode. A zero burn configuration was analyzed at frequencies of 760, 800, and 840 Hz to obtain response to the first tangential mode.

When the finite element model was constructed, the model mass was compared with measured values. The model stiffness was checked out by comparing deflections obtained from a uniform static pressure solution with available measured data. Good agreement was obtained for the mass and static stiffness representation of the model. The clean motor model for the Minuteman T/S motor was assembled by Dr. Dean Wang. The component models were assembled by Mr. Bruce Moore. Neither analyst referred to the accelerometer data available in the Aerojet Acoustics report[1]. No accelerometer data or other response data of any kind were used to modify the models, thus the intent of the "closed envelope" predictions was maintained.

II. RESPONSE PREDICTIONS

The locations of the component attachment points are shown in Figure 1. The acceleration responses predicted for the attachment points are given in Figures 2 through 7. As shown in Figures 2 through 7, the responses calculated for no components attached are quite similar to the responses obtained with components attached.

The responses of the forward dome are shown in Figures 8 through 13. Figures 8, 9, and 10 show the responses to the fundamental longitudinal mode at frequencies of 200, 240, and 300 Hz. The structure analyzed is nearly axisymmetric and the longitudinal acoustic mode shape is nearly axisymmetric. Figure 10 shows that the response to longitudinal modes is nearly axisymmetric. Responses are shown for only one radial line in Figures 8 and 9, but the circumferential variation is small as shown in Figure 10.

For the tangential modes, the response is a maximum along the radial line that corresponds to the maximum acoustic mode pressure. (For tangential modes the pressure varies in the circumferential direction). The full response distribution is shown in Figure 12. Only the response along the maximum pressure radial lines are shown in Figures 11 and 13.

All responses shown in Figures 8 through 13 are for no components attached. Since the attached components did not drastically affect the response at the component attach points on the aft dome, the more remote locations on the forward dome are likely to be less affected by attached components. Data recovery calculations can be performed using data stored on magnetic tapes to obtain the forward dome response with components attached if this appears to be desirable.

REFERENCE

1. Minuteman III Third Stage Pressure Oscillation Study, Final Report, Report No. 1387-01F, Aerojet Solid Propulsion Company, Sacramento, California, August 1971.

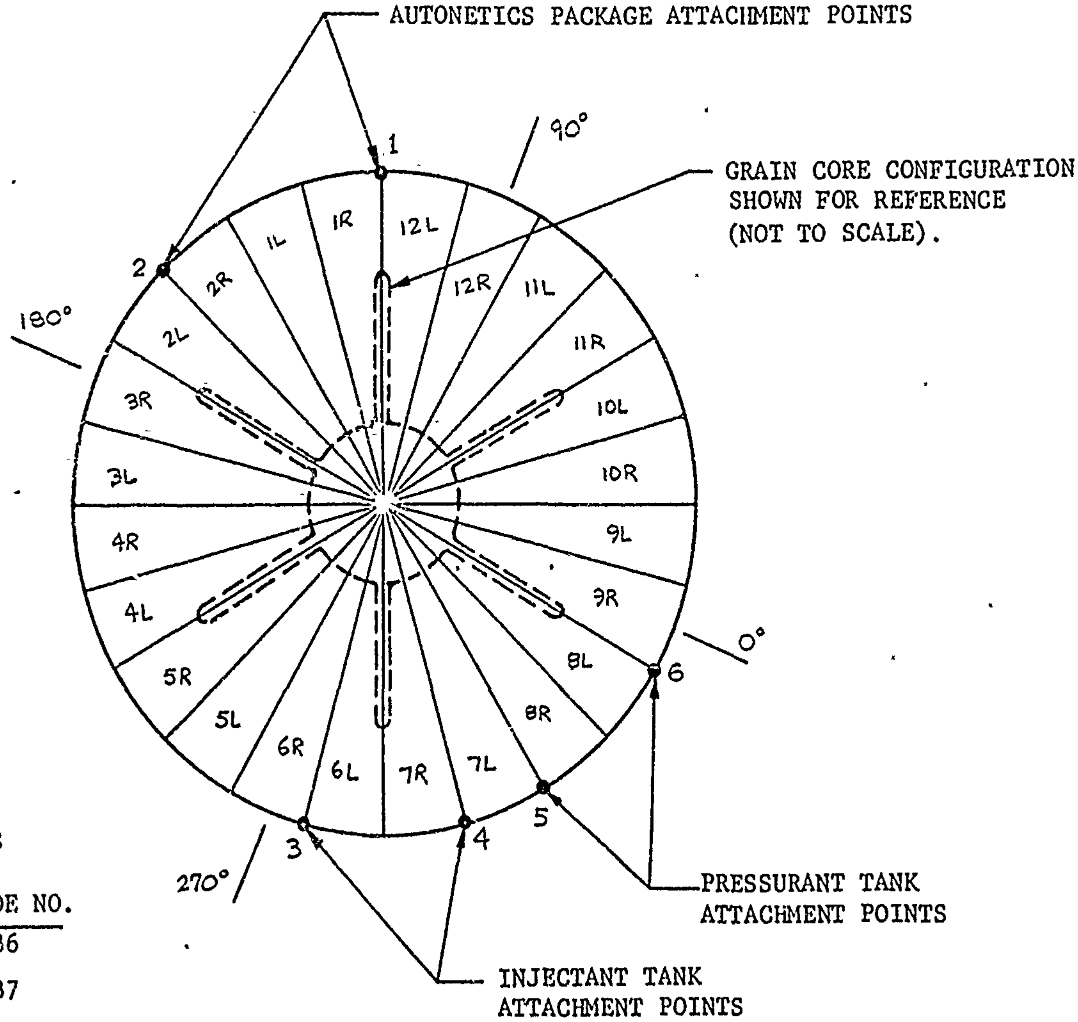

ATTACHMENT POINTS

ORDER IN U_o	SECTION	NODE NO.
U_1	1R	236
U_2	2R	237
U_3	6R	237
U_4	7R	237
U_5	8R	236
U_6	9R	236

VIEW OF THE MINUTEMAN III T/S MOTOR LOOKING AFT
SHOWING CYCLIC SYMMETRY GRID SECTION NUMBERS

Figure 1. Component Attachment Point Locations on the Nozzle Flange.

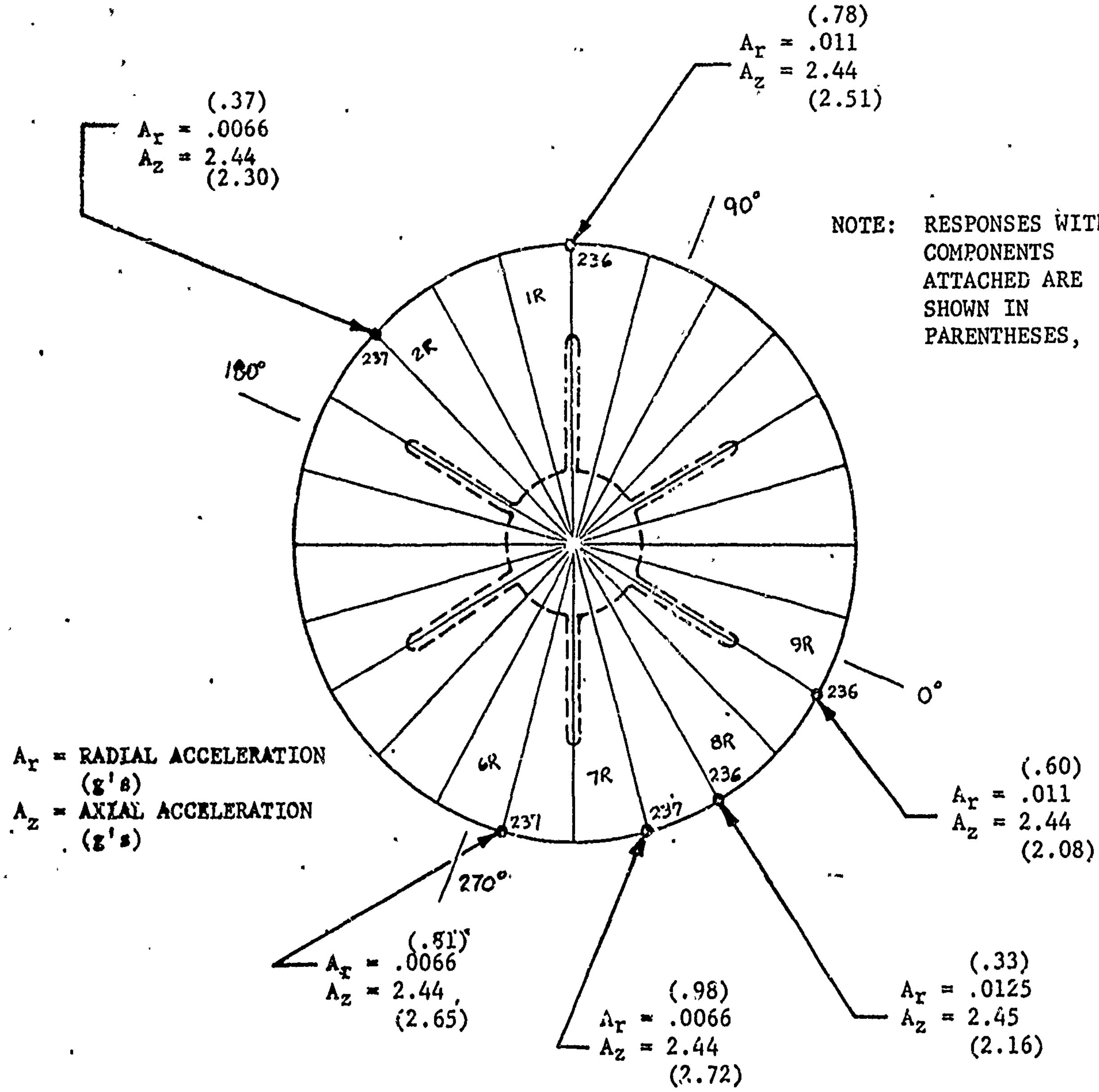

Figure 2. Minuteman III T/S, Acceleration Response at the Attach Points, Long. Mode at 200 Hz, $(P_i)_{max}$ = 1.0 psi, 6 second Burn Time Model.

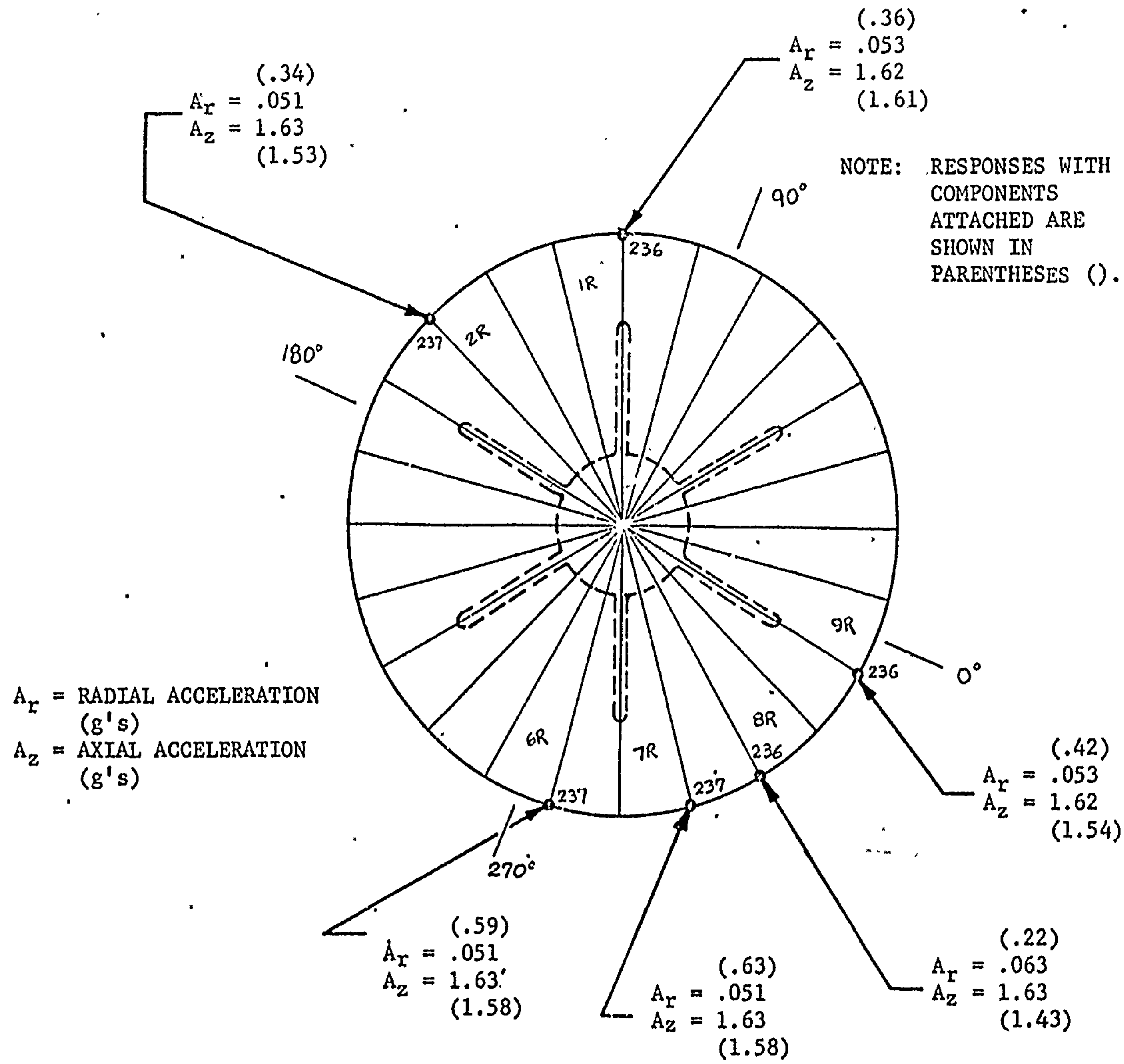

Figure 3. Minuteman III T/S, Acceleration Response at the Attach Points, Long. Mode at 240 Hz, $(P_i)_{max}$ = 1.0 psi, Six second Burn Time Model.

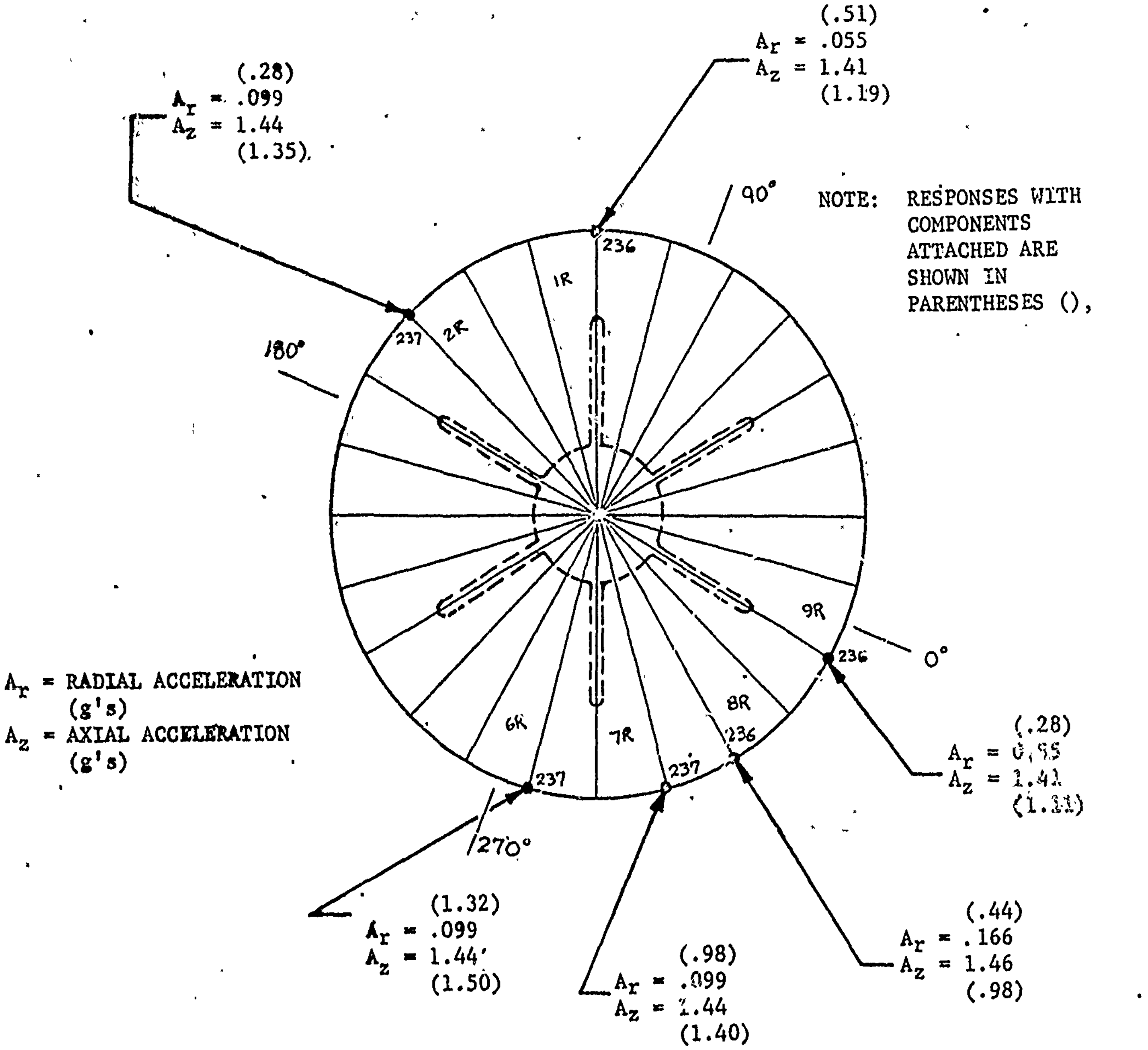

Figure 4. Minuteman III T/S, Acceleration Response at the Attach Points, Long. Mode at 300 Hz, $(P_i)_{max}$ = 1.0 psi, 6 second Burn Time Model.

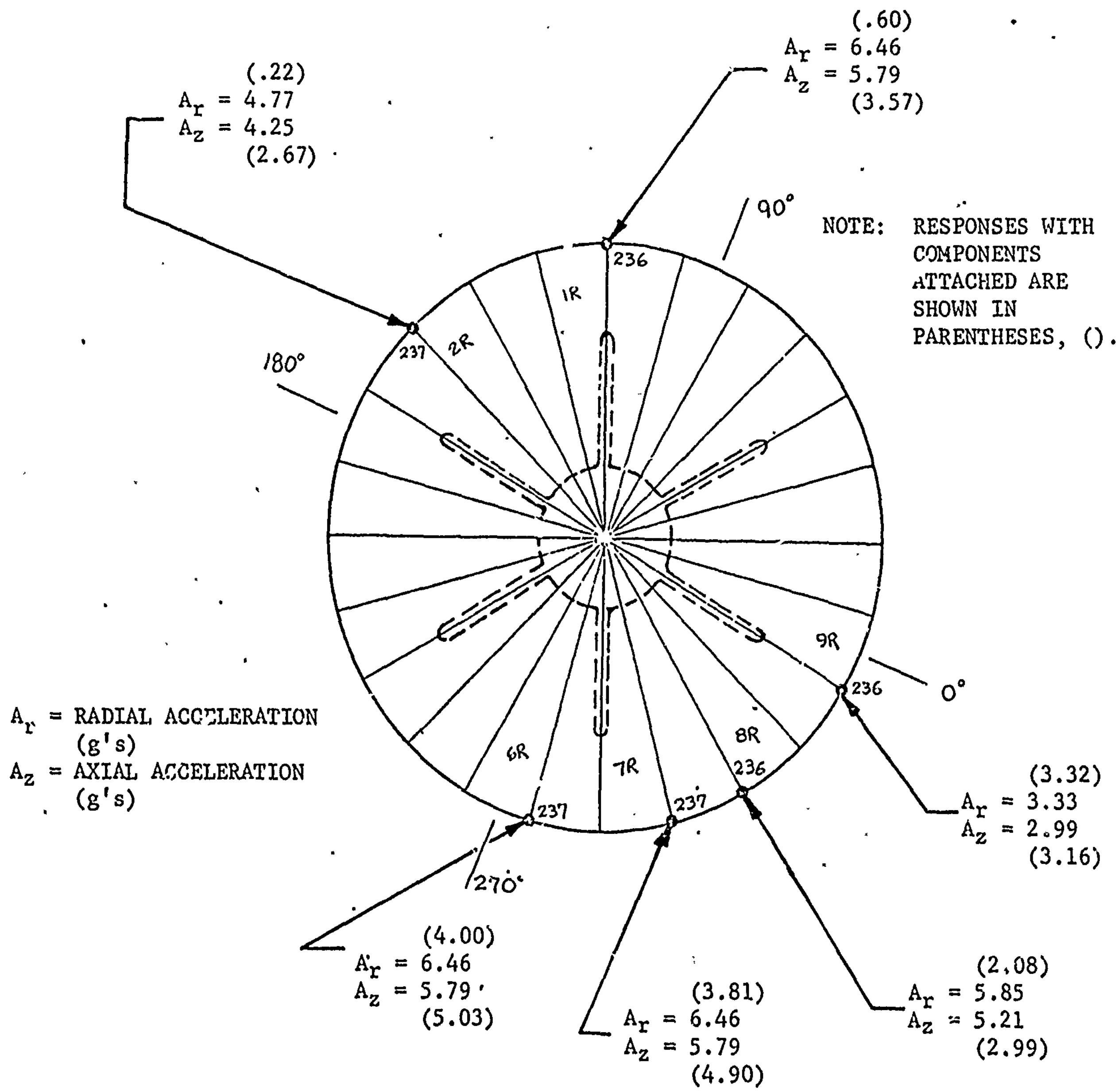

Figure 5. Minuteman III T/S, Acceleration Response at the Attach Points, Tang. Mode at 760 Hz, $(P_{slot})_{max}$ = 100 psi, Zero Burn Time Model.

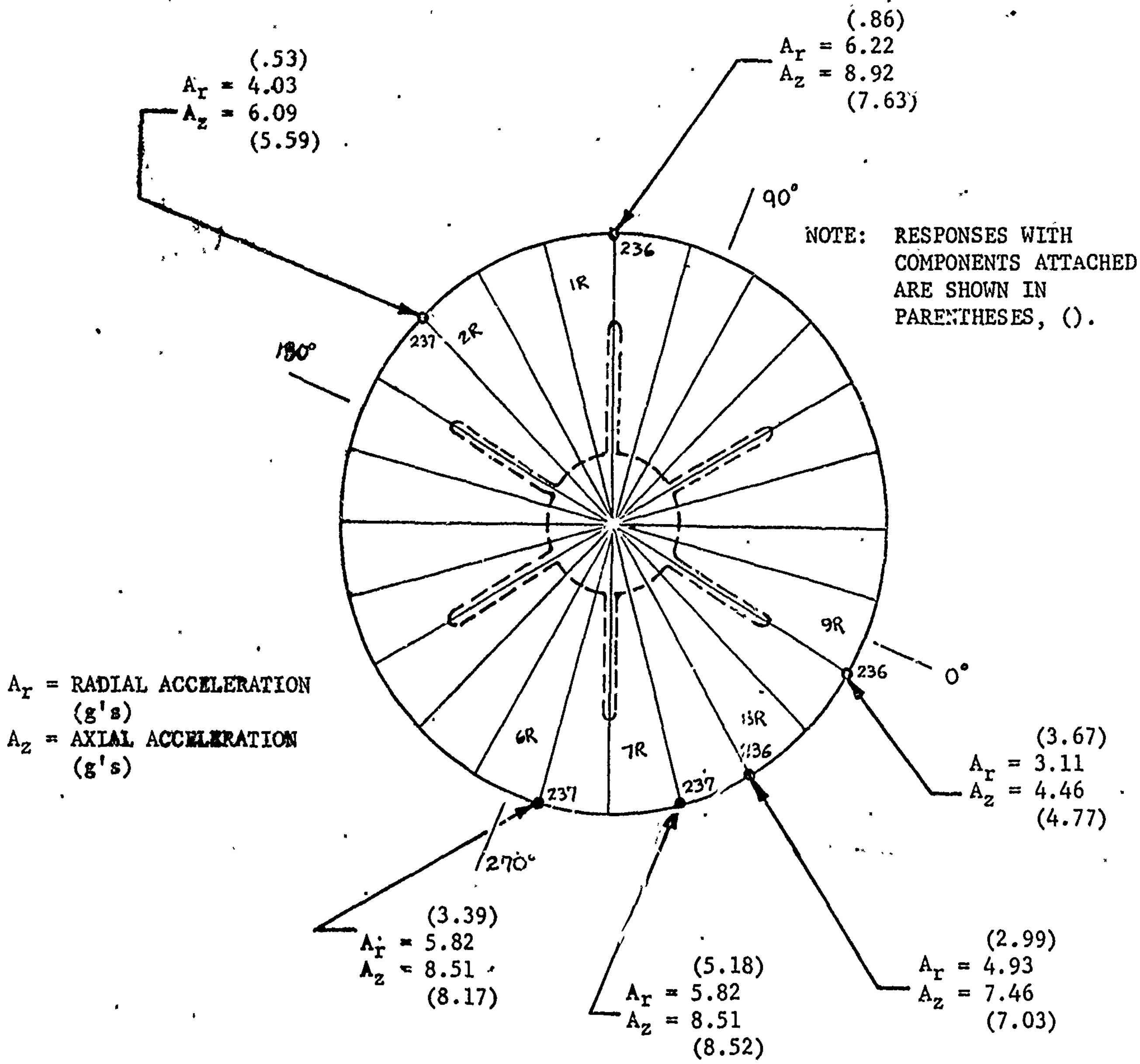

Figure 6. Minuteman III T/S, Acceleration Response at the Attach Points, Tang. Mode at 800 Hz $(P_{slot})_{max}$ = 100 psi, Zero Burn Time Model.

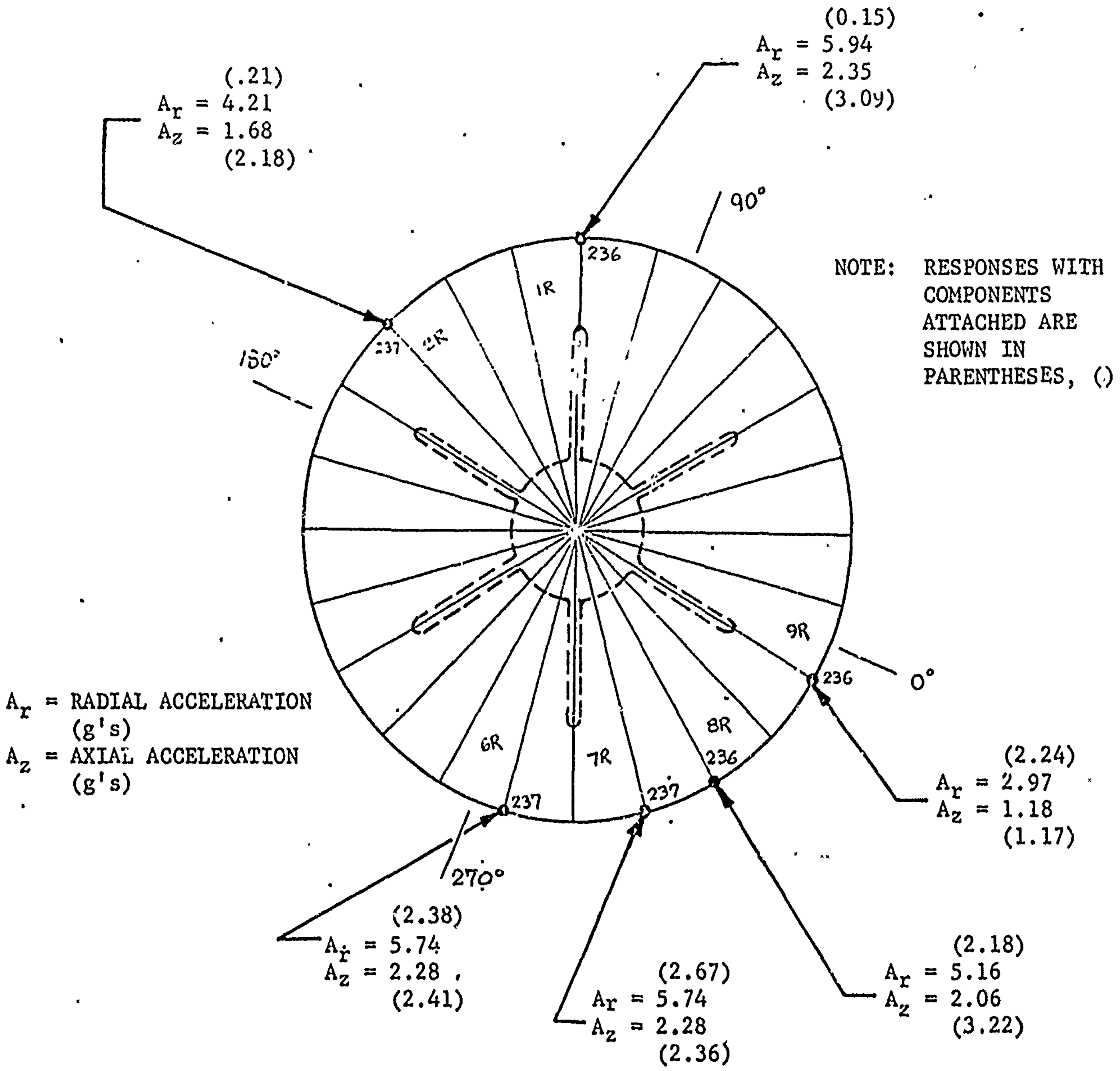

Figure 7. Minuteman III T/S, Acceleration Response at the Attach Points, Tang. Mode at 840 Hz, $(P_{slot})_{max}$ = 100 psi, Zero Burn Time Model.

NOTE: THE NUMBERS SHOWN AT THE GRID LINE INTERSECTIONS REPRESENT THE ACCELERATION RESPONSE IN G'S IN A DIRECTION NORMAL TO THE DOME (FIGURES 8 THROUGH 13)

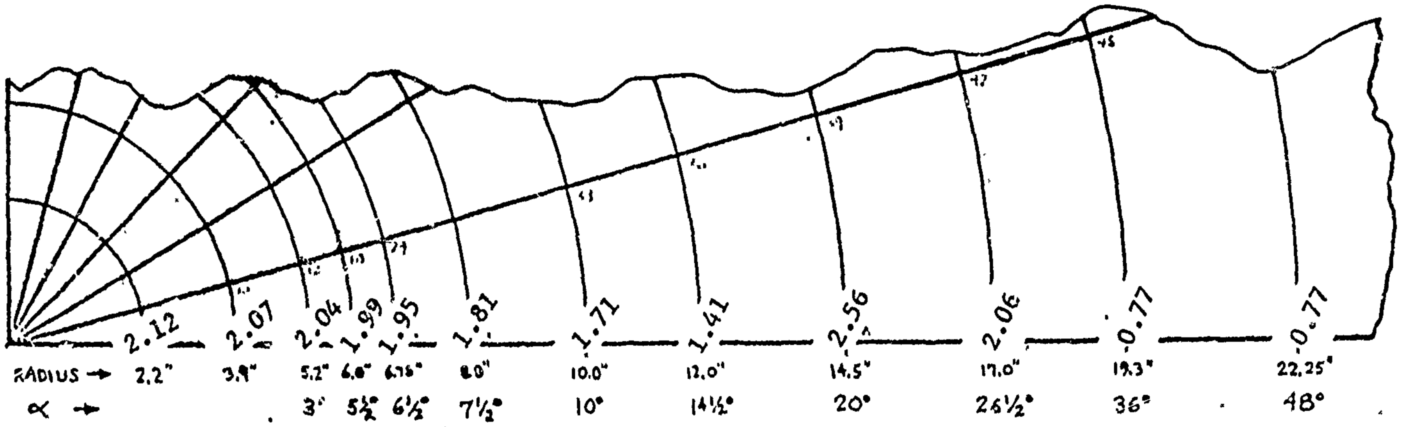

Figure 8. Forward Dome Minuteman III T/S, Response to First Long. Mode at 200 Hz Using 6 Sec. Burn Model, $(P_i)_{Max}$ = 1.0 Psi

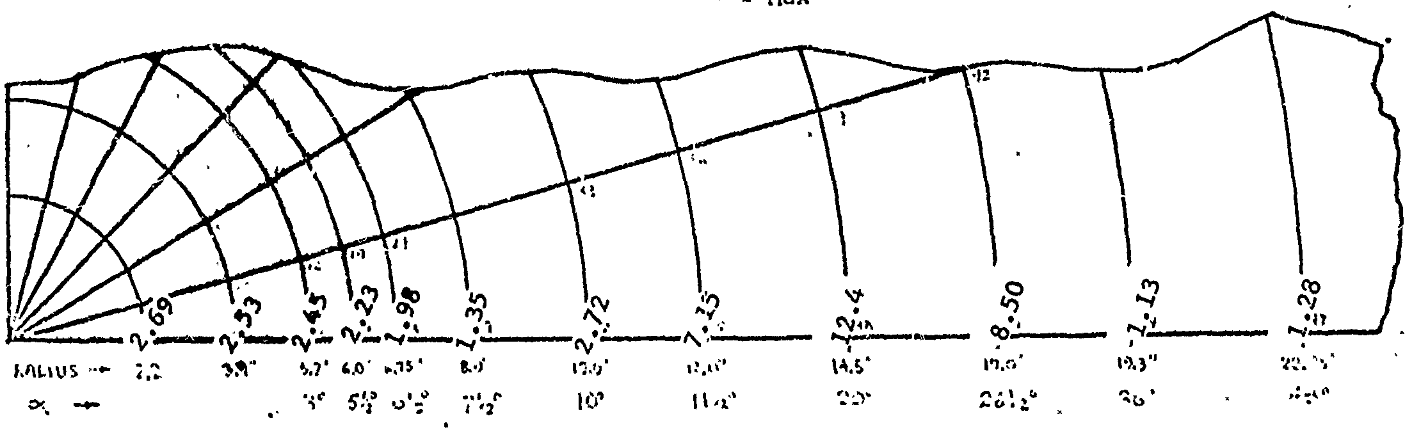

Figure 9. Forward Dome Minuteman III T/S, Response to First Long. Mode at 240 Hz Using 6 Sec. Burn Model, $(P_i)_{Max}$ = 1.0 Psi

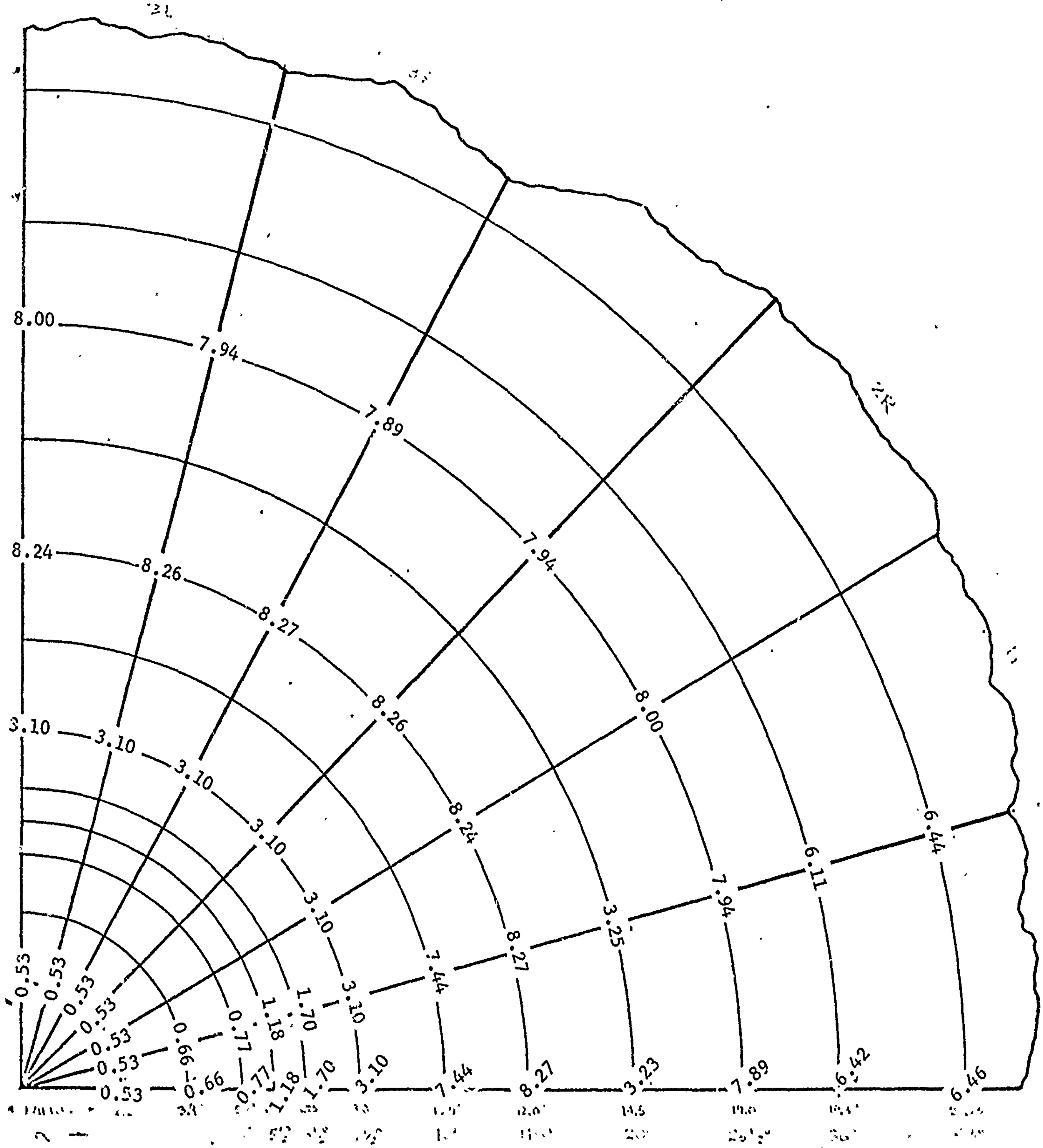

Figure 10. Forward Dome Minuteman III T/S, Response to First Long. Mode at 300 Hz Using 6 Sec. Burn Model, $(P_i)_{Max} = 1.0$ Psi

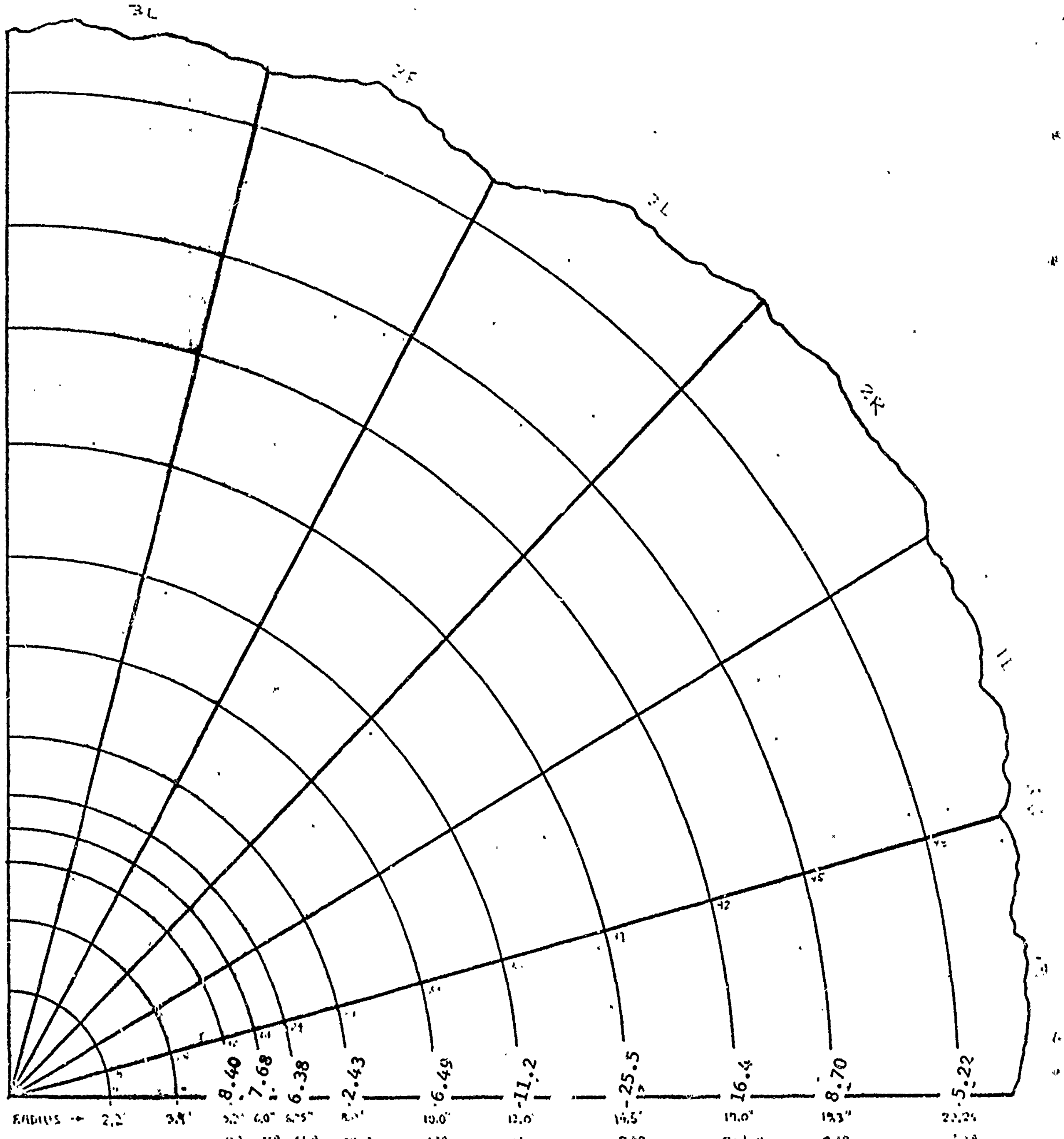

Figure 11. Forward Dome Minuteman III T/S, Response to First Tang. Mode at 760 Hz Using Zero Burn Time Model, $(P_{Slot})_{Max}$ = 100 Psi

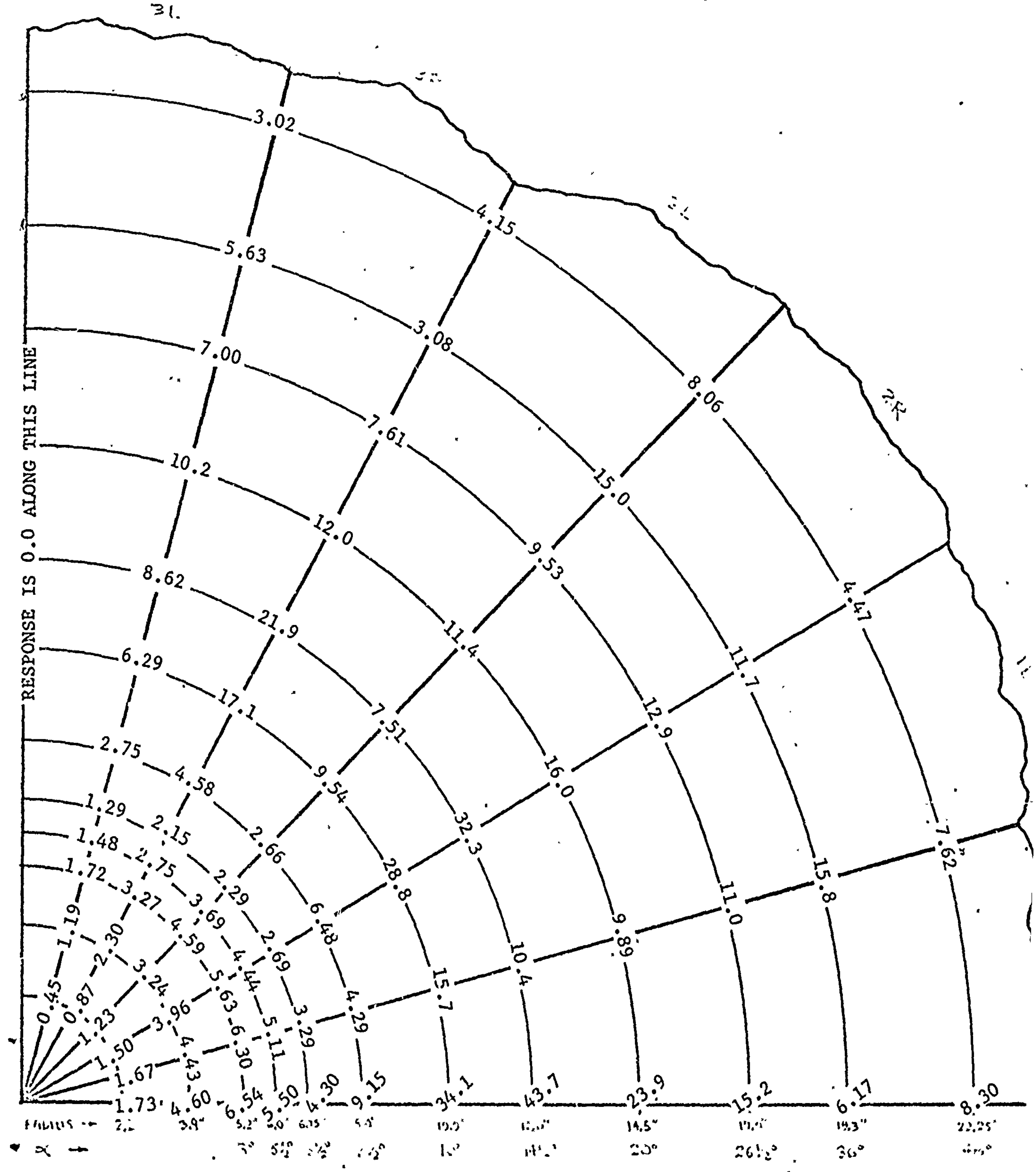

Figure 12. Forward Dome Minuteman III T/S, Response to First Tang. Mode at 800 H:
Using Zero Burn Time Model, $(P_{Slot})_{Max} = 100$ Psi

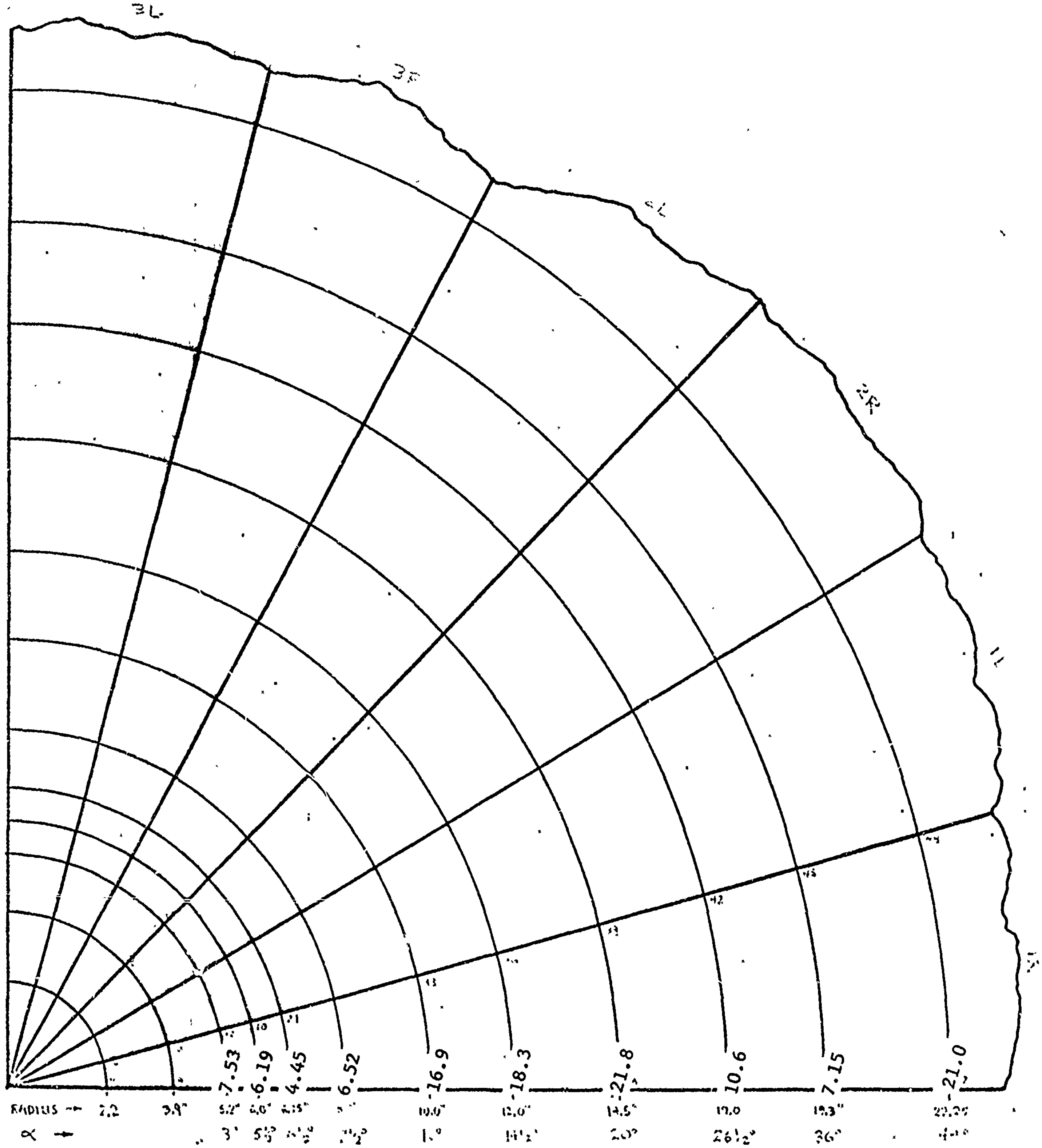

Figure 13. Forward Dome Minuteman III T/S, Response to First Tang. Mode at 840 Hz Using Zero Burn Time Model, $(P_{Slot})_{Max}$ = 100 Psi

APPENDIX I

MODELING TECHNIQUES MANUAL

A GUIDE FOR CONDUCTING
STRUCTURAL DYNAMICS ANALYSIS
ON SOLID ROCKET MOTORS
TO CALCULATE STRUCTURAL RESPONSE TO
INTERNAL ACOUSTIC PRESSURE OSCILLATIONS

By

F. R. Jensen

September 1975

SECTION I

INTRODUCTION

A. BACKGROUND

This modeling techniques manual is a result of work on Air Force Contract F04611-73-C-0025. Hercules Incorporated contracted with the Air Force Rocket Propulsion Laboratory at Edwards Air Force Base, California, to perform a Rocket Motor Component Vibration study program. The manual was submitted as an appendix to the final report for the program. The purpose of the manual is to convey the essential technology from the Component Vibrations Program to prospective analysts. An attempt has been made to put the results in a form that will make them useful for reference when various modeling decisions must be made.

The manual specifically deals with predicting the structural response of a solid rocket motor to internal acoustic pressure oscillations. Predictions of the degree of stability of a particular acoustic mode or definition of the acoustic mode shapes are beyond the scope of the modeling manual. Before the structural dynamics analysis is performed, acoustic modes and corresponding natural frequencies can be obtained either from analysis or testing. Use of the NASTRAN(1) program for calculation of the acoustic modes and natural frequencies is recommended.

B. PHILOSOPHY

The use of the word "modeling" in the title of this manual implies that mathematical models, constructed to represent a rocket motor structure, will be discussed. The most common mathematical models used for analysis of rocket motor structure are those based on use of the finite element method. NASTRAN is one of the most versatile structural analysis programs based on the finite element method. Results given in this manual were obtained using NASTRAN exclusively, but most recommended procedures should apply equally well to any finite element analysis.

The usual procedure consists of constructing a finite element model to represent a rocket motor. The finite element model is characterized by a mesh or grid network superimposed on a drawing of the motor outline. Different models are constructed for different purposes. When stresses are required, a rather fine mesh is generally used. When only displacements are required, less grid refinement is permissible. A grid for a static solution that requires good stiffness modeling may differ from a grid constructed for a dynamic solution where mass distribution is also important.

---

(1) Herting, D. N., Joseph, J. A., Kunsinen, L. R., and MacNeal, R. H., Acoustic Analysis of Solid Rocket Motor Cavities by a Finite Element Method, The MacNeal-Schwendler Corporation, AFRPL-TR-71-96, August 1971.

A significantly finer grid can be used for a two-dimensional (2-D) analysis than for a three-dimensional (3-D) analysis because of the smaller bandwidth associated with 2-D problems. Generally a more refined grid results in a more accurate model. However, the added refinement also results in longer computer run times and thus greater analysis costs. The analyst must weigh all applicable factors and attempt to design a model that will represent the significant motor response at a reasonable analysis cost.

At present, the construction of a finite element model is as much an art as it is a science. To construct a good finite element model, the analyst must be able to visualize the expected structural response of the motor and he must include features in his model that will allow it to simulate the behavior of the real motor. Often, the construction of a finite element model is an iterative process. The model resulting from the first attempt to model a motor is often modified when test results become available, or when comparisons are made with other analyses. Many motors have been found to exhibit behavior that was unexpected or unpredicted by initial models. Thus, past experience has shown that any particular analysis may fail to identify a particular problem. Analyses are performed with the hope that all significant problems will be identified and that response levels will be predicted with reasonable accuracy; however, the possibility of a modeling error or oversight should be kept in mind. This discussion, pointing out uncertainties in finite element analyses, is particularly applicable to the situation when a motor design is analyzed prior to motor fabrication.

Since the quality of the resulting finite element model is dependent on the ability of the analyst to visualize motor response, an attempt has been made to characterize typical motor responses. In addition, general guidelines for model construction are given. Use of the suggested guidelines should be tempered by the analyst's judgment for each individual situation.

C. APPROACH

No situations are on record where the magnitude of acoustic pressure oscillations in a solid rocket motor were sufficiently high to cause damage to the basic motor structure. The motor case, propellant grain, insulation material, nozzle, and igniter of a typical motor are designed to withstand ignition pressurization loads that are considerably more severe than those caused by acoustic pressure oscillations. The concern over effects of acoustic pressure oscillations relates to the components that are attached to the motor. The failure of at least one flight test of a ballistic missile has been traced to failure of a flight control unit mounted on an upper stage motor. The purpose of the analyses discussed in this manual is to predict acceleration levels input to components as a result of an unstable acoustic pressure oscillation.

The second section in this manual discusses some basic modeling considerations by making reference to a simple beam model. Modeling for eigenvalue solutions is compared with modeling for frequency response solutions. The third manual section gives a brief description of applicable analyses that have been performed to date. A fourth section contains modeling guidelines intended to provide direct guidance on model construction. Some test data and analysis results are given in the fifth section to illustrate typical motor response to acoustic pressure oscillations. The sixth section contains conclusions.

SECTION II

BASIC MODELING CONSIDERATIONS

As stated in the introduction, the quality of a finite element model depends on the ability of the analyst to visualize the response mode shapes. Some insight into general dynamic structural behavior can be gained by studying the response of simple uniform beams. Two types of analyses are discussed in this section: (1) Determination of natural frequencies and mode shapes (real eigenvalue analyses), and (2) determination of forced response (frequency response analyses). Results from these analyses are related to the analysis of rocket motors. The results presented were mainly taken from the Task 8 report given in Appendix F of the final report.

A finite element model for a pinned-pinned beam is shown in Figure 1. The model has 8 beam elements and 7 unconstrained displacement coordinates. The displacement coordinates are denoted U_1 through U_7. Theoretical (closed form) solutions for the beam natural frequencies and mode shapes are given by the equations shown in Figure 1. Nearly any standard text on vibrations contains these beam solutions. Rigid Format No. 3 in the NASTRAN program was used to perform a real eigenvalue analysis on the beam. The NASTRAN natural frequencies are compared with the theoretical natural frequencies in Table I. The NASTRAN natural mode shapes are compared with the theoretical natural mode shapes in Figure 2.

The results shown in Table I and Figure 2 illustrate a behavior that is common to all finite element models. The actual beam and the theorectical model both have an infinite number of natural frequencies and mode shapes. By comparison, the finite element model has only a limited number of natural frequencies and mode shapes. A finite element model can have only one natural frequency for each degree of freedom used in the mass matrix for the model. As a result of the limited number of degrees of freedom, the accuracy with which modes and frequencies can be predicted deteriorates for increasing mode numbers. For the beam model, only the first seven natural frequencies and mode shapes could be predicted because only seven degrees of freedom were used in the model. The data in Table I and the mode plots in Figure 2 show that the predicted results become increasingly inaccurate as the mode number approaches seven.

Notice that the eight element beam model yields very good results for the first two mode shapes, as shown in Figure 2. For the first two modes, there are three or more nodes available to define each half wave of the deformed shape. When a grid is constructed to represent a new rocket motor design, the use of a grid refinement that would result in three nodes for each half wave of the expected deformation is suggested as a goal. Grid refinement is discussed in subsequent sections of this manual.

The types of errors that can be expected from using a grid with inadequate refinement are illustrated in Figure 2. One type of error occurs because the location of the maximum response amplitude is not predicted correctly. A second type of error occurs when the predicted peak amplitude is incorrect. A third error type is due to the fact that a model with insufficient grid refinement will exhibit incorrect natural frequencies as shown by the data in Table I. When a real eigenvalue analysis is performed on a finite element model, the resultant mode shapes can be examined to estimate model accuracy as a function of frequency. When jagged mode patterns are found, such as those shown for modes 6 and 7 in Figure 2, chances are high that all three types of errors described above are present in the analysis results. When smoother mode patterns occur, such as those shown for modes 1, 2, and 3 in Figure 2, the analysis results are probably sufficiently accurate.

The criteria for judging the adequacy of a finite element model to be used for calculation of forced response is somewhat different from the criteria explained above for real eigenvalue analyses. The response mode shapes for frequency response analyses are very dependent on load distribution as well as being dependent on load frequency. In general, the response due to a simple distributed load tends to follow the same pattern as the load distribution. If a load is distributed in exactly the same pattern as a natural mode shape, then the response occurs entirely in that mode shape regardless of frequency. In the usual case, where the load is not distributed as a natural mode, various natural modes can participate in forming the response mode shape. The main natural modes that participate in the response are determined by both the load distribution and the forcing frequency. When the excitation frequency is not near a natural frequency, the response mode is likely to be quite similar to the load distribution. When the loading frequency approaches a natural frequency, the response mode may consist of the corresponding natural mode shape combined with the loading distribution mode shape.

The lower plot in Figure 3 shows a loading distribution for the simple beam that somewhat resembles the second natural mode shape. When the load distribution shown in the figure was applied to the beam at a frequency that matched the fourth natural frequency, 630.3 Hz, the response shown in the upper plot of Figure 3 was obtained. The response shown in Figure 3 generally followed the pattern of the loading distribution with a superimposed response in the fourth natural mode.

In a rocket motor, the loading distributions of interest are represented by the various acoustic cavity pressure modes. The finite element grid used to model the motor should be sufficiently refined to allow reasonable resolution for the definition of the pressure mode shapes. The use of a minimum of three nodes per half wave to define any pressure mode is a suggested guideline.

The grid should also be sufficiently refined to yield good definition of the response mode shapes. An after-the-fact examination of the response mode shapes may be used to reveal any potentially poor results, (use Figure 2 as a guide). The guideline of three nodes per half wave of the response mode shape also applies to frequency response analyses.

SECTION III

APPLICABLE EXPERIENCE

In this section, three different programs where rocket motor structural response was calculated are briefly discussed. The first two programs are pressure oscillation studies performed on the Minuteman II and III third stage motors.[2,3,4] The third program is the Component Vibration program for which this modeling manual was written.

A. MINUTEMAN II THIRD STAGE ANALYSIS

The Minuteman II third stage motor was analyzed[2,4] using the SAMIS (Structural Analysis and Matrix Interpretive System) computer program. The analysis was performed by Hercules Incorporated. Only the aft dome and aft dc.. components were included in the model. Due to computer program limitations, a one-quarter dome model (90^{o} slice) was used. The one-quarter model was analyzed four times using different combinations of symmetric and asymmetric boundary conditions to obtain the complete 3-D solution. In addition, the dome models and component models had to be analyzed separately because of problem size limitations of the SAMIS program. The separate solutions were effectively combined to represent the total model solutions by using a Modal Synthesis approach.

The Minuteman II third stage analysis resulted in natural frequencies and mode shapes. Good agreement was obtained between some component measured natural frequencies and calculated natural frequencies, however no attempt was made to calculate the motor response to an acoustic pressure oscillation. Even though the propellant is bonded to the aft dome in many actual motors, only the mass of an arbitrary portion of the propellant was included in the aft dome model. No provision was included in the model to account for effects of omitted motor structure.

The experience gained in constructing component models during the Minuteman II analysis program should be of interest. The analysis experience showed that changes in assumed component connection conditions can have a significant effect on analysis results. Component model response for the Nozzle Control Unit (NCU) was found to be quite sensitive to the torsional stiffness used in the model of the mounting bracket. Grid refinement used in the nozzle and NCU component models is shown in Reference 2.

---

(2) Pressure Osci''‑tions During Firing of Minuteman II Stage III Motor (U), Hercules Inc‹ ‹ated, Final Report Contract No. AF04(694)-903, January 1971 (Confidential).

(3) Minuteman III Third Stage Pressure Oscillation Study, Aerojet Final Report No. 1387-01F, Contract No. F04694-67-C-0004, August 1971.

(4) Jensen, F. R., and Christiansen, H. N., "An Application of Component Mode Synthesis to Rocket Motor Vibration Analysis," The Shock and Vibration Bulletin, The 41st Symposium on Shock, Vibration, and Associ ated Environments, Naval Research Laboratory, Washington, D.C., October 1970.

B. MINUTEMAN III THIRD STAGE ANALYSIS

The Minuteman III third stage motor was analyzed[3] using the NASTRAN computer program. The analysis was performed by the MacNeal Schwendler Corporation working in conjunction with the Aerojet Solid Propulsion Company. Four different types of analyses were conducted: (1) An acoustic analysis, (2) a forward dome modal analysis, (3) a forward half motor analysis, and (4) a nozzle analysis. All analyses are reported in Reference 3.

The acoustic analysis was performed[1] using the then newly-created acoustic analysis capability in the NASTRAN program. The acoustic analysis yields natural frequencies and mode shapes of the combustion gases in the combustion cavity. The program is basically a two-dimensional program, but special provisions have been made to handle tangential modes and slotted grain designs. Good comparisons were reportedly obtained between analysis results and experimentally-measured natural frequencies and mode shapes.

A modal analysis was performed on a model of the forward dome of the Minuteman III third stage motor to determine the natural frequencies and mode shapes below 1000 Hz. The forward dome model was based on a one-quarter (90^o slice) section of the motor. Both symmetic and asymmetric boundary conditions were used in the analyses. The effects of two different components, mounted to the dome in a symmetrical pattern, were studied. The Minuteman III forward dome analysis is of interest mainly because of the way in which differential stiffness was used to model the stiffening effect on the case of the static internal pressure. The procedures for using differential stiffness in a dynamics analysis and the required DMAP alters are given in the Aerojet final report.[3]

The model of the forward dome was incorporated into a model of the forward half of the motor. The dome, propellant, igniter, and TT-ports were included in the forward half motor model. Frequency response analyses were conducted on the forward half motor model at different frequencies and at different burn times. One aspect of the model may be of interest to future analysts. A unique model consisting of scalar springs, scalar masses, and multiple point constraints was used to represent gases physically trapped in the forward dome cavity during motor ignition and shortly thereafter. Figures and test data are given in the Aerojet report so that comparisons between analysis results and firing data may be made.

A fourth analysis was conducted on the Minuteman III third stage motor to determine the vibration modes of the nozzle as an unsupported structure with asymmetrically attached components. This analysis is reported in Appendix A of the Aerojet report.[3]

C. AFRPL COMPONENT VIBRATION PROGRAM

Two motors were analyzed during the Component Vibration program: the Poseidon C-3 second stage motor and the Minuteman III third stage motor. The major difference between these analyses and previous analyses is that the complete motors, including attached components, were included in the models. The use of full motor models was made practical by development of the cyclic symmetry modeling capability. The MacNeal-Schwendler Corporation is responsible for the development of the cyclic symmetry approach. A mechanical impedance approach was used to account for the effects of asymmetrically attached motor components. Comparisons were made between analysis results and experimental results, and several analyses were performed to gain insight into general solid rocket motor structural dynamic behavior. This modeling manual is an appendix to the final report for the Component Vibration program. Refer to the main report for additional detail.

SECTION IV

MODELING GUIDELINES

Section IV is intended to directly address the problem of analyzing a new solid rocket motor design prior to motor manufacture. Some of the basic modeling decisions that must be made are discussed as well as some of the advantages and disadvantages of the suggested analysis approach.

A. INPUT DATA

Before a model can be assembled and analyzed, a certain amount of input data must be collected. The required data usually includes that discussed below.

1. Definition of Motor Geometry and Material Callouts

Drawings are required that give a complete definition of motor geometry including case, grain, nozzle, igniter and other motor hardware such as closures, nozzle adapters, and TT ports. The materials to be used for each motor item must be identified.

2. Material Properties

Generally, the following material properties must be obtained for each material used in the motor:

(a) Material stiffness is required. For isotropic materials, the elastic modulus and Poisson's ratio are sufficient. For orthotropic material (generally composites), the directional stiffness coefficients must be available. For propellant and other viscoelastic materials, dynamic stiffness properties are required (e.g. the loss tangent and shear storage modulus both defined as a function of frequency over the frequency range of interest).

(b) Material density is required for each material which is present in sufficient quantity to warrant inclusion in the mass representation of the motor. Material densities are not needed for items that can be represented by direct input of nodal masses.

(c) Material damping coefficients should be available for each material used in the major load-carrying portions of the structures. Damping for the viscoelastic materials is not required since damping characteristics are included in the stiffness (complex modulus) definition.

3. Loads

The acoustic modes resulting from an acoustic cavity analysis define the input pressure distributions. A uniform internal pressure load system is generally useful for static checkout and evaluation of the model. In the NASTRAN program, pressure loads can be input directly in the static analysis rigid format; however, the frequency response rigid format requires nodal force inputs. A static analysis run, therefore, is generally made for each loading condition to convert pressure loads to nodal forces. An OLOAD (punch) = All NASTRAN instruction is used in the static run to punch the set of generated nodal forces. A FORTRAN program is then used to read the output and punch a new deck in the appropriate format for input to NASTRAN (DAREA cards are required).

4. Mass Data

Masses for component parts of the motor and for the complete motor, obtained by independent calculation or from measurement of available parts, is often useful for preliminary evaluation of the finite element model.

5. Test Data

Any available test data for the motor or for component parts of the motor that relates forces and displacements from static or dynamic tests may be useful for evaluation of the finite element model.

The input data list given above applies to the motor proper. If motor components such as nozzle control units, gas generators, etc., are to be included in the analysis, then similar input data must be gathered for each component of interest. In addition, locations of component centers-of-gravity are useful.

B. FINITE ELEMENT GRID CONSTRUCTION

The usual procedure in finite element grid construction is to make a scale layout of the motor cross-section. Node points are placed at a sufficient number of locations around the motor boundaries to provide a reasonable definition of motor geometry. A typical grid is shown in Figure 4. As shown in the Figure, CHEXA2 elements are used to represent the grain. The use of CHEXA1 elements and CWEDGE elements is not recommended. Uniform symmetrical forces applied to CHEXA1 or CWEDGE elements do not result in exactly uniform and symmetrical displacements as they should.

The use of a large number of nodes around the boundary of the grain is desirable because better definition of the acoustic pressure mode loading is possible. If at least three nodes are used for each half wave of the acoustic mode shape, then at least six nodes would be required for the first longitudinal mode, nine nodes would be required for the second longitudinal mode, etc. Figure 5 shows a way of reducing the total number of nodes in the grid of Figure 4 without changing any of the boundary nodes.

C. CYCLIC SYMMETRY CONSIDERATIONS

Most solid rocket motor designs can be analyzed using the cyclic symmetry option in NASTRAN. (Refer to Appendix C of the Component Vibration final report for a detailed discussion on the use of cyclic symmetry.) When a 3-D solution is required for a rocket motor, the cyclic symmetry capability of NASTRAN can be used to great advantage. The basic requirement for using cyclic symmetry is that the motor can be divided into geometrically identical sections that repeat around the circumference of the motor For example, if the grain design has four evenly spaced identical slots, a 90^o section formed by r-z planes passing through the slot centerlines is one of four identical sections repeating around the circumference. Using cyclic symmetry, such a motor could be modeled by creating a finite element grid for one half of the 90^o section (a grid for a 45^o slice of the motor using the dihedral symmetry option).

Better models can apparently be made for motors with a large number of slots. If a motor has a sufficient number of slots, a grid slice only one element thick can be used as a model. When a large slice is required, several layers of elements may be required to form the slice thickness in the circumferential direction. When more than one layer of elements is required, the bandwidth of the equations increases by a considerable amount. The bandwidth increase means that less grid refinement can be used in a multiple layer model than in a single layer model for a given computer run time.

The finite element model to be used in the analysis usually represents an effort to obtain a grid as refined as possible while still maintaining reasonable computer run times. "Reasonable run times" may have different values depending on the budget of the analysis program and the computer available. A one layer 15^o slice of the grid shown in Figure 4 with 1032 subcases runs approximately 300 CPU minutes on an IBM 370/155. As an aid in making the decision on the maximum slice size to use in the model, results from a previous analysis are shown in Figures 6 and 7. Figure 6 shows the natural frequencies and mode shapes obtained by using a 15^o slice with only one layer of elements.

Figure 7 shows the corresponding results for a 5^o slice. The correspondence between the 5 and 15 degree slice results is not good. The 15 degree slice appears to be too large to provide accurate results.

As discussed, the size of the slice is usually determined by the number of slots in the grain. Another factor that may be important is the number of thrust termination (TT) ports. Depending on the design and location of the TT ports, inclusion of the TT ports as well as the grain slots in the cyclic symmetric structure may be desirable.

Most motors do not have enough slots to warrant the use of a single slice model much smaller than 15 degrees. A motor with 12 slots could be modeled with a 1/24th motor section (15 degree slice). A motor with 15 slots could be modeled with a 1/30th motor section (12 degree slice). There are two ways to obtain effective smaller slice widths for motors without large numbers of slots.

For motors where the TT ports can be represented adequately by smeared properties (i.e., by increasing the stiffness of some case elements near the TT ports in a nearly axisymmetric TT port representation), some dummy grain slots can be introduced so that the slice width required to model the grain can be made as small as desired. The greater the number of dummy slots, the smaller the model slice width. When this procedure is used, the resulting model for a single slice has a small bandwidth and a slice with about 1000 degrees of freedom becomes practical. The introduction of dummy slots is justified by the consideration that the major effect of the slots on the grain structural behavior is to eliminate the capability of the grain to carry a hoop load in the slotted region. Because of the way the slots are modeled (refer to Appendix C of the Acoustic Vibration Final report, example problem), the radial and axial load carrying capacity of the grain should not be affected very much by introduction of additional slots. The use of dummy slots is more straightforward for the longitudinal acoustic pressure modes. For tangential modes, obtaining an equivalent load with a greater number of slots is more difficult.

The second procedure for obtaining smaller slice widths is simply to use a grid section with several layers of elements. A motor with 12 slots could be modeled with a motor section consisting of three 5-degree slices for a total section width of 15 degrees. The disadvantage (increased bandwidth) of this approach has been discussed. A possible solution to this problem is to apply a Guyan reduction to reduce the number of degrees of freedom in the analysis set. No experience with the application of Guyan reduction in a cyclic symmetry problem is available, however, the following should be considered:

(1) Use the OMIT feature in NASTRAN to omit selected degrees of freedom from the analysis set.

(2) Do not omit any degrees of freedom for nodes on the boundaries of the basic grid section, i.e. the nodes that appear on CYJOIN cards.

(3) If the basic grid section is approximately 20° or less, consider OMITing all internal node degrees of freedom.

(4) The reduction process will cause an increase in bandwidth so that a reduction to 200 to 300 degrees of freedom may be necessary to maintain reasonable solution times.

(5) There may be an optimum way to select points to be used in the OMIT set so that a minimum bandwidth results. This may be worth future investigation.

D. ACCOUNTING FOR ATTACHED COMPONENTS

Relatively lightweight components should not be expected to have a significant effect on dome response (or case response if mounted on the cylindrical portion of the case). Heavier components may affect the motor response under certain conditions. To obtain an idea of relative force magnitudes involved, consider that a uniform 1.0 psi pressure distributed over the dome of a motor with a 40-inch radius would apply a distributed net force of about 5000 pounds. By comparison, a 50 pound component vibration at 100 g's would apply a concentrated force of 5000 pounds to the motor. Maximum pressure oscillation levels are generally higher than 1.0 psi while component response levels are usually (but not always) much lower than 100 g's. One exception to the statement about lightweight components occurs in the case of a nozzle actuator that is connected at two widely separated points. The nozzle actuator that couples dome motion with nozzle motion will have a significant effect on overall motor response.

If components mounted on a particular motor are judged most likely not to effect the motor response, the analysis procedure can be greatly simplified. The response of the motor without components can be calculated using the cyclic symmetry model. Accelerations calculated at the component connection points can then be used as input levels for judging the adequacy of component design.

For the situation where components are judged likely to influence motor response, a mechanical impedance procedure is available to allow the response of the coupled motor-components system to be calculated. The discussion on application of the mechanical impedance method from section IV of the Component Vibration final report is partially repeated here. Refer to the report for additional detail.

E. APPLICATION OF MECHANICAL IMPEDANCE

For this discussion consider first a motor with one component attached. The same reasoning is generalized for additional components below. The reason for using the mechanical impedance approach is that it allows the clean motor model (component not attached) and the component model to be analyzed separately, yet results are obtained for the component-mounted-to-motor condition. To make the analysis exact, the component is replaced by the forces that it creates on the clean motor.

Since the motor is oscillating in response to a particular unstable acoustic pressure mode, the motor proper is considered to be acted upon by two separate sets of forces; the oscillating pressure forces are applied internally, and inertia forces due to the attached component are applied at the motor-component interface locations. The solution is obtained by superimposing effects of both loading conditions.

The clean motor model is analyzed with only internal pressure loading to obtain the velocities $\{V_o\}$ at the motor-component interface. The velocities $\{V_1\}$ at the interface caused by component connection forces $\{F_c\}$ can be expressed by using the motor admittance matrix $[Y]$:

$$\{V_1\} = [Y] \{F_c\}$$

The total velocity $\{V_t\}$ is obtained by superimposing the effects of the two loading conditions:

$$\{V_t\} = \{V_o\} + \{V_1\}$$

Substituting from above gives

$$\{V_t\} = \{V_o\} + [Y] \{F_c\}$$

The forces $\{F_c\}$ at the interface are unknown, but they can be expressed in terms of the total velocity by considering the component impedance relationship:

$$\{F_c\} = - \{Z_c\} \{V_t\}$$

where $\{Z_c\}$ represents the component impedance matrix. The minus sign occurs because forces applied to the component are equal and opposite to those applied to the motor. Substituting $\{F_c\}$ in the equation for $\{V_t\}$ gives:

$$\{V_t\} = \{V_o\} - [Y] [Z_c] \{V_t\}$$

Rearranging:

$$\{V_t\} = \left([I] + [Y] [Z_c] \right)^{-1} \{V_o\}$$

where $[I]$ is the identity matrix. Each matrix must be complex to handle the magnitude and phase information required for characterization of damped systems. The solution represented by the last equation given above for $\{V_t\}$ must be repeated at each frequency of interest. Solution of the last equation results in response at the component connection points for the coupled motor-components system.

SECTION V

TYPICAL MOTOR BEHAVIOR

The purpose of this brief section is to present some analysis results and some test data to aid in the visualization of likely motor response modes. The better the dynamic response of a motor is understood, the more likely a meaningful finite element analysis can be conducted. The analysis results shown here were taken from the Task 8 report, Appendix F of the Component Vibration final report. The test data were taken from Appendix B of the same report.

Figures 6 and 7 show results from real eigenvalue analyses on an aft dome model. The model was a single slice with symmetry boundary conditions applied along each slice face. The model was constrained at the Y-joint in a direction parallel to the motor axis. The small lines plotted normal to the dome are displacement vectors plotted to an exaggerated scale. In addition to the symmetric modes shown in Figures 6 and 7, the dome can exhibit many unsymmetric modes including lobar type modes.

Real eigenvalue analyses were also applied to a one-half grain model. The motor axis is normal to the motor mid-plane that divides the grain into halves. The grain model was analyzed both with symmetry and with asymmetry boundary conditions at the motor mid-plane, the results are shown in Figures 8 and 9, respectively.

Typical motor response to frequency-dependent loads is shown in Figures 10 and 11. Figure 10 shows the axisymmetric aft dome response of the motor to the axisymmetric third longitudinal acoustic mode. The response of the grain surface along the centerbore to the same mode (but at the hot gas frequency) is shown in Figure 11. The response mode crosses the zero reference three times and therefore has the equivalent of four half waves in the deformed shape.

Figures 12 and 13 show plots of response amplitude as a function of frequency for an aft dome model loaded with three different loading distributions. The response at the peaks and the width of the peaks in the response plots is dependent on the damping used in the model.

Figure 14 shows how radial motion at the Y-joint of an aft dome can be transformed to axial motion of the nozzle and nozzle adapter.

In spite of the numerous natural frequencies and mode shapes exhibited by motor finite element models, vibration tests often excite only a few of the total possible modes.* For example, when a motor is vibrated in an axial direction by attachment to the motor skirts, the grain exhibits

*Information in this paragraph is given with reference to a personal conversation with Mr. T. E. Depkovich of the Aerojet Solid Propulsion Company.

only 2 or 3 resonances (peaks in the frequency response curve). Apparently the higher natural frequencies are so heavily damped that they do not respond during the low level vibration test. This motor behavior has caused measurement methods for grain dynamic moduli to be questioned. In transverse axis tests, lobar modes higher than the first mode are very difficult to excite and the response is generally similar to response in the axial direction as higher modes seem to be heavily damped.

Figures 15 and 16 show two types of responses to acoustic oscillations that occur in a typical motor. Figure 15 shows a single frequency sinusoidal response that occurs at 730 Hz between approximately 2-1/2 and 4-1/2 seconds. Figure 16 characterizes a common response type that changes frequency rapidly with increasing motor burn time. The oscillation characterized in Figure 16 begins at 1320 Hz at about 3.8 seconds. As the burn surface progresses, the frequency of the oscillation increases to about 1450 Hz at 6.5 seconds. Some acoustic modes decrease in frequency with advancing burn time.

SECTION VI

CONCLUSIONS

The objective of this modeling techniques manual was to convey information that would provide guidance to the analyst assigned to the task of calculating the response of a solid rocket motor to acoustic pressure oscillations. The objective has been achieved since guidance has been provided. Providing a complete set of analysis instructions would not be possible since each analysis problem is different in some respect than all previous analyses. The discussions given hopefully pointed out potential problem areas and, in some cases, suggested solutions. No attempt was made to provide "Cook Book" type instructions on how to perform the analyses. Instead, reference and background material were given to provide the analyst with a basis for some of the required modeling decisions.

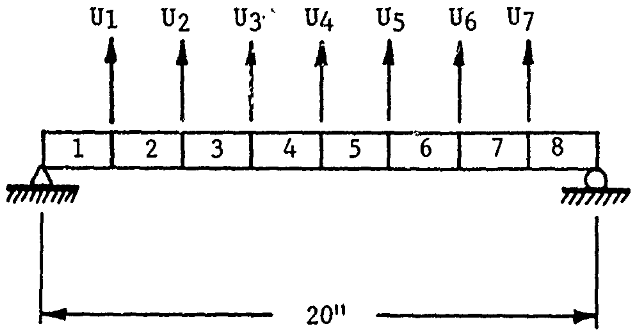

FINITE ELEMENT BEAM MODEL

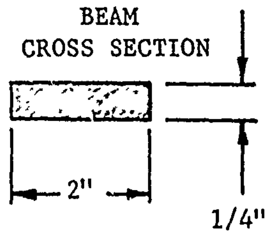

$I = 0.002604 \text{ IN.}^4$
$E = 5 \times 10^6 \text{ PSI}$
$\rho = 2.58799 \times 10^{-4}$

$$f_n = \frac{n^2 \pi}{2 \ell^2} \sqrt{\frac{EI}{m}} = (39.3911)\, n^2$$

$$\varphi_n (X) = \text{Sin} \frac{n \pi X}{\ell}$$

f_n = NATURAL FREQUENCY OF NTH MODE

φ_n = NATURAL MODE SHAPE

Figure 1. Beam Model Used to Study Mode Shapes

TABLE I

COMPARISON BETWEEN FINITE ELEMENT AND CLOSED-FORM NATURAL FREQUENCIES

n	f_n (NASTRAN) (Hz)	f_n (Theory) (Hz)	Error (%)
1	39.39	39.39	0.0
2	157.52	157.57	0.032
3	353.87	354.53	0.186
4	625.68	630.28	0.730
5	962.04	984.81	2.312
6	1328.46	1418.13	6.323
7	1641.03	1930.23	14.983

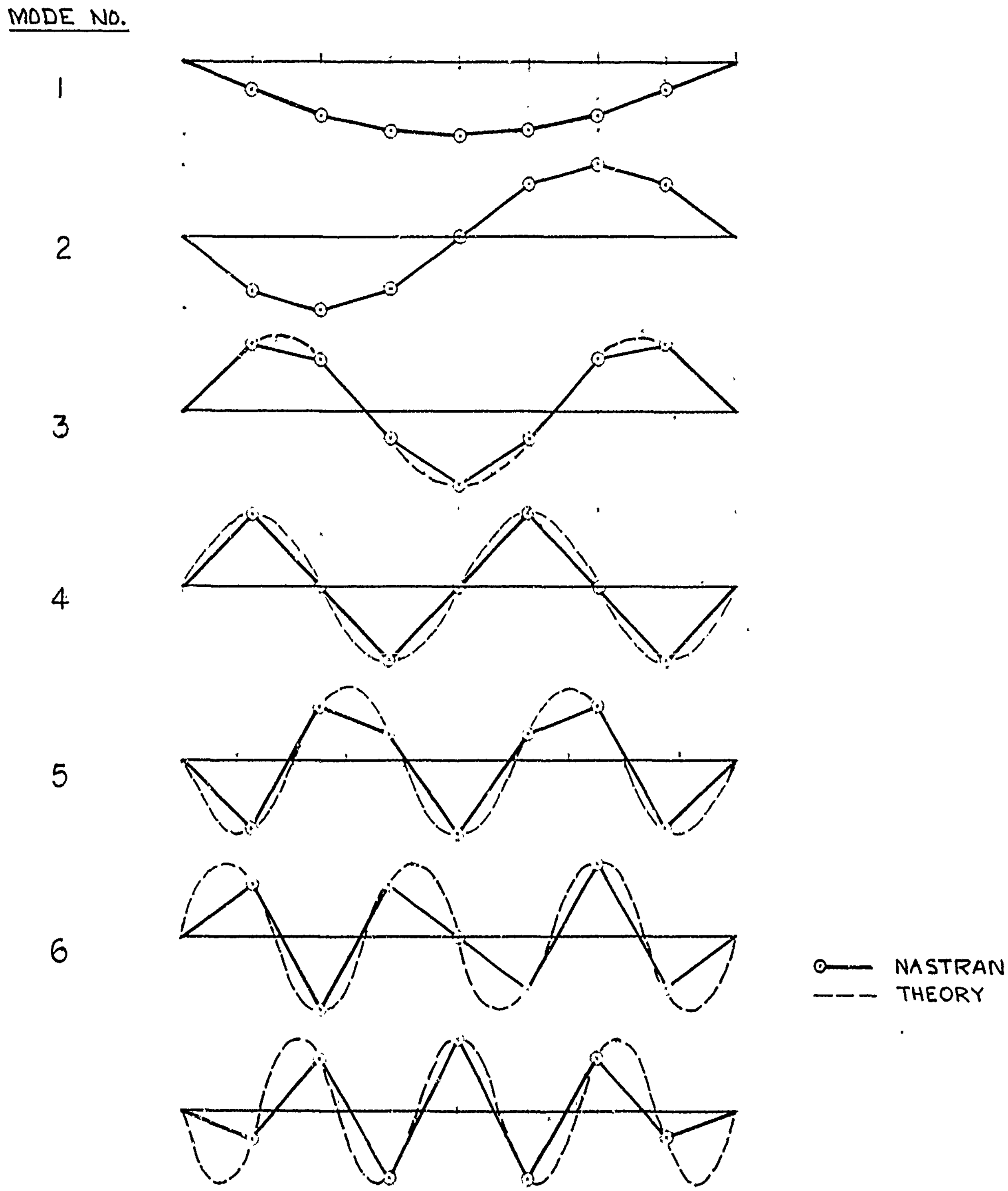

Figure 2. Comparison Between NASTRAN Calculated Mode Shapes and Theoretical Mode Shapes

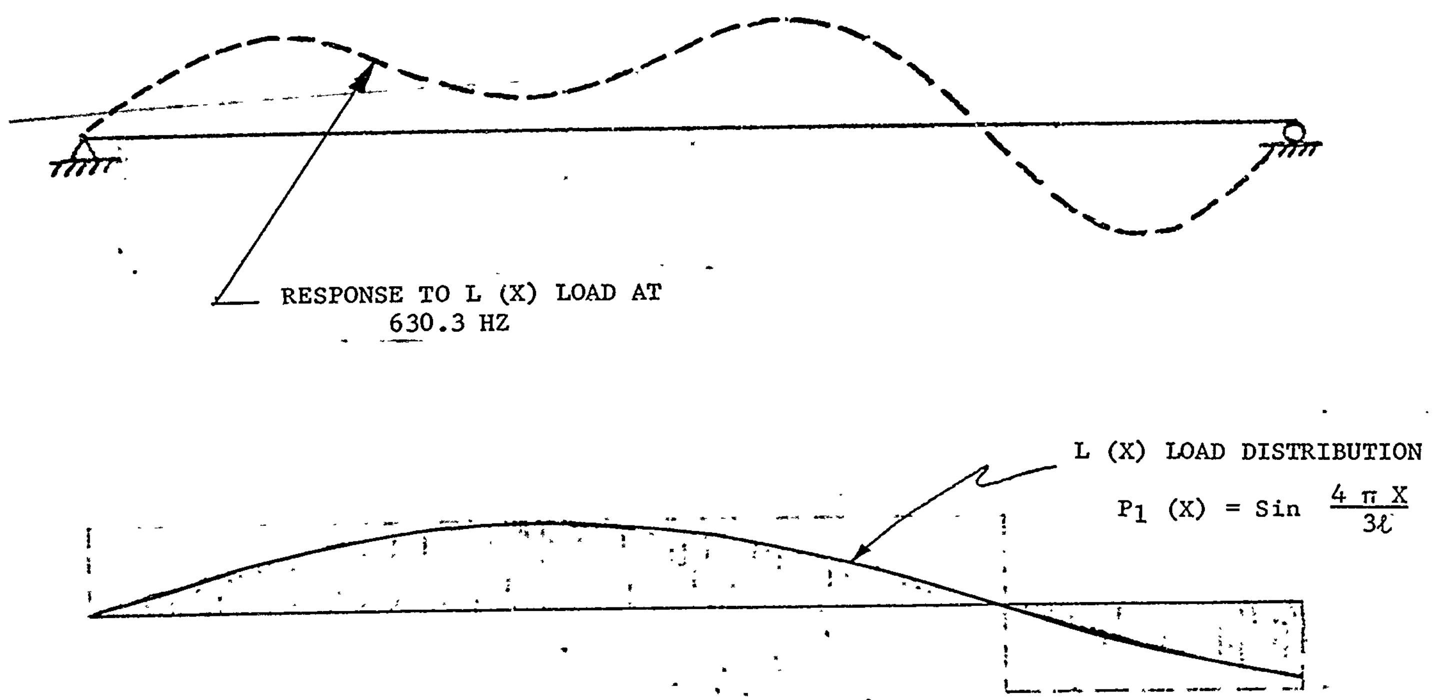

Figure 3. Response of Beam to Arbitrary Smooth Loading Distribution

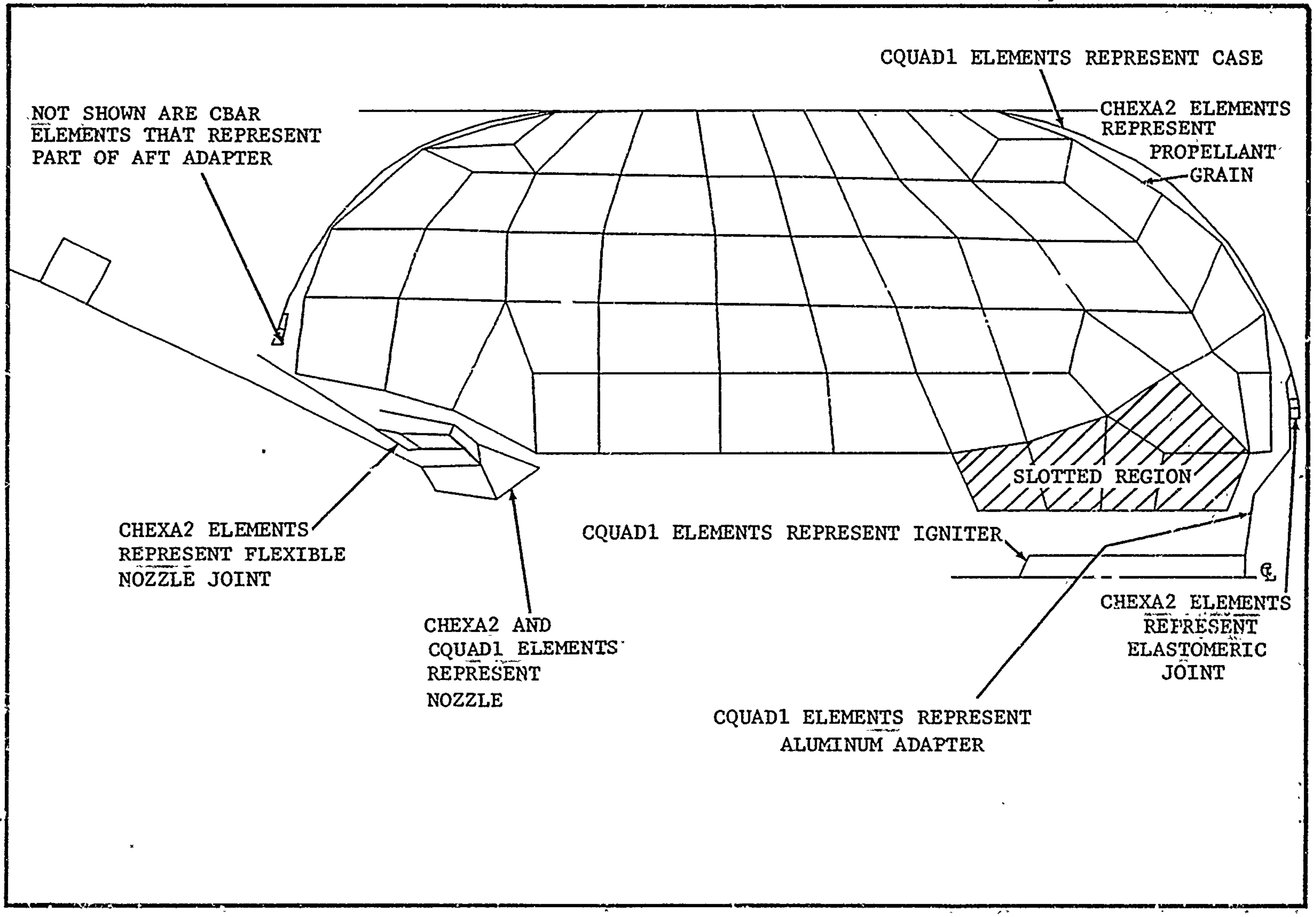

Figure 4. Typical Finite Element Grid for Upper Stage Ballistic Missile Motor

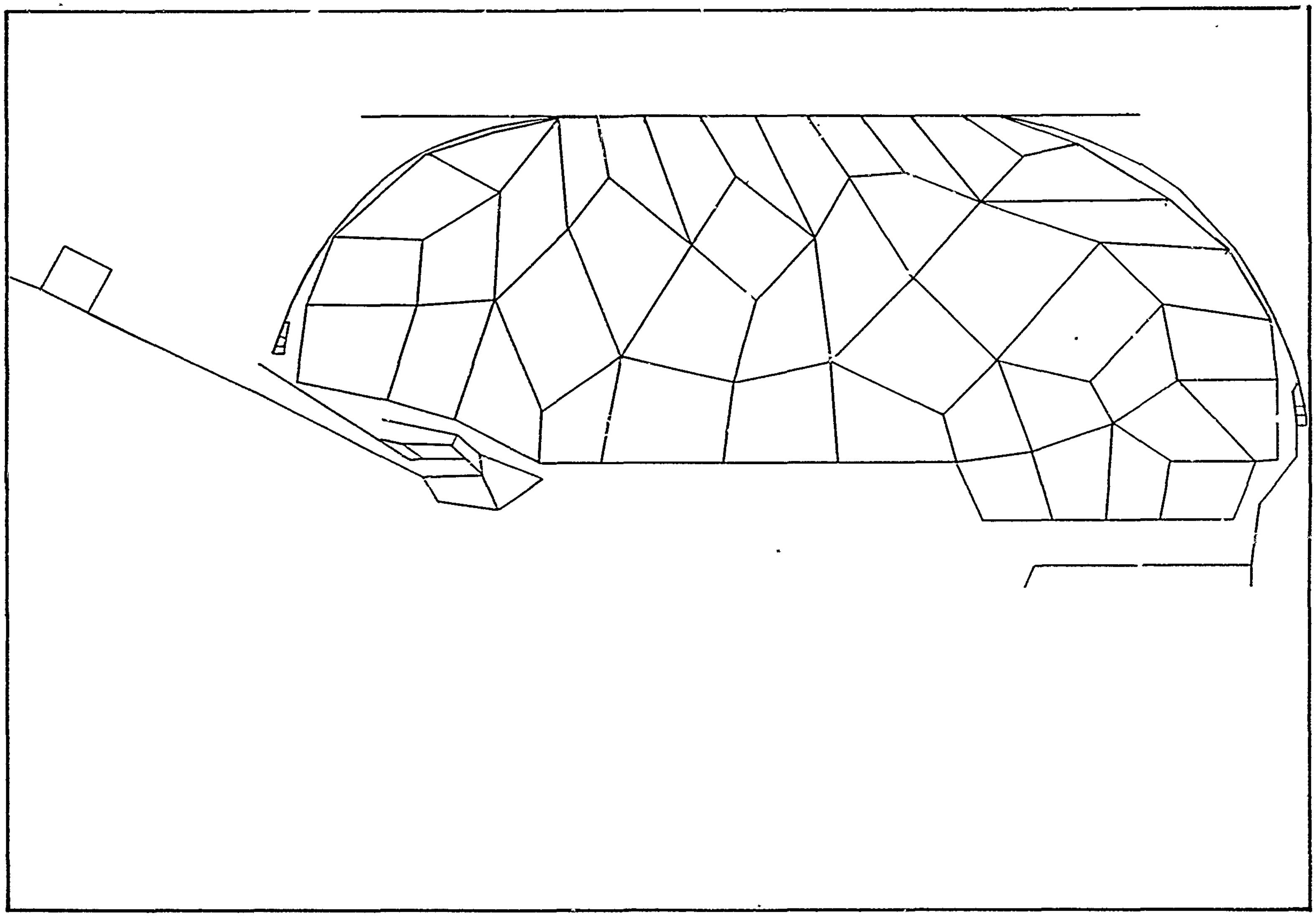

Figure 5. Irregular Grid Used to Reduce Number of Internal Nodes From Number Used in Figure 4

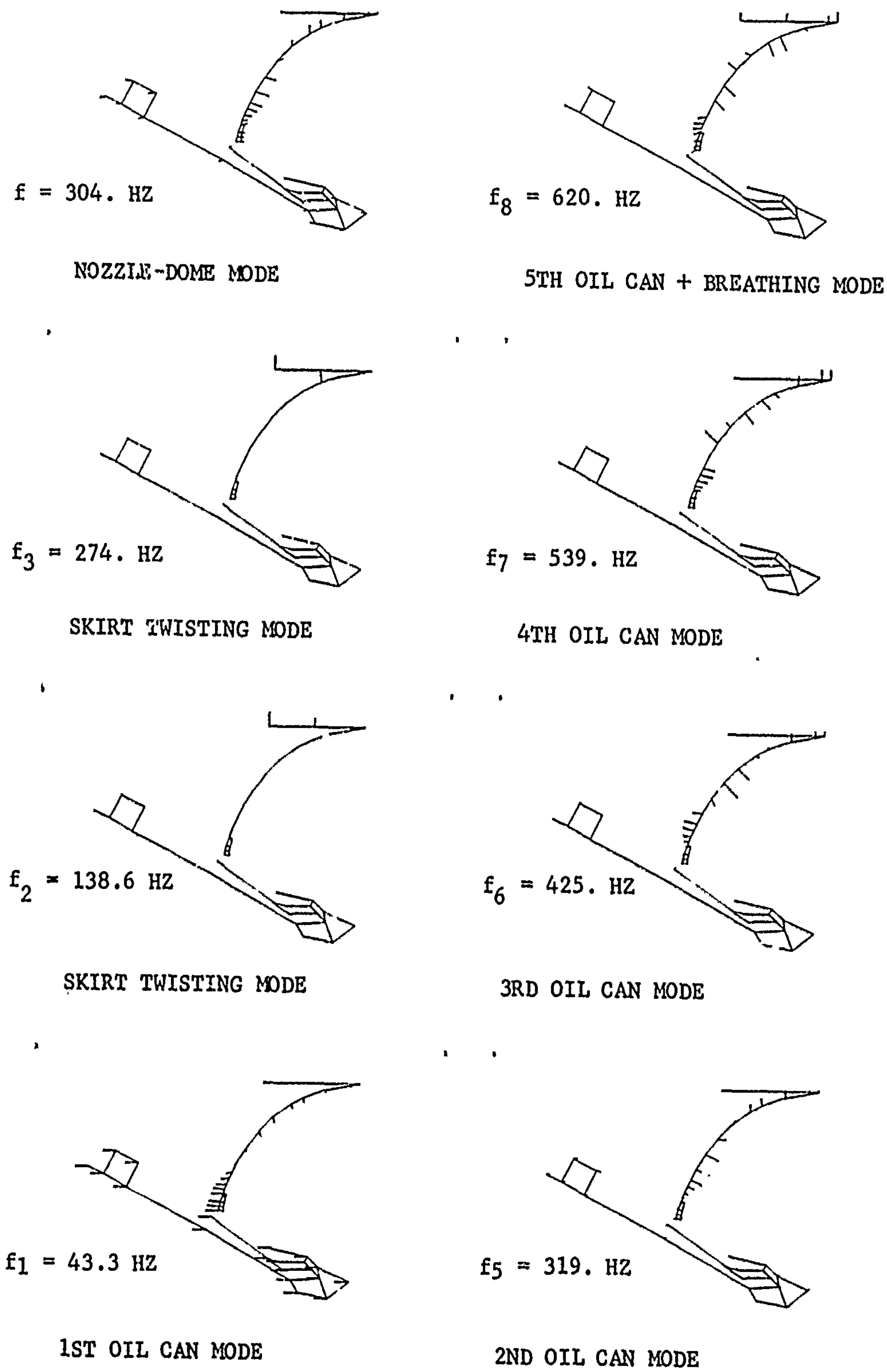

Figure 6. Poseidon C-3 Second Stage Aft Dome Mode Shapes Using a 15° Slice Finite Element Grid

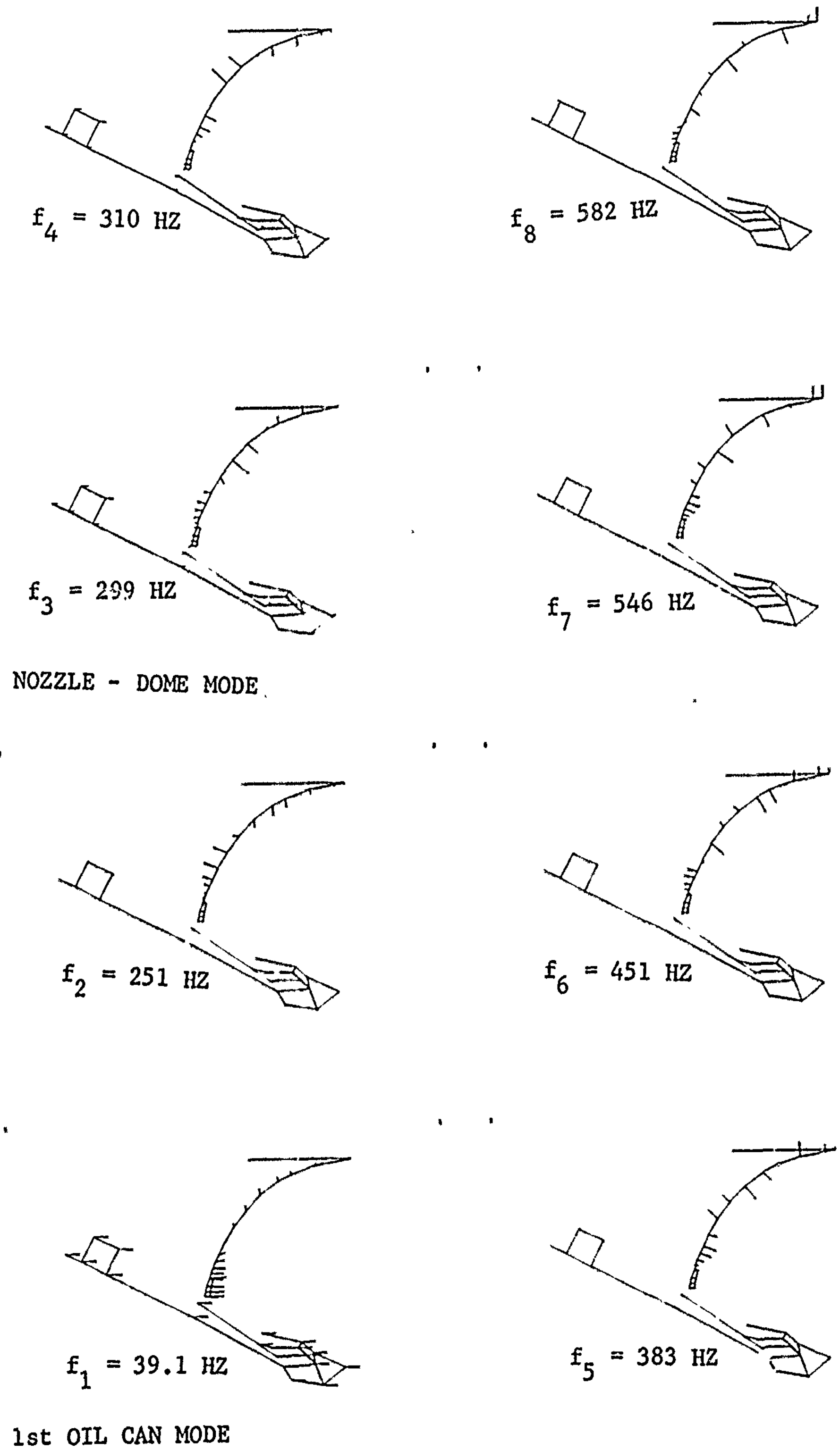

Figure 7. Poseidon C-3 Second Stage Aft Dome Mode Shapes Using a 5° Slice Finite Element Model.

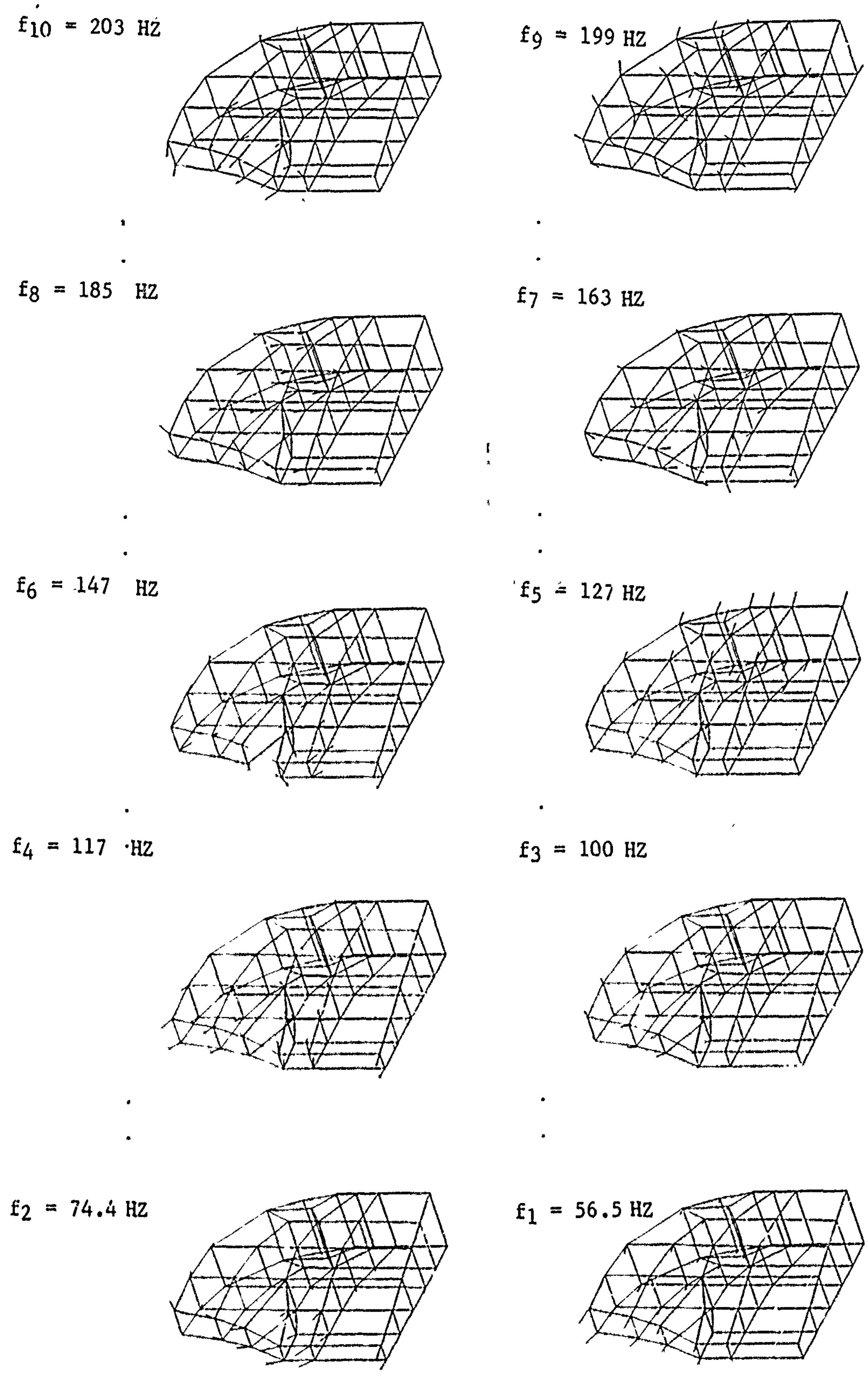

Figure 8. Poseidon C3 Second Stage Aft Half Grain Model Natural Modes for Symmetry Boundary Conditions.

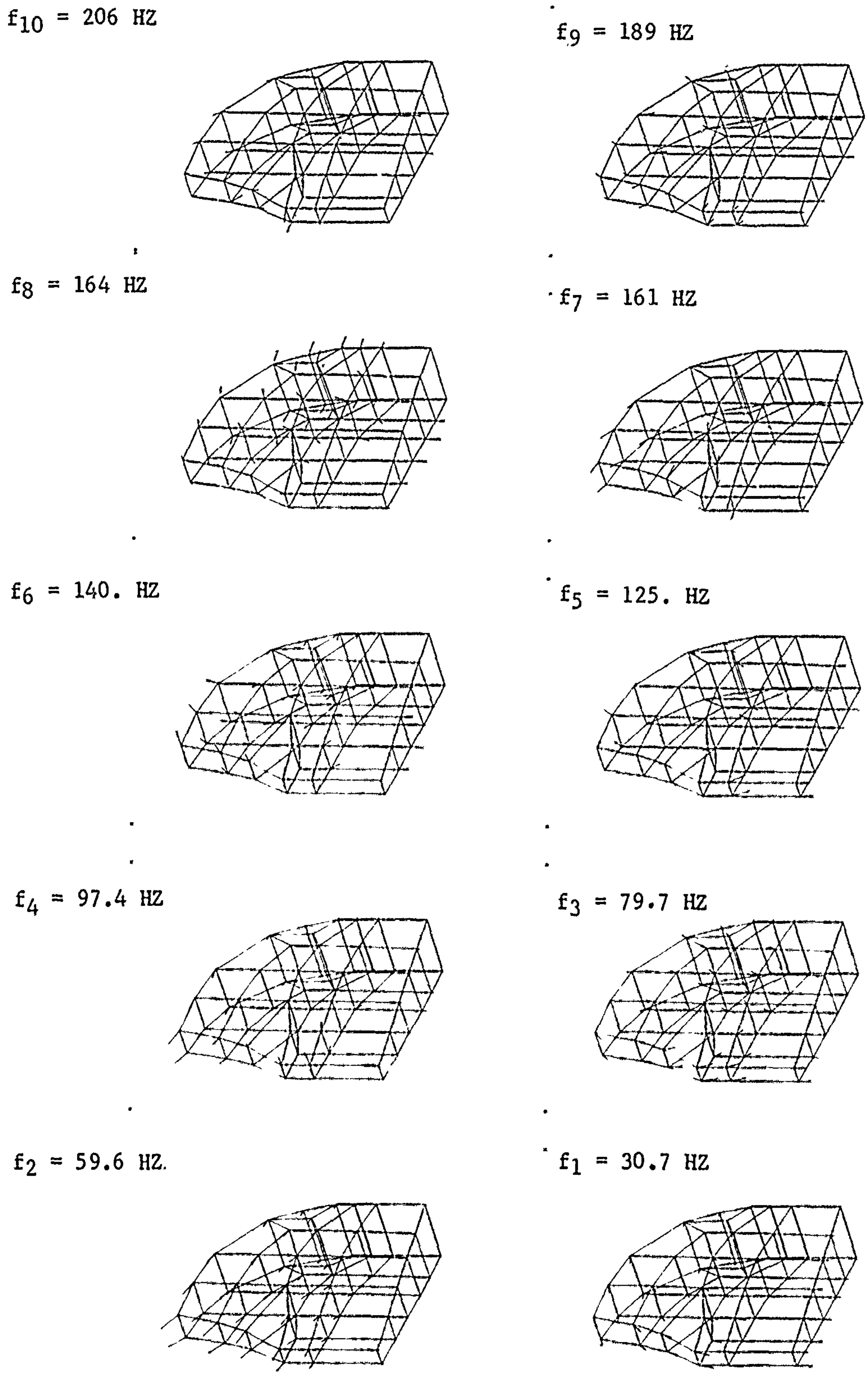

Figure 9. Poseidon C3 Second Stage Aft Half Grain Model Natural Modes for Asymmetric Boundary Conditions

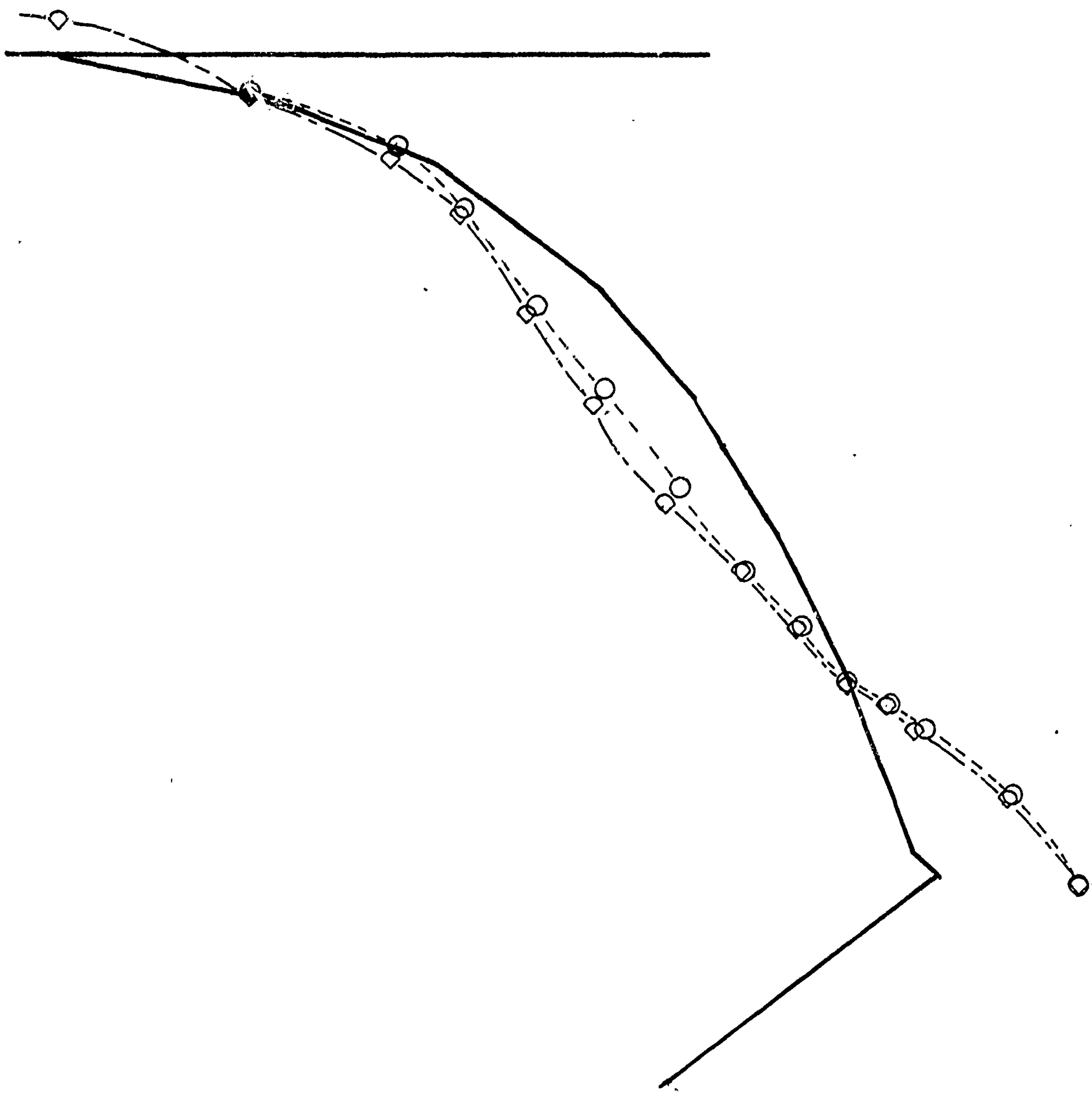

Figure 10. Typical Aft Dome Mode Shapes with and without Scalar Springs for the C-3 Poseidon S/S Motor, Response to the L_3 Mode at 265 Hz

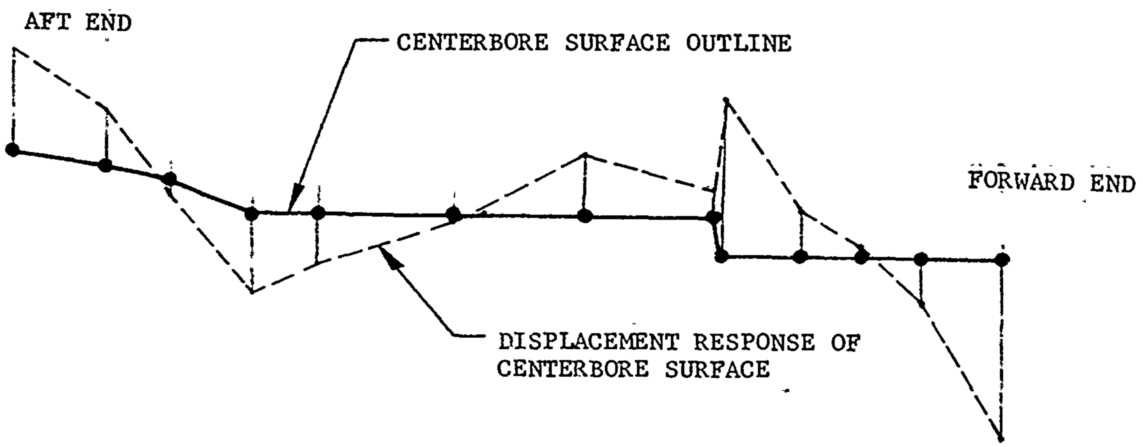

Figure 11. Response of the Poseidon S/S Grain Along the Centerbore to the 770 Hz L_3 Acoustic Mode

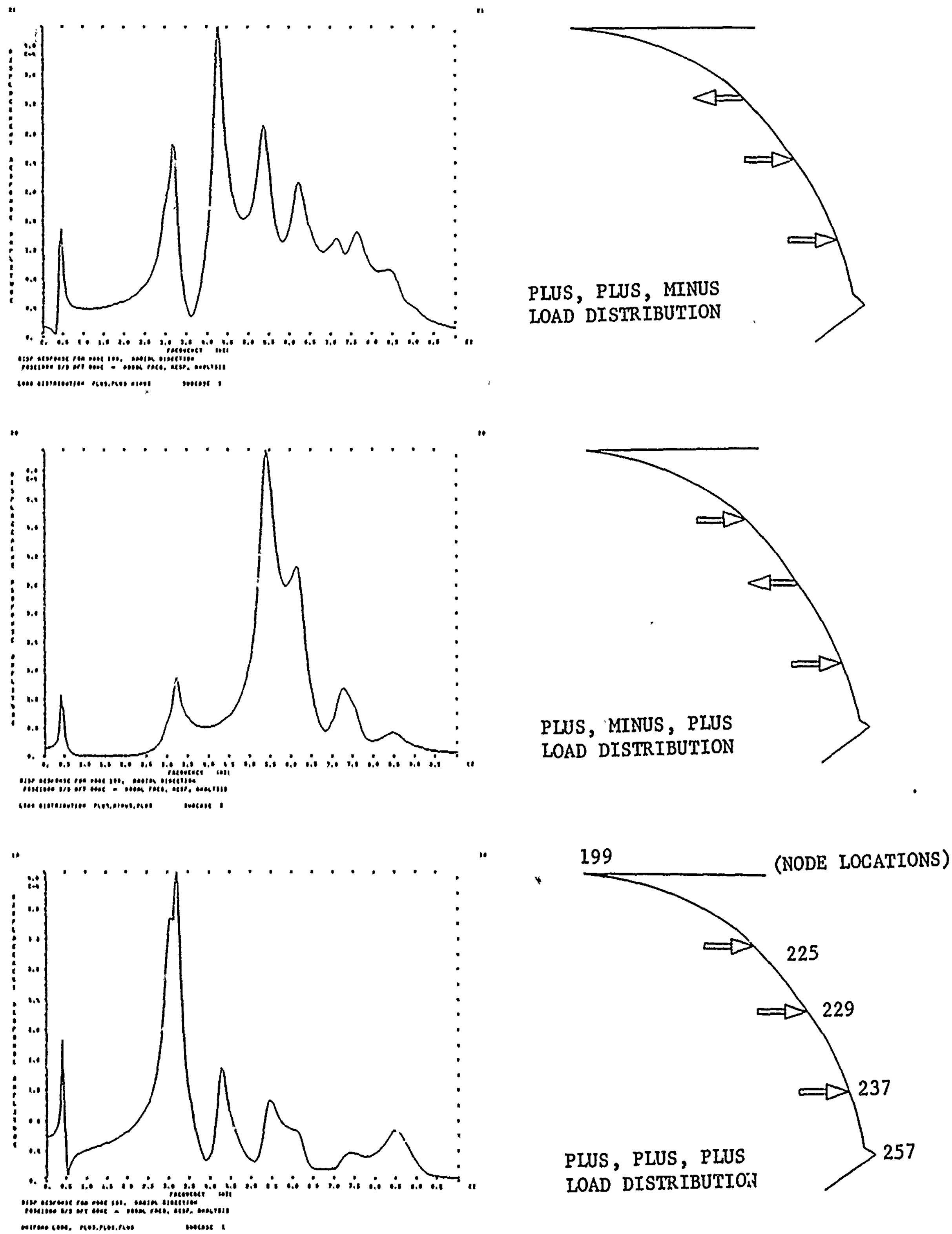

Figure 12 Aft Dome Load Distributions and Frequency Response Plots for Node 199

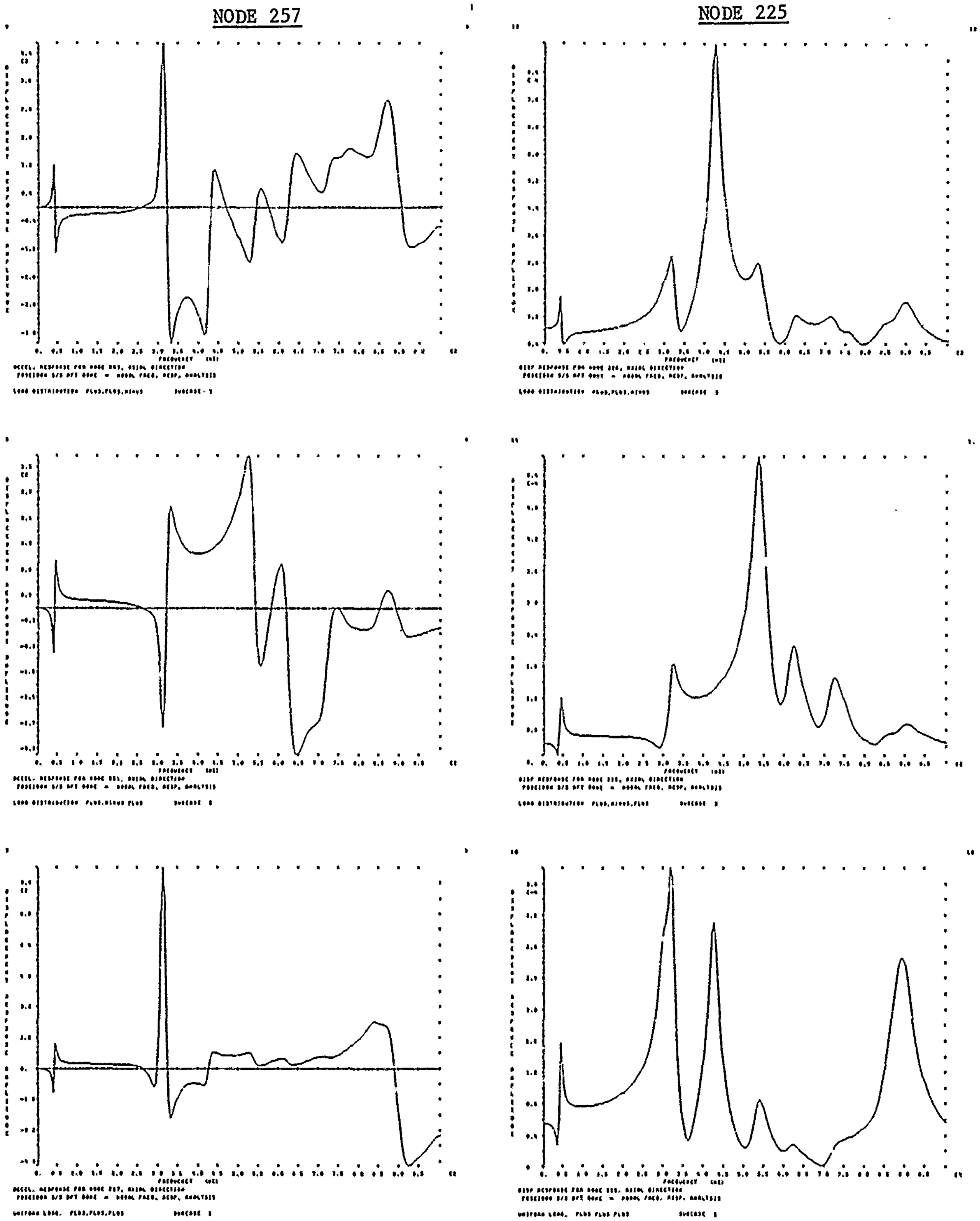

Figure 13. Axial Acceleration Frequency Response Plots for Node 257 and Axial Displacement Response Plots for Node 225

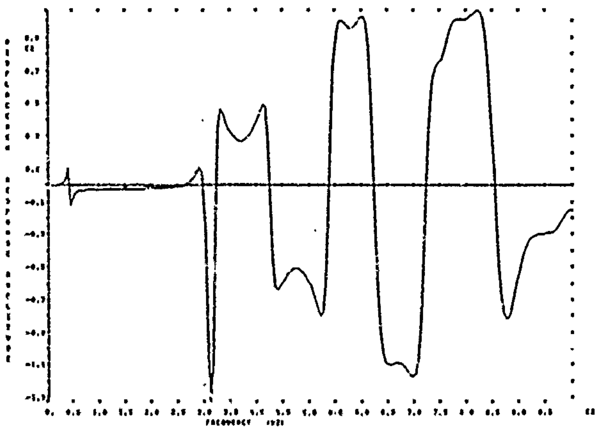

DISPLACEMENT RESPONSE FOR 257 -
AXIAL DIRECTION

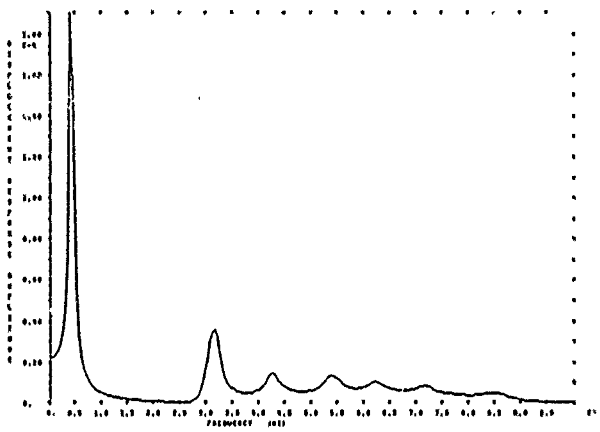

ACCELERATION RESPONSE FOR 257 -
AXIAL DIRECTION

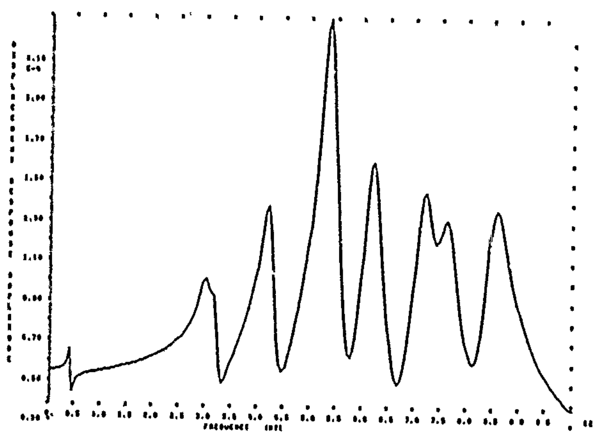

DISPLACEMENT RESPONSE FOR 199-
RADIAL DIRECTION

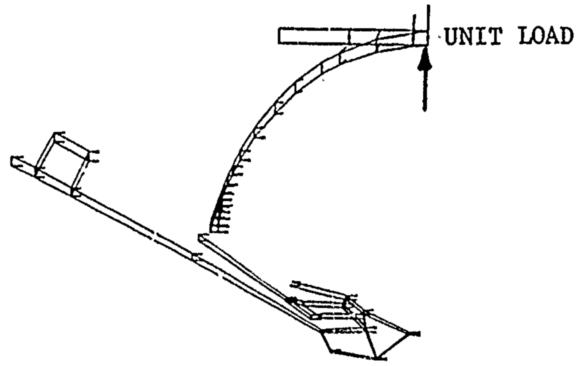

DISPLACEMENTS SHOWN BY VECTORS

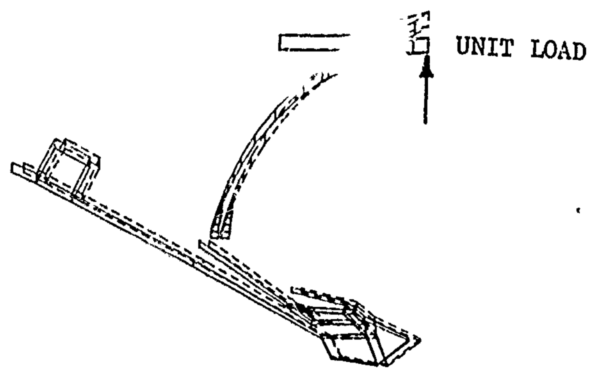

DISPLACED POSITION SHOWN BY DASHED LINES

Figure 14. Aft Dome Static Deformations for a Radial Unit Load Applied at the Wye Joint and Corresponding Response Plots for Load Frequencies Between 0 and 1000 Hz

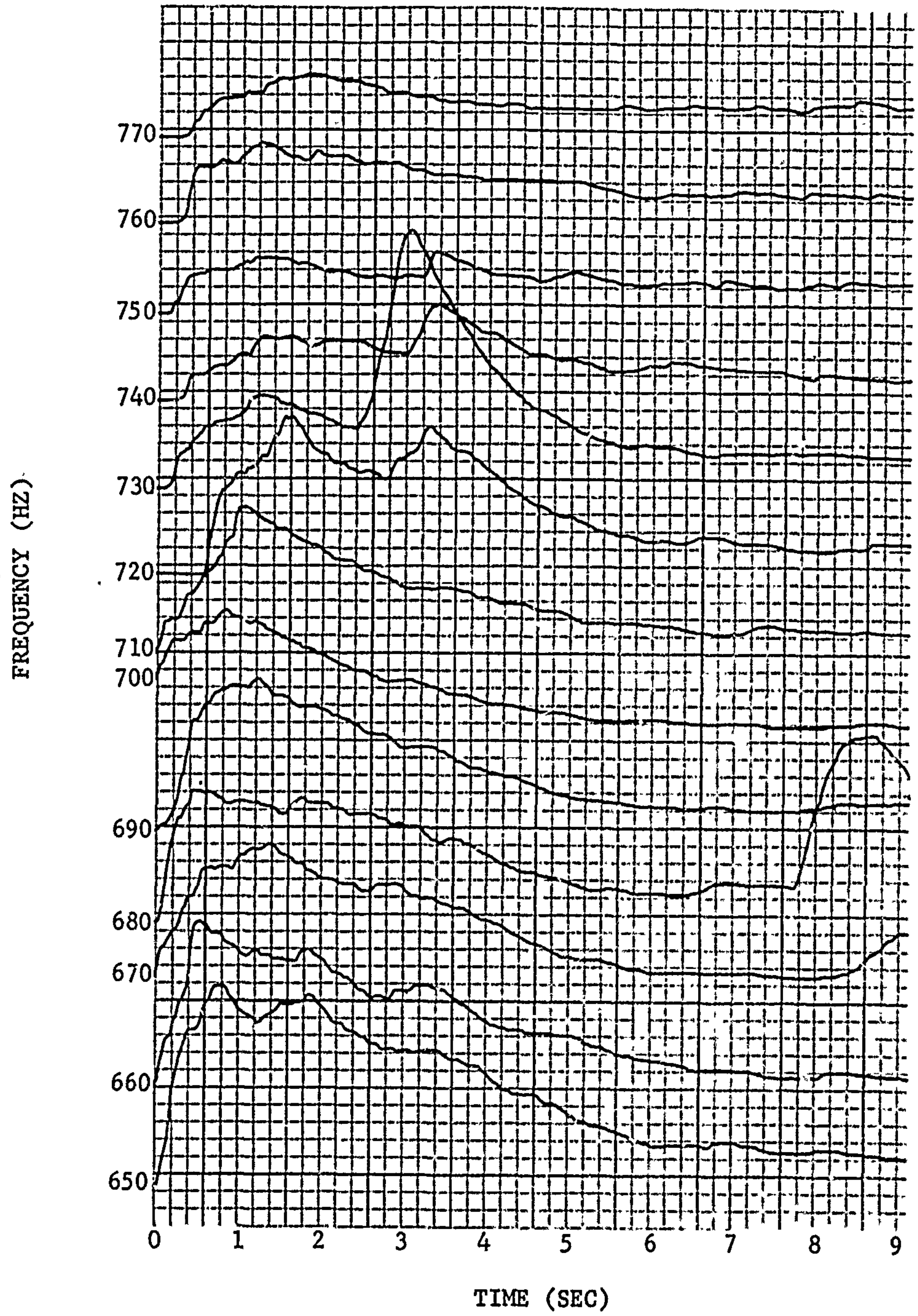

Figure 15. Frequency Mapping for Poseidon ` Motor SP-0160, Accelerometer No. AC-250, Frequency Range 650 ., 770 Hz, Each Curve Showing Acceleration Magnitude

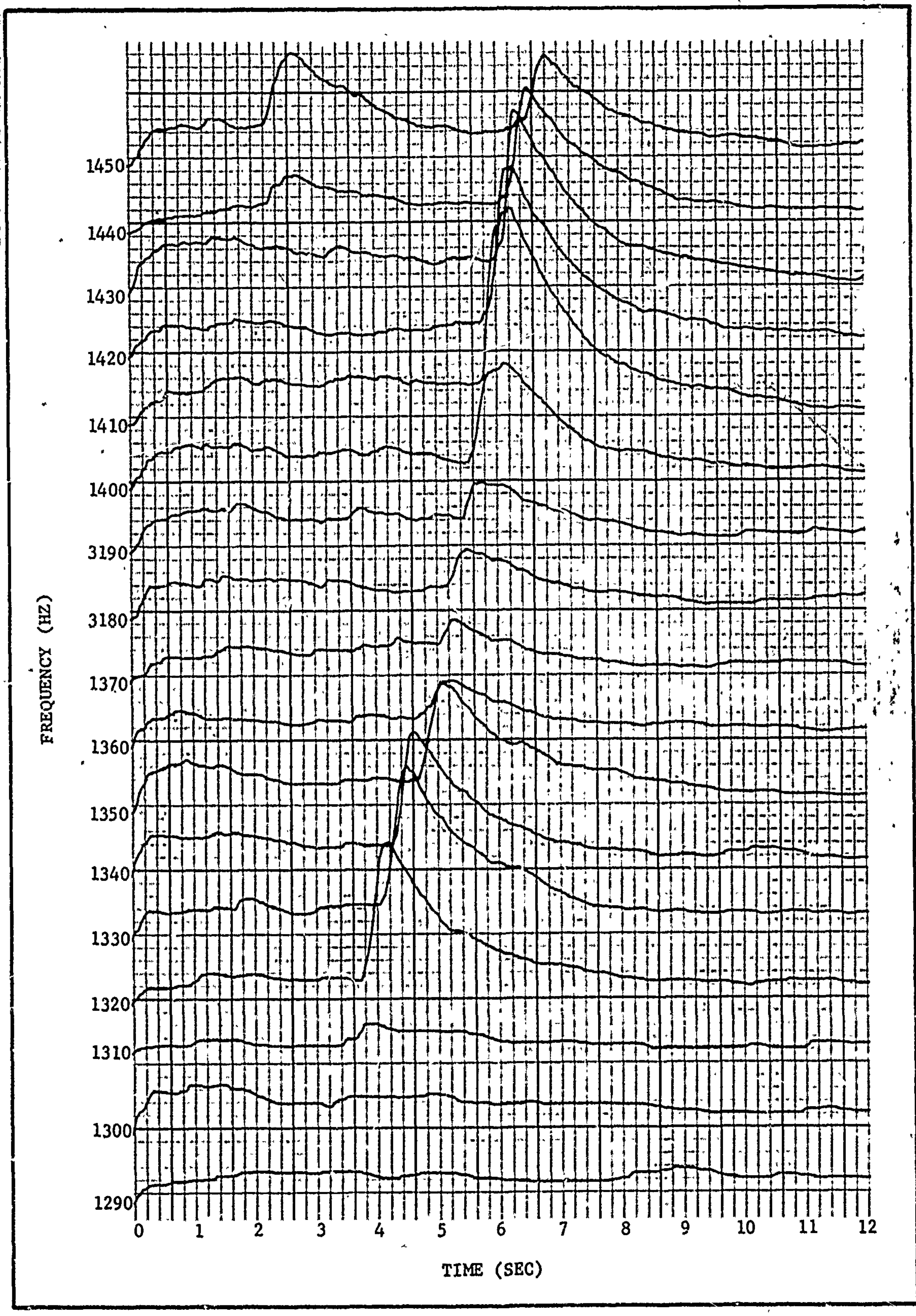

Figure 16. Frequency Mapping for Poseidon S/S Motor SP-0131, Accelerometer No. AC-250, Frequency Range 1290 to 1450 Hz, Each Curve Showing Acceleration Magnitude